Historical warming has almost tripled global population annually exposed to extreme events: Supplementary information

Stefan Lange[1], Jan Volkholz[1], Tobias Geiger[1], Fang Zhao[27], Iliusi Vega del Valle[1], Ted Veldkamp[2,3], Christopher P.O. Reyer[1], Lila Warszawski[1], Veronika Huber[1,4], Jonas Jägermeyr[1,5,6], Jacob Schewe[1], David N. Bresch[7,8], Matthias Büchner[1], Jinfeng Chang[3,9], Philippe Ciais[9], Marie Dury[10], Kerry Emanuel[11], Christian Folberth[3], Dieter Gerten[1,13], Simon N. Gosling[14], Naota Hanasaki[15], Alexandra-Jane Henrot[10], Thomas Hickler[16,17], Yasushi Honda[18], Akihito Ito[15], Nikolay Khabarov[3], Wenfeng Liu[9,19], Christoph Müller[1], Kazuya Nishina[15], Sebastian Ostberg[1], Hannes Müller Schmied[16,17], Sonia I. Seneviratne[20], Tobias Stacke[21], Jörg Steinkamp[16,22], Wim Thiery[20,23], Yoshihide Wada[3], Hong Yang[19,24], Minoru Yoshikawa[25], Chao Yue[26,9], Katja Frieler[1]

[1] Potsdam Institute for Climate Impact Research (PIK), Member of the Leibniz Association, Germany; [2] Institute for Environmental Studies, VU Amsterdam, Netherlands; [3] International Institute for Applied Systems Analysis (IIASA), Laxenburg, Austria; [4] Universidad Pablo de Olavide Sevilla, Spain; [5] NASA Goddard Institute for Space Studies, New York, NY 10025, USA; [6] Department of Computer Science, University of Chicago, Chicago, IL 60637, USA [7] Institute for Environmental Decisions, ETH Zurich, Switzerland; [8] Federal Office of Meteorology and Climatology MeteoSwiss, Switzerland; [9] Laboratoire des Sciences du Climat et de l'Environnement, CEA CNRS UVSQ, Institut Pierre Simon Laplace, Gif sur Yvette, France; [10] Unit for Modelling of Climate and Biogeochemical Cycles, University of Liege, Belgium; [11] Lorenz Center, Massachusetts Institute of Technology, USA; [13] Geography Department, Humboldt-Universität zu Berlin, Germany; [14] School of Geography, University of Nottingham, Nottingham, UK; [15] National Institute for Environmental Studies, Tsukuba, Japan; [16] Senckenberg Biodiversity and Climate Research Centre (SBiK-F), Germany; [17] Institute of Physical Geography, Goethe-University Frankfurt, Germany; [18] University of Tsukuba, Japan; [19] Swiss Federal Institute of Aquatic Science and Technology (Eawag), Switzerland; [20] Institute for Atmospheric and Climate Science, ETH Zurich, Switzerland; [21] Max Planck Institute for Meteorology, Germany; [22] Johannes Gutenberg-Universität Mainz, Anselm-Franz-von-Bentzel-Weg 12, 55128 Mainz, Germany; [23] Department of Hydrology and Hydraulic Engineering, Vrije Universiteit Brussel, Belgium; [24] Department of Environmental Sciences, MUG, University of Basel, Switzerland; [25] Mizuho Information & Research Institute Inc., Tokyo, Japan; [26] State Key Laboratory of Soil Erosion and Dryland Farming on the Loess Plateau, Northwest A&F University, Yangling, Shaanxi 712100, P.R. China; [27] School of Geographic Sciences, East China Normal University, Shanghai 200241, China

Contents

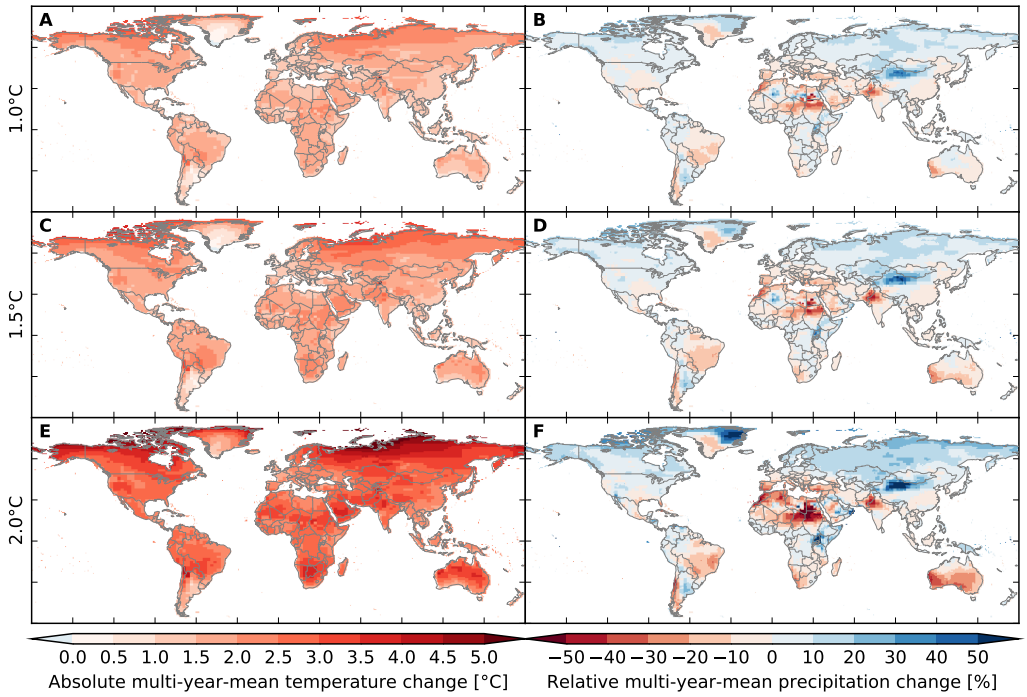

Figure S1: Warming patterns (left) and precipitation changes (right) projected by GFDL-ESM2M for different levels of global warming (rows) relative to preindustrial climate conditions. To calculate multi-year-mean temperature and precipitation for different warming levels, simulation years are pooled in the same way as for the calculation of changes in areas affected by and people exposed to extremes.

1 Climate and impact model characteristics

Table S1 provides the GCM-specific number of simulation years per global warming level bin for bins centered at 1 °C, 1.5 °C, and 2 °C global warming that are used to quantify the pure effect of climate change on extremes.

Based on these warming level bins, spatial warming and precipitation change patterns at 1 °C, 1.5 °C, and 2 °C global warming for GFDL-ESM2M, IPSL-CM5A-LR and MIROC5 are depicted in Figs. S1, S2 and S3, respectively.

Table S2 summarizes which direct human influences were considered in the impact model simulations analysed in this study. For details see Tables S5, S6 and S7.

Table S1: GCM-specific number of simulation years (from the historical, RCP2.6 and RCP6.0 simulations done within CMIP5) per global warming level bin of 1 °C width centered at different global warming levels ΔT.

	GFDL-ESM2M	IPSL-CM5A-LR	MIROC5
ΔT = 1.0 °C	157	56	279
ΔT = 1.5 °C	139	143	324
ΔT = 2.0 °C	44	322	115

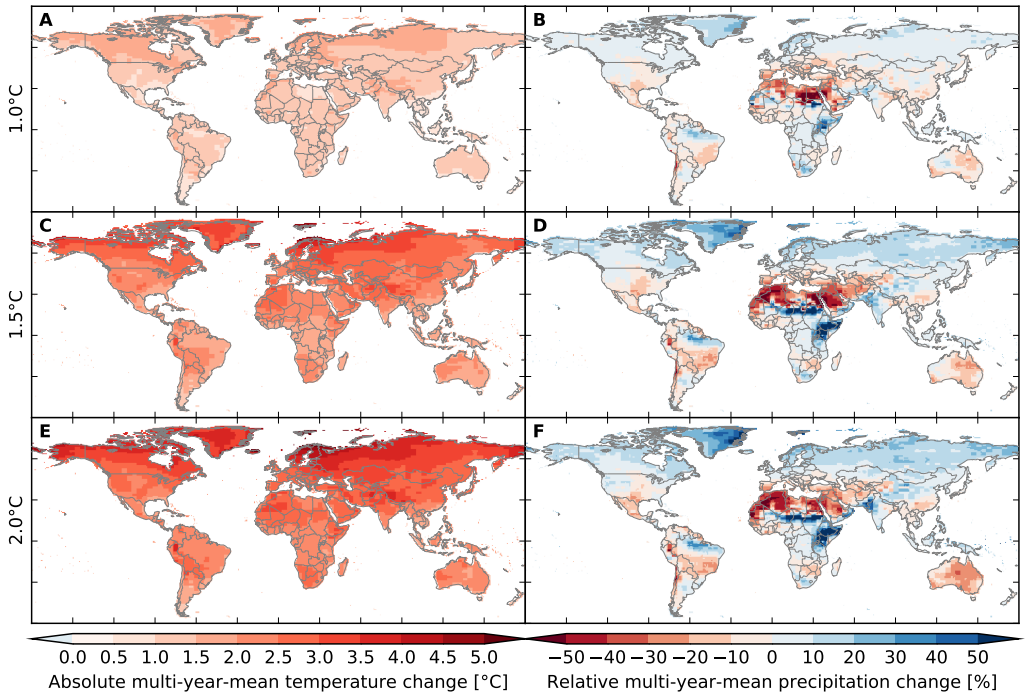

Figure S2: Same as Fig. S1 but for IPSL-CM5A-LR.

2 Multi-model ensemble statistics

2.1 Emulation of missing values in the climate model-impact model matrix of results

Missing values in the climate model-impact model matrix of results are emulated based on available results using the following procedure, which is independently applied to results for different global warming levels and categories of extremes.

Let x_{ij} denote an available result for climate model i and impact model j. Let further J be the set of all impact models for which results are available for all three climate models, and let $n = \sum_{j \in J} 1$ be the number of those impact models. Let μ_i denote the sample mean value of x_{ij} over all impact models in J,

$$\mu_i = \frac{1}{n} \sum_{j \in J} x_{ij}, \tag{1}$$

and let σ_i denote the sample standard deviation of x_{ij} over all impact models in J,

$$\sigma_i^2 = \frac{1}{n-1} \sum_{j \in J} (x_{ij} - \mu_i)^2. \tag{2}$$

Let further I_{ij} be the set of all climate models $k \neq i$ for which x_{kj} is available, and let $n_{ij} = \sum_{k \in I_{ij}} 1$ be the number of those climate models. Then we emulate $\hat{x}_{ij}$, the formerly missing result for climate model i and impact model j, by

$$\hat{x}_{ij} = \mu_i + \frac{1}{n_{ij}} \sum_{k \in I_{ij}} \frac{\sigma_i}{\sigma_k} (x_{kj} - \mu_k). \tag{3}$$

2.2 Multi-model ensemble statistics of changes in global land area affected by and global population exposed to extremes

We use the annual data behind Figures S1 and S3 of the main text to calculate multi-model ensemble statistics over all climate model-impact model combinations of the change in global land area (absolute

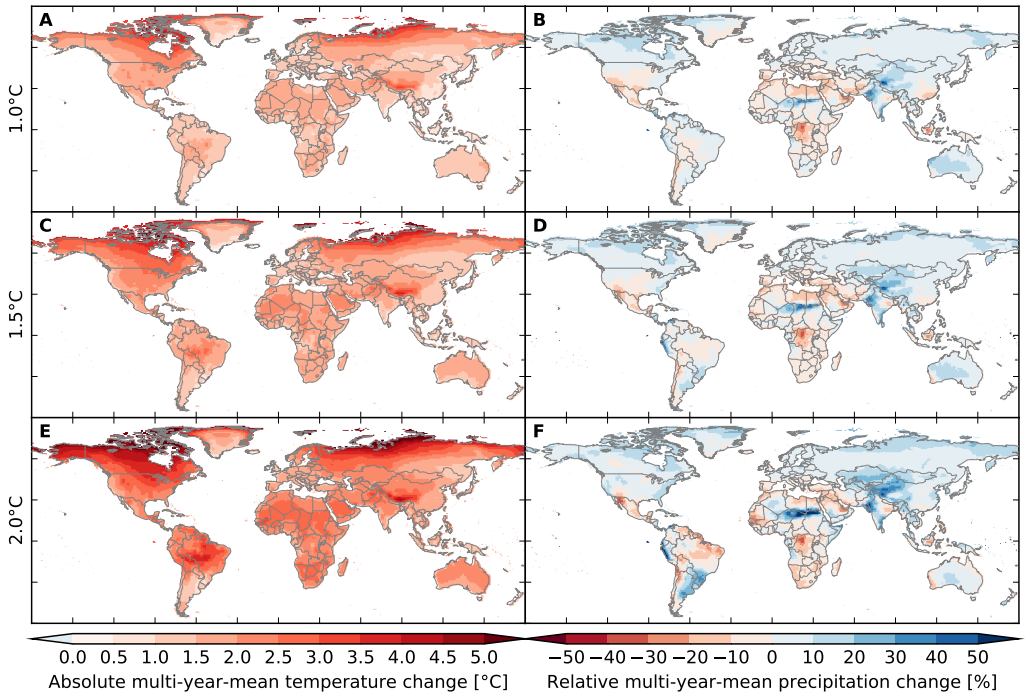

Figure S3: Same as Fig. S1 but for MIROC5.

numbers in million hectar) affected by and global population (absolute numbers in million, based on 2005 population) exposed to extremes related to different levels of global mean temperature change (Tables S3 and S4).

Also shown in those tables are the results of an analysis of variance (ANOVA) of the changes simulated by or emulated for all climate model-impact model combinations. The contributions of climate models and impact models to the overall variance were quantified applying the ANOVA with subsampling introduced by (6). The last column of Tables S3 and S4 shows the contribution of climate model-impact model interactions to the multi-model variance of multi-year mean changes of the global land area affected by and the global population exposed to extremes, respectively. The sum of the contributions by climate models, impact models and climate model-impact model interactions always equals 100%.

Table S2: Direct human influences (DHIs) considered in impact model simulations analysed in this study. The following abbreviations are used: hist, historical changes of DHIs considered up to 2005 and fixed at 2005 levels thereafter (histsoc and 2005soc according to ISIMIP2b protocol, respectively); fixed, DHIs considered fixed at 2005 levels (2005soc according to ISIMIP2b protocol); fixed*, DHIs considered fixed at levels representative of some recent historical period (see Section 5); NA, DHIs not considered. For details see Tables S5, S6 and S7.

Global hydrological model	land-use patterns	irrigation patterns	domestic and industrial water use	livestock water use	dams and reservoirs
CLM4.5	fixed	fixed	NA	NA	NA
H08	fixed	fixed	fixed	NA	fixed
LPJmL	hist	hist	hist	NA	hist
JULES-W1	fixed	fixed	NA	NA	NA
MPI-HM	hist	hist	NA	NA	NA
ORCHIDEE	hist	hist	NA	NA	NA
PCR-GLOBWB	hist	hist	hist	hist	hist
WaterGAP2	fixed	hist	hist	hist	hist

Global vegetation model	land-use patterns	irrigation patterns	influence on fire ignition and suppression
CARAIB	hist	NA	NA
LPJ-GUESS	hist	NA	NA
LPJmL	hist	hist	NA
ORCHIDEE	hist	hist	hist
VISIT	hist	NA	NA

Global gridded crop model	land-use patterns	irrigation patterns	cultivars	sowing dates	fertilizer input
GEPIC	hist	hist	fixed*	fixed*	fixed
LPJmL	hist	hist	fixed*	fixed*	NA
PEPIC	hist	hist	fixed*	fixed*	fixed

Table S3: Multi-climate model-impact model-ensemble statistics of absolute changes in multi-year mean annual global land area affected by different categories of extreme events at different levels of global warming relative to preindustrial climate conditions. Asterisks (plus signs) in column 3 indicate that at least 80% of all model combinations agree on an increase or decrease (a change) that is larger than 2 standard deviations (smaller than 1 standard deviation) of the preindustrial interannual variability. Values in columns 4–6 represent percentages of the global land area. Columns 7–9 show ANOVA results, where CM, IM, and VF abbreviate climate model, impact model, and variance fraction, respectively. Column 10 shows the multi-model-median pure effect of socioeconomic development (PESED) from 1860 to 2005 in both absolute and relative terms (CF abbreviates change factor). The last column shows the multi-model-median baseline under preindustrial climate and 2005 socioeconomic conditions.

event category	warming (°C)	median (Mha)	median (%)	mean (%)	std (%)	CM VF (%)	IM VF (%)	interaction VF (%)	PESED (Mha, CF)	baseline (Mha)
River Flood	1.0	13	0.082	0.076	0.024	86	8.3	6.1	0.52, 1.049x	13
	1.5	17*	0.11	0.11	0.020	24	59	18		
	2.0	28*	0.18	0.18	0.035	61	24	15		
Tropical Cyclone	1.0	5.5	0.034	0.084	0.10	99	0.15	0.38	−1.8, 0.966x	42
	1.5	7.9	0.049	0.11	0.10	99	0.16	0.37		
	2.0	16	0.10	0.14	0.093	99	0.32	0.67		
Crop Failure	1.0	6.4	0.040	0.056	0.050	60	20	20	7.2, 2.5x	13
	1.5	11	0.066	0.086	0.072	70	17	13		
	2.0	19	0.12	0.12	0.066	56	32	12		
Wildfire	1.0	8.4	0.052	0.084	0.25	8.0	91	1.4	−28, 0.930x	105
	1.5	11	0.065	0.10	0.36	4.2	94	1.5		
	2.0	14	0.086	0.15	0.51	5.1	93	1.6		
Drought	1.0	235	1.5	1.3	0.75	7.8	83	9.4	−3.5, 0.950x	150
	1.5	356	2.2	1.9	1.1	29	66	5.0		
	2.0	486*	3.0	2.6	1.5	18	73	9.3		
Heatwave	1.0	381*	2.4	2.2	0.72	100	0	0	0.55, 1.059x	37
	1.5	638*	4.0	3.8	0.64	100	0	0		
	2.0	1060*	6.6	6.3	1.0	100	0	0		
Drought/Heatwave	1.0	596*	3.7	3.6	1.1	32	63	5.2	−2.7, 0.973x	172
	1.5	911*	5.7	5.7	1.3	41	55	3.6		
	2.0	1451*	9.0	8.8	1.5	10	80	9.6		
River Flood/Crop Failure/	1.0	40	0.25	0.30	0.23	33	65	2.3	−20, 0.978x	168
Tropical Cyclone/Wildfire	1.5	61	0.38	0.39	0.34	21	77	1.9		
	2.0	83	0.52	0.57	0.47	17	81	2.1		
River Flood/Crop Failure/	1.0	660*	4.1	3.9	0.90	26	61	13	−26, 0.968x	352
Tropical Cyclone/Wildfire/	1.5	935*	5.8	5.7	1.2	46	52	2.4		
Drought/Heatwave	2.0	1503*	9.3	8.9	1.4	26	68	5.6		

Table S4: Multi-climate model-impact model-ensemble statistics of absolute changes in multi-year mean annual global population exposed to different categories of extreme events at different levels of global warming relative to preindustrial climate conditions. Asterisks (plus signs) in column 3 indicate that at least 80% of all model combinations agree on an increase or decrease (a change) that is larger than 2 standard deviations (smaller than 1 standard deviation) of the preindustrial interannual variability. Values in columns 4–6 represent percentages of the global population. Columns 7–9 show ANOVA results, where CM, IM, and VF abbreviate climate model, impact model, and variance fraction, respectively. Column 10 shows the multi-model-median pure effect of socioeconomic development (PESED) from 1860 to 2005 in both absolute and relative terms (CF abbreviates change factor). The last column shows the multi-model-median baseline under preindustrial climate and 2005 socioeconomic conditions.

event category	warming (°C)	median (million)	median (%)	mean (%)	std (%)	CM VF (%)	IM VF (%)	interaction VF (%)	PESED (million, CF)	baseline (million)
River Flood	1.0	6.7	0.10	0.10	0.086	91	7.6	1.1	−0.046, 0.9940x	11
	1.5	8.5	0.13	0.16	0.070	90	8.3	1.9		
	2.0	13	0.20	0.24	0.11	84	13	2.8		
Tropical Cyclone	1.0	5.8	0.090	0.25	0.28	98	0.41	1.2	13, 1.45x	52
	1.5	14	0.21	0.33	0.28	98	0.58	1.0		
	2.0	17	0.27	0.40	0.27	96	1.3	2.4		
Crop Failure	1.0	18	0.27	0.28	0.24	39	37	24	−8.0, 0.68x	25
	1.5	27	0.41	0.52	0.45	60	25	15		
	2.0	51	0.78	0.76	0.44	43	43	14		
Wildfire	1.0	4.2	0.064	0.0010	0.36	9.7	80	10	−6.6, 0.88x	53
	1.5	7.0	0.11	−0.015	0.49	4.6	89	6.2		
	2.0	9.6	0.15	−0.0023	0.64	6.1	87	7.1		
Drought	1.0	32	0.50	0.57	0.40	15	77	7.8	−7.0, 0.58x	17
	1.5	48	0.74	0.74	0.49	18	75	7.6		
	2.0	70	1.1	1.1	0.75	20	69	11		
Heatwave	1.0	211*	3.3	3.6	0.82	100	0	0	3.5, 1.63x	39
	1.5	474*	7.3	6.8	2.1	100	0	0		
	2.0	762*	12	12	0.94	100	0	0		
Drought/Heatwave	1.0	272*	4.2	4.3	0.89	54	33	13	−8.5, 0.80x	51
	1.5	512*	7.9	7.4	1.9	94	4.2	2.1		
	2.0	819*	13	12	0.84	58	34	7.1		
River Flood/Crop Failure/ Tropical Cyclone/Wildfire	1.0	47	0.72	0.62	0.42	44	43	13	−4.9, 0.959x	131
	1.5	66	1.0	0.90	0.58	49	44	7.6		
	2.0	90*	1.4	1.3	0.69	35	56	8.1		
River Flood/Crop Failure/ Tropical Cyclone/Wildfire/ Drought/Heatwave	1.0	337*	5.2	5.0	1.1	56	22	22	−28, 0.89x	188
	1.5	555*	8.6	7.9	2.2	93	7.0	0.43		
	2.0	867*	13	13	1.2	64	33	2.9		

2.3 Relative change in annual national land area affected by and population exposed to aggregated extremes

Relative changes corresponding to absolute changes shown in Figures S2 and S4 of the main text are shown in Figures S4 and S5, respectively.

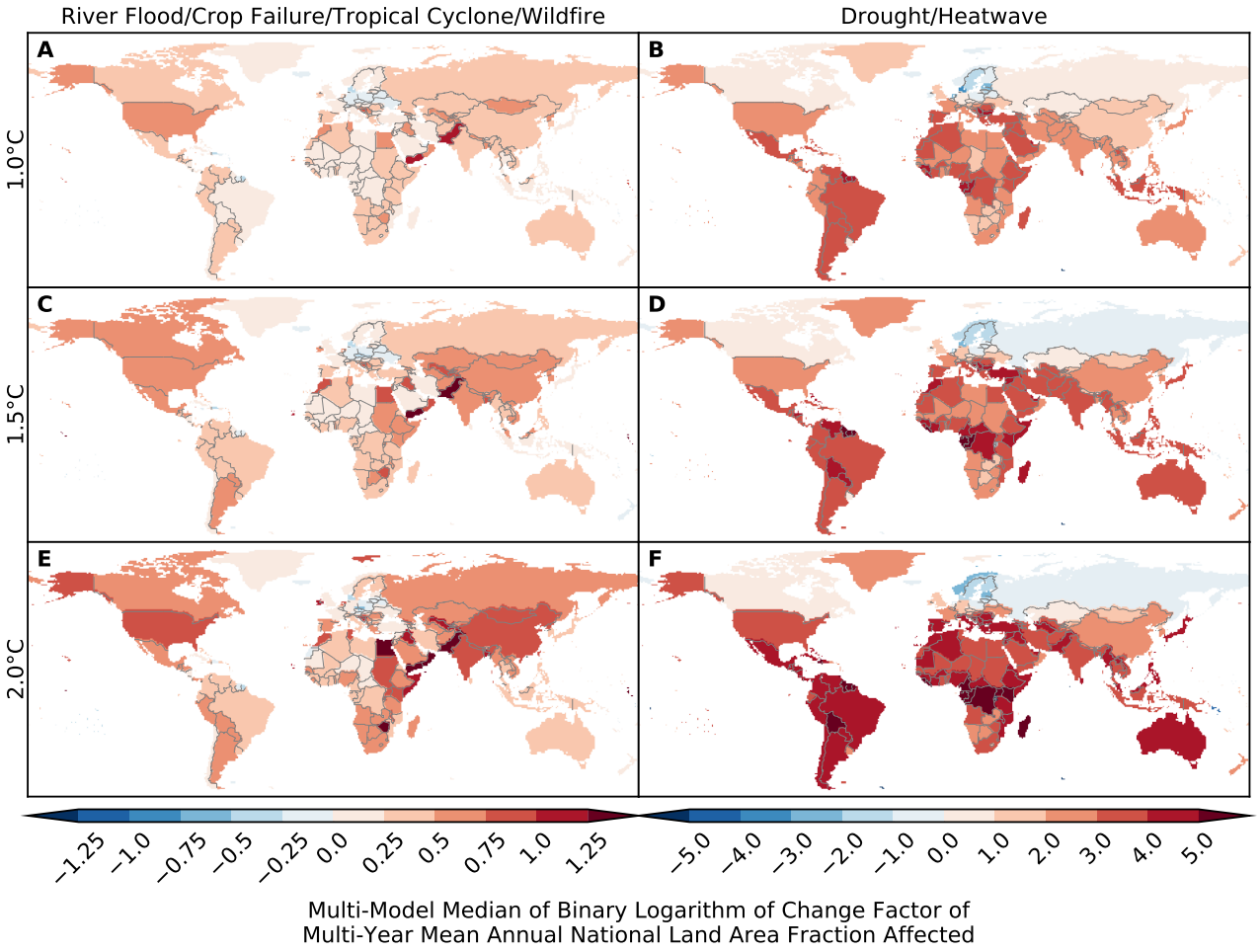

Figure S4: **Pure effect of climate change on the annual national land area fraction affected by aggregated extremes.** Multi-model median relative change in multi-year mean annual national land area fraction affected by (A, C, E) river flood/crop failure/tropical cyclone/wildfire and (B, D, F) drought/heatwave at (A, B) 1 °C, (C, D) 1.5 °C and (E, F) 2 °C global warming. Shown are the binary logarithms of the change factors, i.e. −2, −1, 0, 1, 2 means that the new value is 1/4, 1/2, 1, 2, 4 times the old value, which is equivalent to a relative change by −75 %, −50 %, 0 %, +100 %, +300 %, respectively.

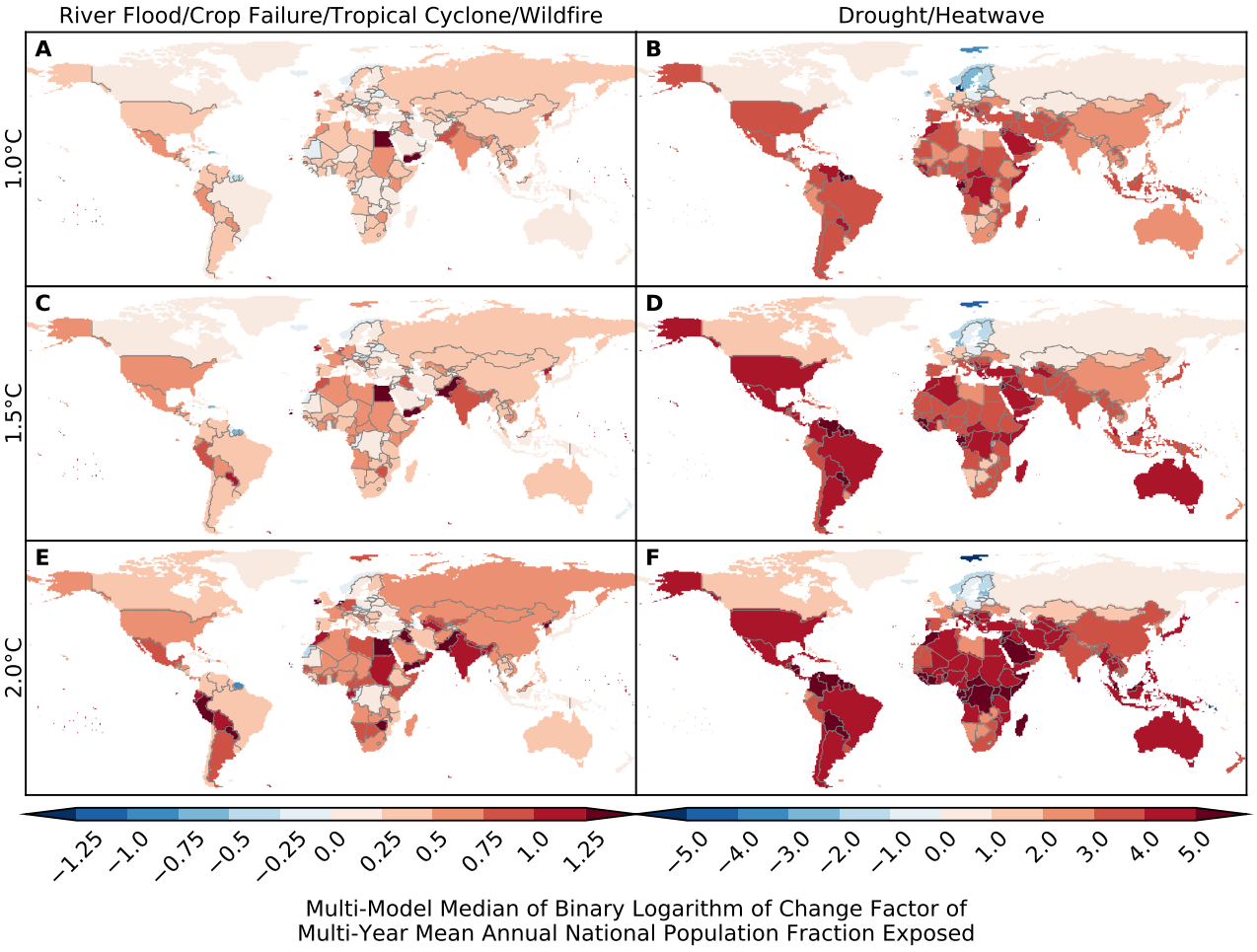

Figure S5: **Pure effect of climate change on the annual national population fraction exposed to aggregated extremes.** Same as Figure S4 but for the annual national population fraction exposed.

3 Calculation of land area affected by and number of people exposed to river floods

Flooded areas are derived from seven Global Hydrological Models (GHM) (see Table S5. All models are forced by bias-corrected daily climate data provided within ISIMIP2b (20). They assume fixed socioeconomic conditions (e.g. changes in land-use patterns) before 1860 (1860soc for 1661–1860 according to the ISIMIP2b protocol), and if possible account for varying socioeconomic drivers during the historical period (indicated with "histsoc" for 1861–2005 according to the ISIMIP2b protocol, Table S5). After 2005 socioeconomic conditions are held constant at present-day levels (2005soc for 2005–2099 or 2005–2299, respectively, according to the ISIMIP2b protocol).

Table S5: Main characteristics of the Global Hydrological Models (GHMs)

Global Hydrological Model	Energy balance	Soil scheme	Evaporation scheme	Runoff scheme	Snow scheme	Direct Human influences
CLM45 (45; 57)	Yes	15 soil layers with variable thickness down to 42 m	Monin-Obukhov similarity theory	Saturation excess, fractional area	Energy balance, up to 5 layers	Time-varying irrigation amount depending on crop water demand; land use and irrigation area fixed at 2005 levels; no domestic or industrial water use, no reservoir operation considered
H08 (30)	Yes	1 soil layer with a depth of 1 m	Bulk formula	Saturation excess, non-linear	Energy balance	Land use, irrigation, domestic and industrial water use, and reservoir operation always ixed at 2005 levels
JULES-W1 (4; 59)	Yes	4 soil layers of 10, 25, 65 and 200 cm thickness	Penman-Monteith	Hortonian infiltration excess mechanism enhanced by vegetation specific factors	Energy balance	Land use always fixed at 2005 levels; no other human influences considered
LPJmL (66; 70)	No	5 soil layers of 20, 30, 50, 100 and 100 cm thickness	Priestley-Taylor	Saturation excess	Degree Day	Time-varying rainfed agriculture, irrigation area, irrigation, domestic and industrial water use, and reservoir operation until 2005, fixed at 2005 levels afterwards
MPI-HM (29; 80)	No	Prescribed by plant rooting depth	Penman-Monteith	Saturation excess, non-linear	Degree Day	Time-varying rainfed and irrigated crops until 2005, fixed at 2005 levels afterwards; no other human influences considered
PCR-GLOBWB (90; 91)	No	2 soil layers of 0.3 and 1.2 m depth	Hamon	Saturation excess, beta function	Degree Day	Time-varying rainfed agriculture, irrigation area, irrigation, livestock and domestic and industrial water use, and reservoir operation until 2005, fixed at 2005 levels afterwards
ORCHIDEE (28)	Yes	11 soil layers down to 2 m depth	Bulk formula	Infiltration excess	Energy balance	Time-varying land use until 2005, fixed at 2005 levels afterwards; no other human influences considered
WaterGAP2 (55; 54)	No	1 soil layer with varying depth of 0.1 to 4 m depending on land cover type	Priestley Taylor with two alpha factors depending on grid cell aridity	Saturation excess, beta function	Degree Day	Time-varying irrigation area, irrigation, domestic and industrial and livestock water use, and reservoir operation until 2005, fixed at 2005 levels afterwards

3.1 Land area affected

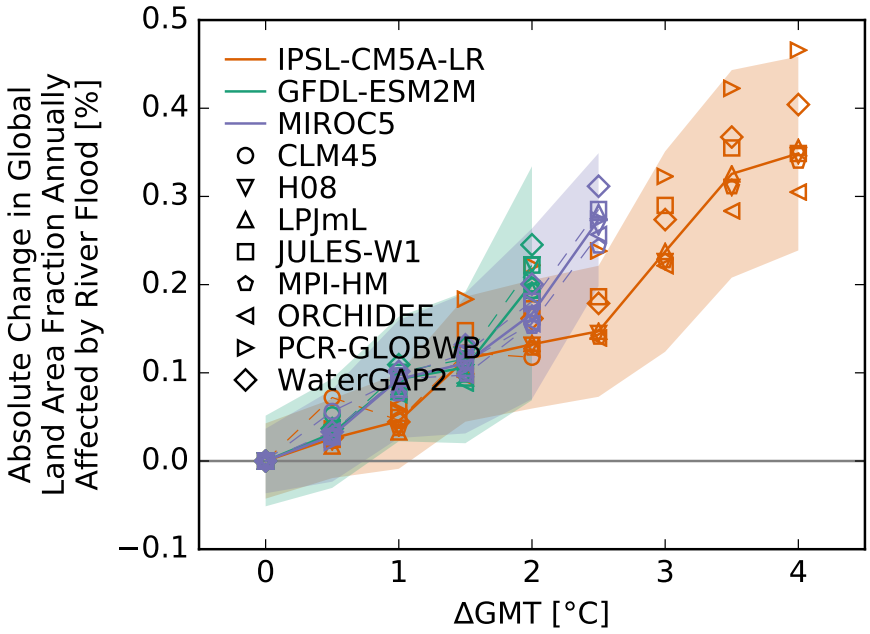

Figure S6: **Pure effect of climate change on global land area fraction annually affected by river floods.** Absolute change in global land area fraction annually affected by river floods at different levels of global mean temperature (GMT) change relative to the long-term preindustrial mean GMT as simulated by different impact models (symbols) driven by different climate models (colors). Symbols indicate the climate model-impact model combination-specific multi-year mean change caused by global warming (these are identical to the red solid lines in Panel D of Figures S49 … S67). Symbols connected by dashed lines represent emulated multi-year mean changes. Solid lines are the medians over all impact models per climate model. Shaded areas represent the multi-impact model median ±1 standard deviation range of the interannual variability of the global land area fraction annually affected by river floods.

Since the GHMs provide grid-scale river discharge and runoff instead of flooded area, it is necessary to apply the global river model CaMa-Flood (94; 95), which is forced only by the runoff simulations of each GHM. Simulated daily runoff is translated into the annual maximum daily discharge by CaMa-Flood to estimate the fraction of each grid cell that has been affected by a river flood event at least once in a considered year. CaMa-Flood has been shown to improve the reproduction of the multi-model ensemble mean of observed peak discharge in a majority of areas compared to the original routing schemes used within the GHMs, although individual GHM discharge might still fit better to observations (98). The river flood inundation scheme enables simulation of global gridded flooded area and depth, and the model is widely used to estimate global river flood risk under climate change (43; 32; 60).

A grid cell is considered to be affected by river flooding if the maximum annual discharge exceeds the 100-year return level derived from the preindustrial simulations. While dams and levees are often effective measures to prevent river flooding, river flood defense in most developing regions are currently insufficient to prevent large floods with return periods longer than 100 years (73). Assuming universal protection against river floods with return periods shorter than 100 years is thus expected to underestimate flooded land area in developing countries, but overestimate it in some industrialized countries. Since regions with protection levels higher than 100-year return levels are small (see Figure S8), our default projections of areas affected by river flooding are expected to be conservative.

Specifically, for each GCM-GHM combination and at every grid cell, a Generalized Extreme Value (GEV) distribution (38) is fitted to the distribution of annual maximum discharge (up to 639 years) using L-moment estimators (37). The considered preindustrial reference samples are much larger than the 30

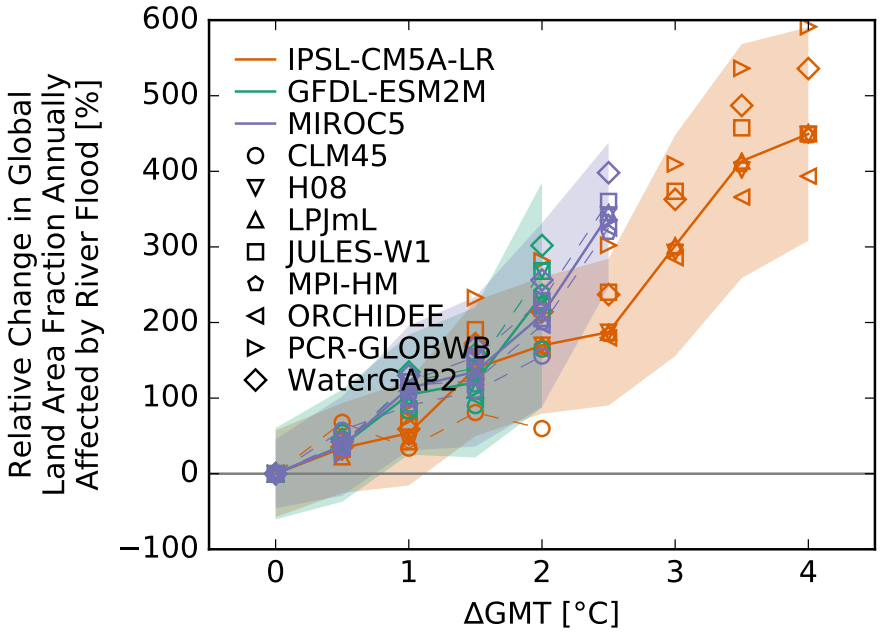

Figure S7: **Pure effect of climate change on global land area fraction annually affected by river floods.** Same as Figure S6 but for the relative change in global land area fraction annually affected by river floods.

historical years often considered in previous studies and allow for a more robust estimate of return periods. Since the climate forcing could still contain biases, the frequency distribution of annual maximum daily discharge, instead of flood depth and area directly simulated by CaMa-Flood, is used. Following the approach by (32), annual maximum daily discharge with a return period of more than 100 years is mapped to corresponding river flood depth from a retrospective CaMa-Flood run with MATSIRO (82) runoff, driven by observed climate forcing. To estimate the fraction of the 0.5°× 0.5° grid cell that is affected by the flood, the flood depth mapped to the retrospective MATSIRO run is then downscaled by CaMa-Flood based on high resolution topography data (about 100 m spatial resolution) to yield the annual maximum flood inundation area fraction on a 2.5'× 2.5' grid.

Separation of pure effect of climate change from direct human influences Changing human water management and use in the historical period mostly affects river discharge (e.g. through water abstraction from rivers, lakes, and reservoir management) but only has a minor effect on gridded runoff. As CaMa-Flood uses the gridded daily runoff instead of routed discharge from the GHMs, the majority of human water management, such as dams and reservoirs (not simulated by CaMa-Flood), has a negligible effect on the derived land area affected by river flooding. In those cases where water demand is satisfied from groundwater resources, a reasonable reduction of groundwater runoff (one component of runoff) can be expected. However, for flooded area this effect seems to be negligible (see preindustrial and future segments of the reference simulations shown in Panel A (gray dots) from multiple GHM-GCM combinations).

3.2 Number of people exposed

For each cell we multiplied the annual inundated area fraction by the cell population in the corresponding year. Before 1860 and after 2005, population data were held fixed at 1860 and 2005 levels, respectively. The estimates of exposed people on the 2.5'×2.5' grid were aggregated to the common ISIMIP2b 0.5°×0.5° grid.

Compared to the area fraction affected, the fraction of population exposed to river flooding increases faster with increasing global warming levels. This suggests that river floods with a return period of over

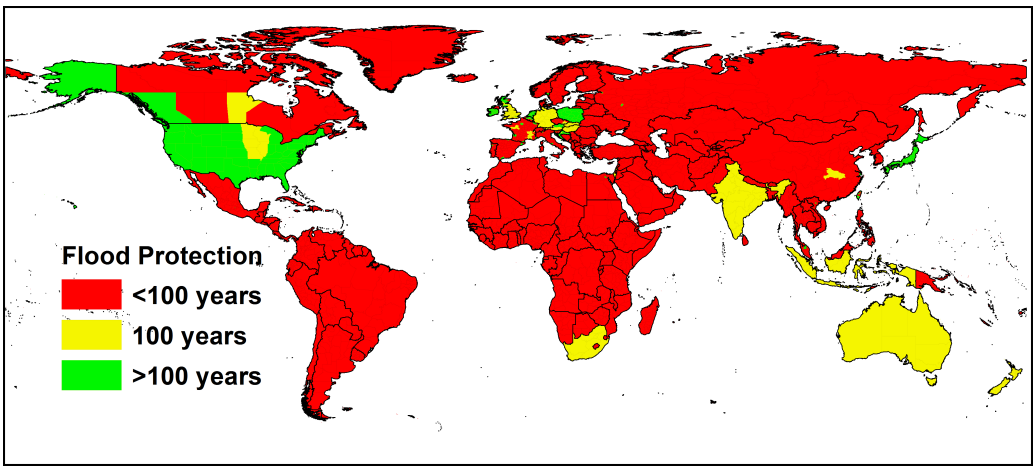

Figure S8: **Estimated present day protection levels against river floods expressed in return levels of discharge based on the FLOPROS database** (73). Red areas: Flood protection is lower than the river flood protection assumed in our default simulations. Yellow areas: Flood protection corresponds to the protection assumed in the default simulations. Green areas: Flood protection exceeds the level of protection considered in our default calculations.

100 years increase more in areas with denser population (while change in population distribution in the historical period may play a role, it should not affect the change at higher warming levels where population is fixed at 2005 levels).

Differences between projected relative changes are much larger between GCMs (for a fixed GHM) than between GHMs (for a fixed GCM). This suggests that river flood projections are mainly driven by high precipitation as provided by the climate projections and less dependent on e.g. the implementation of evapotranspiration in the GHMs.

Separation of pure effect of climate change from direct human influences As shown in the previous section, direct human influences only have a minor influence on the extent of river flooded land area derived by CaMaFlood. The additional effect of the historical changes in population patterns (1860–2005) on people exposed to river flooding is minor, too (see preindustrial and future segments of the reference simulations shown in Panel A (median values for the gray dots), the differences shown in some individual GCM-GHM combinations are likely due to difference in population patterns, although they are also possibly affected by different climate realizations).

3.3 Land area affected and number of people exposed at the national scale

Figure S11 shows, in absolute terms, how the national land area affected by and population exposed to river floods change under the different warming levels. As a general trend one can see that the area affected by river flood events with a larger than 100 year return period increase with global warming. The increase is largest in the tropical regions (most notably East Africa, with the aforementioned caveat, and Southeast Asia) and particularly pronounced under 2 °C global warming. Some boreal regions, such as in Russia or Argentina experience a substantial increase as well. In a few countries the affected area decreases, most notably in South Europe and Northwest Africa. Most of the changes are already visible under 1.0 °C global warming and are further enhanced under 2 °C warming. These spatial patterns largely agree with previous findings on projected changes in the frequency of river floods (32).

A rather similar picture emerges for the exposed population. In some countries in Southeast Asia, such as Myanmar or Vietnam, the exposed population rises in particular. The same phenomenon occurs in Egypt and in Sudan. Both of these thrends are particularly noticable under 2.0 °C of global warming.

Figure S12 shows the same results, albeit this time they are depicted as relative changes. The patterns

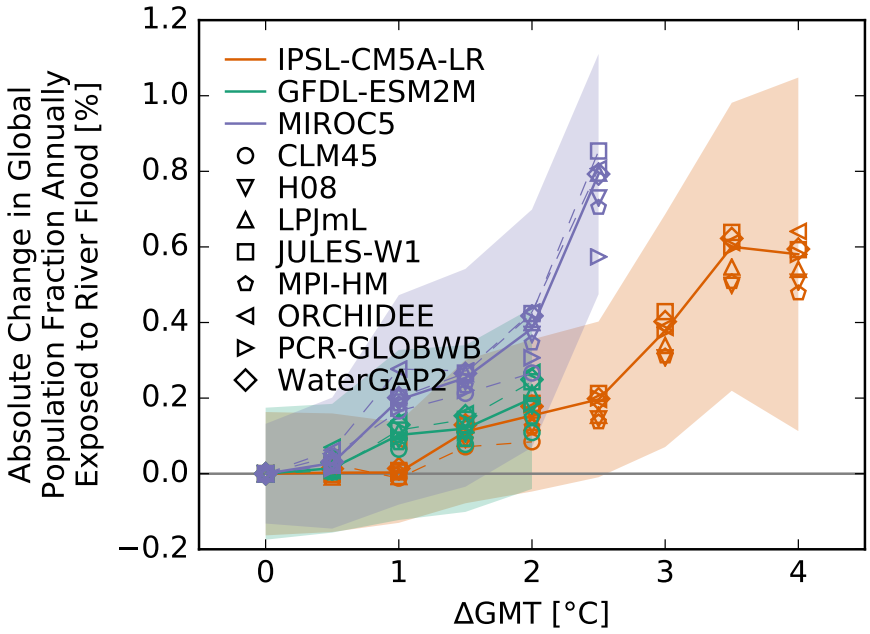

Figure S9: **Pure effect of climate change on global population fraction annually exposed to river floods.** Absolute change in global population fraction annually exposed to river floods at different levels of global mean temperature (GMT) change relative to the long-term preindustrial mean GMT as simulated by different impact models (symbols) driven by different climate models (colors). Symbols indicate the climate model-impact model combination-specific multi-year mean change caused by global warming (these are identical to the red solid lines in Panel D of Figures S68 … S86). Symbols connected by dashed lines represent emulated multi-year mean changes. Solid lines are the medians over all impact models per climate model. Shaded areas represent the multi-impact model median ±1 standard deviation range of the interannual variability of the global population fraction annually exposed to river floods.

in both plots are largely the same, i.e. often the countries with large absolute changes experience large relative changes as well. However, there are a few countries, suche as Syria or Ethiopia, where the relative changes are particularly severe. This is effect is exacerbated with increased global warming.

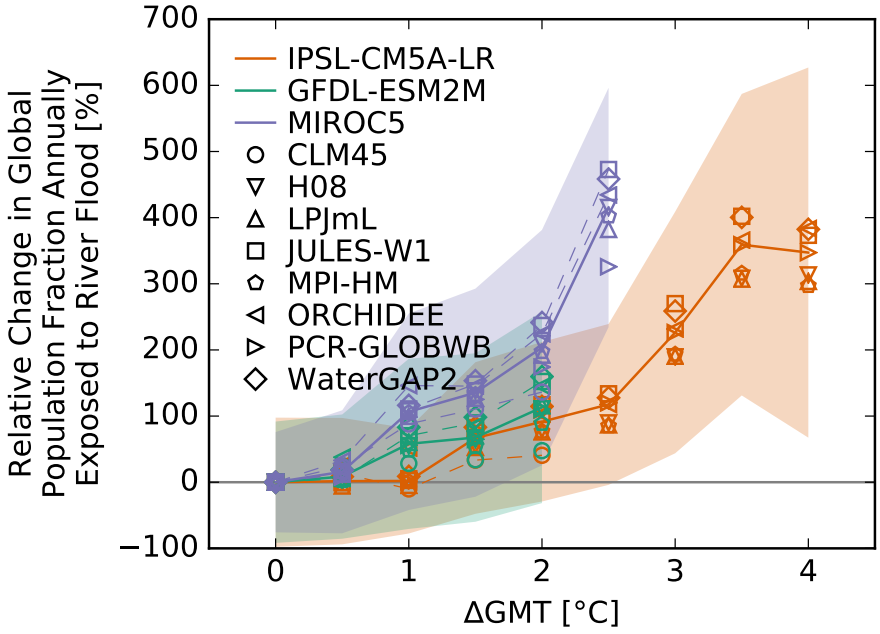

Figure S10: **Pure effect of climate change on global population fraction annually exposed to river floods.** Same as Figure S9 but for the relative change in global population fraction annually exposed to river floods.

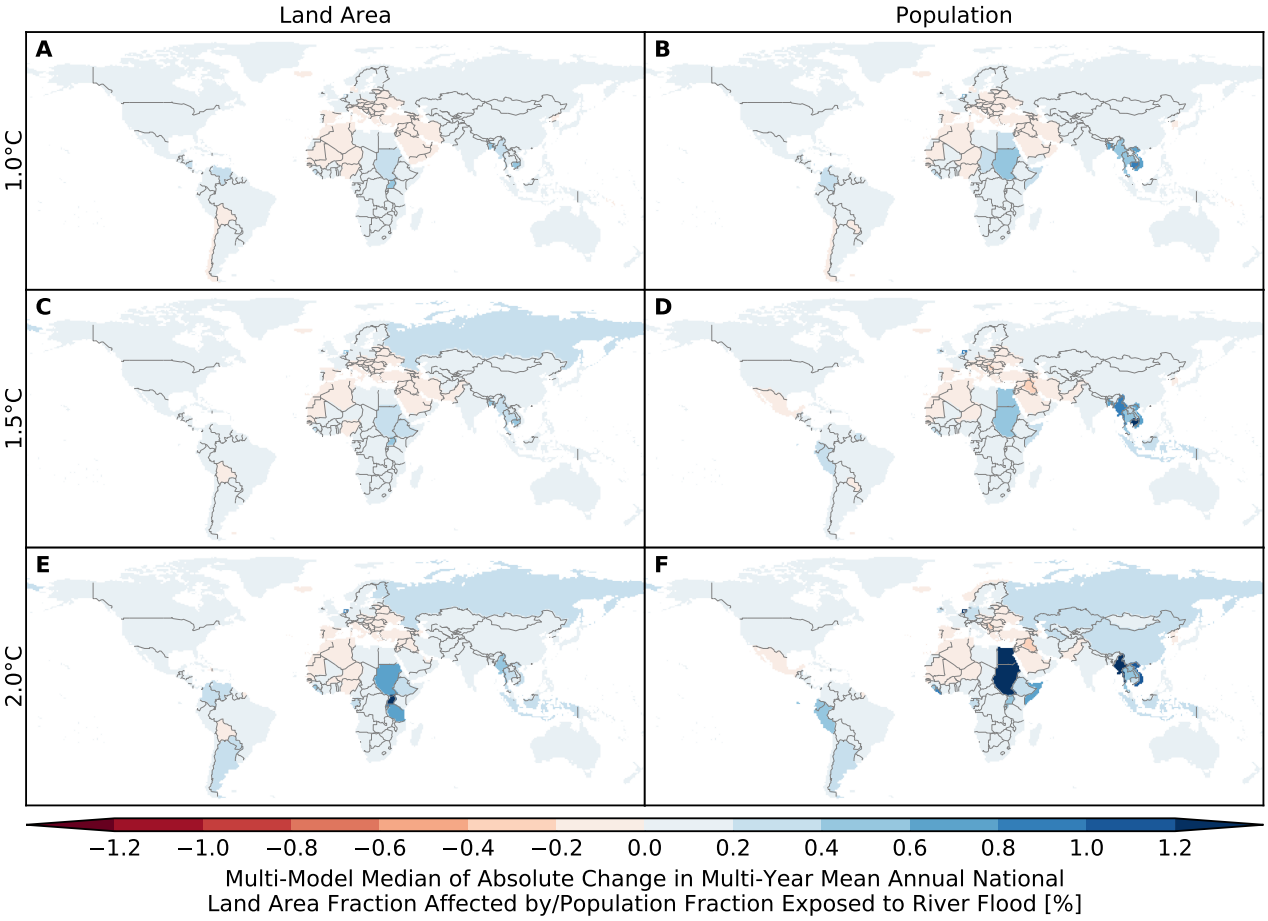

Figure S11: **Pure effect of climate change on annual national land area fraction affected by and population fraction exposed to river floods.** Colors indicate multi-model median absolute changes in multi-year mean annual national (A, C, E) land area fraction affected by and (B, D, F) population fraction exposed to river floods at (A, B) 1 °C, (C, D) 1.5 °C and (E, F) 2 °C global warming. Stippling indicates that at least 80% of all model combinations agree on an increase or decrease that is larger than 2σ of the preindustrial interannual variability. Hatching indicates that at least 80% of all model combinations agree that the change is smaller than 1σ of the preindustrial interannual variability. The climate model-impact model combination-specific results are shown in Figures S87 … S123.

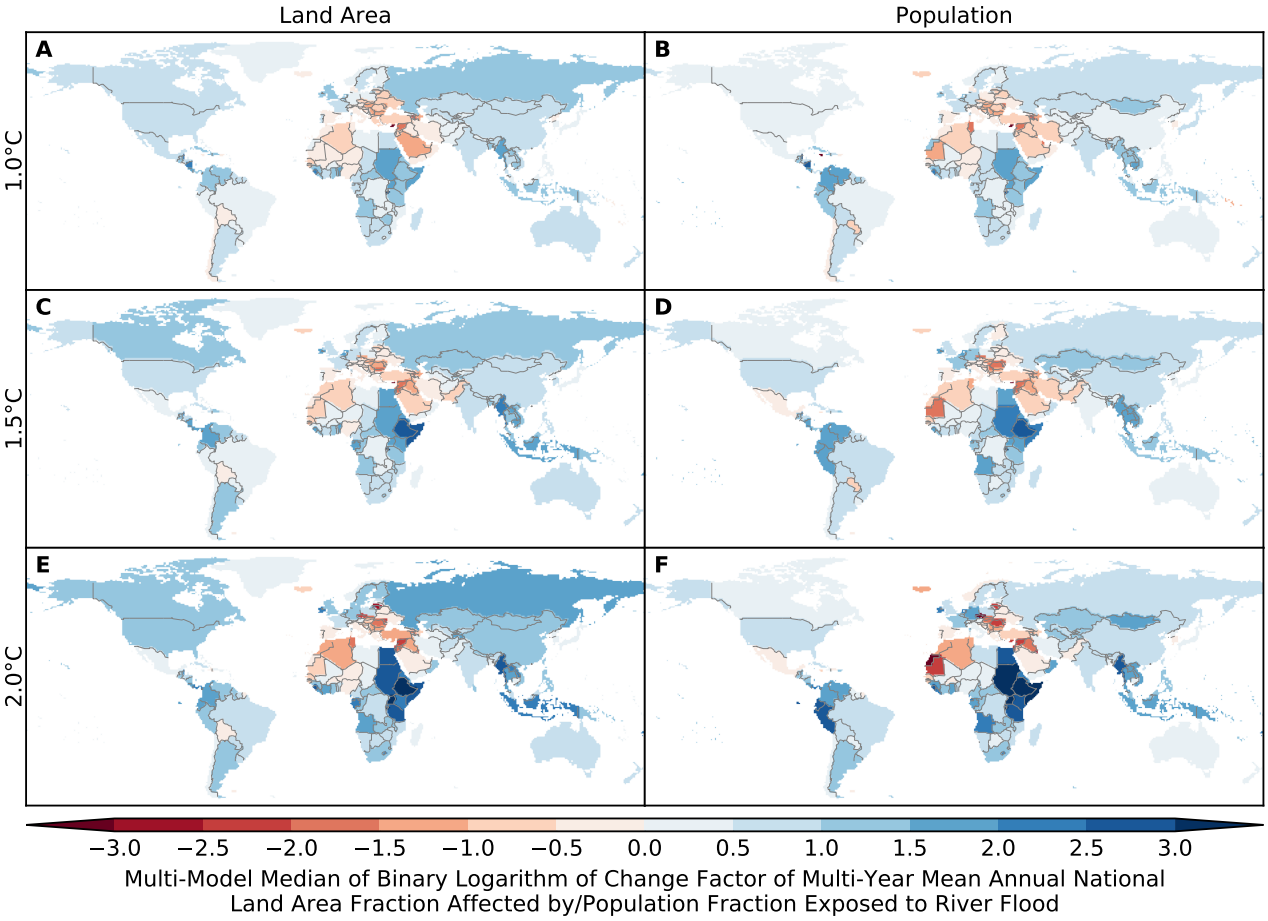

Figure S12: **Pure effect of climate change on annual national land area fraction affected by and population fraction exposed to river floods.** Same as Figure S11 but for relative changes expressed in terms of binary logarithms of change factors, i.e. −2, −1, 0, 1, 2 means that the new value is 1/4, 1/2, 1, 2, 4 times the old value, which is equivalent to a relative change by −75 %, −50 %, 0 %, +100 %, +300 %, respectively. White indicates undefined relative changes due to division by zero. The climate model-impact model combination-specific results are shown in Figures S88 … S124.

4 Calculation of land area affected by and number of people exposed to tropical cyclones

4.1 Land area affected

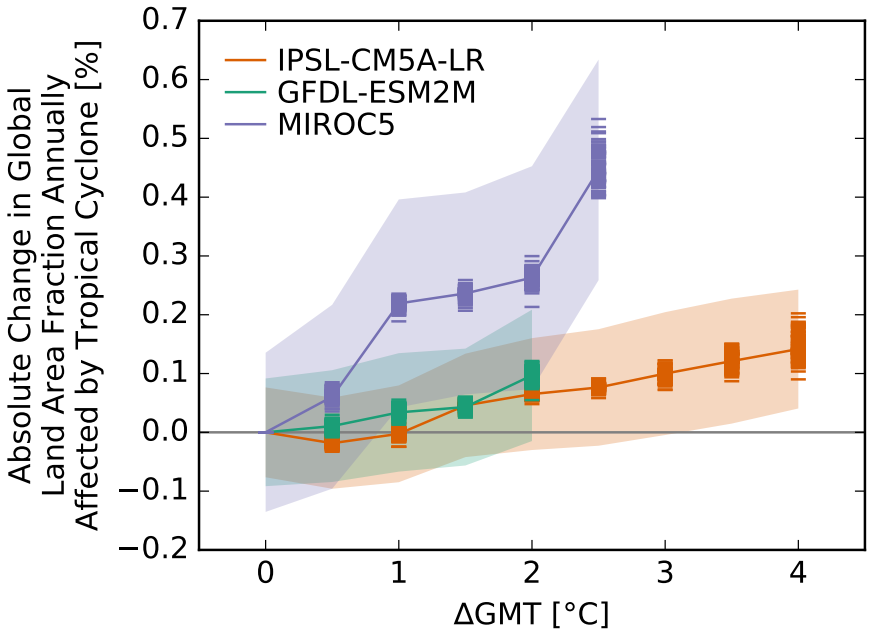

Figure S13: **Pure effect of climate change on global land area fraction annually affected by tropical cyclones.** Absolute change in global land area fraction annually affected by tropical cyclones at different levels of global mean temperature (GMT) change relative to the long-term preindustrial mean GMT as simulated by different model realizations (bars) driven by different climate models (colors). Bars indicate the climate model-model realization combination-specific multi-year mean change caused by global warming (these are identical to the red solid lines in Panel D of Figures S125 … S127). Symbols connected by dashed lines represent emulated multi-year mean changes. Solid lines are the medians over all model realizations per climate model. Shaded areas represent the multi-model realization median ±1 standard deviation range of the interannual variability of the global land area fraction annually affected by tropical cyclones.

Land area affected by tropical cyclones (TCs) is defined as all grid cells subject to 1-minute sustained hurricane-force winds (wind speed larger or equal to 64 knots) at least once a year. Potential TC tracks are simulated using a dynamical tropical cyclone model (14) forced by GCM data. Affected land area is derived from a windfield model (33) providing bare track coordinates with a realistic extension of winds around the TC center, and implemented in the open-source climate risk modeling toolbox climada (8; 24; 22). The dynamical downscaling approach (15) as well as the windfield model have been shown to realistically reproduce observational TC data (33; 22), and have been applied to project socioeconomic TC impacts (50; 23).

Generation of 100 potential realizations of tropical cyclones for each year of the historical period and the RCP scenarios For each of the considered years a global total of 300 potential TCs per year and the expected number of cyclones for each year are provided. For the scenario runs, each underlying GCM year corresponds to the same year considered within all other sectors. To provide 100 sets of potential hurricane realizations for each year, we randomly draw the expected number of tracks from the sample of 300 tracks provided for each year. Each set of tracks is referred to as one realization in the following.

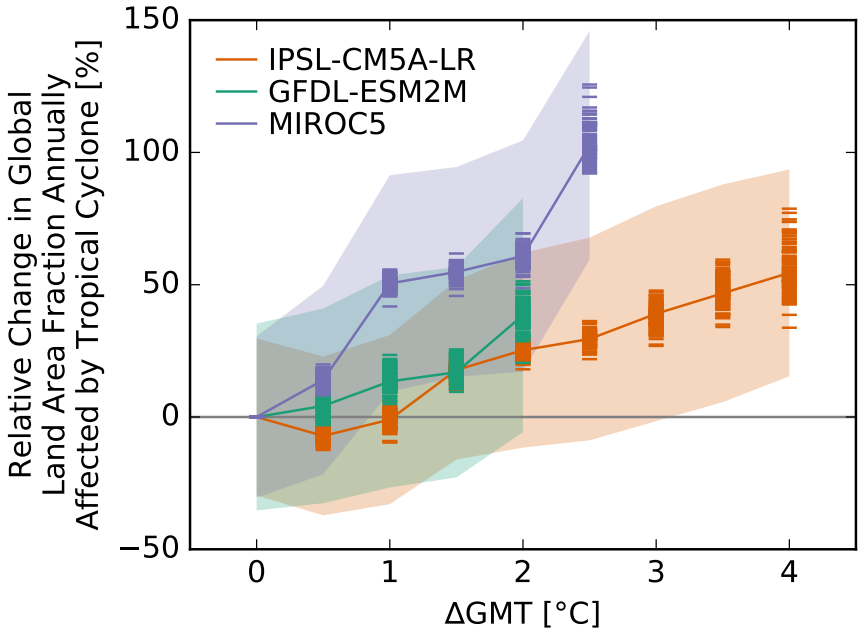

Figure S14: **Pure effect of climate change on global land area fraction annually affected by tropical cyclones.** Same as Figure S13 but for the relative change in global land area fraction annually affected by tropical cyclones.

Generation of 100 potential realizations of tropical cyclones for each year of the preindustrial reference scenario The preindustrial control simulations only comprise 100 TCs tracks per year. In addition, the underlying GCM years do not necessarily match the years considered within all other sectors as the downscaling is partly forced by other segments of the preindustrial GCM runs. To generate a sample of 100 potential realizations of cyclone tracks that correspond to the individual year considered within the other sectors, we select at least three years of cyclone simulations that match a considered year in the other sectors in terms of the low frequency variability of global mean temperature (21-year running-mean) and the 3-month running-mean of the Equatorial Southern Oscillation Index (as defined by NOAA's Climate Prediction Center http://www.cpc.ncep.noaa.gov/data/indices/). The algorithm initially sets a very strong threshold of similarity and iteratively and alternatively for GMT and ESOI lowers the threshold until at least three years have been selected. In this way we create a sample of at least 300 TCs we can draw from. The expected number of TCs to draw is randomly selected from the expected numbers of cyclones associated with the years contributing to the sample. As both GMT and ESOI (or variants thereof) have been shown to significantly modulate the occurrence of climate extremes, see e.g. Ref. (19; 92), we thereby account for relevant regional climate extreme patterns within this sector and across sectors.

For each year and each realization of tracks a binary map of affected land area with hurricane-force winds is generated with 0.1°×0.1° spatial resolution. This map is then aggregated to a grid with 0.5° spatial resolution and the area fraction affected of the larger grid cell is then saved and compared to the other climate extremes.

Discussion of Results The absolute change in global land area fraction affected (AFA) by TCs shows an increase across all models with increasing GMT (Fig. S13). Two GCMs (GFDL-ESM2M and IPSL-CM5A-LR) show a comparable result with less than 0.1 % rise in AFA for 2 °C of warming, while for MIROC5 the AFA rises by almost 0.3 %. Since TCs only affect a small portion of the global land mass, these small absolute increases translate to large relative increases, e.g. to a greater than 50 % rise in TC-affected global land area for MIROC5 (Fig. S14).

The difference in AFA changes for different GCMs can be explained by how TC characteristics change

in different models and ocean basins. While GFDL-ESM2M and IPSL-CM5A-LR predict large changes in annual TC frequency with rising GMT (see Figures S16 and S17), MIROC5 additionally predicts large changes in annual maximum TC intensities (see Figure S15). Both, changes in frequency and intensity result in rising AFA as more events can potentially cause more landfalls and more intense events cause higher wind speeds that can exceed the here-applied threshold of 64 knots over land.

Across all GCMs and all basins we observe similar changes in TC frequency and intensity with rising GMT for both RCP scenarios, indicating that GMT is sufficient to explain most changes in TC-specific impacts under global warming.

4.2 Number of people exposed

On the high resolution grid (0.1° × 0.1°) all people living in a grid cell affected by hurricane-force winds are considered to be exposed to the respective tropical cyclone. The number of people living in these grid cells is taken from the SSP2-based population distribution on the 0.1° grid provided within ISIMIP2b. The high resolution maps of people exposed are then spatially aggregated to obtain the global population fraction exposed (PFE) by TCs on the 0.5° grid.

Discussion of Results For PFE we obtain similar findings as for AFA (Figs. S18 and S19). For all GCMs we sind increases in the number of exposed people with rising GMT, with MIROC5 again simulating an increase that is about three times as large as the increases simulated by GFDL-ESM2M and IPSL-CM5A-LR. Changes in PFE are somewhat larger than changes in AFA, which can be explained by the fact that a large fraction of global population resides close to the coast. Hence, an additional unit of coastal AFA hosts over-proportionally more people than a non-coastal area, and thus small changes in AFA can cause larger changes in PFE.

For PFE we also find larger interannual variability than for AFA (shaded areas in Figs. S18 and S19). This is related to the stochastic nature of TC occurrence (see also the large variability of the thin lines in Figures S15…S17). This stochasticity also affects the specific landfall location and the associated number of people exposed: Whether a major city is directly hit or barely missed contributes significantly to the interannual variability of the population exposed.

4.3 Land area affected and number of people exposed at the national scale

Absolute changes in country area affected by and population exposed to TCs under various levels of warming are positive almost everywhere (Fig. S20). Only some countries with very little historical TC experience in Southern America, Africa, and the South Pacific show some tendency for a decrease in absolute terms, in particular, for very low levels of warming. On the other side, there exist hot-spot regions, namely Mexico and some parts of the Caribbean, the South-East coast of Africa, in particular Madagascar, South-East Asia, in particular the Philippines and Vietnam, and Japan and the Korean Peninsula that show rather large and rising increases in absolute terms and with higher levels of global warming. These hot-spot regions are consistently found in terms of affected land area and exposed population. Nonetheless, none of these country-level changes in absolute terms are large relative to the year-to-year variability under preindustrial climate conditions. This is not surprising in particular for rather small countries, for which the year-to-year variability is tremendous.

When analyzing relative changes in country area affected by and population exposed to TCs under various levels of warming one similarly observes the hot-spot regions mentioned above (Fig. S21). In addition, the USA, Australia, China, India, and the countries in the Bay of Bengal show major positive changes. This is caused by the fact that these countries have large areas of which only a small fraction is regularly affected by TCs and hence changes in absolute terms are small while relative changes can be large. We also find that relative changes in terms of population exposed are somewhat larger than for area affected. This is in line with the fact that the coastal regions in those large countries are usually more

densely populated and thus exposure increases over-proportionally.

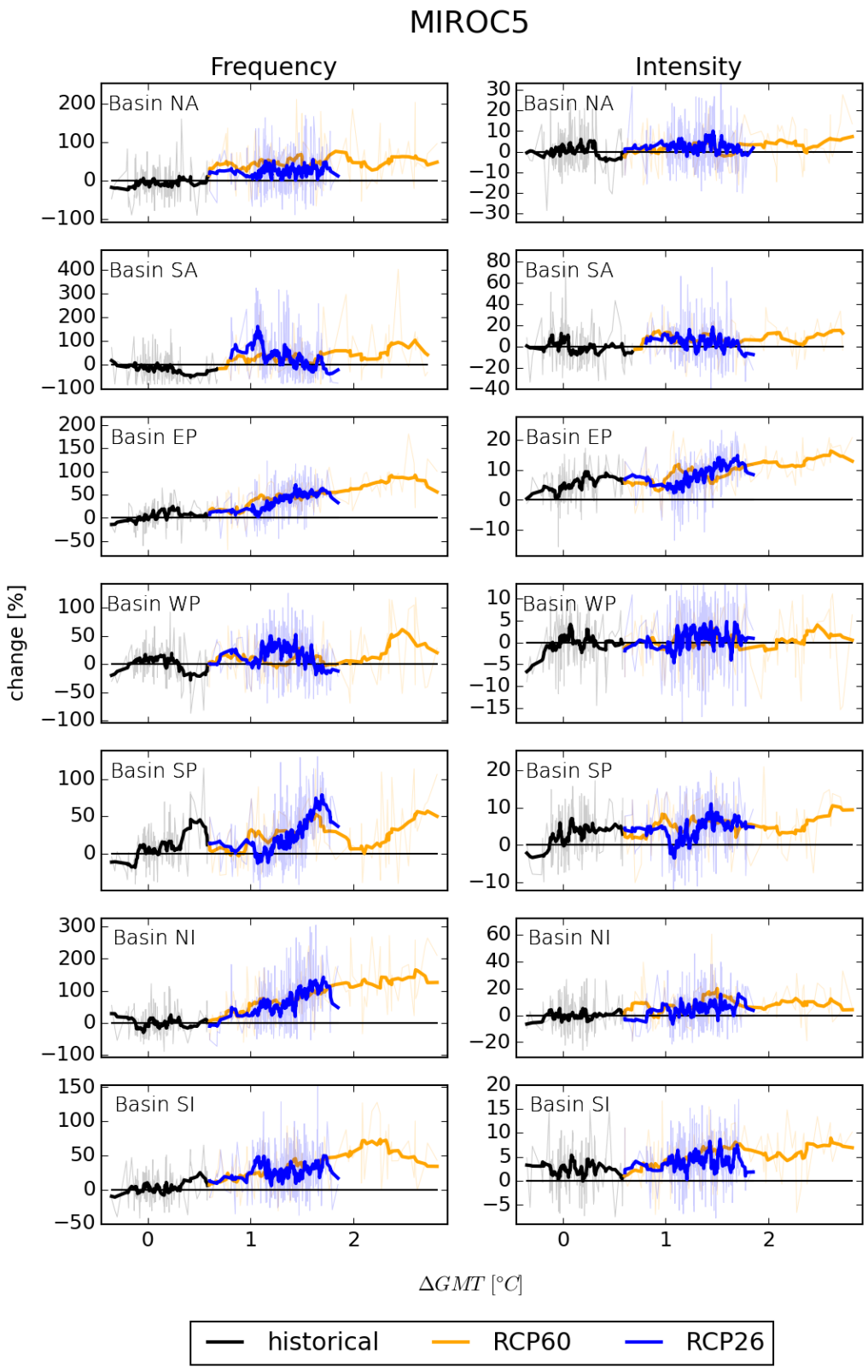

Figure S15: **Changes in annual ocean basin-specific TC frequency and intensity for different levels of global mean temperature for GCM MIROC5.** Per-cent changes relative to the long-term preindustrial mean in ocean basin-specific annual TC frequency (left column) and mean annual maximum TC intensity (right column) analyzed over all simulated TCs for each year. Annual changes (thin colored lines) are overlaid with 11-year running-mean changes (thick colored lines) for the historical period (black), and the RCP26 (blue) and RCP60 (orange) scenarios. Basin abbreviations are as follows: NA – North Atlantic Ocean, SA – South Atlantic Ocean, EP – East Pacific Ocean, WP – West Pacific Ocean, SP – South Pacific Ocean, NI – North Indian Ocean, SI – South Indian Ocean. The line of zero change is marked with a thin black line.

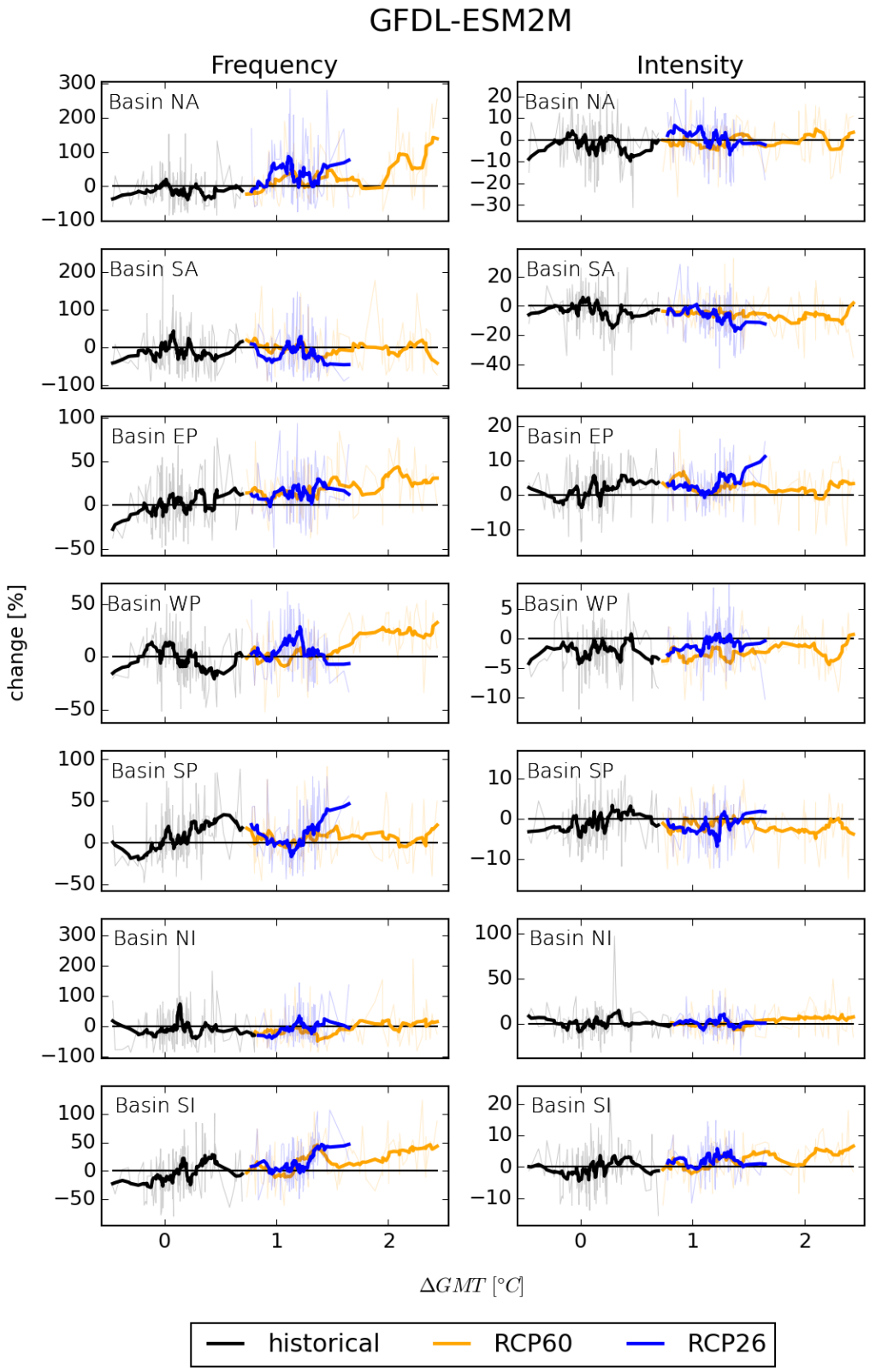

Figure S16: **Changes in annual ocean basin-specific TC frequency and intensity for different levels of global mean temperature for GCM GFDL-ESM2M.** Similar to Figure S15 but for GCM GFDL-ESM2M.

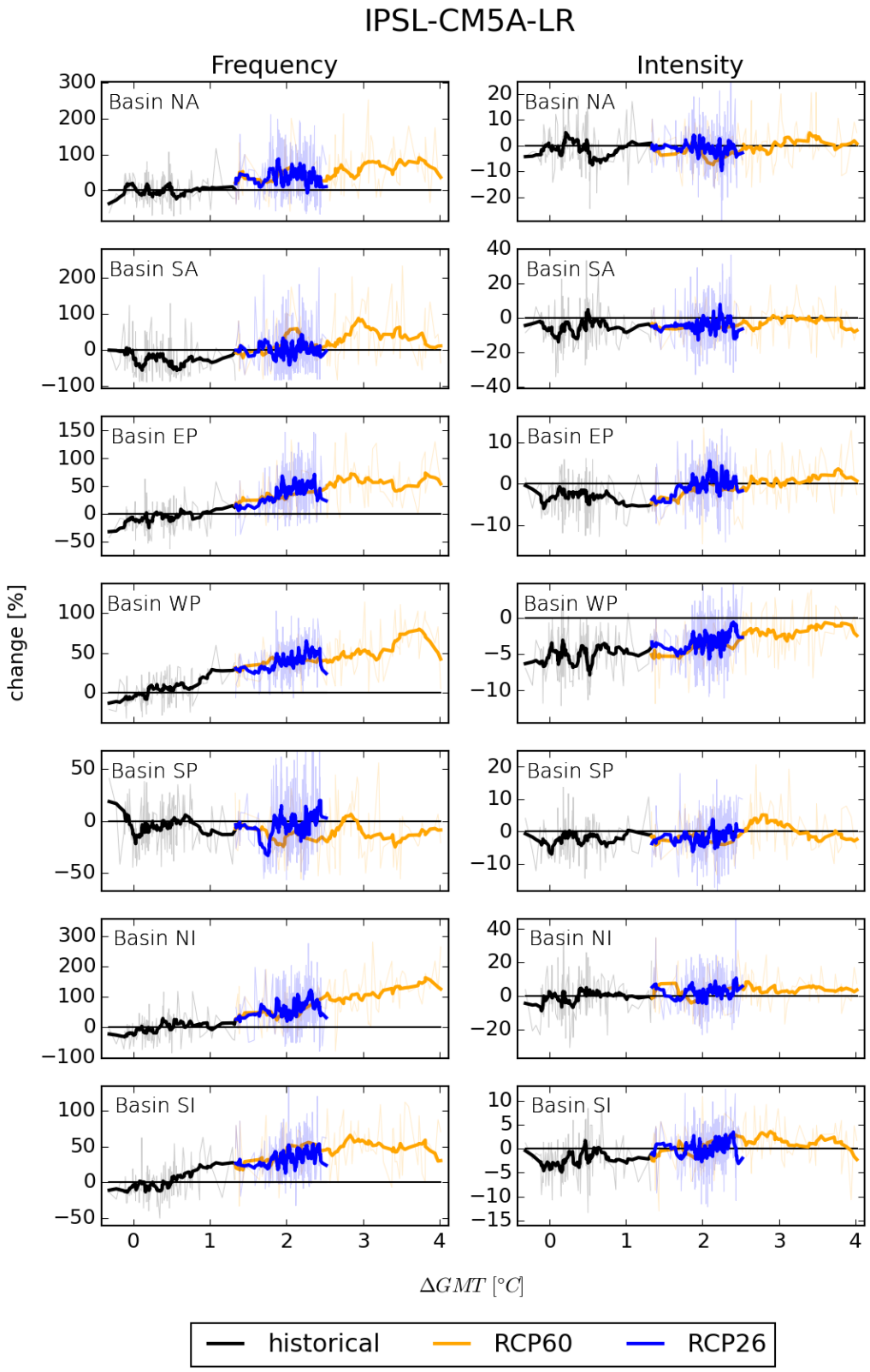

Figure S17: **Changes in annual ocean basin-specific TC frequency and intensity for different levels of global mean temperature for GCM IPSL-CM5A-LR.** Similar to Figure S15 but for GCM IPSL-CM5A-LR.

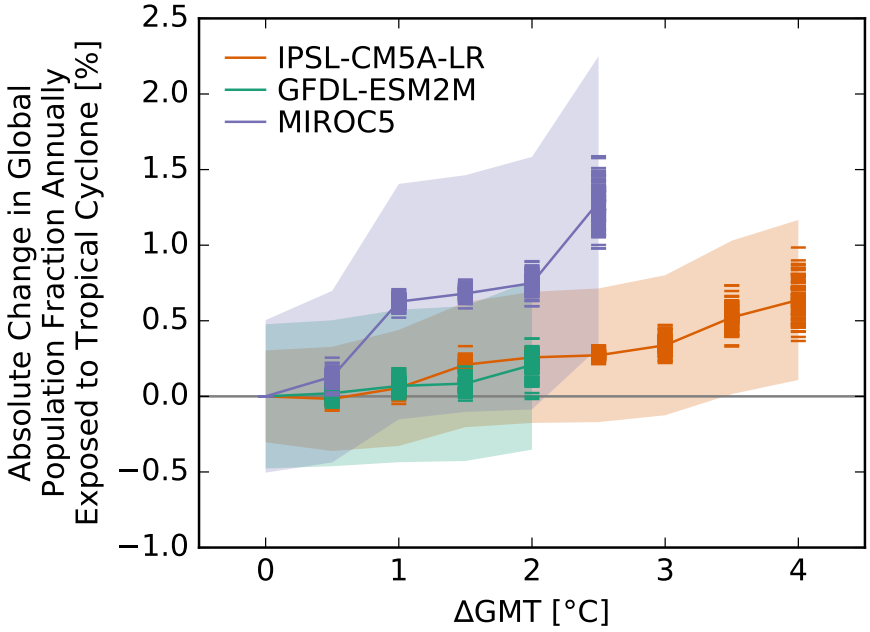

Figure S18: **Pure effect of climate change on global population fraction annually exposed to tropical cyclones.** Absolute change in global population fraction annually exposed to tropical cyclones at different levels of global mean temperature (GMT) change relative to the long-term preindustrial mean GMT as simulated by different model realizations (bars) driven by different climate models (colors). Bars indicate the climate model-model realization combination-specific multi-year mean change caused by global warming (these are identical to the red solid lines in Panel D of Figures S128 … S130). Symbols connected by dashed lines represent emulated multi-year mean changes. Solid lines are the medians over all model realizations per climate model. Shaded areas represent the multi-model realization median ±1 standard deviation range of the interannual variability of the global population fraction annually exposed to tropical cyclones.

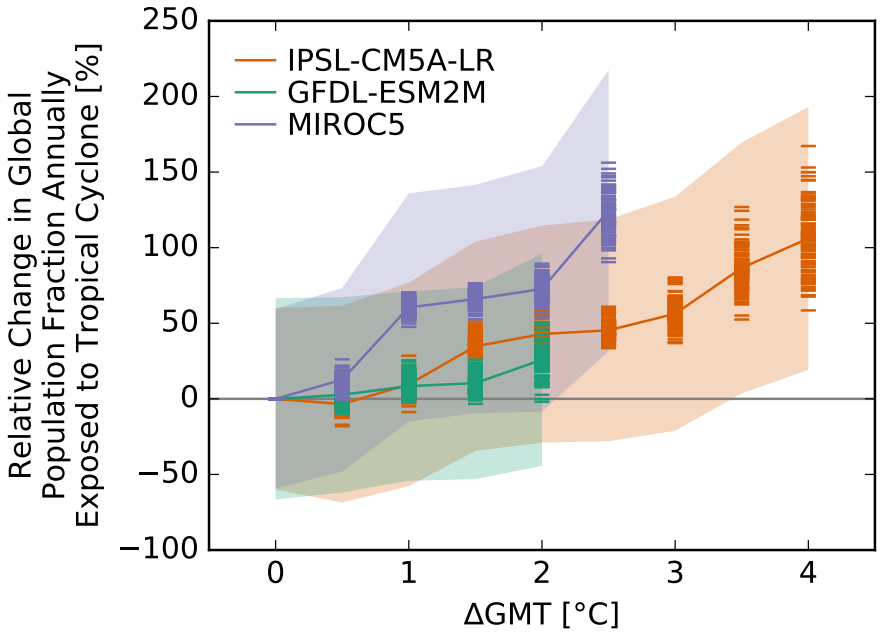

Figure S19: **Pure effect of climate change on global population fraction annually exposed to tropical cyclones.** Same as Figure S18 but for the relative change in global population fraction annually exposed to tropical cyclones.

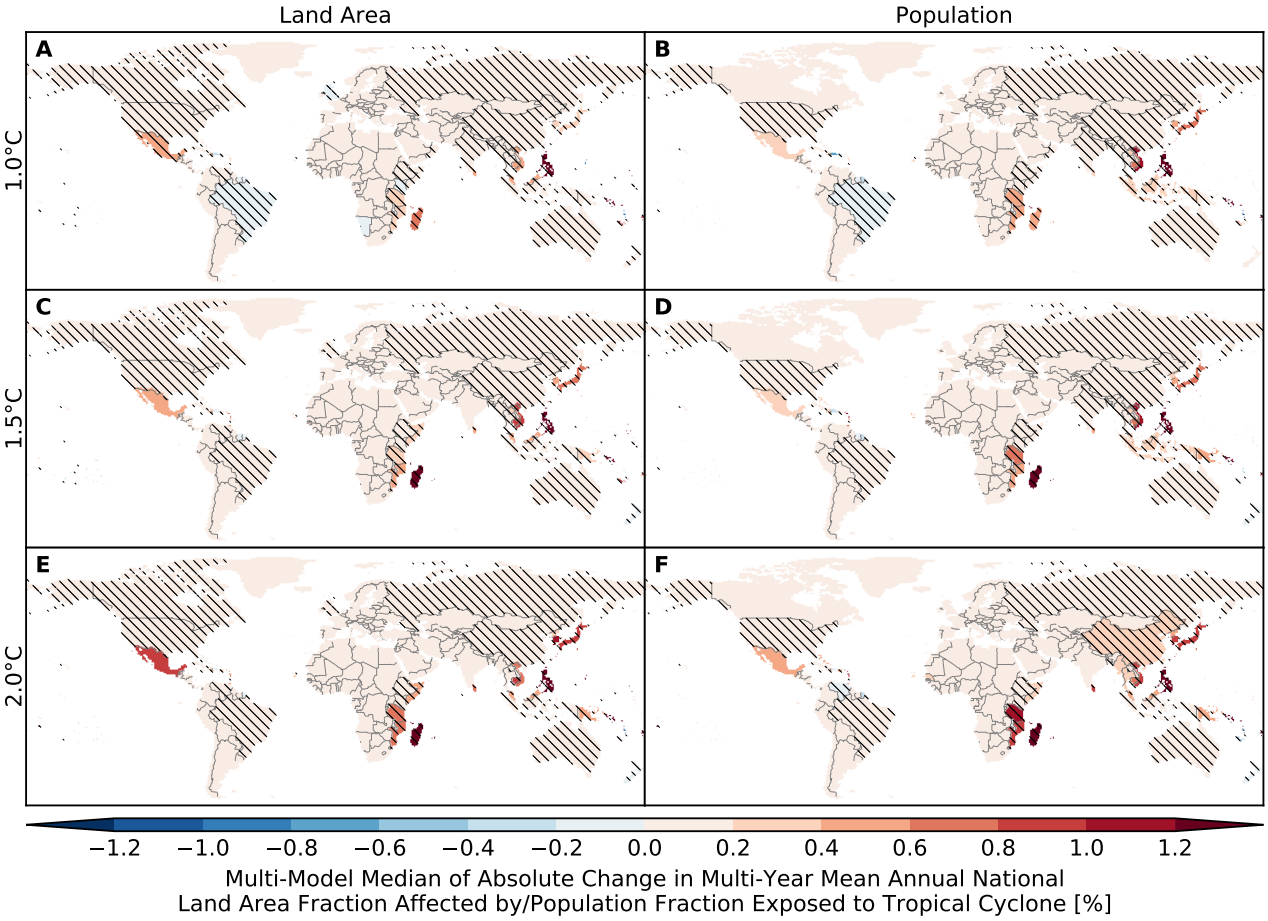

Figure S20: **Pure effect of climate change on annual national land area fraction affected by and population fraction exposed to tropical cyclone.** Colors indicate multi-climate model-model realization median absolute changes in multi-year mean annual national (A, C, E) land area fraction affected by and (B, D, F) population fraction exposed to tropical cyclone at (A, B) 1 °C, (C, D) 1.5 °C and (E, F) 2 °C global warming. Stippling indicates that at least 80% of all climate model-model realization combinations agree on an increase or decrease that is larger than 2σ of the preindustrial interannual variability. Hatching indicates that at least 80% of all climate model-model realization combinations agree that the change is smaller than 1σ of the preindustrial interannual variability. Results for one specific climate model-model realization combination are shown in Figures S131 … S135.

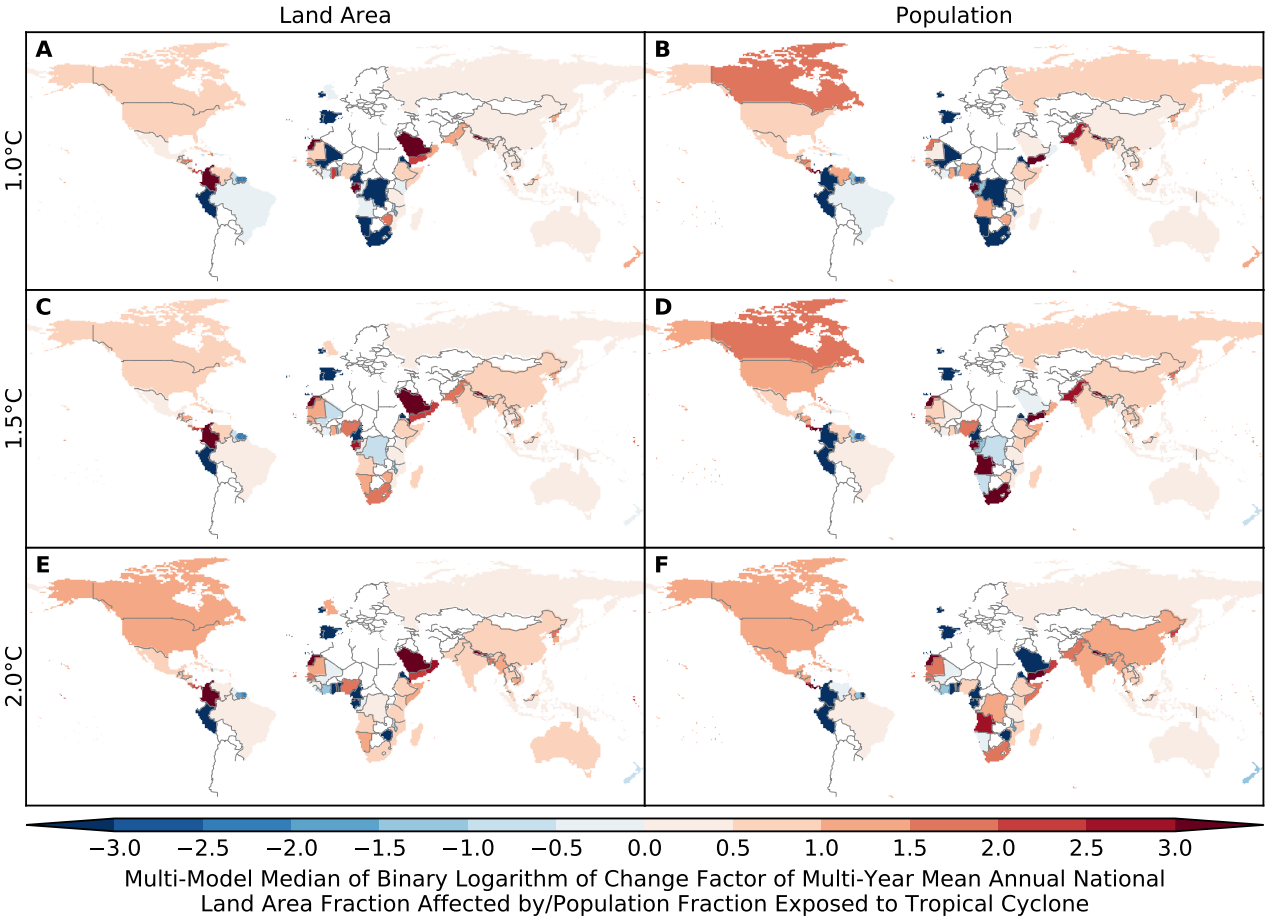

Figure S21: **Pure effect of climate change on annual national land area fraction affected by and population fraction exposed to tropical cyclone.** Same as Figure S20 but for relative changes expressed in terms of binary logarithms of change factors, i.e. −2, −1, 0, 1, 2 means that the new value is 1/4, 1/2, 1, 2, 4 times the old value, which is equivalent to a relative change by −75 %, −50 %, 0 %, +100 %, +300 %, respectively. White indicates undefined relative changes due to division by zero. Results for one specific climate model-model realization combination are shown in Figures S132 … S136.

5 Calculation of land area affected by and number of people exposed to crop failure

Crop failure is derived from three process-based crop models (GEPIC, LPJmL and PEPIC, see Table S6 for their basic characteristics) providing yields [t/ha] of wheat, maize, rice and soy on the ISIMIP2b 0.5° grid. The original simulations do not account for land use patterns. Instead, models provide pure crop runs assuming that each crop grows everywhere. For each crop, the individual modeling groups provide simulations assuming fully irrigated conditions, ignoring potential constraints on water availability and a separate set of simulations assuming purely rainfed management conditions everywhere. In this way LU patterns can be applied in post-processing ensuring maximum flexibility. Here, we apply historical land use and irrigation patterns for 5 crop classes (21) that have been downscaled to maize, rice, and soy (20). The ISIMIP2b LU patterns only provide grid cell fractions for "temperate cereals" without considering wheat separately. The wheat patterns considered within this study are derived from the "annual C3 crops" category in LUH2 assuming constant wheat shares according to (51). Before 1860 and after 2005 land use and irrigation patterns were held constant. Model simulations do not account for water constraints but assume that crops are fully irrigated on irrigated areas. All models provide 2005soc simulations according to the ISIMIP2b protocol, i.e. they do not account for historical or future management changes or technological progress but assume a fixed management setting described in Table S6. Yields are provided as annual output, assuming one single cropping cycle per crop and year. All considered crop models account for the CO_2 fertilization effects (See Table S6).

Table S6: Basic characteristics of the considered global gridded crop models. More detailed information on model setups are provided in (16) and (53).

Crop model	CO_2 fertilization	Representation of human management	Calibration
GEPIC (47; 48; 93)	RUE, TE	No representation of historical changes in management (2005soc simulations according to the ISIMIP2b protocol). Representation of nutrient constraints: N application based on HYDE3.2 (41) dataset provided within ISIMIP2b. 1/3 of total dose applied at planting, 2/3 about 40 days after germination. Implementation of growing seasons: Planting dates are based on the data provided within the global gridded crop model inter-comparison project (13); total heat units to reach maturity remain constant over time but vary spatially according to reported growing seasons for the recent historic period. Winter and spring wheat are distributed according to (81): Winter wheat is planted in grid cells with a minimum temperature in the coldest month of the year of > −10 °C and < 5 °C based on decadal monthly means during the recent historic time period and kept constant over time.	The model is not calibrated explicitly but has been evaluated in detail (17). Maize cultivars are distributed based on the human development index (HDI) with high-yielding cultivars in countries with HDI > 80 and low-yielding in all others. Soils were pre-conditioned in a spin-up run as described in (17). Subsequently, soils were treated statically in the model with an annual re-initialization of all soil properties except soil humidity and mineral N.
LPJmL (5)	LLP, CC	No representation of historical changes in management (2005soc simulations according to the ISIMIP2b protocol). Representation of nutrient constraints: Soil nutrient limiting factors are not accounted for. Implementation of growing seasons: Planting dates are based on the data provided within the global gridded crop model inter-comparison project (13); total heat units to reach maturity remain constant over time but vary spatially according to reported growing seasons for the recent historic period.	Leaf Area Index (LAI), Harvest Index (HI), and a scaling factor that scales leaf-level photosynthesis to stand level are adjusted to reproduce observed yields on country level (1996–2000).
PEPIC (47; 48; 93)	RUE, TE	No representation of historical changes in management (2005soc simulations according to the ISIMIP2b protocol). Representation of nutrient constraints: Flexible N application based on N stress > 10 % with a maximum value according to the ISIMIP2b input data; phosphorus deficiency not considered. Implementation of growing seasons: Fixed sowing dates (69); potential heat units to reach maturity based on average growing season temperature between 1980 and 2010, i.e. they vary spatially but stay constant over time.	Model parameters are adjusted to reproduce average (1998–2002) reported yields (FAO) on national level.

Crop failure at each grid cell and for irrigated and rainfed yields is defined of simulated yields falling below the 2.5th percentile of the associated reference distribution based on the model simulations forced by preindustrial climate. As the crop models do not account for management changes the entire time series of reference simulations has been used.

5.1 Land area affected

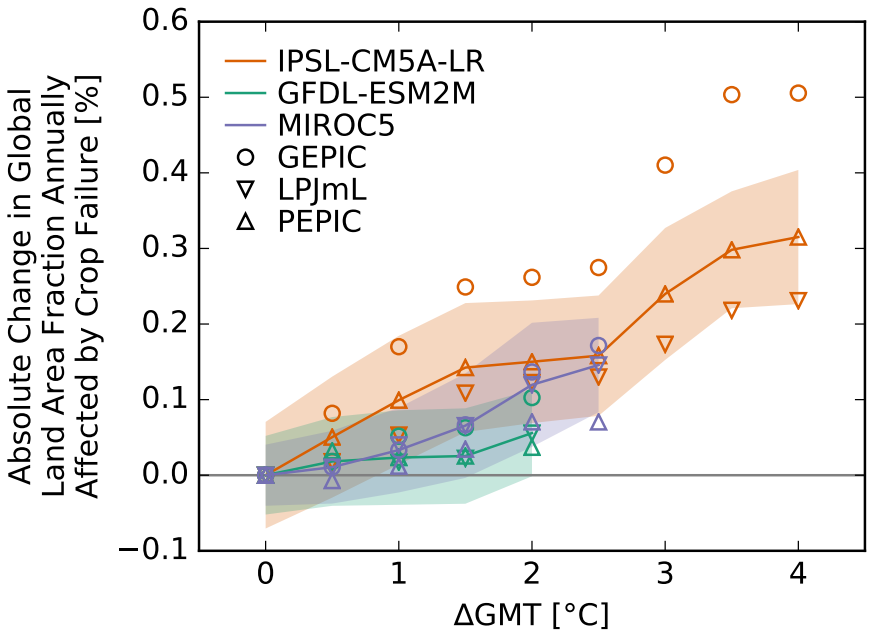

Figure S22: **Pure effect of climate change on global land area fraction annually affected by crop failures.** Absolute change in global land area fraction annually affected by crop failures at different levels of global mean temperature (GMT) change relative to the long-term preindustrial mean GMT as simulated by different impact models (symbols) driven by different climate models (colors). Symbols indicate the climate model-impact model combination-specific multi-year mean change caused by global warming (these are identical to the red solid lines in Panel D of Figures S137 … S145). Symbols connected by dashed lines represent emulated multi-year mean changes. Solid lines are the medians over all impact models per climate model. Shaded areas represent the multi-impact model median ±1 standard deviation range of the interannual variability of the global land area fraction annually affected by crop failures.

To estimate the area affected by crop failure we assume that it only affects the fraction of the grid cell where the crop is grown under irrigated and rainfed conditions, respectively. To estimate the total area affected the individual affected areas are added up across the different crops and irrigation settings.

Historical expansion of cropland alone lead to an increase in land area affected by crop failure (as a fraction of the global land area) simply because more land is used for cropping activities and all cropland is subject to crop failure (2.5th percentile). This is visible in the results of the crop models assuming preindustrial climate (see gray dots in panel A of Figures S137 … S145). In addition, the annual variability of the global land area affected by crop failure increases with the expansion of global cropland. On top of this increase in variability that is driven by the expansion of cropland, we find that climate change drives further increases in crop failure. In spite of the CO_2 fertilization effect all models show an increase in land area affected by crop failure with increasing levels of global warming (see dots with color of black, yellow, and blue in Figures S137 … S145). This increase in area affected is robust across all GCMs and GGCMs, even though the uncertainty between different climate scenarios and crop models is substantial. For the climate scenarios, this is mainly due to how spatial and temporal patterns of climate change overlap with cropland and growing seasons, whereas the differences between GGCMs stem from

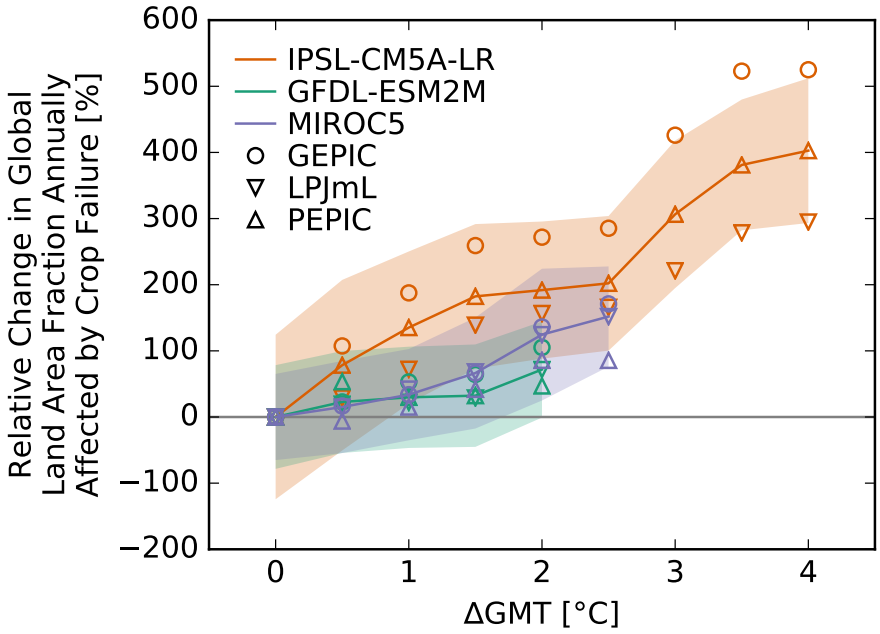

Figure S23: **Pure effect of climate change on global land area fraction annually affected by crop failures.** Same as Figure S22 but for the relative change in global land area fraction annually affected by crop failures.

different assumptions in crop management systems and model-specific differences (16; 53). There is no evident difference between the impacts of the concentration pathways RCP2.6 and 6.0 for a given change in GMT (Figures S137 … S145). An exception is MIROC5, where impacts are often stronger for RCP2.6 in the +1 °C to +2 °C bin than for RCP 6.0 (Figures S139, S142, S145).

5.2 Number of people exposed

When calculating the number of people exposed to crop failure we only account for local effects on people working in agriculture. Large-scale market effects cannot be captured here with biophysical impact models. Also, we argue that most crop failure events are too small-scale to significantly affect consumers thanks to buffering by the market.

If fraction A_{failure} of the land area of a grid cell is affected by crop failure, then the fraction P of the population of that grid cell that is exposed to that crop failure is calculated as

$$P = F\frac{A_{\text{failure}}}{A_{\text{agriculture}}},$$

where F is a national estimate of the employment in agriculture as a fraction of total employment (34), and $A_{\text{agriculture}}$ is the area fraction of the grid cell used for agriculture. The factor $A_{\text{failure}}/A_{\text{agriculture}}$ is supposed to estimate the fraction of the local population working in agriculture that is exposed to the crop failure. This factor is smaller than one in cases where not all of the crops grown in the grid cell failed. Gaps in the national time series of employment in agriculture have been filled by linear interpolation and the fraction is assumed to stay constant before the first and the last available data point at the first and last available value, respectively.

In contrast to the land area affected, the historical reduction in employment in agriculture leads to decreasing numbers of people directly (see definition above) exposed to crop failure under preindustrial climate conditions over the historical period according to the applied definition (see gray dots in Panel A of Figures S146 … S154). In addition the inter-annual variability of the numbers also decreases. However, the number of people exposed to crop failure is consistently increasing with global warming, which is mainly due to the expanded land area affected despite population reduction in employment in agriculture.

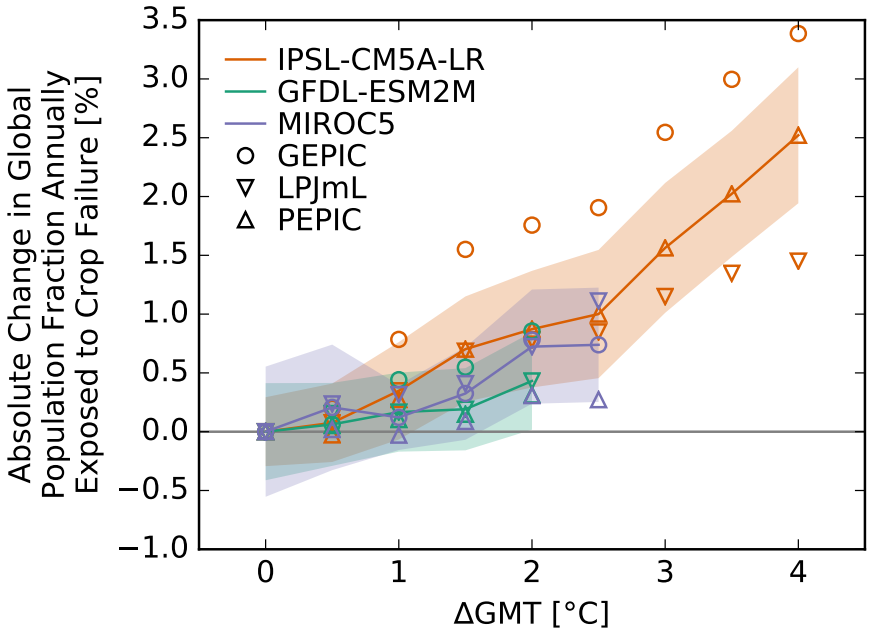

Figure S24: **Pure effect of climate change on global population fraction annually exposed to crop failures.** Absolute change in global population fraction annually exposed to crop failures at different levels of global mean temperature (GMT) change relative to the long-term preindustrial mean GMT as simulated by different impact models (symbols) driven by different climate models (colors). Symbols indicate the climate model-impact model combination-specific multi-year mean change caused by global warming (these are identical to the red solid lines in Panel D of Figures S146 … S154). Symbols connected by dashed lines represent emulated multi-year mean changes. Solid lines are the medians over all impact models per climate model. Shaded areas represent the multi-impact model median ±1 standard deviation range of the interannual variability of the global population fraction annually exposed to crop failures.

5.3 Land area affected and number of people exposed at the national scale

In Figure S26 the changes in crop failures on the country levels are depicted. More specifically, absolute changes in the affected land area and the exposed population at various warming levels are shown. Similar to earlier findings (65; 9), tropical regions see an increase in the frequency of crop failure with global warming. The highest increases are simulated in presently semi-arid regions or tropical and temperate regions that are prone to crop failure also under preindustrial climate conditions. Hotspots are the Indo-Gangetic Plain, Sudano-Sahelian belt and Central America. The temperate latitudes, on the other hand, experience only a moderate increase in crop failures, or even decline, as in large parts of northern Europe, Russia or Argentina. These patterns intensify with increased warming.

As before, relative changes in the affected land area/number of exposed people are shown as well, see Figure S27. Here one can see that in terms of relative changes central Africa and the Sahel zone are particularly struck by an increase in the affected land area and the number of people exposed.

The aforementioned hotspot regions of adverse impacts are also the locations in which most climate model-crop model combinations agree on the sign of the impact (Figures S155 … S171). Noticeable differences in impact estimates among climate model-crop model combinations occur e.g. for Central to Southern Africa and North America, which is – depending on the crop – in agreement with an earlier crop model intercomparison study (65).

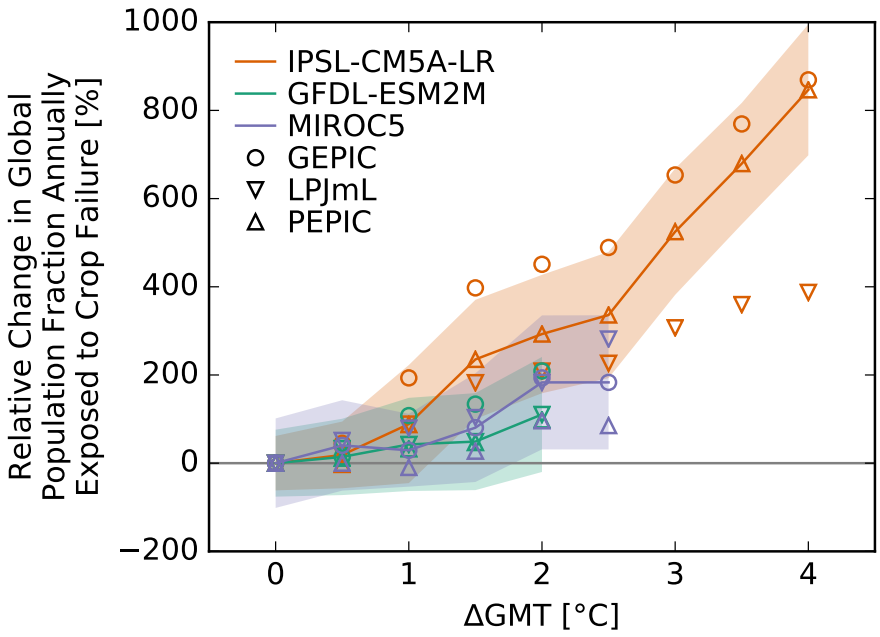

Figure S25: **Pure effect of climate change on global population fraction annually exposed to crop failures.** Same as Figure S24 but for the relative change in global population fraction annually exposed to crop failures.

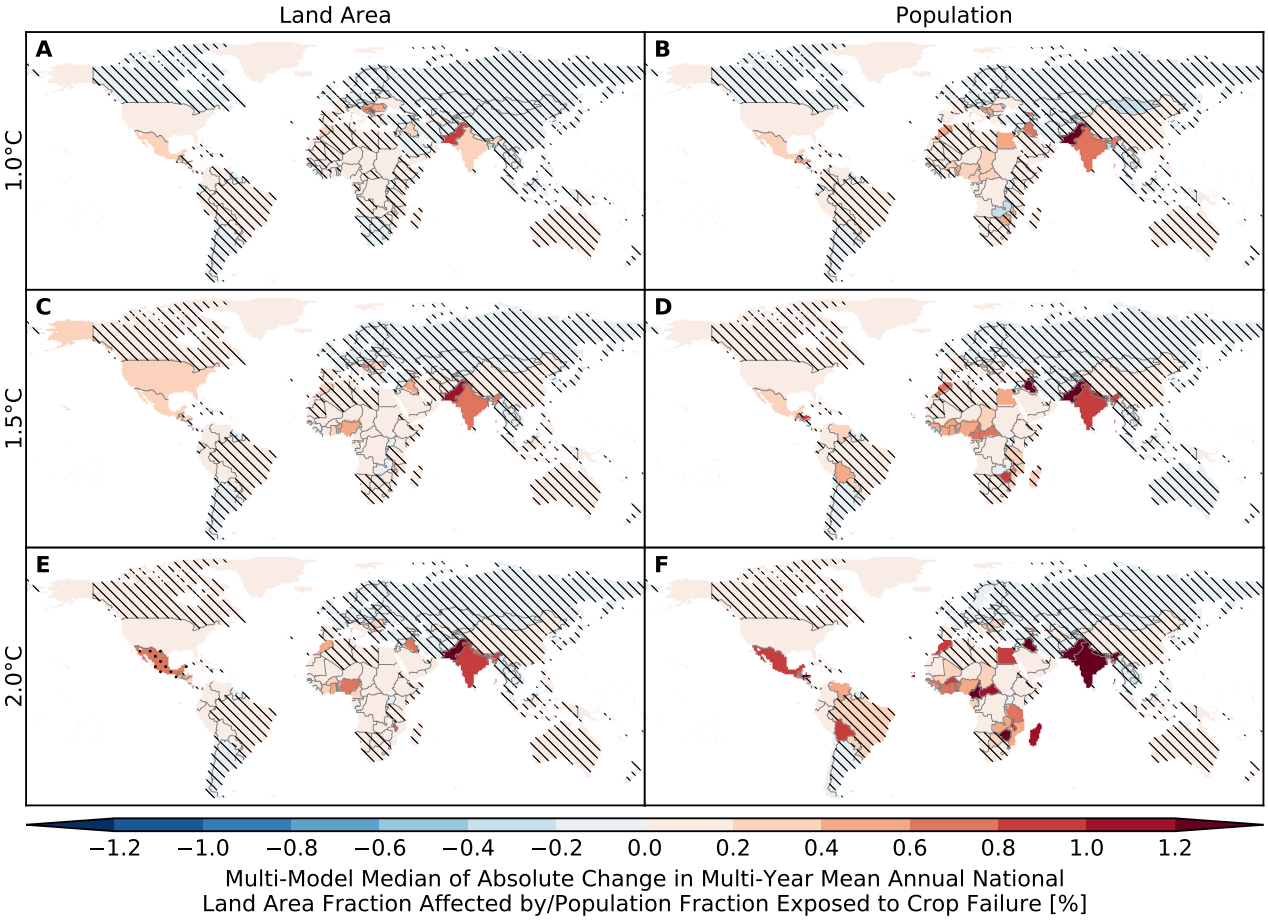

Figure S26: **Pure effect of climate change on annual national land area fraction affected by and population fraction exposed to crop failure.** Colors indicate multi-model median absolute changes in multi-year mean annual national (A, C, E) land area fraction affected by and (B, D, F) population fraction exposed to crop failure at (A, B) 1 °C, (C, D) 1.5 °C and (E, F) 2 °C global warming. Stippling indicates that at least 80% of all model combinations agree on an increase or decrease that is larger than 2σ of the preindustrial interannual variability. Hatching indicates that at least 80% of all model combinations agree that the change is smaller than 1σ of the preindustrial interannual variability. The climate model-impact model combination-specific results are shown in Figures S155 … S171.

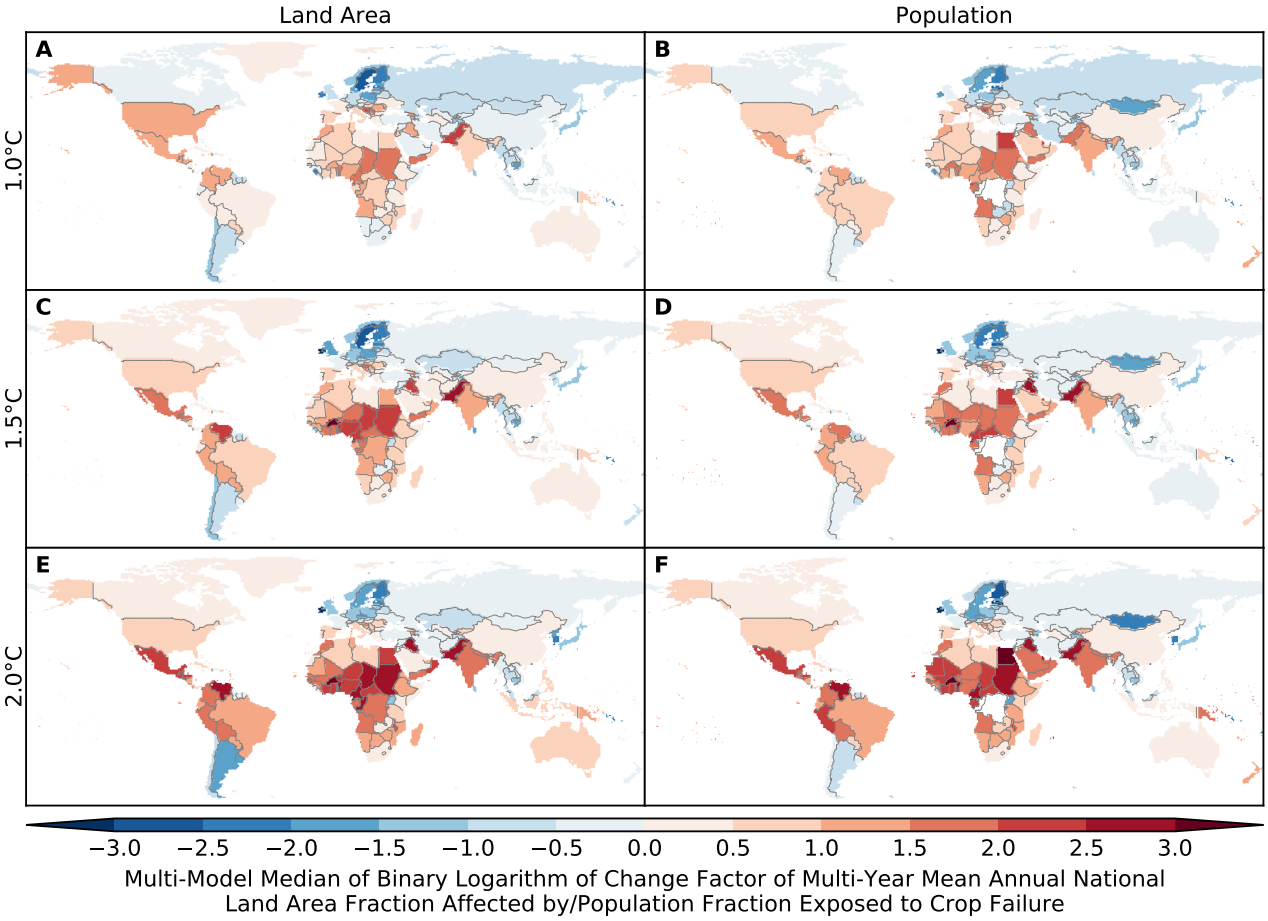

Figure S27: **Pure effect of climate change on annual national land area fraction affected by and population fraction exposed to crop failure.** Same as Figure S26 but for relative changes expressed in terms of binary logarithms of change factors, i.e. −2, −1, 0, 1, 2 means that the new value is 1/4, 1/2, 1, 2, 4 times the old value, which is equivalent to a relative change by −75 %, −50 %, 0 %, +100 %, +300 %, respectively. White indicates undefined relative changes due to division by zero. The climate model-impact model combination-specific results are shown in Figures S156 … S172.

6 Calculation of land area affected by and number of people exposed to wildfires

Grid-cell area fractions affected by wildfire are derived directly from the output of burned area by five Global Vegetation Models (GVMs; see Table S7). All GVMs are forced by bias-corrected daily climate data provided within ISIMIP2b (20). With the exception of ORCHIDEE, all GVMs have been run at a 0.5° grid resolution. ORCHIDEE has been run on a 1° grid because of computational constraints. All GVMs assume fixed socioeconomic conditions (e.g. changes in land use patterns) before 1860 (1860soc for 1661–1860 according to the ISIMIP2b protocol) and account for land-use changes and nitrogen deposition during the historical period (histsoc for 1861–2005 according to the ISIMIP2b protocol). After 2005 socioeconomic conditions including land-use patterns are held constant at present-day levels (2005soc for 2005–2100 or 2005–2300, respectively, according to the ISIMIP2b protocol). All GVMs except VISIT simulate dynamic natural vegetation distribution over time where the total area of natural vegetation is externally described by the ISIMIP2b land-use patterns. VISIT's fixed vegetation distribution is based on Olson's vegetation map (58) with modification by the potential vegetation data by (64).

All GVMs assume that fires burn natural vegetation. Pasture is not considered as natural vegetation and therefore not subject to dynamic vegetation changes simulated by the models but externally prescribed by land use patterns. LPJ-GUESS, ORCHIDEE and VISIT allow pastures to burn. LPJ-GUESS is the only model additionally allowing even croplands to burn. Thus, for most models land-use changes from natural vegetation to cropland reduce the area potentially subject to wildfires, whereas land use change from natural vegetation to pasture only reduces the area for CARAIB and LPJmL. The main elements of the fire modules used in the GVMs are described in Table S7.

Table S7: Main characteristics of the GVM fire models.

GVM	Fire ignition factors	Human influence on fire ignition and/or suppression included	How is fire spread/extent modelled	Minimum burned area fraction at grid level	Vegetation types allowed to burn besides natural vegetation
CARAIB (12)	availability of fuel, combustibility of fuel (soil moisture), presence of natural ignition source (lightning flash data)	no	function of soil moisture and wind speed	0	none
LPJmL (85; 5; 71)	ignition occurs once soil moisture threshold for available litter associated with plant productivity is reached	no	empirical relationship between the length of the fire season and the annual area burned, where the length of the fire season is derived from the number of fires initialized in the considered year	0.001	none
LPJ-GUESS (85; 78)	as in LPJmL	no	as in LPJmL	0.001	managed pastures, rangeland, cropland
ORCHIDEE (84; 96; 97)	ignitions from anthropogenic and lightning sources (lightening flash data) based on availability of fuel, combustibility of fuel (soil moisture), presence of ignition source	both human ignitions and suppressions are implicitly included in a single equation based on population density, only anthropogenic fires are suppressed	fire spread simulated as a function of fuel load, fuel compact status, fire intensity and wind speed; final fire extent is determined by an assumed mean fire size derived from fire spread rate and duration, and the number of effective ignitions	0	managed pastures, rangeland
VISIT (36; 35)	natural ignition based on availability of fuel, combustibility of fuel (soil moisture)	no	fire extent is an empirical function of soil moisture and fuel load	0	managed pastures, rangeland

6.1 Land area affected

The global land area fraction affected by wildfire is directly derived from monthly or annual data of burned area provided by the five GVMs. LPJmL and LPJ-GUESS provided annual burned area while VISIT, ORCHIDEE and CARAIB provided monthly data. For the latter three models, the annual area fraction affected by wildfire is calculated as the sum of the monthly values (capped at 100%) assuming that an area that has burned during one month of a year is unlikely to burn again during the same year, because fires would reduce the available fuel for the next burning and in most GVMs fire ignitions are limited by fuel availability. This mechanism holds true for most of the globe (3; 87; 1) even though fire return intervals may be smaller than one year in strongly fire-dominated ecosystems such as in Sub-Saharan Africa (2).

CARAIB, LPJmL and LPJ-GUESS simulate a global land area affected by wildfire in the 20th century ranging from 0.05 to 1.2 % per year while the global land area affected by wildfire in the 20th century reaches about 5.5 % and even up to 12.0 % per year for some years for VISIT and ORCHIDEE, respectively. Hence, three GVMs underestimate and two overestimate the global land area affected by wildfire compared to a reconstruction from a wide array of sources over the same period of about 4.0 % per year by (52). As shown in Figures S12–14, this pattern remains the same when the simulated burned area is compared to three satellite-derived burned area datasets, namely GLOBCARBON (63), L3JRC (83) and GFED3.1 (25). However, this comparison has to be interpreted with caution given that the satellite data only cover a short time period (2001–2005) and the climate data used to drive the GVM simulations during this time period do not correspond to the actual, observed climate.

The underestimation of burned area by some GVMs might be partly explained by an underestimation of fire return intervals in strongly fire-dominated ecosystem as outlined above. However, we expect a more important factor to be the neglectance of GVMs to account for fire being intentionally or unintentionally used to clear natural vegetation as part of land-use changes. Even though the reconstruction by (52) does not account for burning of agricultural wastes, nor for prescribed burning as part of landscape clearing or deforestation, overall, it does account for a wider range of fires than considered by the GVMs such as fires escaping from agricultural lands and during land clearing (as long as these have been reported by firefighters). Additionally, there are model-specific reasons for an underestimation of burned area: CARAIB only considers natural ignitions from lightning and the fire model parameters are uncalibrated, i.e. have not been adjusted to observed burned area. LPJmL underestimates fire occurrence in savannah regions due to lack of human ignition, and also defines rangelands and other extensively managed grasslands as pastures that cannot burn. LPJ-GUESS, despite allowing fire to occur on croplands and pastures, features a rather small burned area. LPJ-GUESS has been found to be very sensitive to the choice of the fire module (1) and the fire module used in this study (GlobFIRM; (86)) is known to underestimate burned area, since at the time it was developed estimates of burned area were lower (26) and GlobFIRM was calibrated with data on fire return intervals rather than burned area (86).

The reasons for overestimating the global burned area are also model specific. One reason why VISIT is slightly overestimating the global burned area might be that VISIT is the only GVM in our ensemble that does not simulate dynamic vegetation, which might lead to increasing maladaptation of regrowing vegetation after a fire to climate change-induced changes in fire risk. Additionally, the overestimation of fire in boreal regions and in Northern China/India and several other regions due to a lack of fire suppression in VISIT is known to outweigh the underestimation of fire in savannah regions due to lacking human ignitions (40). ORCHIDEE overestimates global burned area because of the large grassland and pasture fraction available to burn and a lower tree fraction as compared to previous burned area evaluations of the model (96). In ORCHIDEE, the fire spread rate is inversely linked with the fuel bulk density. Grassland have a low fuel bulk density (more loosely packed fuel) so a higher grassland fraction leads to lower fuel bulk density and a high spread rate, which leads to higher burned area. Another reason for the difference between the burned area simulations of ORCHIDEE in this study and the ORCHIDEE model evaluation study presented in (96) could be the different climate input data used.

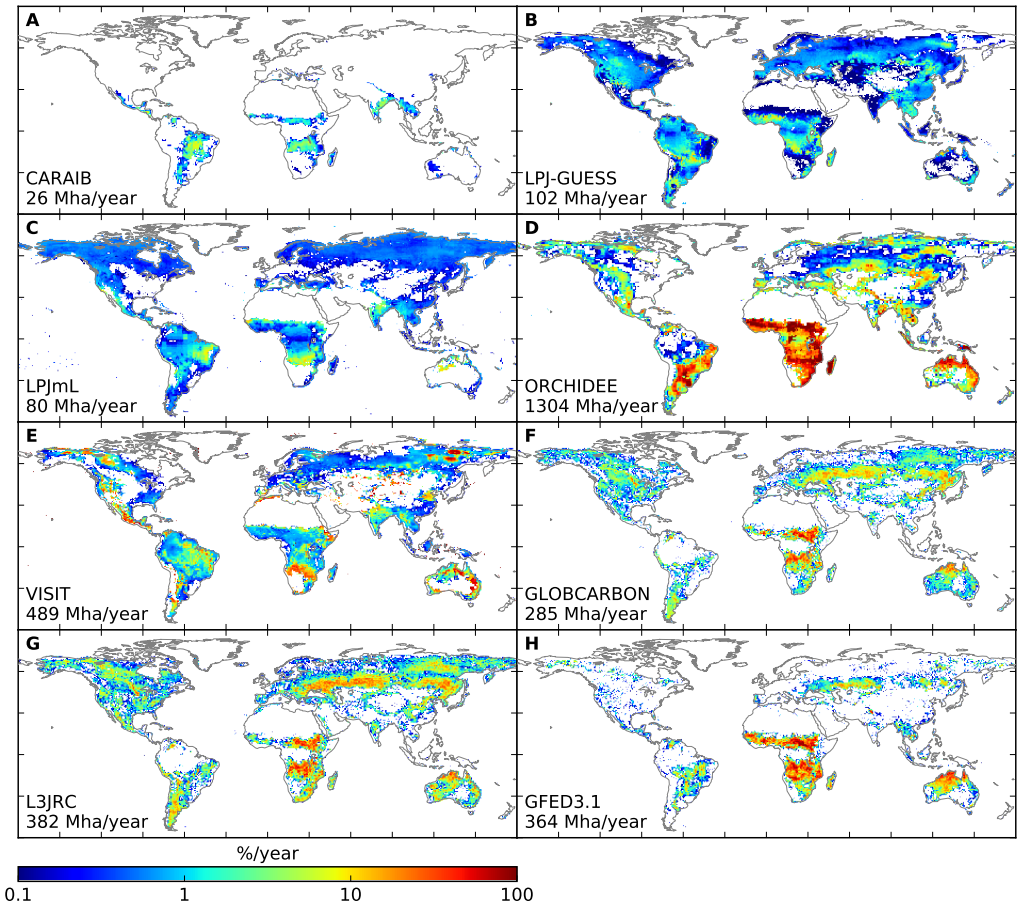

Figure S28: Mean annual burned area fraction at grid scale (color, in percent) and annual global burned area (annotated in the lower left corner of each panel) over 2001–2005 as simulated by (A) CARAIB, (B) LPJ-GUESS, (C) LPJmL, (D) ORCHIDEE and (E) VISIT driven with IPSL-CM5A-LR historical climate input data, and as observed according to the satellite-derived burned area datasets (F) GLOBCARBON (63), (G) L3JRC (83) and (H) GFED3.1 (25).

Separation of pure effect of climate change from direct human influences

CARAIB and especially LPJmL show a clear decrease of the global area affected by wildfire in the 1860–2005 period in the simulations driven with preindustrial climate and changing land use. This trend can be explained by the set-up of these models and the land-use change dynamics because CARAIB and LPJmL do not allow pastures and cropland to burn and hence because the pasture and cropland area increases during the historical time period, the area available to burn decreases. This effect of land-use change also dominates the historical simulations of CARAIB and LPJmL including land-use and climate change where burned area substantially decreases. The patterns of decreasing global land area affected by wildfire with increasing land-use change in CARAIB and LPJmL seem counter-intuitive at a first glance because, historically, fire has been a key tool to clear natural vegetation (7). However, as noted above, the current GVM setup does neither capture the application of fire as a way to clear land nor the associated risk of burning adjacent natural vegetation unintendedly through escaping fires. The decrease of global land area affected by wildfire as a result of changing land use mimics historical tendencies to suppress fires on agricultural and other human-dominated lands (61; 42).

ORCHIDEE, VISIT and LPJ-GUESS only show minor changes in burned area over the 1860–2005 period in the simulations driven by preindustrial climate and changing land use (see gray dots in panels A of Figures S173 … S186). Because these models do allow pastures, and in the case of LPJ-GUESS even croplands, to burn the small changes in burned area can possibly be attributed to the effects of decreasing natural vegetation available to burn (as outlined above) and increasing pastures (and croplands in the case

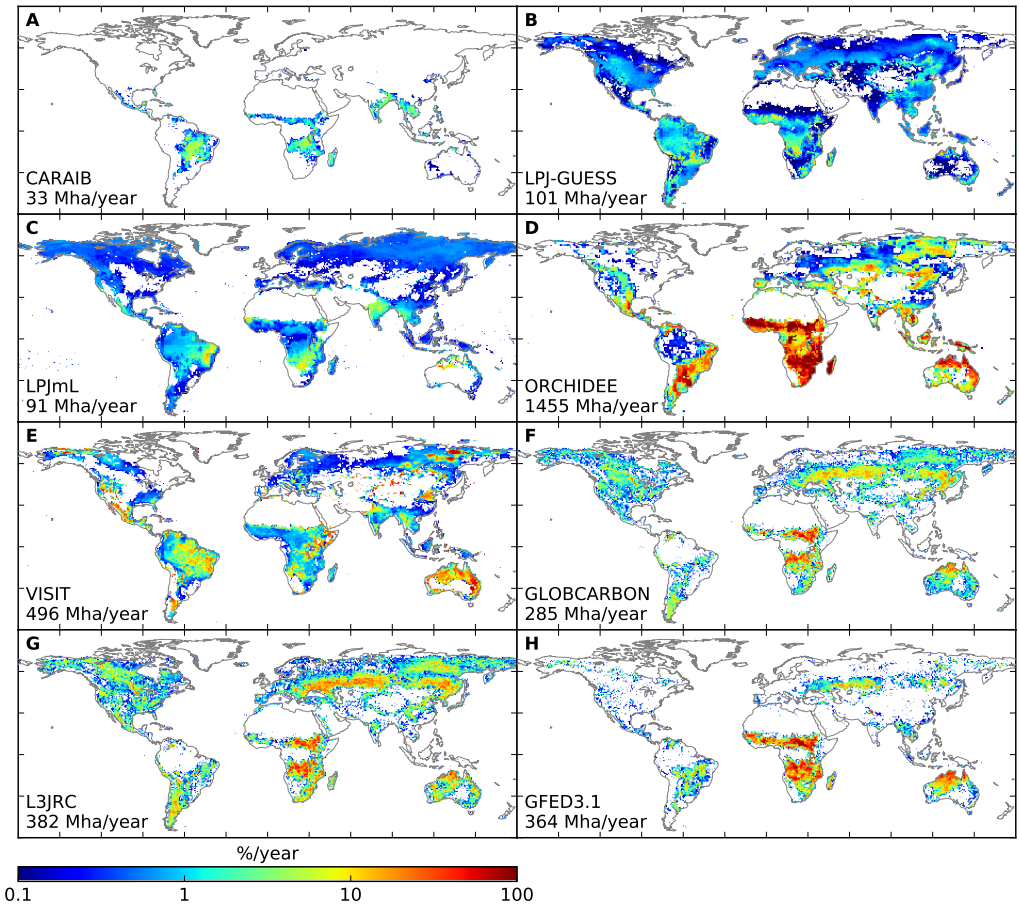

Figure S29: Same as Figure S28 but for GVMs driven with GFDL-ESM2M historical climate input data.

of LPJ-GUESS) available to burn largely cancelling each other off. The pure climatic effect on burned area during the 1860–2005 period is weak for most GVM-GCM combinations (black dots in panel C of Figures S173 … S186) but shows slightly increasing global area affected by wildfire, most visibly for VISIT and CARAIB.

ORCHIDEE, VISIT and LPJ-GUESS only show minor changes in burned area over the 1860–2005 period in the simulations driven by preindustrial climate and changing land use (see gray dots in panels A of Figures S173 … S186). Because these models do allow pastures, and in the case of LPJ-GUESS even croplands, to burn the small changes in burned area can possibly be attributed to the effects of decreasing natural vegetation available to burn (as outlined above) and increasing pastures (and croplands in the case of LPJ-GUESS) available to burn largely cancelling each other off. The pure climatic effect on burned area during the 1860–2005 period is weak for most GVM-GCM combinations (black dots in panel C of Figures S173 … S186) but shows slightly increasing global area affected by wildfire, most visibly for VISIT and CARAIB.

In ORCHIDEE, the decline in burned area mainly occurs in the grassland areas that burn so much during the historical simulations. Because of the strong contribution of grasses to burned area (due to the inverse relationship of fire spread and fuel bulk density described above), the decrease in burned area is explained by a decrease in grassland available to burn. In fact, an additional analysis has revealed that ORCHIDEE simulates substantial vegetation shifts from grassland to forest in response to global warming in most parts of the world, arguably because higher atmospheric CO_2 concentrations favor C3 over C4 plants. Compared to grassland, forests are characterised by more compact fuel, which decreases the fire spread rate and hence burned area. Additionally, the effects of increasing CO_2 on plant water relations might increase soil moisture and hence reduce combustibility of the fuel, counterbalancing increasing climatic fire risk.

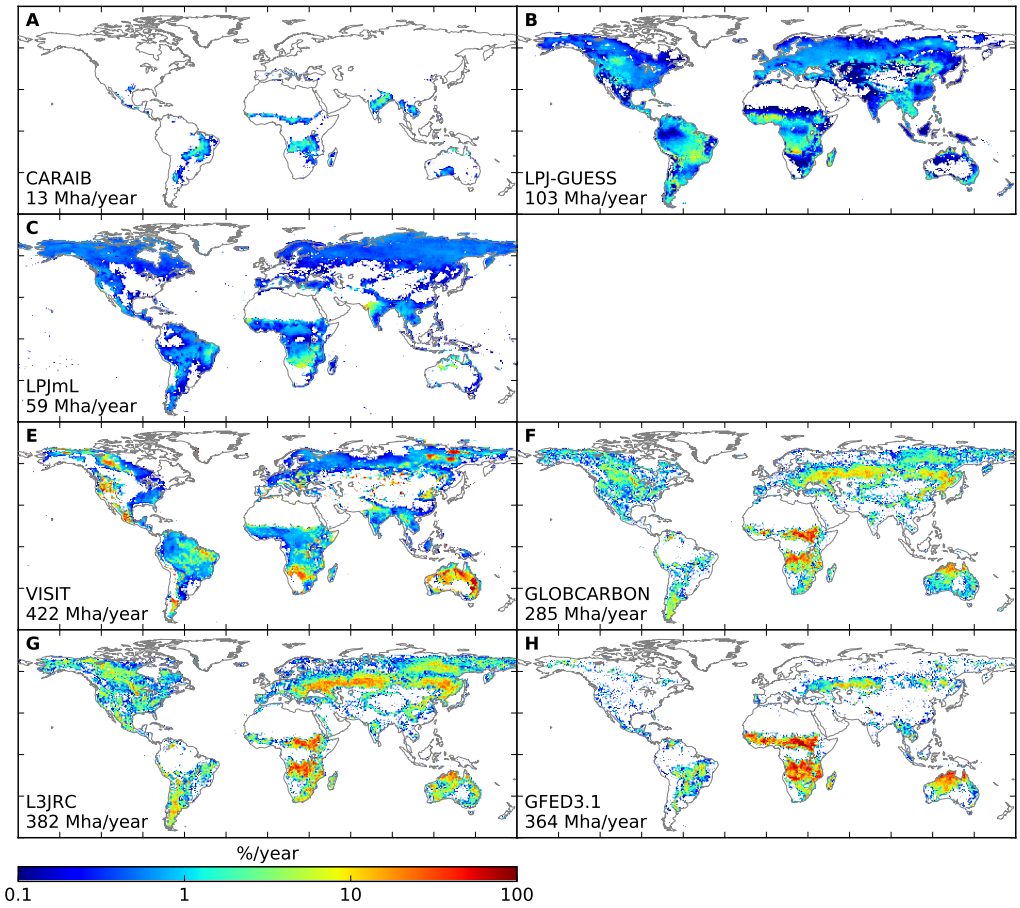

Figure S30: Same as Figure S28 but for GVMs driven with MIROC5 historical climate input data.

6.2 Number of people exposed

We assume that the fraction of the population of a grid cell that is exposed to a wildfire occurring in that grid cell scales with the grid cell's area fraction affected by the wildfire. Therefore, the fraction of the population exposed to wildfire is set equal to the fraction of the grid cell area affected by wildfire at the 0.5° grid level. This reasoning is based on the assumption that densely populated area such as cities, even though not being able to burn in the GVMs, will still be exposed to a fire in the same grid cell, for example due to air pollution from smoke (44). Before 1860 and after 2005, population data are held fixed at 1860 and 2005 levels, respectively.

Compared to the global land area fraction affected by wildfire, the fraction of the global population exposed to wildfire is slightly higher throughout all GVMs and GCM combinations with value ranges of 2–12 % per year for VISIT, 7–12 % per year for ORCHIDEE and 0–1.2 % per year for all other models. This suggests that an area affected by wildfire houses slightly more people than an average area.

Separation of pure effect of climate change from direct human influences

LPJmL, ORCHIDEE, CARAIB and VISIT (the latter two only when driven by MIROC5) show a decrease of the global population affected by wildfire over the 1860–2005 period in the simulations driven with preindustrial climate and changing land use (see gray dots in panels A of Figures S187 … S200). CARAIB and VISIT, when driven by GFDL-ESM2M and IPSL-CM5A-LR, do not show a clear trend. In general the trends of CARAIB and VISIT are small and the different responses to the different GCMs might simply be explained by the climatic differences underlying these forcings. The clear decrease in LPJmL can be explained by the decreasing area affected by wildfire due to changes from natural vegetation to cropland and pastures (as explained above). In ORCHIDEE, the increasing population leads to increasing fire sup-

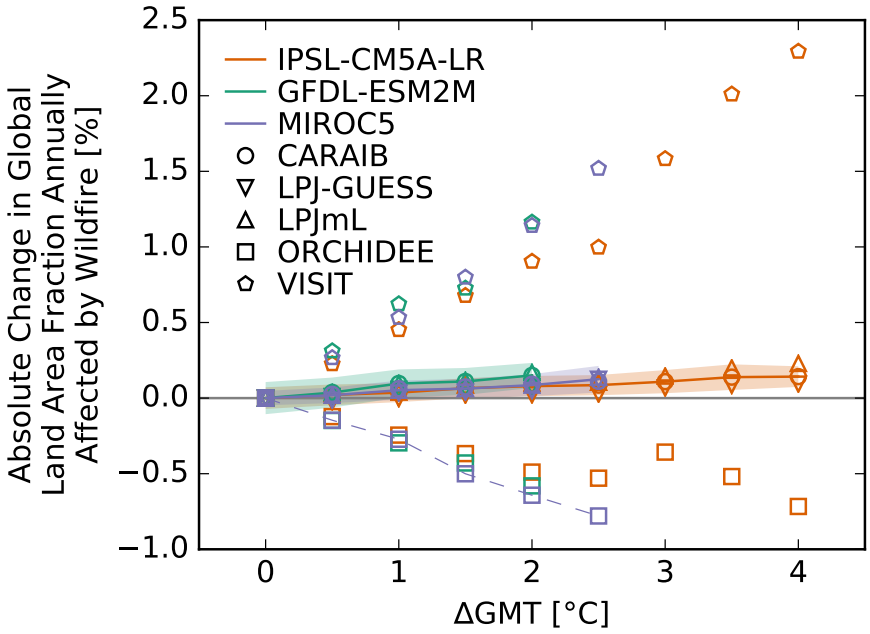

Figure S31: **Pure effect of climate change on global land area fraction annually affected by wildfires.** Absolute change in global land area fraction annually affected by wildfires at different levels of global mean temperature (GMT) change relative to the long-term preindustrial mean GMT as simulated by different impact models (symbols) driven by different climate models (colors). Symbols indicate the climate model-impact model combination-specific multi-year mean change caused by global warming (these are identical to the red solid lines in Panel D of Figures S173 … S186). Symbols connected by dashed lines represent emulated multi-year mean changes. Solid lines are the medians over all impact models per climate model. Shaded areas represent the multi-impact model median ±1 standard deviation range of the interannual variability of the global land area fraction annually affected by wildfires.

pression (see Table S7). LPJ-GUESS shows an slightly increasing trend in population affected by wildfire over the 1860–2005 period that is consistent with the increasing area affected by wildfire due to an increasing area of pastures and cropland available to burn. The simulations driven with changing climate and land-use change during the 1860–2005 period show the same patterns. The pure climatic effect during the historical period is rather weak but for most GVM-GCM combinations (with the exception of ORCHIDEE) there is an increasing trend of population affected by wildfire over time (black dots in panel C). For ORCHIDEE, the clearly negative pure climatic effect on the global population exposed is possibly due to the corresponding decrease in burned area.

In the 21st century, the pure climatic effect leads to an increasing trend in the global population exposed to wildfire for CARAIB, LPJ-GUESS, LPJmL and VISIT (blue and yellow dots in panel C of Figures S187 … S200). For ORCHIDEE, the pure climatic effect in the 21st century is decreasing the population exposed to wildfire. For the longer-term simulations covering 2100–2300 under RCP2.6 there is no clear trend in the global population exposed to wildfire for most of the GVM-GCM combinations. Generally, increasing global mean temperature leads to an increase in global population exposed to wildfire beyond the preindustrial and historical levels according to all considered GVMs except ORCHIDEE (blue and yellow dots in panel D of Figures S173 … S186). The decreasing population exposed to wildfire in ORCHIDEE can possibly be explained by the decrease in burned area discussed above.

6.3 Land area affected and number of people exposed at the national scale

Spatial multi-model median change patterns (Figures S35 and S36) show increases in land area affected by and population exposed to wildwire for almost all countries of the world. Exceptions include Indonesia as well as a few Sub-Saharan and Latin-American countries. The largest absolute increases in burnt land

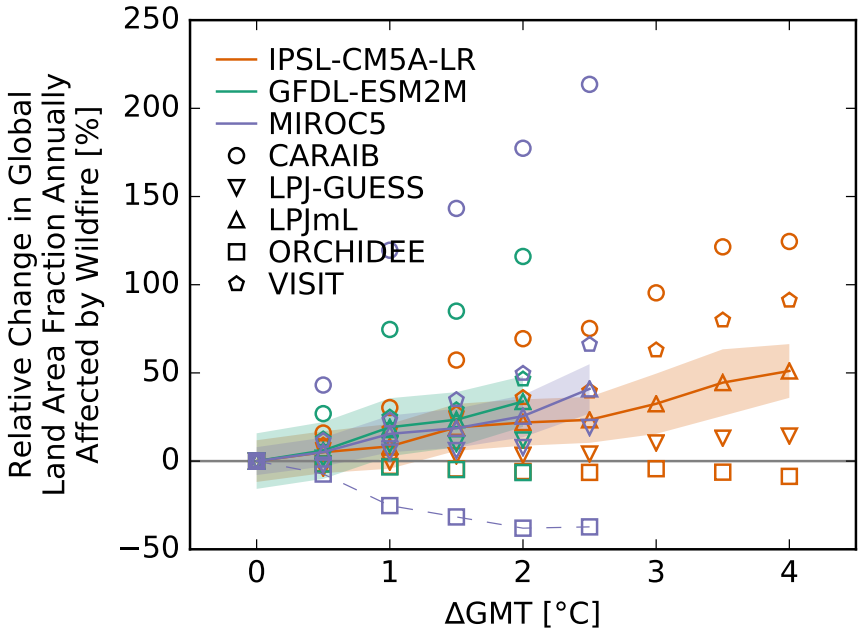

Figure S32: **Pure effect of climate change on global land area fraction annually affected by wildfires.** Same as Figure S31 but for the relative change in global land area fraction annually affected by wildfires.

area are simulated for some South African countries, but even at 2°C global warming for no country at least 80% of all model combinations simulate a change in the multi-year mean national burned land area that is larger than 2σ of the preindustrial interannual variability. This is due to the substantial differences in signs and magnitudes of the pure effect of climate change on wildfire occurrences simulated with the different GVMs. While CARAIB simulates increasing burned area in response to global warming for almost all countries, ORCHIDEE simulates a decreasing burned area over large parts of the tropics and high latitudes. Decreasing fire danger is also simulated by LPJmL for North Europe, and by VISIT for Indonesia, India, parts of Central, East and North Africa, and some Central American countries. Model agreement is high about an increasing fire danger in southern South America, the USA, South Europe, the Middle East, Central Asia, East Asia, South Africa and parts of East Africa.

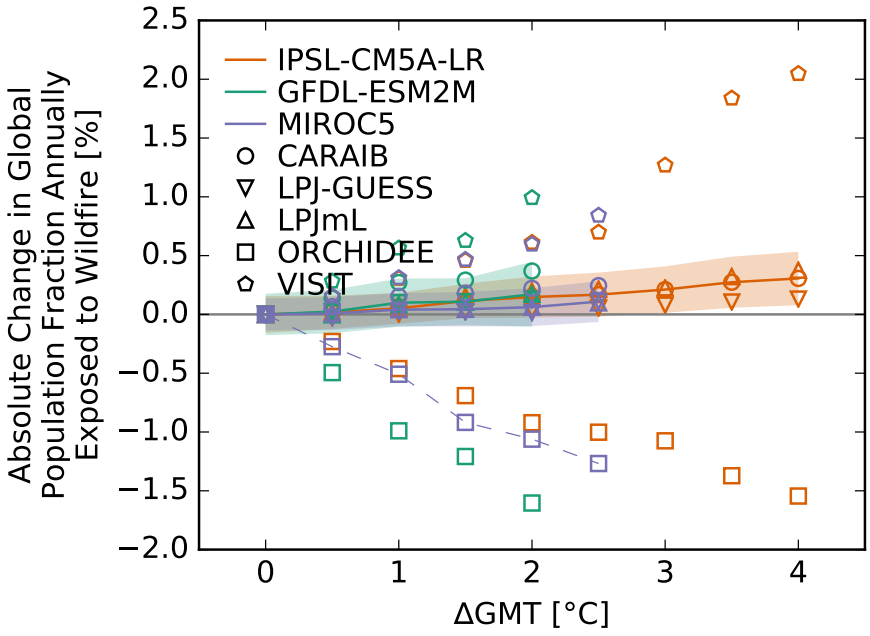

Figure S33: **Pure effect of climate change on global population fraction annually exposed to wildfires.** Absolute change in global population fraction annually exposed to wildfires at different levels of global mean temperature (GMT) change relative to the long-term preindustrial mean GMT as simulated by different impact models (symbols) driven by different climate models (colors). Symbols indicate the climate model-impact model combination-specific multi-year mean change caused by global warming (these are identical to the red solid lines in Panel D of Figures S187 … S200). Symbols connected by dashed lines represent emulated multi-year mean changes. Solid lines are the medians over all impact models per climate model. Shaded areas represent the multi-impact model median ±1 standard deviation range of the interannual variability of the global population fraction annually exposed to wildfires.

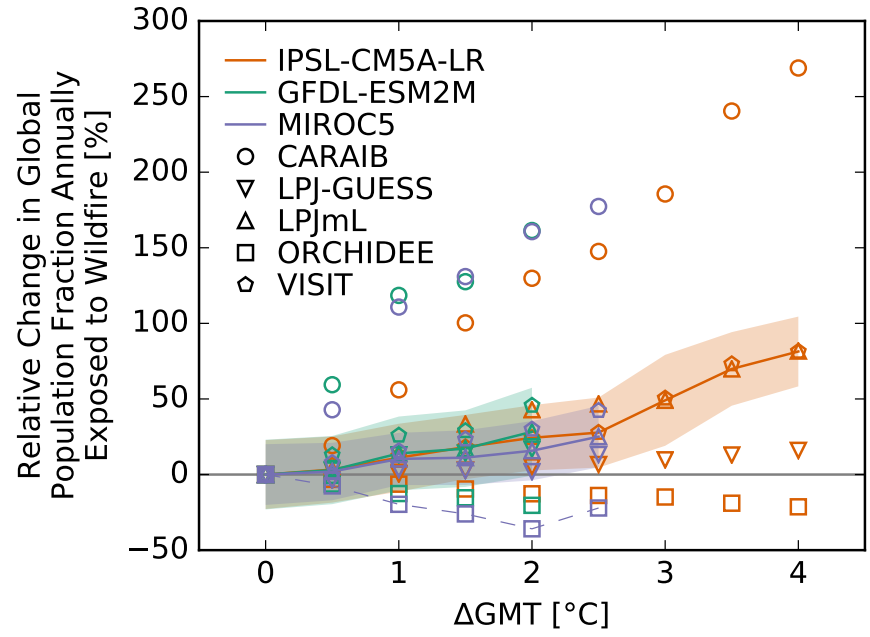

Figure S34: **Pure effect of climate change on global population fraction annually exposed to wildfires.** Same as Figure S33 but for the relative change in global population fraction annually exposed to wildfires.

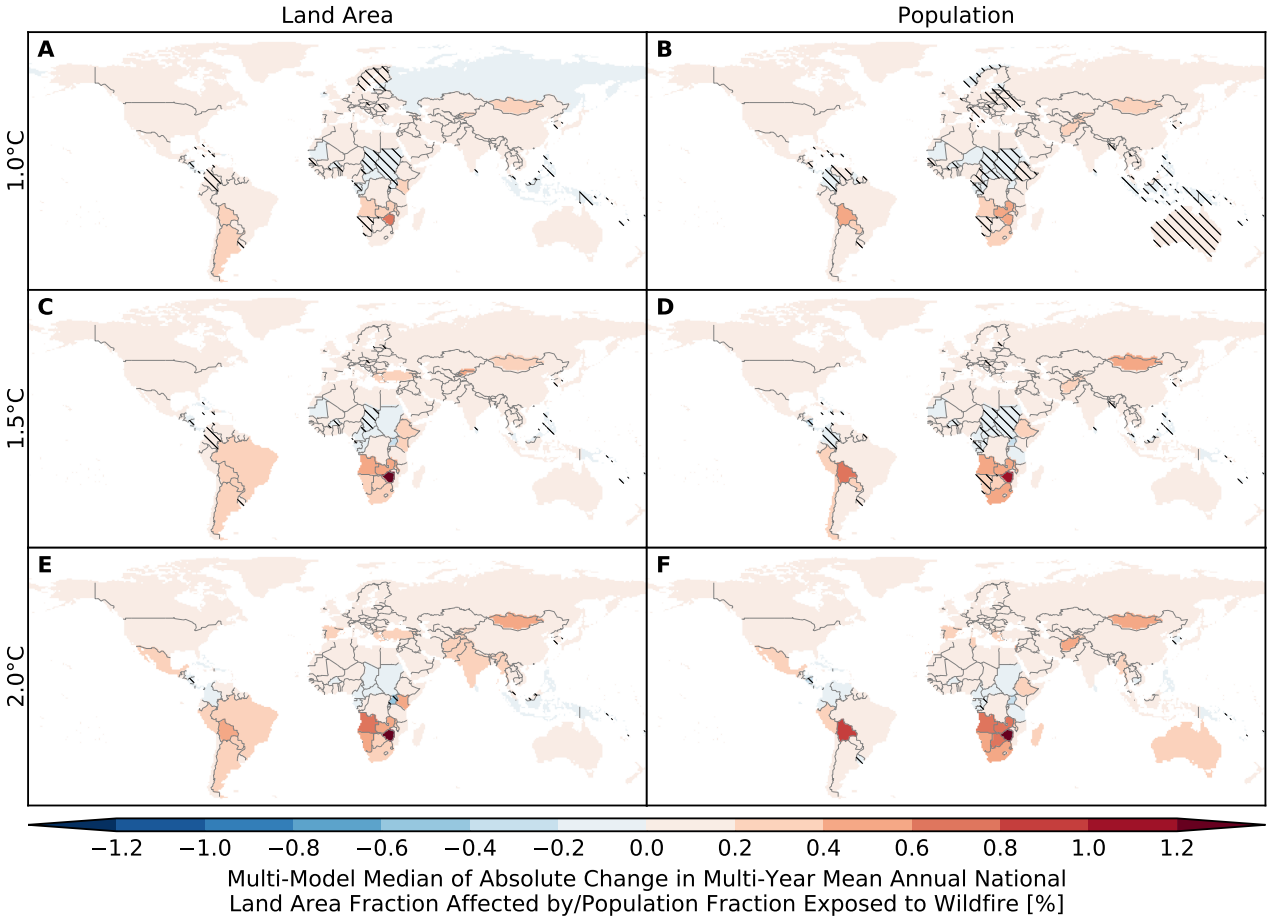

Figure S35: **Pure effect of climate change on annual national land area fraction affected by and population fraction exposed to wildfire.** Colors indicate multi-model median absolute changes in multi-year mean annual national (A, C, E) land area fraction affected by and (B, D, F) population fraction exposed to wildfire at (A, B) 1 °C, (C, D) 1.5 °C and (E, F) 2 °C global warming. Stippling indicates that at least 80% of all model combinations agree on an increase or decrease that is larger than 2σ of the preindustrial interannual variability. Hatching indicates that at least 80% of all model combinations agree that the change is smaller than 1σ of the preindustrial interannual variability. The climate model-impact model combination-specific results are shown in Figures S201 … S227.

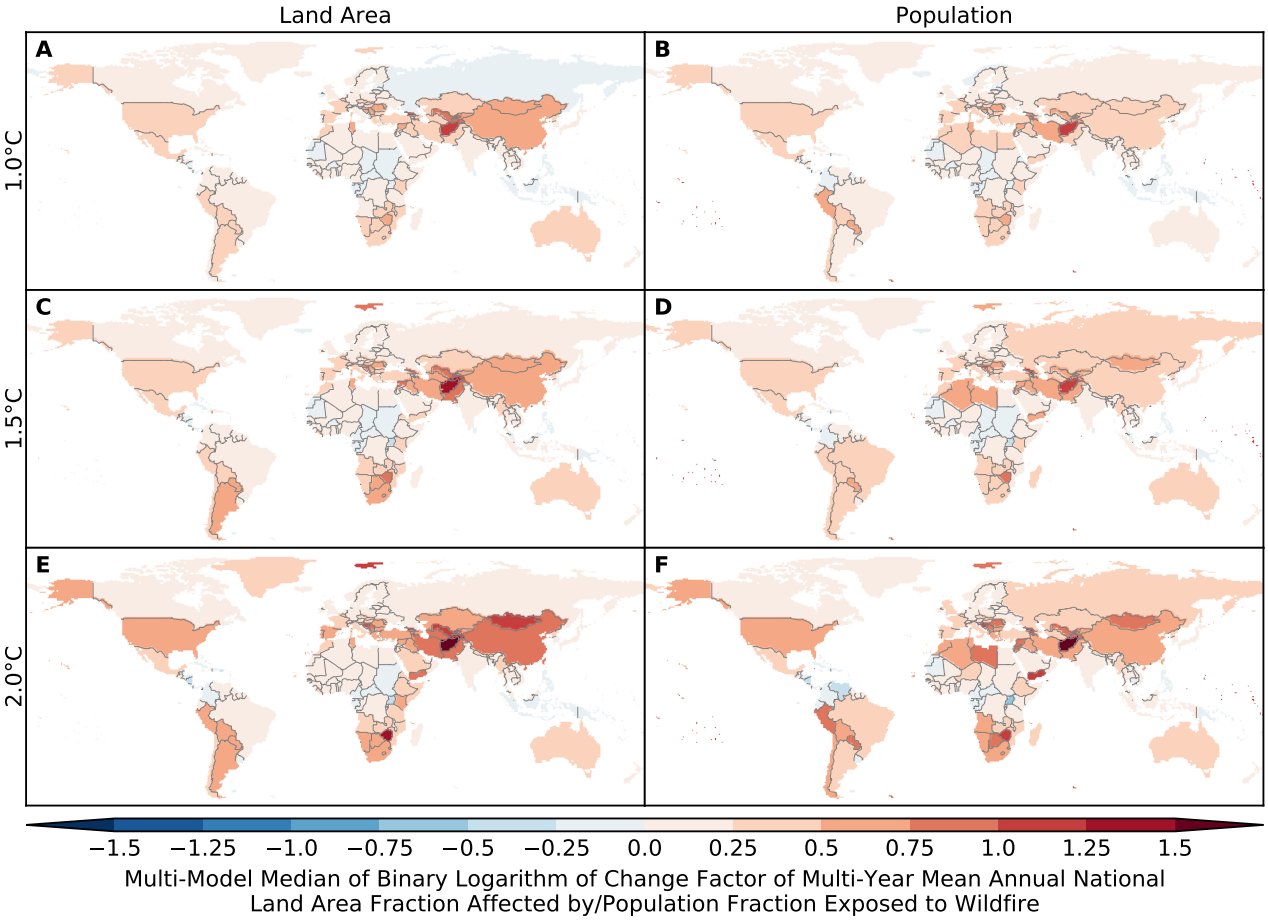

Figure S36: **Pure effect of climate change on annual national land area fraction affected by and population fraction exposed to wildfire.** Same as Figure S35 but for relative changes expressed in terms of binary logarithms of change factors, i.e. −2, −1, 0, 1, 2 means that the new value is 1/4, 1/2, 1, 2, 4 times the old value, which is equivalent to a relative change by −75 %, −50 %, 0 %, +100 %, +300 %, respectively. White indicates undefined relative changes due to division by zero. The climate model-impact model combination-specific results are shown in Figures S202 … S228.

7 Calculation of land area affected by and number of people exposed to droughts

Severe drought conditions are defined by monthly soil moisture (10; 75) falling below the 2.5th percentile variable monthly threshold, based on using of the preindustrial reference distribution (1661–1859), for at least 7 consecutive months (74). Moisture in the top meter of soil shows the combined effects of processes like precipitation, soil evaporation, plant transpiration, infiltration, runoff, snow accumulation and melt, and is therefore a good indicator for drought conditions (76). The monthly soil moisture information used in this study that was provided by the individual hydrological models refers to soil layers of different thicknesses (see Table S5). Here we use root moisture as directly provided by H08, MPI-HM, PCR-GLOBWB, and WaterGAP2. To approximate this variable we integrated soil moisture across the first seven soil layers of CLM45 (down to a depth of 78 cm), the first three layers of JULES-W1 (down to a depth of 1 m), the first three layers of LPJmL (down to a depth of 1m), and the first 9 layers of ORCHIDEE (down to a depth of 75 cm). Further properties of the models are shown in Table S5.

The variable monthly threshold level method (88; 39; 56; 31; 89) was applied here to distinguish periods of soil moisture drought from periods of no drought. The use of a variable monthly threshold accounts for seasonal climatology (76; 31), which is relevant for the management of water resources.

For each month individually we identified per model and climatological forcing combination the 2.5th percentile soil moisture value at the grid-level, using the preindustrial scenario as reference period. Using these spatially and monthly explicit threshold-levels we, subsequently, evaluated for the different scenarios applied how often the soil moisture conditions fall below this threshold. Subsequently, we applied a six-month threshold to distinguish the longer, prolonged drought events from the short, incidental ones (75). Only these prolonged droughts were taken into account when evaluating the land area and population exposed to drought conditions at the yearly scale. In doing so, we checked for each year whether a grid-cell was exposed to at least one of a period of prolonged droughts (i.e. drought conditions that last longer than 6 months). In case the grid-cell was exposed this cell was accounted as 'being exposed to drought' for that respective year, in case the grid-cell was not exposed to drought conditions or only to relatively short drought conditions, the grid-cell was classified as 'not exposed to drought' for that respective year.

To evaluate the impacts of human actions and climate change on the occurrence and spatial extent of droughts we superimpose the critical drought thresholds that were defined for the preindustrial reference period over the scenarios that represent the historical (including human actions) and/or climate change conditions (including both human actions and climate change impacts). Hence, the difference in exposure between these scenarios give indication to the attribution of climate change and human activities to droughts. It must be said, though, that with such an approach we only evaluate the attribution of climate change and human activities to the increase in the exposure of drought events in time and place. Any changes in the severity of drought conditions, nor in the duration or of frequency (if consistently lower or higher than 6 months) of drought events at sub-yearly scales were not accounted for in this evaluation.

7.1 Land area affected

To estimate the area affected by drought, we sum the grid cells with a fraction of the grid cell suffering drought. To estimate the total area affected the individual affected areas are added up.

For preindustrial climate conditions and 1860/2005 socioeconomic conditions, the distribution of the annual global land area fraction affected (AFA) remains almost constant for all model and GCM combinations. Such ranges vary depending on the model and GCM combination, but are mostly within the 2 % and never go beyond the 5 %.

For historical climate conditions, the pure effect of climate change in AFA by drought for H08 and WaterGAP2 is small, as the differences between the annual AFA by drought and the median of the sim-

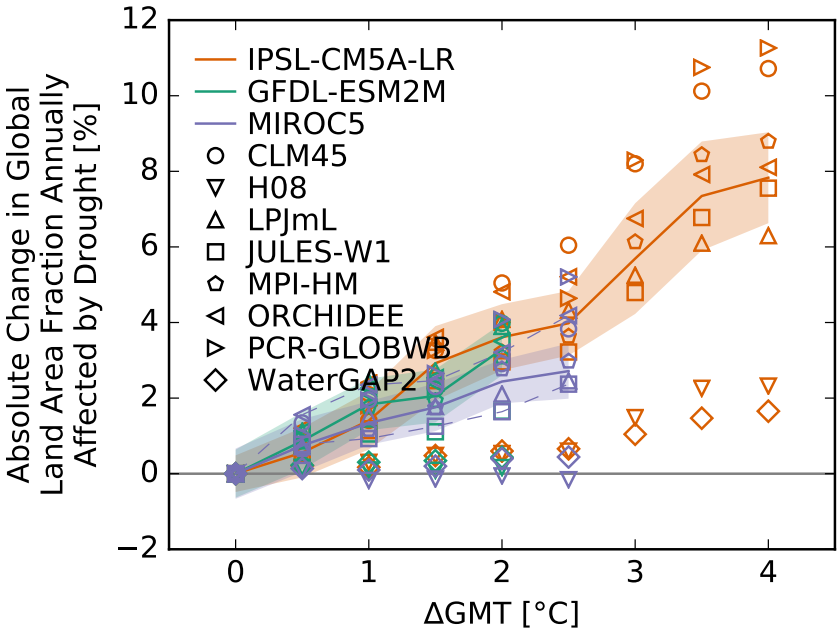

Figure S37: **Pure effect of climate change on global land area fraction annually affected by drought.** Absolute change in global land area fraction annually affected by drought at different levels of global mean temperature (GMT) change relative to the long-term preindustrial mean GMT as simulated by different impact models (symbols) driven by different climate models (colors). Symbols indicate the climate model-impact model combination-specific multi-year mean change caused by global warming (these are identical to the red solid lines in Panel D of Figures S229 … S250). Symbols connected by dashed lines represent emulated multi-year mean changes. Solid lines are the medians over all impact models per climate model. Shaded areas represent the multi-impact model median ±1 standard deviation range of the interannual variability of the global land area fraction annually affected by drought.

ulations assuming preindustrial climate conditions are of at most 2 %. For JULES-W1, PCR-GLOBWB, ORCHIDEE, MPI-HM and LPJmL, the change in AFA by drought increases over time, and such ranges depend on the model and GCM, but in general reach the 4 %. These results are in line with Dai (10), who showed an increasing trend in drought exposure between 1950 and 2010 using a Palmer Drought Severity Index (PDSI) based drought indicator. According to Dai (10), the global land area affected by drought has an initial increase of around 0.5 % by 1950, which grows up to 5 % by 2010. Dai (10) showed that increasing global temperatures since the 1980s have contributed significantly to the increase in land area affected by drought globally (+8 %), mainly as a result of increased evaporation.

The increase in AFA by drought starting in the historical period highlights the effects of human forcing. WaterGAP2 and H08 models show little increase in the AFA by drought, while other models show significantly larger effects. All models include human impacts, but they do so in a different way. Methods of human impact parameterization may give rise to the differences in the observed impacts and it would be worth to analyze this further.

For RCP2.6 climate conditions, the change in AFA by drought for H08 and WaterGAP2 follows the same behavior as for the historical climate conditions. For all other models, the change in AFA by drought increases in time, reaching up to 8 %. For RCP6.0 climate conditions, the change in AFA by drought increases over time for all models. Such change is small for H08 and WaterGAP2, where the largest change occurs for H08 + IPSL-CM5A-LR, reaching the 8 %, but remains under 2 % for all other cases. For all other models and GCMs, the change is larger, reaching up to 15 % for PCR-GLOBWB + IPSL-CM5A-LR. All of Dai (10), Lehner et al. (46) and Sheffield & Wood (75) support our observations of increases in drought exposure under climate change. Dai (10) suggest that severe and widespread droughts will occur in the next decades in many regions as a result of either decreased precipitation and/or increased evapotranspi-

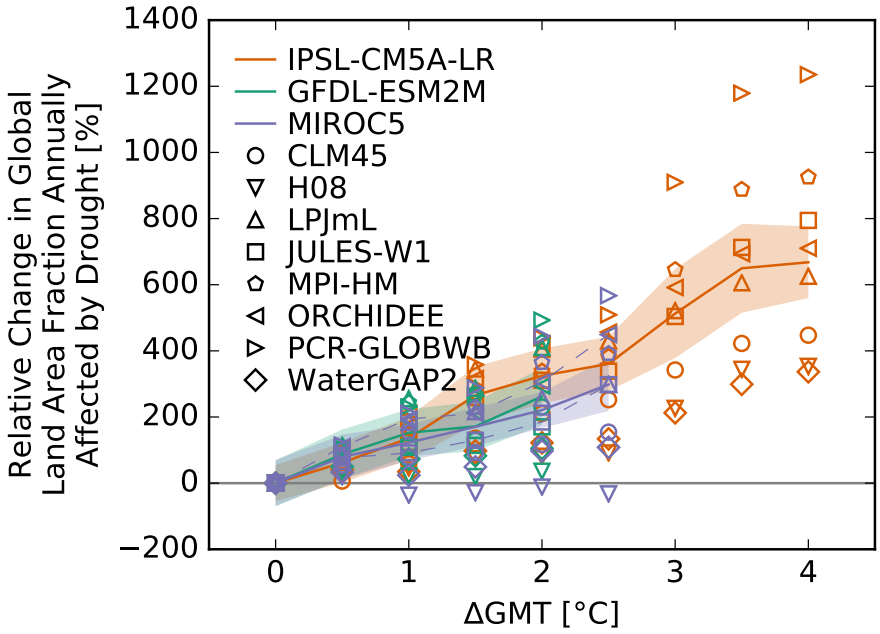

Figure S38: **Pure effect of climate change on global land area fraction annually affected by drought.** Same as Figure S37 but for the relative change in global land area fraction annually affected by drought.

ration. The results of Lehner et al. (46) indicate a widespread drying under both 1.5 °C and 2.0 °C degree climates, for example in the Mediterranean, central Europe, the Amazon, and southern Africa. Sheffield & Wood (75) show that most models show decreases in soil moisture globally under future projections which results in a doubling of the area exposed to severe soil moisture deficits and the frequency of short term soil moisture droughts. Longer, prolonged droughts triple under the scenarios applied by Sheffield & Wood (75), although model results vary.

7.2 Number of people exposed

The fraction of the population of a grid cell exposed to drought scales with the area of the grid cell affected by drought at the 0.5° grid level. Before 1860, the population is fixed at 1860 levels, and after 2005, the population is fixed at 2005 levels.

The behavior of the time series of annual global population fraction exposed (PFE) to drought is very similar to the one seen in the AFA by drought. The difference is in the percentage of change due to the pure effect of climate change in PFE, which is considerably smaller.

For preindustrial climate conditions, the percentage of the global population exposed to drought ranges for all models between 0.2 % and 5 %, being H08 and WaterGAP2 the models with smaller percentages of PFE, up to 2 %. The change of PFE due to historical climate conditions shows a small increase over time for all models, being IPSL-CM5A-LR + MPI-HM the one with the largest change over time, from 3 % to 6 %. For RCP2.6 and RCP6.0 climate conditions we see consistent increments in the PFE to drought over time, being the largest changes under the IPSL-CM5A-LR GCM, which reaches up to 10 % change for PCR-GLOBWB and 12 % for MPI-HM.

Despite the similar behavior in trends for the AFA and PFE to drought, the lower percentages found in the pure effect of climate change may be due to the population being unequally distributed, which introduces changes in exposure of to soil moisture.

An interesting feature of these results is the decrease in the PFE to drought for historical climate conditions for most models, being the decrease more significant for LPJmL and PCR-GLOBWB, two models considering reservoir storage and detailed land-use classification (79). This finding also suggests a strong effect of the population density, growth and distribution, which should be considered for further

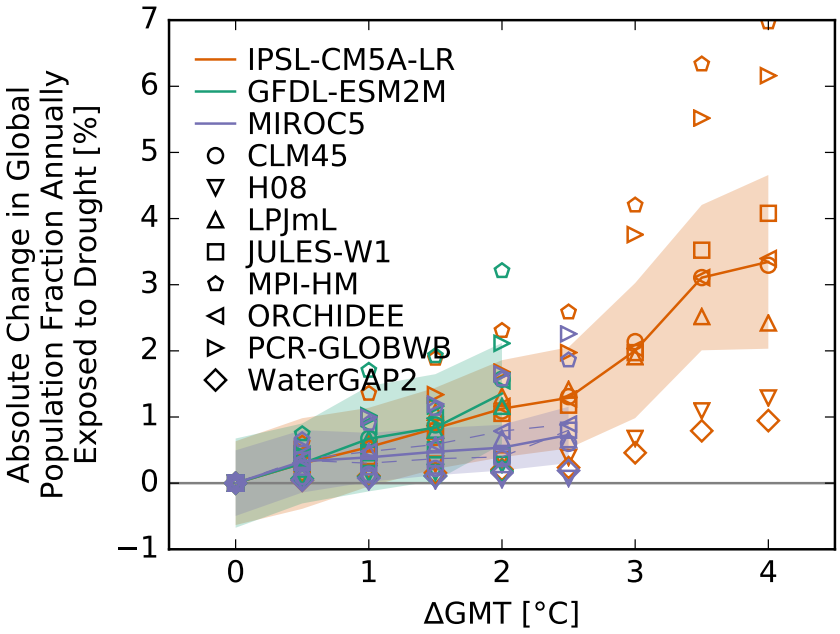

Figure S39: **Pure effect of climate change on global population fraction annually exposed to drought.** Absolute change in global population fraction annually exposed to drought at different levels of global mean temperature (GMT) change relative to the long-term preindustrial mean GMT as simulated by different impact models (symbols) driven by different climate models (colors). Symbols indicate the climate model-impact model combination-specific multi-year mean change caused by global warming (these are identical to the red solid lines in Panel D of Figures S251 … S272). Symbols connected by dashed lines represent emulated multi-year mean changes. Solid lines are the medians over all impact models per climate model. Shaded areas represent the multi-impact model median ±1 standard deviation range of the interannual variability of the global population fraction annually exposed to drought.

analysis.

It is also worth mentioning that the exposure to this drought calculation does not take into account vulnerability, i.e. how much water one would need to accommodate its daily needs (27). This, being a relative threshold on a specific hydrological condition, does not consider the absolute water availability. Therefore, exposure to drought should not be confused with exposure to water scarcity (water-demand versus water-supply).

7.3 Land area affected and number of people exposed at the national scale

Figure S41 shows absolute changes in the national land area affected by as well as the national population exposed to droughts. For most countries of the world, the occurrence of as well as the exposure to droughts are projected to increase with global warming. A decline in the national land area affected is only simulated for Russia and parts of northern Europe. The largest changes are projected for South America, North Africa, South Europe, the Middle East and China. These patterns do not agree well with those found in other studies (10; 46), yet comparisons are difficult due to the different drought indicators used and because drought modelling uncertainty is so large (see Figs. S37 and S39).

The largest relative changes in drought occurrences (Fig. S42) are projected for Latin America, Southern Europe, the Middle East, Africa and Australia.

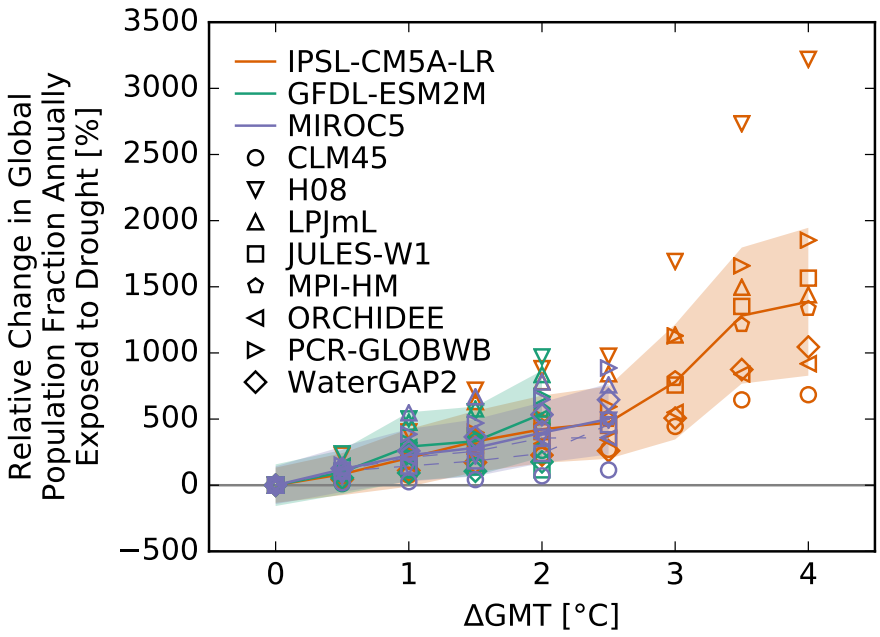

Figure S40: **Pure effect of climate change on global population fraction annually exposed to drought.** Same as Figure S39 but for the relative change in global population fraction annually exposed to drought.

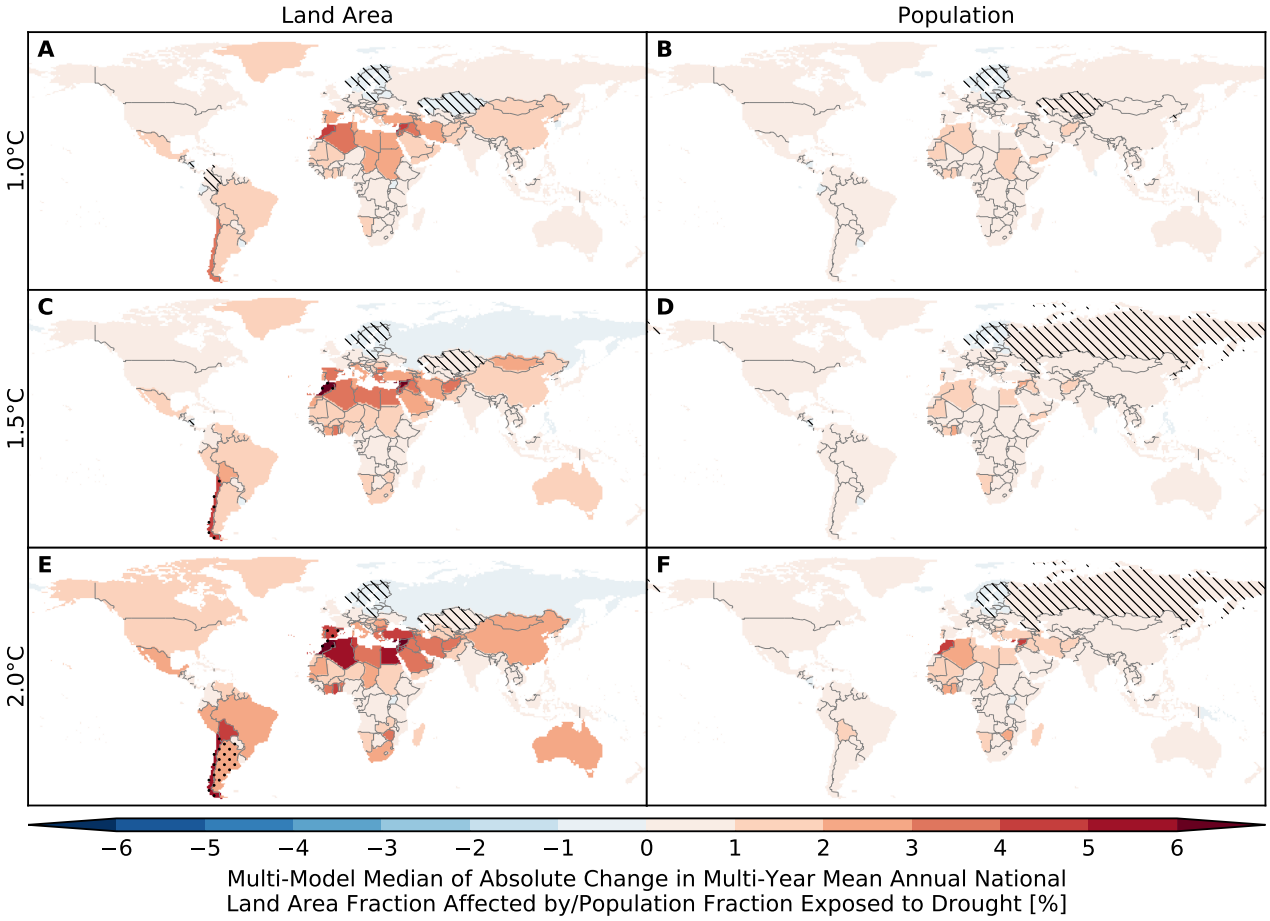

Figure S41: **Pure effect of climate change on annual national land area fraction affected by and population fraction exposed to drought.** Colors indicate multi-model median absolute changes in multi-year mean annual national (A, C, E) land area fraction affected by and (B, D, F) population fraction exposed to drought at (A, B) 1 °C, (C, D) 1.5 °C and (E, F) 2 °C global warming. Stippling indicates that at least 80% of all model combinations agree on an increase or decrease that is larger than 2σ of the preindustrial interannual variability. Hatching indicates that at least 80% of all model combinations agree that the change is smaller than 1σ of the preindustrial interannual variability. The climate model-impact model combination-specific results are shown in Figures S273 … S315.

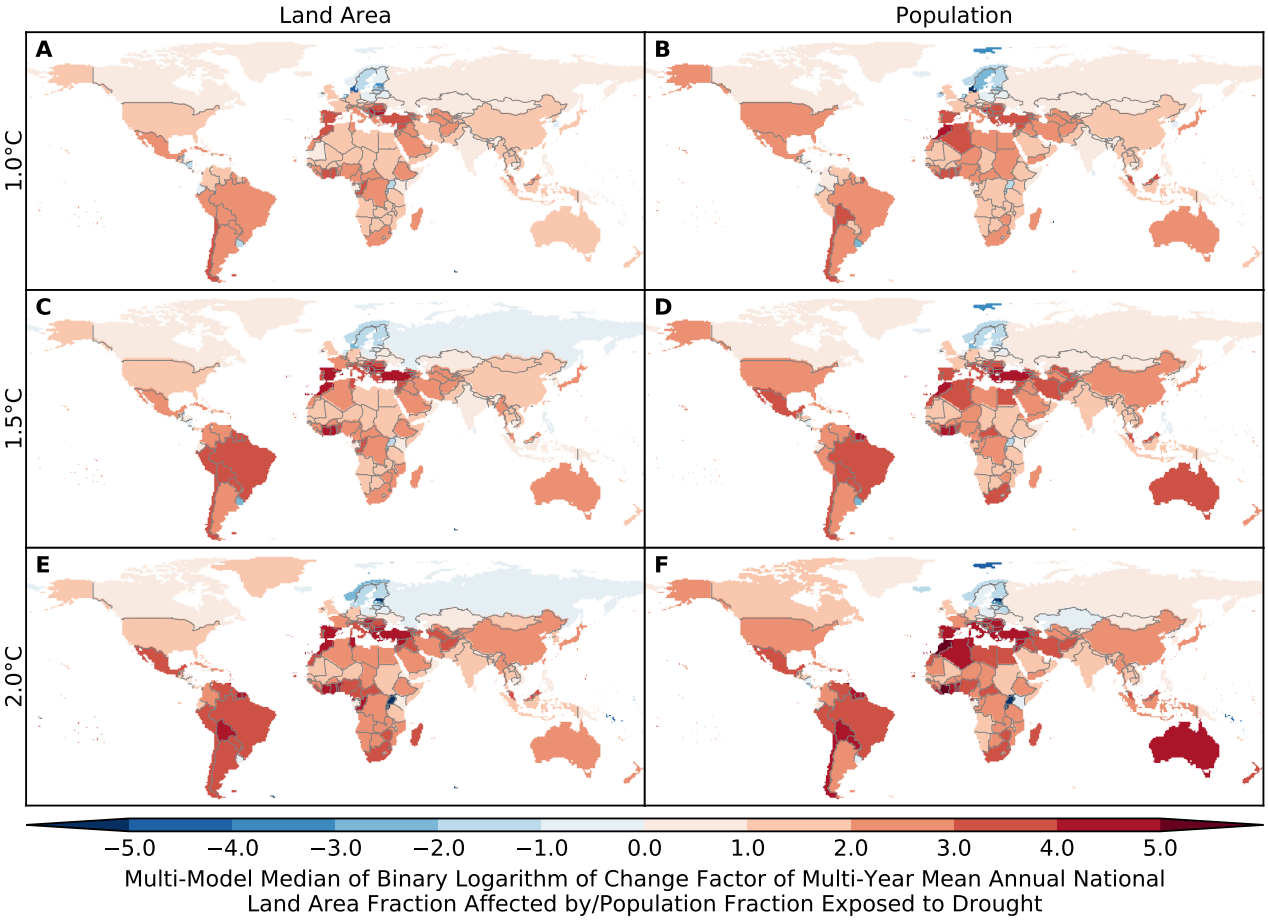

Figure S42: **Pure effect of climate change on annual national land area fraction affected by and population fraction exposed to drought.** Same as Figure S41 but for relative changes expressed in terms of binary logarithms of change factors, i.e. −2, −1, 0, 1, 2 means that the new value is 1/4, 1/2, 1, 2, 4 times the old value, which is equivalent to a relative change by −75 %, −50 %, 0 %, +100 %, +300 %, respectively. White indicates undefined relative changes due to division by zero. The climate model-impact model combination-specific results are shown in Figures S274 … S316.

8 Calculation of land area affected by and number of people exposed to heatwaves

8.1 Land area affected

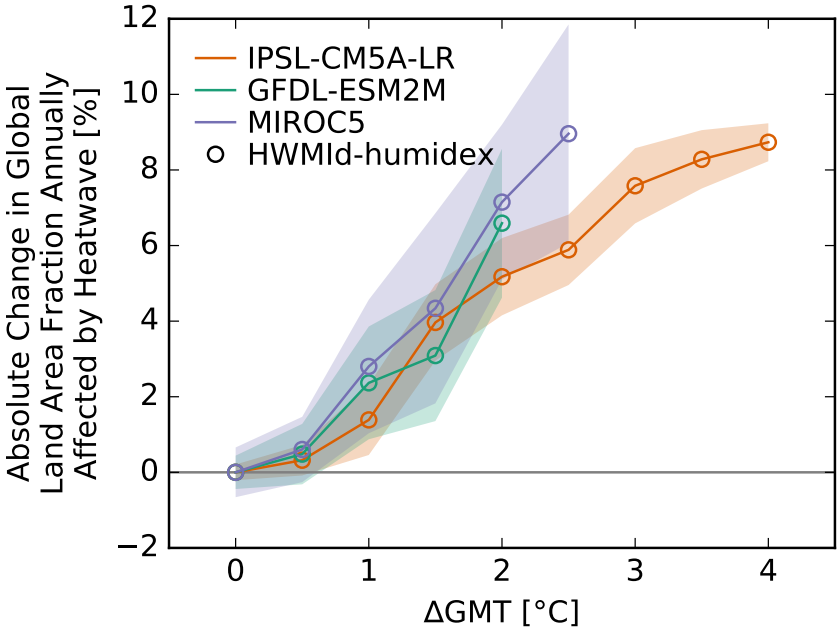

Figure S43: **Pure effect of climate change on global land area fraction annually affected by heatwaves.** Absolute change in global land area fraction annually affected by heatwaves at different levels of global mean temperature (GMT) change relative to the long-term preindustrial mean GMT as simulated by different impact models (symbols) driven by different climate models (colors). Symbols indicate the climate model-impact model combination-specific multi-year mean change caused by global warming (these are identical to the red solid lines in Panel D of Figures S317 … S319). Symbols connected by dashed lines represent emulated multi-year mean changes. Solid lines are the medians over all impact models per climate model. Shaded areas represent the multi-impact model median ±1 standard deviation range of the interannual variability of the global land area fraction annually affected by heatwaves.

Heatwaves are defined based on GCM output of daily mean relative humidity and daily mean and maximum temperature. A grid cell is considered to be affected by a heatwave in a given year if (i) the Heat Wave Magnitude Index daily (HWMId, 67; 68) of that year exceeds the 97.5th percentile of the HWMId distribution under preindustrial climate conditions of that grid cell, and if (ii) the humidex exceeds 45 on all days of heatwave period corresponding to the HWMId. If both criteria are fulfilled then the area fraction affected by heatwave of the grid cell in that year is set to one, otherwise it is set to zero.

Our heatwave definition combines a relative criterion, which assesses the magnitude of a heatwave relative to magnitudes that are normal under preindustrial climate conditions, with an absolute criterion that is to prevent us from labeling a period that would be considered exceptionally warm under preindustrial climate conditions as a heatwave even though the period is not hot enough in an absolute sense to have a negative impact on human health. In the following we describe how HWMId and humidex are defined and computed here.

The HWMId is defined as the maximum magnitude of all hot periods occurring in a year, where a hot period is a period of at least 3 consecutive days with daily maximum temperature exceeding a threshold value T_{pi90} which is defined as the 90th percentile of daily maximum temperatures under preindustrial climate conditions, centered on a 31-day window. The magnitude of each hot period in a year is the sum of the daily magnitudes on the consecutive days composing the hot period, with daily magnitude calculated

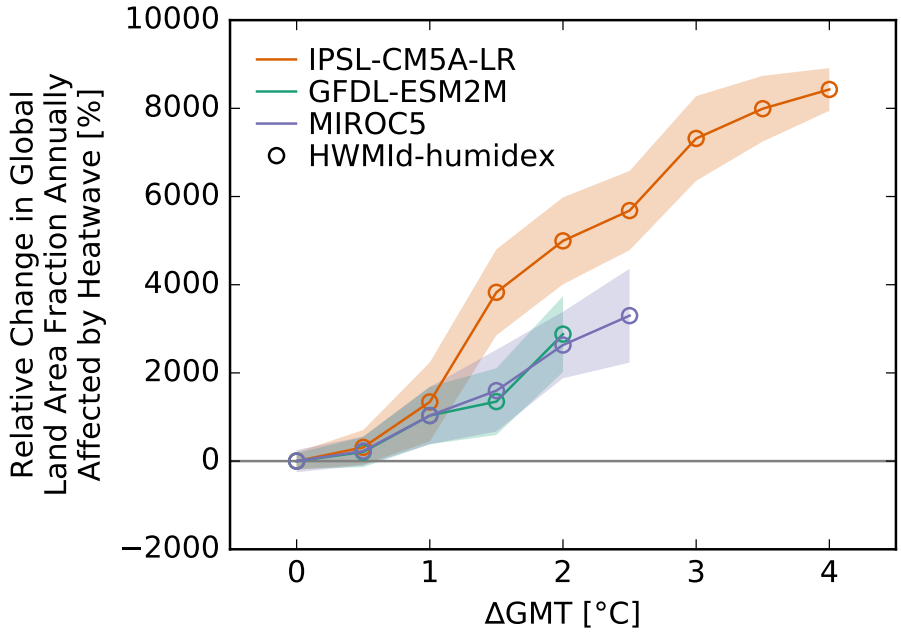

Figure S44: **Pure effect of climate change on global land area fraction annually affected by heatwaves.** Same as Figure S43 but for the relative change in global land area fraction annually affected by heatwaves.

according to $M_{\mathrm{d}}(T_{\mathrm{d}}) = 0$ if $T_{\mathrm{d}} \leq T_{\mathrm{pi25}}$ else $(T_{\mathrm{d}} - T_{\mathrm{pi25}})/(T_{\mathrm{pi75}} - T_{\mathrm{pi25}})$ where T_{d} is the daily maximum temperature on day d of the hot period, and T_{pi25} and T_{pi75} are the 25th and 75th percentile, respectively, of the annual maximum of the daily maximum temperature under preindustrial climate conditions. In order to estimate T_{pi90}, T_{pi25} and T_{pi75}, we use more than 400 years of daily maximum temperature data of 0.5° spatial resolution representing preindustrial climate conditions as available from the ISIMIP2b climate input data set. Based on these more than 400 years of temperature data we then derive $M_{\mathrm{pi97.5}}$, the 97.5th percentile of the HWMId distribution under preindustrial climate conditions.

The humidex (49) was developed to capture the experienced effects of hot weather on the human body by combining temperature and relative humidity via the dew point to an effective temperature:

$$\text{Humidex} = T_{\mathrm{max}} + 0.5555\,[6.11\,\mathrm{e}^{5417.7530\,(\frac{1}{273.16} - \frac{1}{273.15+T_{\mathrm{dew}}})} - 10]\,.$$

We calculate the humidex at the time of maximum daily temperature using the above formula, the daily maximum temperature for T_{max}, and the daily mean temperature and relative humidity to approximately compute the dew point temperature T_{dew} at the time of maximum daily temperature, exploiting that the dew point does usually not vary much over the course of a day (62; 72). The Canadian Center for Occupational Health and Safety links the humidex to human stress as follows (18).

20–29	comfortable
30–39	some discomfort
40–45	great discomfort, avoid exertion
above 45	dangerous, heat stroke possible

The resulting probabilities of occurrence are very low under preindustrial climate conditions, with less than 1 % of the global land area being affected by heatwaves annually. This area fraction rises to about 7 % at 2 °C of global warming, and to about 10 % at 4 °C of global warming. The emissions scenario-dependence of the relationship between global mean temperature change and global land area affected by heatwave is low as are differences between GCMs.

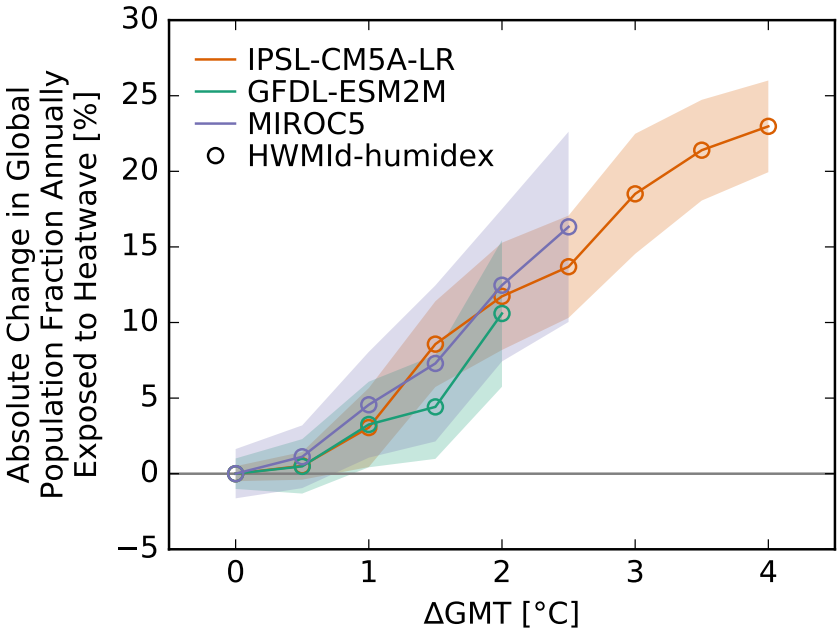

Figure S45: **Pure effect of climate change on global population fraction annually exposed to heatwaves.** Absolute change in global population fraction annually exposed to heatwaves at different levels of global mean temperature (GMT) change relative to the long-term preindustrial mean GMT as simulated by different impact models (symbols) driven by different climate models (colors). Symbols indicate the climate model-impact model combination-specific multi-year mean change caused by global warming (these are identical to the red solid lines in Panel D of Figures S320 … S322). Symbols connected by dashed lines represent emulated multi-year mean changes. Solid lines are the medians over all impact models per climate model. Shaded areas represent the multi-impact model median ±1 standard deviation range of the interannual variability of the global population fraction annually exposed to heatwaves.

8.2 Number of people exposed

It is assumed that if a grid cell is struck by a heatwave, then all people living in that grid cell are affected by that heatwave. Therefore, the population fraction exposed to heatwave is set equal to the area fraction affected by heatwave at the 0.5° grid level. Less than 1 % of the global population is exposed to heatwaves annually under preindustrial climate conditions. This fraction rises to about 12 % at 2 °C of global warming, and to 24 % at 4 °C of global warming. Interestingly, the global population fraction exposed to heatwaves increases with about twice as large a rate as the global area fraction affected by heatwaves. This is because many people currently live (and arguably will continue to live) in those areas that are projected to be most increasingly struck by heatwaves in the future, in particular West, Central and East Africa as well as South and Southeast Asia (see Fig. S47). The emissions scenario-dependence of the relationship between global mean temperature change and heatwave exposure of the global population is low as are differences between GCMs.

8.3 Land area affected and number of people exposed at the national scale

Figures S47 and S48 show how the affected national land area and exposed national population change under global warming, both in terms of absolute changes (Figure S47) and relative changes (Figure S48). As expected global warming increases the area affected by and the number of people exposed to heatwaves in practically all parts of the world. The spatial patterns of increases in heatwave occurrence do not differ much between GCMs (Figures S317 … S319). For many countries, the increases are large relative to preindustrial interannual variability. We find the strongest increases in the tropical regions, in particular in Central America and northern South America, large parts of Africa, around the Persian Gulf,

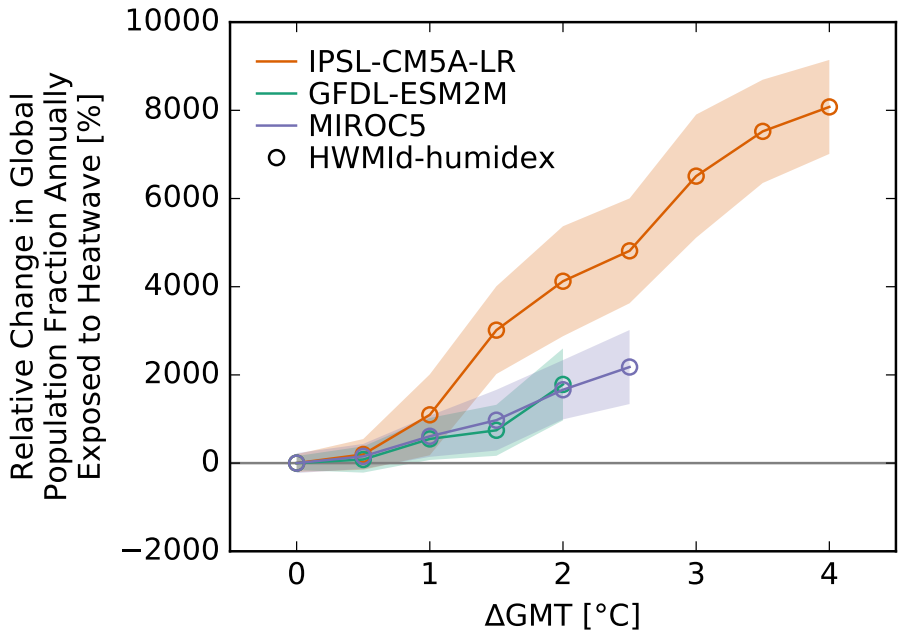

Figure S46: **Pure effect of climate change on global population fraction annually exposed to heatwaves.** Same as Figure S45 but for the relative change in global population fraction annually exposed to heatwaves.

and in South and Southeast Asia. These regions are largely consistent with the areas projected to witness dangerous wet-bulb (globe) temperature increases in response to global warming (77; 11). Figure S48 demonstrates drastic relative changes in both, the affected land area and the number of exposed people. At 2 °C global warming, a rather large number of countries experience increases by a factor of 30 or more.

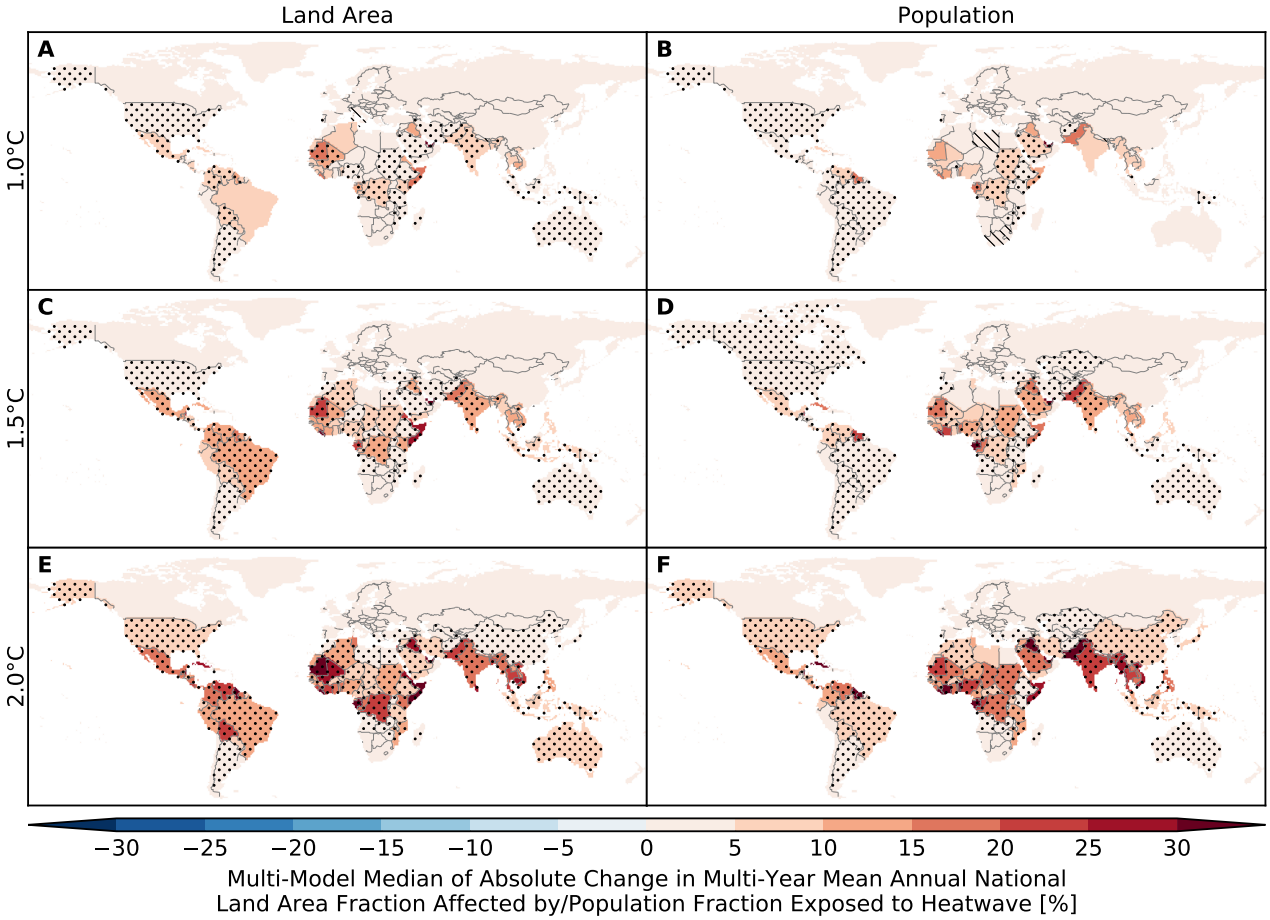

Figure S47: **Pure effect of climate change on annual national land area fraction affected by and population fraction exposed to heatwave.** Colors indicate multi-model median absolute changes in multi-year mean annual national (A, C, E) land area fraction affected by and (B, D, F) population fraction exposed to heatwave at (A, B) 1 °C, (C, D) 1.5 °C and (E, F) 2 °C global warming. Stippling indicates that at least 80% of all model combinations agree on an increase or decrease that is larger than 2σ of the preindustrial interannual variability. Hatching indicates that at least 80% of all model combinations agree that the change is smaller than 1σ of the preindustrial interannual variability. The climate model-impact model combination-specific results are shown in Figures S323 … S327.

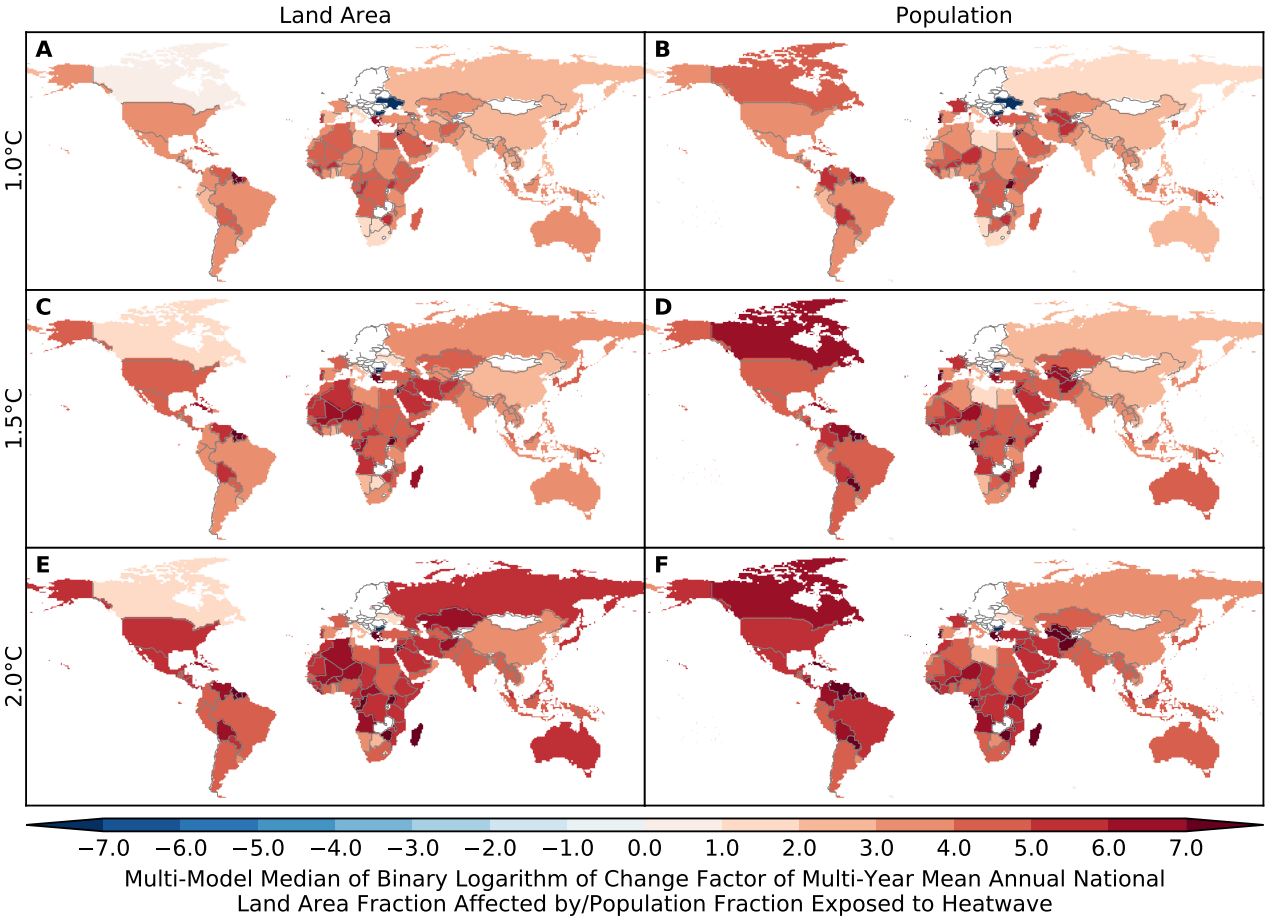

Figure S48: **Pure effect of climate change on annual national land area fraction affected by and population fraction exposed to heatwave.** Same as Figure S47 but for relative changes expressed in terms of binary logarithms of change factors, i.e. −2, −1, 0, 1, 2 means that the new value is 1/4, 1/2, 1, 2, 4 times the old value, which is equivalent to a relative change by −75 %, −50 %, 0 %, +100 %, +300 %, respectively. White indicates undefined relative changes due to division by zero. The climate model-impact model combination-specific results are shown in Figures S324 … S328.

9 Model specific results

9.1 River floods

Land area affected

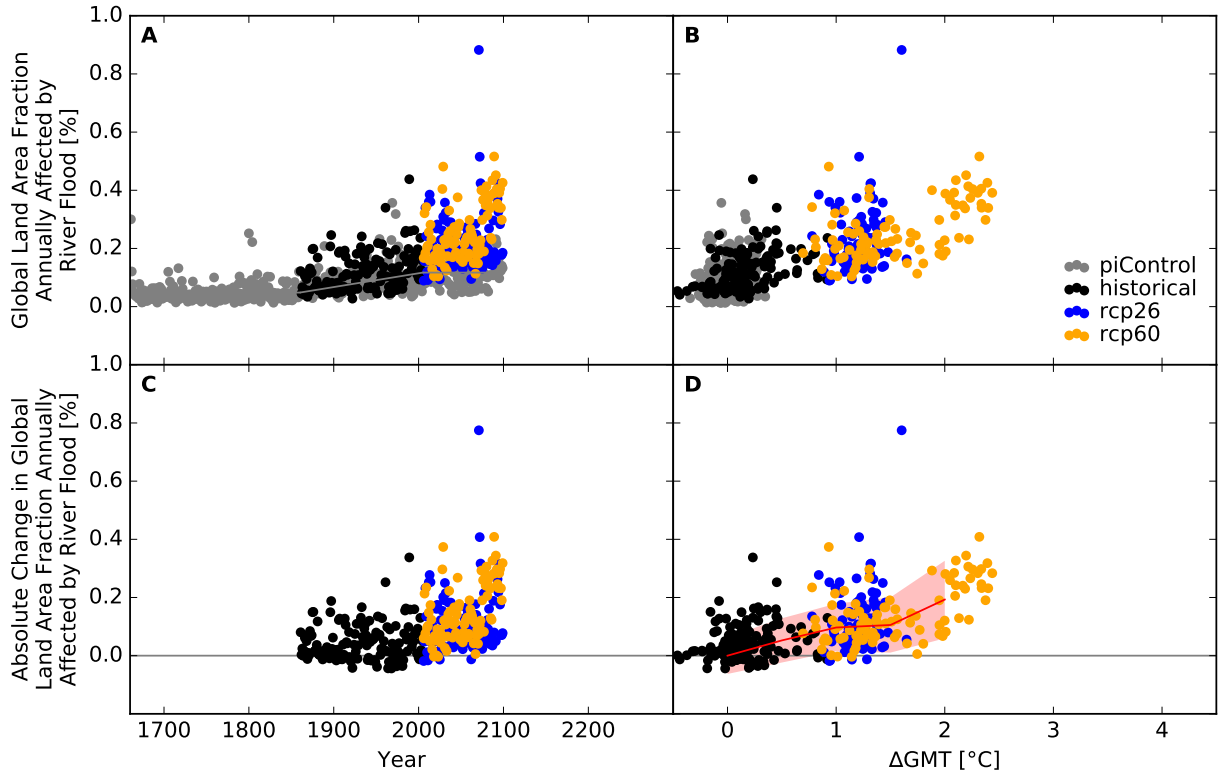

Figure S49: **Derivation of the pure effect of climate change on the global land area fraction annually affected by river flood (GFDL-ESM2M + CLM45).** Panel A: Time series of annual global land area fraction affected (AFA) by river flood for preindustrial climate (grey dots), historical climate (black dots), climate projections for RCP2.6 (blue dots), and RCP6.0 (orange dots). In all simulations, socioeconomic conditions are varied according to the historically observed development between 1860 and 2005, and held fixed at 1860 conditions before 1860 and at 2005 conditions after 2005. The horizontal gray lines before 1860 and after 2005 represent the multi-year mean global land area fraction annually affected by river flood under preindustrial climate conditions and socioeconomic conditions of 1860 and 2005, respectively. The gray line between 1860 and 2005 is a linear interpolation of these mean values. Panel B: Data shown in Panel A plotted against the associated GCM-specific annual global mean temperature (GMT) change relative to the long-term preindustrial mean GMT. Panel C: Pure effect of climate change on AFA, calculated as the difference between the annual data shown in Panel A and the multi-year mean AFA under preindustrial climate conditions (gray line in Panel A). Panel D: Data shown in Panel C plotted against annual GMT change. The red line represents the mean values of the annual data points per 1 °C-wide GMT change bin, with bins centered at GMT change levels increasing from 0 °C to 4 °C in steps of 0.5 °C. The area shaded in red represents the mean value ±1 standard deviation ranges of the annual data points per GMT change bin.

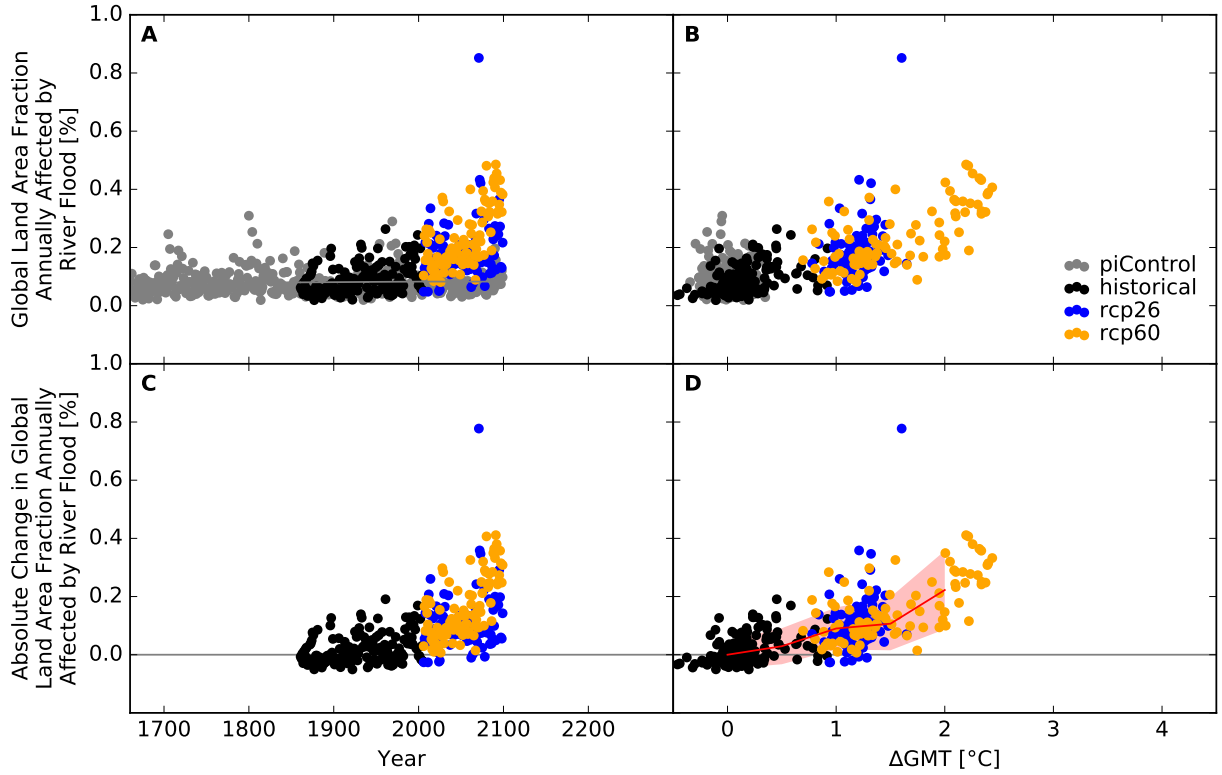

Figure S50: **Derivation of the pure effect of climate change on the global land area fraction annually affected by river flood (GFDL-ESM2M + H08).** Analogous to Figure S49.

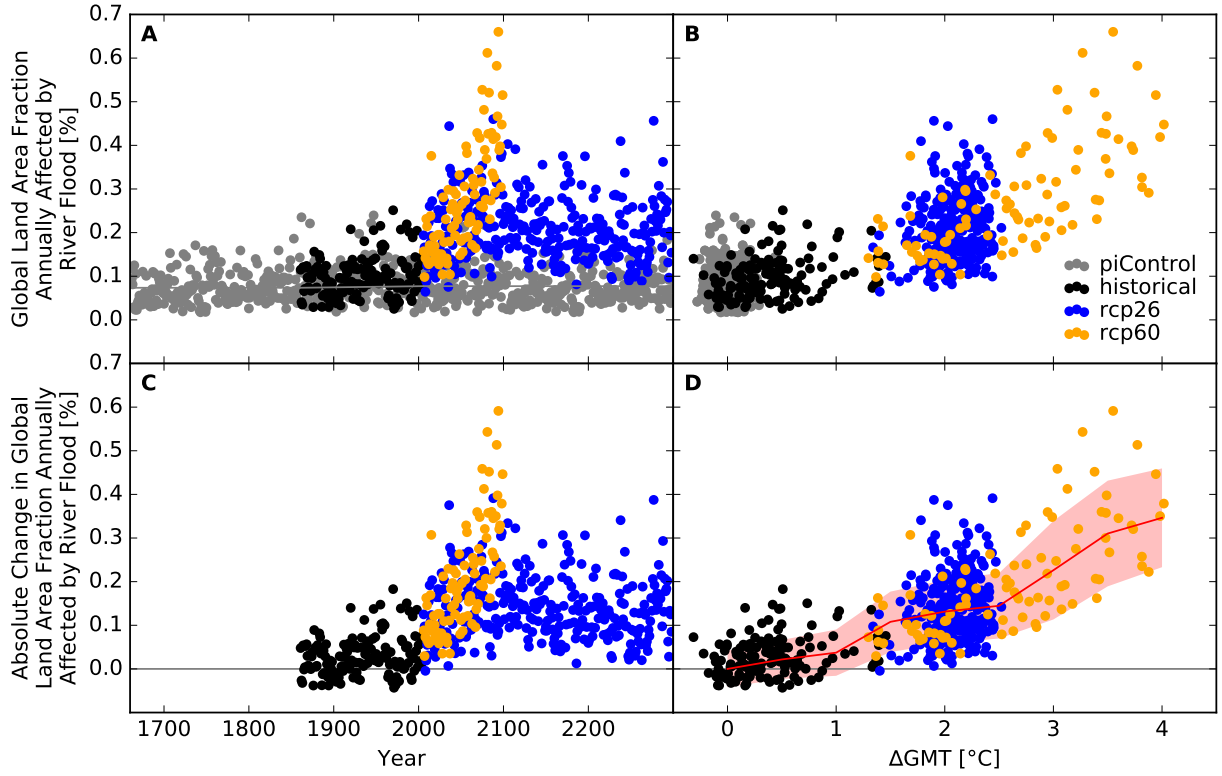

Figure S51: **Derivation of the pure effect of climate change on the global land area fraction annually affected by river flood (IPSL-CM5A-LR + H08).** Analogous to Figure S49.

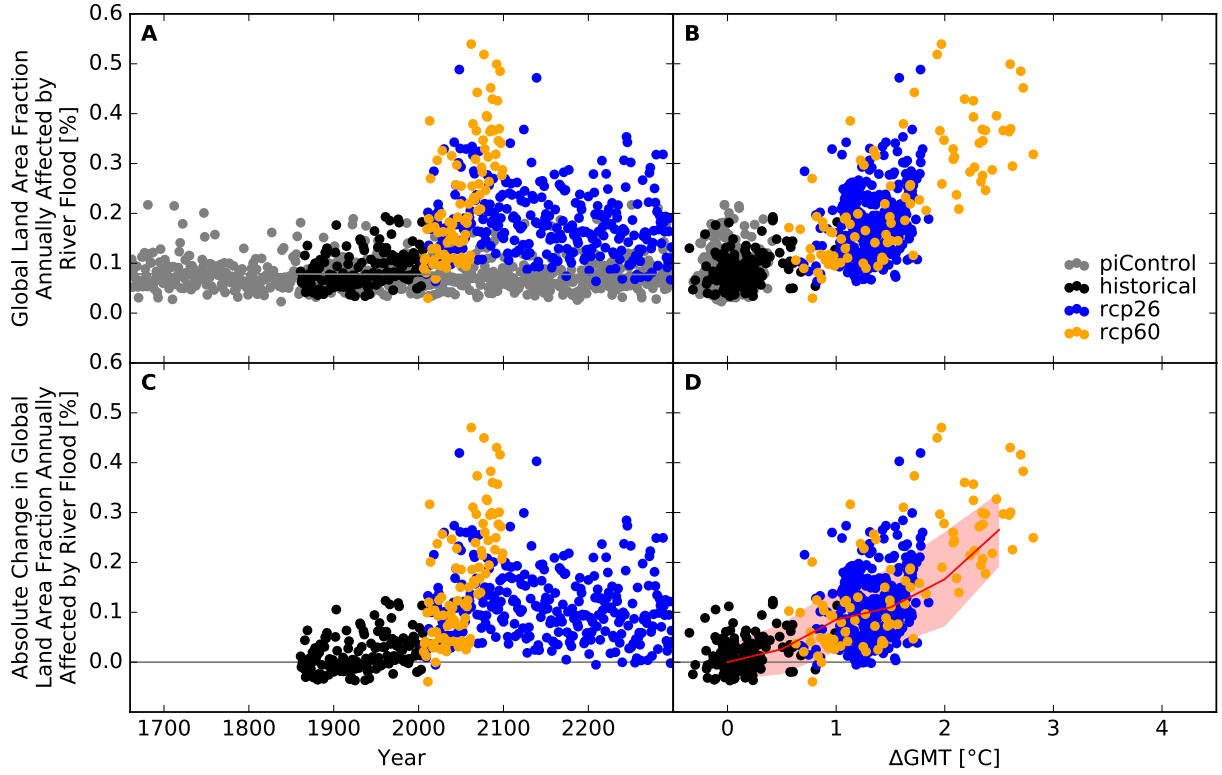

Figure S52: **Derivation of the pure effect of climate change on the global land area fraction annually affected by river flood (MIROC5 + H08).** Analogous to Figure S49.

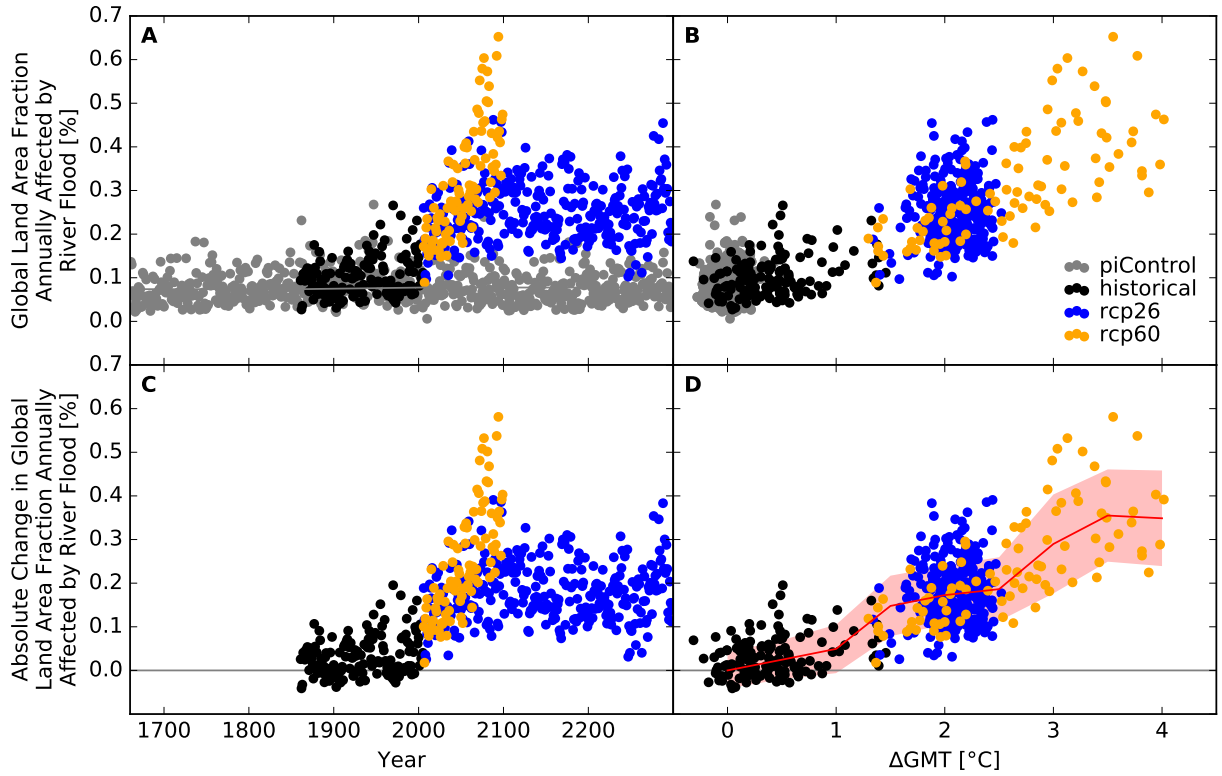

Figure S53: **Derivation of the pure effect of climate change on the global land area fraction annually affected by river flood (IPSL-CM5A-LR + JULES-W1).** Analogous to Figure S49.

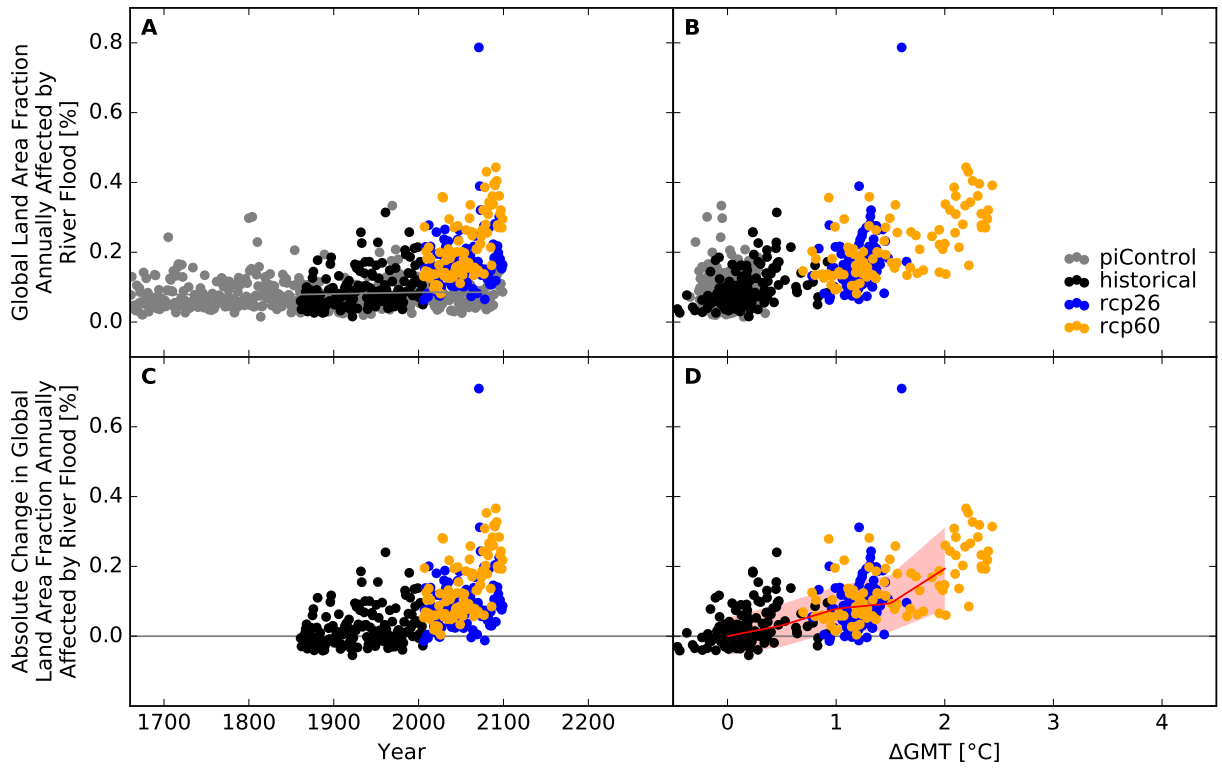

Figure S54: **Derivation of the pure effect of climate change on the global land area fraction annually affected by river flood (GFDL-ESM2M + LPJmL).** Analogous to Figure S49.

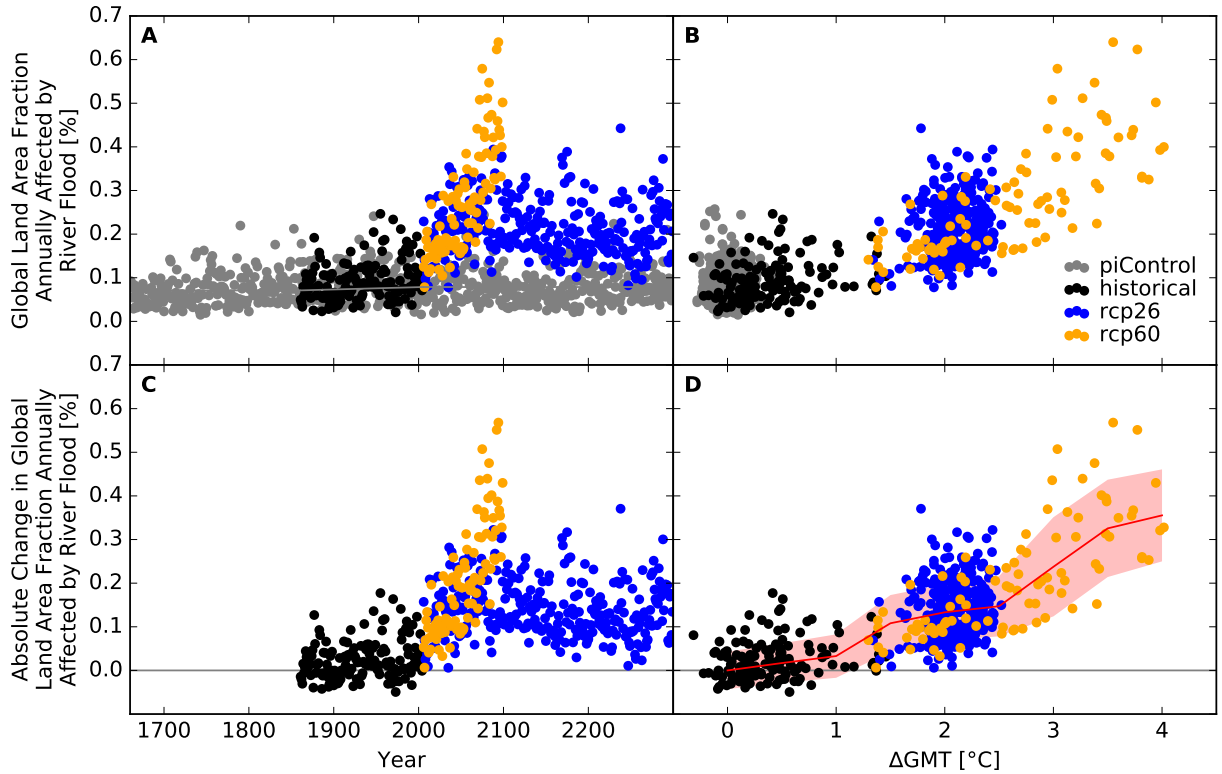

Figure S55: **Derivation of the pure effect of climate change on the global land area fraction annually affected by river flood (IPSL-CM5A-LR + LPJmL).** Analogous to Figure S49.

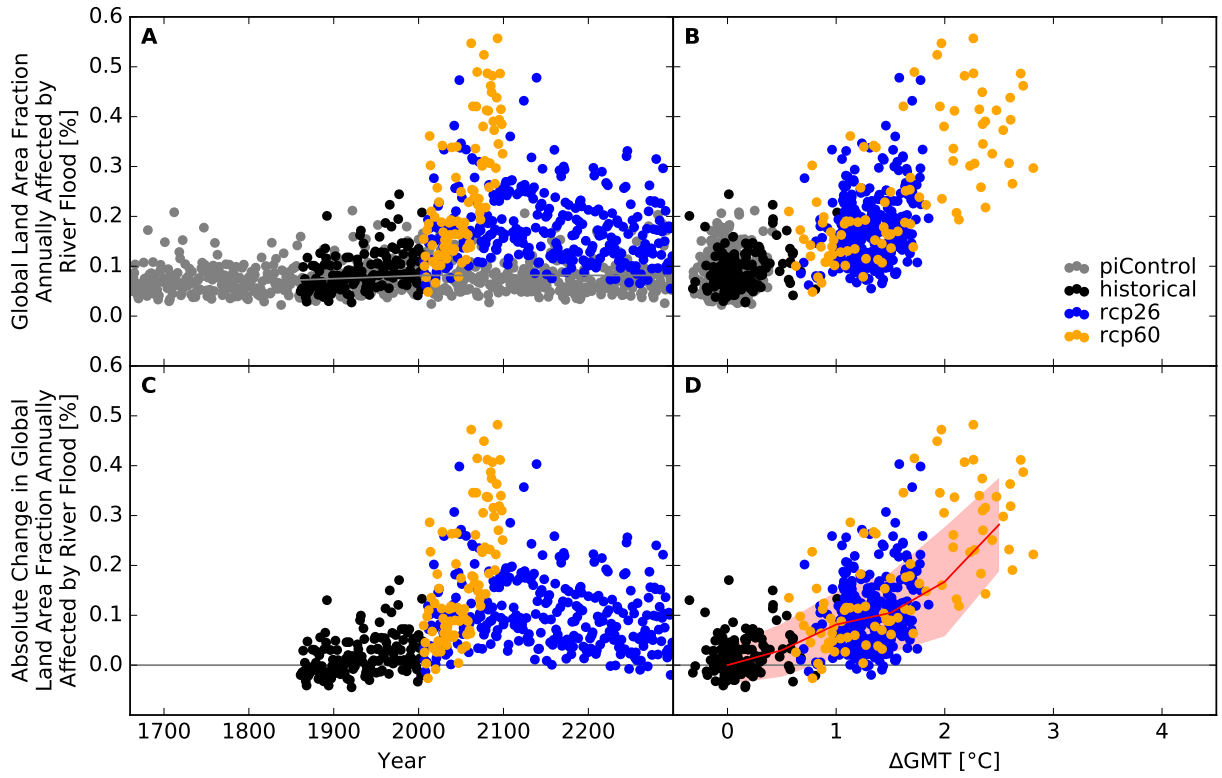

Figure S56: **Derivation of the pure effect of climate change on the global land area fraction annually affected by river flood (MIROC5 + LPJmL).** Analogous to Figure S49.

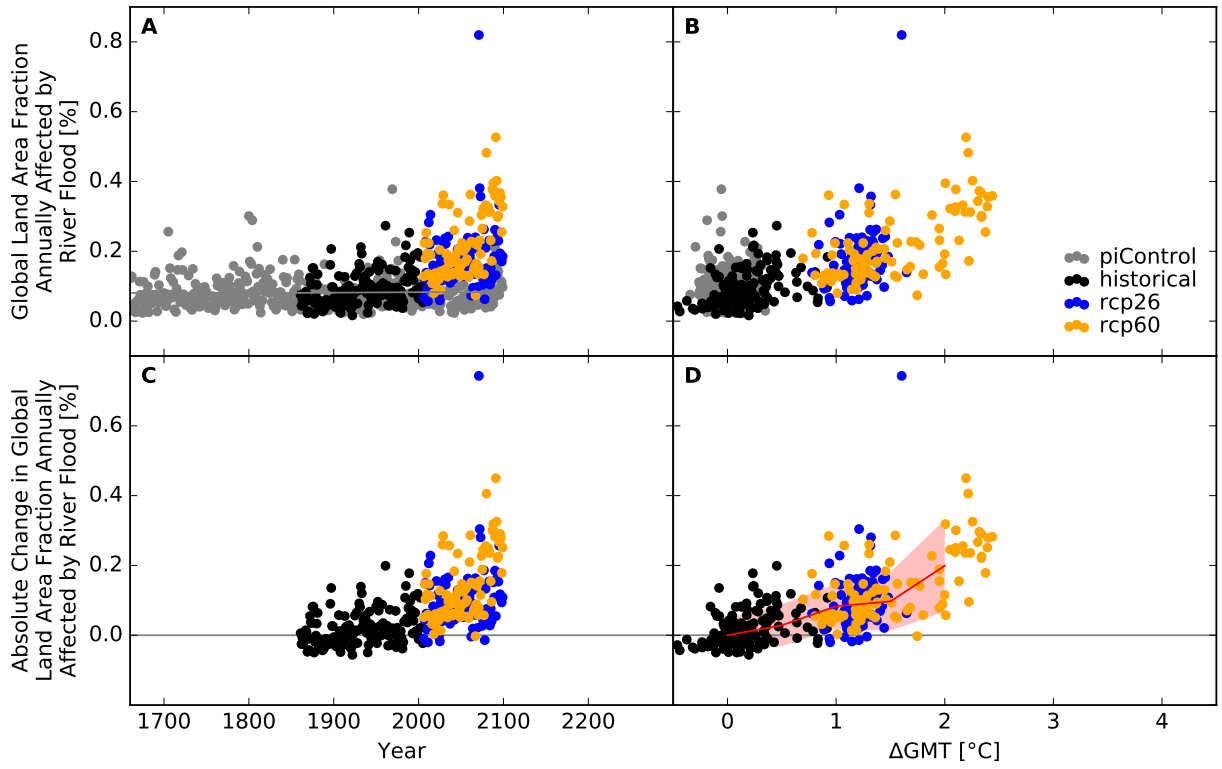

Figure S57: **Derivation of the pure effect of climate change on the global land area fraction annually affected by river flood (GFDL-ESM2M + MPI-HM).** Analogous to Figure S49.

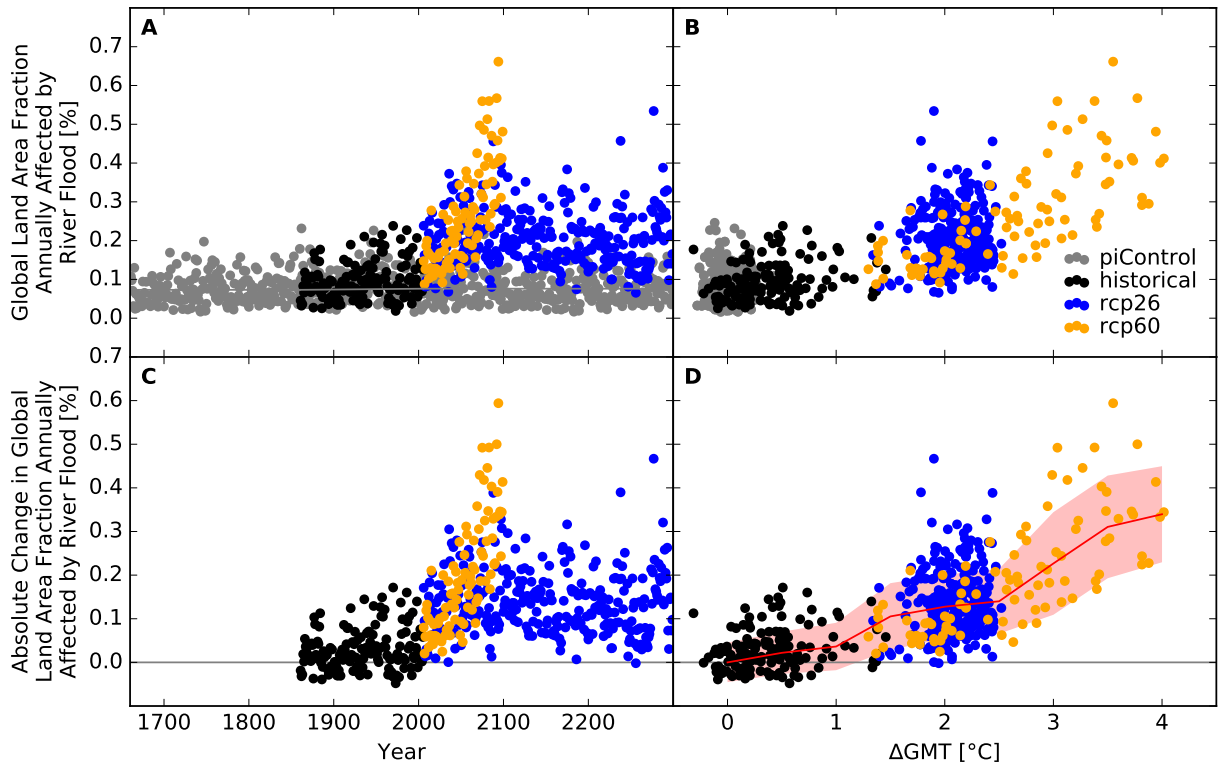

Figure S58: **Derivation of the pure effect of climate change on the global land area fraction annually affected by river flood (IPSL-CM5A-LR + MPI-HM).** Analogous to Figure S49.

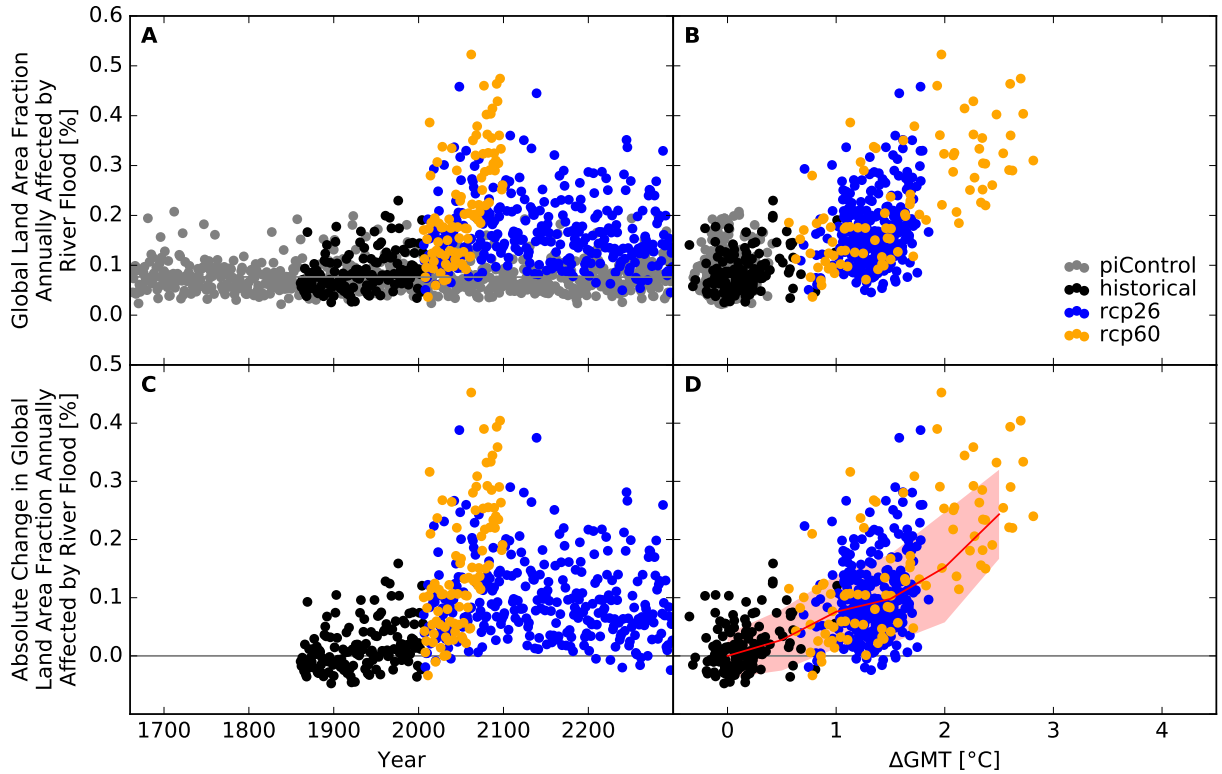

Figure S59: **Derivation of the pure effect of climate change on the global land area fraction annually affected by river flood (MIROC5 + MPI-HM).** Analogous to Figure S49.

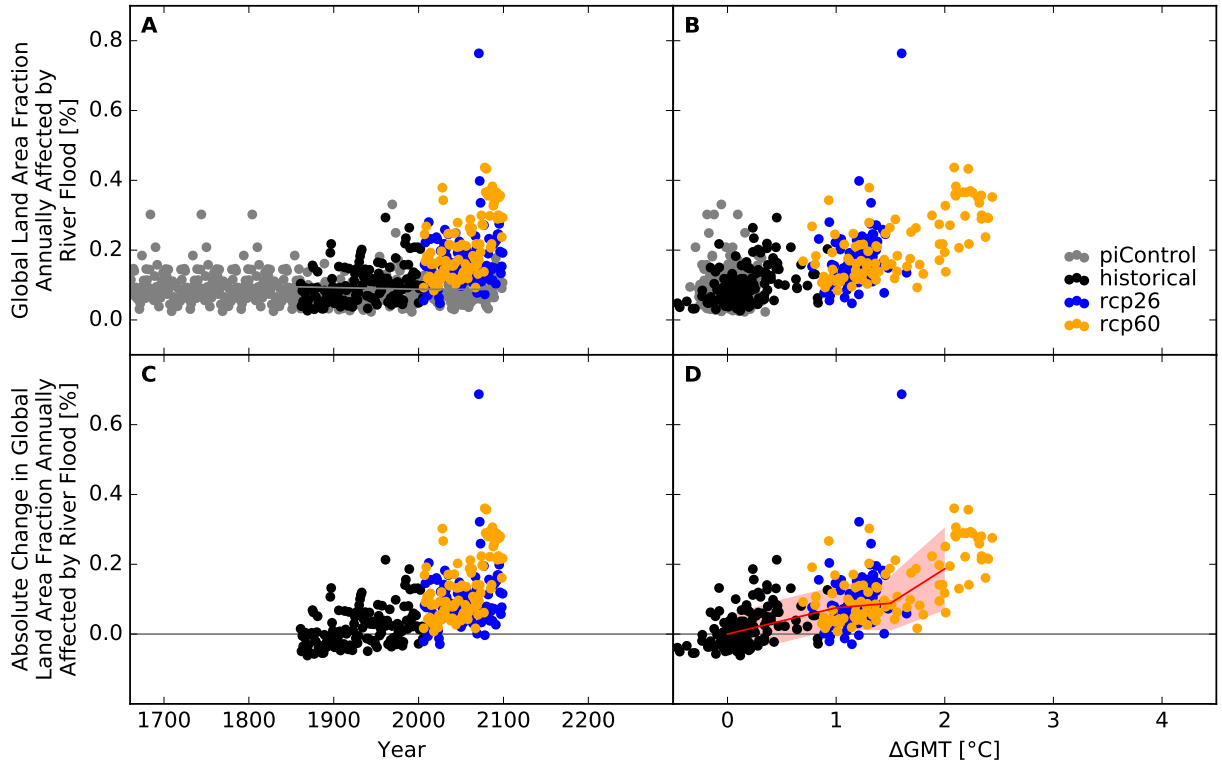

Figure S60: **Derivation of the pure effect of climate change on the global land area fraction annually affected by river flood (GFDL-ESM2M + ORCHIDEE).** Analogous to Figure S49.

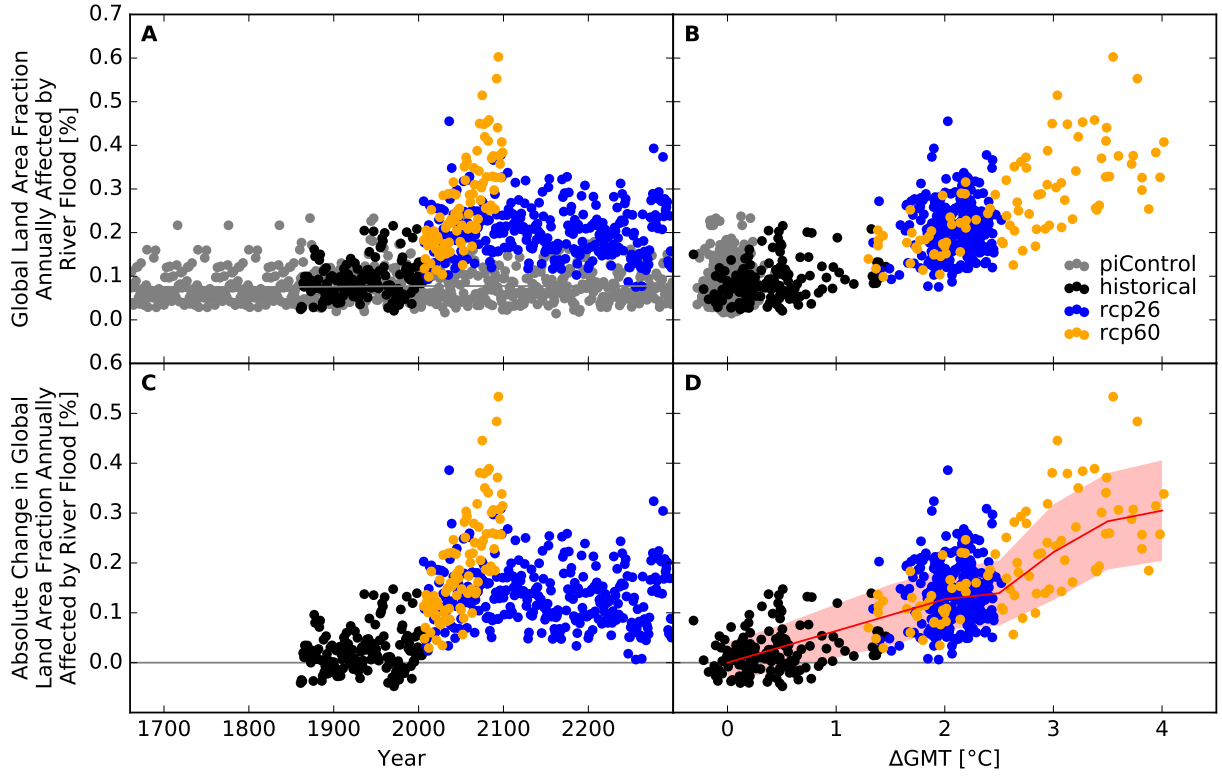

Figure S61: **Derivation of the pure effect of climate change on the global land area fraction annually affected by river flood (IPSL-CM5A-LR + ORCHIDEE).** Analogous to Figure S49.

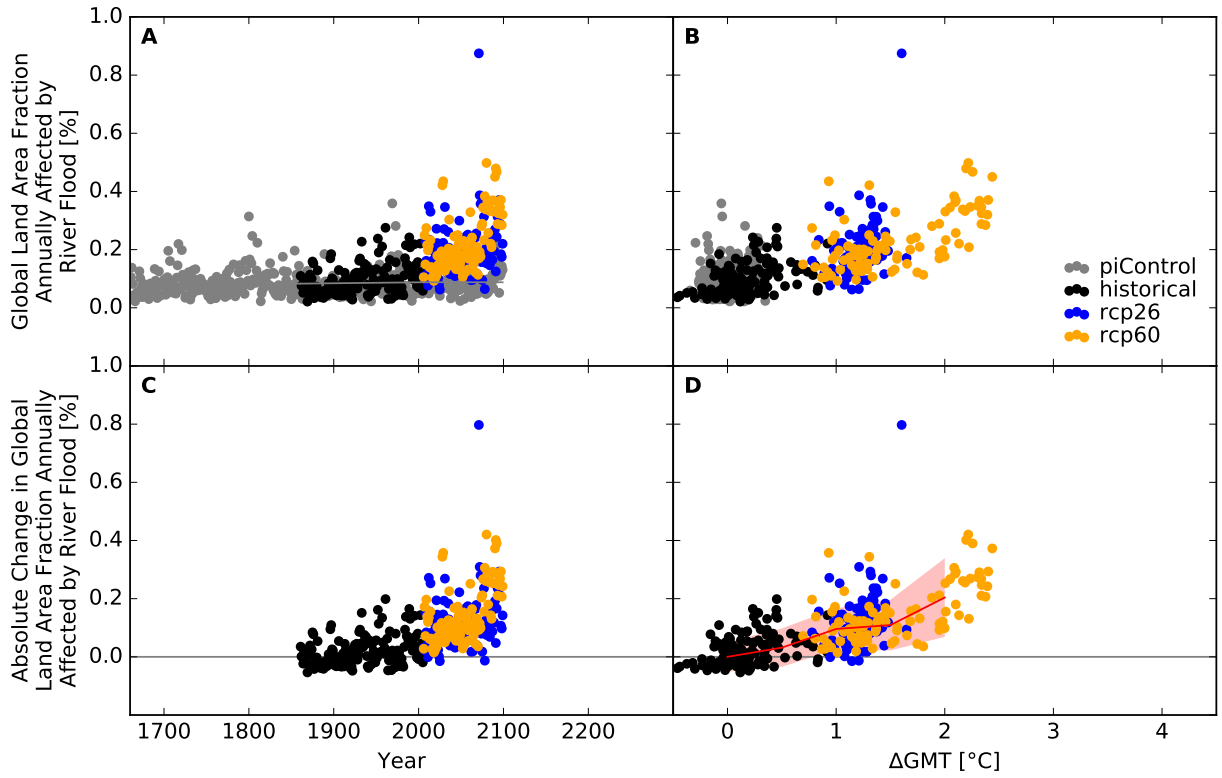

Figure S62: **Derivation of the pure effect of climate change on the global land area fraction annually affected by river flood (GFDL-ESM2M + PCR-GLOBWB).** Analogous to Figure S49.

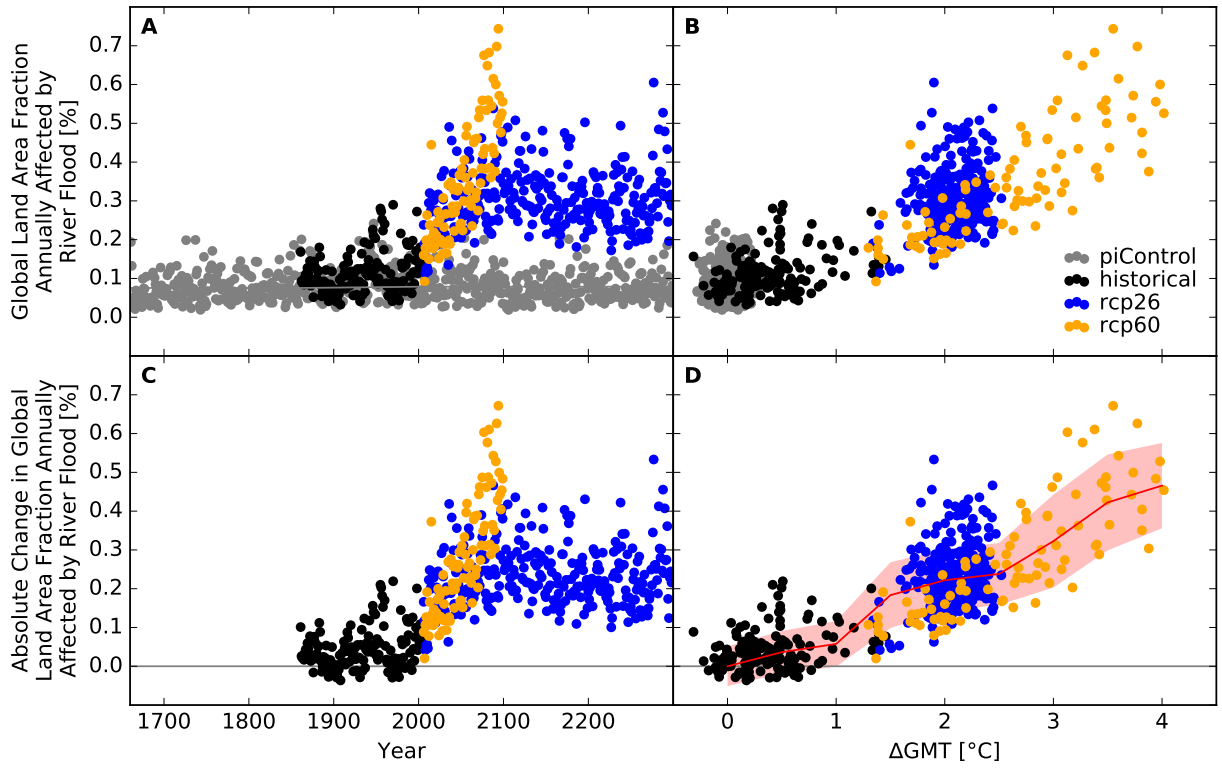

Figure S63: **Derivation of the pure effect of climate change on the global land area fraction annually affected by river flood (IPSL-CM5A-LR + PCR-GLOBWB).** Analogous to Figure S49.

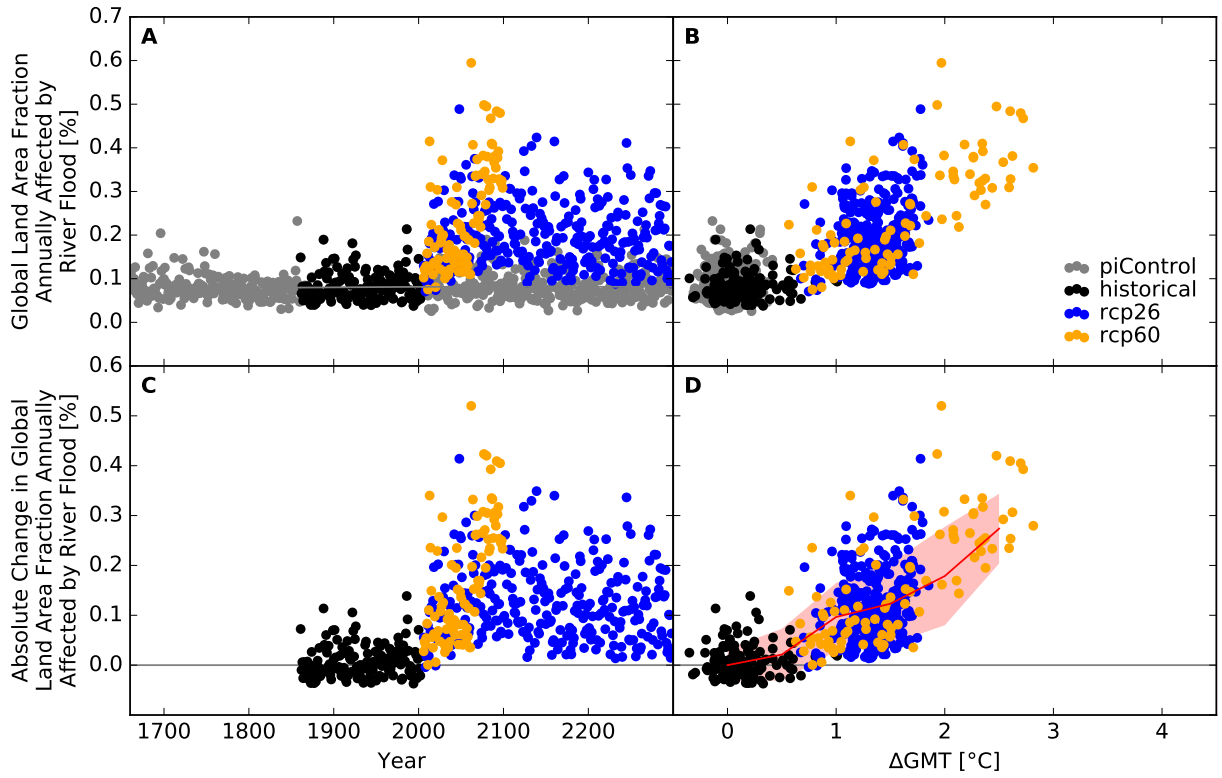

Figure S64: **Derivation of the pure effect of climate change on the global land area fraction annually affected by river flood (MIROC5 + PCR-GLOBWB).** Analogous to Figure S49.

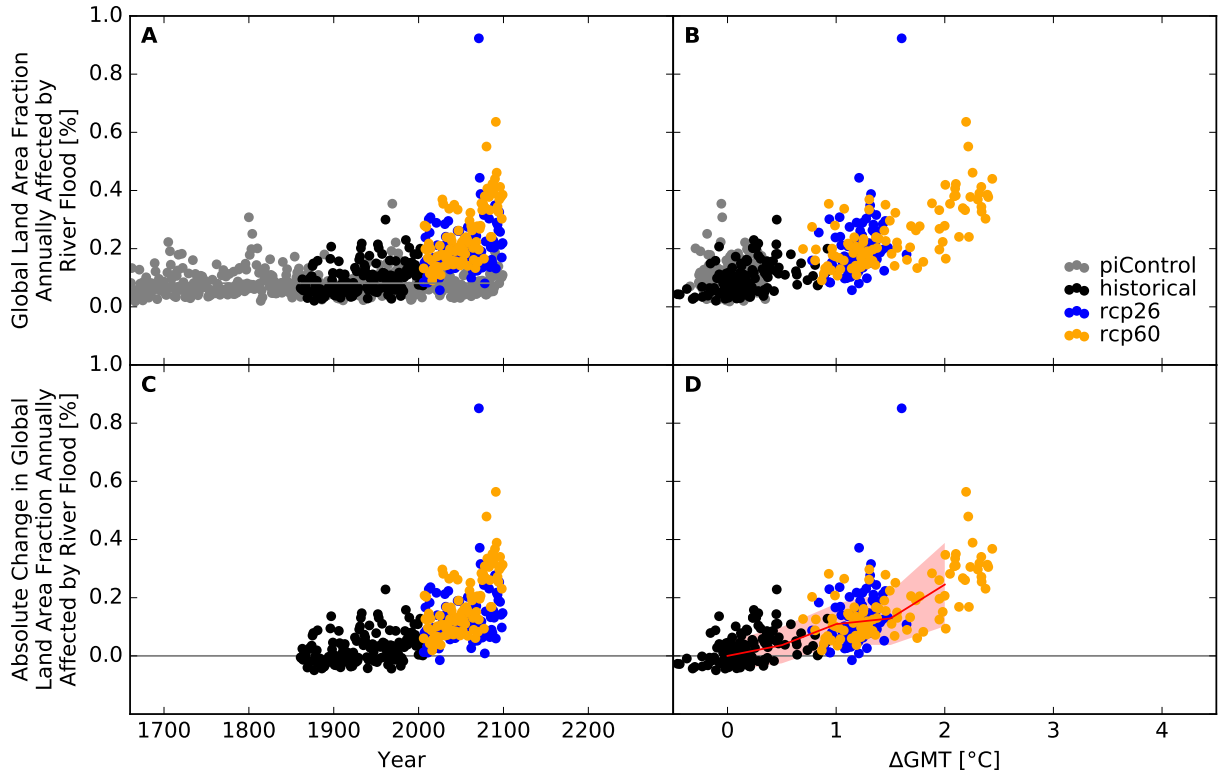

Figure S65: **Derivation of the pure effect of climate change on the global land area fraction annually affected by river flood (GFDL-ESM2M + WaterGAP2).** Analogous to Figure S49.

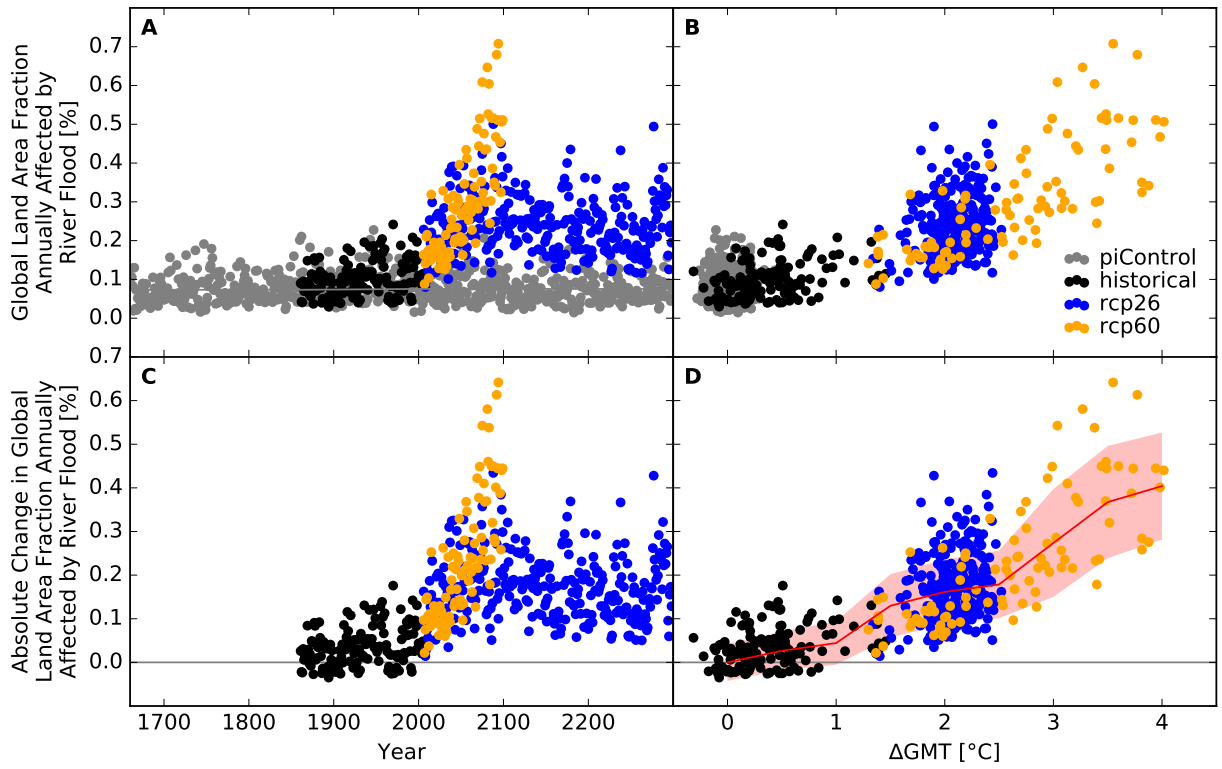

Figure S66: **Derivation of the pure effect of climate change on the global land area fraction annually affected by river flood (IPSL-CM5A-LR + WaterGAP2).** Analogous to Figure S49.

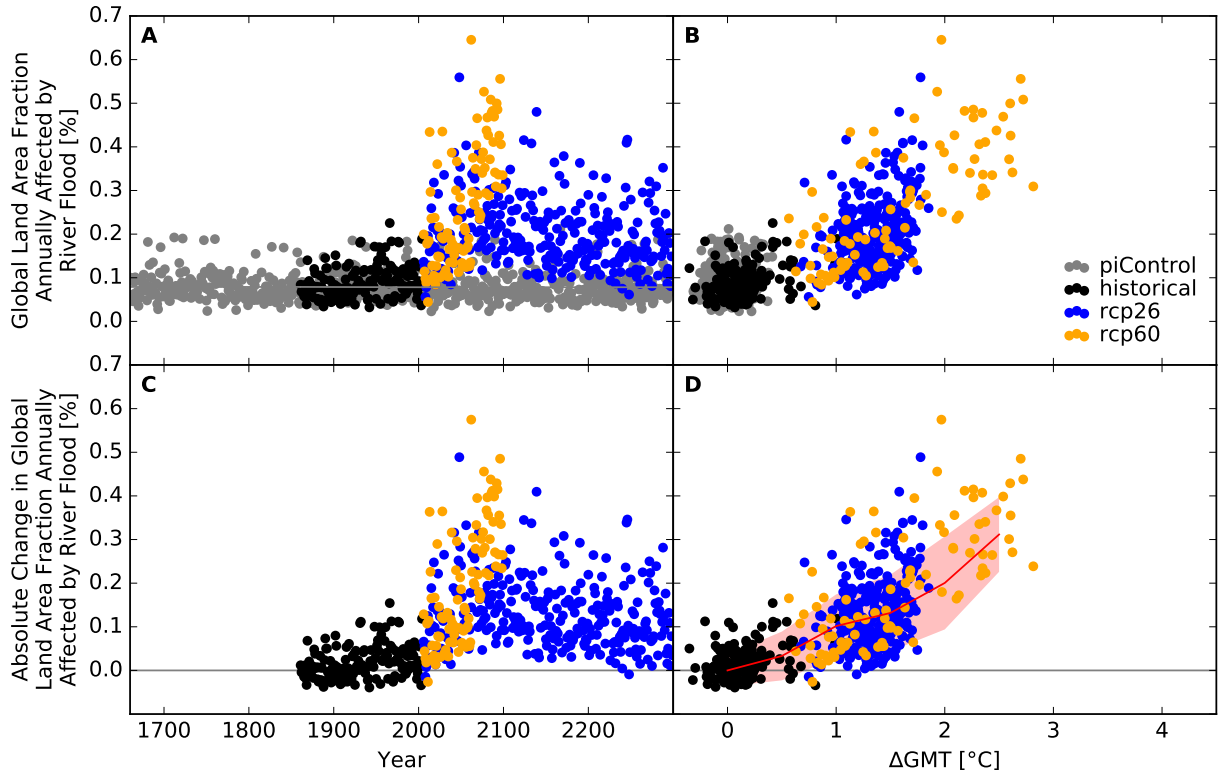

Figure S67: **Derivation of the pure effect of climate change on the global land area fraction annually affected by river flood (MIROC5 + WaterGAP2).** Analogous to Figure S49.

Number of people exposed

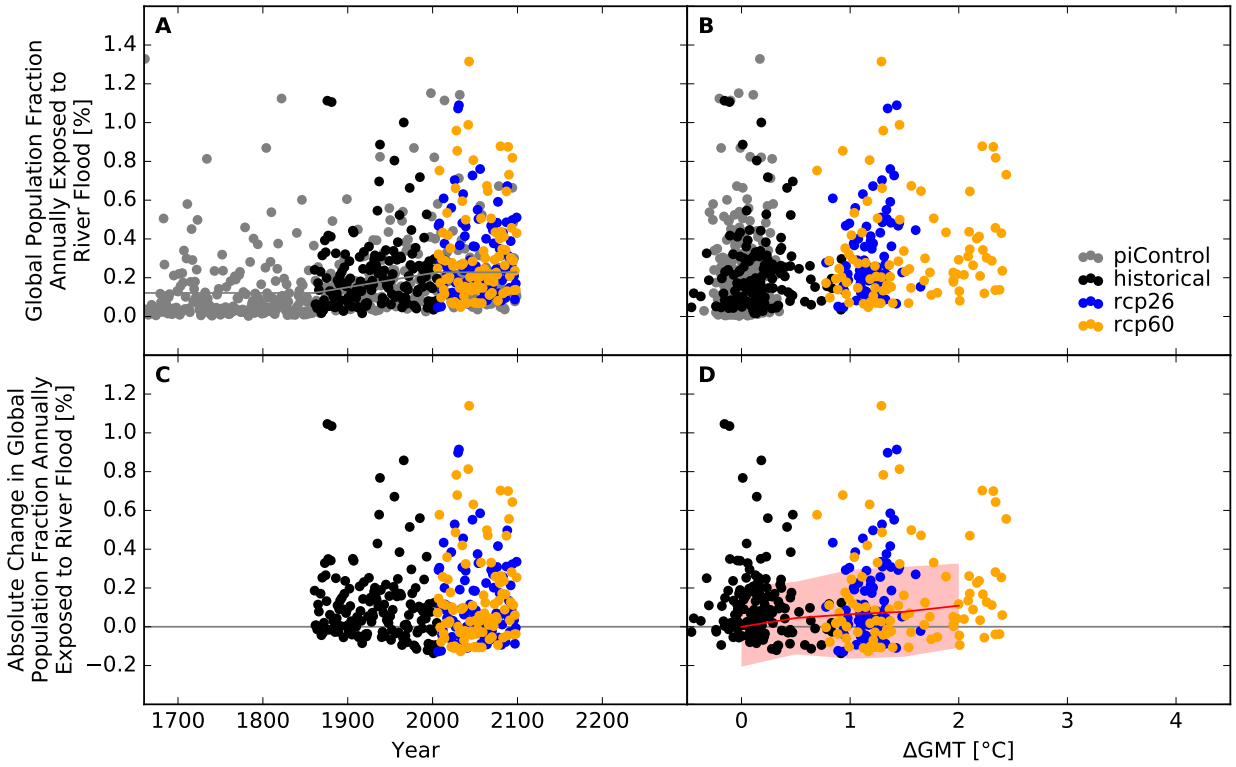

Figure S68: **Derivation of the pure effect of climate change on the global population fraction annually exposed to river flood (GFDL-ESM2M + CLM45).** Panel A: Time series of annual global population fraction exposed (PFE) to river flood for preindustrial climate (grey dots), historical climate (black dots), climate projections for RCP2.6 (blue dots), and RCP6.0 (orange dots). In all simulations, socioeconomic conditions are varied according to the historically observed development between 1860 and 2005, and held fixed at 1860 conditions before 1860 and at 2005 conditions after 2005. The horizontal gray lines before 1860 and after 2005 represent the multi-year mean global population fraction annually exposed to river flood under preindustrial climate conditions and socioeconomic conditions of 1860 and 2005, respectively. The gray line between 1860 and 2005 is a linear interpolation of these mean values. Panel B: Data shown in Panel A plotted against the associated GCM-specific annual global mean temperature (GMT) change relative to the long-term preindustrial mean GMT. Panel C: Pure effect of climate change on PFE, calculated as the difference between the annual data shown in Panel A and the multi-year mean PFE under preindustrial climate conditions (gray line in Panel A). Panel D: Data shown in Panel C plotted against annual GMT change. The red line represents the mean values of the annual data points per 1 °C-wide GMT change bin, with bins centered at GMT change levels increasing from 0 °C to 4 °C in steps of 0.5 °C. The area shaded in red represents the mean value ±1 standard deviation ranges of the annual data points per GMT change bin.

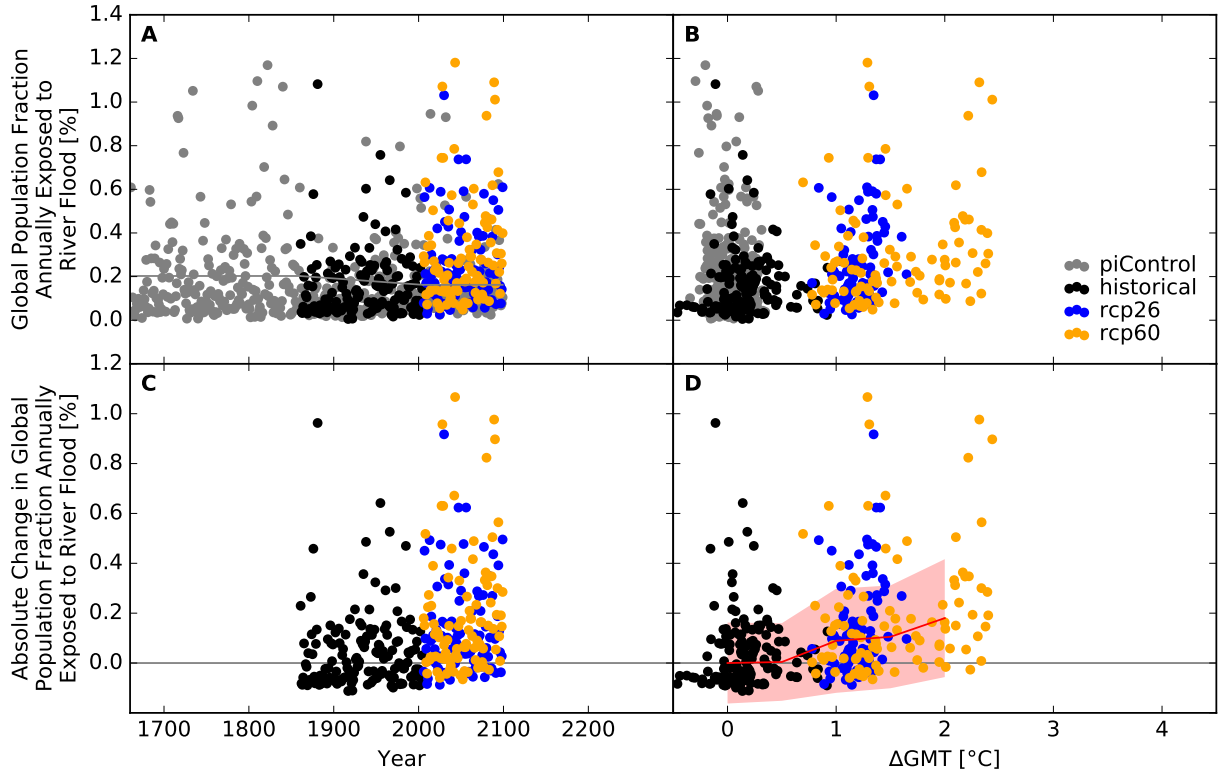

Figure S69: **Derivation of the pure effect of climate change on the global population fraction annually exposed to river flood (GFDL-ESM2M + H08).** Analogous to Figure S68.

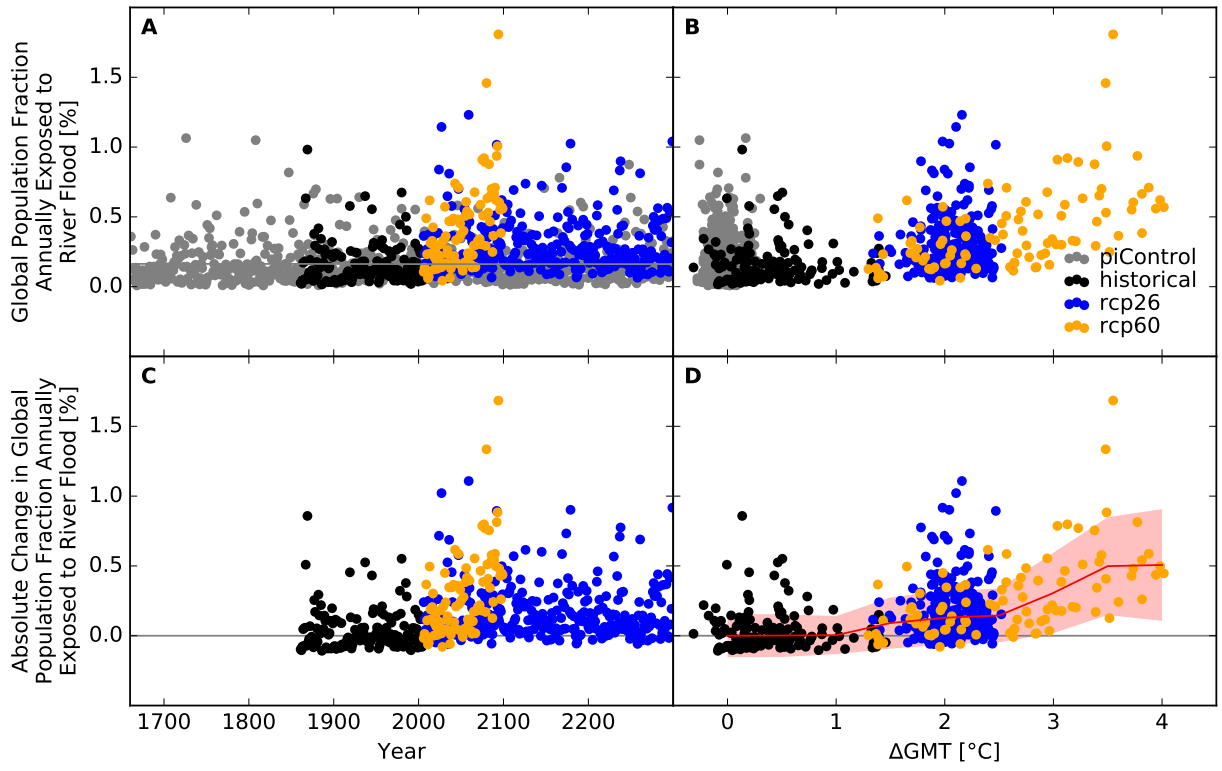

Figure S70: **Derivation of the pure effect of climate change on the global population fraction annually exposed to river flood (IPSL-CM5A-LR + H08).** Analogous to Figure S68.

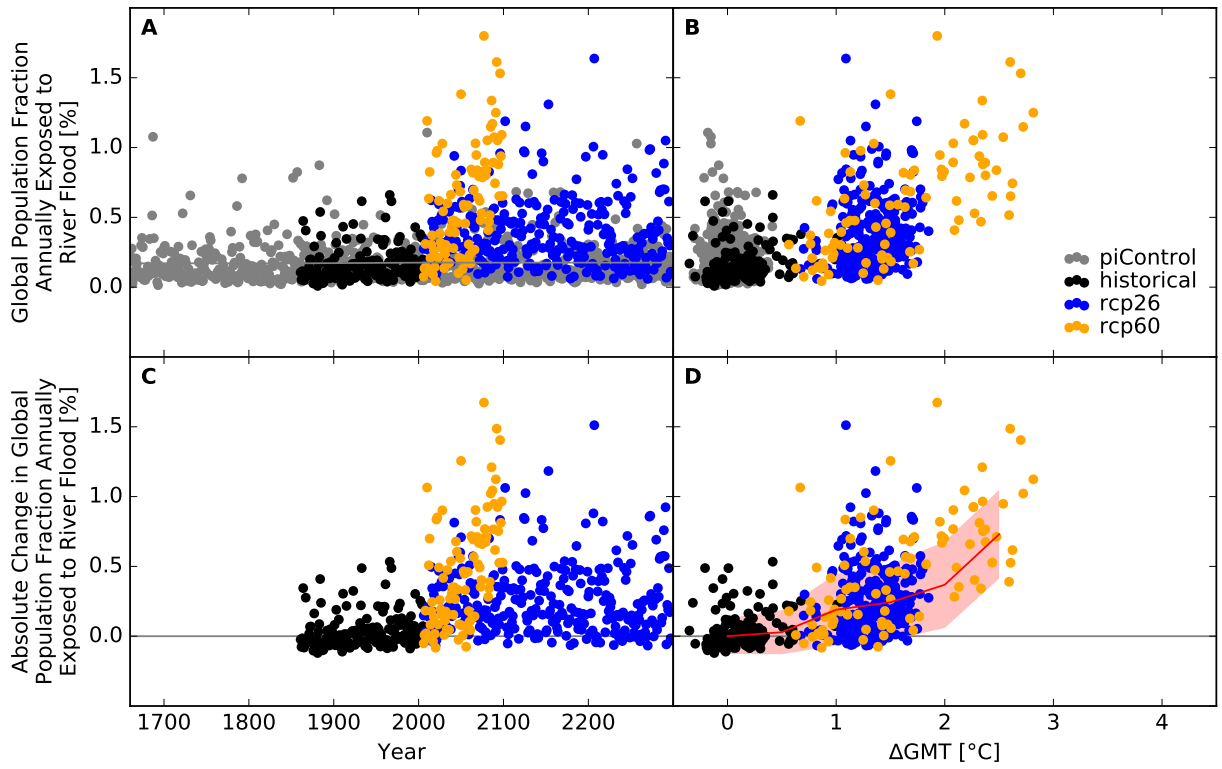

Figure S71: **Derivation of the pure effect of climate change on the global population fraction annually exposed to river flood (MIROC5 + H08).** Analogous to Figure S68.

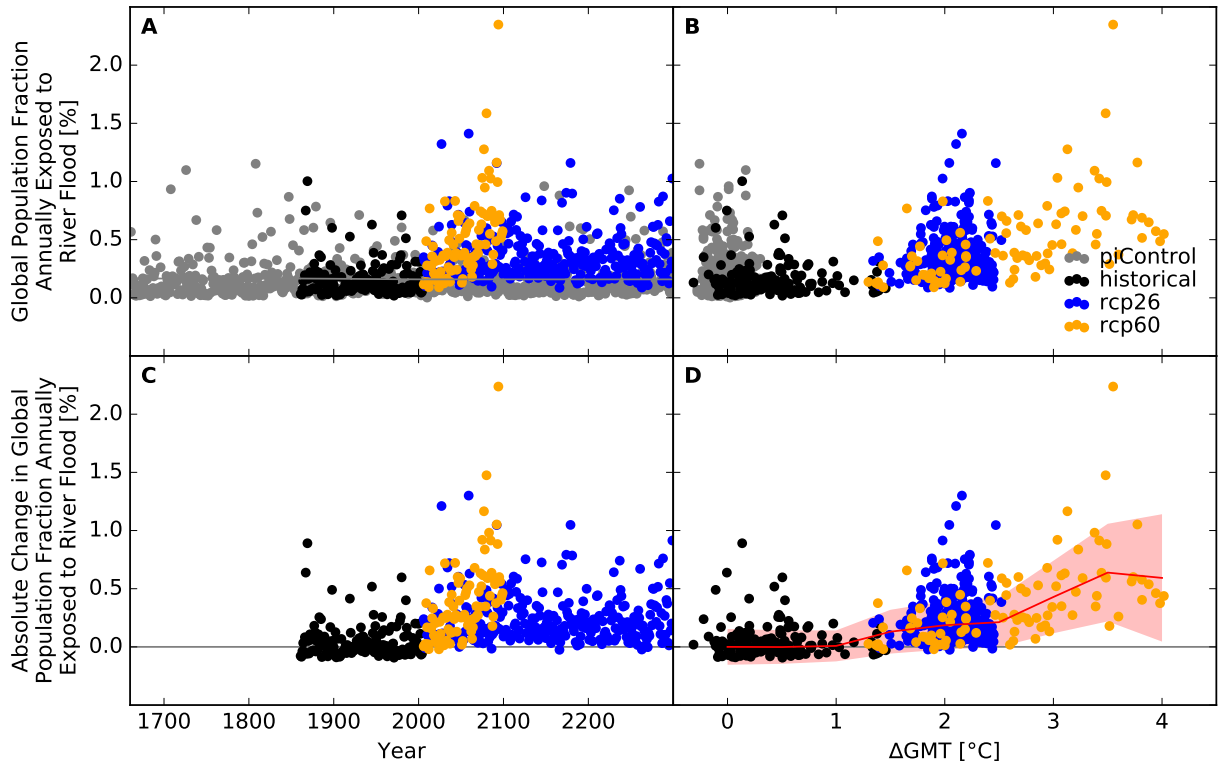

Figure S72: **Derivation of the pure effect of climate change on the global population fraction annually exposed to river flood (IPSL-CM5A-LR + JULES-W1).** Analogous to Figure S68.

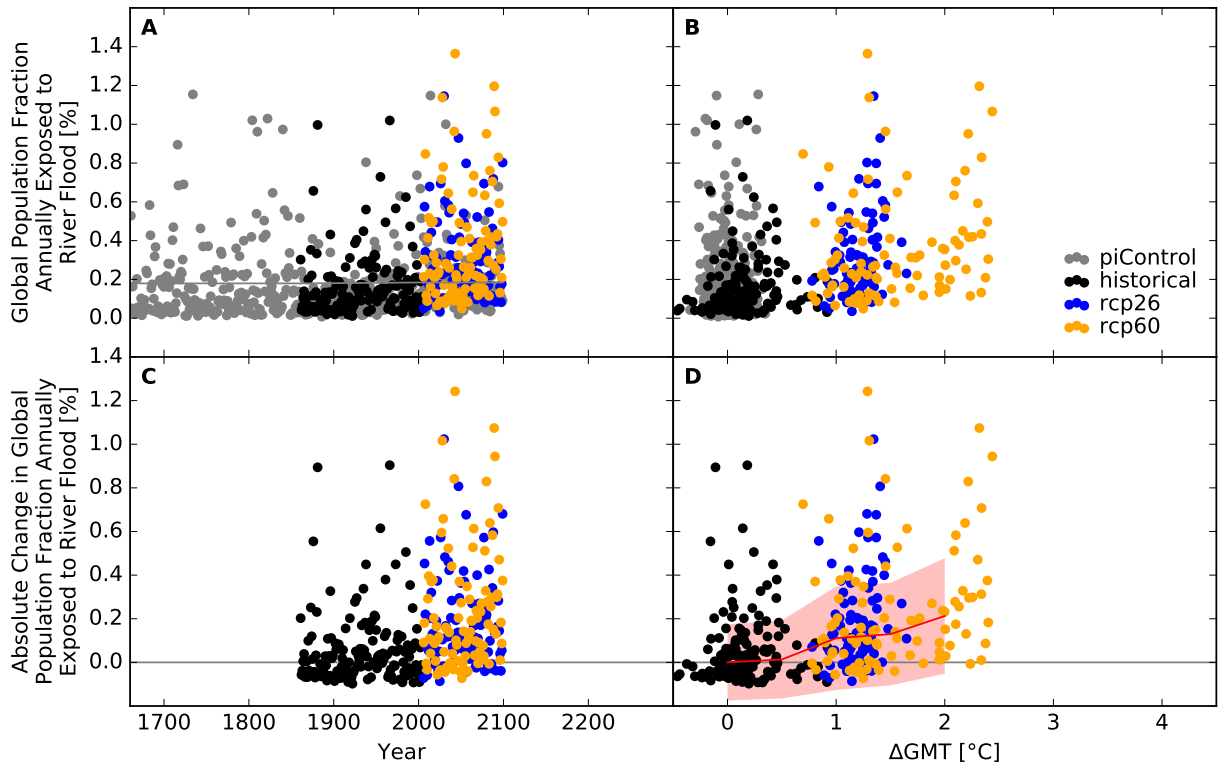

Figure S73: **Derivation of the pure effect of climate change on the global population fraction annually exposed to river flood (GFDL-ESM2M + LPJmL).** Analogous to Figure S68.

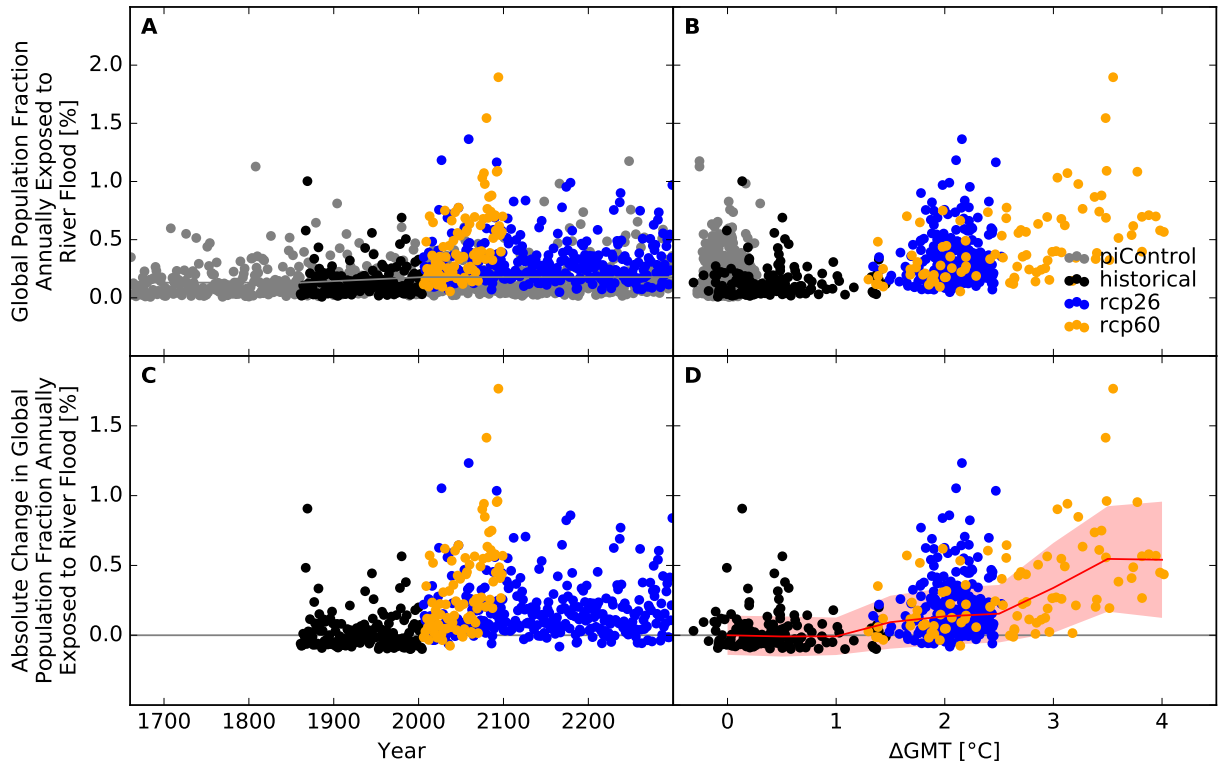

Figure S74: **Derivation of the pure effect of climate change on the global population fraction annually exposed to river flood (IPSL-CM5A-LR + LPJmL).** Analogous to Figure S68.

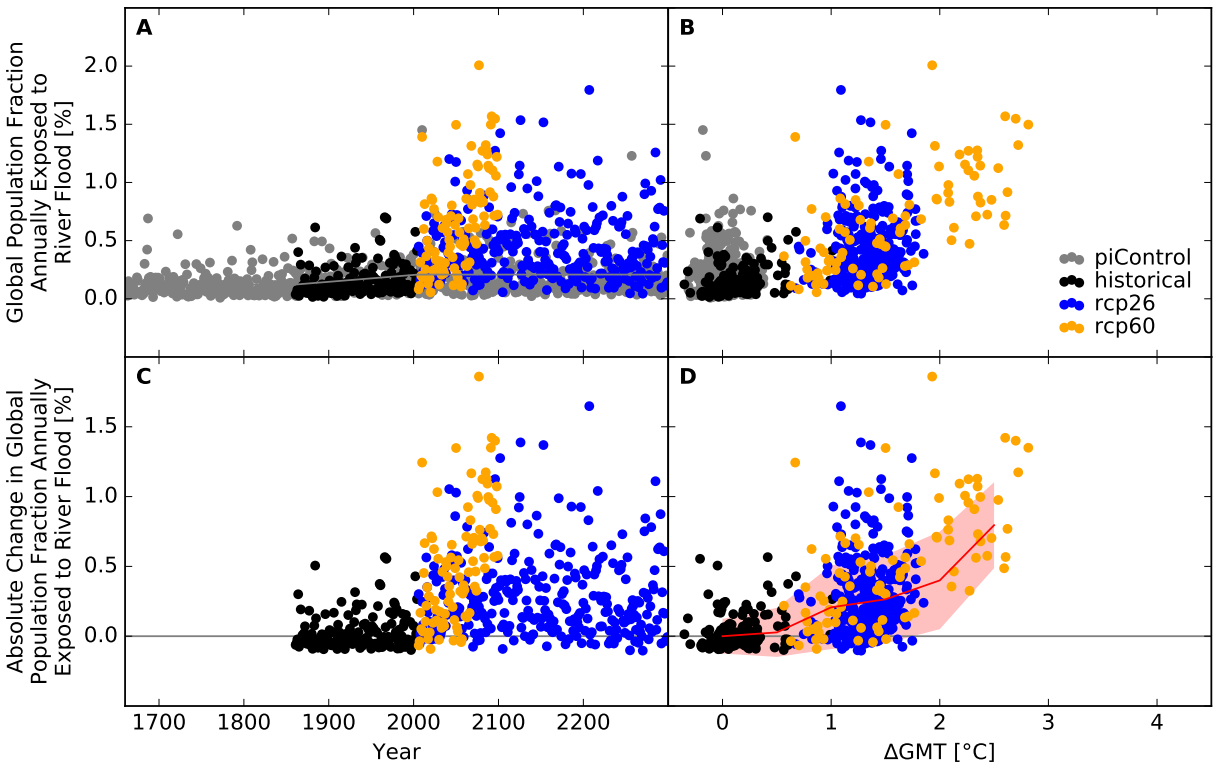

Figure S75: **Derivation of the pure effect of climate change on the global population fraction annually exposed to river flood (MIROC5 + LPJmL).** Analogous to Figure S68.

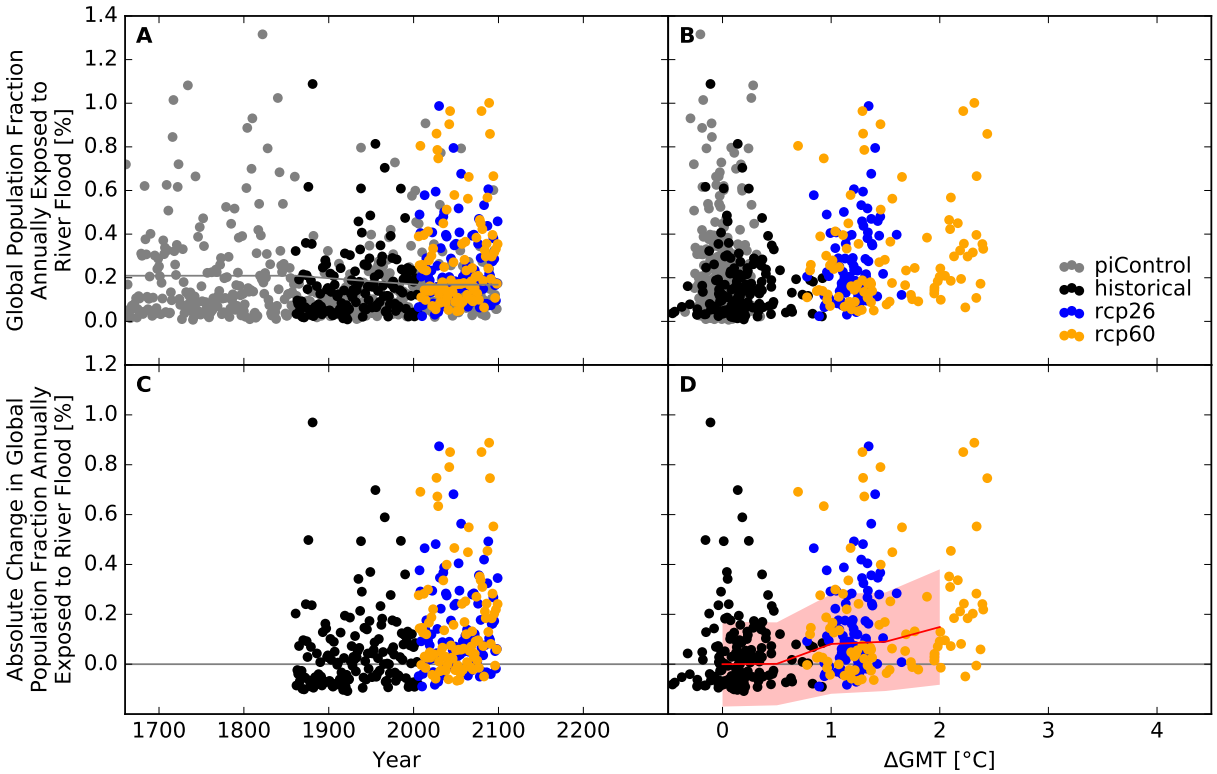

Figure S76: **Derivation of the pure effect of climate change on the global population fraction annually exposed to river flood (GFDL-ESM2M + MPI-HM).** Analogous to Figure S68.

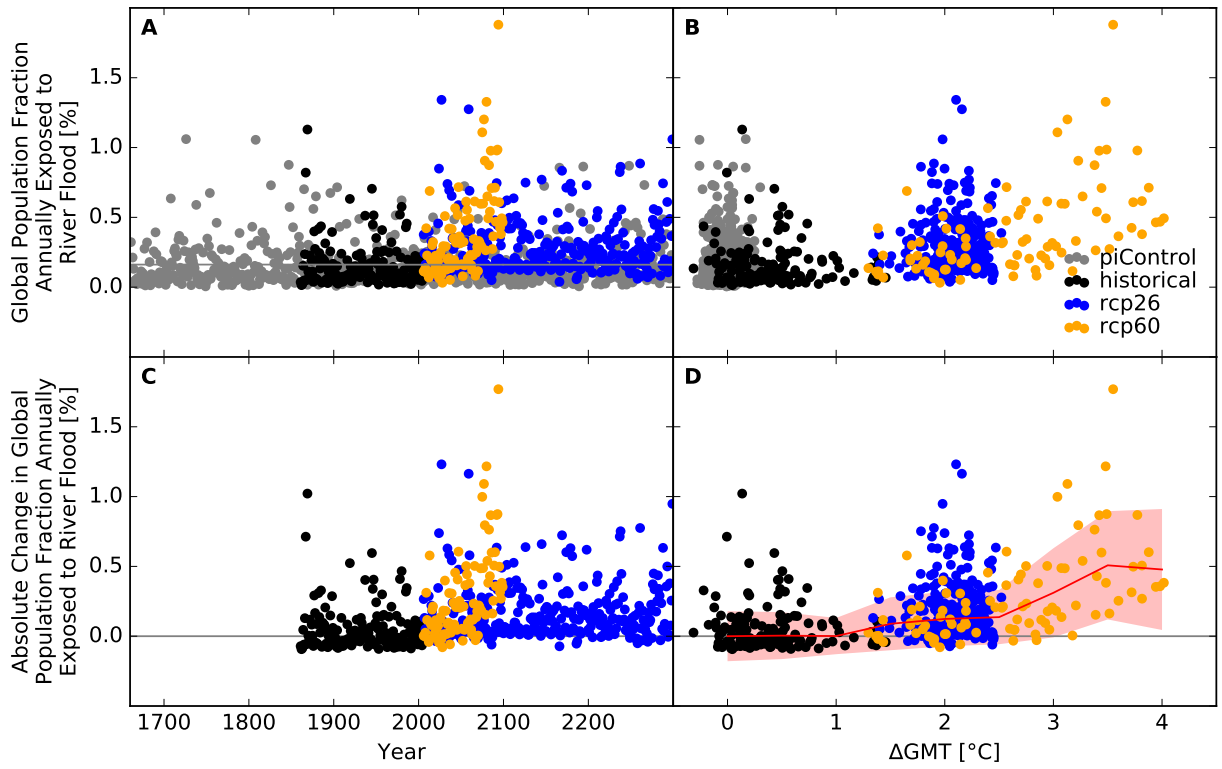

Figure S77: **Derivation of the pure effect of climate change on the global population fraction annually exposed to river flood (IPSL-CM5A-LR + MPI-HM).** Analogous to Figure S68.

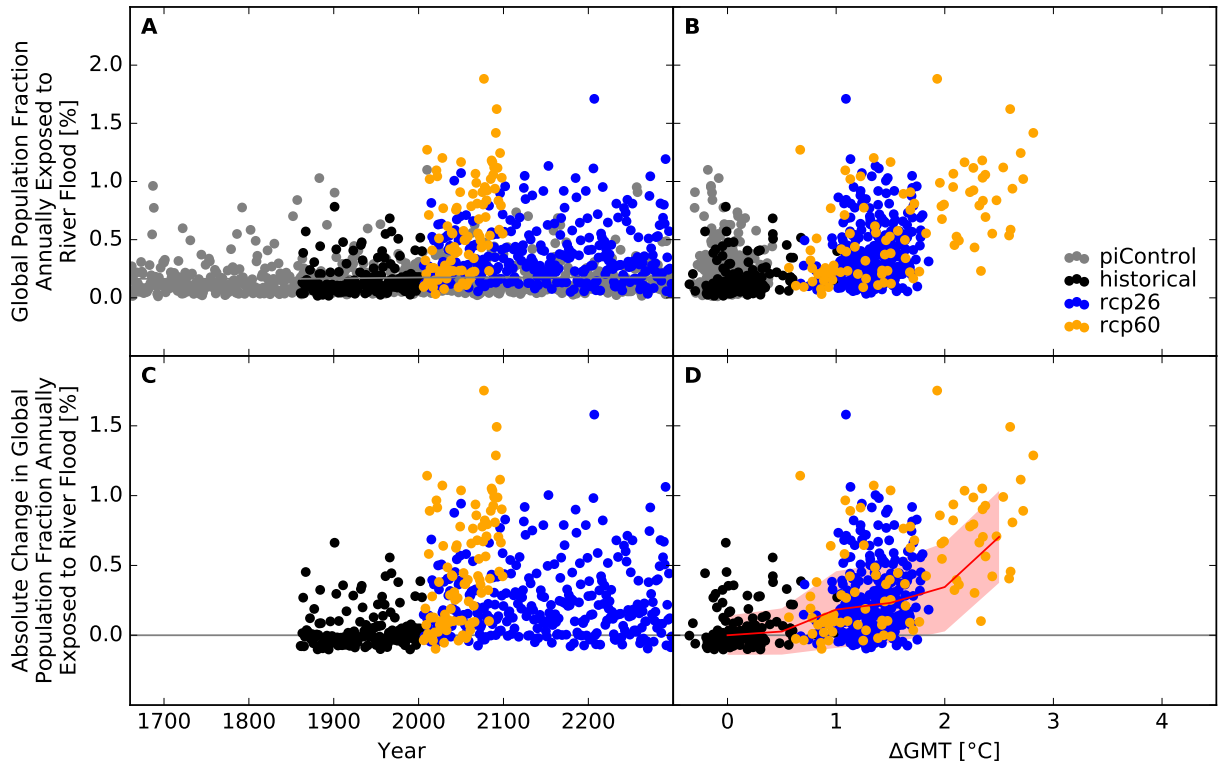

Figure S78: **Derivation of the pure effect of climate change on the global population fraction annually exposed to river flood (MIROC5 + MPI-HM).** Analogous to Figure S68.

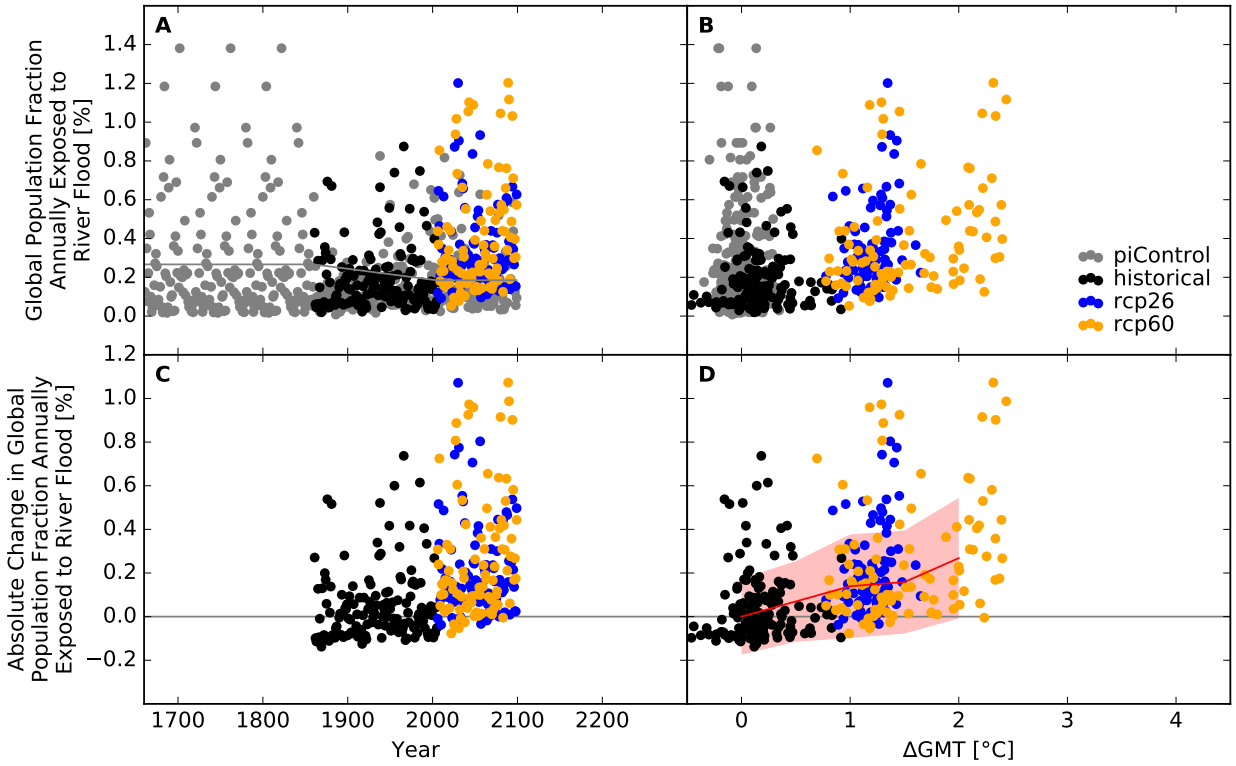

Figure S79: **Derivation of the pure effect of climate change on the global population fraction annually exposed to river flood (GFDL-ESM2M + ORCHIDEE).** Analogous to Figure S68.

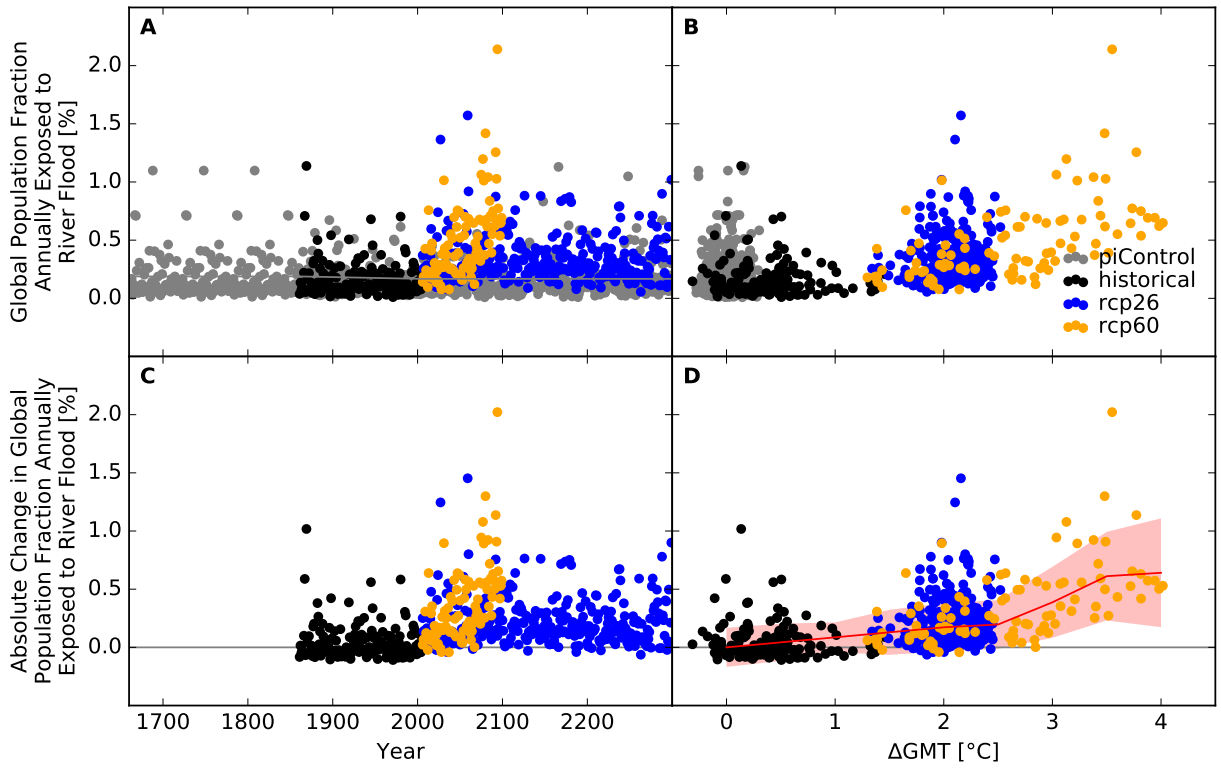

Figure S80: **Derivation of the pure effect of climate change on the global population fraction annually exposed to river flood (IPSL-CM5A-LR + ORCHIDEE).** Analogous to Figure S68.

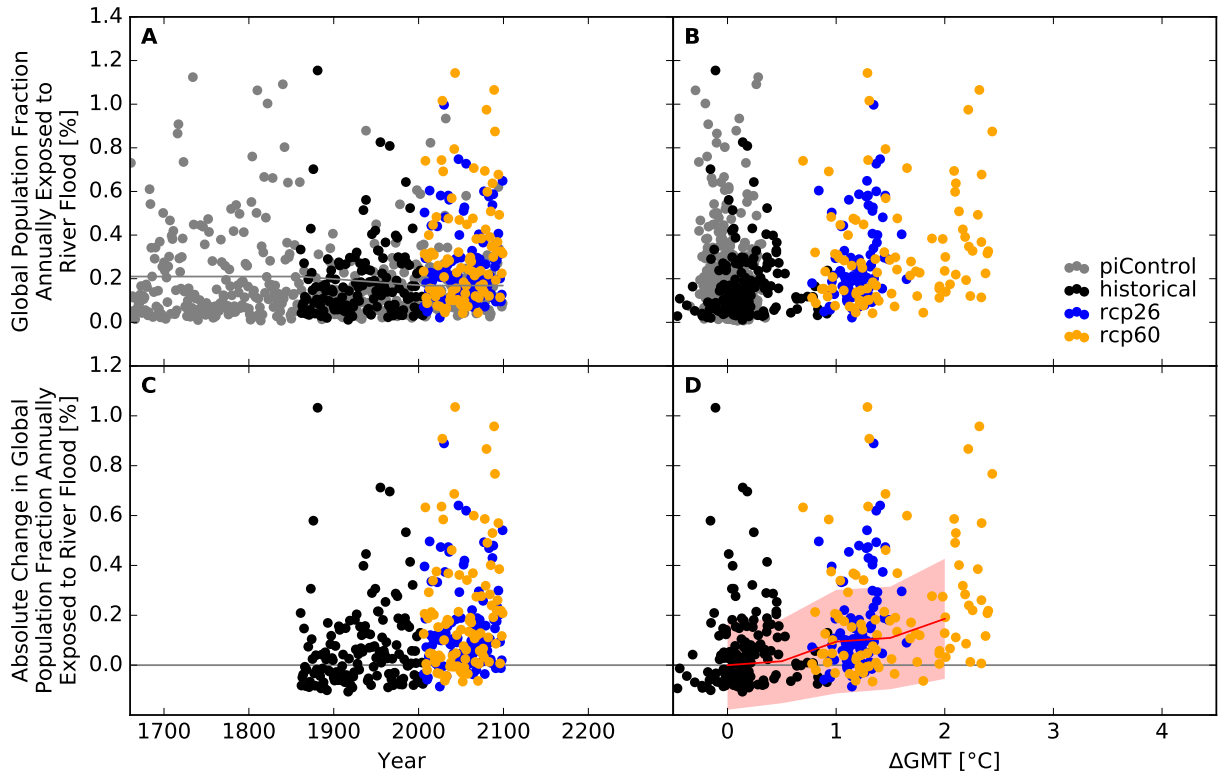

Figure S81: **Derivation of the pure effect of climate change on the global population fraction annually exposed to river flood (GFDL-ESM2M + PCR-GLOBWB).** Analogous to Figure S68.

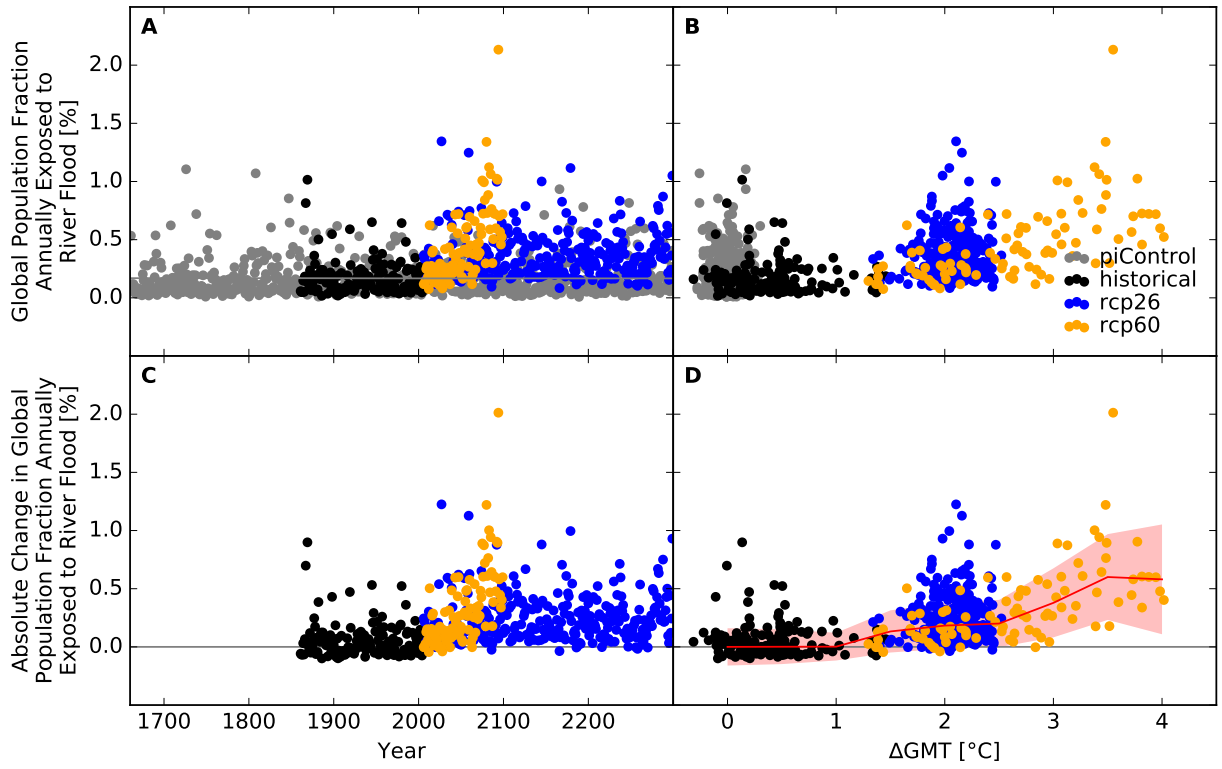

Figure S82: **Derivation of the pure effect of climate change on the global population fraction annually exposed to river flood (IPSL-CM5A-LR + PCR-GLOBWB).** Analogous to Figure S68.

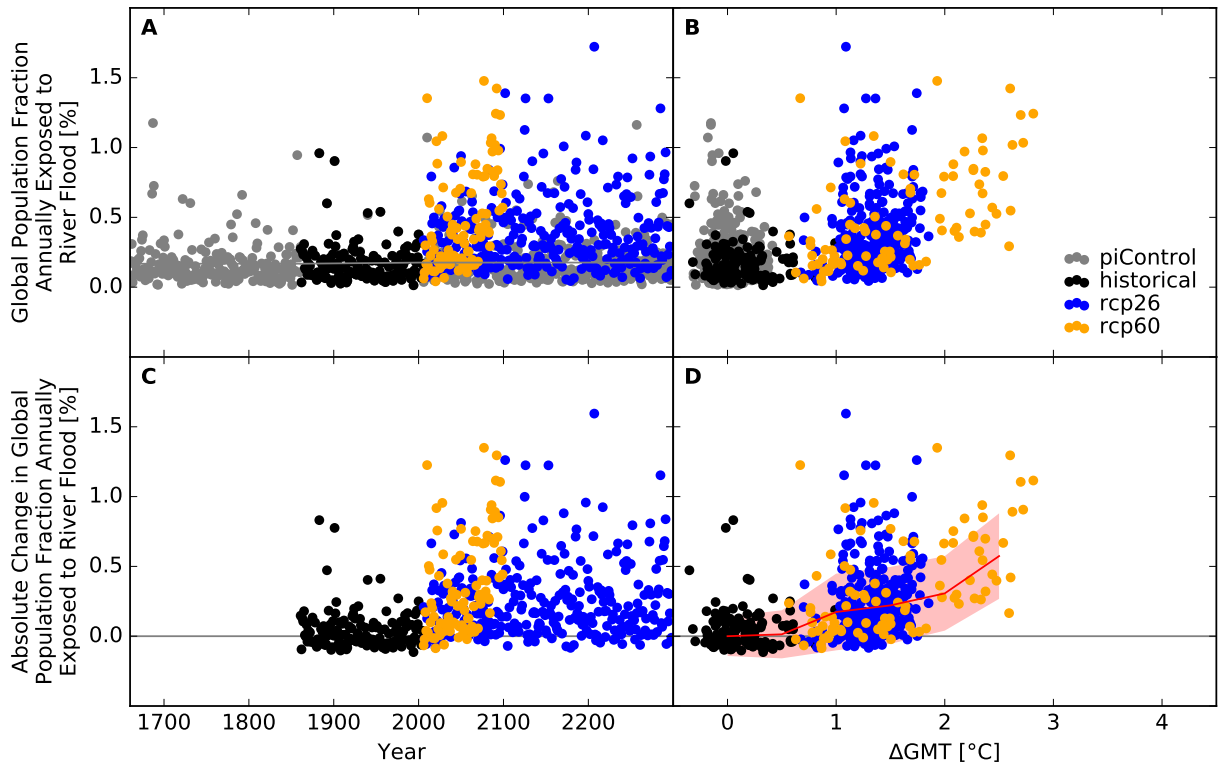

Figure S83: **Derivation of the pure effect of climate change on the global population fraction annually exposed to river flood (MIROC5 + PCR-GLOBWB).** Analogous to Figure S68.

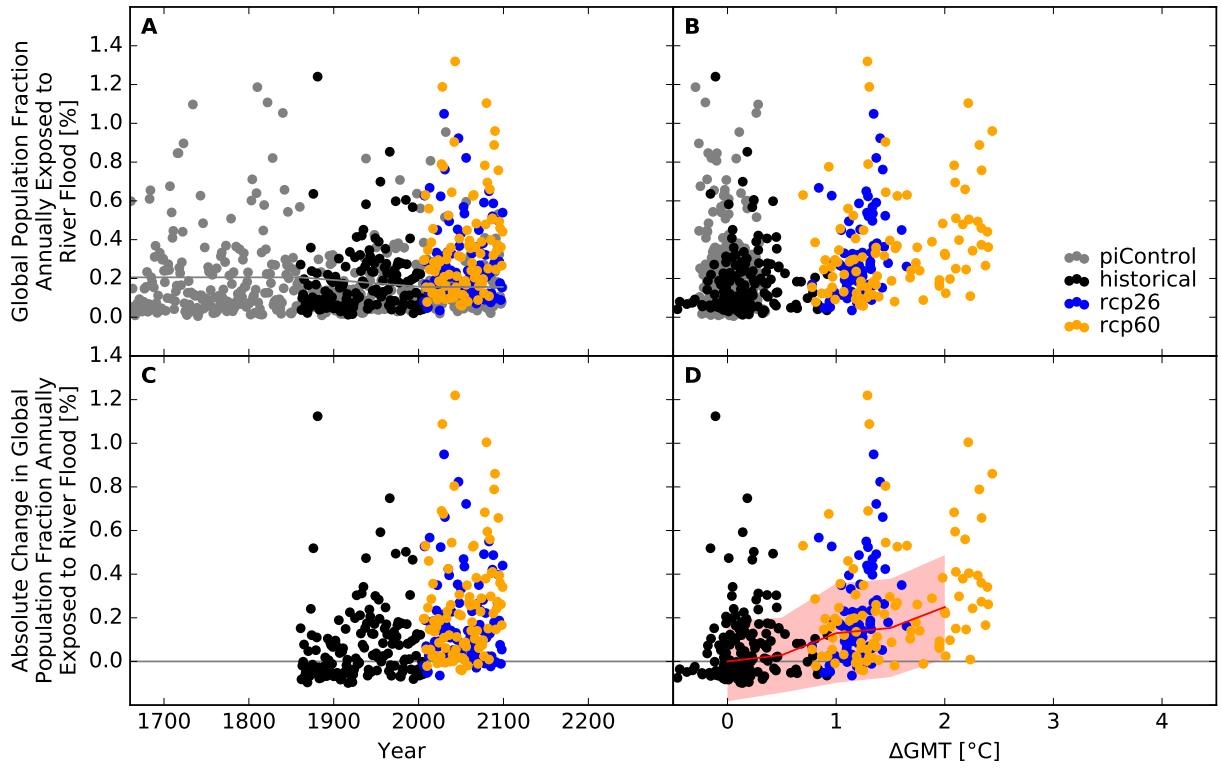

Figure S84: **Derivation of the pure effect of climate change on the global population fraction annually exposed to river flood (GFDL-ESM2M + WaterGAP2).** Analogous to Figure S68.

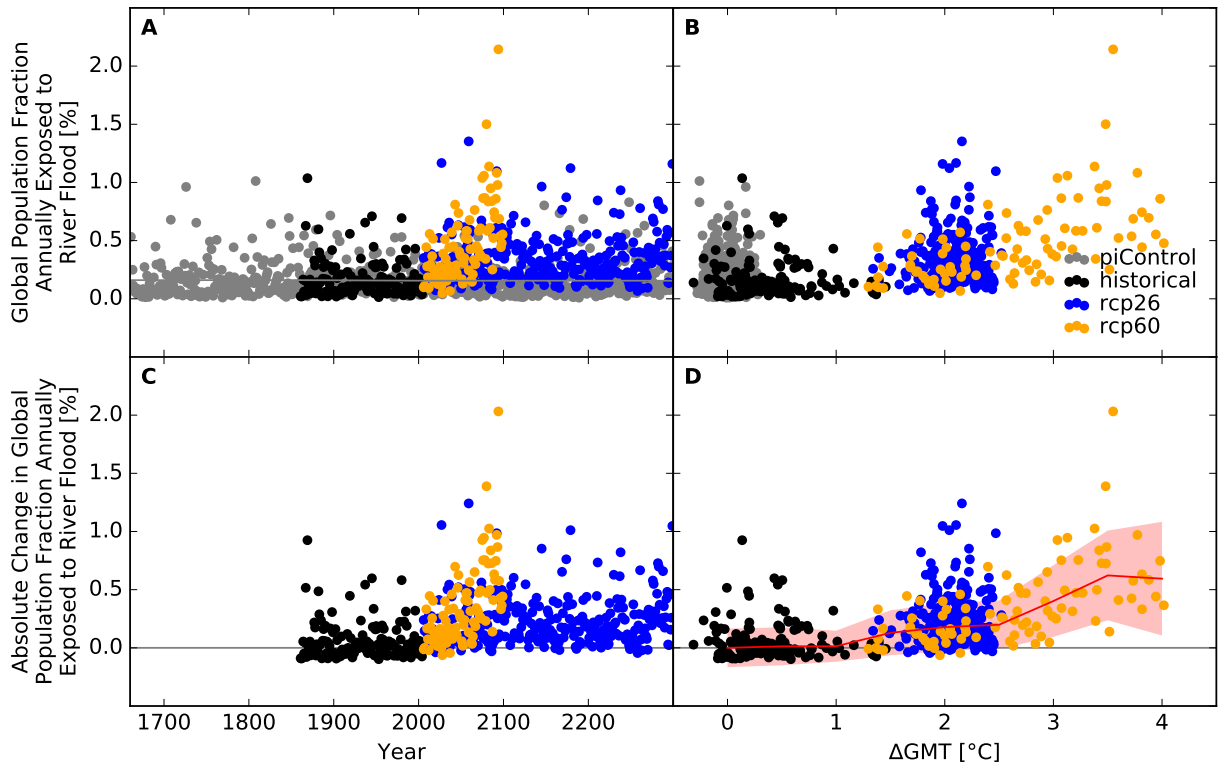

Figure S85: **Derivation of the pure effect of climate change on the global population fraction annually exposed to river flood (IPSL-CM5A-LR + WaterGAP2).** Analogous to Figure S68.

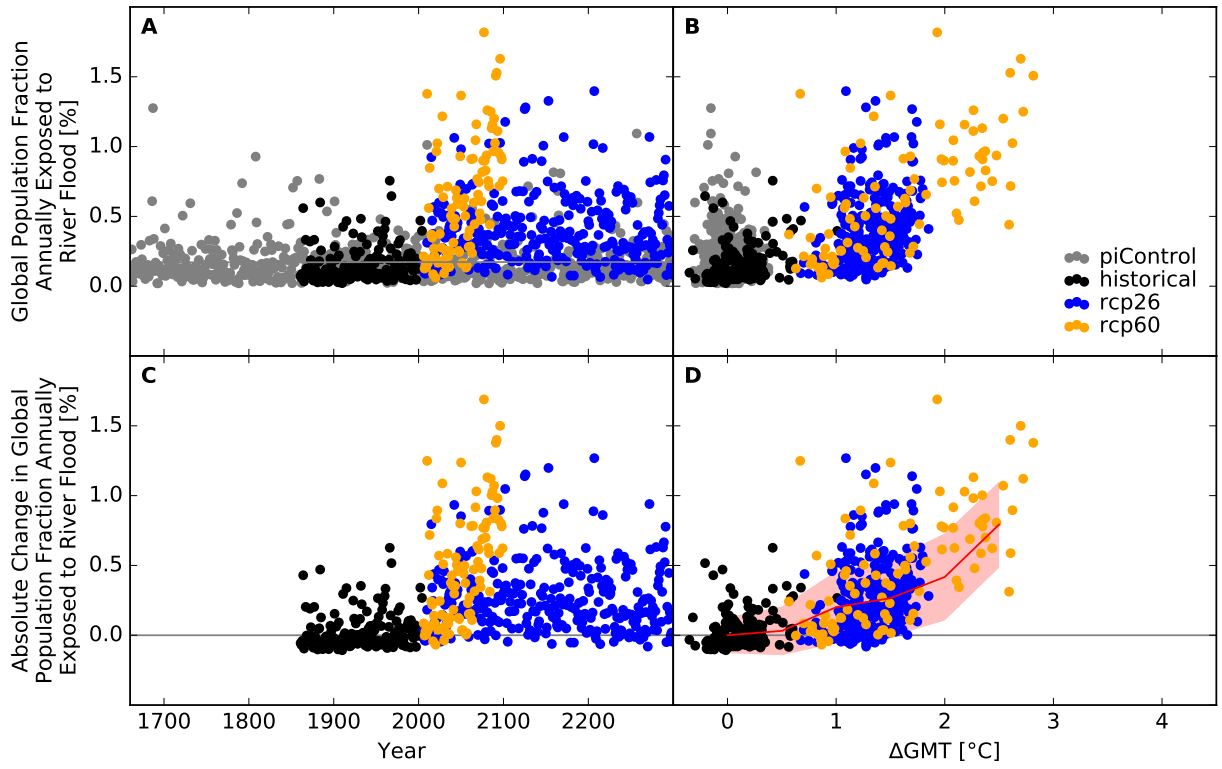

Figure S86: **Derivation of the pure effect of climate change on the global population fraction annually exposed to river flood (MIROC5 + WaterGAP2).** Analogous to Figure S68.

Land area affected and number of people exposed at the national scale

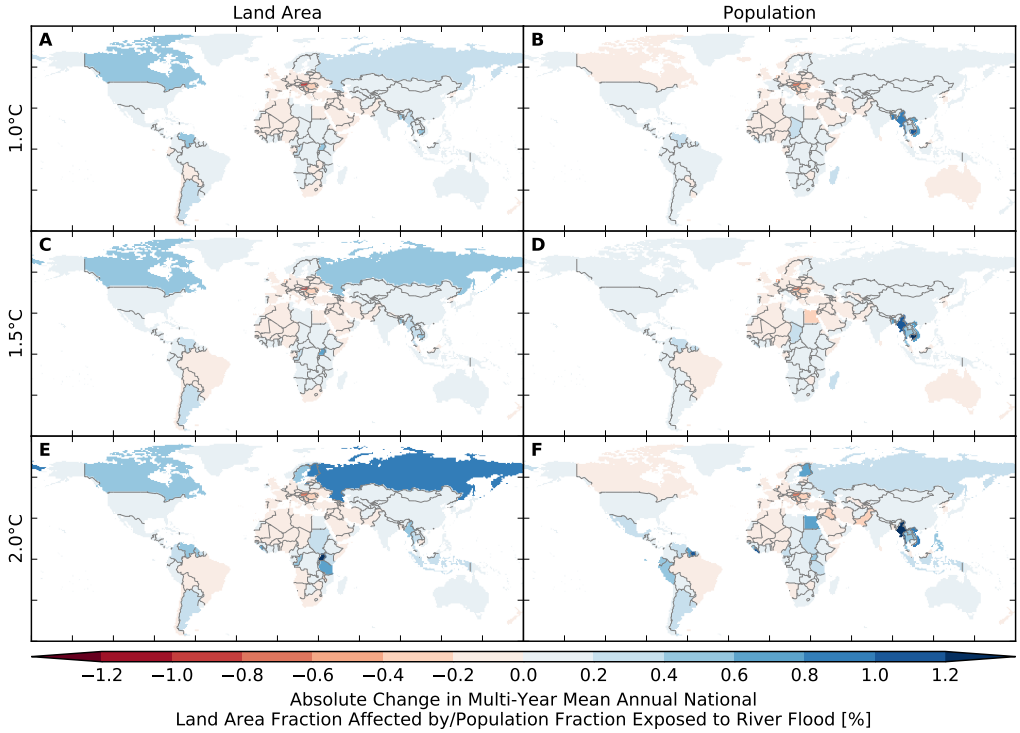

Figure S87: **Pure effect of climate change on annual national land area fraction affected by and population fraction exposed to river flood (GFDL-ESM2M + CLM45).** Absolute changes in multi-year mean annual national (A, C, E) land area fraction affected by and (B, D, F) population fraction exposed to river flood at (A, B) 1 °C, (C, D) 1.5 °C and (E, F) 2 °C global warming.

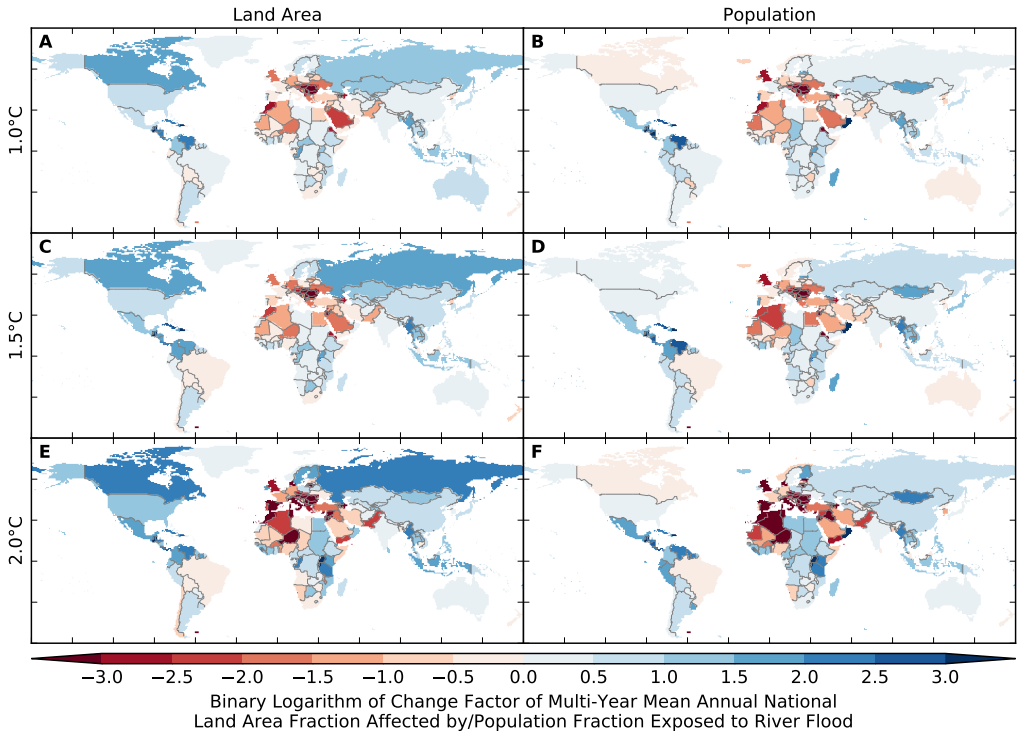

Figure S88: **Pure effect of climate change on annual national land area fraction affected by and population fraction exposed to river flood (GFDL-ESM2M + CLM45).** Same as Figure S87 but for relative changes expressed in terms of binary logarithms of change factors, i.e. −1 means a change by a factor of 0.5, 0 means no change, and 1 means a change by a factor of 2. White indicates undefined relative changes due to division by zero.

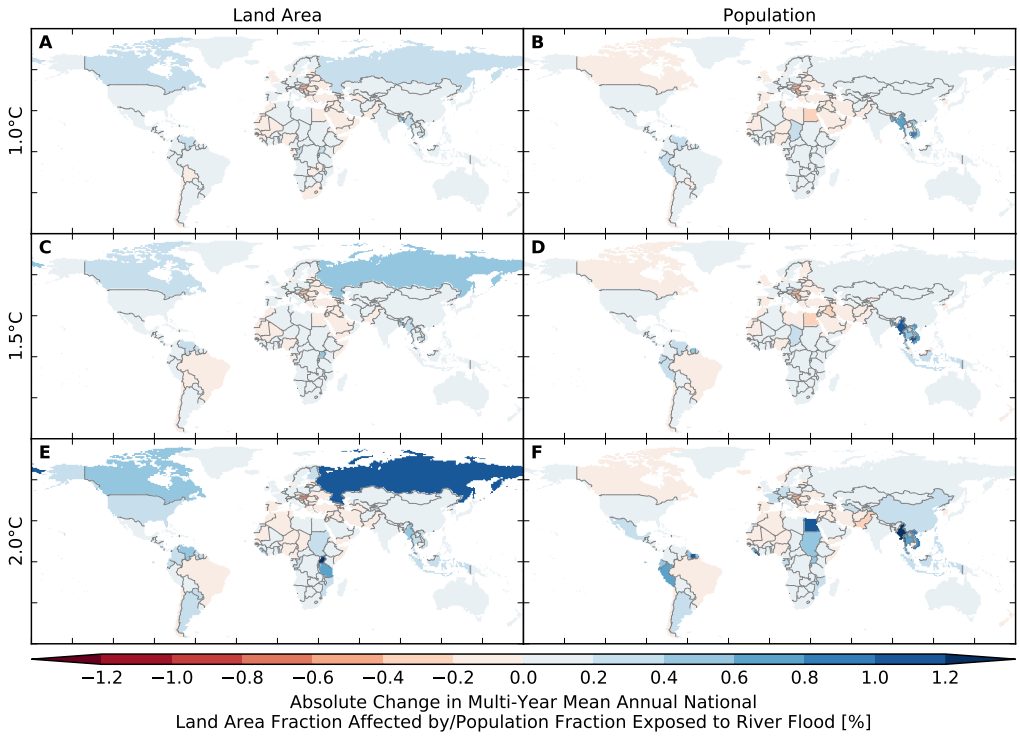

Figure S89: **Pure effect of climate change on annual national land area fraction affected by and population fraction exposed to river flood (GFDL-ESM2M + H08).** Analogous to Figure S87.

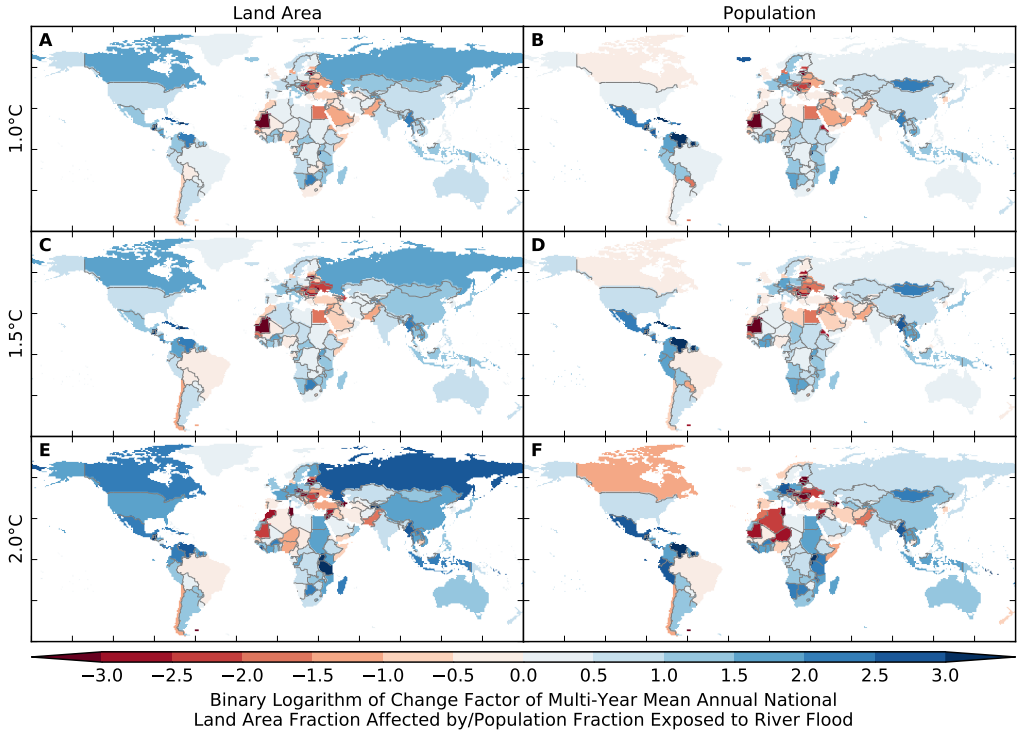

Figure S90: **Pure effect of climate change on annual national land area fraction affected by and population fraction exposed to river flood (GFDL-ESM2M + H08).** Analogous to Figure S88.

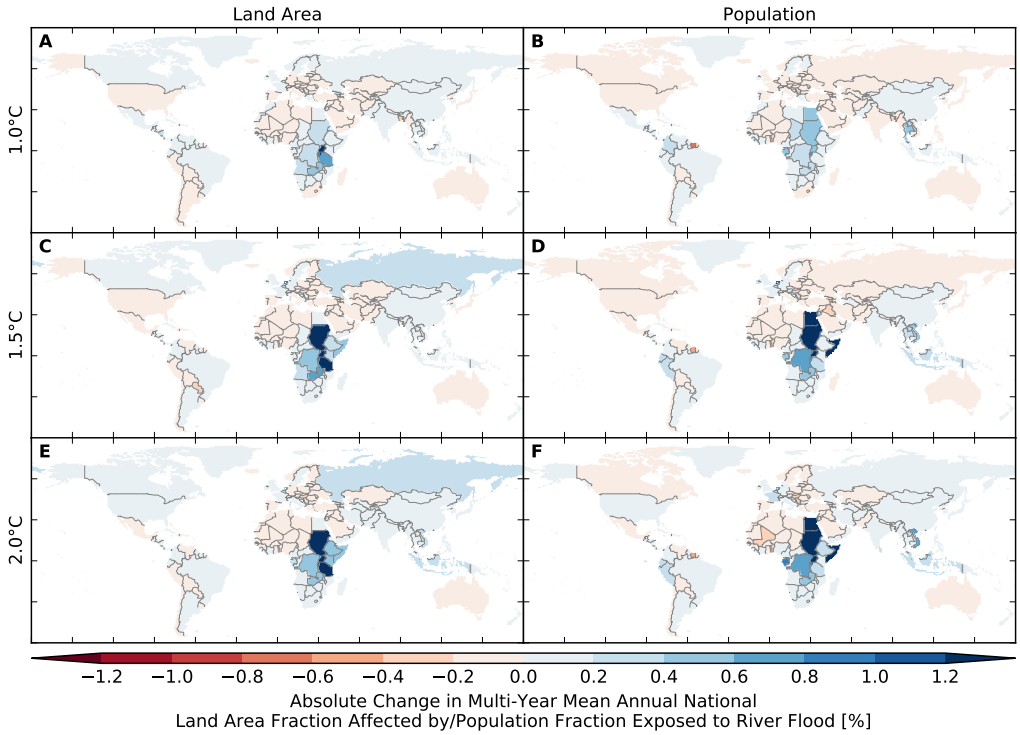

Figure S91: **Pure effect of climate change on annual national land area fraction affected by and population fraction exposed to river flood (IPSL-CM5A-LR + H08).** Analogous to Figure S87.

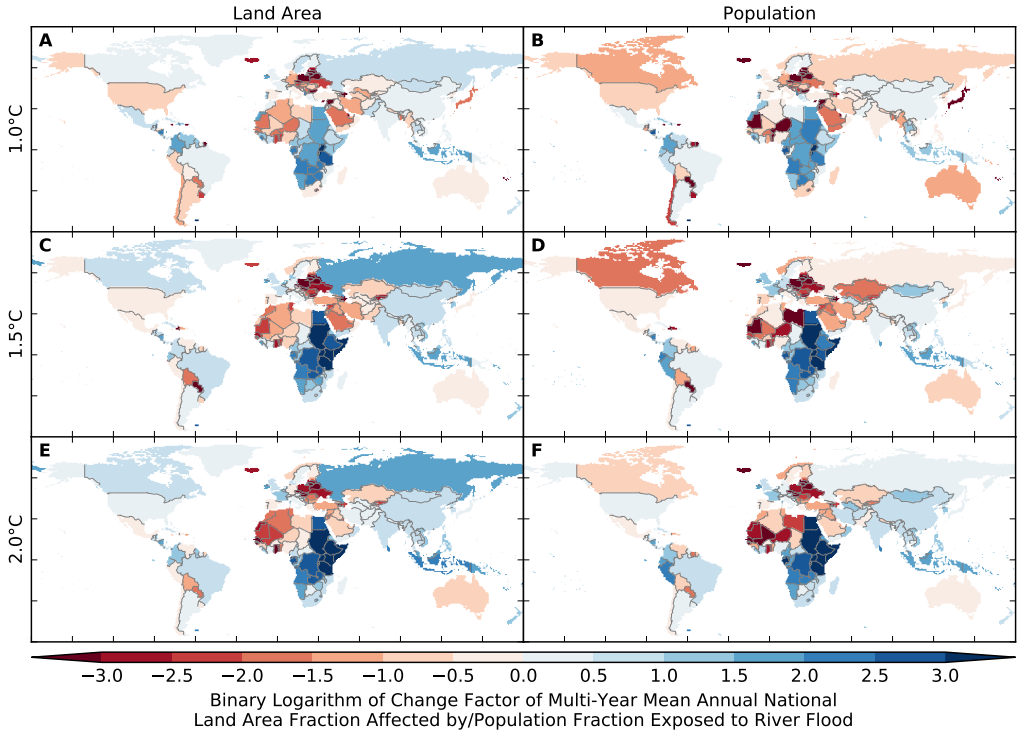

Figure S92: **Pure effect of climate change on annual national land area fraction affected by and population fraction exposed to river flood (IPSL-CM5A-LR + H08).** Analogous to Figure S88.

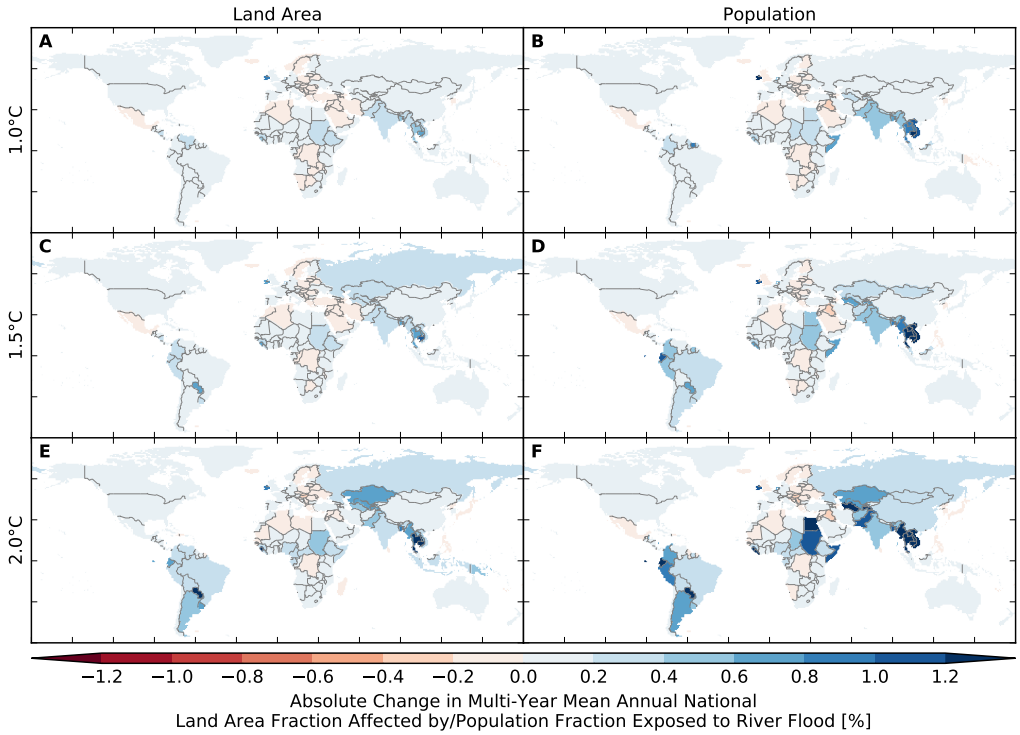

Figure S93: **Pure effect of climate change on annual national land area fraction affected by and population fraction exposed to river flood (MIROC5 + H08).** Analogous to Figure S87.

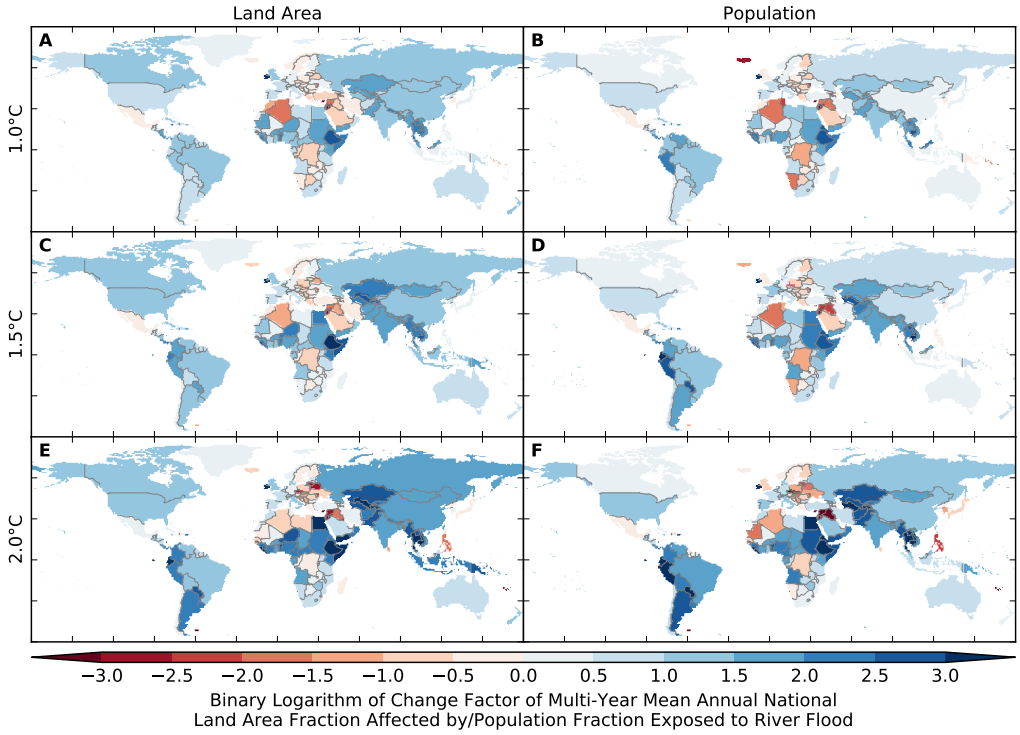

Figure S94: **Pure effect of climate change on annual national land area fraction affected by and population fraction exposed to river flood (MIROC5 + H08).** Analogous to Figure S88.

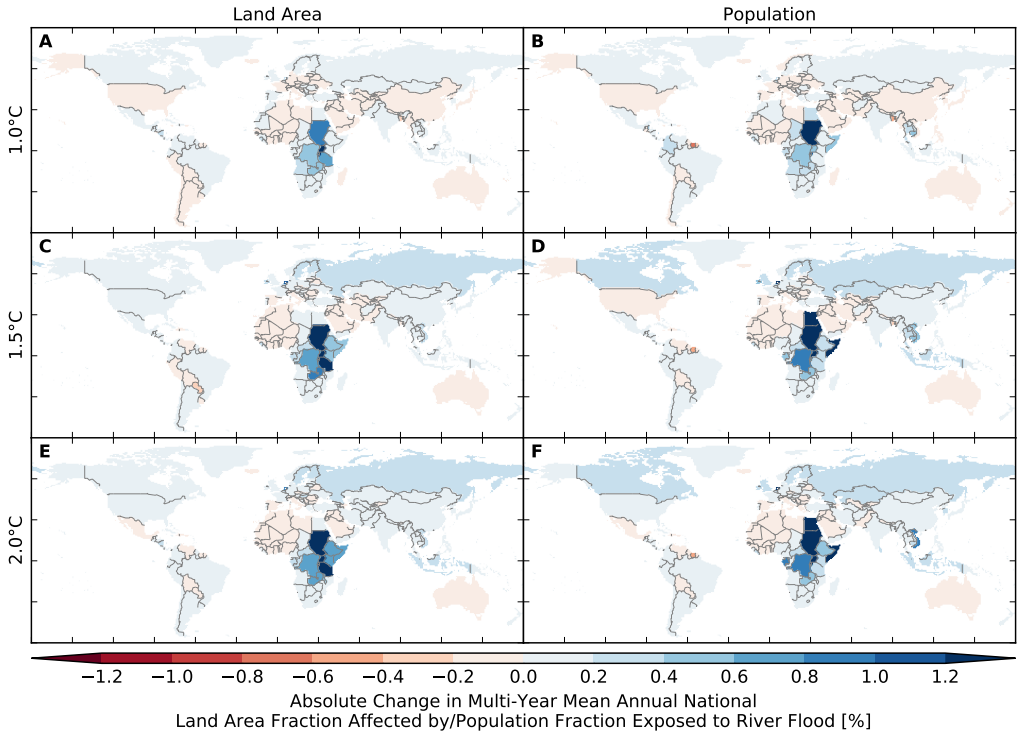

Figure S95: **Pure effect of climate change on annual national land area fraction affected by and population fraction exposed to river flood (IPSL-CM5A-LR + JULES-W1).** Analogous to Figure S87.

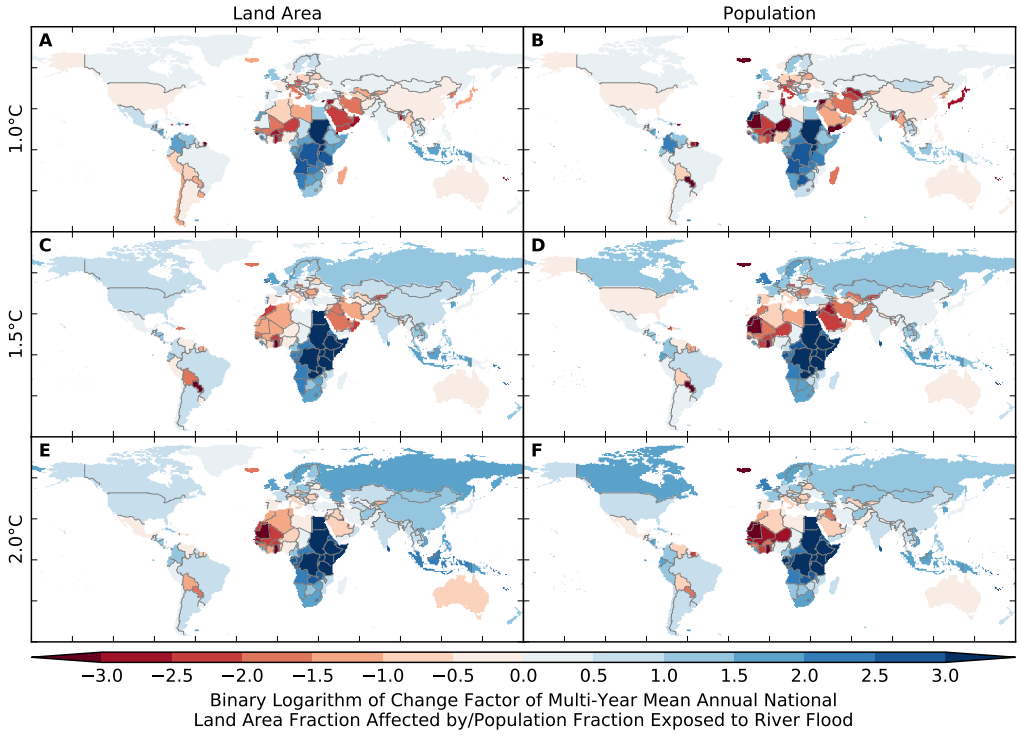

Figure S96: **Pure effect of climate change on annual national land area fraction affected by and population fraction exposed to river flood (IPSL-CM5A-LR + JULES-W1).** Analogous to Figure S88.

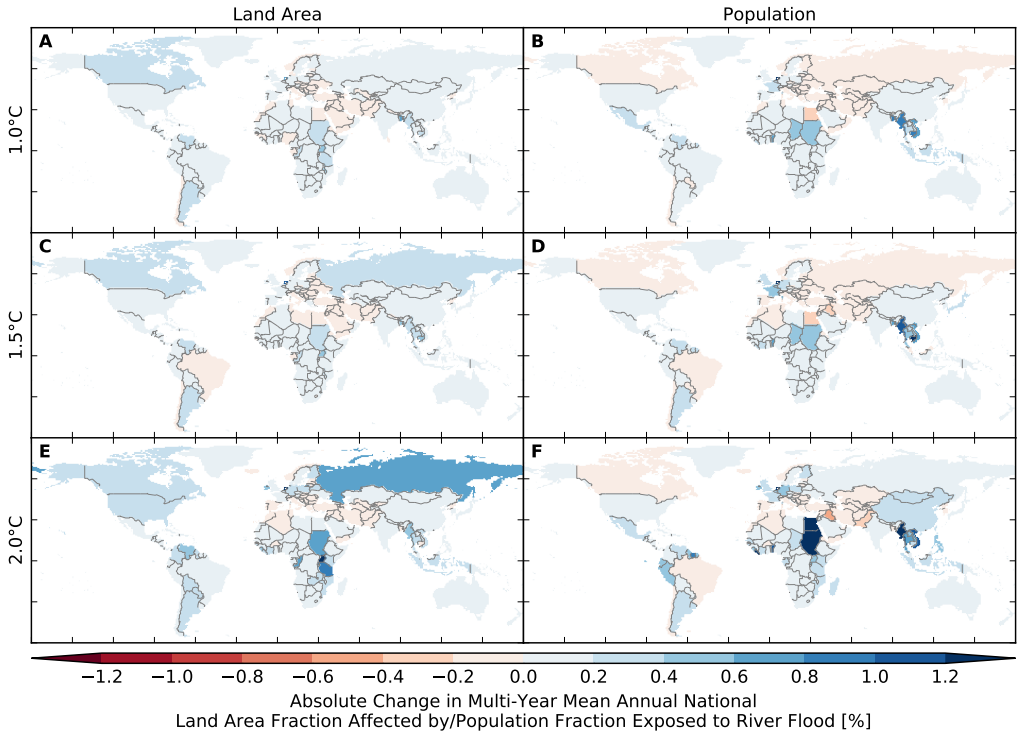

Figure S97: **Pure effect of climate change on annual national land area fraction affected by and population fraction exposed to river flood (GFDL-ESM2M + LPJmL).** Analogous to Figure S87.

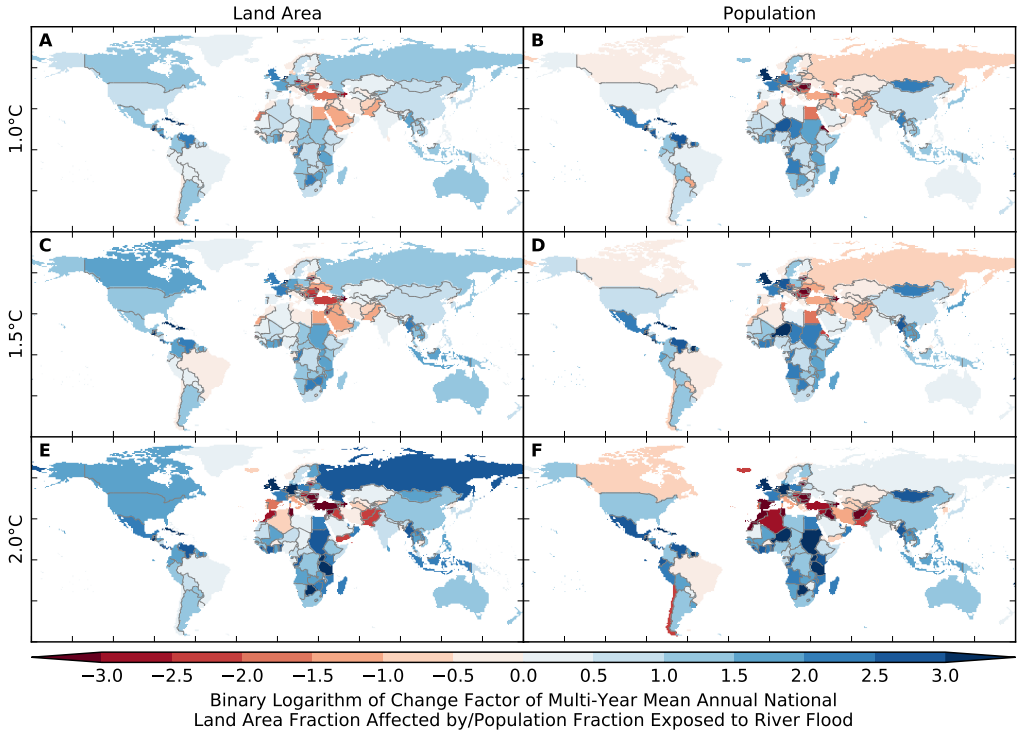

Figure S98: **Pure effect of climate change on annual national land area fraction affected by and population fraction exposed to river flood (GFDL-ESM2M + LPJmL).** Analogous to Figure S88.

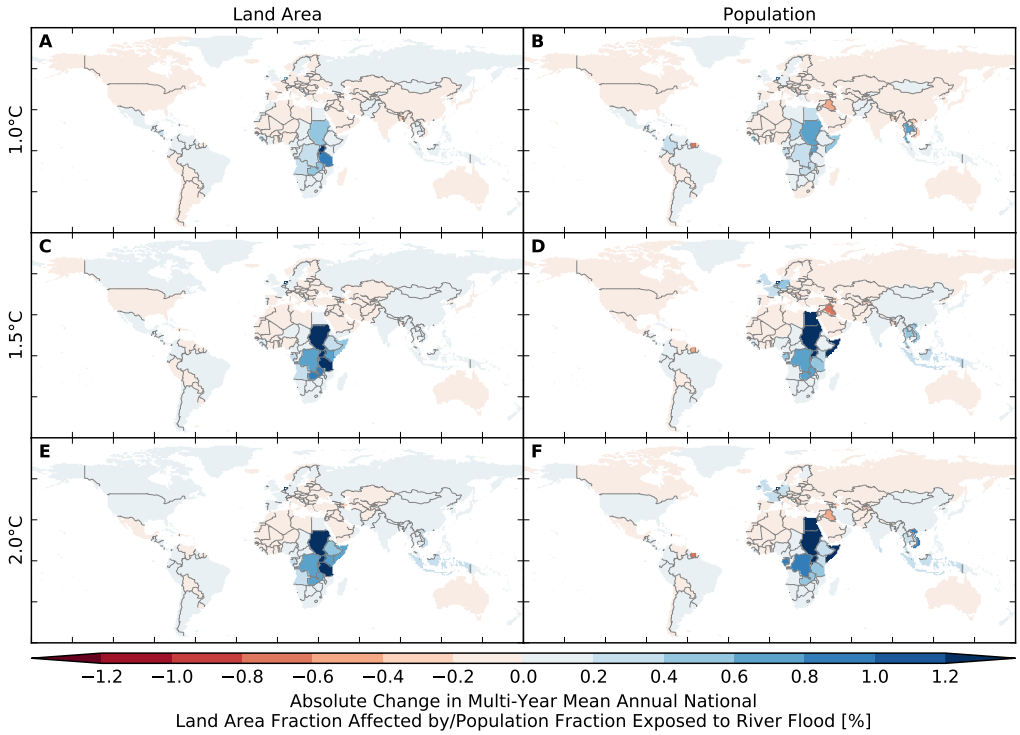

Figure S99: **Pure effect of climate change on annual national land area fraction affected by and population fraction exposed to river flood (IPSL-CM5A-LR + LPJmL).** Analogous to Figure S87.

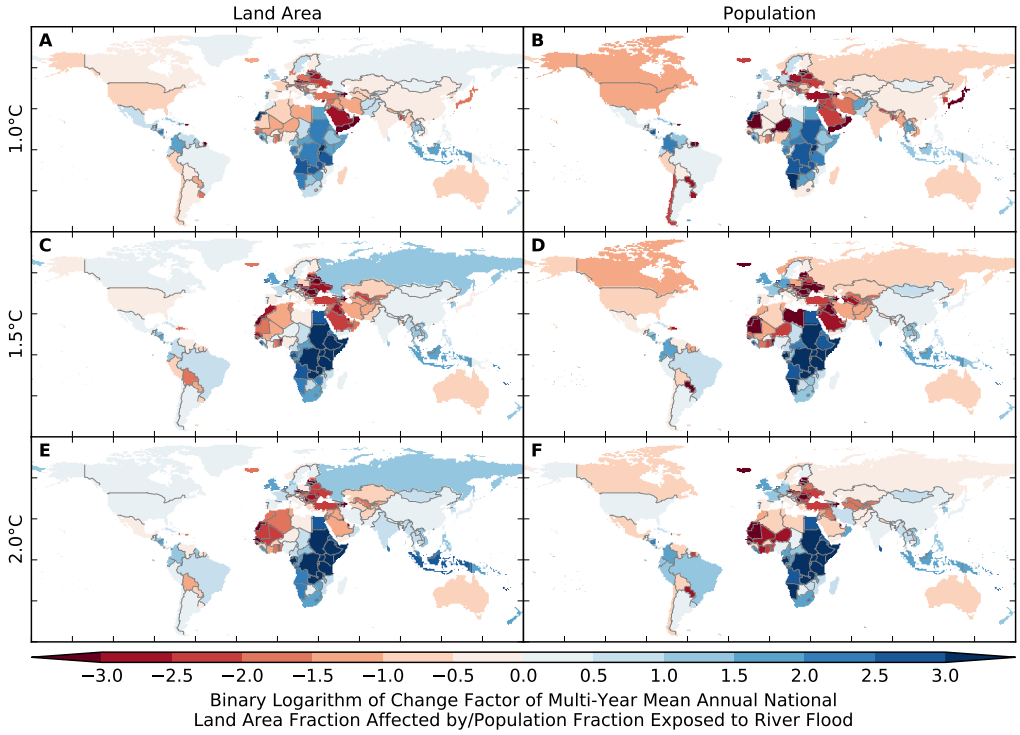

Figure S100: **Pure effect of climate change on annual national land area fraction affected by and population fraction exposed to river flood (IPSL-CM5A-LR + LPJmL).** Analogous to Figure S88.

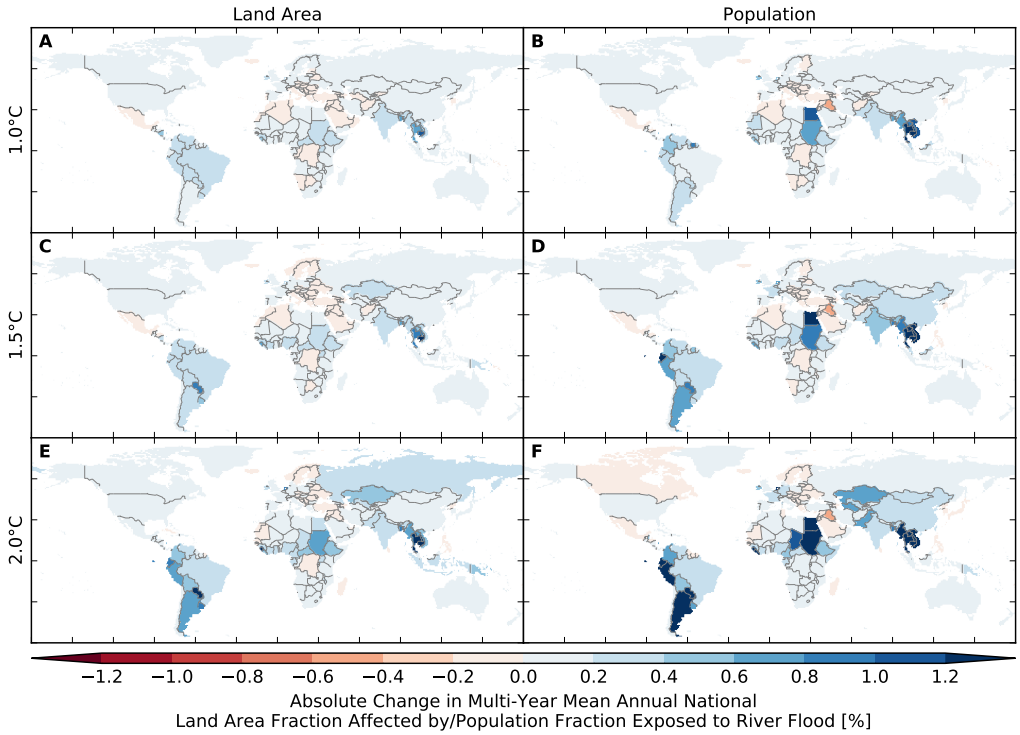

Figure S101: **Pure effect of climate change on annual national land area fraction affected by and population fraction exposed to river flood (MIROC5 + LPJmL).** Analogous to Figure S87.

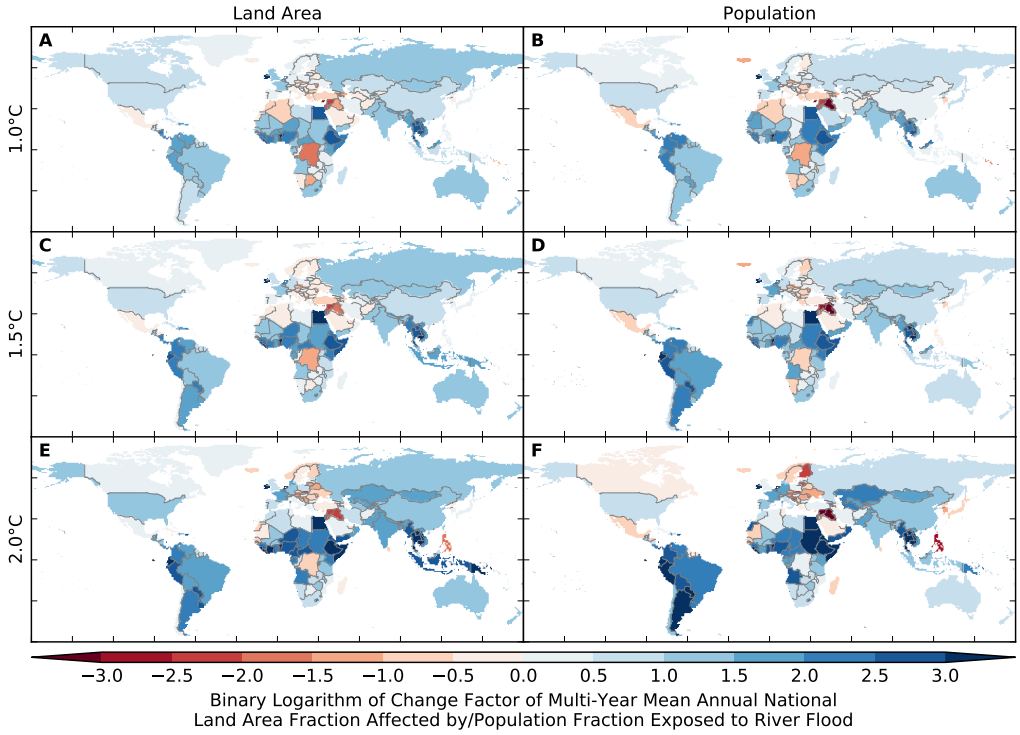

Figure S102: **Pure effect of climate change on annual national land area fraction affected by and population fraction exposed to river flood (MIROC5 + LPJmL).** Analogous to Figure S88.

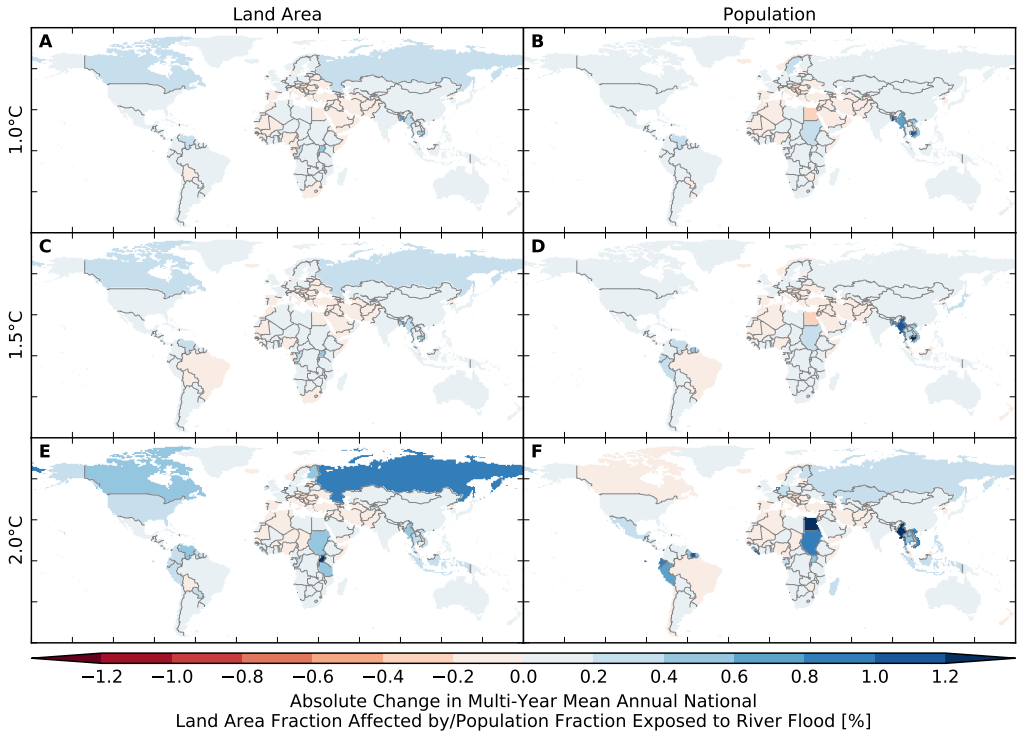

Figure S103: **Pure effect of climate change on annual national land area fraction affected by and population fraction exposed to river flood (GFDL-ESM2M + MPI-HM).** Analogous to Figure S87.

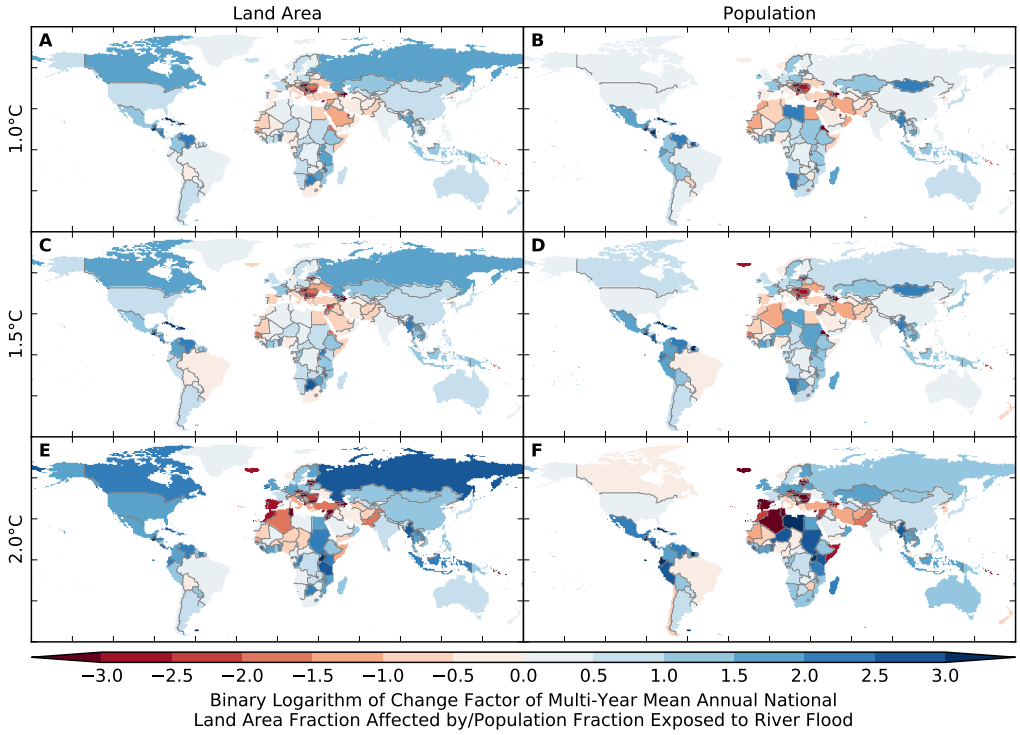

Figure S104: **Pure effect of climate change on annual national land area fraction affected by and population fraction exposed to river flood (GFDL-ESM2M + MPI-HM).** Analogous to Figure S88.

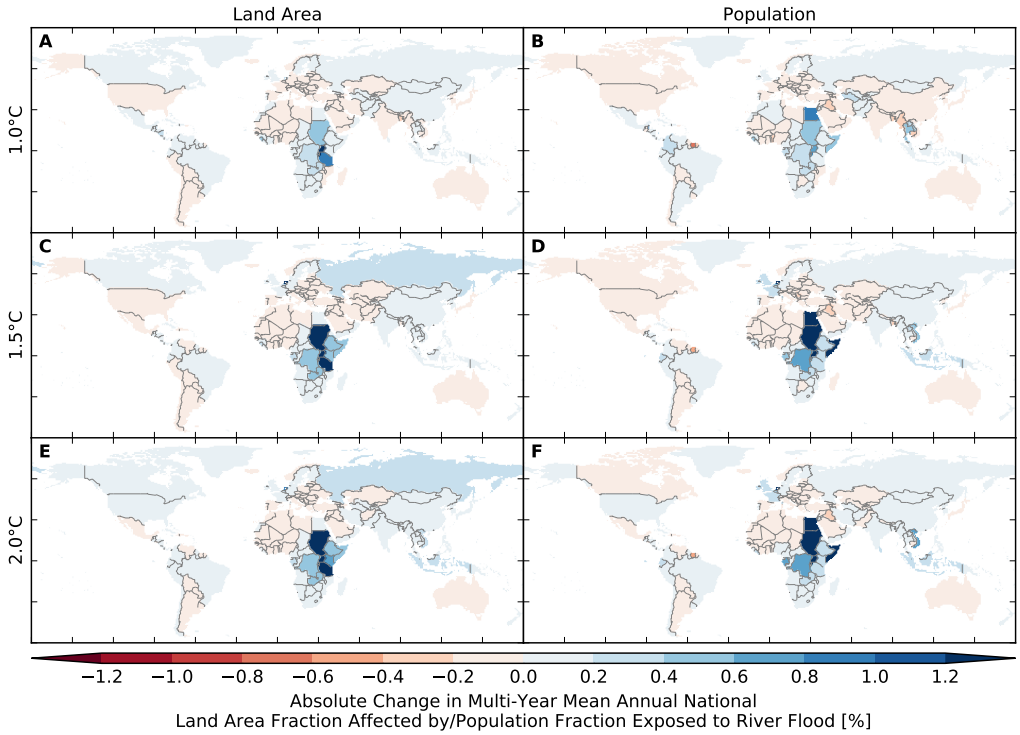

Figure S105: **Pure effect of climate change on annual national land area fraction affected by and population fraction exposed to river flood (IPSL-CM5A-LR + MPI-HM).** Analogous to Figure S87.

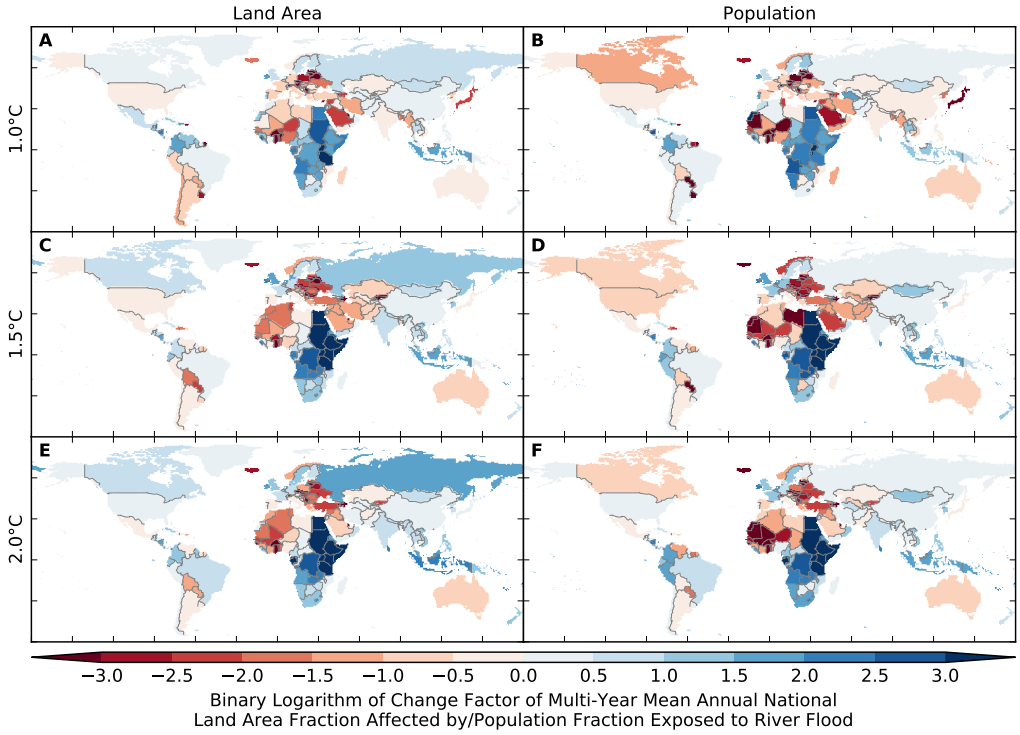

Figure S106: **Pure effect of climate change on annual national land area fraction affected by and population fraction exposed to river flood (IPSL-CM5A-LR + MPI-HM).** Analogous to Figure S88.

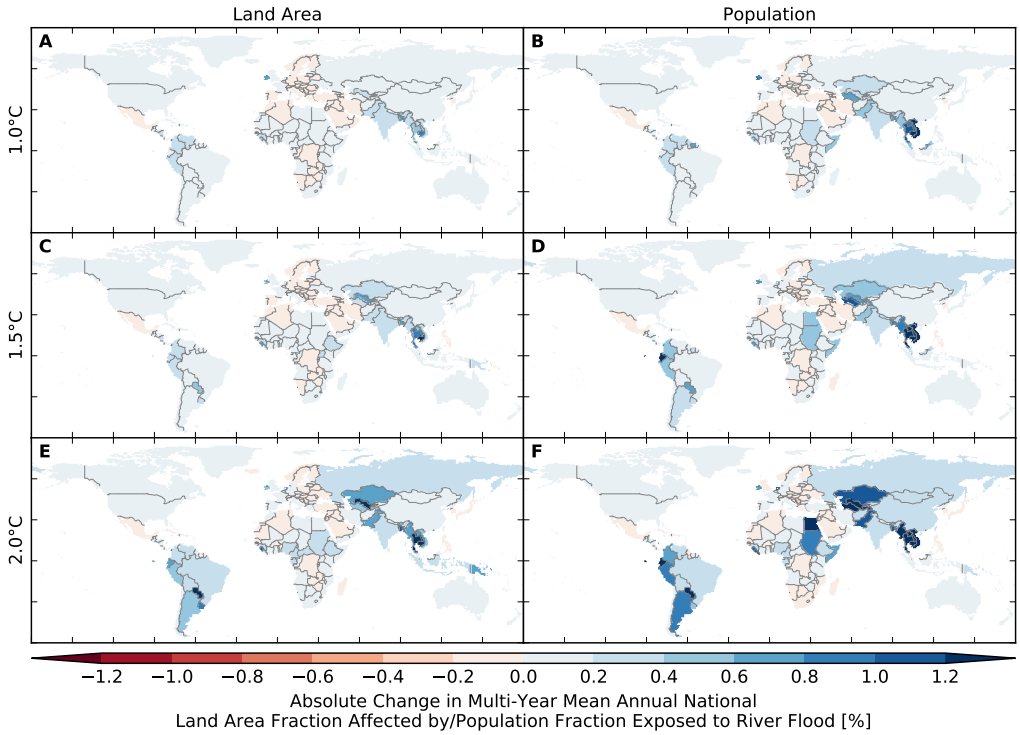

Figure S107: **Pure effect of climate change on annual national land area fraction affected by and population fraction exposed to river flood (MIROC5 + MPI-HM).** Analogous to Figure S87.

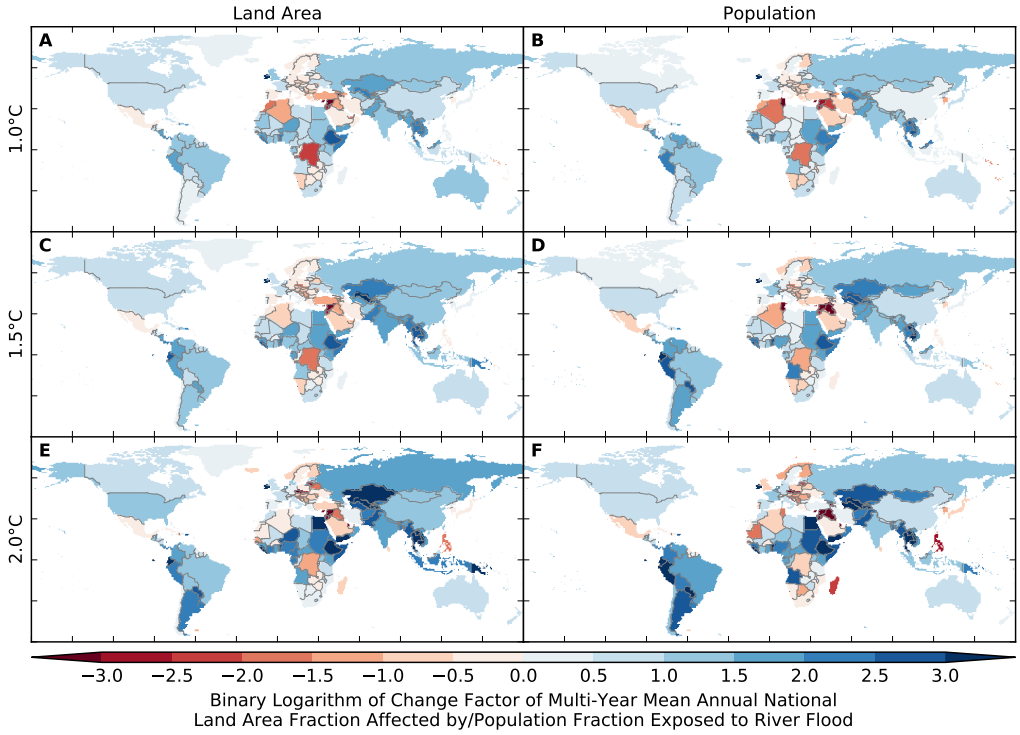

Figure S108: **Pure effect of climate change on annual national land area fraction affected by and population fraction exposed to river flood (MIROC5 + MPI-HM).** Analogous to Figure S88.

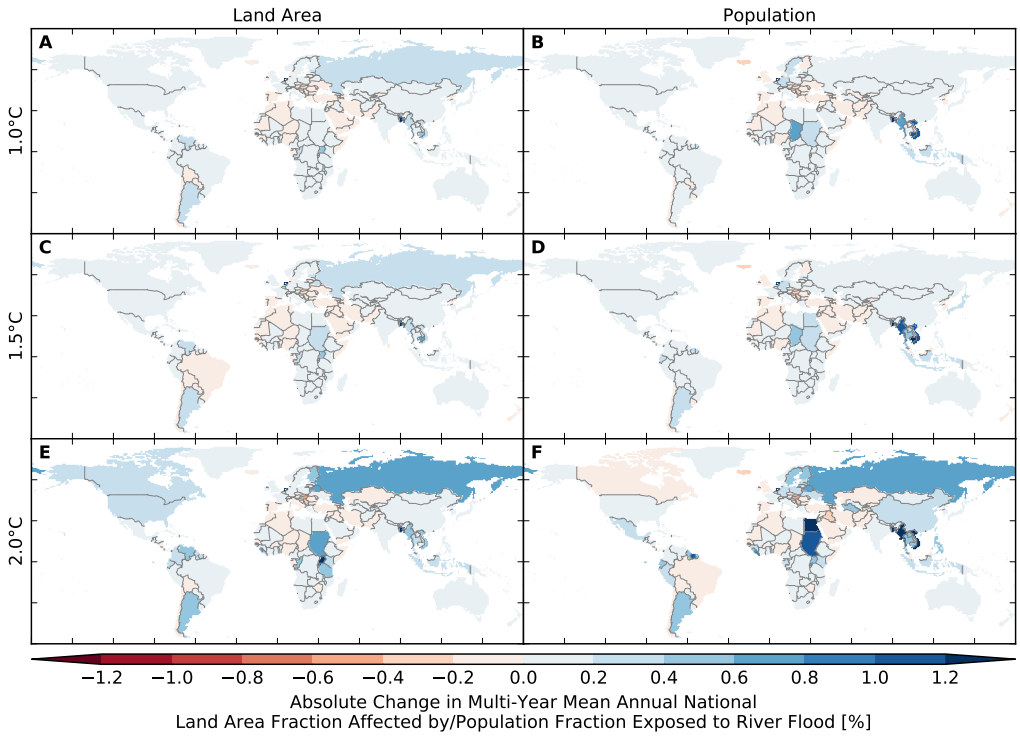

Figure S109: **Pure effect of climate change on annual national land area fraction affected by and population fraction exposed to river flood (GFDL-ESM2M + ORCHIDEE).** Analogous to Figure S87.

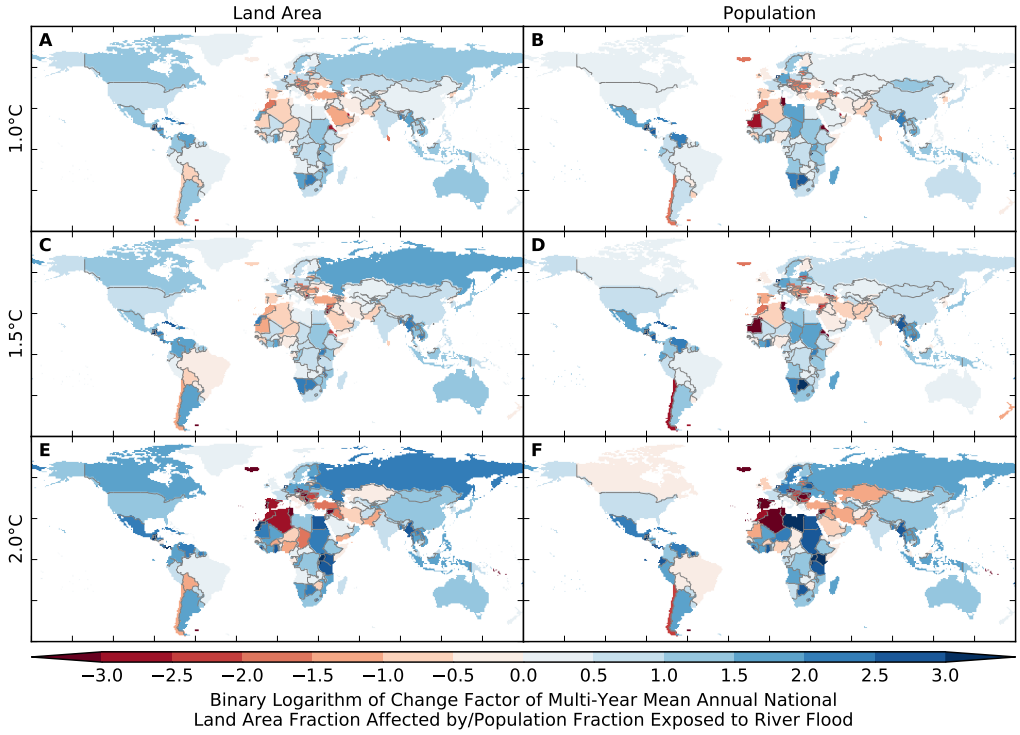

Figure S110: **Pure effect of climate change on annual national land area fraction affected by and population fraction exposed to river flood (GFDL-ESM2M + ORCHIDEE).** Analogous to Figure S88.

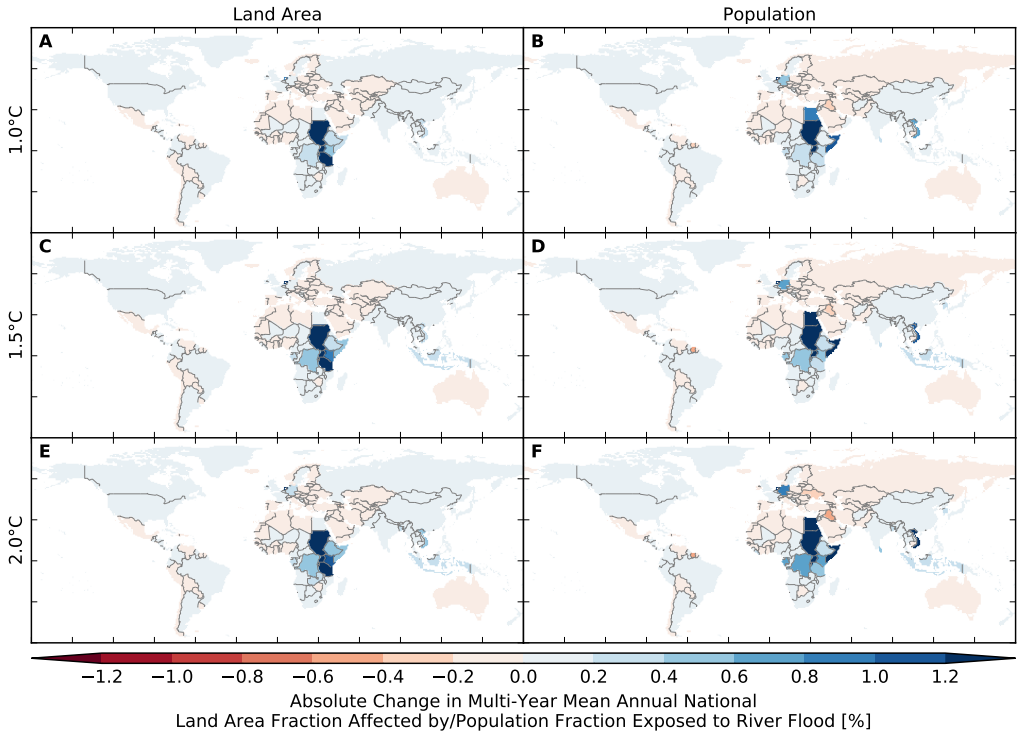

Figure S111: **Pure effect of climate change on annual national land area fraction affected by and population fraction exposed to river flood (IPSL-CM5A-LR + ORCHIDEE).** Analogous to Figure S87.

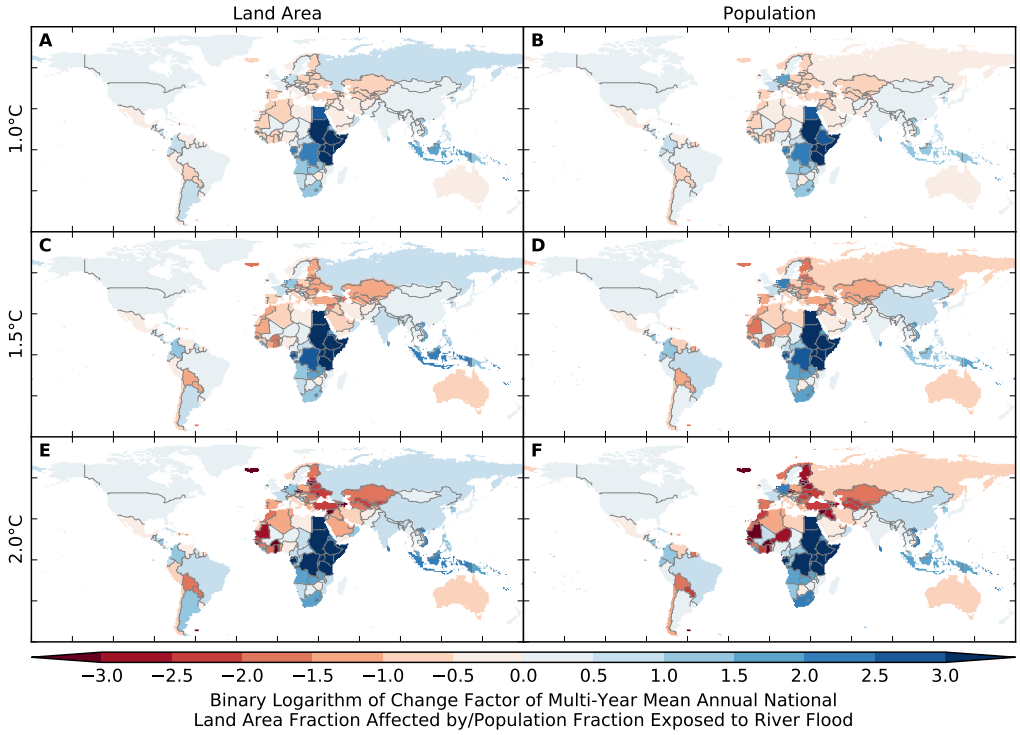

Figure S112: **Pure effect of climate change on annual national land area fraction affected by and population fraction exposed to river flood (IPSL-CM5A-LR + ORCHIDEE).** Analogous to Figure S88.

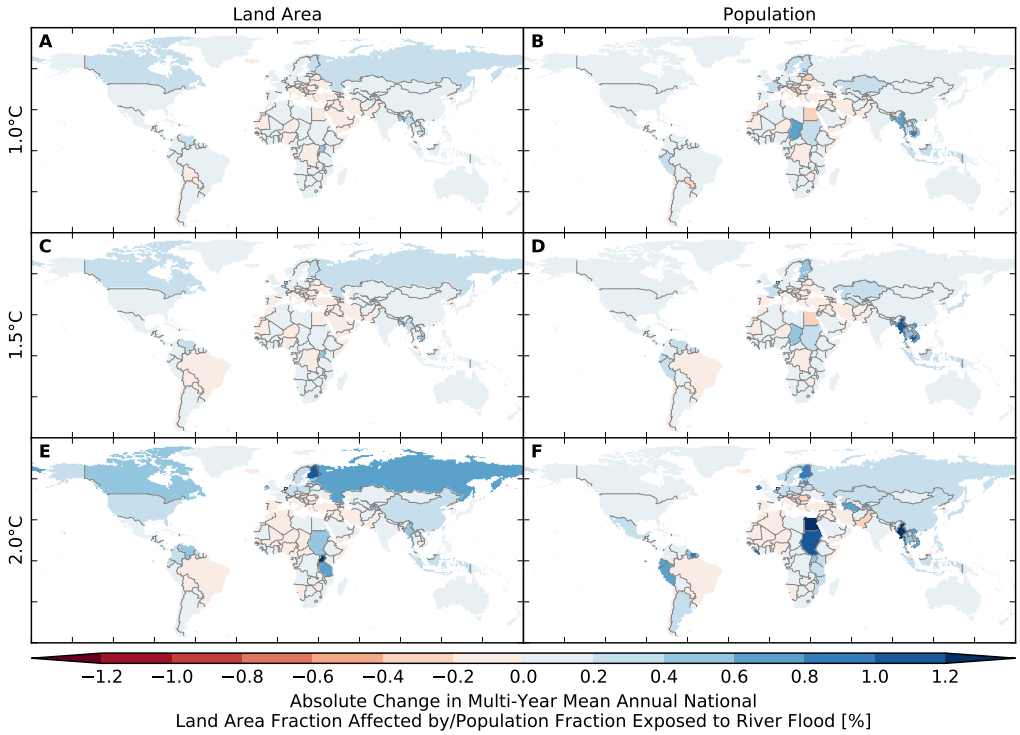

Figure S113: **Pure effect of climate change on annual national land area fraction affected by and population fraction exposed to river flood (GFDL-ESM2M + PCR-GLOBWB).** Analogous to Figure S87.

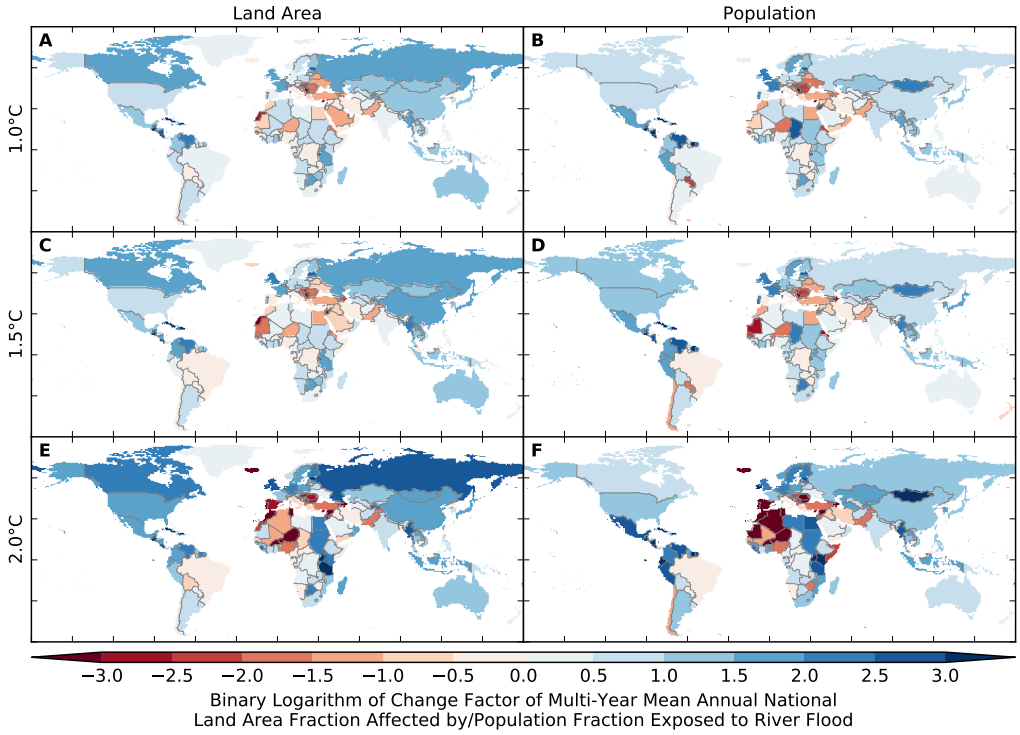

Figure S114: **Pure effect of climate change on annual national land area fraction affected by and population fraction exposed to river flood (GFDL-ESM2M + PCR-GLOBWB).** Analogous to Figure S88.

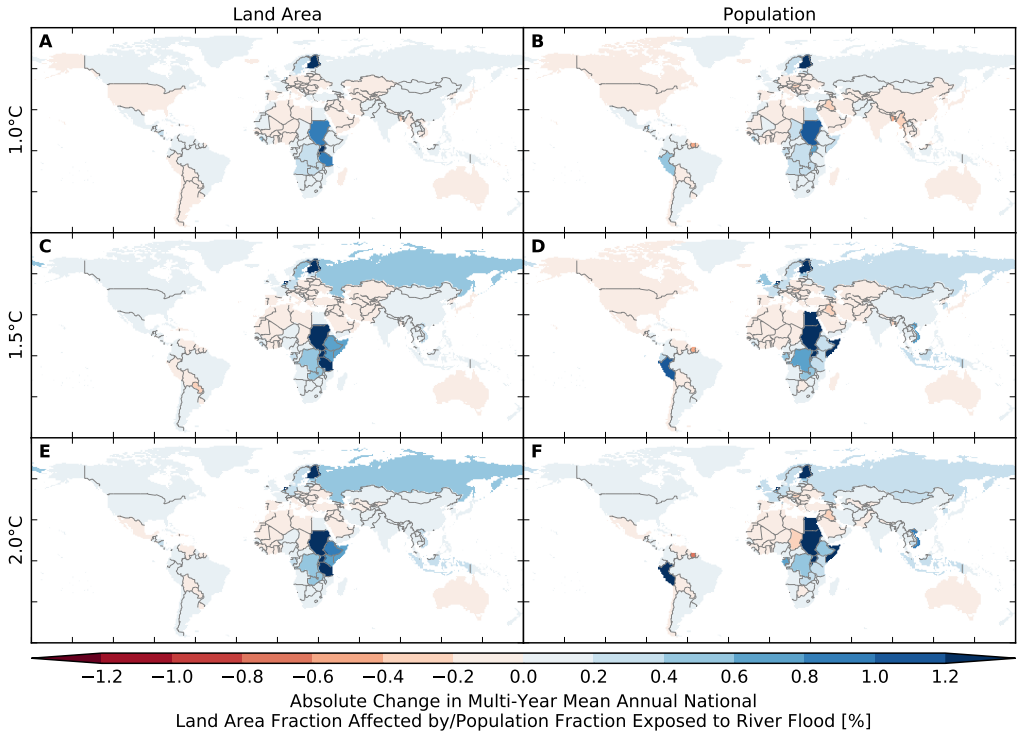

Figure S115: **Pure effect of climate change on annual national land area fraction affected by and population fraction exposed to river flood (IPSL-CM5A-LR + PCR-GLOBWB).** Analogous to Figure S87.

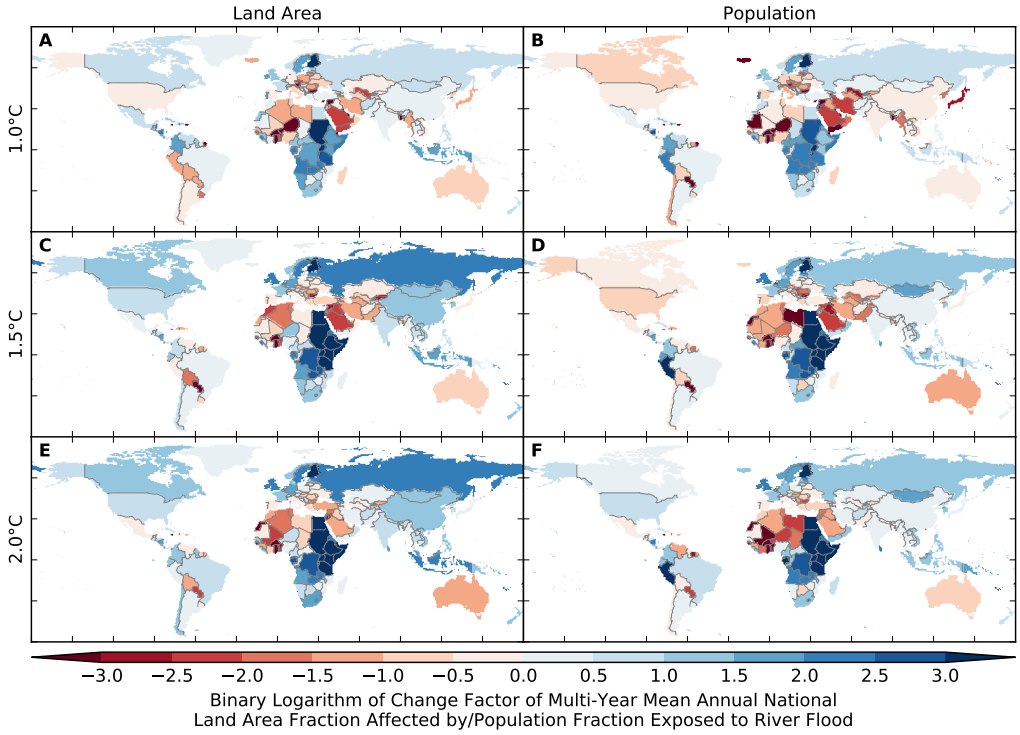

Figure S116: **Pure effect of climate change on annual national land area fraction affected by and population fraction exposed to river flood (IPSL-CM5A-LR + PCR-GLOBWB).** Analogous to Figure S88.

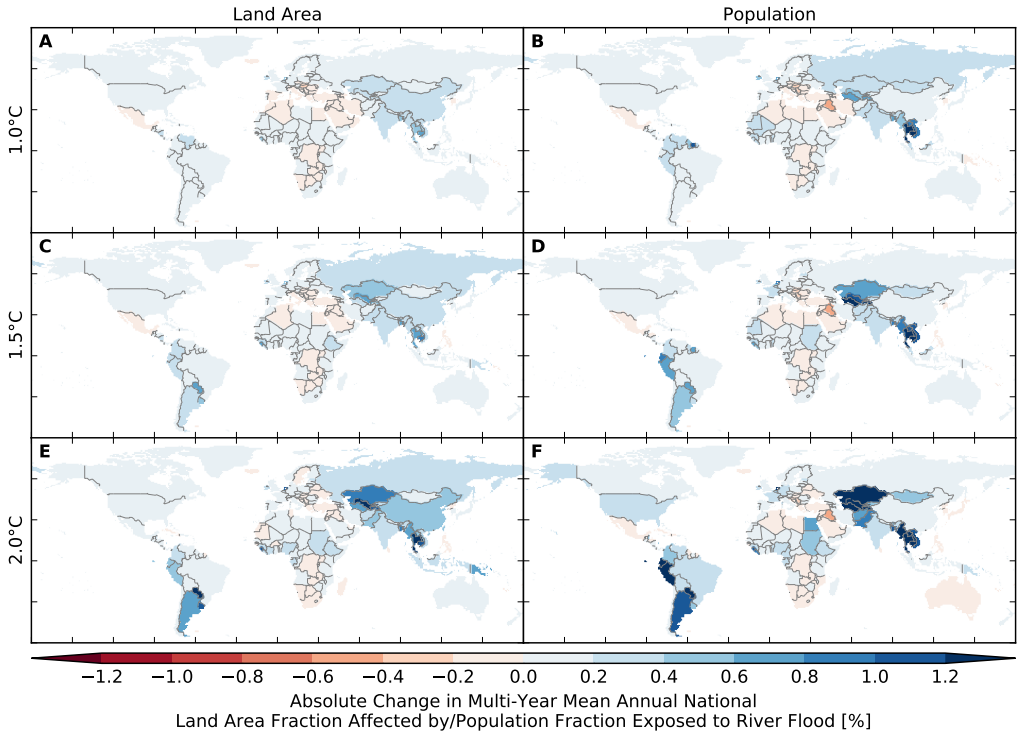

Figure S117: **Pure effect of climate change on annual national land area fraction affected by and population fraction exposed to river flood (MIROC5 + PCR-GLOBWB).** Analogous to Figure S87.

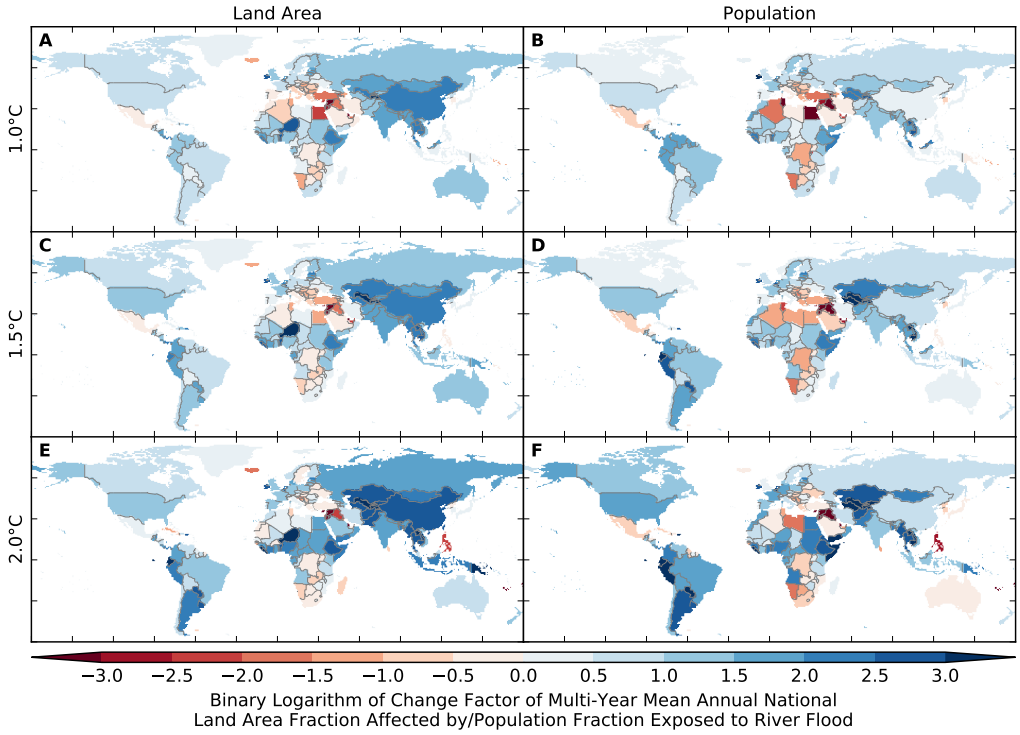

Figure S118: **Pure effect of climate change on annual national land area fraction affected by and population fraction exposed to river flood (MIROC5 + PCR-GLOBWB).** Analogous to Figure S88.

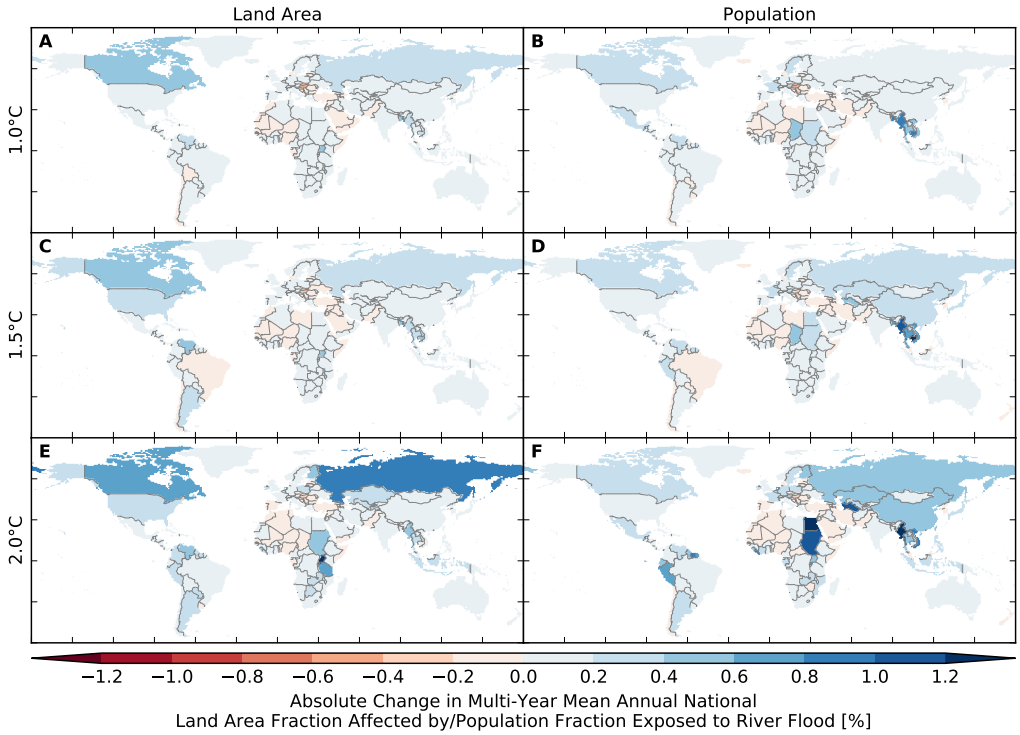

Figure S119: **Pure effect of climate change on annual national land area fraction affected by and population fraction exposed to river flood (GFDL-ESM2M + WaterGAP2).** Analogous to Figure S87.

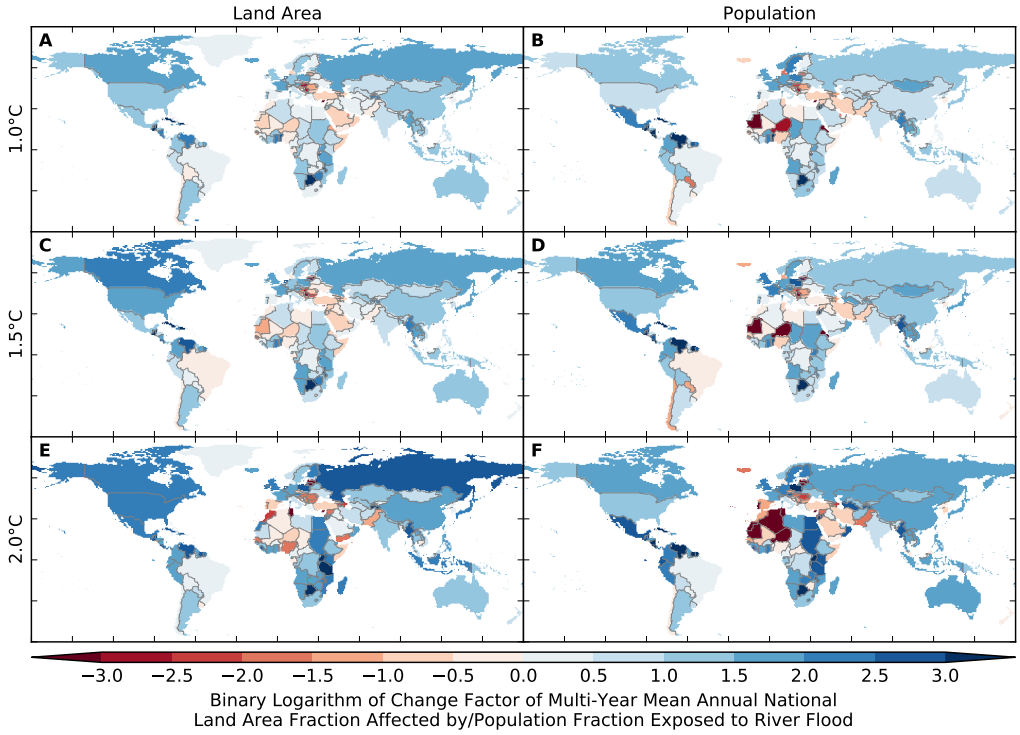

Figure S120: **Pure effect of climate change on annual national land area fraction affected by and population fraction exposed to river flood (GFDL-ESM2M + WaterGAP2).** Analogous to Figure S88.

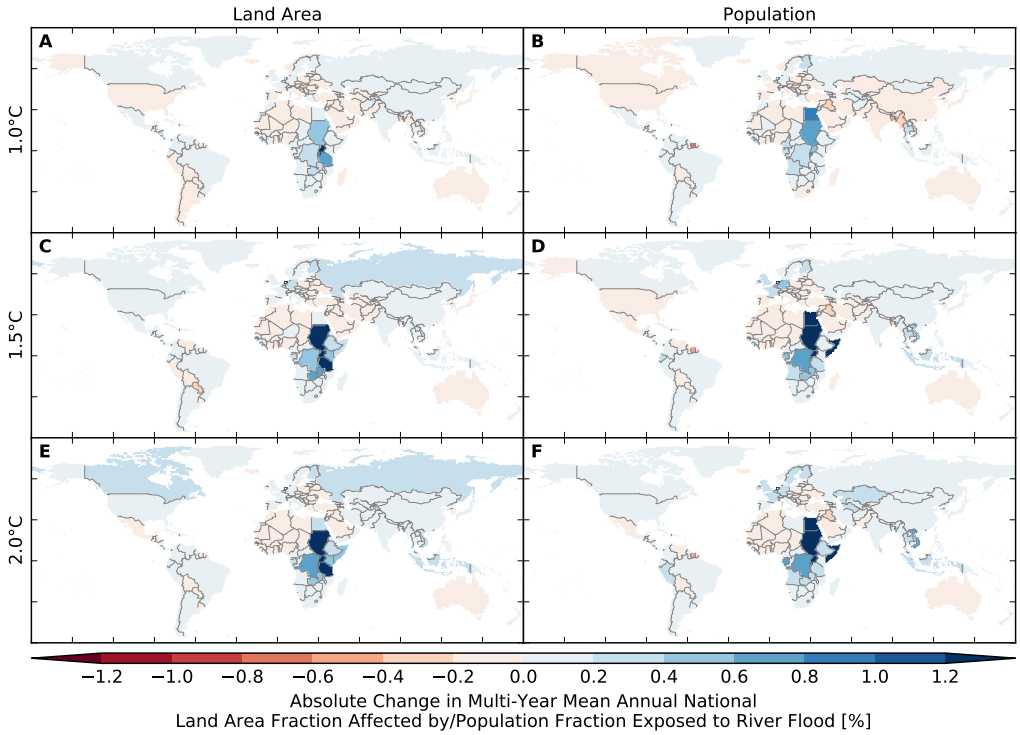

Figure S121: **Pure effect of climate change on annual national land area fraction affected by and population fraction exposed to river flood (IPSL-CM5A-LR + WaterGAP2).** Analogous to Figure S87.

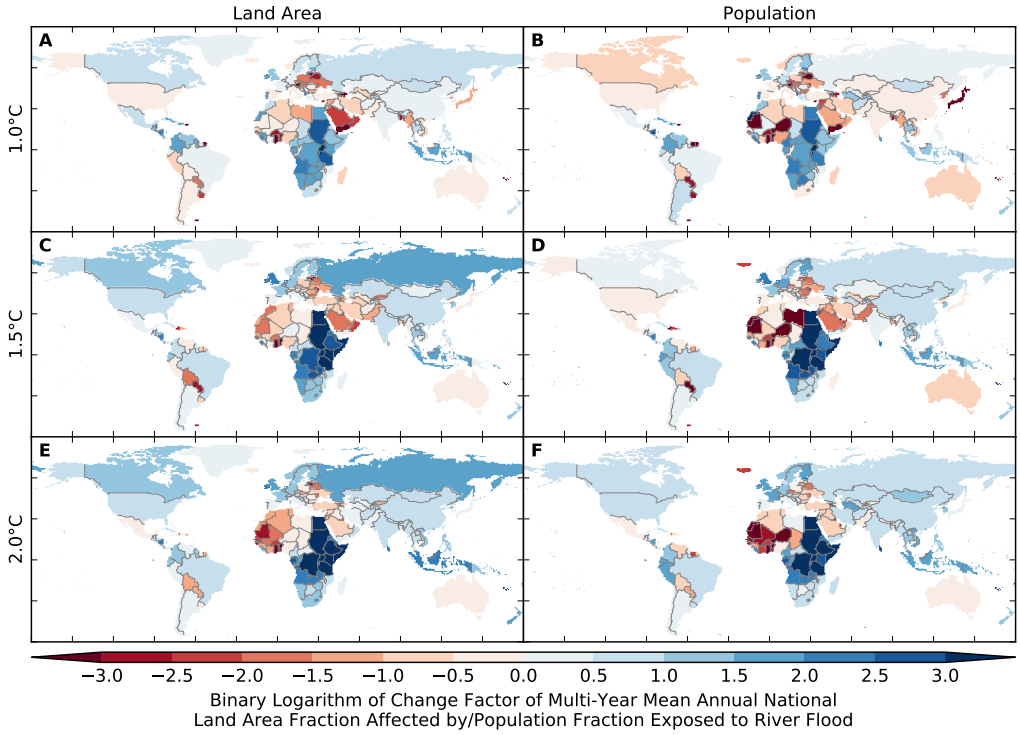

Figure S122: **Pure effect of climate change on annual national land area fraction affected by and population fraction exposed to river flood (IPSL-CM5A-LR + WaterGAP2).** Analogous to Figure S88.

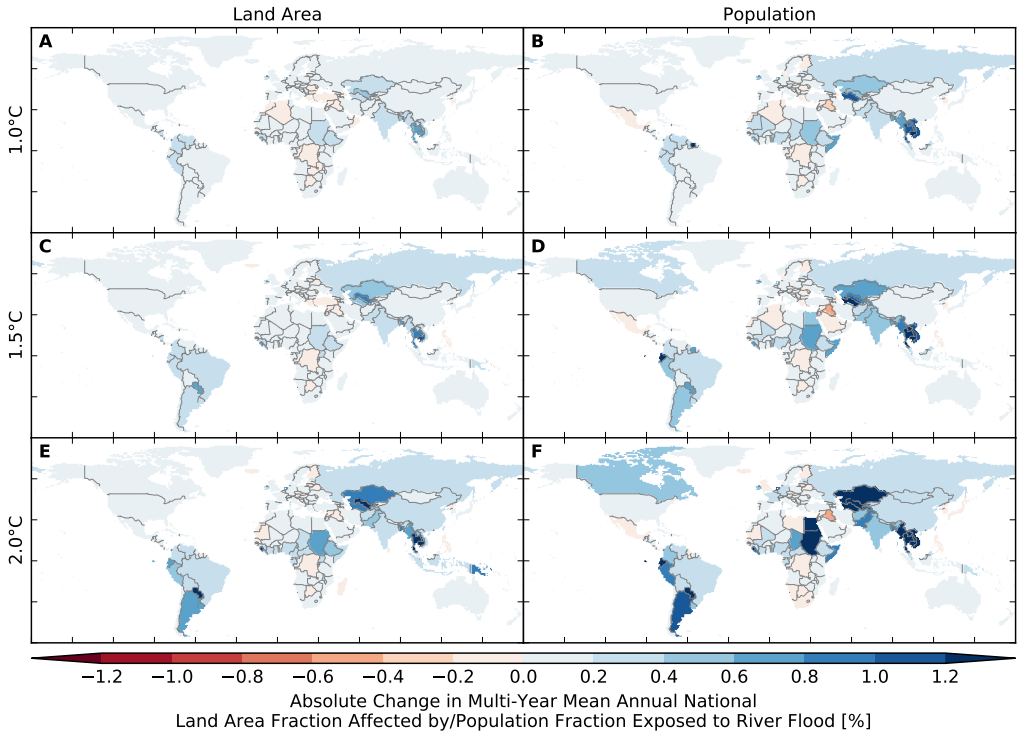

Figure S123: **Pure effect of climate change on annual national land area fraction affected by and population fraction exposed to river flood (MIROC5 + WaterGAP2).** Analogous to Figure S87.

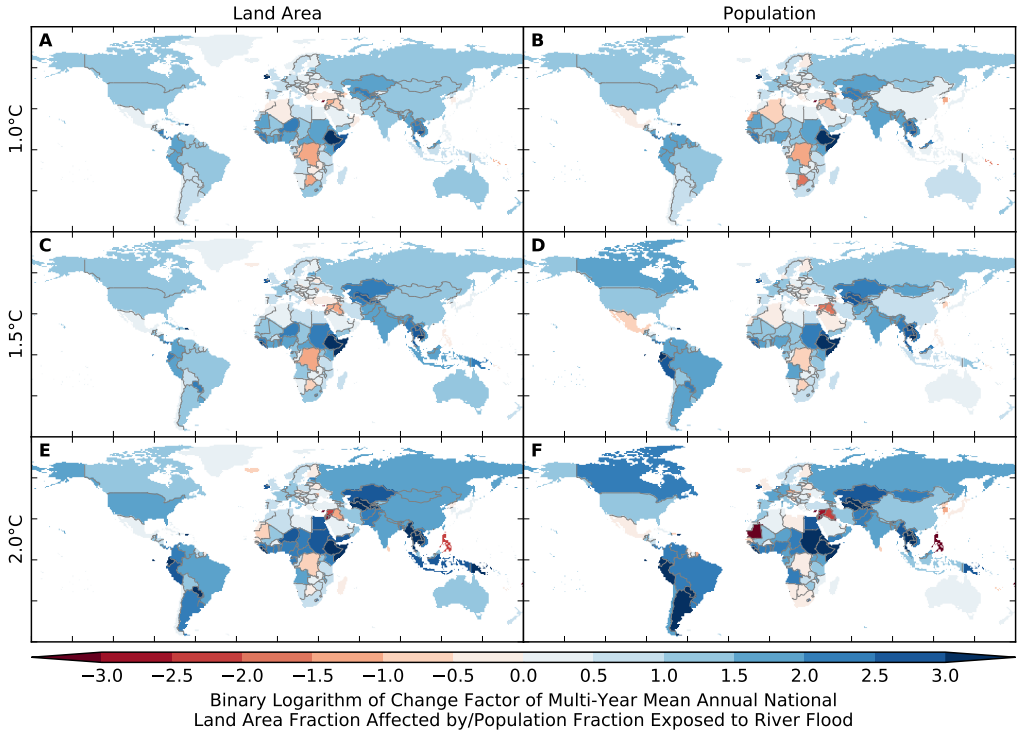

Figure S124: **Pure effect of climate change on annual national land area fraction affected by and population fraction exposed to river flood (MIROC5 + WaterGAP2).** Analogous to Figure S88.

9.2 Tropical cyclones

For tropical cyclones we provide 100 model realizations of the same model. Here we show one example, i.e. one realization for each GCM. Despite slight differences between different realizations, that account for the stochasticity of tropical cyclone impacts, we do not observe relevant realization-specific deviations that require a detailed discussion. All climate model-model realizations combinations are available on request.

Land area affected

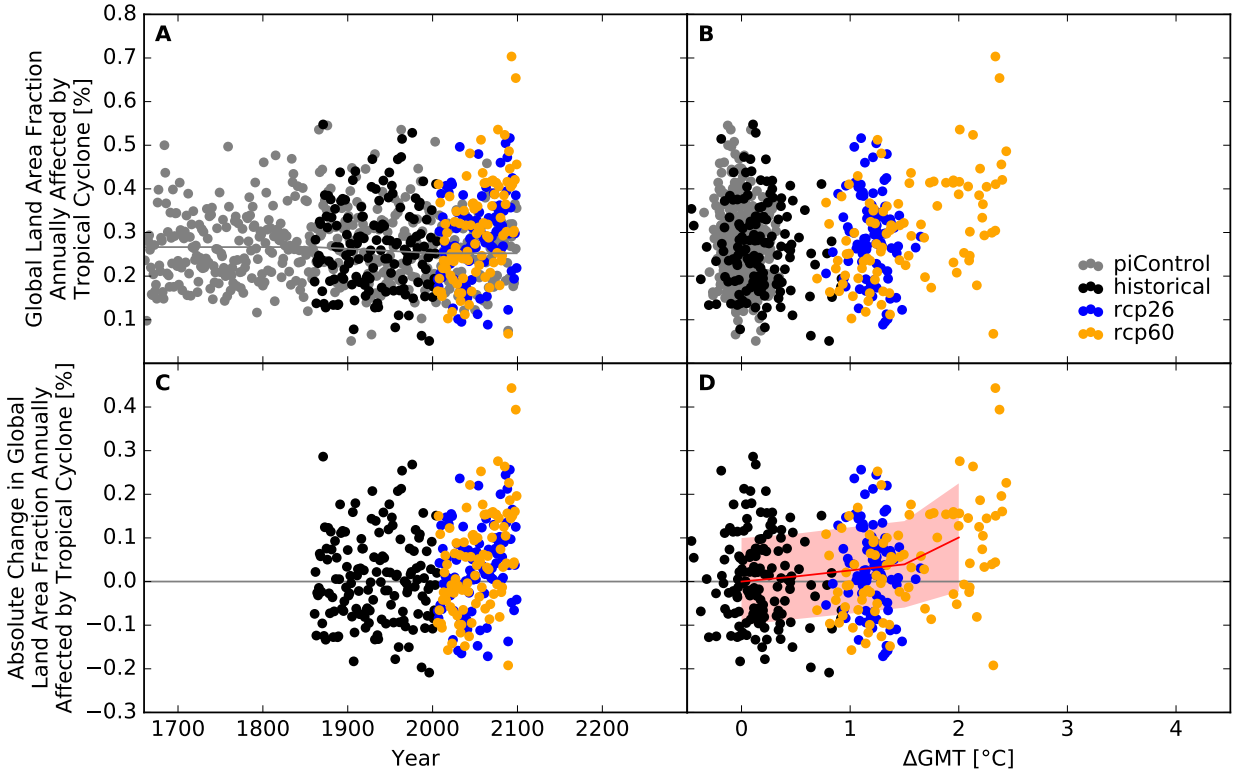

Figure S125: **Derivation of the pure effect of climate change on the global land area fraction annually affected by tropical cyclone (GFDL-ESM2M + KE-TG-001).** Panel A: Time series of annual global land area fraction affected (AFA) by tropical cyclone for preindustrial climate (grey dots), historical climate (black dots), climate projections for RCP2.6 (blue dots), and RCP6.0 (orange dots). In all simulations, socioeconomic conditions are varied according to the historically observed development between 1860 and 2005, and held fixed at 1860 conditions before 1860 and at 2005 conditions after 2005. The horizontal gray lines before 1860 and after 2005 represent the multi-year mean global land area fraction annually affected by tropical cyclone under preindustrial climate conditions and socioeconomic conditions of 1860 and 2005, respectively. The gray line between 1860 and 2005 is a linear interpolation of these mean values. Panel B: Data shown in Panel A plotted against the associated GCM-specific annual global mean temperature (GMT) change relative to the long-term preindustrial mean GMT. Panel C: Pure effect of climate change on AFA, calculated as the difference between the annual data shown in Panel A and the multi-year mean AFA under preindustrial climate conditions (gray line in Panel A). Panel D: Data shown in Panel C plotted against annual GMT change. The red line represents the mean values of the annual data points per 1 °C-wide GMT change bin, with bins centered at GMT change levels increasing from 0 °C to 4 °C in steps of 0.5 °C. The area shaded in red represents the mean value ±1 standard deviation ranges of the annual data points per GMT change bin.

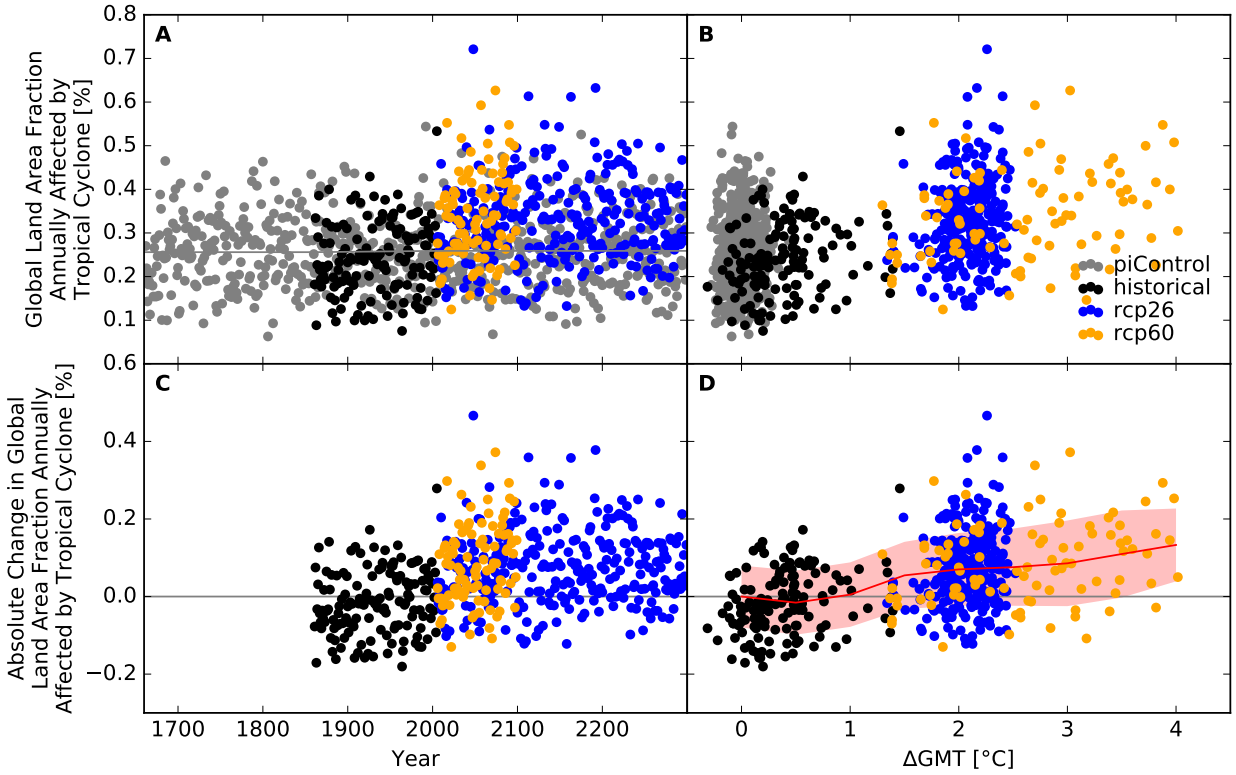

Figure S126: **Derivation of the pure effect of climate change on the global land area fraction annually affected by tropical cyclone (IPSL-CM5A-LR + KE-TG-001).** Analogous to Figure S125.

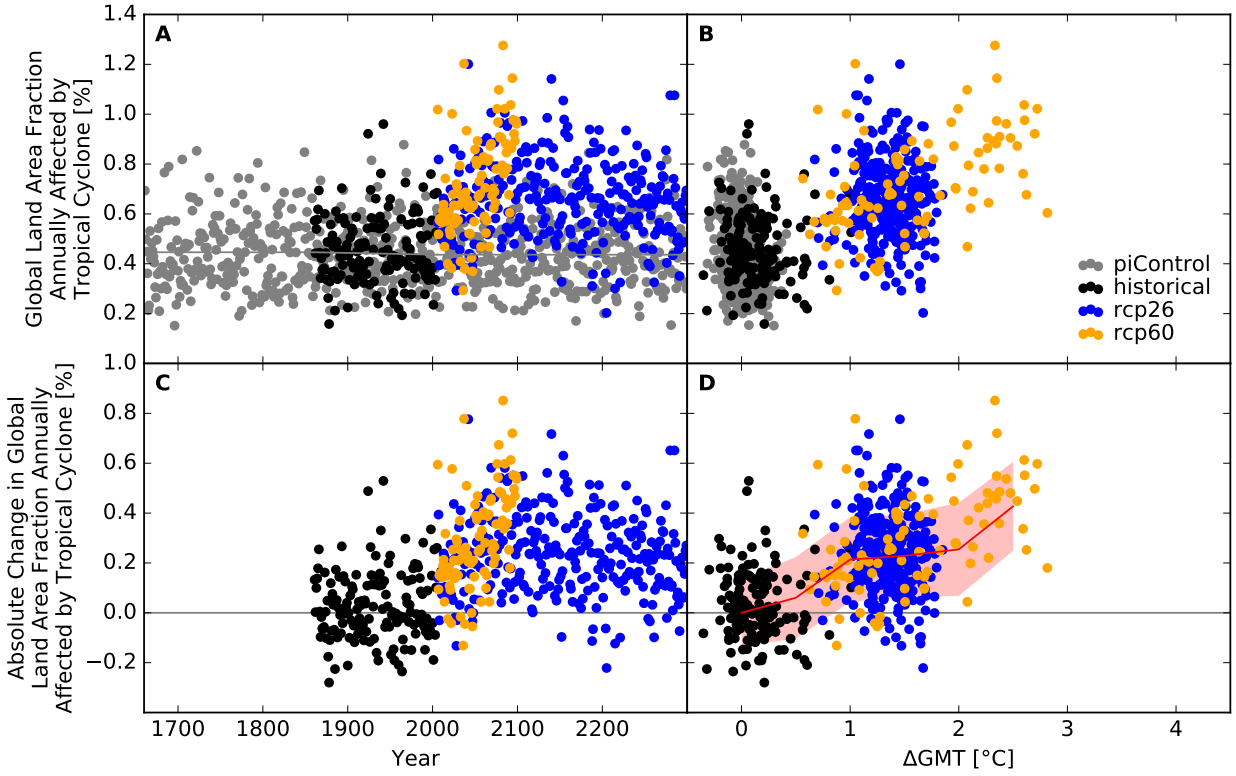

Figure S127: **Derivation of the pure effect of climate change on the global land area fraction annually affected by tropical cyclone (MIROC5 + KE-TG-001).** Analogous to Figure S125.

Number of people exposed

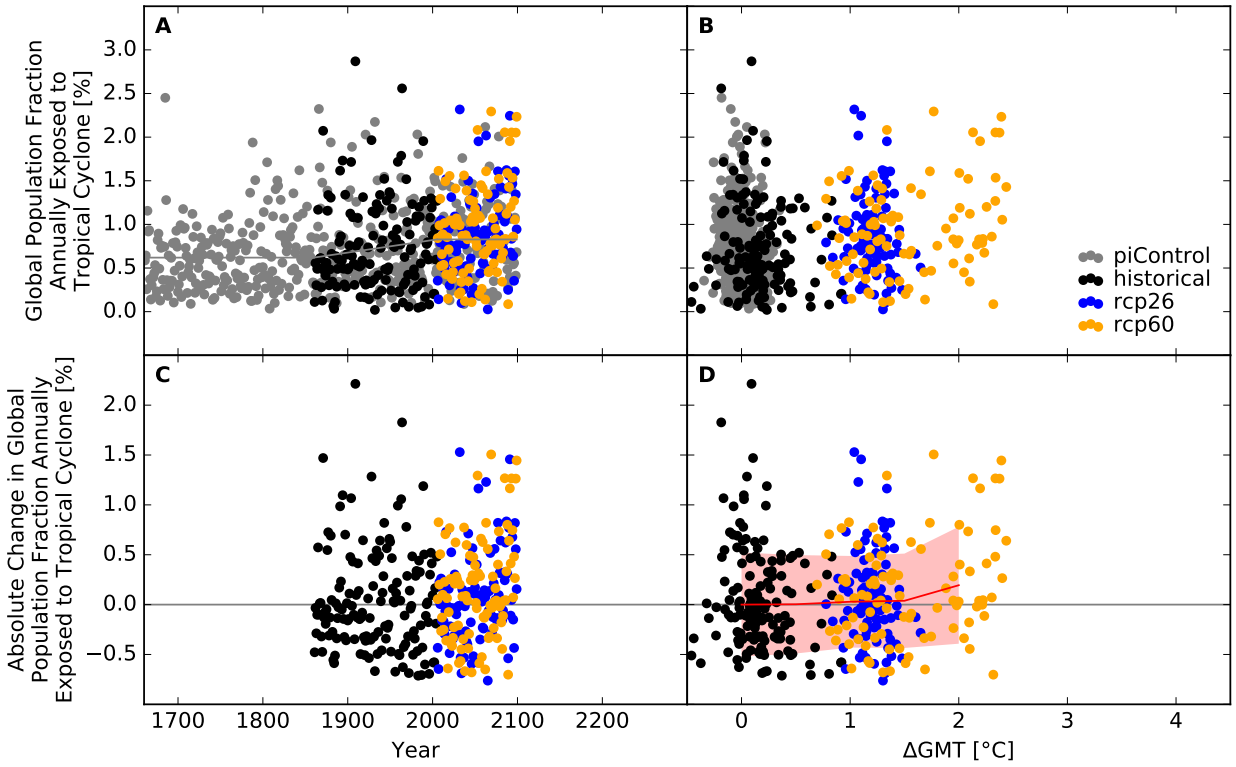

Figure S128: **Derivation of the pure effect of climate change on the global population fraction annually exposed to tropical cyclone (GFDL-ESM2M + KE-TG-001).** Panel A: Time series of annual global population fraction exposed (PFE) to tropical cyclone for preindustrial climate (grey dots), historical climate (black dots), climate projections for RCP2.6 (blue dots), and RCP6.0 (orange dots). In all simulations, socioeconomic conditions are varied according to the historically observed development between 1860 and 2005, and held fixed at 1860 conditions before 1860 and at 2005 conditions after 2005. The horizontal gray lines before 1860 and after 2005 represent the multi-year mean global population fraction annually exposed to tropical cyclone under preindustrial climate conditions and socioeconomic conditions of 1860 and 2005, respectively. The gray line between 1860 and 2005 is a linear interpolation of these mean values. Panel B: Data shown in Panel A plotted against the associated GCM-specific annual global mean temperature (GMT) change relative to the long-term preindustrial mean GMT. Panel C: Pure effect of climate change on PFE, calculated as the difference between the annual data shown in Panel A and the multi-year mean PFE under preindustrial climate conditions (gray line in Panel A). Panel D: Data shown in Panel C plotted against annual GMT change. The red line represents the mean values of the annual data points per 1 °C-wide GMT change bin, with bins centered at GMT change levels increasing from 0 °C to 4 °C in steps of 0.5 °C. The area shaded in red represents the mean value ±1 standard deviation ranges of the annual data points per GMT change bin.

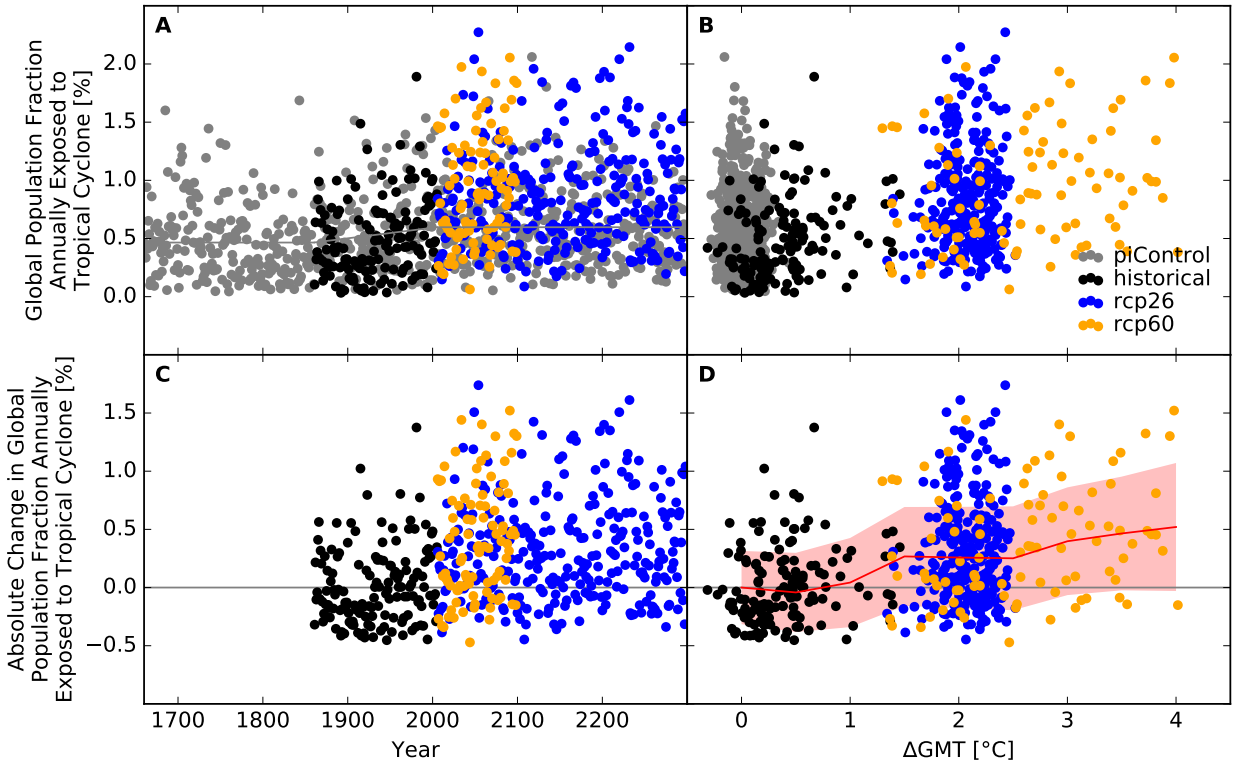

Figure S129: **Derivation of the pure effect of climate change on the global population fraction annually exposed to tropical cyclone (IPSL-CM5A-LR + KE-TG-001).** Analogous to Figure S128.

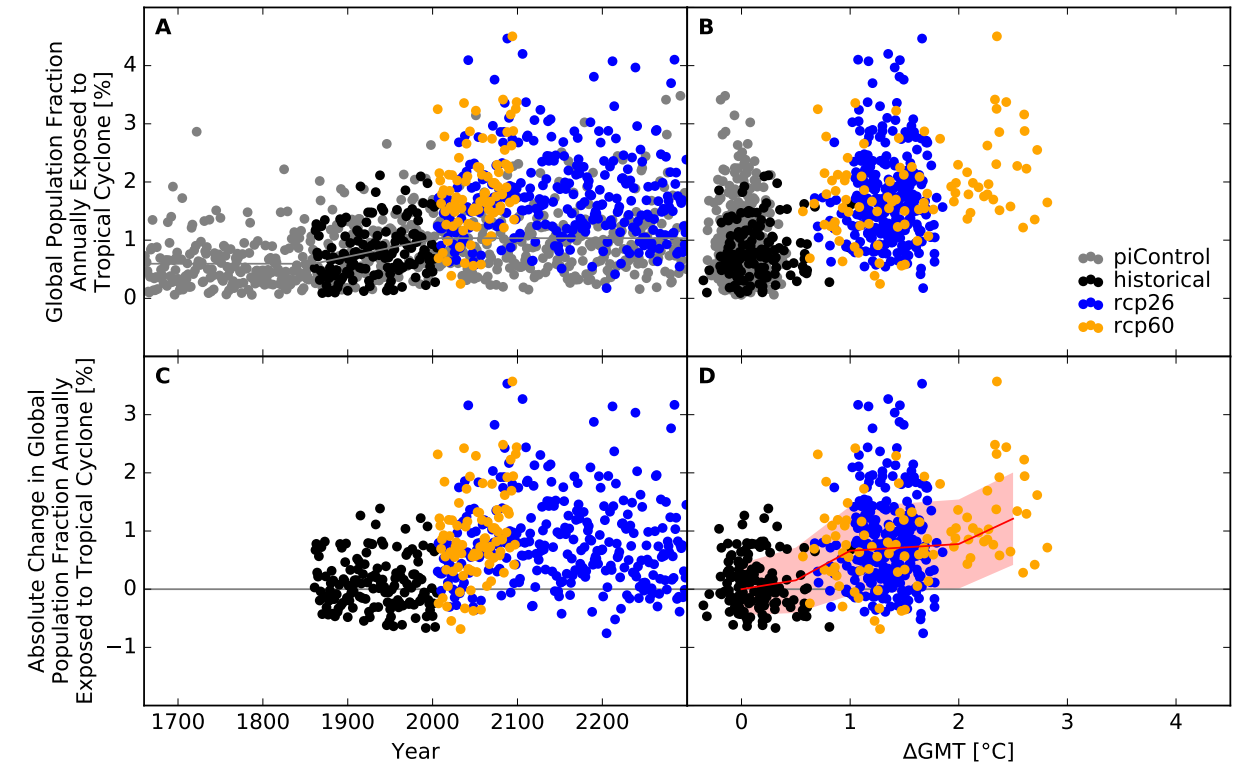

Figure S130: **Derivation of the pure effect of climate change on the global population fraction annually exposed to tropical cyclone (MIROC5 + KE-TG-001).** Analogous to Figure S128.

Land area affected and number of people exposed at the national scale

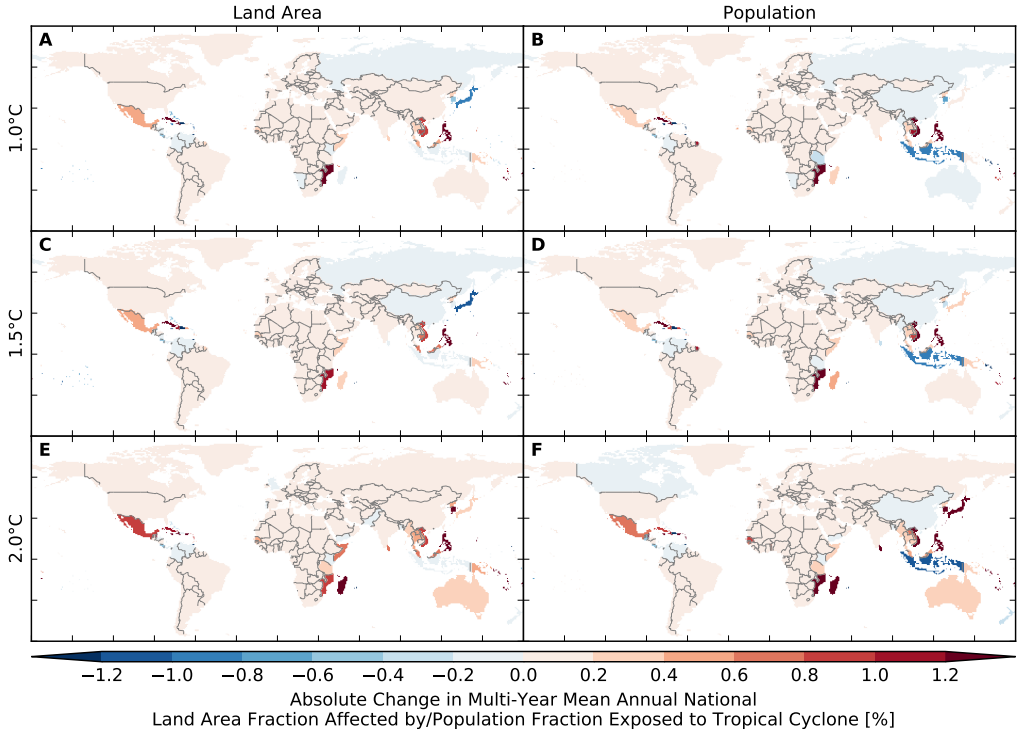

Figure S131: **Pure effect of climate change on annual national land area fraction affected by and population fraction exposed to tropical cyclone (GFDL-ESM2M + KE-TG-001).** Absolute changes in multi-year mean annual national (A, C, E) land area fraction affected by and (B, D, F) population fraction exposed to tropical cyclone at (A, B) 1 °C, (C, D) 1.5 °C and (E, F) 2 °C global warming.

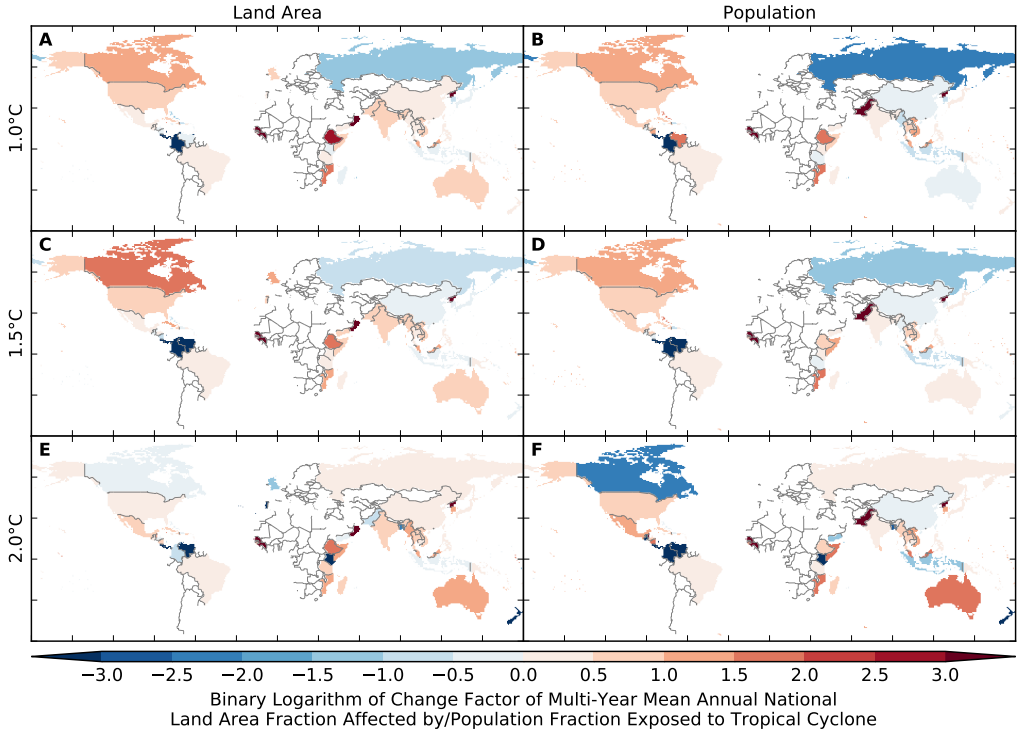

Figure S132: **Pure effect of climate change on annual national land area fraction affected by and population fraction exposed to tropical cyclone (GFDL-ESM2M + KE-TG-001).** Same as Figure S131 but for relative changes expressed in terms of binary logarithms of change factors, i.e. −1 means a change by a factor of 0.5, 0 means no change, and 1 means a change by a factor of 2. White indicates undefined relative changes due to division by zero.

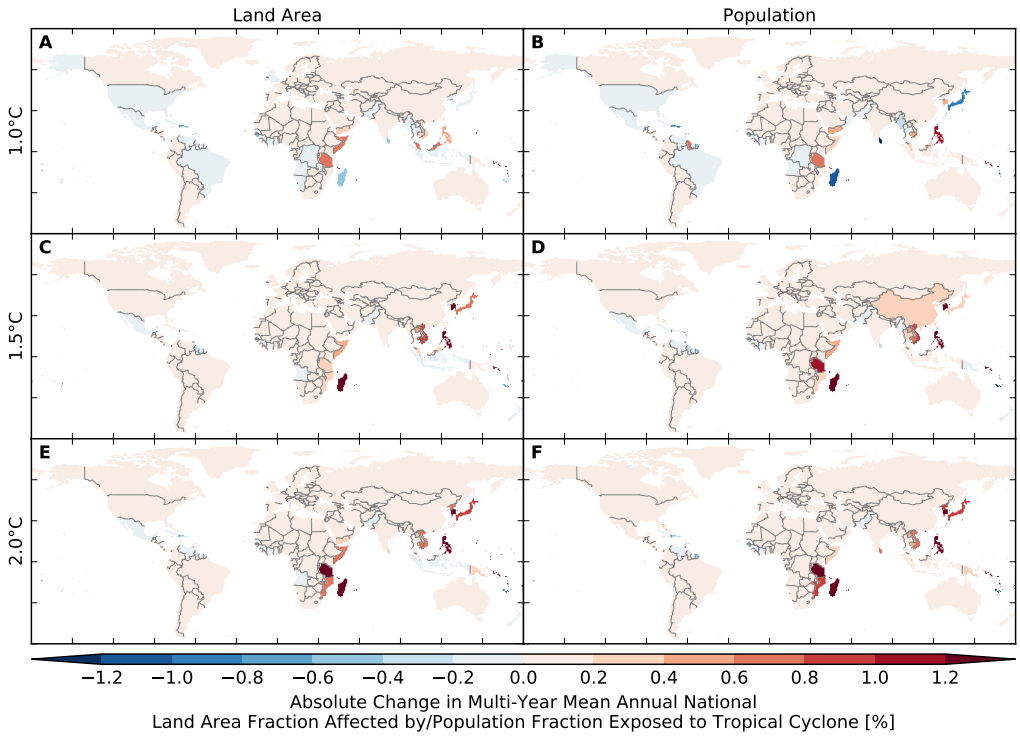

Figure S133: **Pure effect of climate change on annual national land area fraction affected by and population fraction exposed to tropical cyclone (IPSL-CM5A-LR + KE-TG-001).** Analogous to Figure S131.

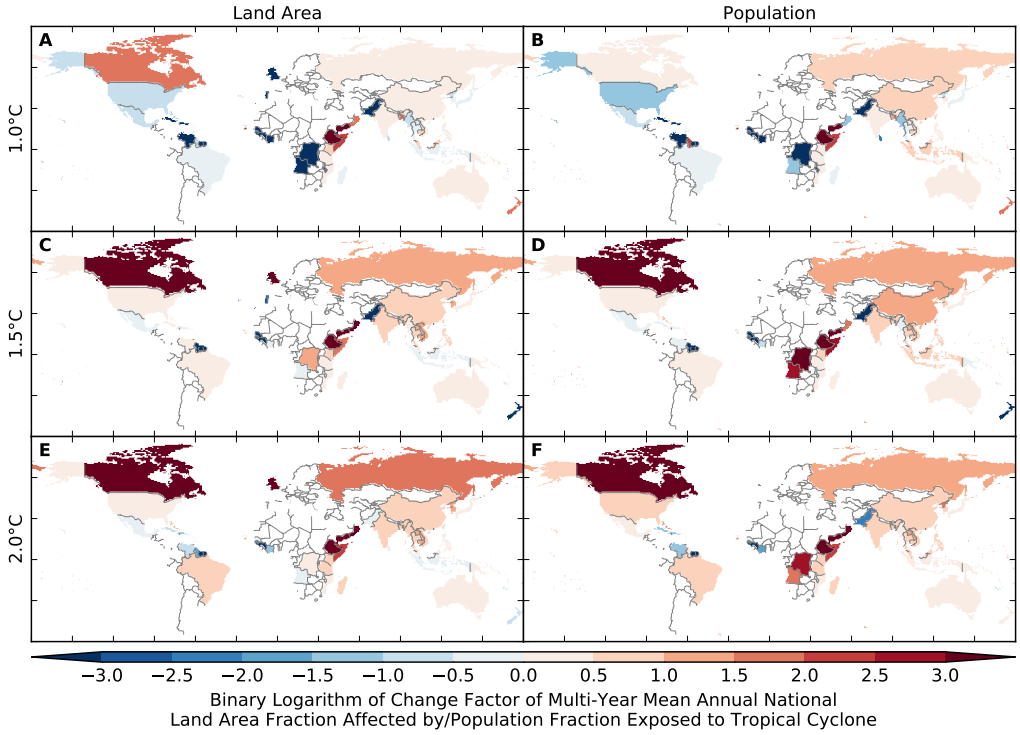

Figure S134: **Pure effect of climate change on annual national land area fraction affected by and population fraction exposed to tropical cyclone (IPSL-CM5A-LR + KE-TG-001).** Analogous to Figure S132.

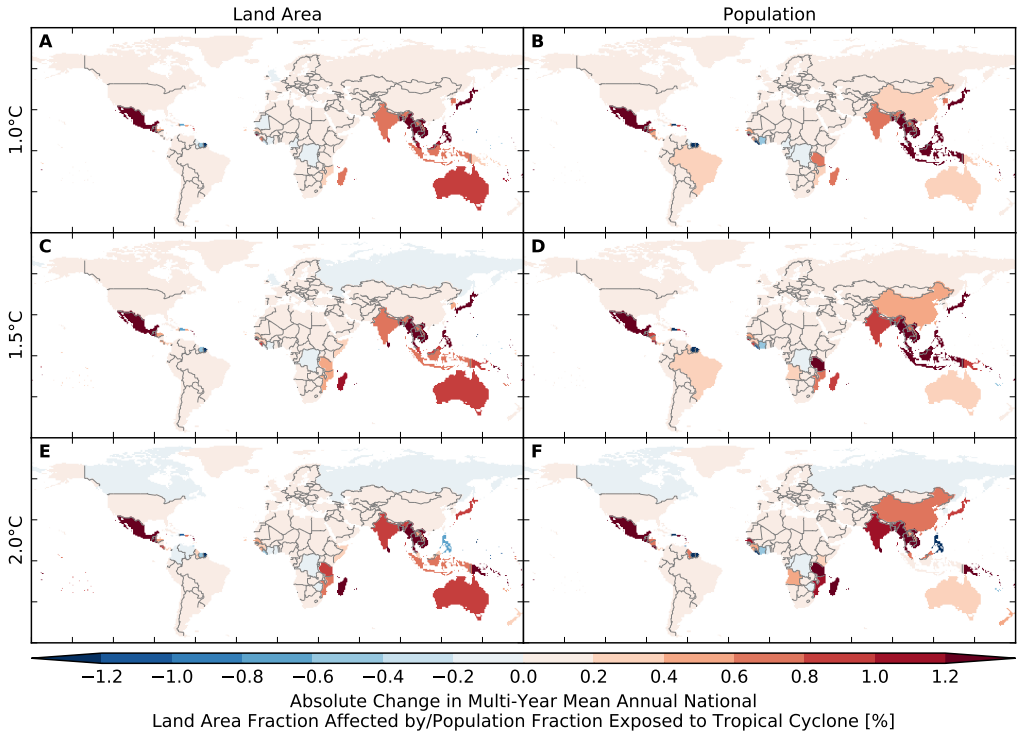

Figure S135: **Pure effect of climate change on annual national land area fraction affected by and population fraction exposed to tropical cyclone (MIROC5 + KE-TG-001).** Analogous to Figure S131.

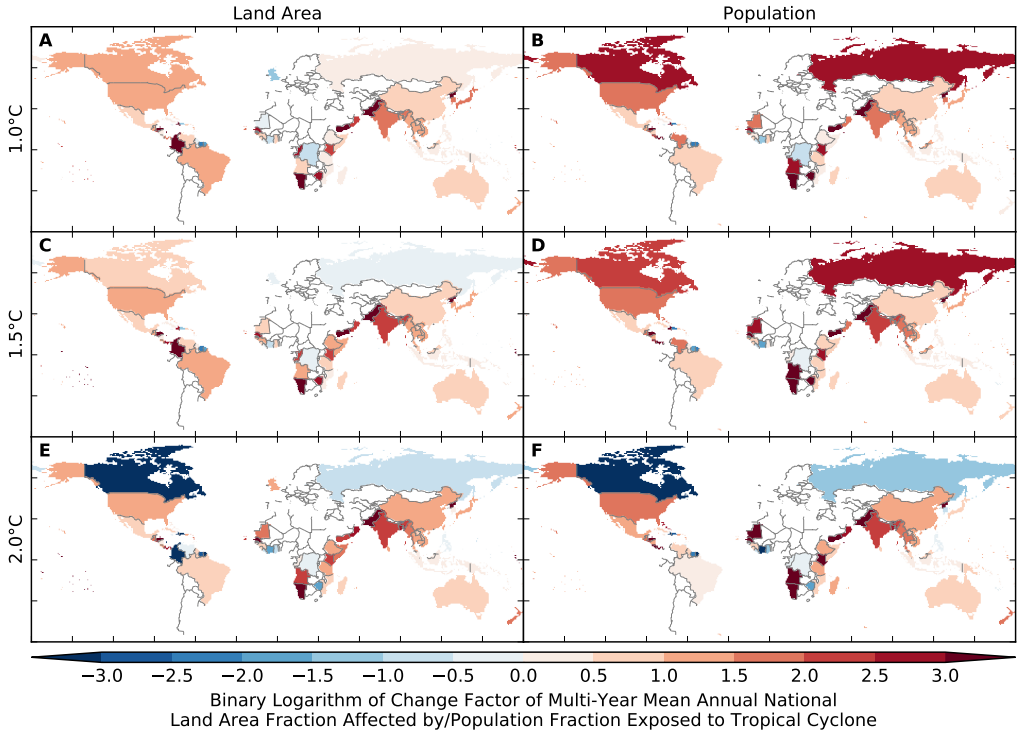

Figure S136: **Pure effect of climate change on annual national land area fraction affected by and population fraction exposed to tropical cyclone (MIROC5 + KE-TG-001).** Analogous to Figure S132.

9.3 Crop failure

Land area affected

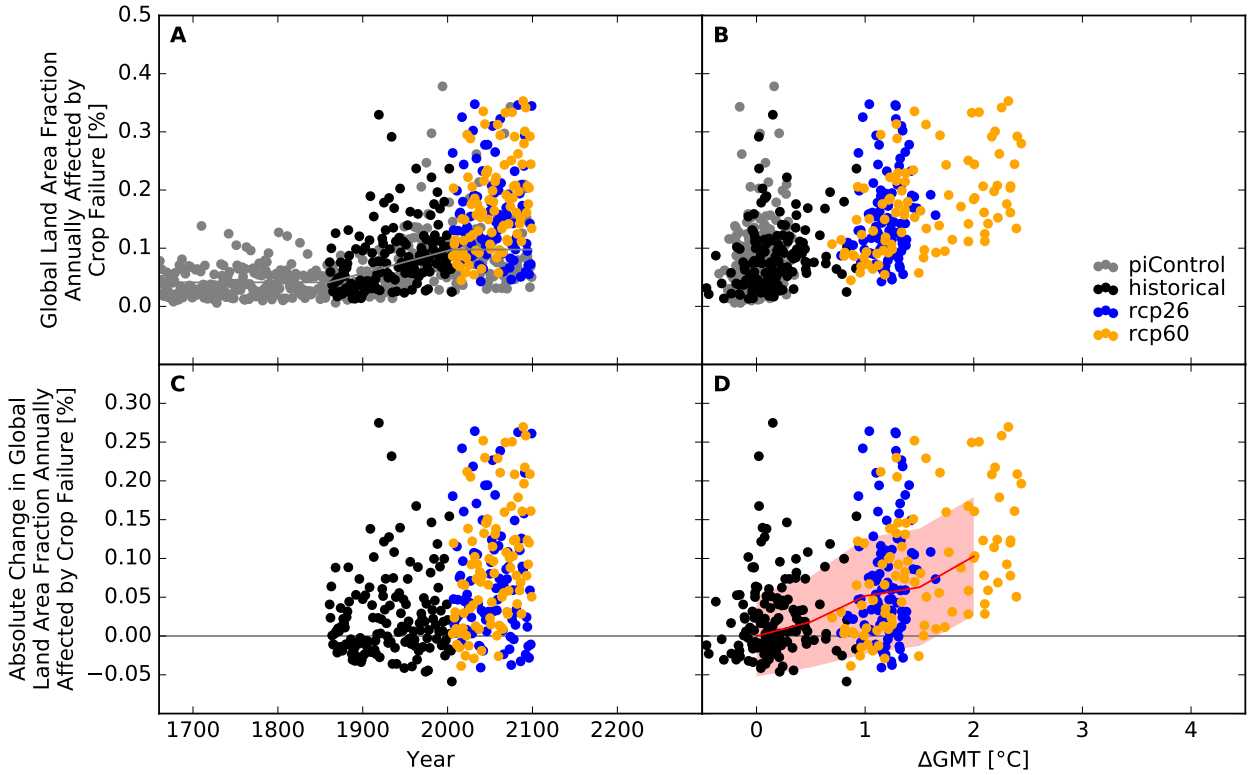

Figure S137: **Derivation of the pure effect of climate change on the global land area fraction annually affected by crop failure (GFDL-ESM2M + GEPIC).** Panel A: Time series of annual global land area fraction affected (AFA) by crop failure for preindustrial climate (grey dots), historical climate (black dots), climate projections for RCP2.6 (blue dots), and RCP6.0 (orange dots). In all simulations, socioeconomic conditions are varied according to the historically observed development between 1860 and 2005, and held fixed at 1860 conditions before 1860 and at 2005 conditions after 2005. The horizontal gray lines before 1860 and after 2005 represent the multi-year mean global land area fraction annually affected by crop failure under preindustrial climate conditions and socioeconomic conditions of 1860 and 2005, respectively. The gray line between 1860 and 2005 is a linear interpolation of these mean values. Panel B: Data shown in Panel A plotted against the associated GCM-specific annual global mean temperature (GMT) change relative to the long-term preindustrial mean GMT. Panel C: Pure effect of climate change on AFA, calculated as the difference between the annual data shown in Panel A and the multi-year mean AFA under preindustrial climate conditions (gray line in Panel A). Panel D: Data shown in Panel C plotted against annual GMT change. The red line represents the mean values of the annual data points per 1 °C-wide GMT change bin, with bins centered at GMT change levels increasing from 0 °C to 4 °C in steps of 0.5 °C. The area shaded in red represents the mean value ±1 standard deviation ranges of the annual data points per GMT change bin.

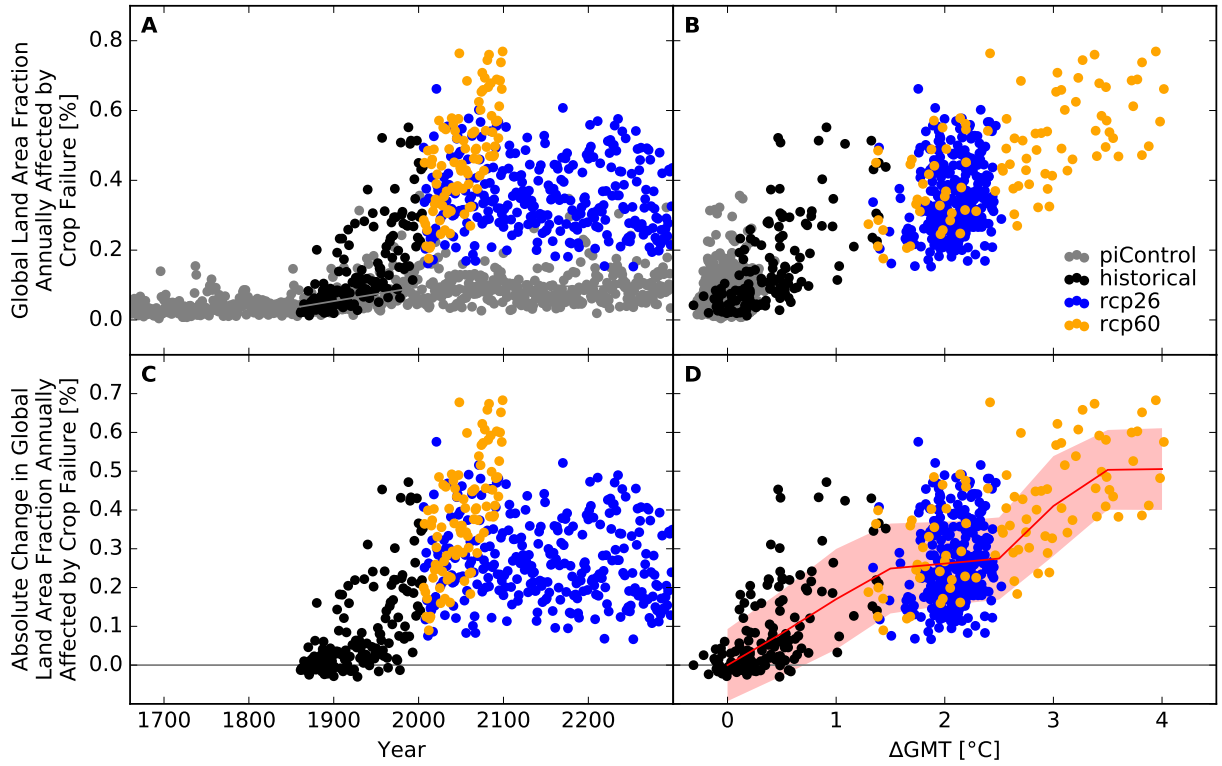

Figure S138: **Derivation of the pure effect of climate change on the global land area fraction annually affected by crop failure (IPSL-CM5A-LR + GEPIC).** Analogous to Figure S137.

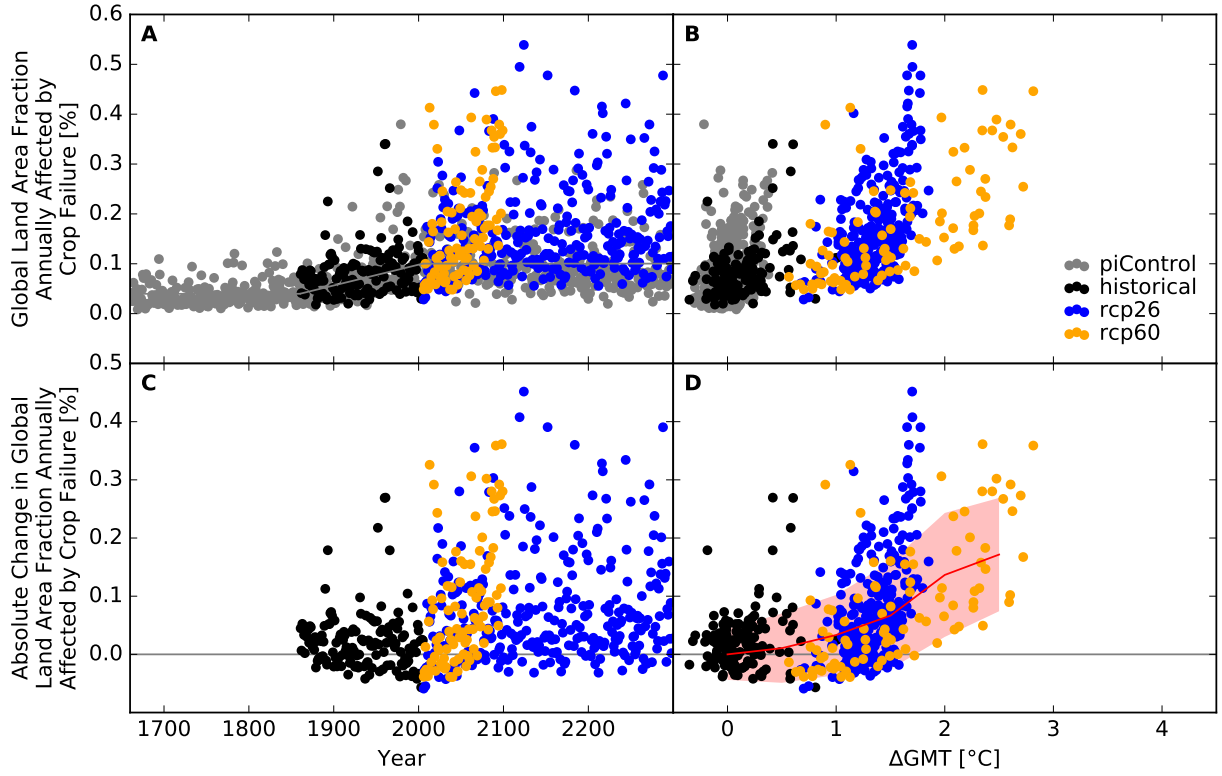

Figure S139: **Derivation of the pure effect of climate change on the global land area fraction annually affected by crop failure (MIROC5 + GEPIC).** Analogous to Figure S137.

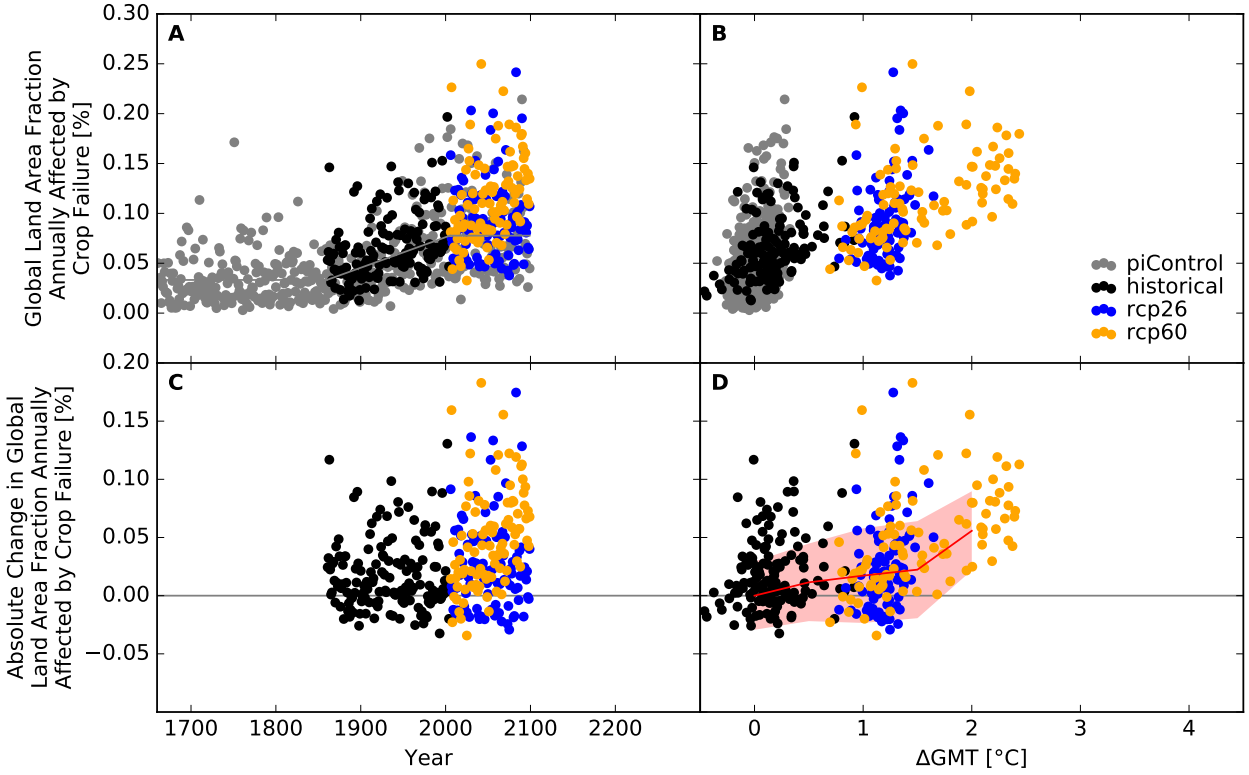

Figure S140: **Derivation of the pure effect of climate change on the global land area fraction annually affected by crop failure (GFDL-ESM2M + LPJmL).** Analogous to Figure S137.

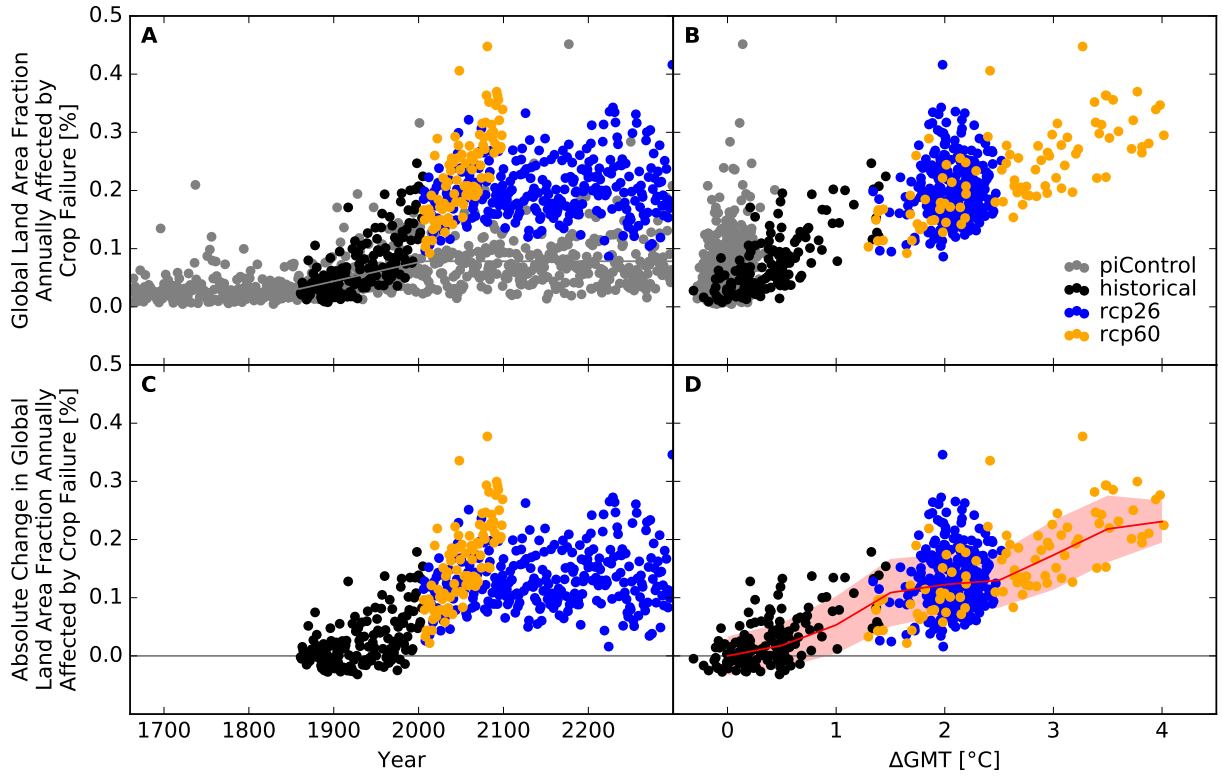

Figure S141: **Derivation of the pure effect of climate change on the global land area fraction annually affected by crop failure (IPSL-CM5A-LR + LPJmL).** Analogous to Figure S137.

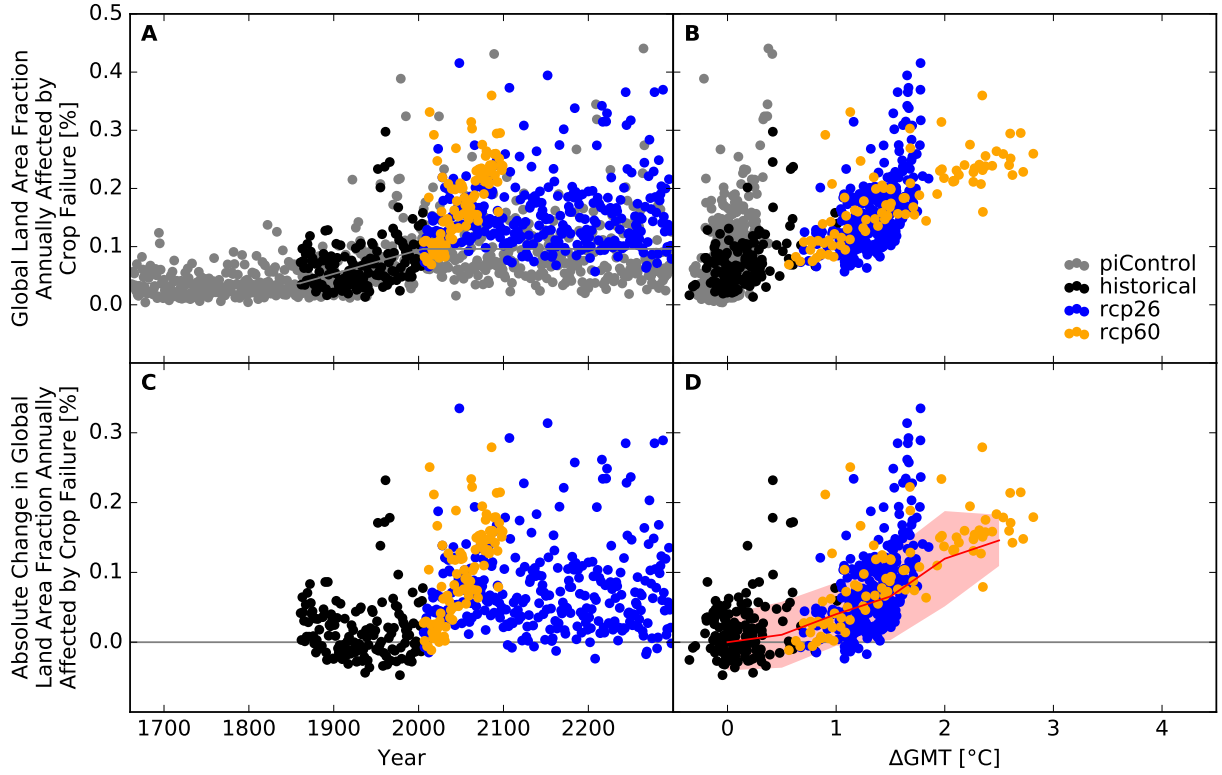

Figure S142: **Derivation of the pure effect of climate change on the global land area fraction annually affected by crop failure (MIROC5 + LPJmL).** Analogous to Figure S137.

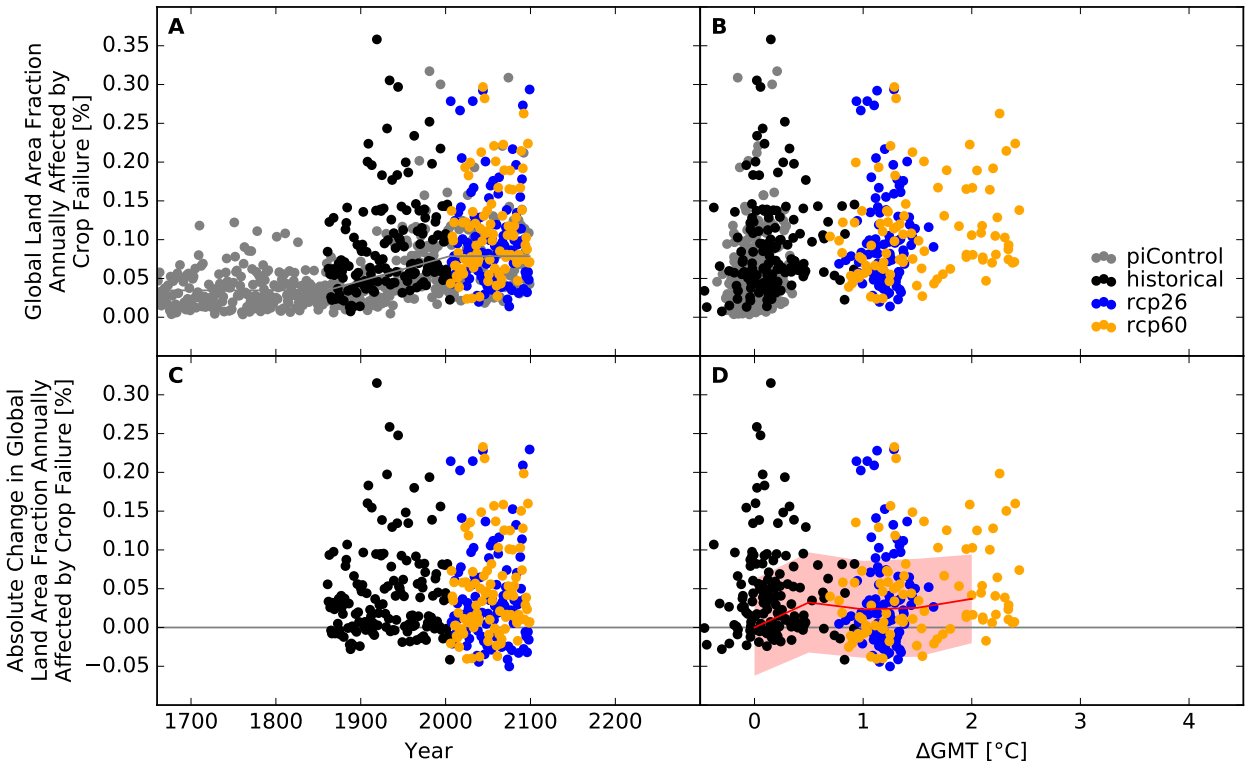

Figure S143: **Derivation of the pure effect of climate change on the global land area fraction annually affected by crop failure (GFDL-ESM2M + PEPIC).** Analogous to Figure S137.

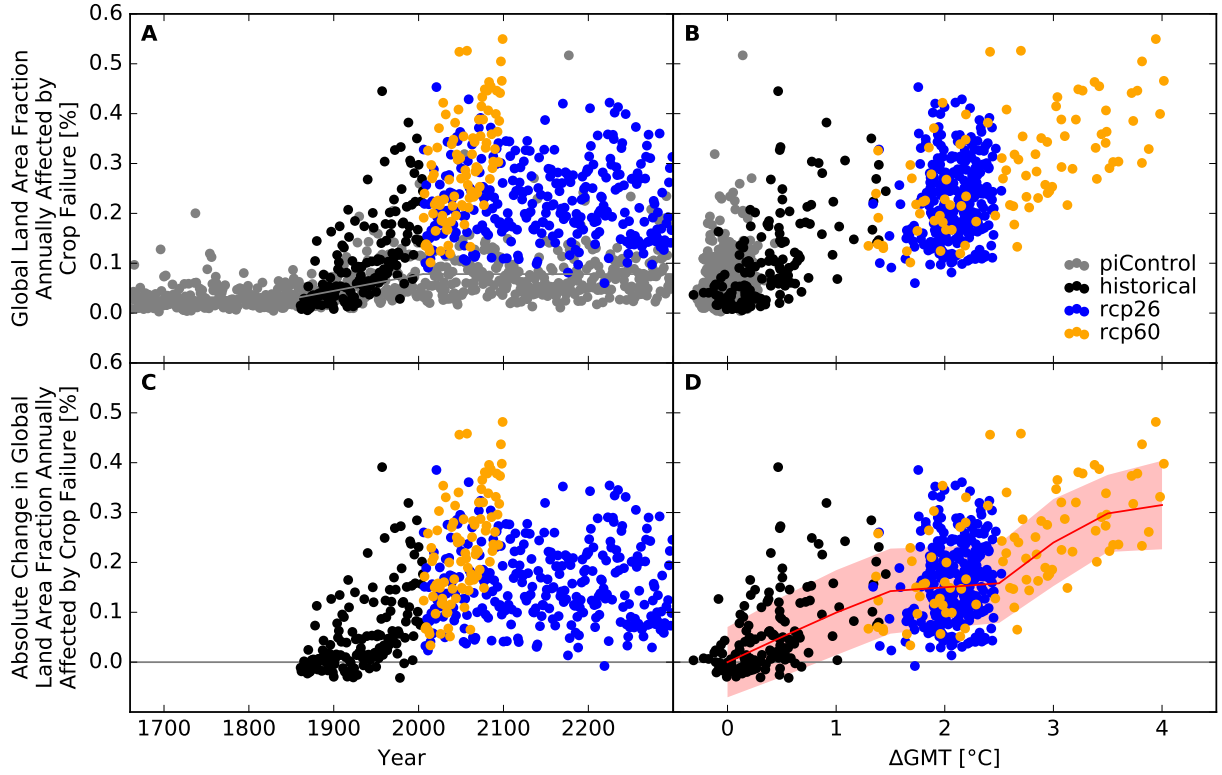

Figure S144: **Derivation of the pure effect of climate change on the global land area fraction annually affected by crop failure (IPSL-CM5A-LR + PEPIC).** Analogous to Figure S137.

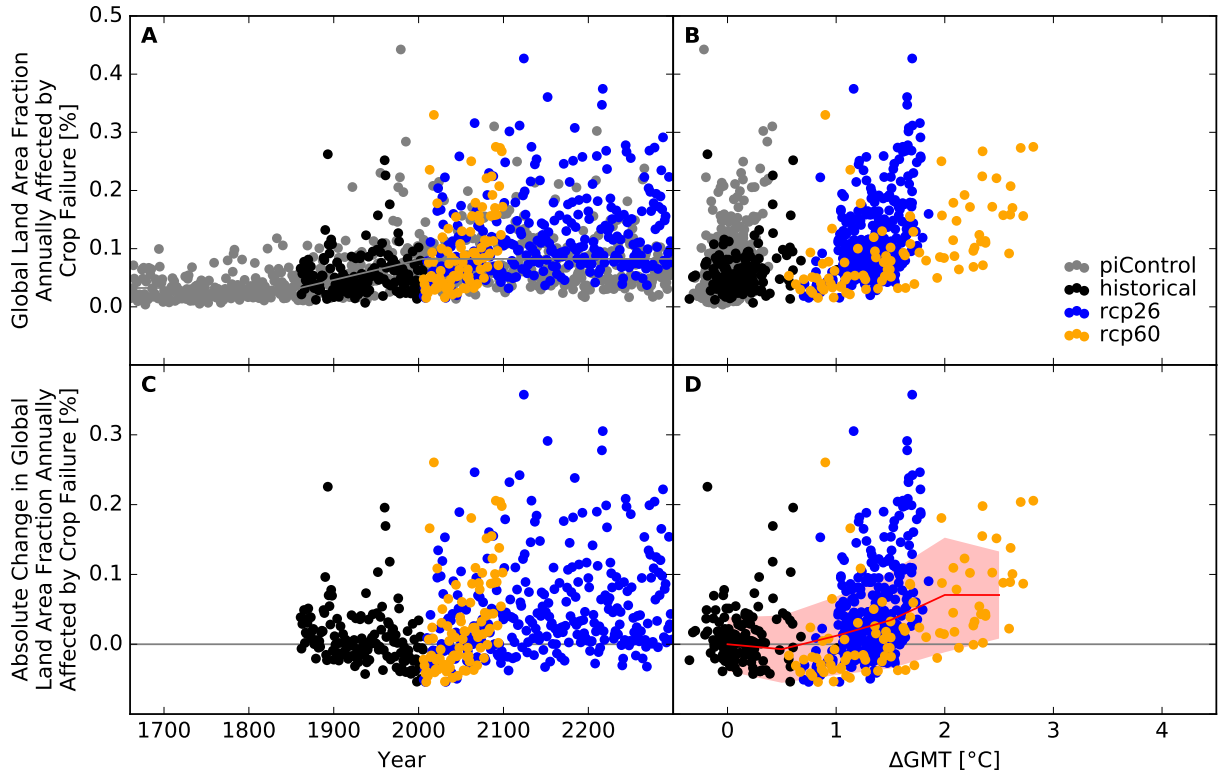

Figure S145: **Derivation of the pure effect of climate change on the global land area fraction annually affected by crop failure (MIROC5 + PEPIC).** Analogous to Figure S137.

Number of people exposed

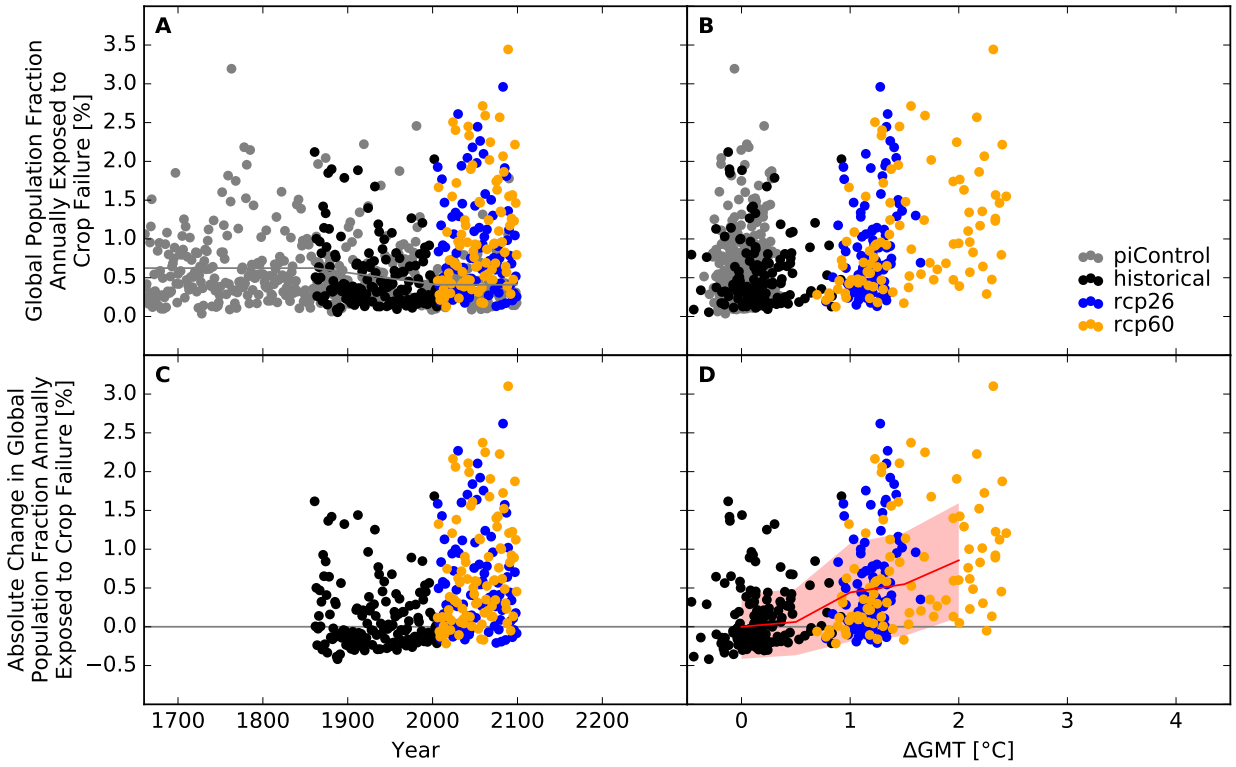

Figure S146: **Derivation of the pure effect of climate change on the global population fraction annually exposed to crop failure (GFDL-ESM2M + GEPIC).** Panel A: Time series of annual global population fraction exposed (PFE) to crop failure for preindustrial climate (grey dots), historical climate (black dots), climate projections for RCP2.6 (blue dots), and RCP6.0 (orange dots). In all simulations, socioeconomic conditions are varied according to the historically observed development between 1860 and 2005, and held fixed at 1860 conditions before 1860 and at 2005 conditions after 2005. The horizontal gray lines before 1860 and after 2005 represent the multi-year mean global population fraction annually exposed to crop failure under preindustrial climate conditions and socioeconomic conditions of 1860 and 2005, respectively. The gray line between 1860 and 2005 is a linear interpolation of these mean values. Panel B: Data shown in Panel A plotted against the associated GCM-specific annual global mean temperature (GMT) change relative to the long-term preindustrial mean GMT. Panel C: Pure effect of climate change on PFE, calculated as the difference between the annual data shown in Panel A and the multi-year mean PFE under preindustrial climate conditions (gray line in Panel A). Panel D: Data shown in Panel C plotted against annual GMT change. The red line represents the mean values of the annual data points per 1 °C-wide GMT change bin, with bins centered at GMT change levels increasing from 0 °C to 4 °C in steps of 0.5 °C. The area shaded in red represents the mean value ±1 standard deviation ranges of the annual data points per GMT change bin.

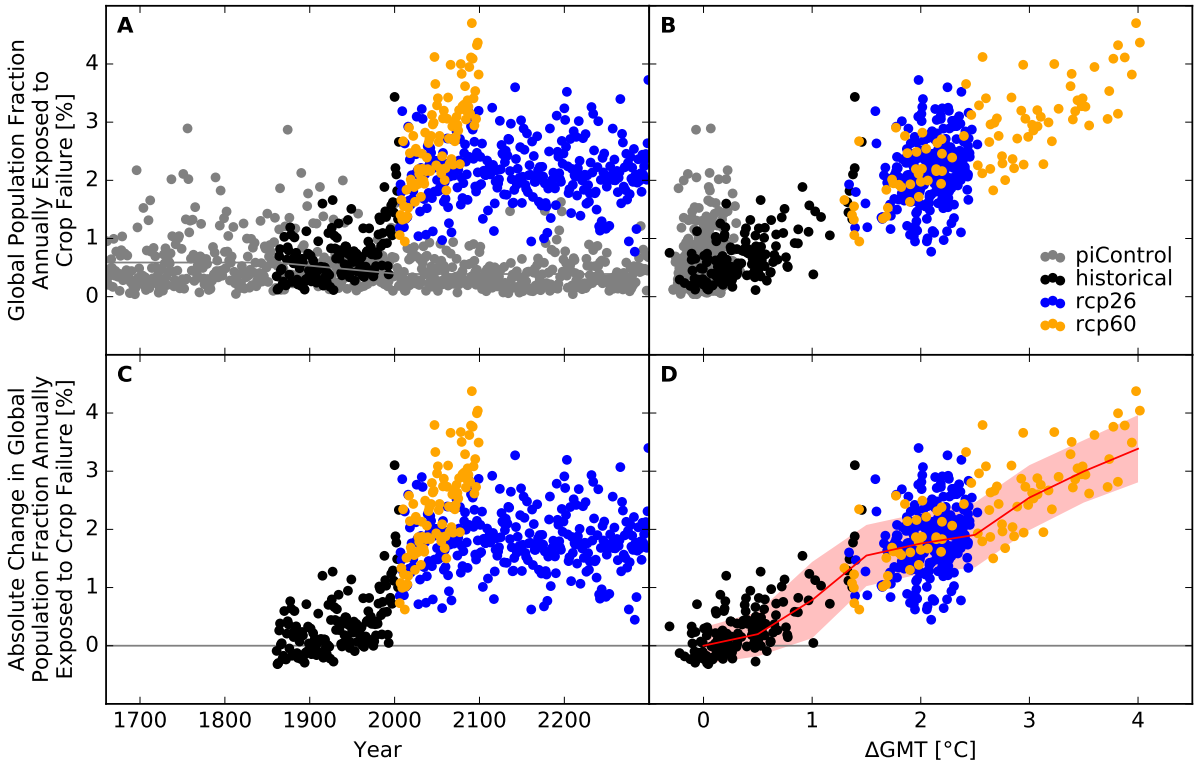

Figure S147: **Derivation of the pure effect of climate change on the global population fraction annually exposed to crop failure (IPSL-CM5A-LR + GEPIC).** Analogous to Figure S146.

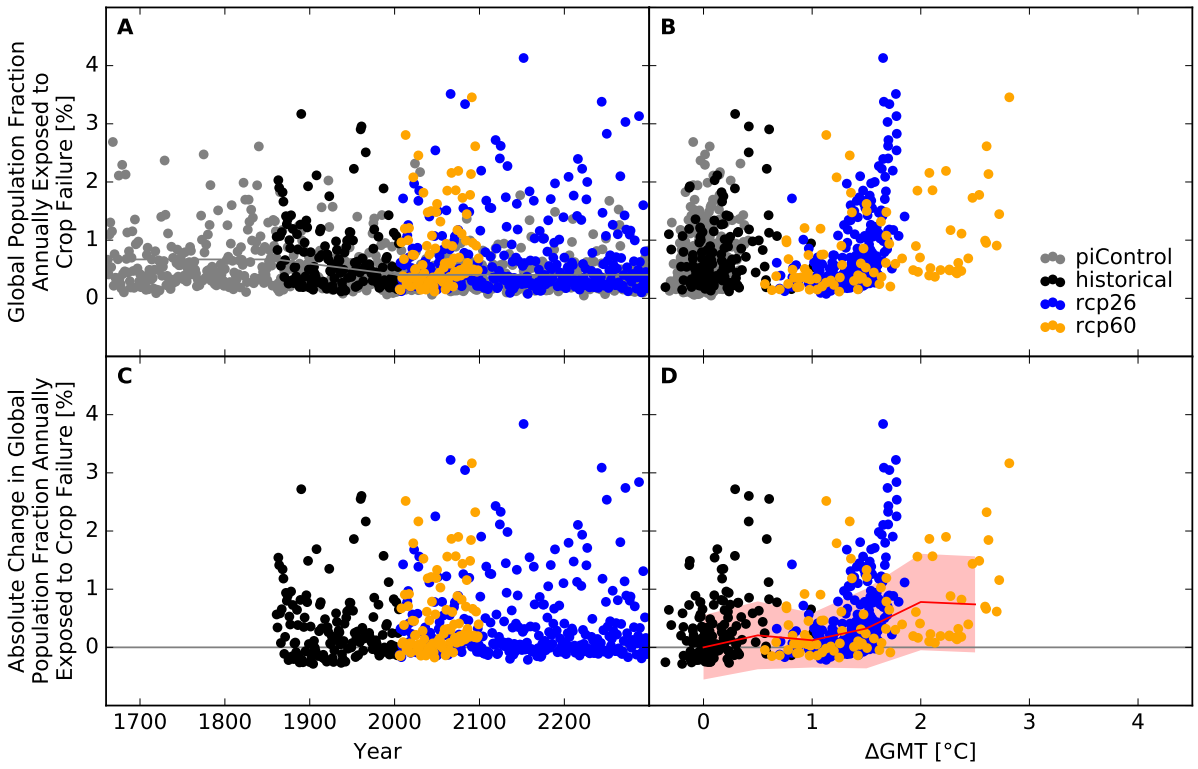

Figure S148: **Derivation of the pure effect of climate change on the global population fraction annually exposed to crop failure (MIROC5 + GEPIC).** Analogous to Figure S146.

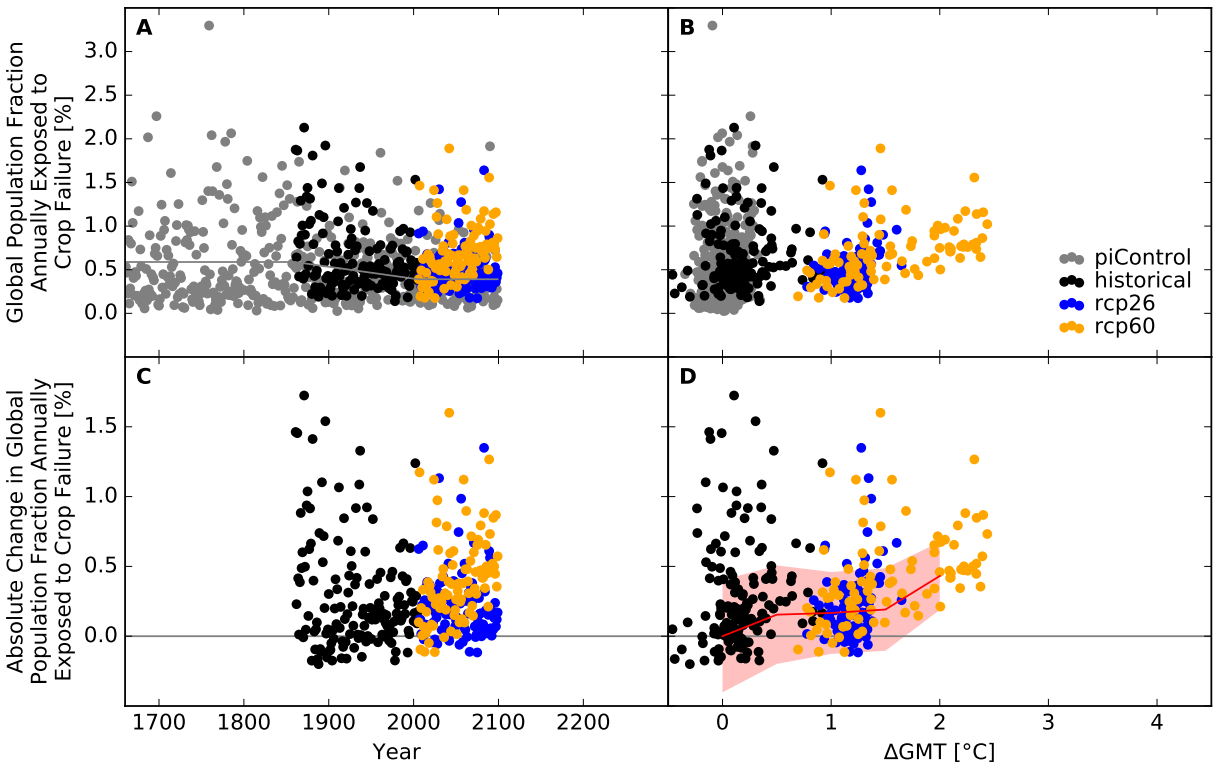

Figure S149: **Derivation of the pure effect of climate change on the global population fraction annually exposed to crop failure (GFDL-ESM2M + LPJmL).** Analogous to Figure S146.

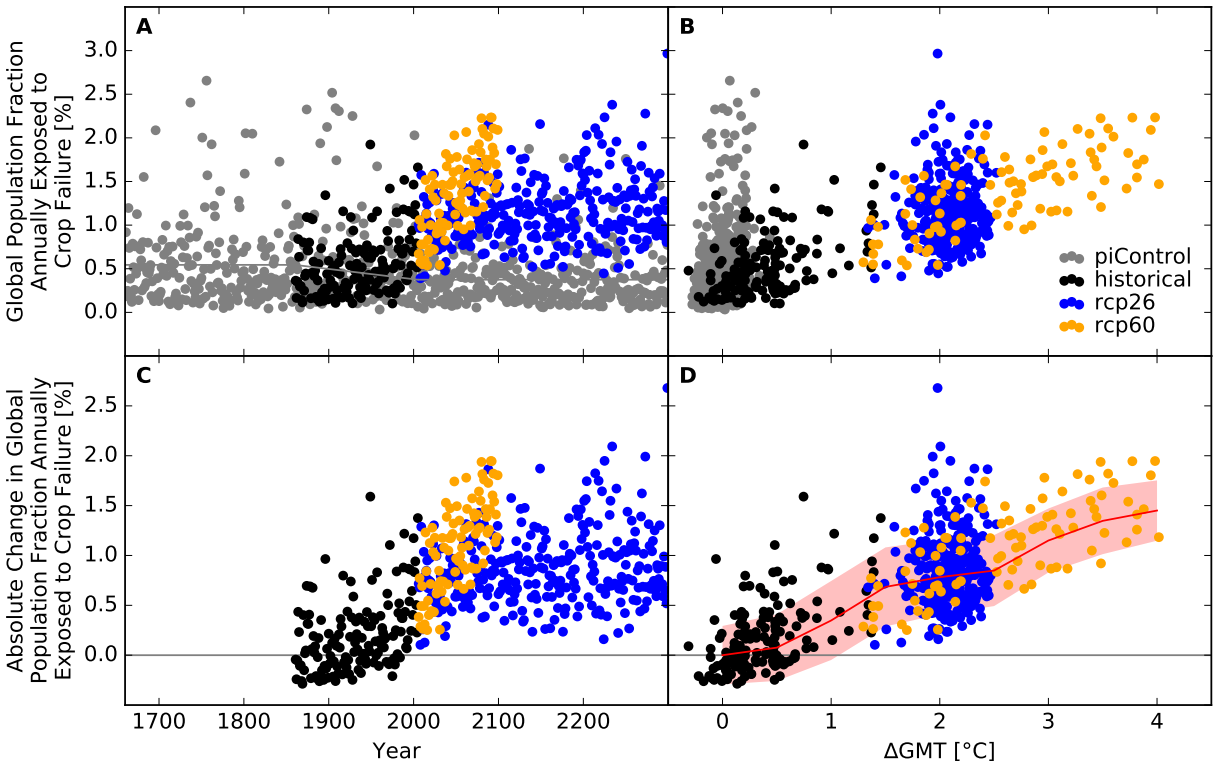

Figure S150: **Derivation of the pure effect of climate change on the global population fraction annually exposed to crop failure (IPSL-CM5A-LR + LPJmL).** Analogous to Figure S146.

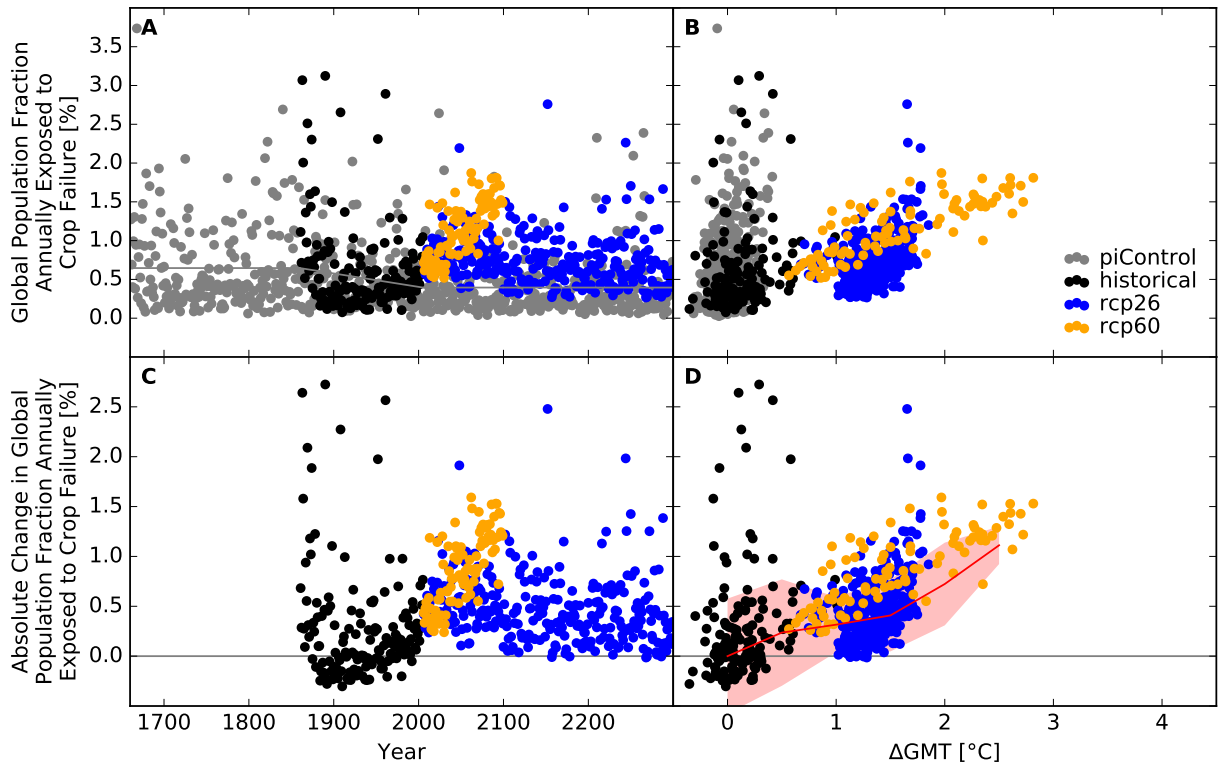

Figure S151: **Derivation of the pure effect of climate change on the global population fraction annually exposed to crop failure (MIROC5 + LPJmL).** Analogous to Figure S146.

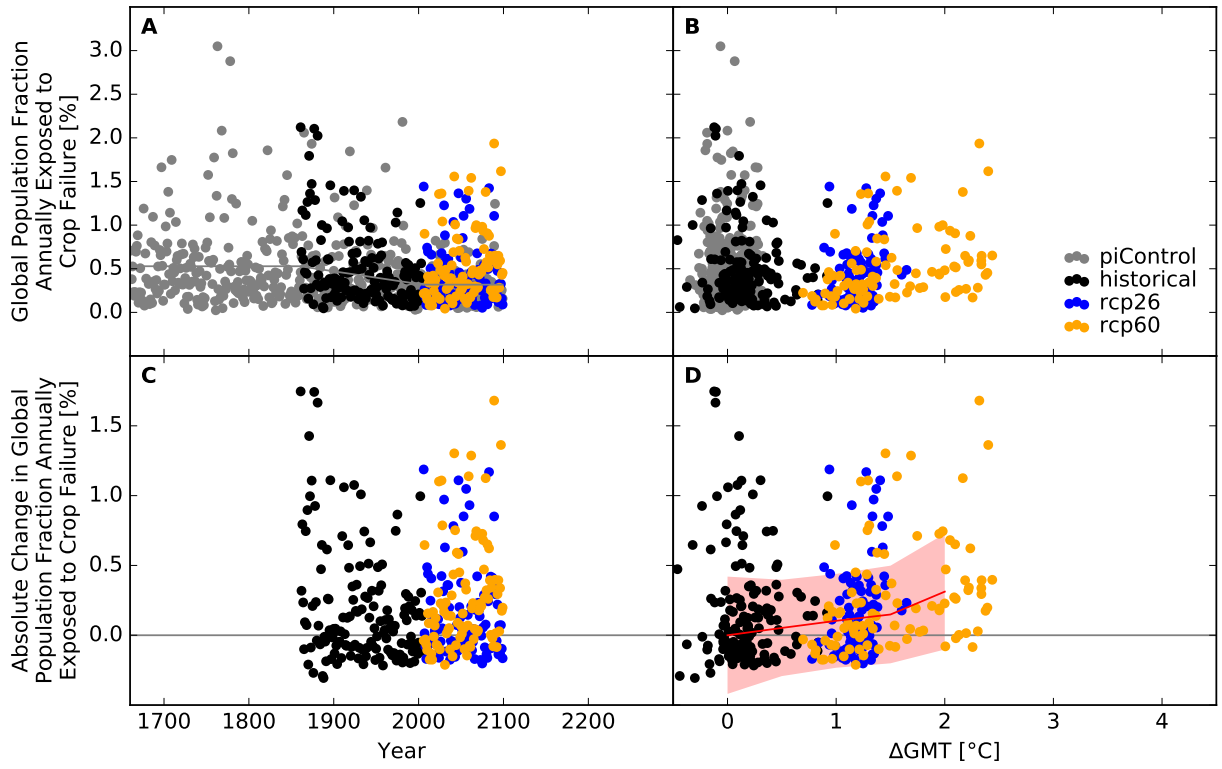

Figure S152: **Derivation of the pure effect of climate change on the global population fraction annually exposed to crop failure (GFDL-ESM2M + PEPIC).** Analogous to Figure S146.

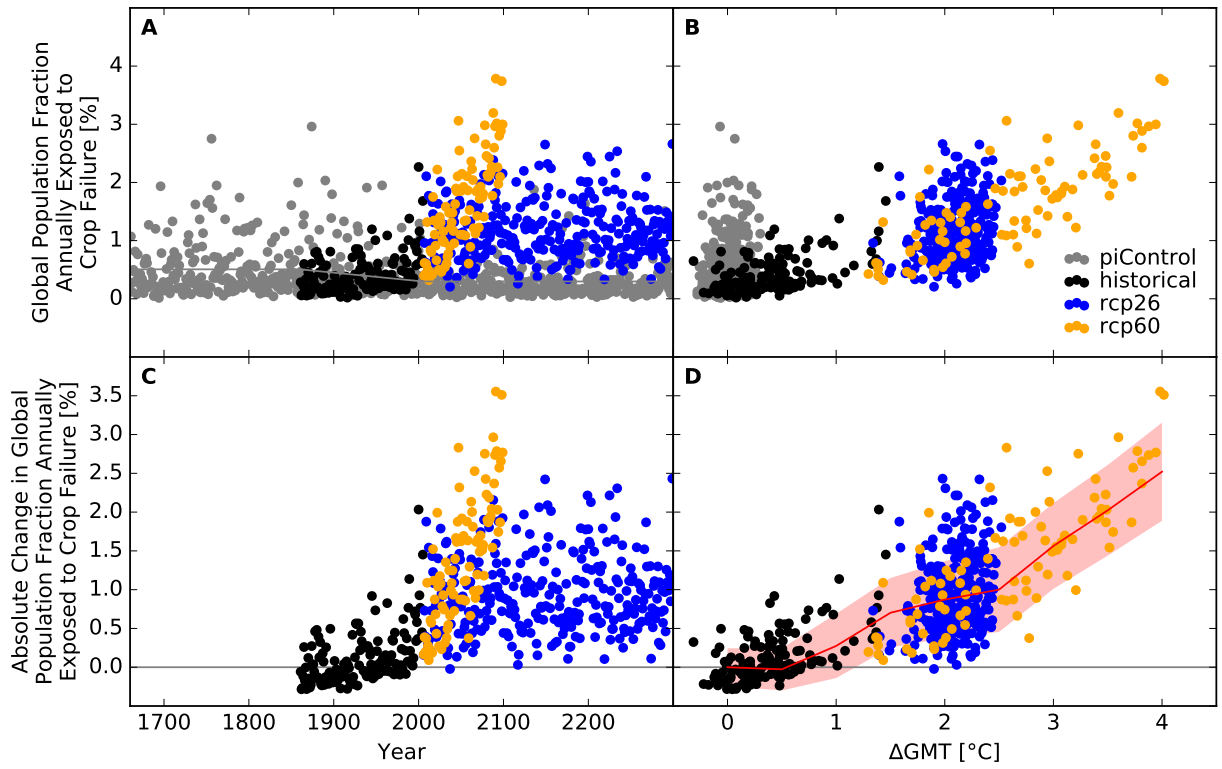

Figure S153: **Derivation of the pure effect of climate change on the global population fraction annually exposed to crop failure (IPSL-CM5A-LR + PEPIC).** Analogous to Figure S146.

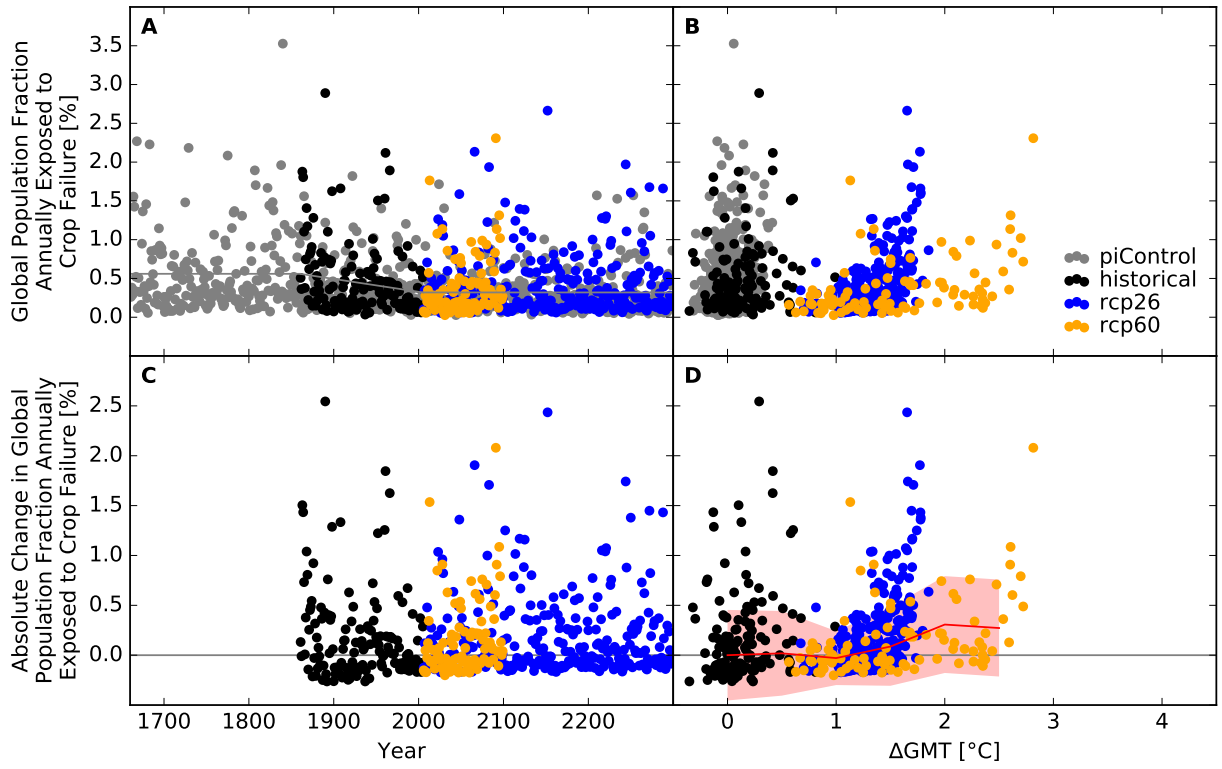

Figure S154: **Derivation of the pure effect of climate change on the global population fraction annually exposed to crop failure (MIROC5 + PEPIC).** Analogous to Figure S146.

Land area affected and number of people exposed at the national scale

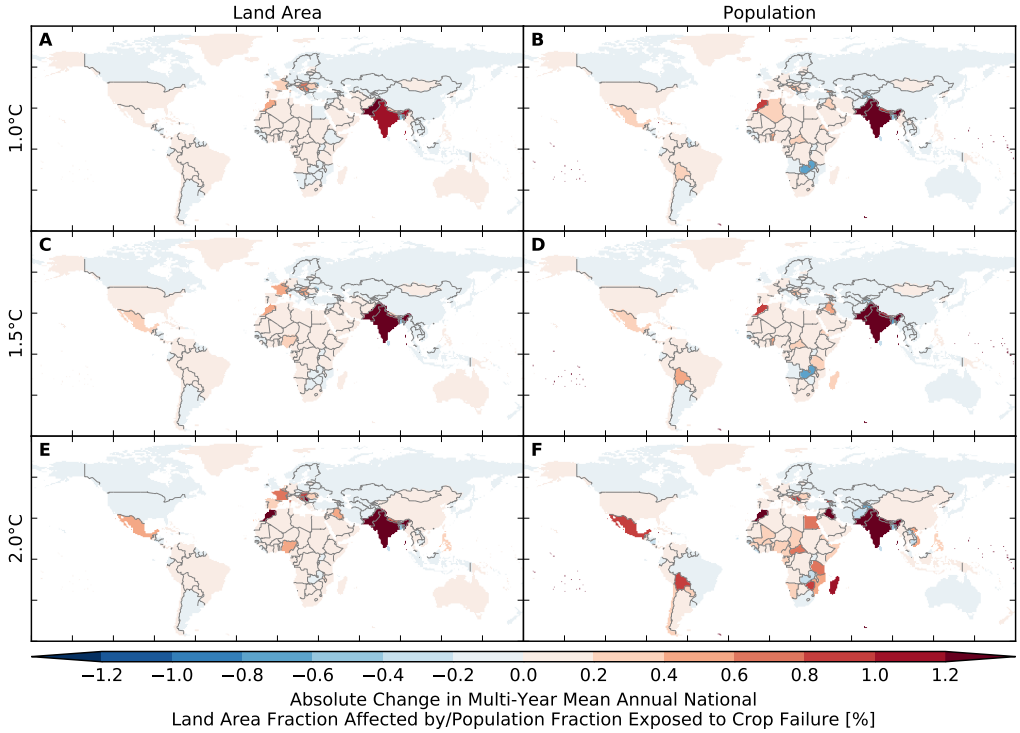

Figure S155: **Pure effect of climate change on annual national land area fraction affected by and population fraction exposed to crop failure (GFDL-ESM2M + GEPIC).** Absolute changes in multi-year mean annual national (A, C, E) land area fraction affected by and (B, D, F) population fraction exposed to crop failure at (A, B) 1 °C, (C, D) 1.5 °C and (E, F) 2 °C global warming.

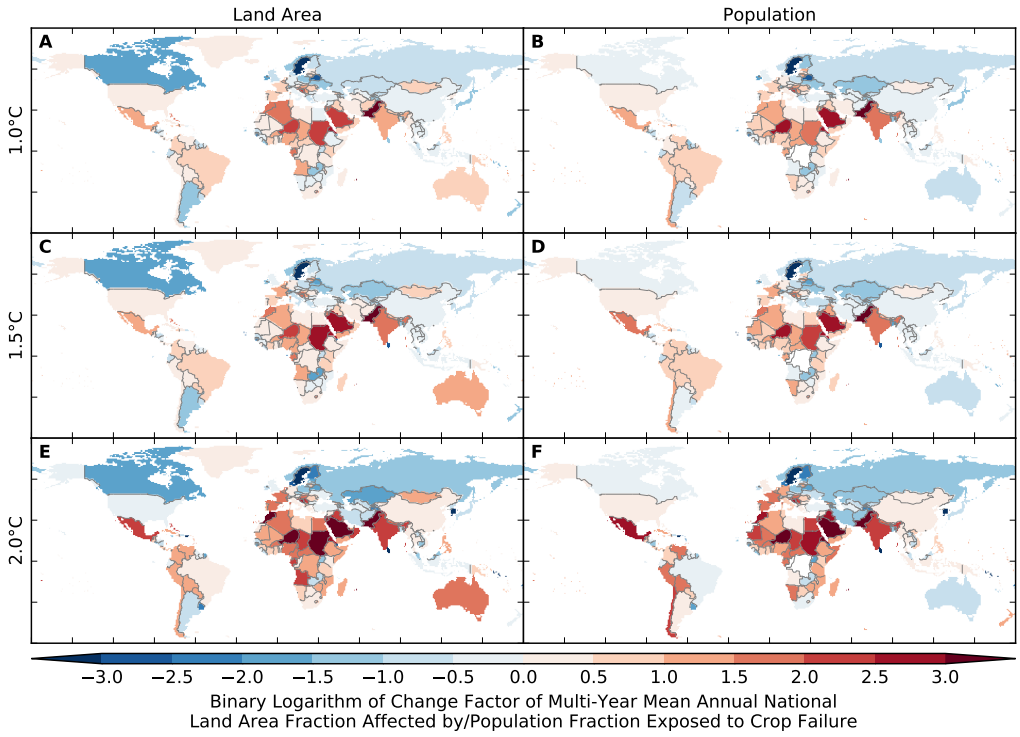

Figure S156: **Pure effect of climate change on annual national land area fraction affected by and population fraction exposed to crop failure (GFDL-ESM2M + GEPIC).** Same as Figure S155 but for relative changes expressed in terms of binary logarithms of change factors, i.e. −1 means a change by a factor of 0.5, 0 means no change, and 1 means a change by a factor of 2. White indicates undefined relative changes due to division by zero.

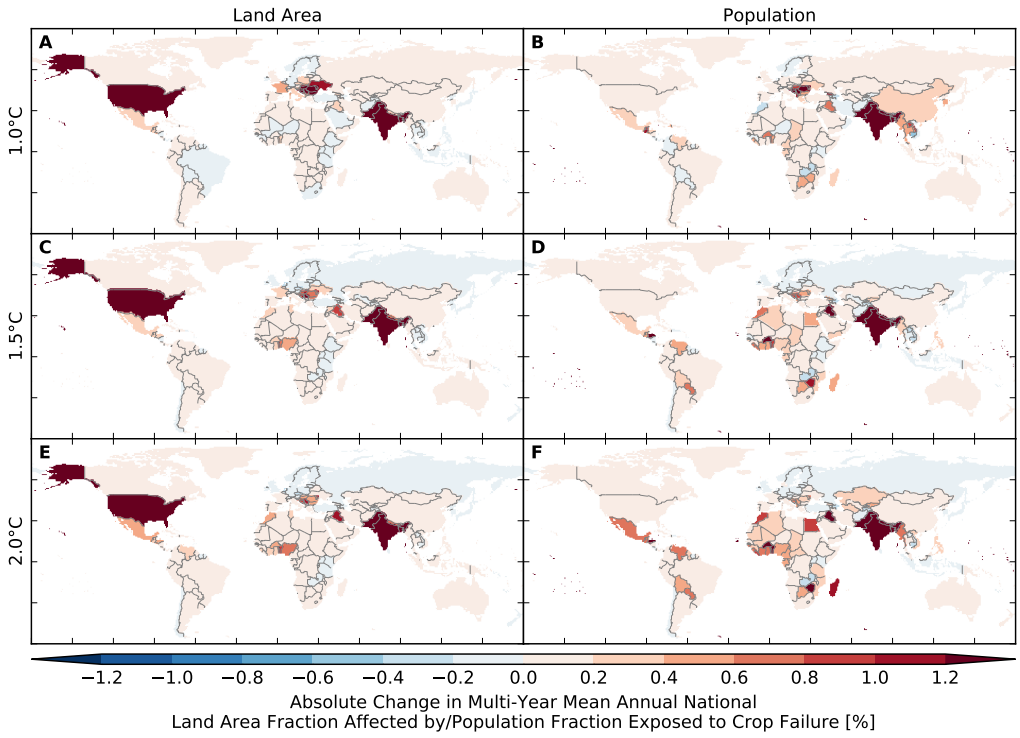

Figure S157: **Pure effect of climate change on annual national land area fraction affected by and population fraction exposed to crop failure (IPSL-CM5A-LR + GEPIC).** Analogous to Figure S155.

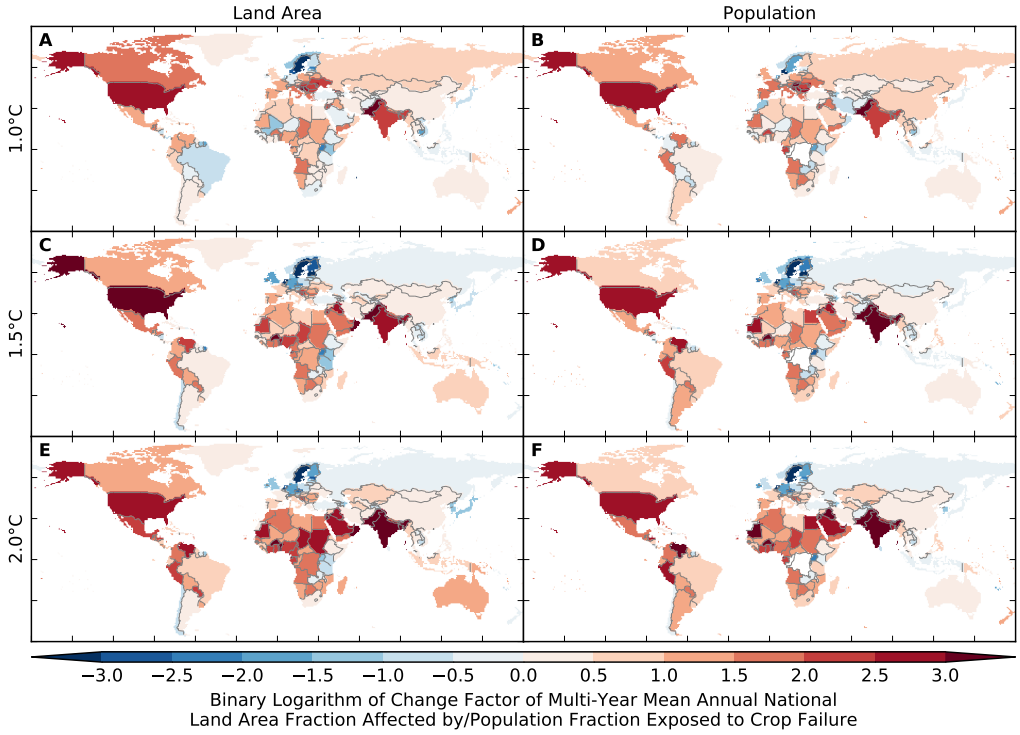

Figure S158: **Pure effect of climate change on annual national land area fraction affected by and population fraction exposed to crop failure (IPSL-CM5A-LR + GEPIC).** Analogous to Figure S156.

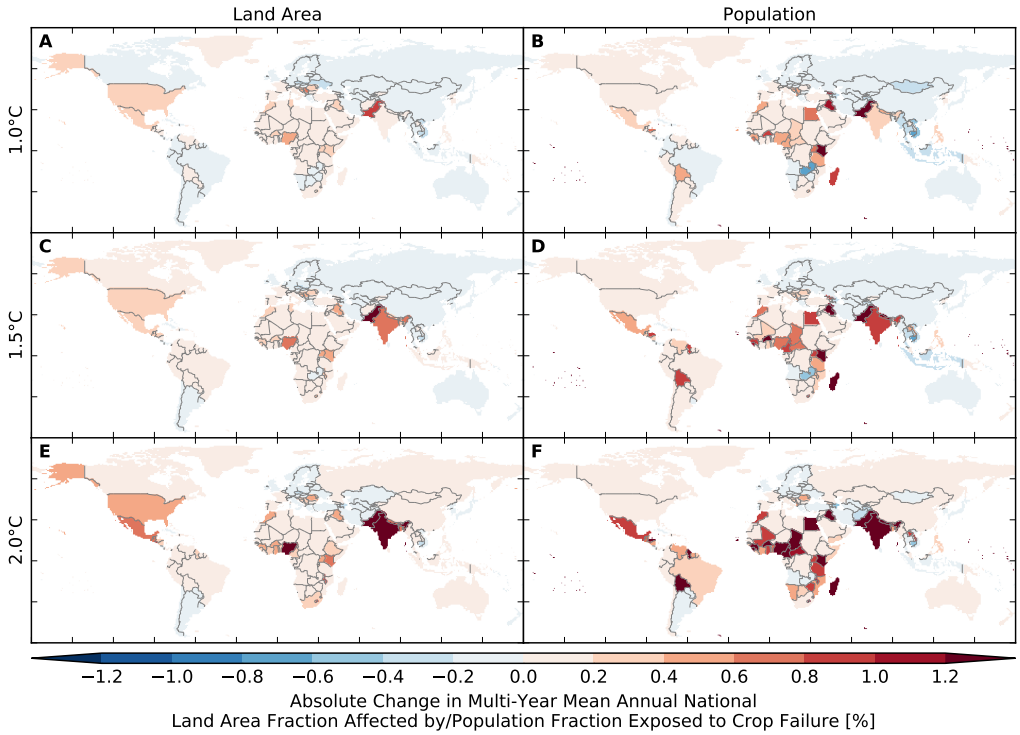

Figure S159: **Pure effect of climate change on annual national land area fraction affected by and population fraction exposed to crop failure (MIROC5 + GEPIC).** Analogous to Figure S155.

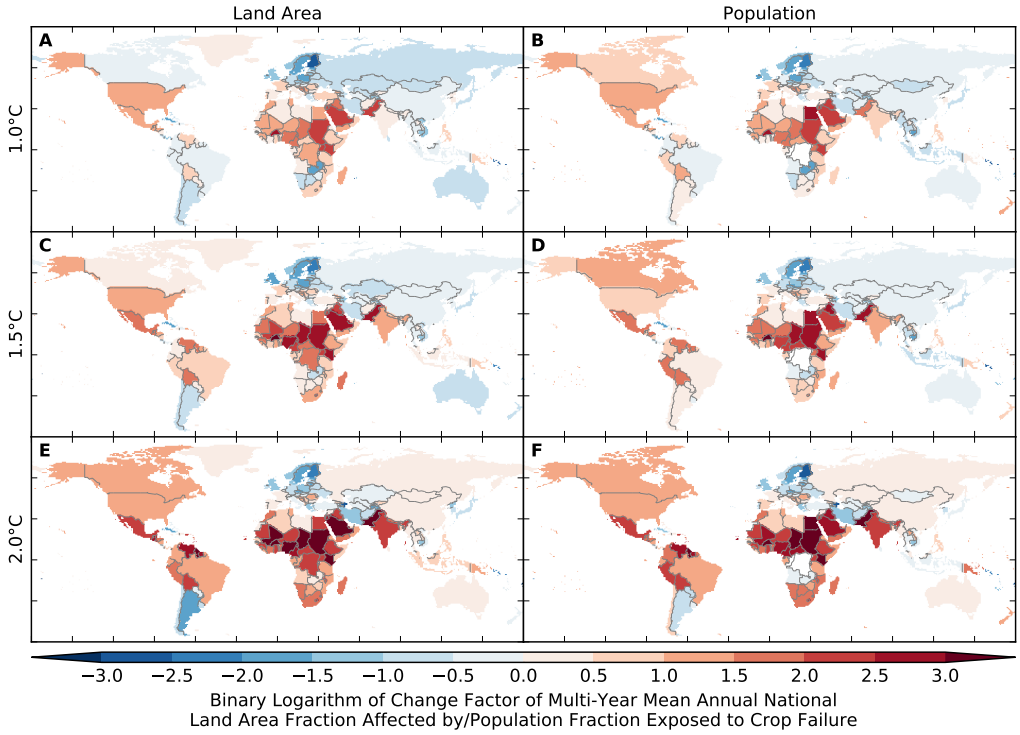

Figure S160: **Pure effect of climate change on annual national land area fraction affected by and population fraction exposed to crop failure (MIROC5 + GEPIC).** Analogous to Figure S156.

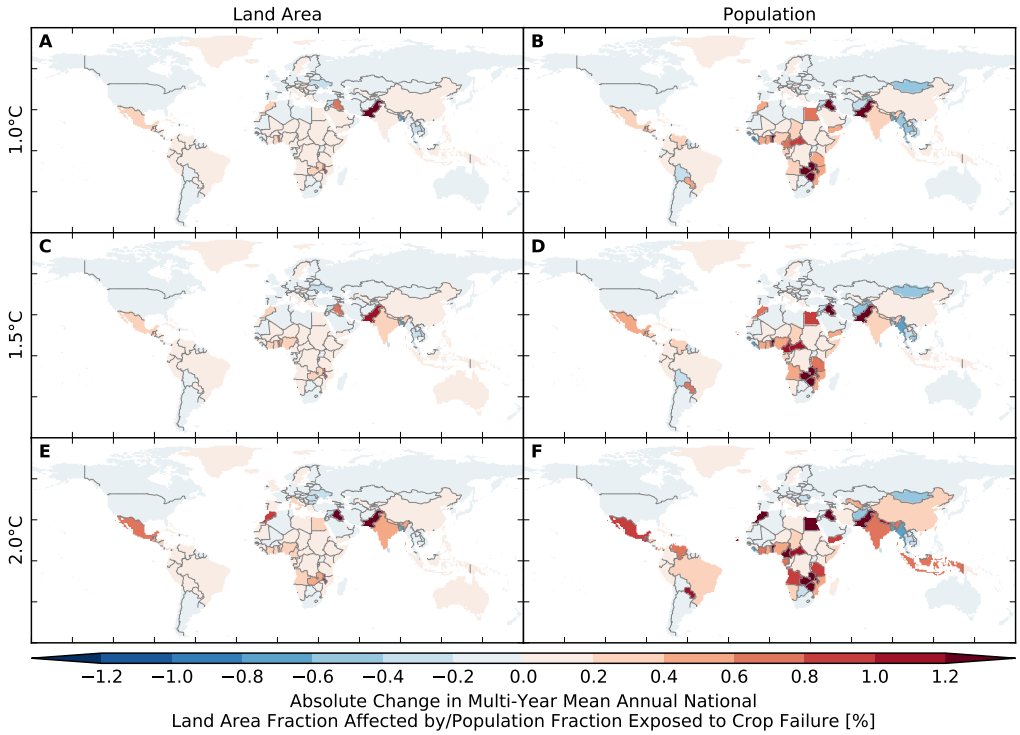

Figure S161: **Pure effect of climate change on annual national land area fraction affected by and population fraction exposed to crop failure (GFDL-ESM2M + LPJmL).** Analogous to Figure S155.

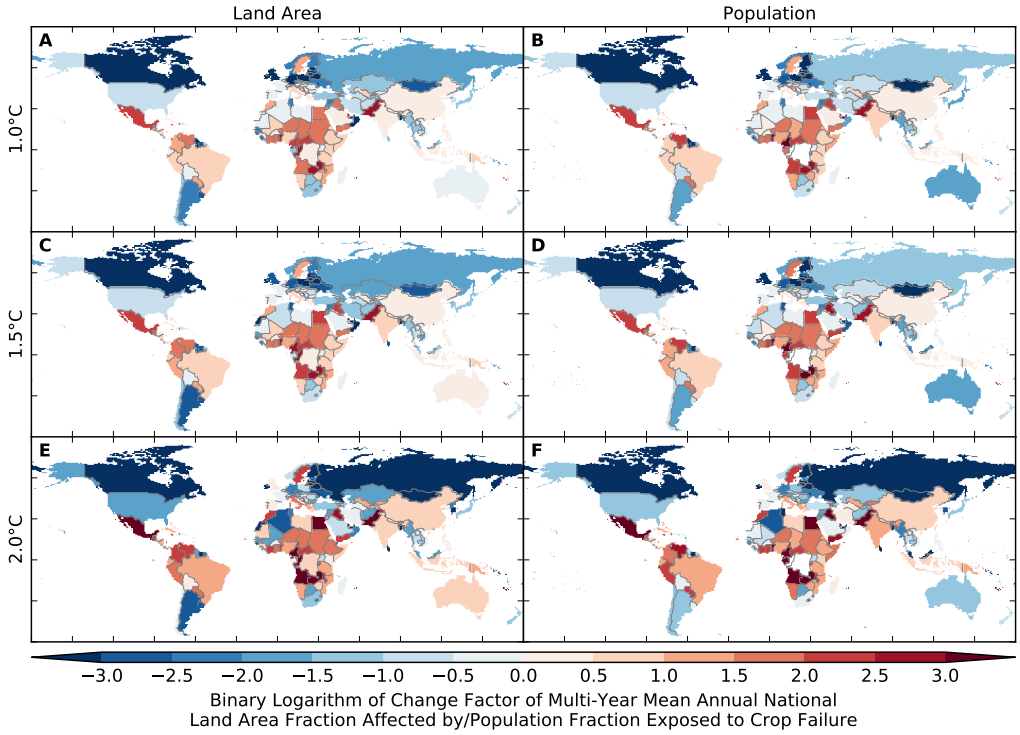

Figure S162: **Pure effect of climate change on annual national land area fraction affected by and population fraction exposed to crop failure (GFDL-ESM2M + LPJmL).** Analogous to Figure S156.

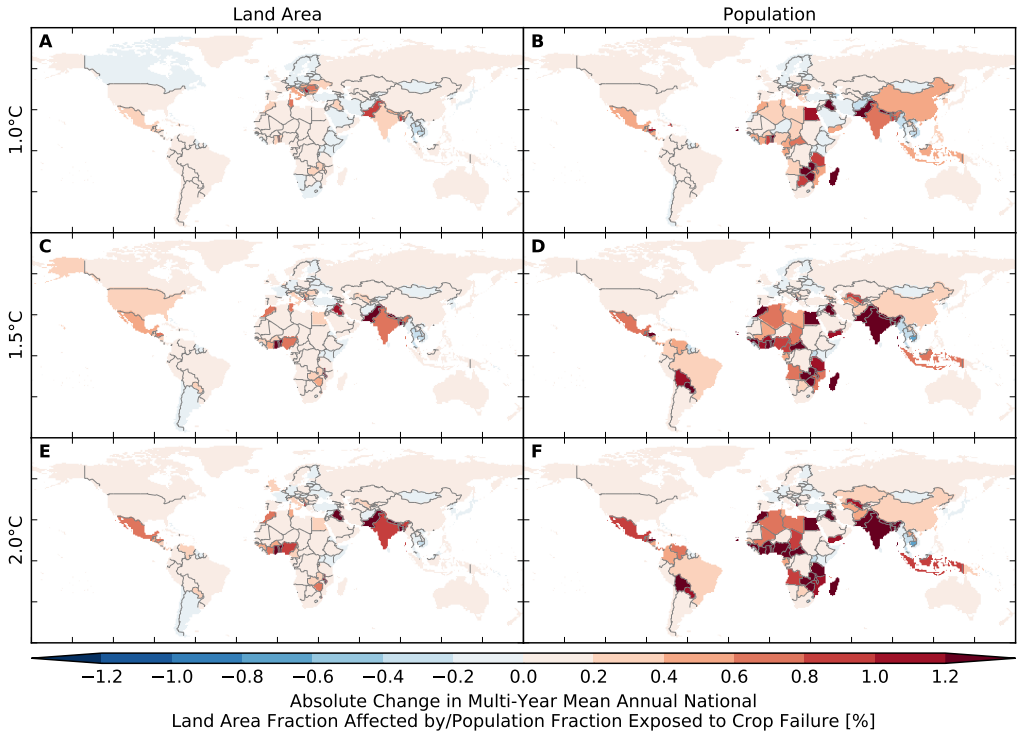

Figure S163: **Pure effect of climate change on annual national land area fraction affected by and population fraction exposed to crop failure (IPSL-CM5A-LR + LPJmL).** Analogous to Figure S155.

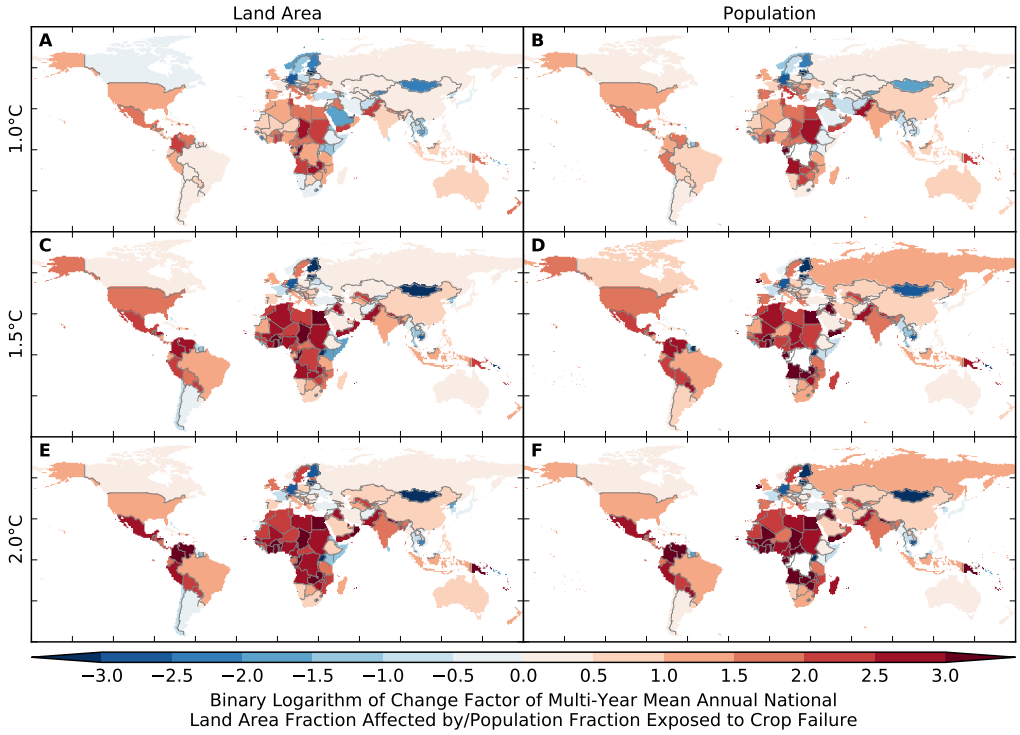

Figure S164: **Pure effect of climate change on annual national land area fraction affected by and population fraction exposed to crop failure (IPSL-CM5A-LR + LPJmL).** Analogous to Figure S156.

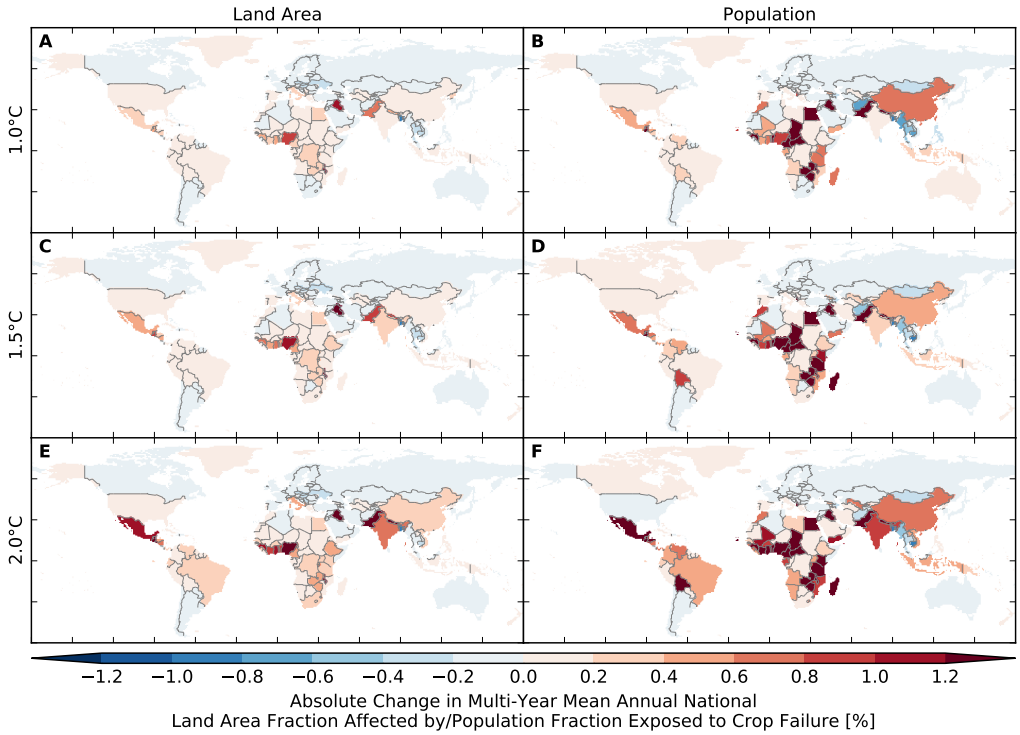

Figure S165: **Pure effect of climate change on annual national land area fraction affected by and population fraction exposed to crop failure (MIROC5 + LPJmL).** Analogous to Figure S155.

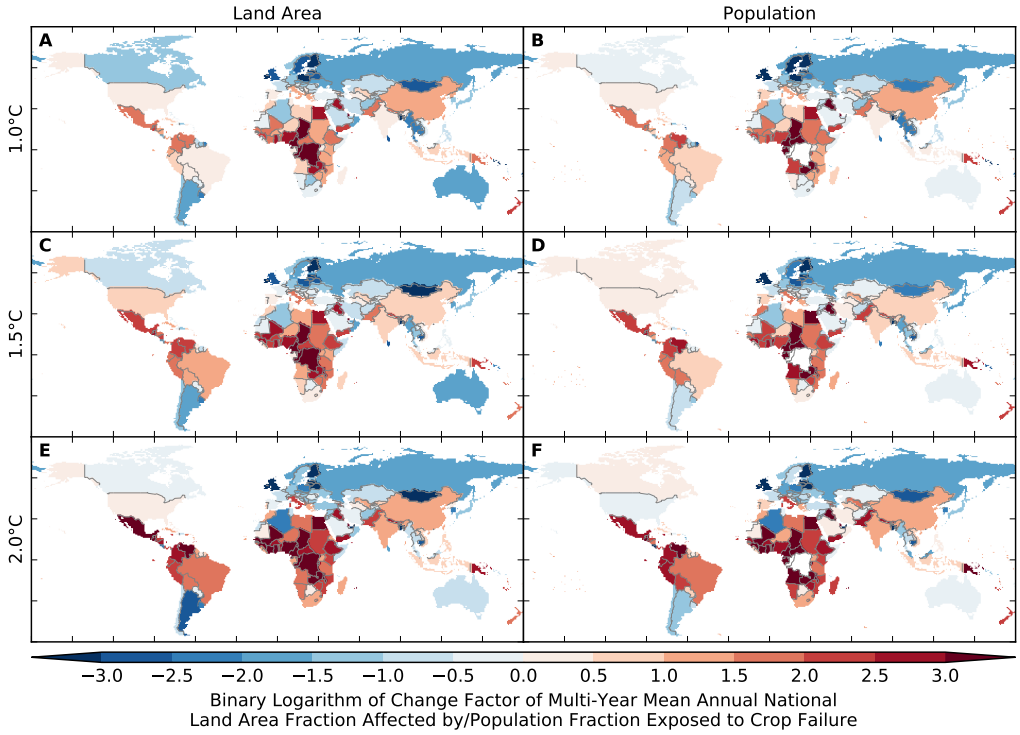

Figure S166: **Pure effect of climate change on annual national land area fraction affected by and population fraction exposed to crop failure (MIROC5 + LPJmL).** Analogous to Figure S156.

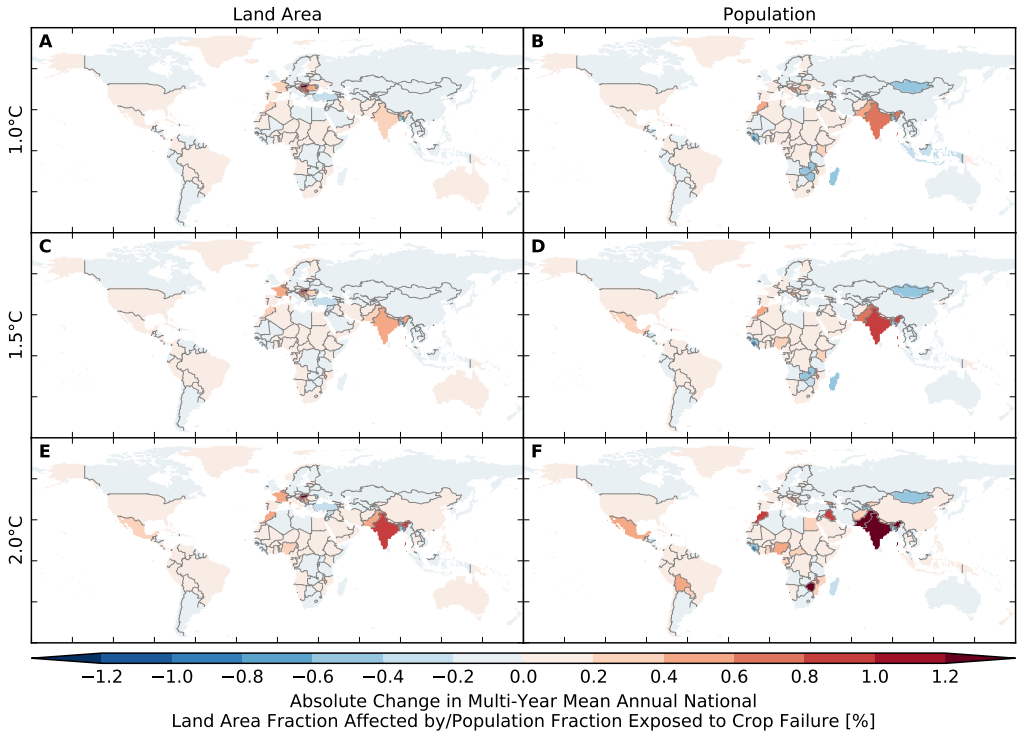

Figure S167: **Pure effect of climate change on annual national land area fraction affected by and population fraction exposed to crop failure (GFDL-ESM2M + PEPIC).** Analogous to Figure S155.

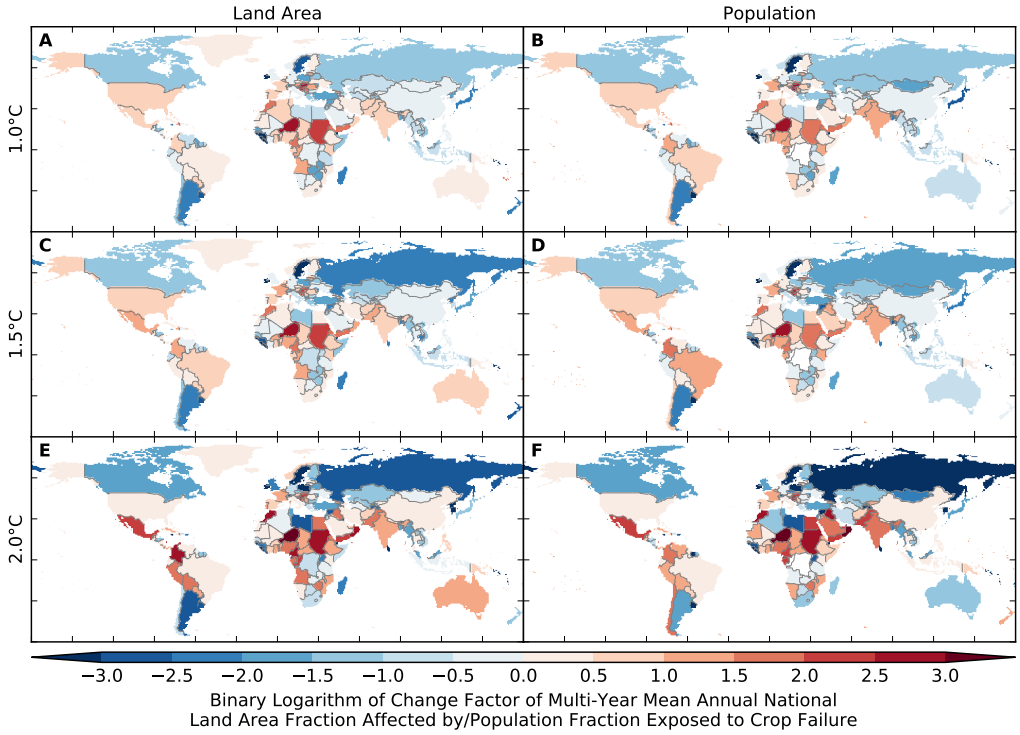

Figure S168: **Pure effect of climate change on annual national land area fraction affected by and population fraction exposed to crop failure (GFDL-ESM2M + PEPIC).** Analogous to Figure S156.

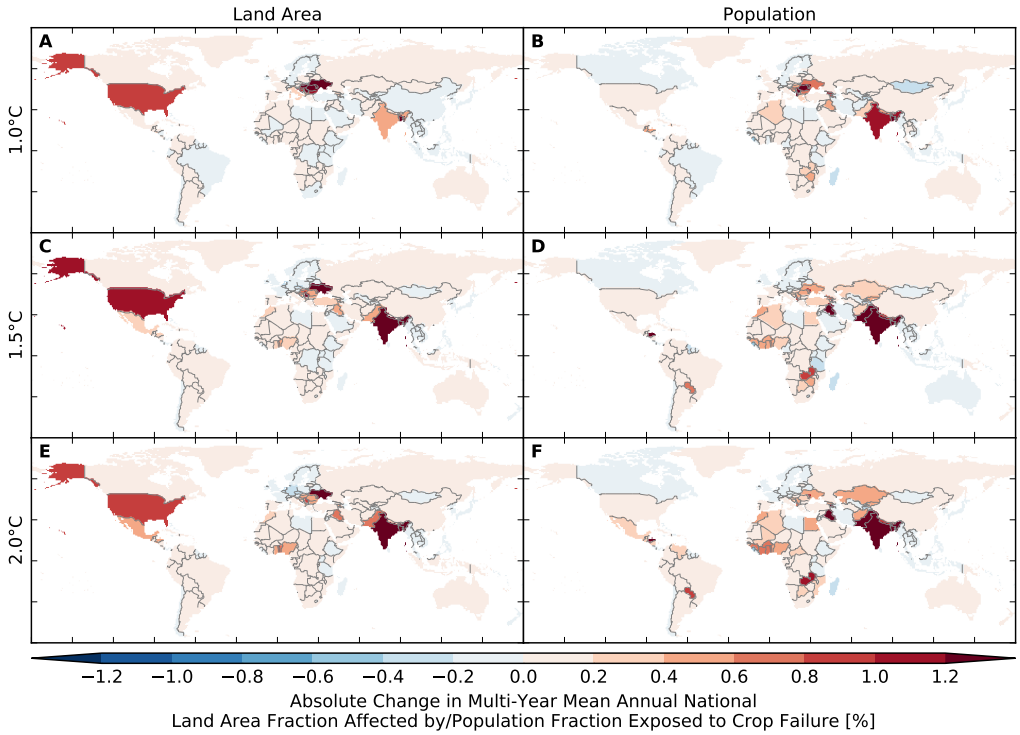

Figure S169: **Pure effect of climate change on annual national land area fraction affected by and population fraction exposed to crop failure (IPSL-CM5A-LR + PEPIC).** Analogous to Figure S155.

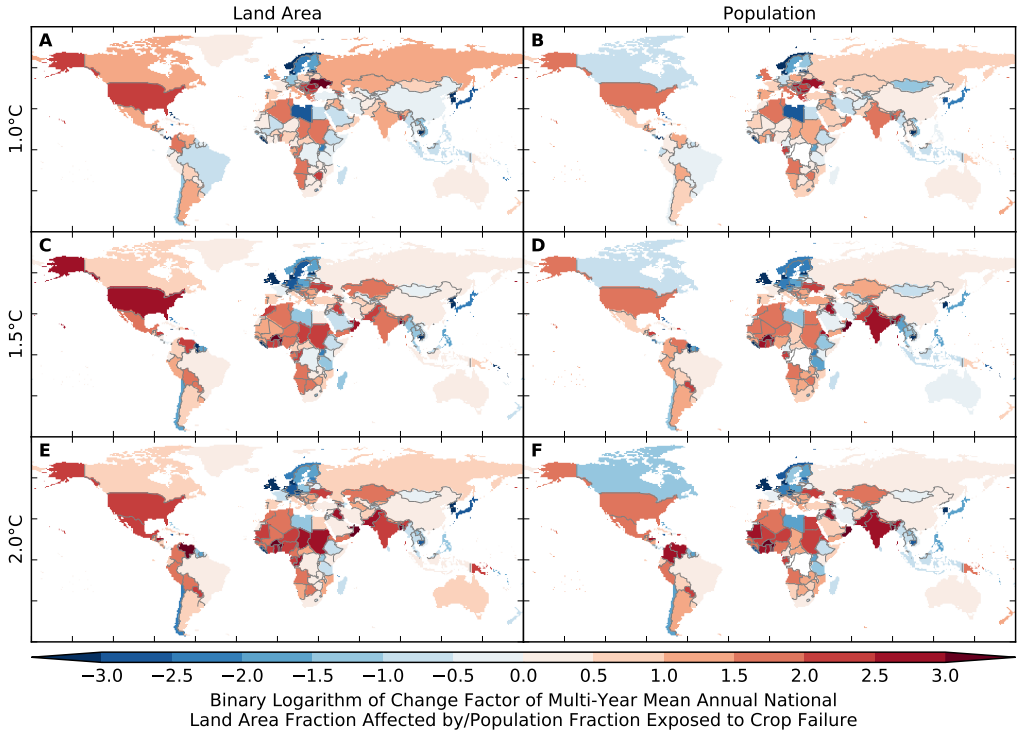

Figure S170: **Pure effect of climate change on annual national land area fraction affected by and population fraction exposed to crop failure (IPSL-CM5A-LR + PEPIC).** Analogous to Figure S156.

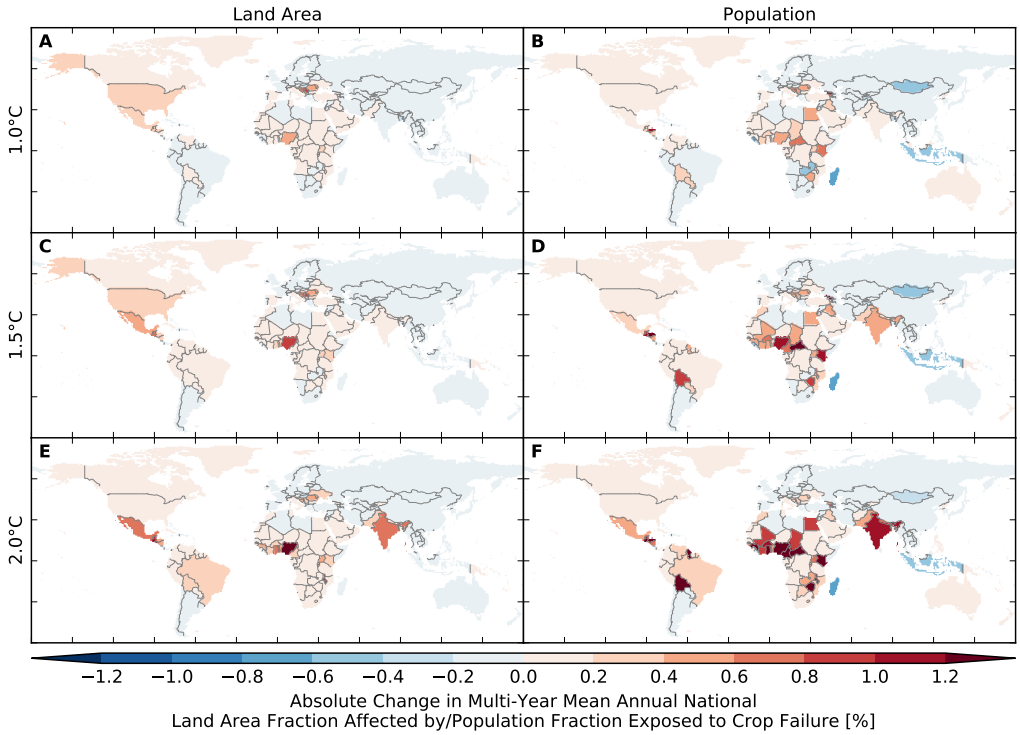

Figure S171: **Pure effect of climate change on annual national land area fraction affected by and population fraction exposed to crop failure (MIROC5 + PEPIC).** Analogous to Figure S155.

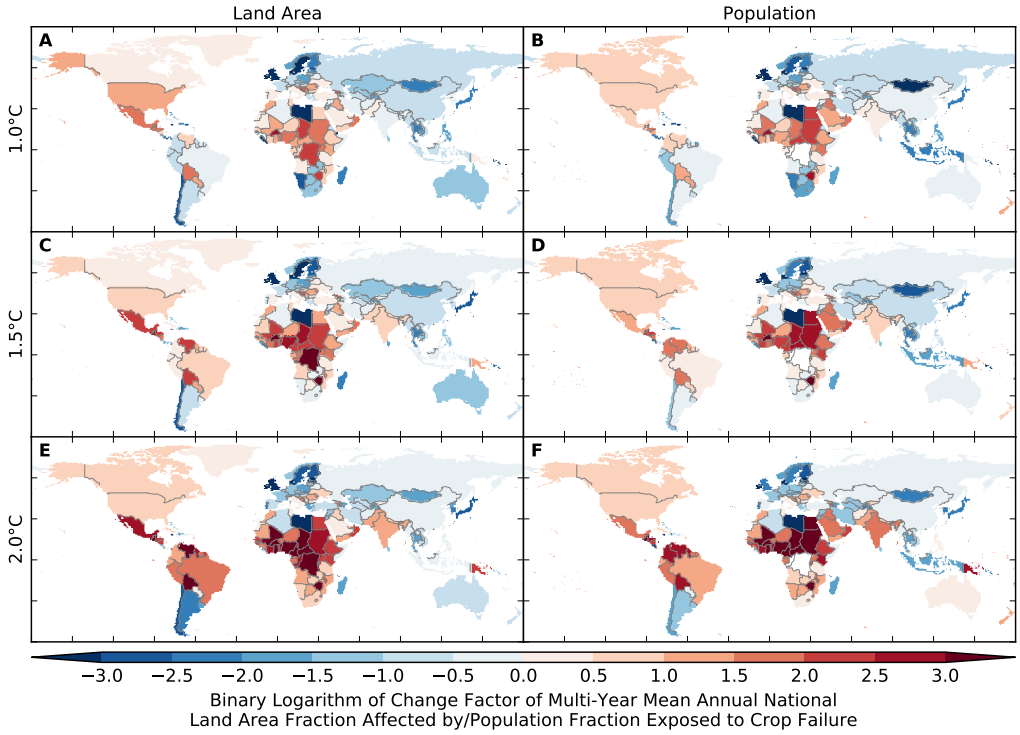

Figure S172: **Pure effect of climate change on annual national land area fraction affected by and population fraction exposed to crop failure (MIROC5 + PEPIC).** Analogous to Figure S156.

9.4 Wildfires

Land area affected

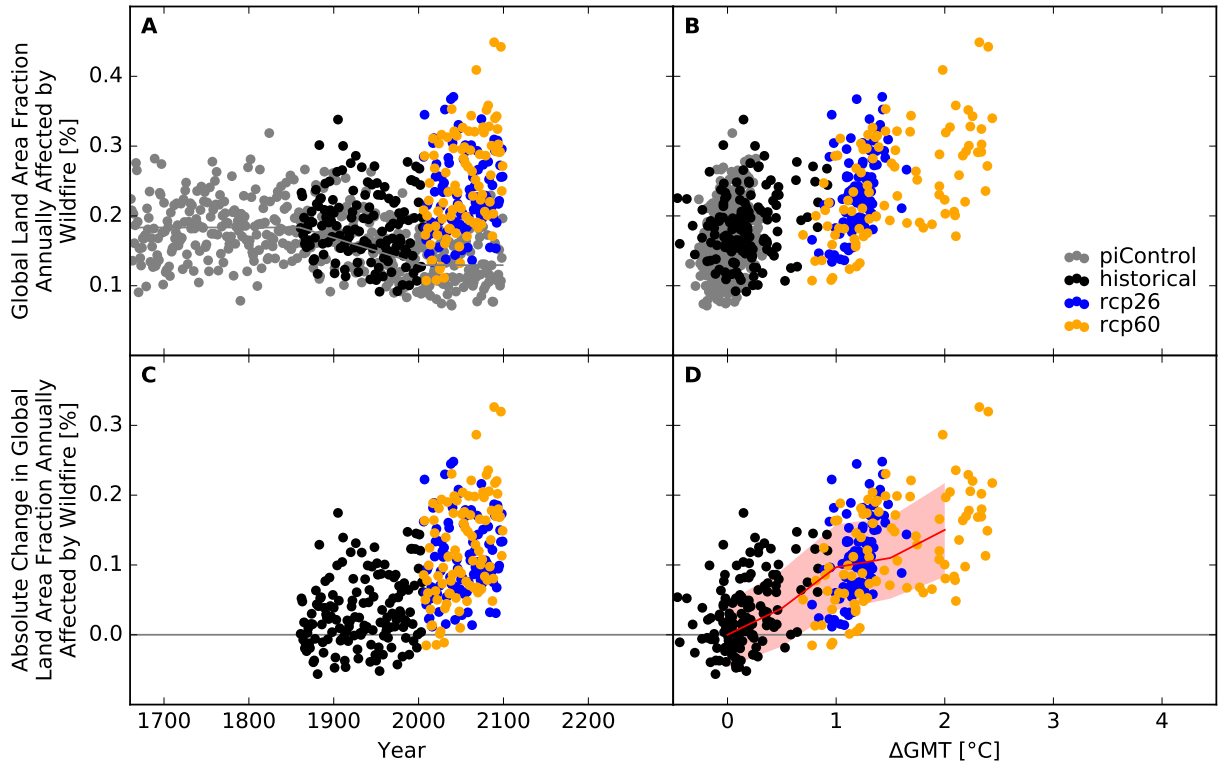

Figure S173: **Derivation of the pure effect of climate change on the global land area fraction annually affected by wildfire (GFDL-ESM2M + CARAIB).** Panel A: Time series of annual global land area fraction affected (AFA) by wildfire for preindustrial climate (grey dots), historical climate (black dots), climate projections for RCP2.6 (blue dots), and RCP6.0 (orange dots). In all simulations, socioeconomic conditions are varied according to the historically observed development between 1860 and 2005, and held fixed at 1860 conditions before 1860 and at 2005 conditions after 2005. The horizontal gray lines before 1860 and after 2005 represent the multi-year mean global land area fraction annually affected by wildfire under preindustrial climate conditions and socioeconomic conditions of 1860 and 2005, respectively. The gray line between 1860 and 2005 is a linear interpolation of these mean values. Panel B: Data shown in Panel A plotted against the associated GCM-specific annual global mean temperature (GMT) change relative to the long-term preindustrial mean GMT. Panel C: Pure effect of climate change on AFA, calculated as the difference between the annual data shown in Panel A and the multi-year mean AFA under preindustrial climate conditions (gray line in Panel A). Panel D: Data shown in Panel C plotted against annual GMT change. The red line represents the mean values of the annual data points per 1 °C-wide GMT change bin, with bins centered at GMT change levels increasing from 0 °C to 4 °C in steps of 0.5 °C. The area shaded in red represents the mean value ±1 standard deviation ranges of the annual data points per GMT change bin.

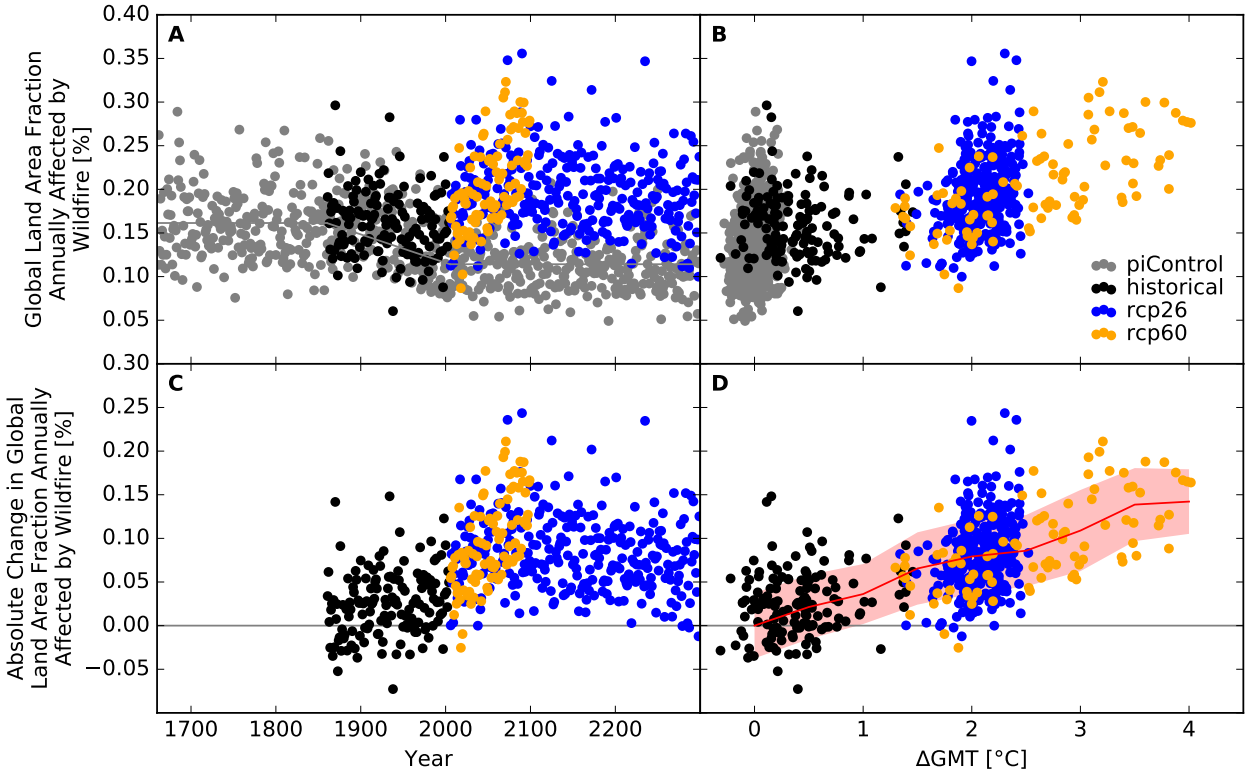

Figure S174: **Derivation of the pure effect of climate change on the global land area fraction annually affected by wildfire (IPSL-CM5A-LR + CARAIB).** Analogous to Figure S173.

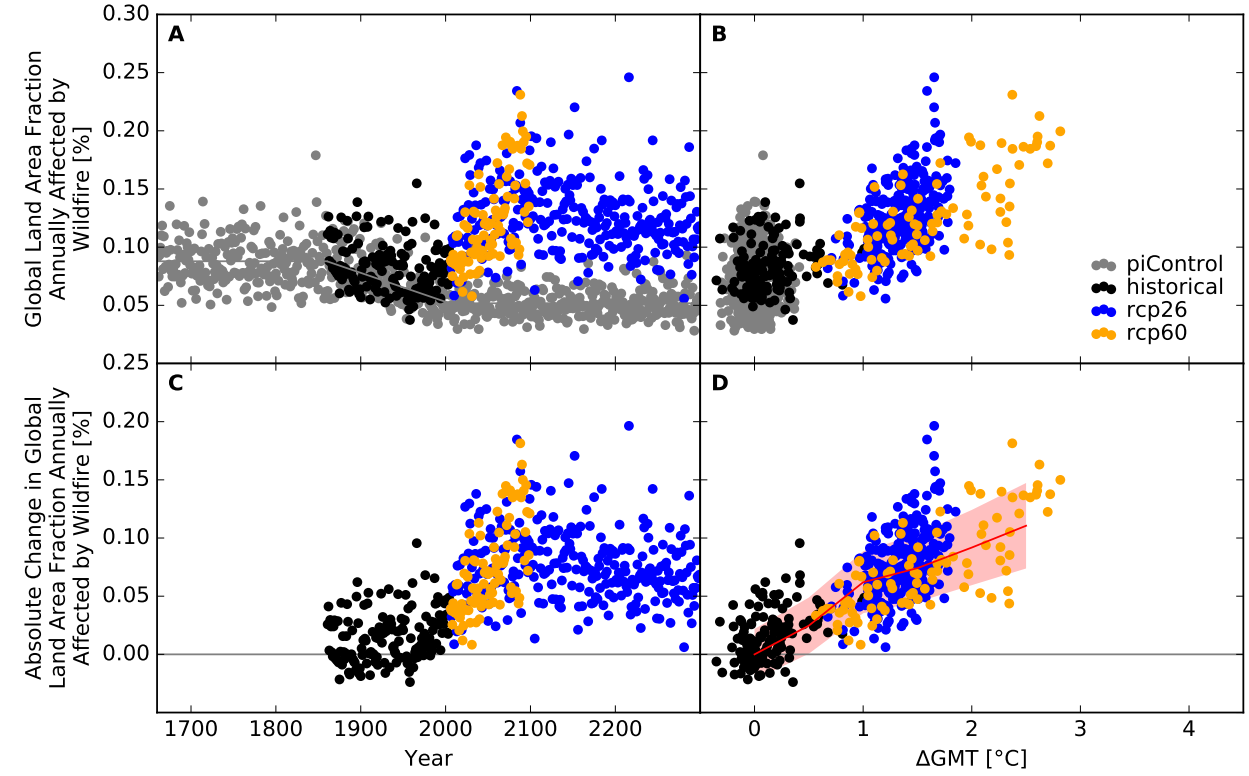

Figure S175: **Derivation of the pure effect of climate change on the global land area fraction annually affected by wildfire (MIROC5 + CARAIB).** Analogous to Figure S173.

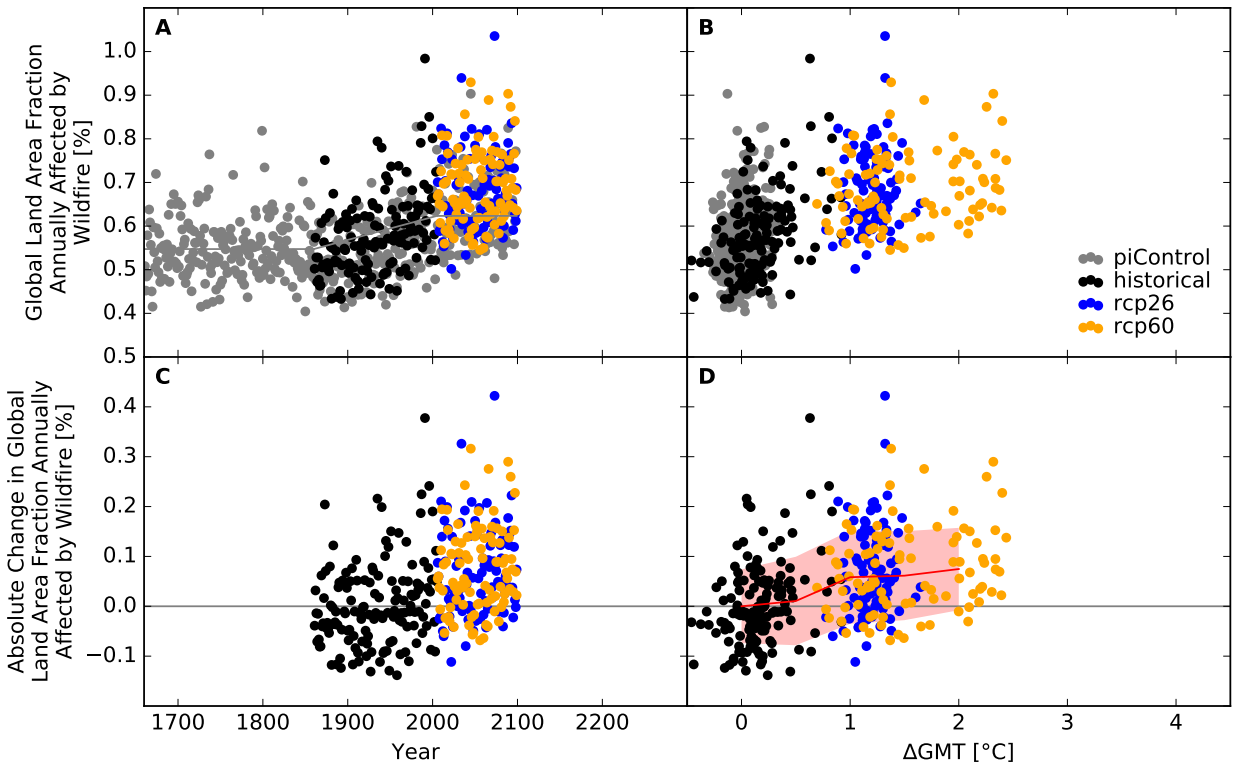

Figure S176: **Derivation of the pure effect of climate change on the global land area fraction annually affected by wildfire (GFDL-ESM2M + LPJ-GUESS).** Analogous to Figure S173.

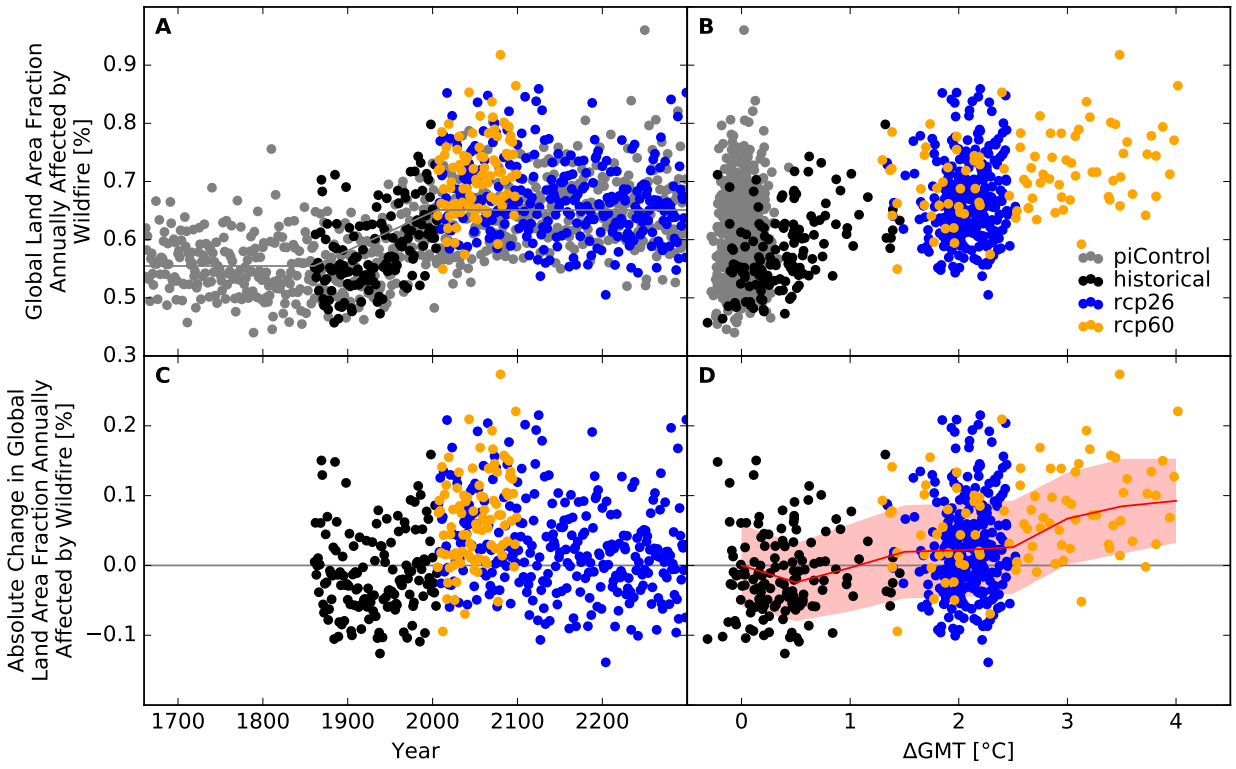

Figure S177: **Derivation of the pure effect of climate change on the global land area fraction annually affected by wildfire (IPSL-CM5A-LR + LPJ-GUESS).** Analogous to Figure S173.

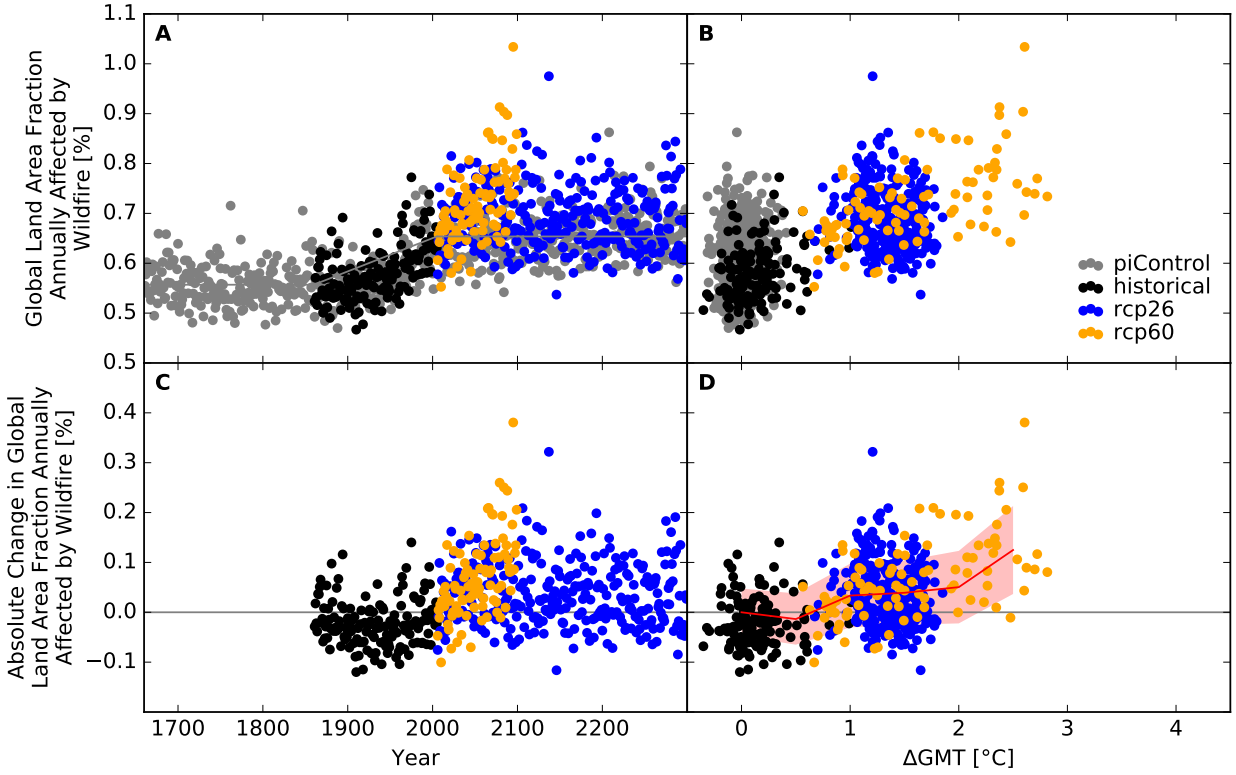

Figure S178: **Derivation of the pure effect of climate change on the global land area fraction annually affected by wildfire (MIROC5 + LPJ-GUESS).** Analogous to Figure S173.

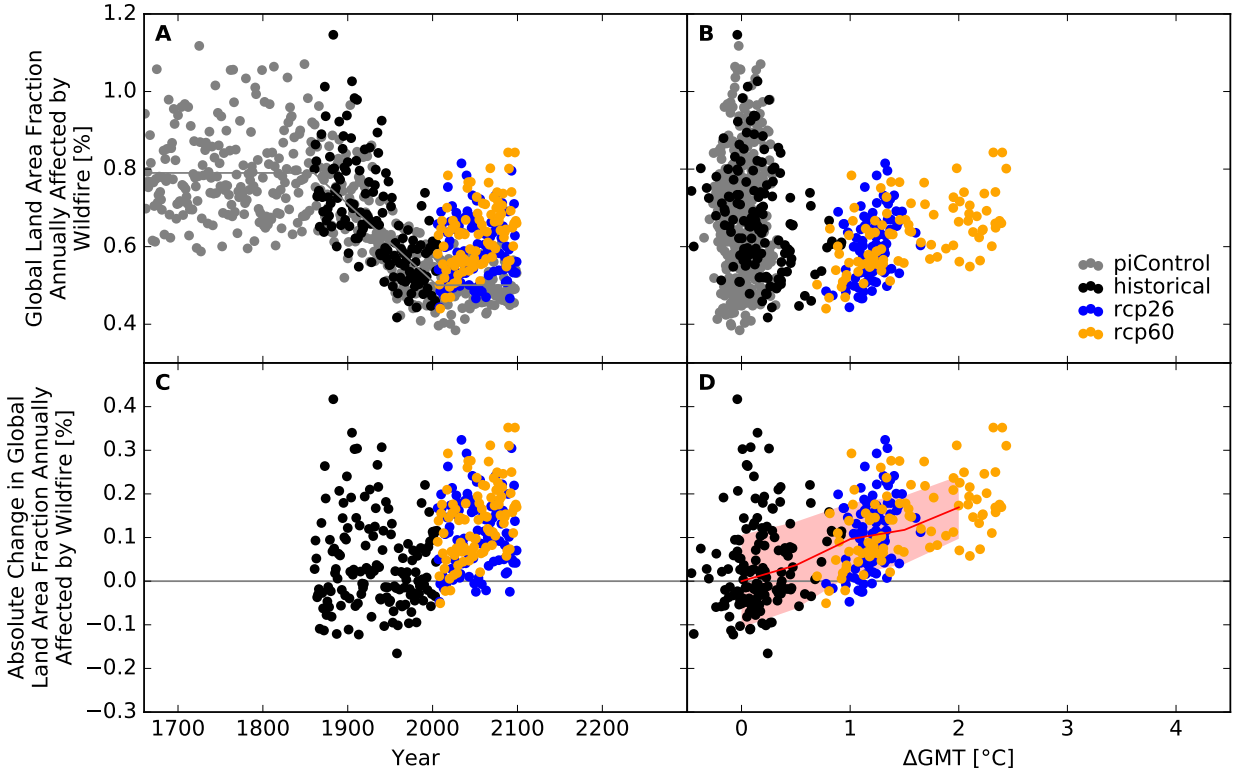

Figure S179: **Derivation of the pure effect of climate change on the global land area fraction annually affected by wildfire (GFDL-ESM2M + LPJmL).** Analogous to Figure S173.

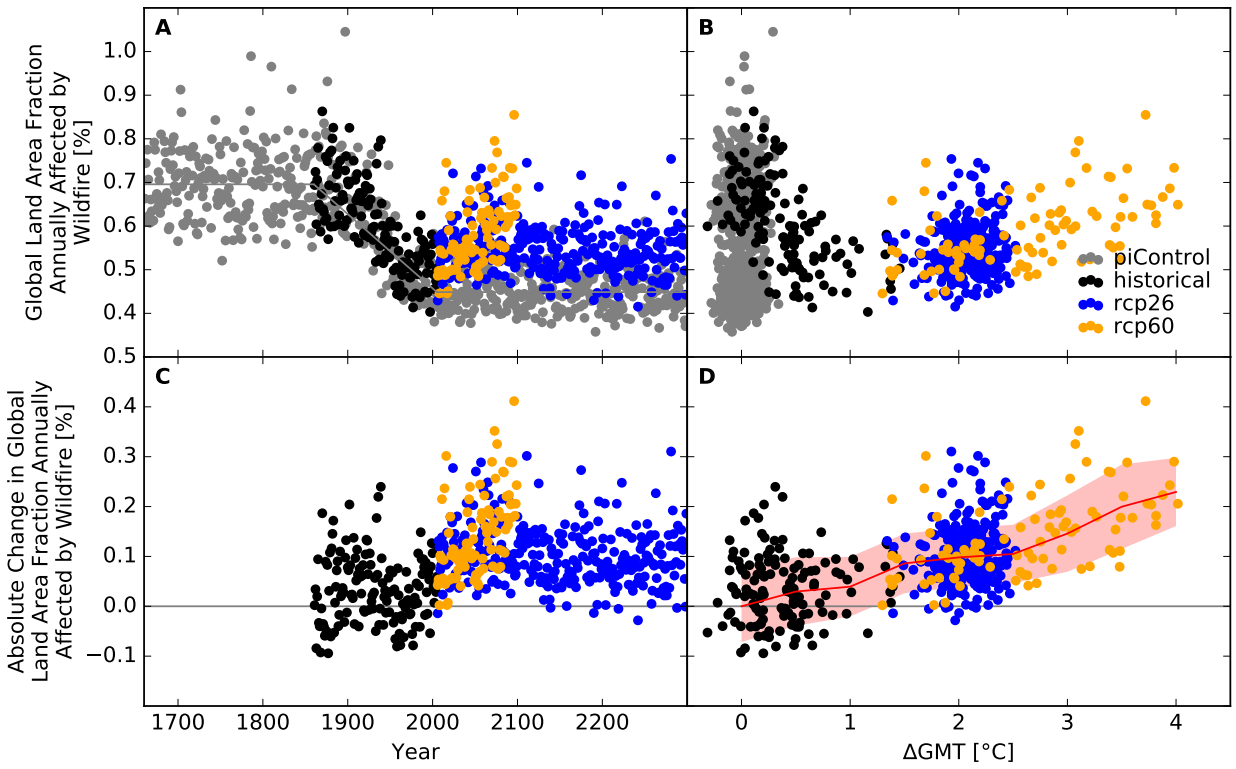

Figure S180: **Derivation of the pure effect of climate change on the global land area fraction annually affected by wildfire (IPSL-CM5A-LR + LPJmL).** Analogous to Figure S173.

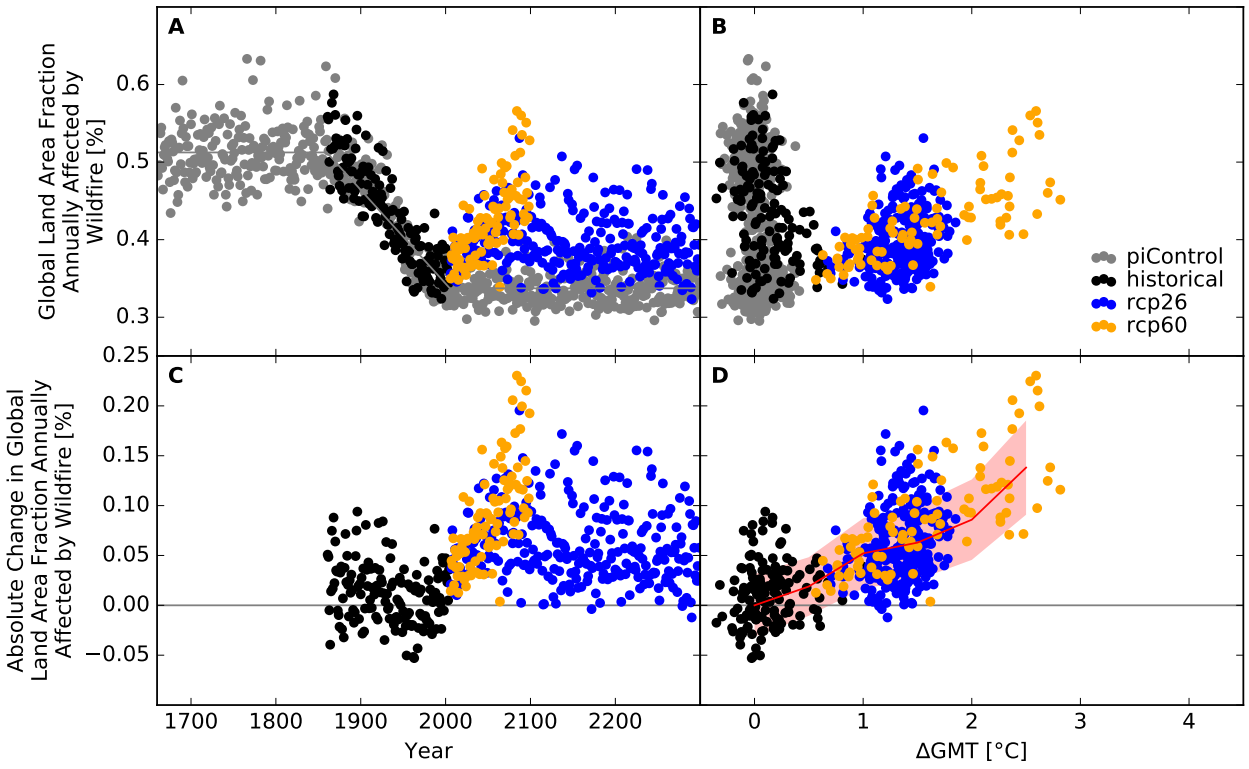

Figure S181: **Derivation of the pure effect of climate change on the global land area fraction annually affected by wildfire (MIROC5 + LPJmL).** Analogous to Figure S173.

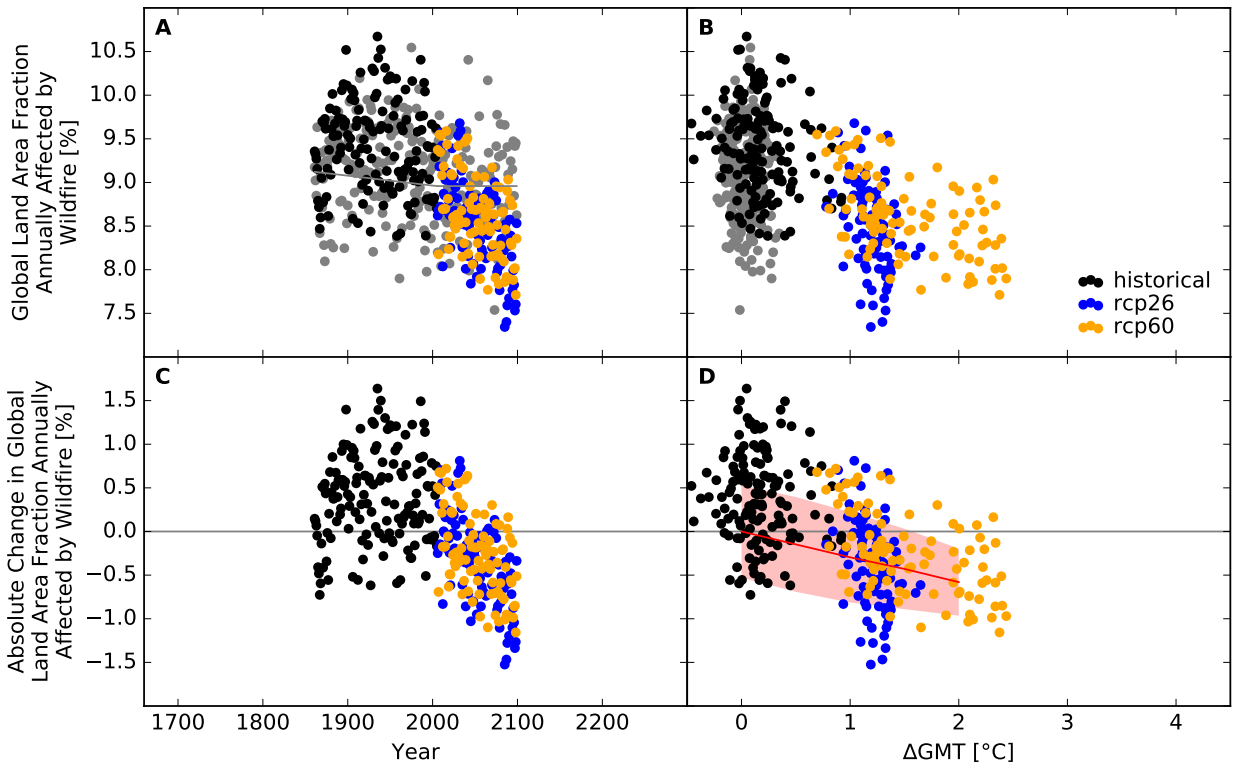

Figure S182: **Derivation of the pure effect of climate change on the global land area fraction annually affected by wildfire (GFDL-ESM2M + ORCHIDEE).** Analogous to Figure S173.

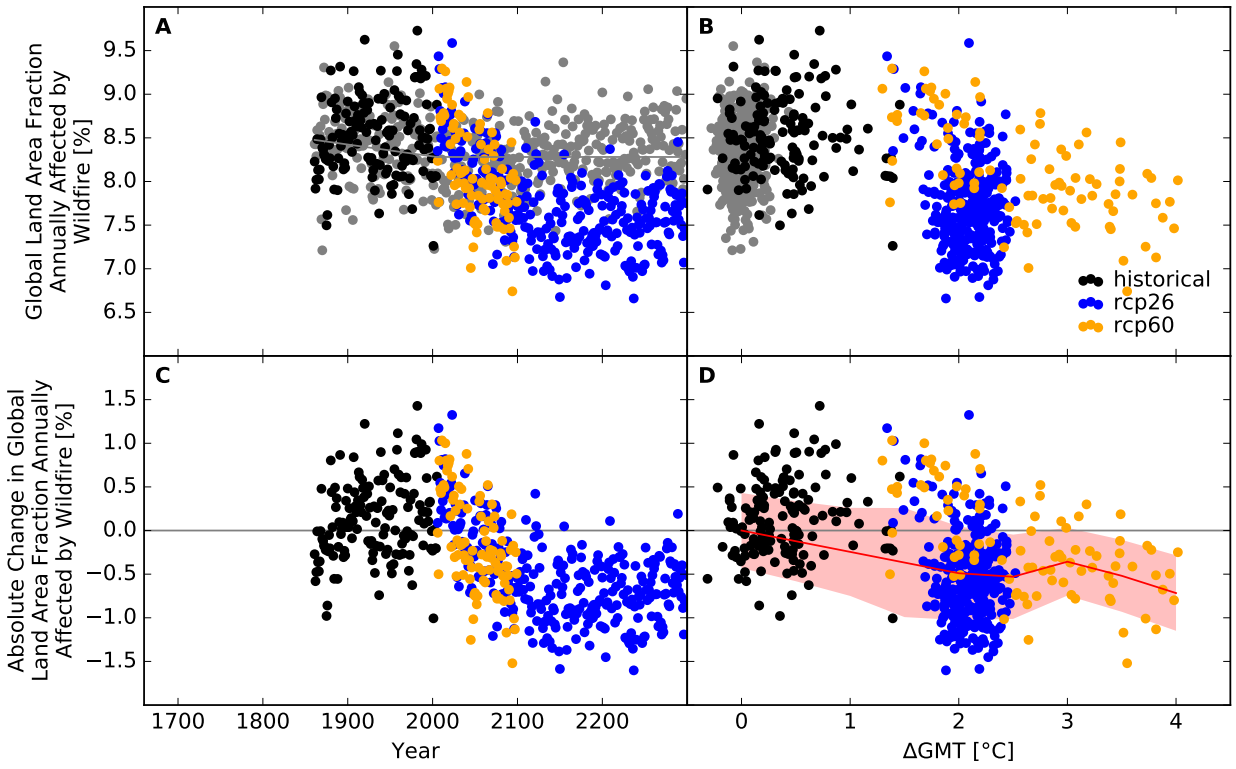

Figure S183: **Derivation of the pure effect of climate change on the global land area fraction annually affected by wildfire (IPSL-CM5A-LR + ORCHIDEE).** Analogous to Figure S173.

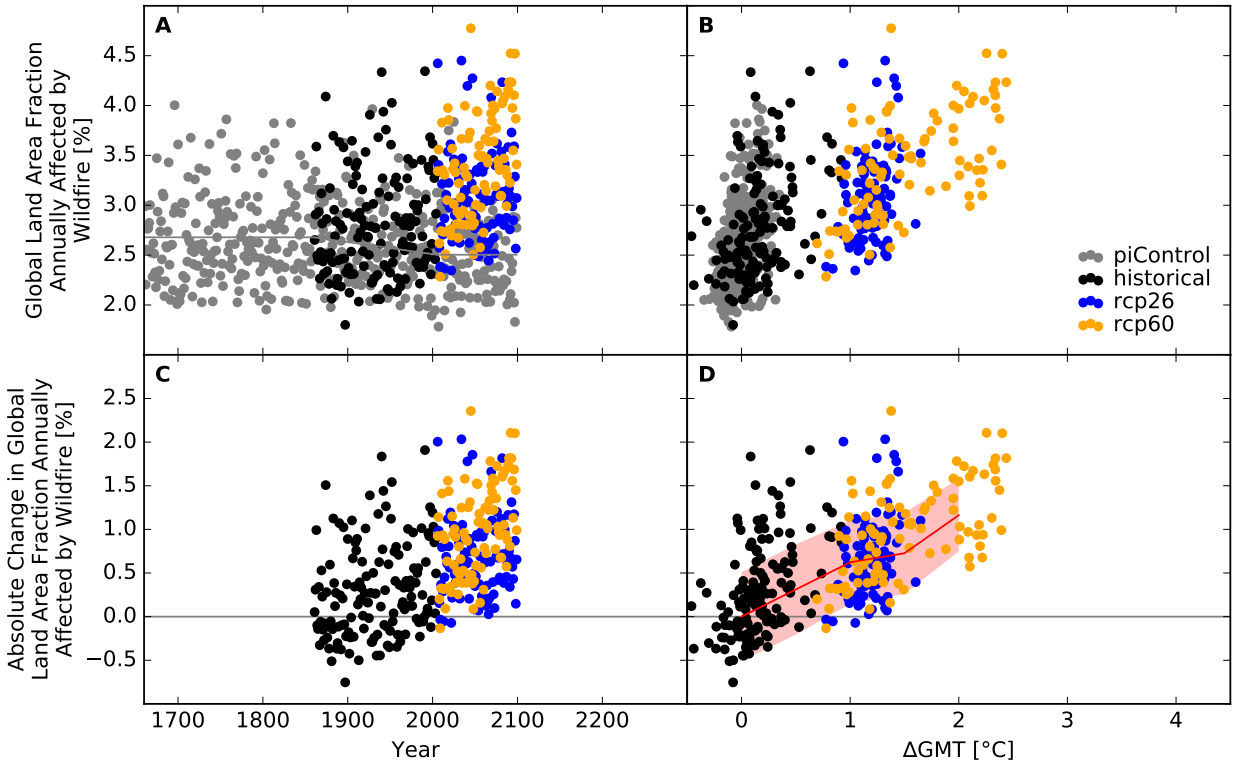

Figure S184: **Derivation of the pure effect of climate change on the global land area fraction annually affected by wildfire (GFDL-ESM2M + VISIT).** Analogous to Figure S173.

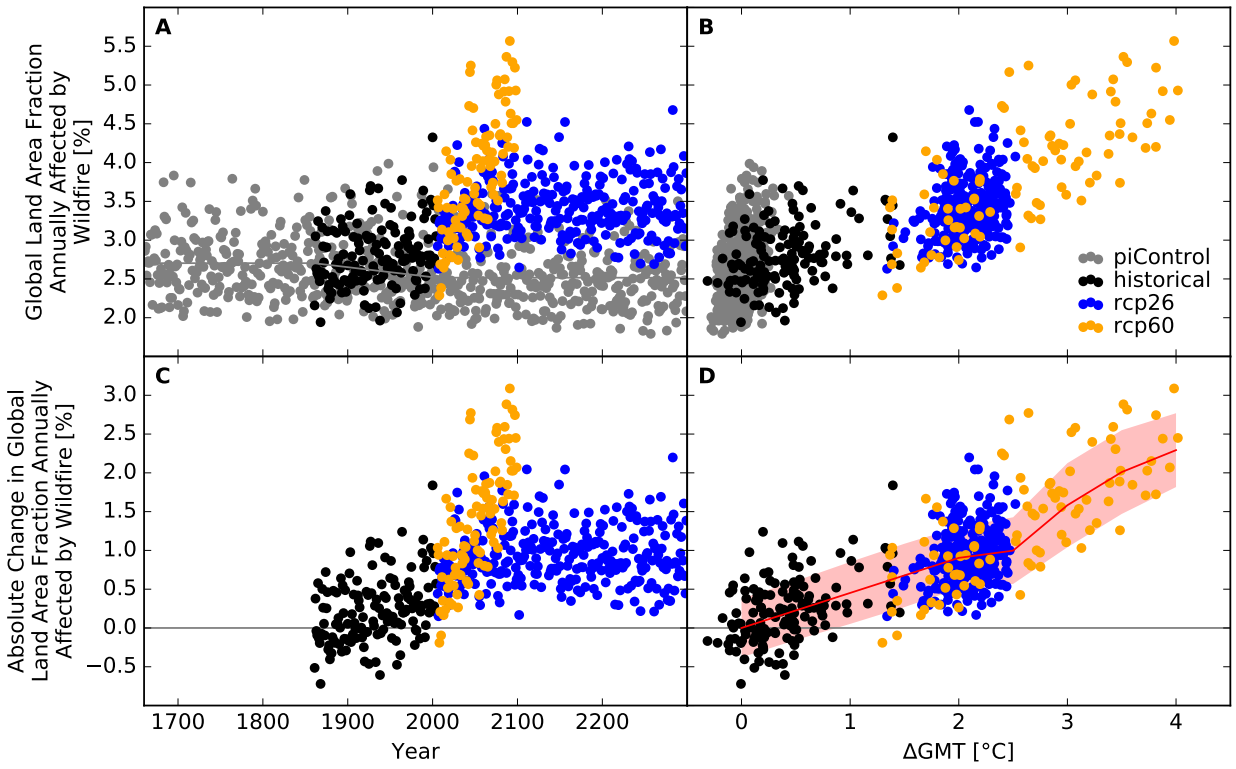

Figure S185: **Derivation of the pure effect of climate change on the global land area fraction annually affected by wildfire (IPSL-CM5A-LR + VISIT).** Analogous to Figure S173.

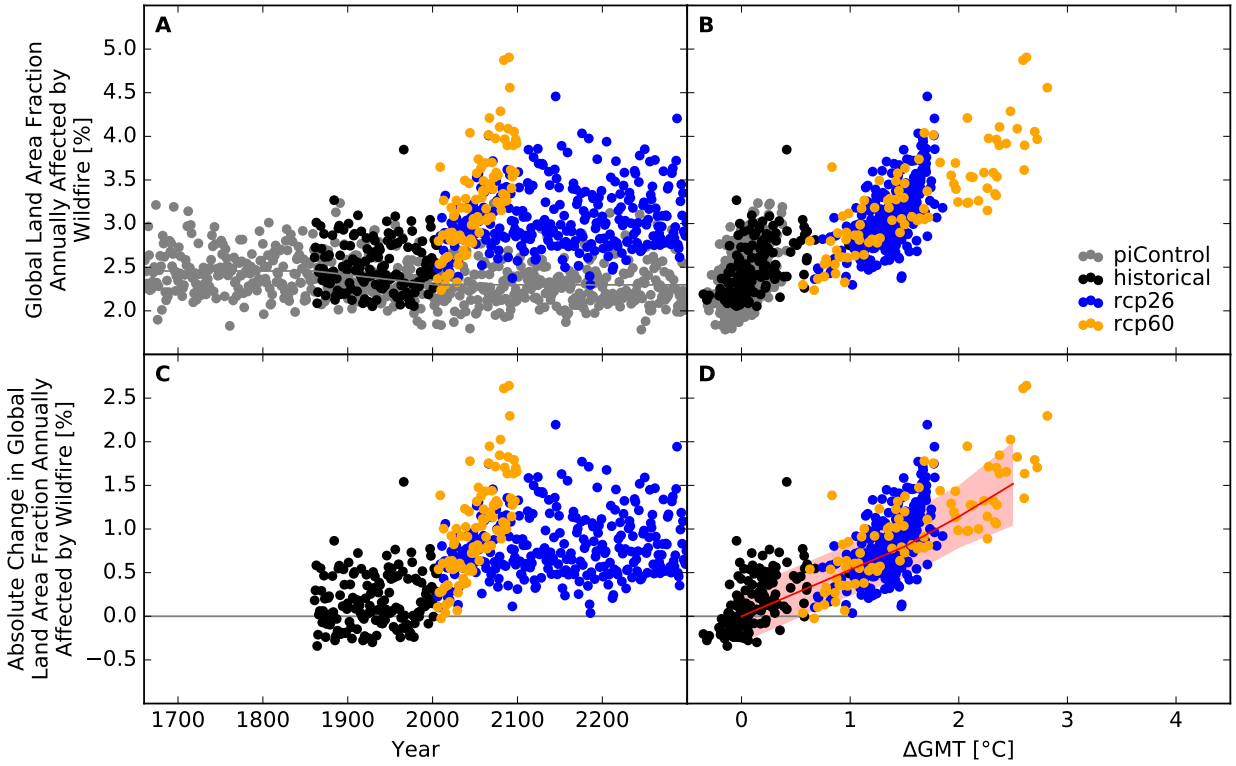

Figure S186: **Derivation of the pure effect of climate change on the global land area fraction annually affected by wildfire (MIROC5 + VISIT).** Analogous to Figure S173.

Number of people exposed

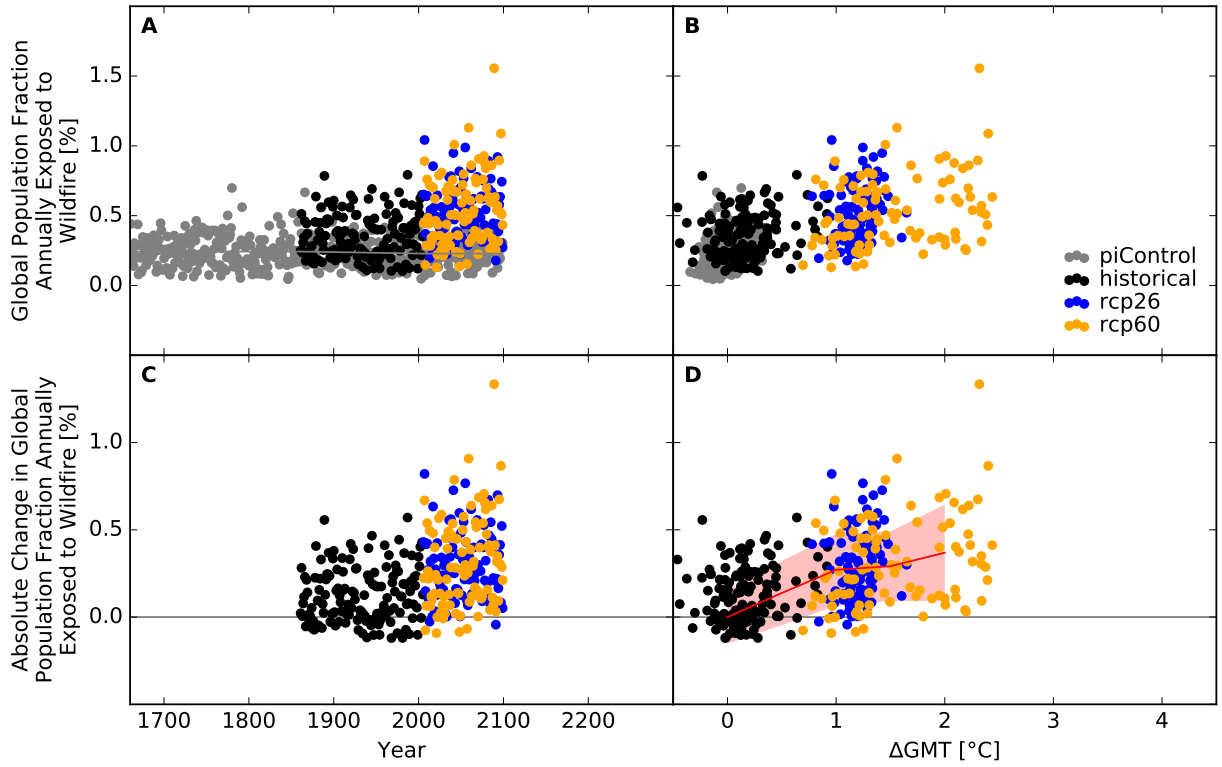

Figure S187: **Derivation of the pure effect of climate change on the global population fraction annually exposed to wildfire (GFDL-ESM2M + CARAIB).** Panel A: Time series of annual global population fraction exposed (PFE) to wildfire for preindustrial climate (grey dots), historical climate (black dots), climate projections for RCP2.6 (blue dots), and RCP6.0 (orange dots). In all simulations, socioeconomic conditions are varied according to the historically observed development between 1860 and 2005, and held fixed at 1860 conditions before 1860 and at 2005 conditions after 2005. The horizontal gray lines before 1860 and after 2005 represent the multi-year mean global population fraction annually exposed to wildfire under preindustrial climate conditions and socioeconomic conditions of 1860 and 2005, respectively. The gray line between 1860 and 2005 is a linear interpolation of these mean values. Panel B: Data shown in Panel A plotted against the associated GCM-specific annual global mean temperature (GMT) change relative to the long-term preindustrial mean GMT. Panel C: Pure effect of climate change on PFE, calculated as the difference between the annual data shown in Panel A and the multi-year mean PFE under preindustrial climate conditions (gray line in Panel A). Panel D: Data shown in Panel C plotted against annual GMT change. The red line represents the mean values of the annual data points per 1 °C-wide GMT change bin, with bins centered at GMT change levels increasing from 0 °C to 4 °C in steps of 0.5 °C. The area shaded in red represents the mean value ±1 standard deviation ranges of the annual data points per GMT change bin.

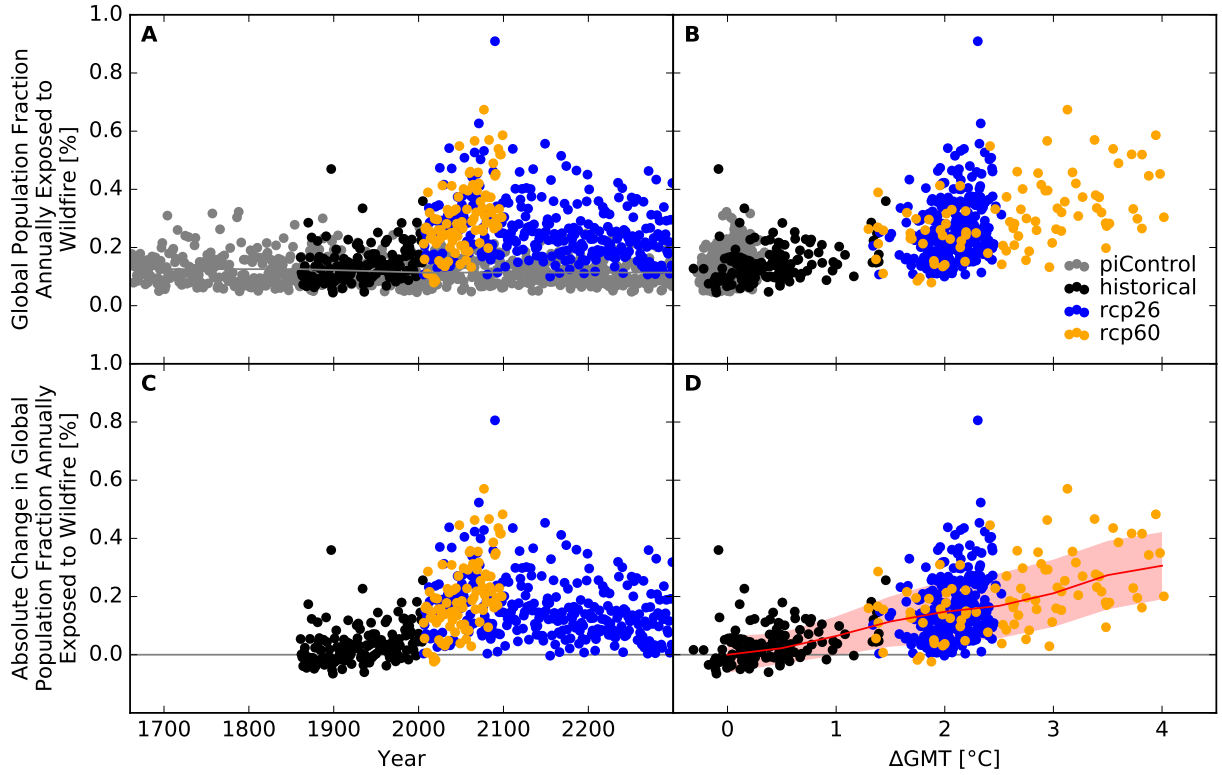

Figure S188: **Derivation of the pure effect of climate change on the global population fraction annually exposed to wildfire (IPSL-CM5A-LR + CARAIB).** Analogous to Figure S187.

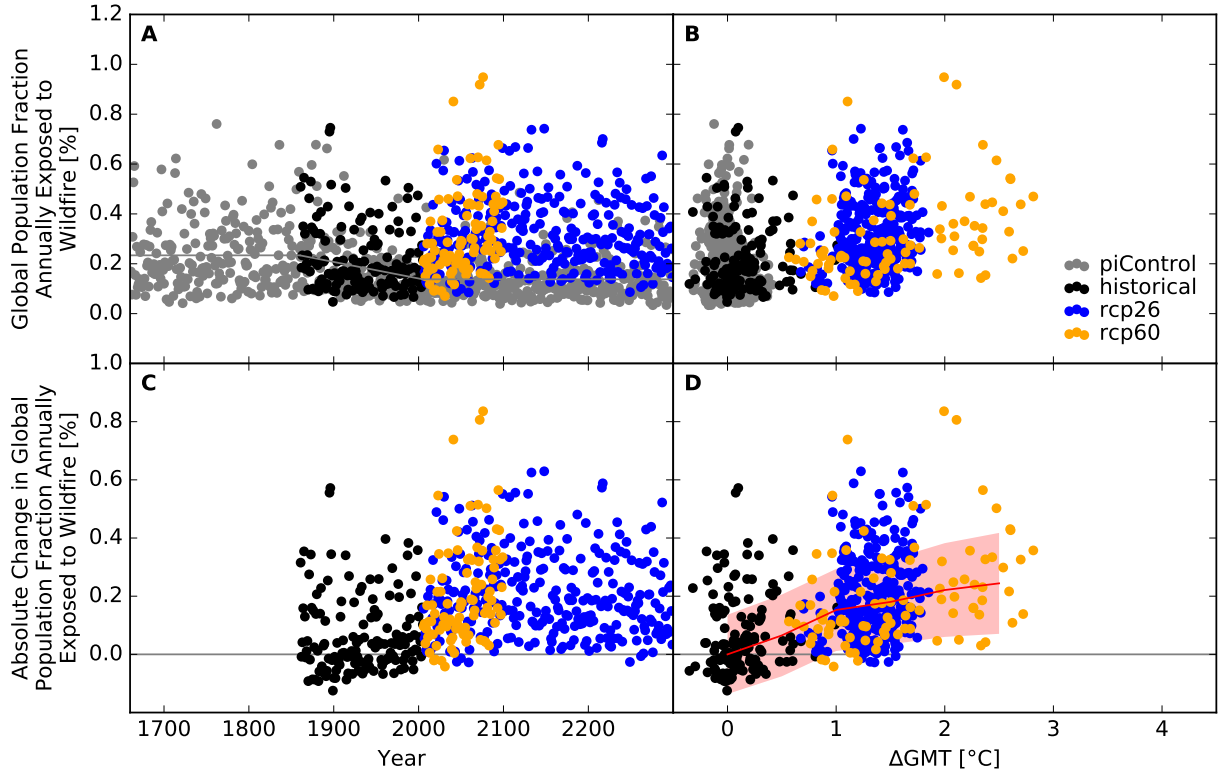

Figure S189: **Derivation of the pure effect of climate change on the global population fraction annually exposed to wildfire (MIROC5 + CARAIB).** Analogous to Figure S187.

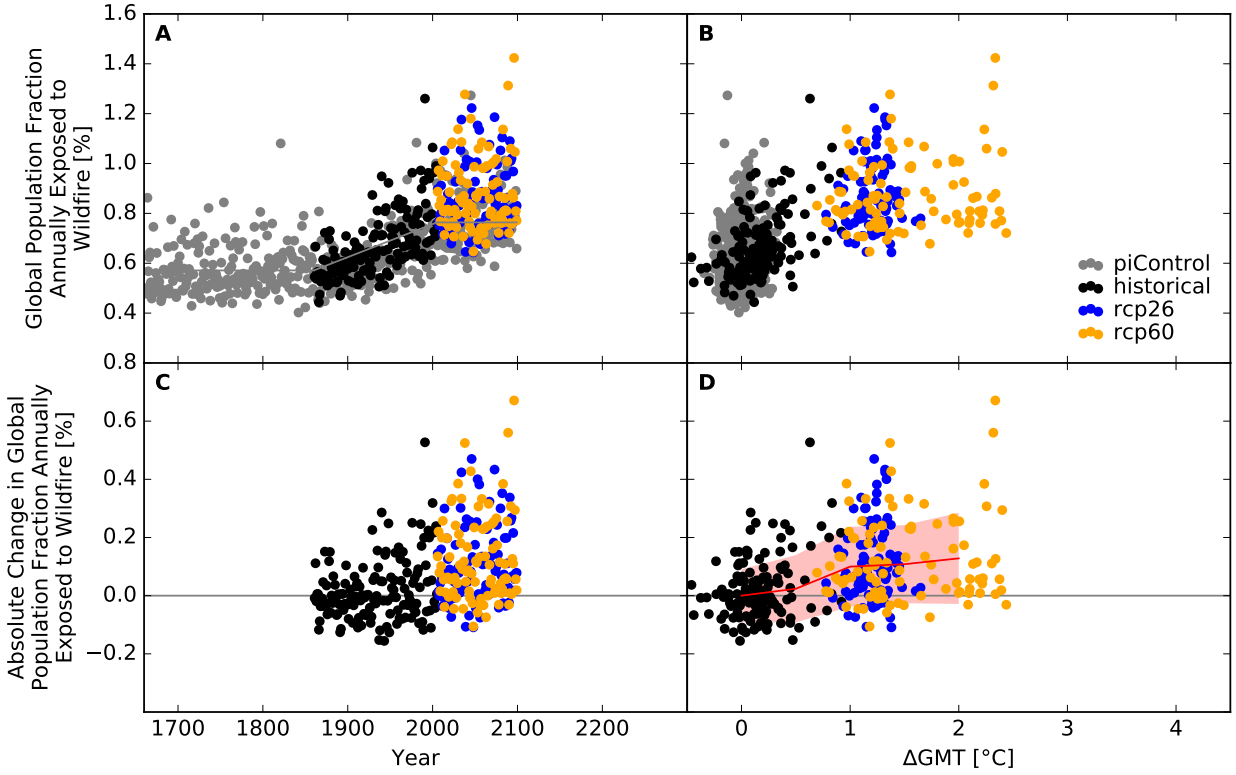

Figure S190: **Derivation of the pure effect of climate change on the global population fraction annually exposed to wildfire (GFDL-ESM2M + LPJ-GUESS).** Analogous to Figure S187.

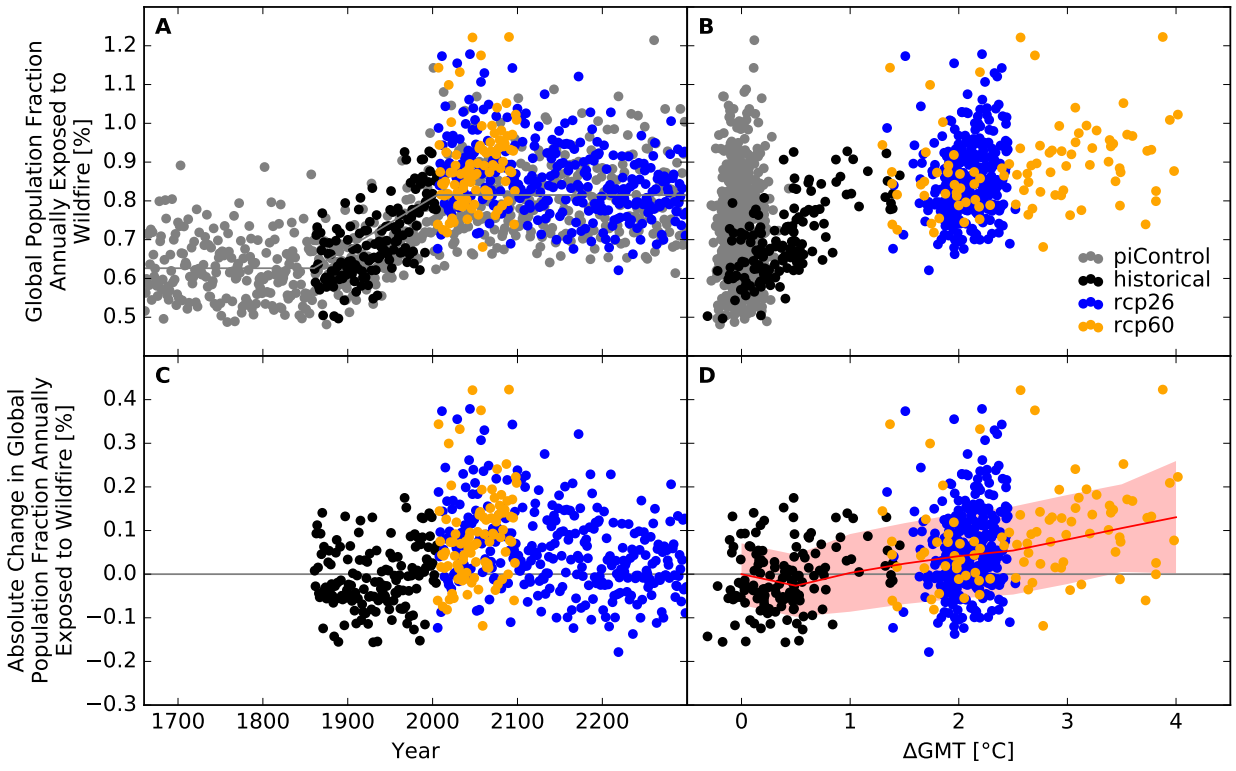

Figure S191: **Derivation of the pure effect of climate change on the global population fraction annually exposed to wildfire (IPSL-CM5A-LR + LPJ-GUESS).** Analogous to Figure S187.

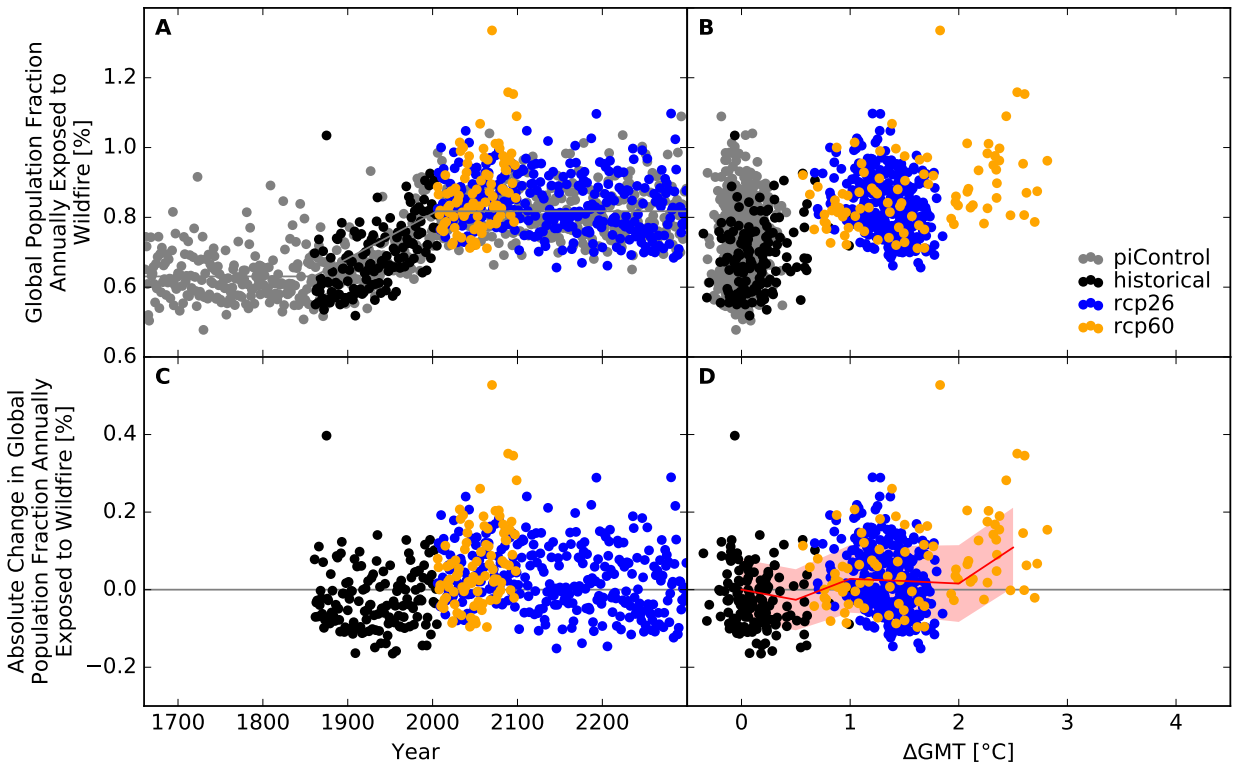

Figure S192: **Derivation of the pure effect of climate change on the global population fraction annually exposed to wildfire (MIROC5 + LPJ-GUESS).** Analogous to Figure S187.

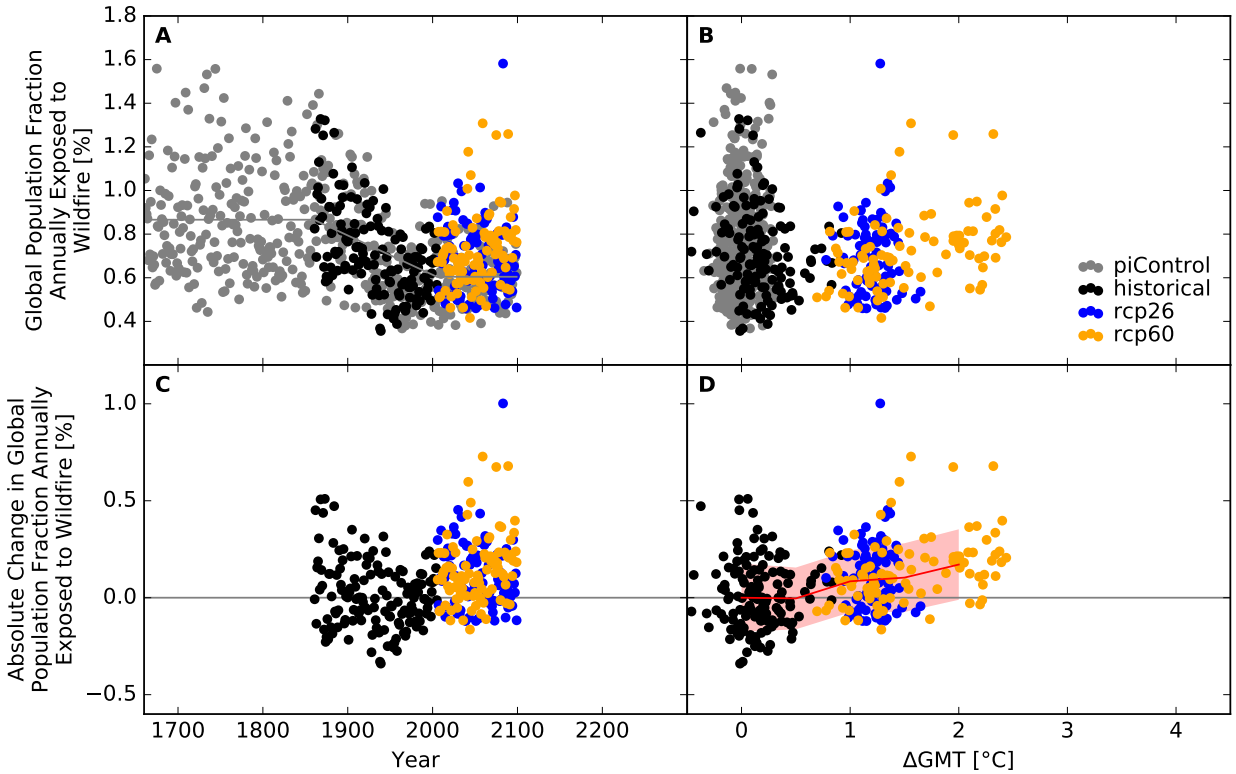

Figure S193: **Derivation of the pure effect of climate change on the global population fraction annually exposed to wildfire (GFDL-ESM2M + LPJmL).** Analogous to Figure S187.

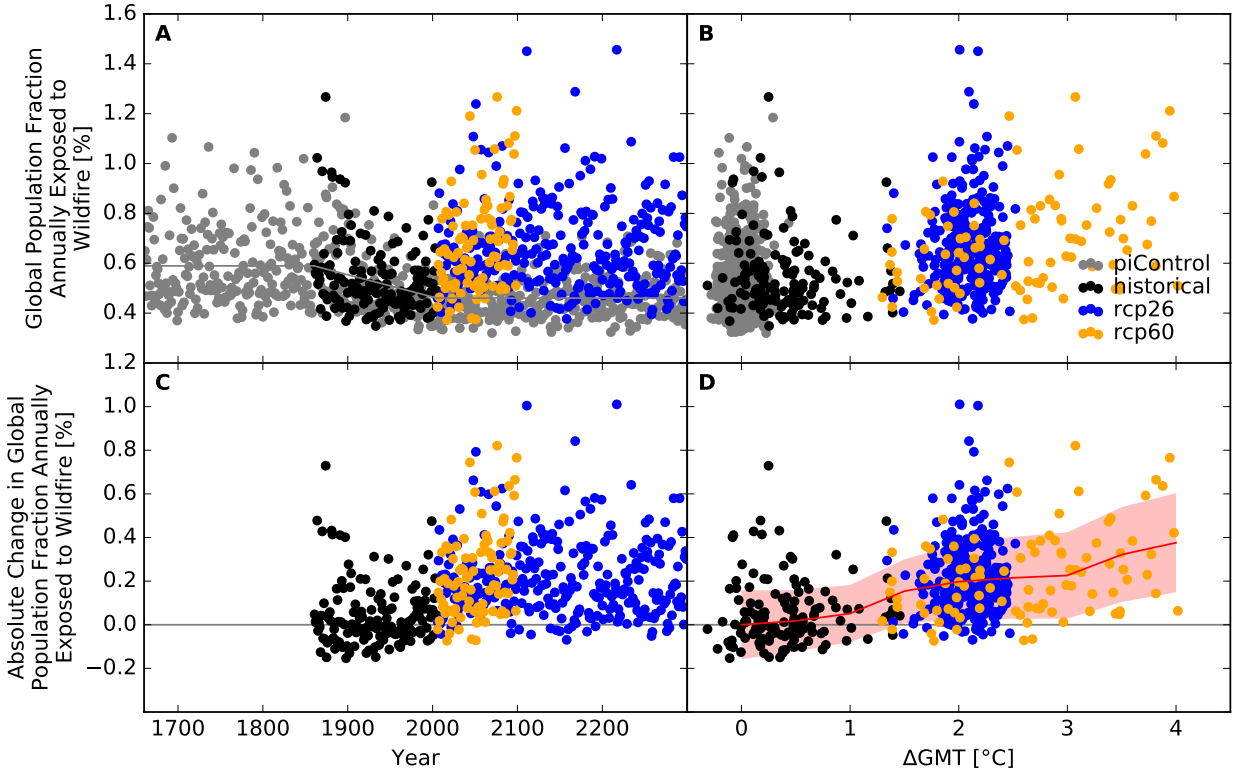

Figure S194: **Derivation of the pure effect of climate change on the global population fraction annually exposed to wildfire (IPSL-CM5A-LR + LPJmL).** Analogous to Figure S187.

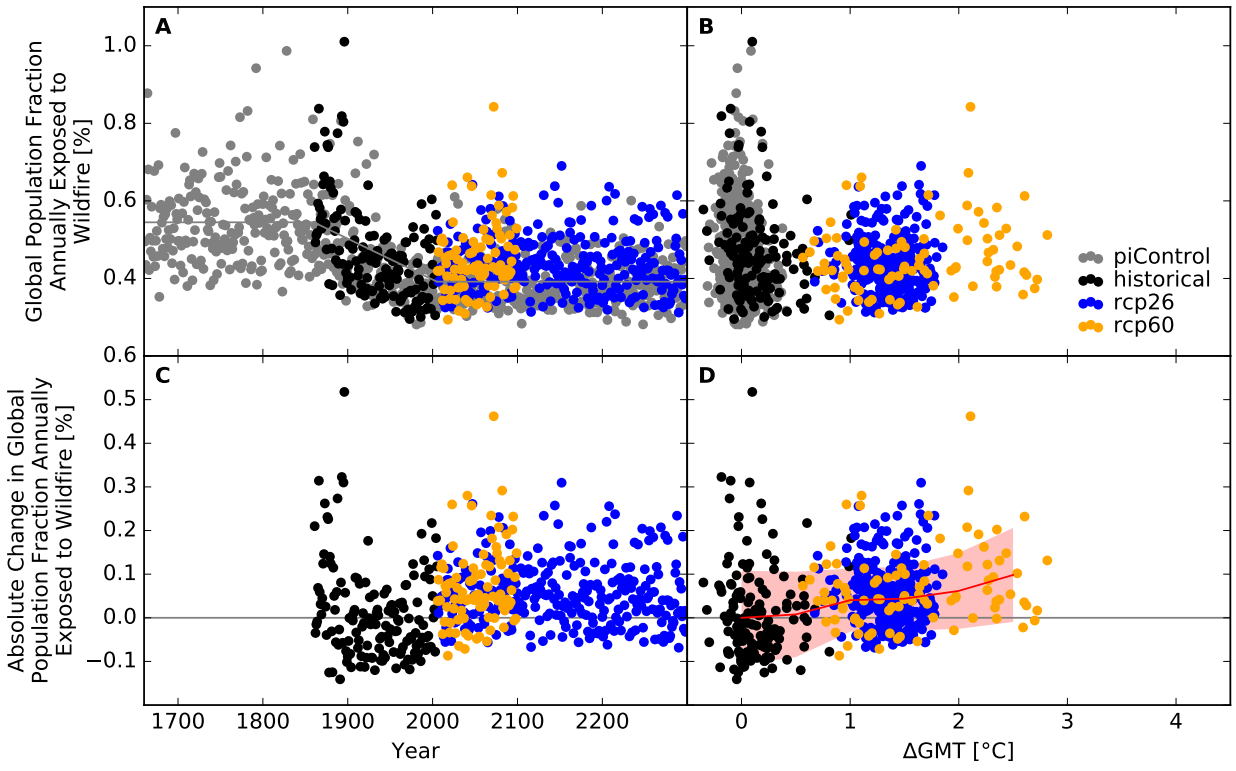

Figure S195: **Derivation of the pure effect of climate change on the global population fraction annually exposed to wildfire (MIROC5 + LPJmL).** Analogous to Figure S187.

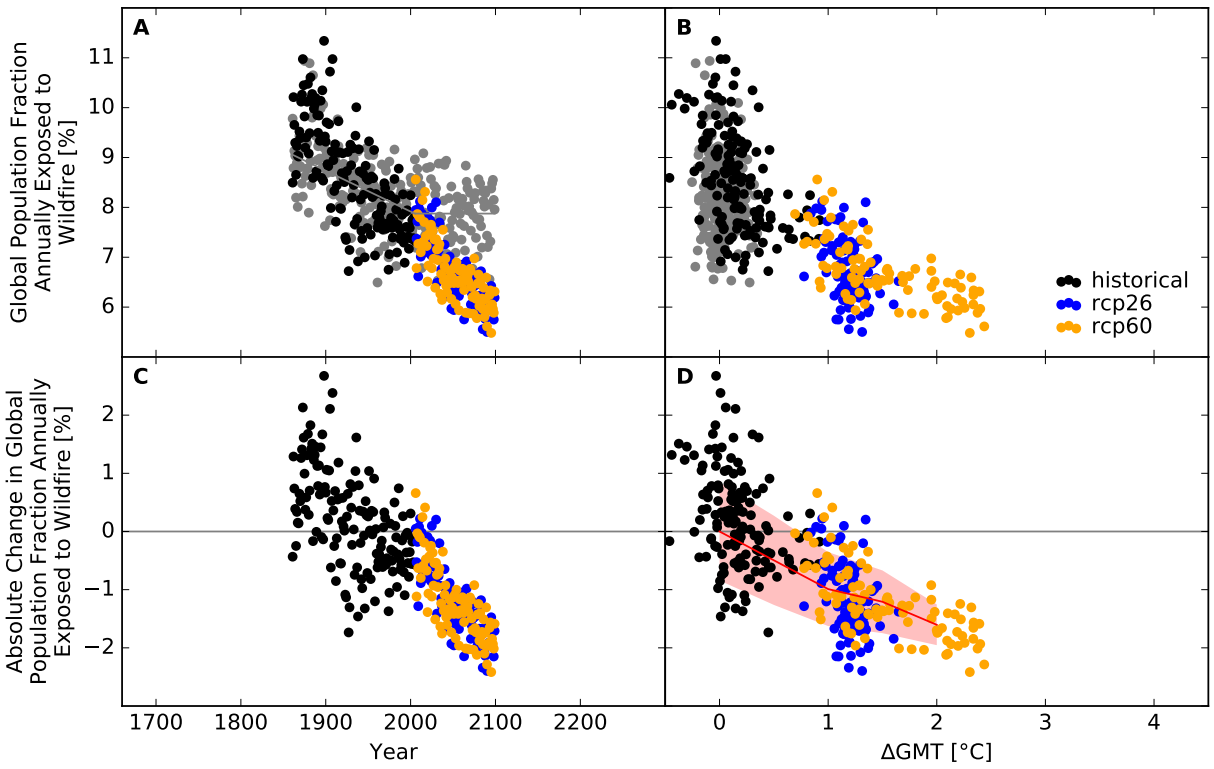

Figure S196: **Derivation of the pure effect of climate change on the global population fraction annually exposed to wildfire (GFDL-ESM2M + ORCHIDEE).** Analogous to Figure S187.

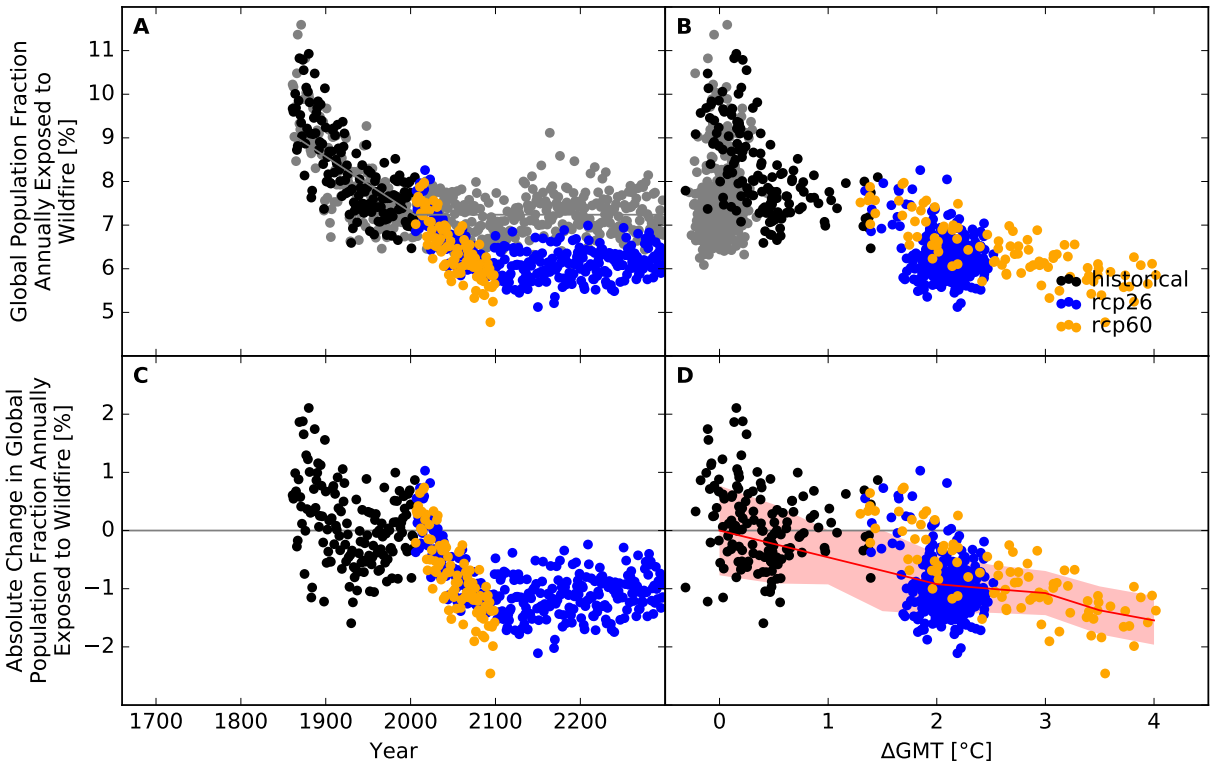

Figure S197: **Derivation of the pure effect of climate change on the global population fraction annually exposed to wildfire (IPSL-CM5A-LR + ORCHIDEE).** Analogous to Figure S187.

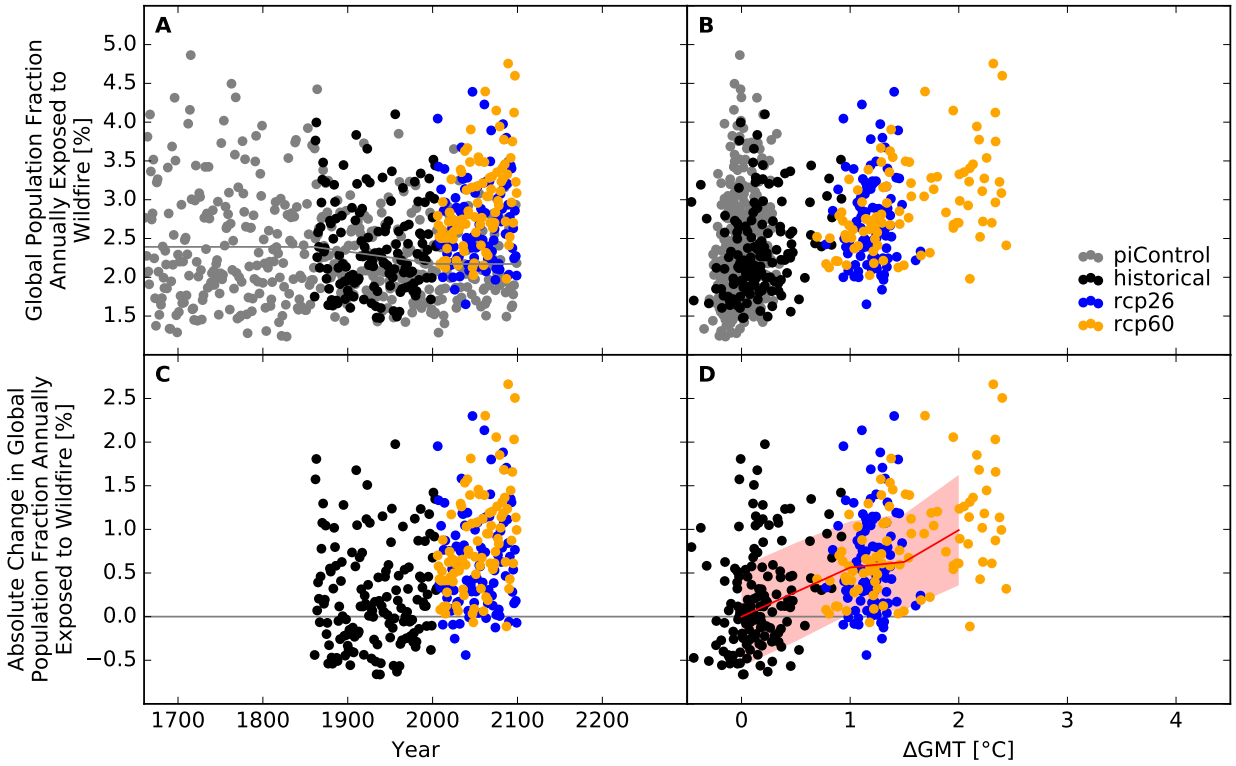

Figure S198: **Derivation of the pure effect of climate change on the global population fraction annually exposed to wildfire (GFDL-ESM2M + VISIT).** Analogous to Figure S187.

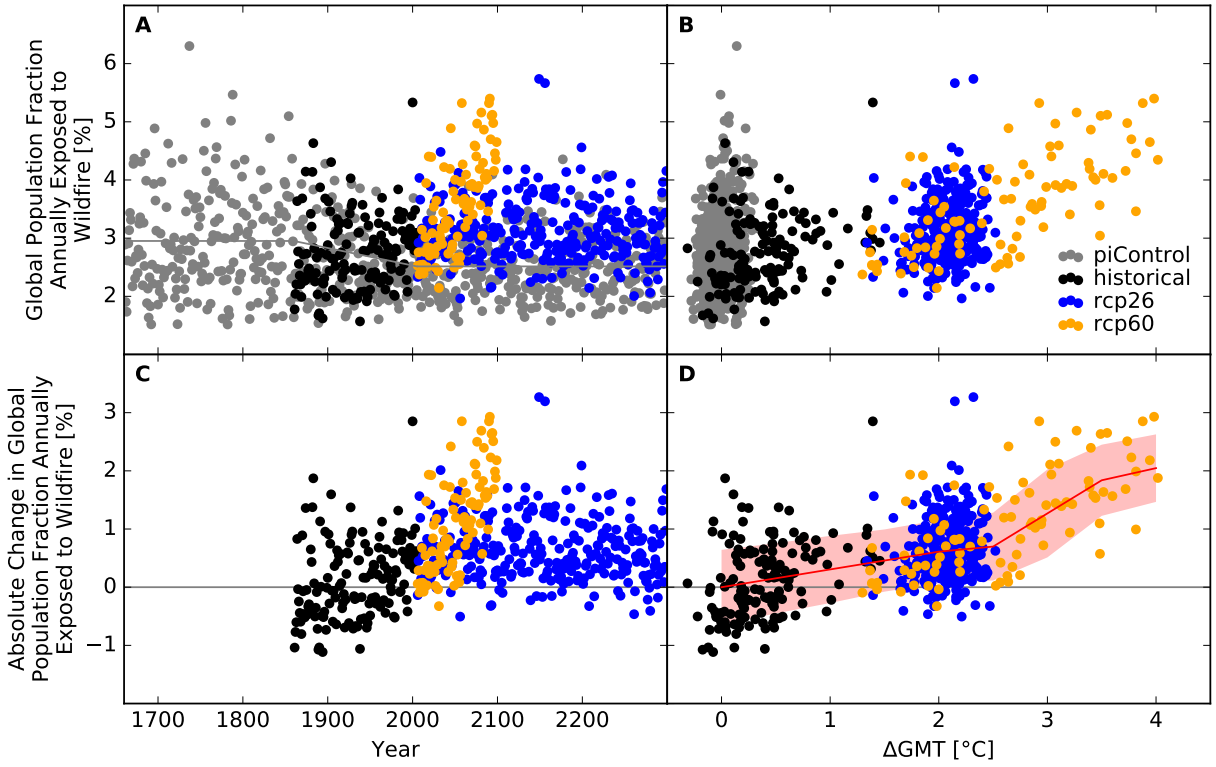

Figure S199: **Derivation of the pure effect of climate change on the global population fraction annually exposed to wildfire (IPSL-CM5A-LR + VISIT).** Analogous to Figure S187.

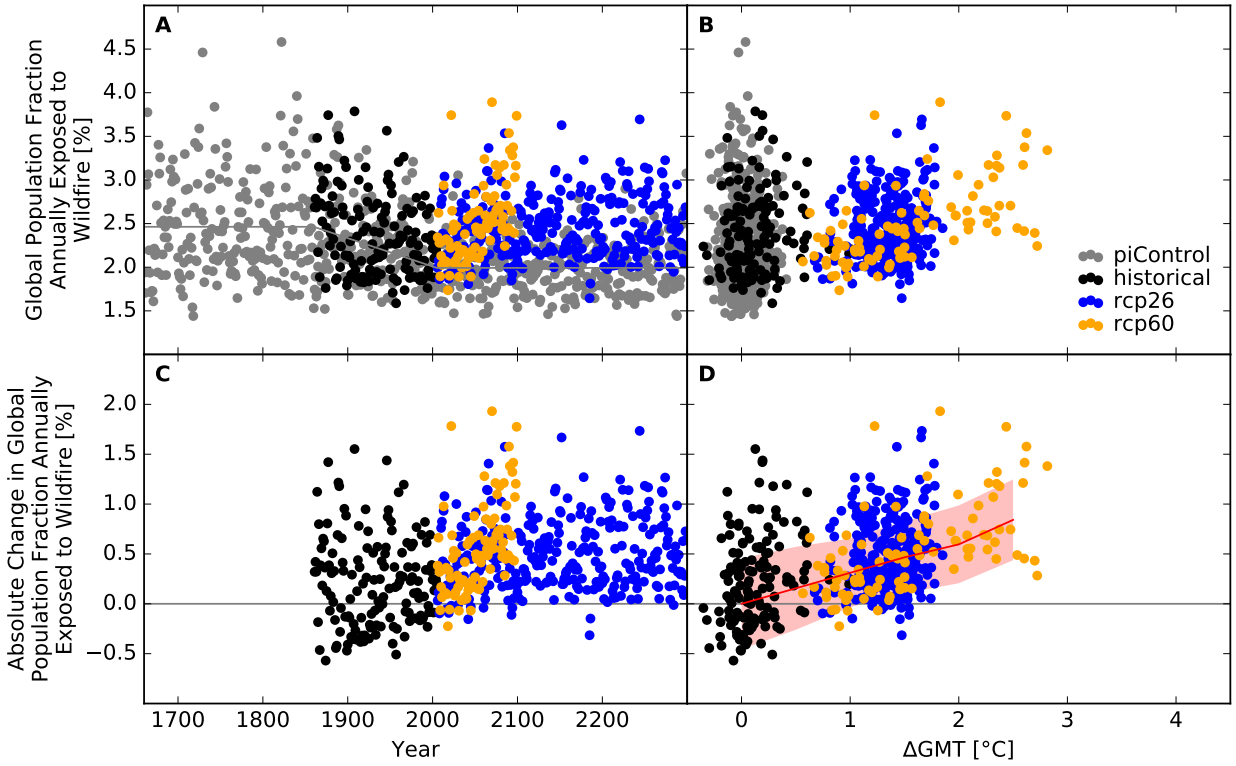

Figure S200: **Derivation of the pure effect of climate change on the global population fraction annually exposed to wildfire (MIROC5 + VISIT).** Analogous to Figure S187.

Land area affected and number of people exposed at the national scale

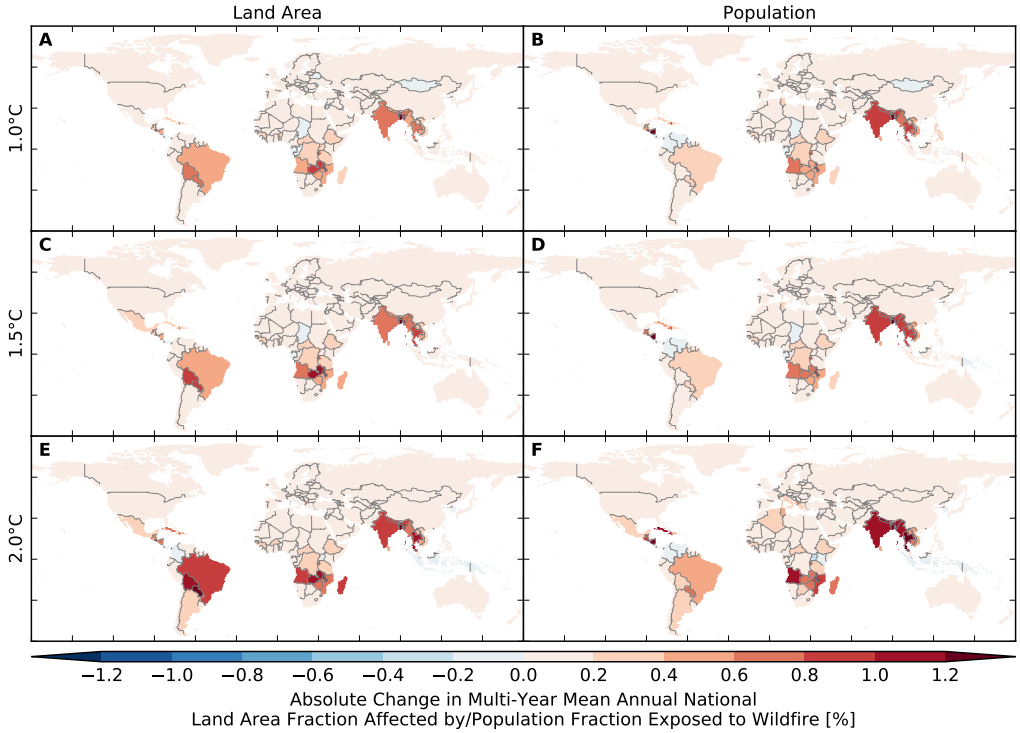

Figure S201: **Pure effect of climate change on annual national land area fraction affected by and population fraction exposed to wildfire (GFDL-ESM2M + CARAIB).** Absolute changes in multi-year mean annual national (A, C, E) land area fraction affected by and (B, D, F) population fraction exposed to wildfire at (A, B) 1 °C, (C, D) 1.5 °C and (E, F) 2 °C global warming.

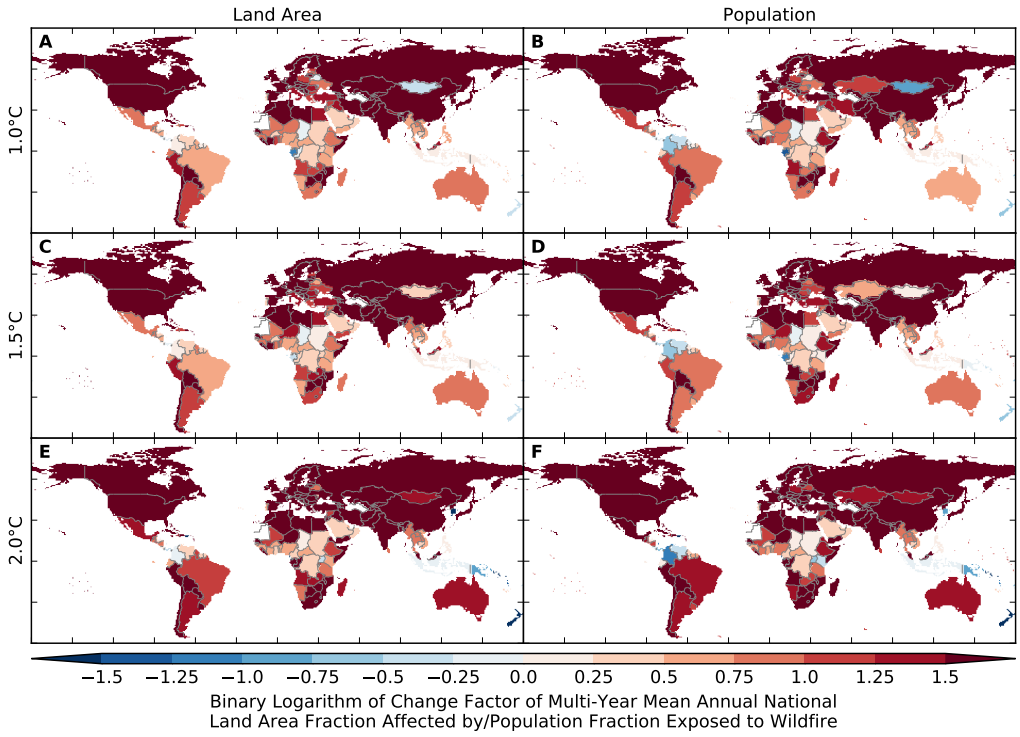

Figure S202: **Pure effect of climate change on annual national land area fraction affected by and population fraction exposed to wildfire (GFDL-ESM2M + CARAIB).** Same as Figure S201 but for relative changes expressed in terms of binary logarithms of change factors, i.e. −1 means a change by a factor of 0.5, 0 means no change, and 1 means a change by a factor of 2. White indicates undefined relative changes due to division by zero.

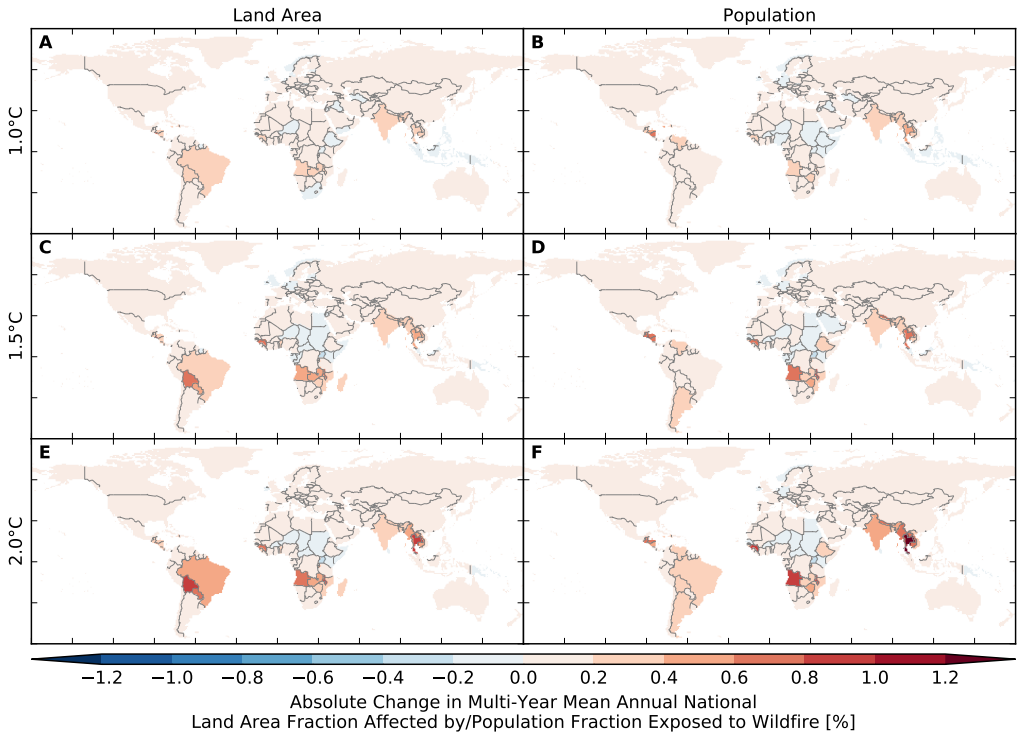

Figure S203: **Pure effect of climate change on annual national land area fraction affected by and population fraction exposed to wildfire (IPSL-CM5A-LR + CARAIB).** Analogous to Figure S201.

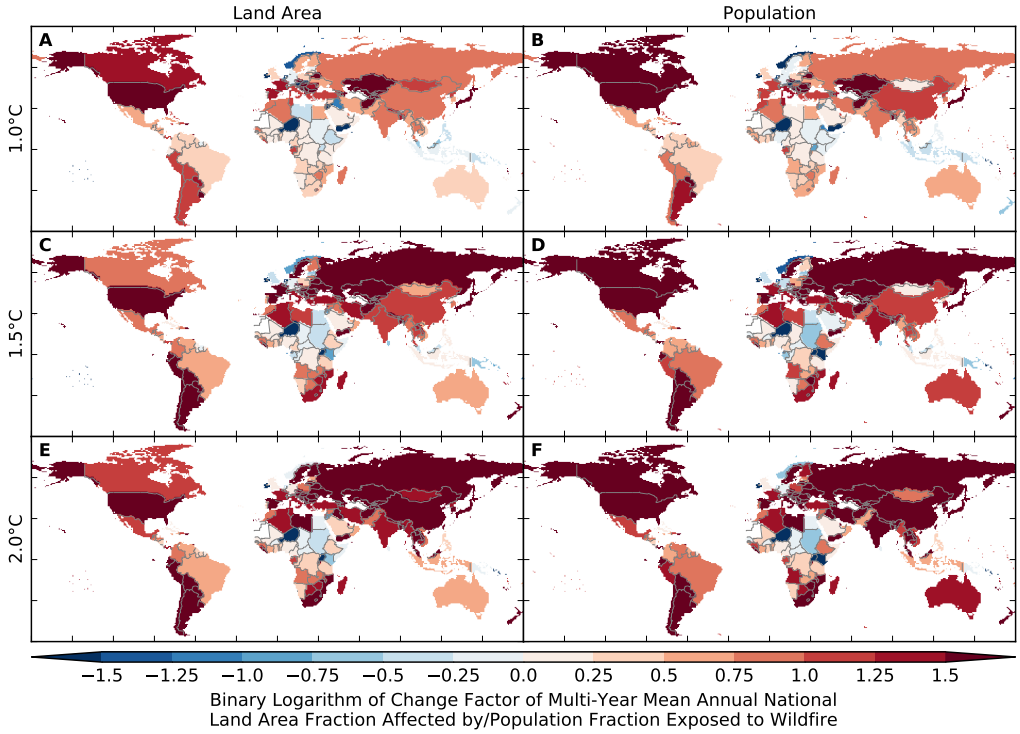

Figure S204: **Pure effect of climate change on annual national land area fraction affected by and population fraction exposed to wildfire (IPSL-CM5A-LR + CARAIB).** Analogous to Figure S202.

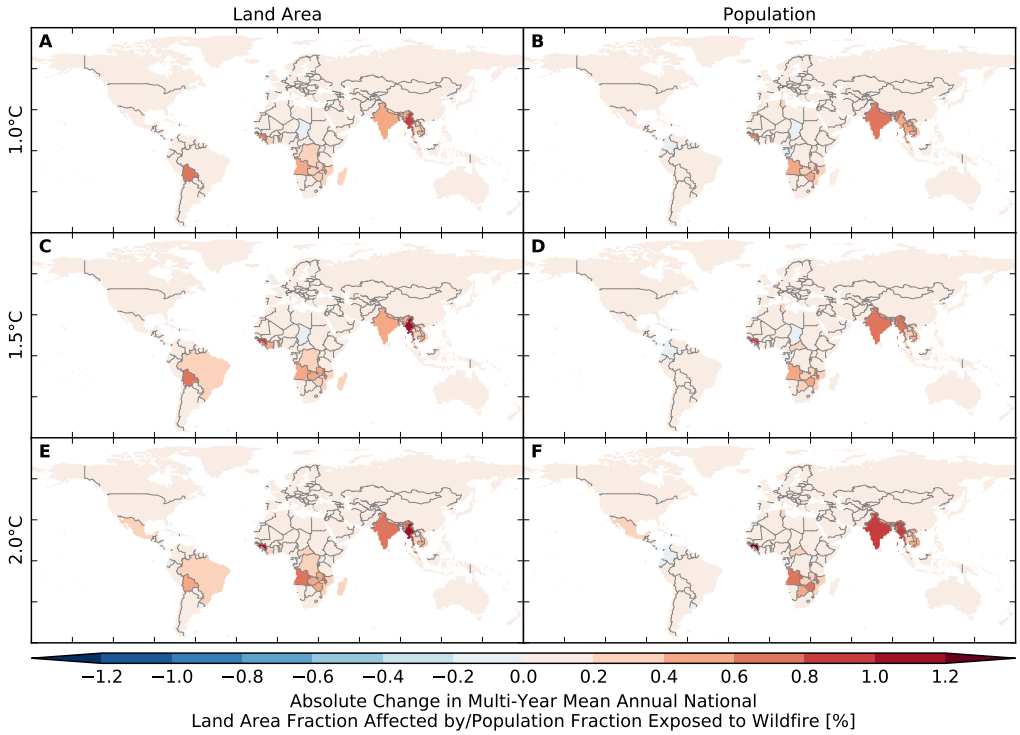

Figure S205: **Pure effect of climate change on annual national land area fraction affected by and population fraction exposed to wildfire (MIROC5 + CARAIB).** Analogous to Figure S201.

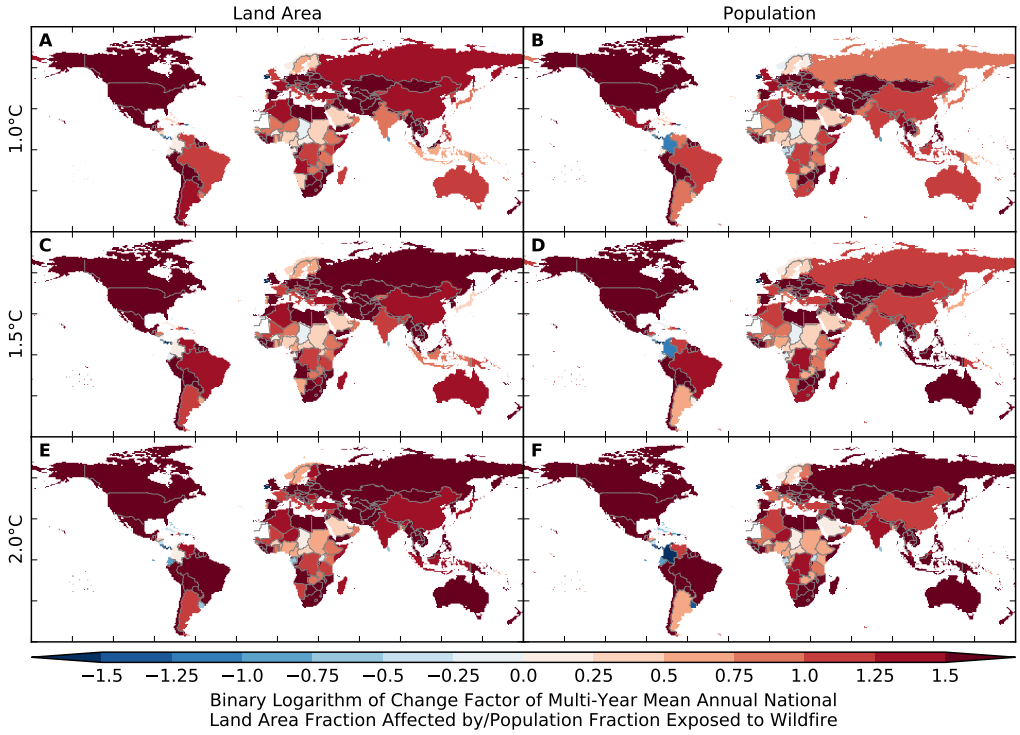

Figure S206: **Pure effect of climate change on annual national land area fraction affected by and population fraction exposed to wildfire (MIROC5 + CARAIB).** Analogous to Figure S202.

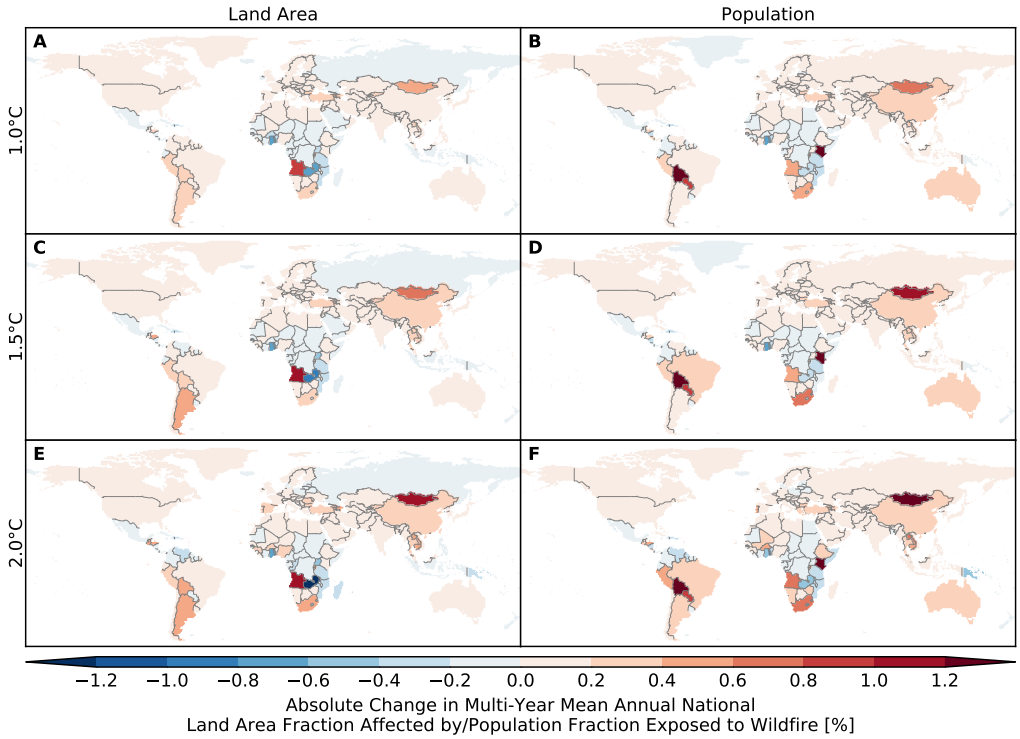

Figure S207: **Pure effect of climate change on annual national land area fraction affected by and population fraction exposed to wildfire (GFDL-ESM2M + LPJ-GUESS).** Analogous to Figure S201.

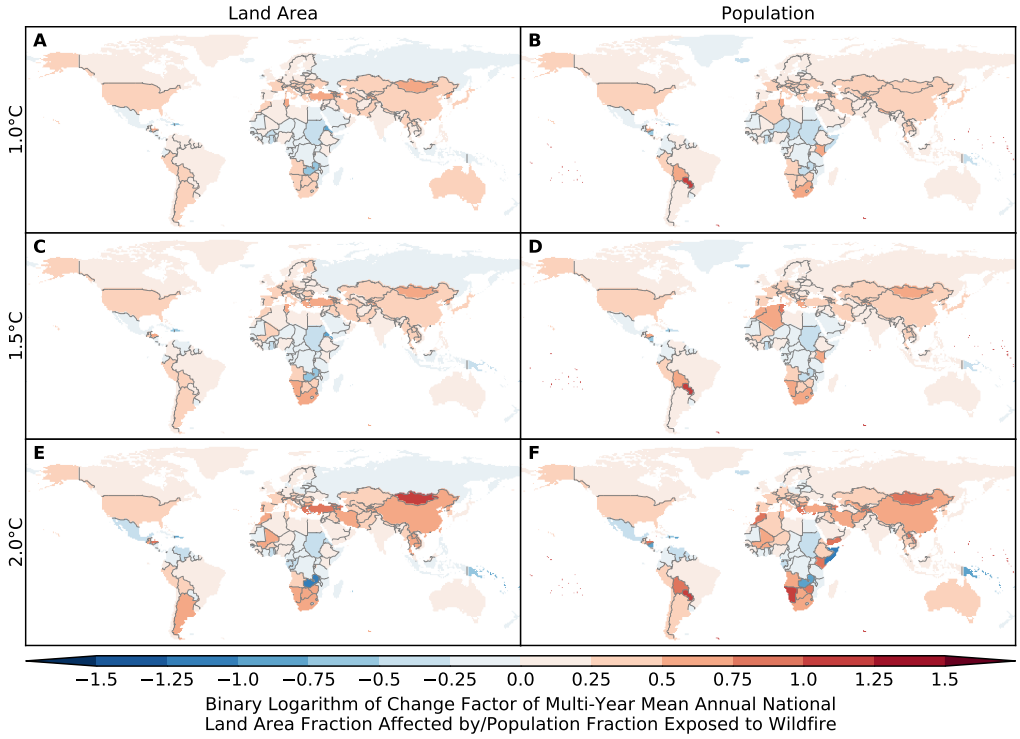

Figure S208: **Pure effect of climate change on annual national land area fraction affected by and population fraction exposed to wildfire (GFDL-ESM2M + LPJ-GUESS).** Analogous to Figure S202.

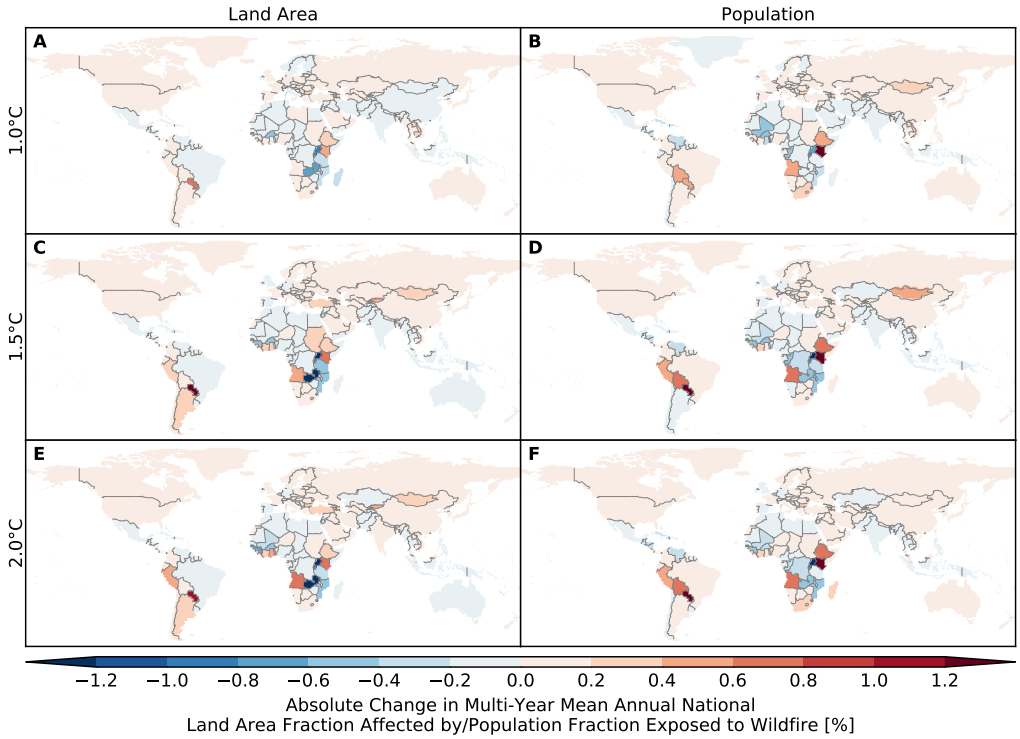

Figure S209: **Pure effect of climate change on annual national land area fraction affected by and population fraction exposed to wildfire (IPSL-CM5A-LR + LPJ-GUESS).** Analogous to Figure S201.

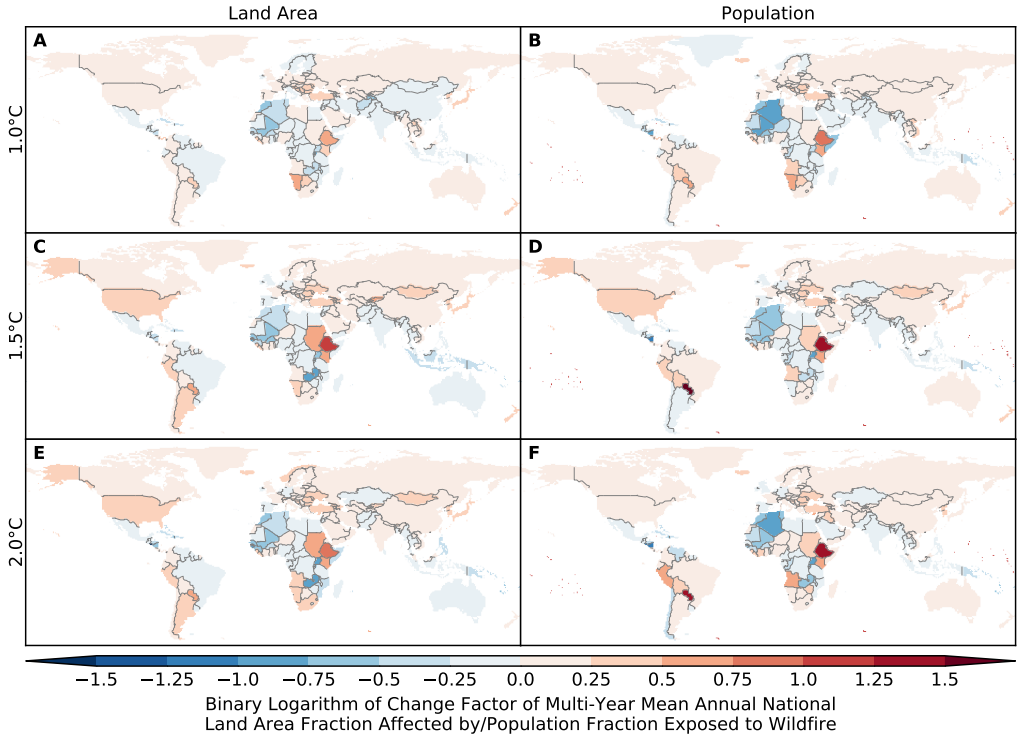

Figure S210: **Pure effect of climate change on annual national land area fraction affected by and population fraction exposed to wildfire (IPSL-CM5A-LR + LPJ-GUESS).** Analogous to Figure S202.

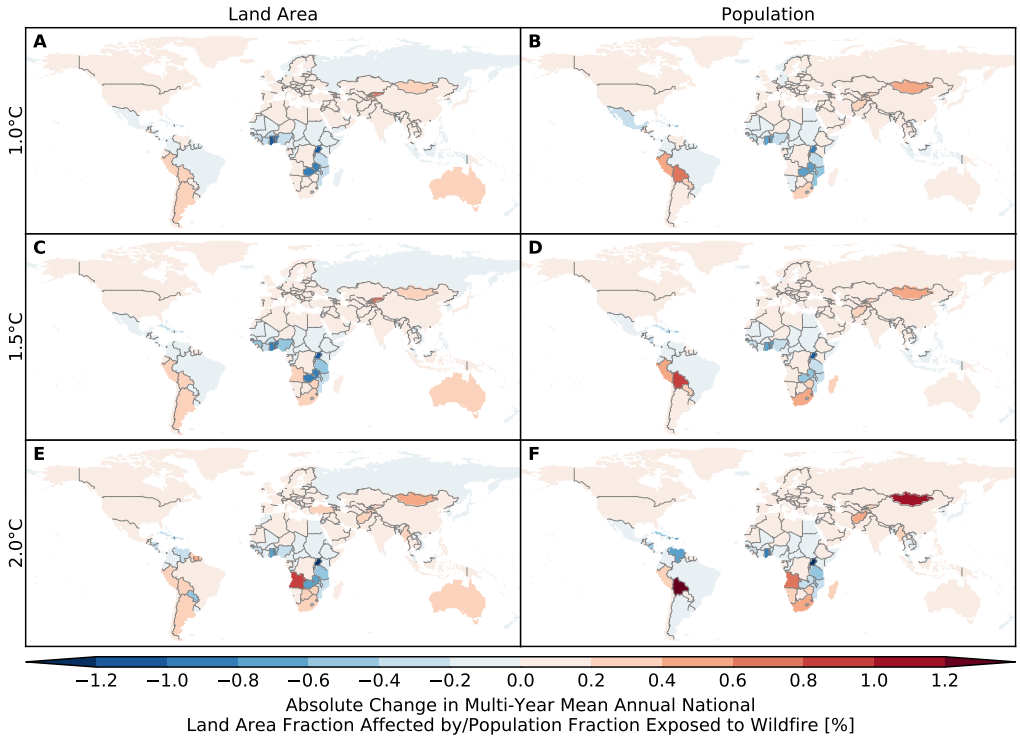

Figure S211: **Pure effect of climate change on annual national land area fraction affected by and population fraction exposed to wildfire (MIROC5 + LPJ-GUESS).** Analogous to Figure S201.

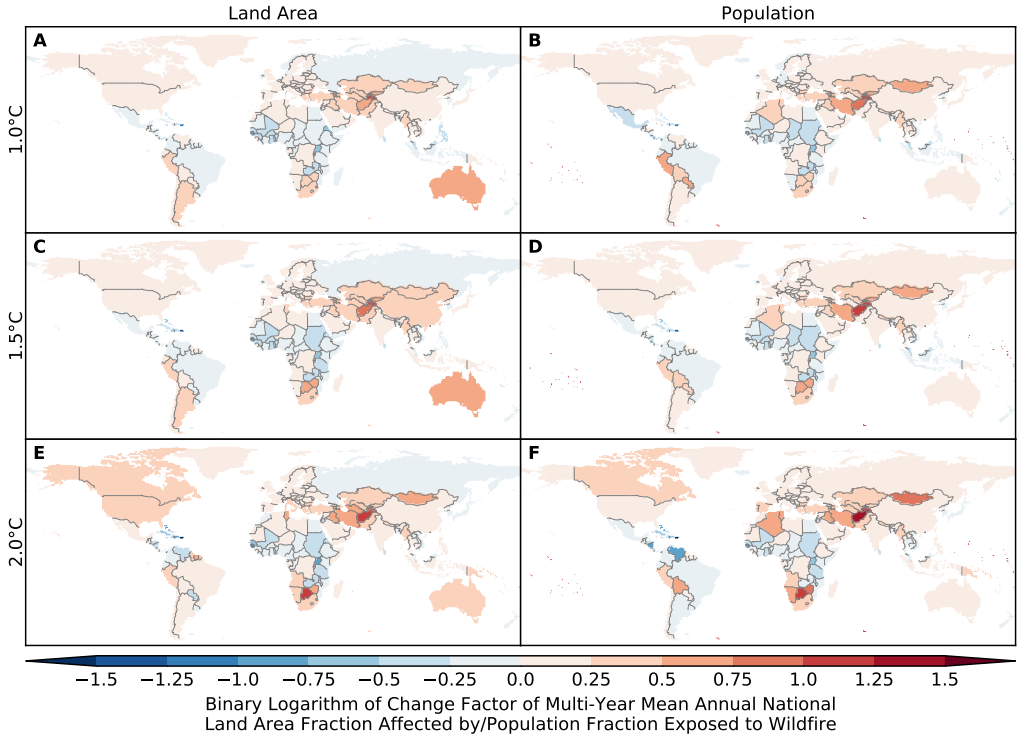

Figure S212: **Pure effect of climate change on annual national land area fraction affected by and population fraction exposed to wildfire (MIROC5 + LPJ-GUESS).** Analogous to Figure S202.

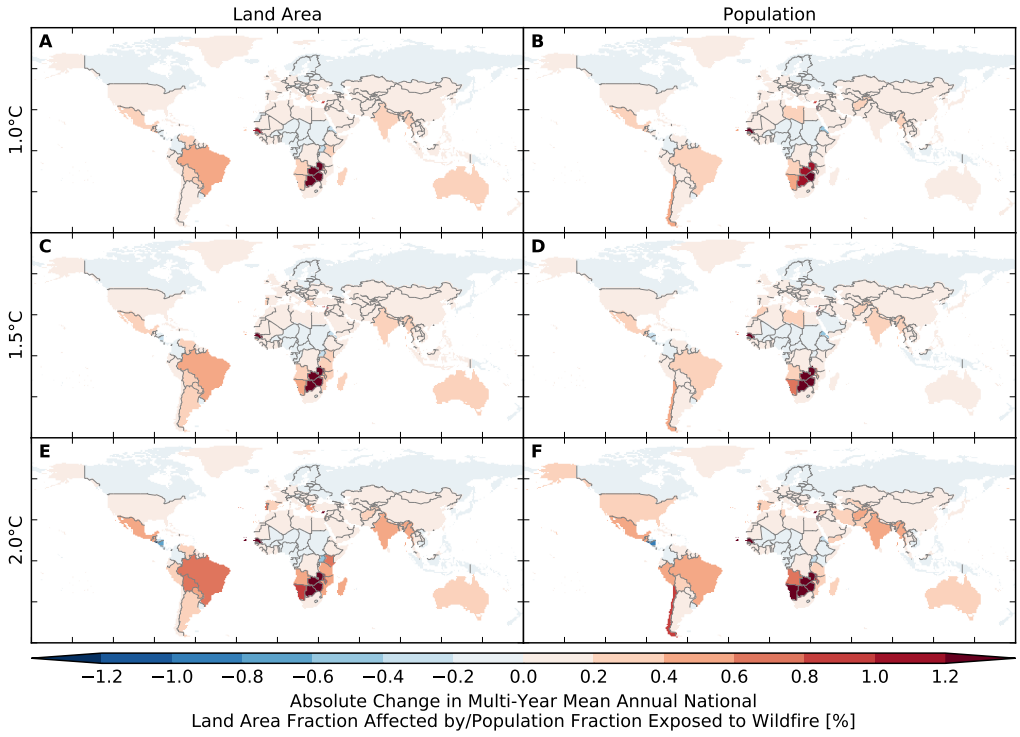

Figure S213: **Pure effect of climate change on annual national land area fraction affected by and population fraction exposed to wildfire (GFDL-ESM2M + LPJmL).** Analogous to Figure S201.

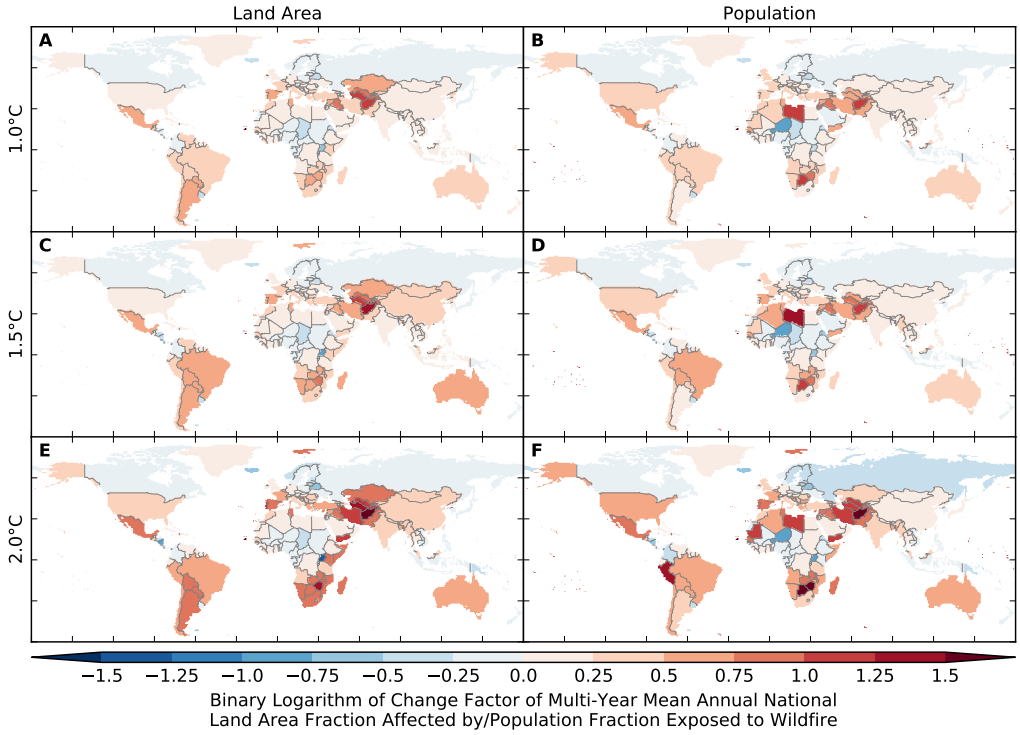

Figure S214: **Pure effect of climate change on annual national land area fraction affected by and population fraction exposed to wildfire (GFDL-ESM2M + LPJmL).** Analogous to Figure S202.

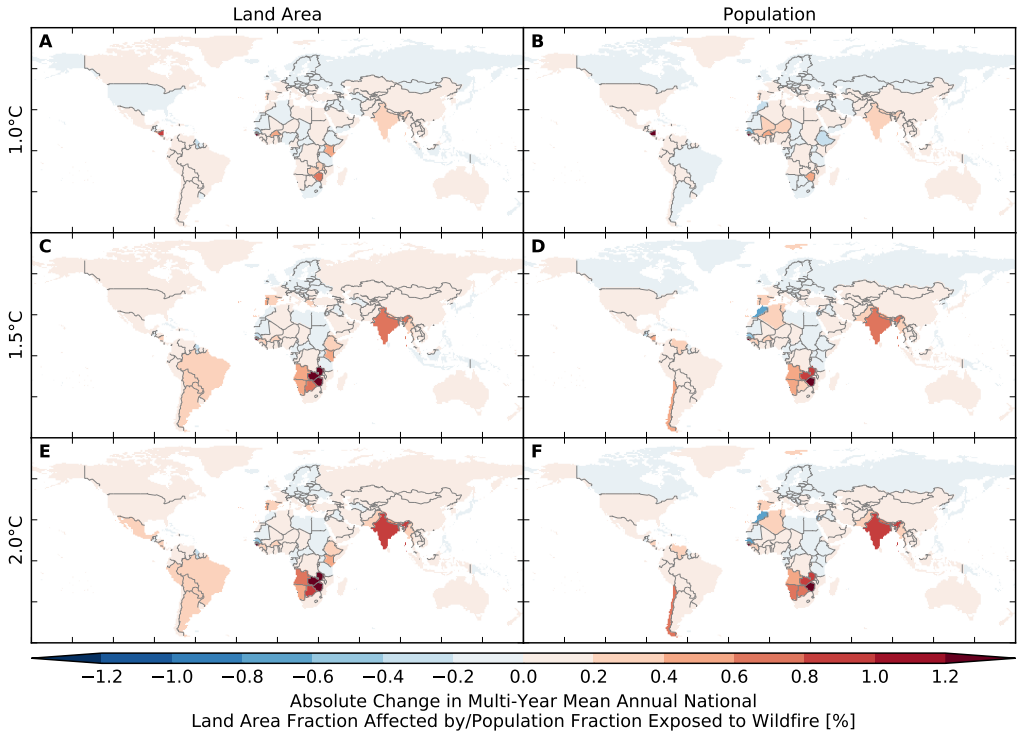

Figure S215: **Pure effect of climate change on annual national land area fraction affected by and population fraction exposed to wildfire (IPSL-CM5A-LR + LPJmL).** Analogous to Figure S201.

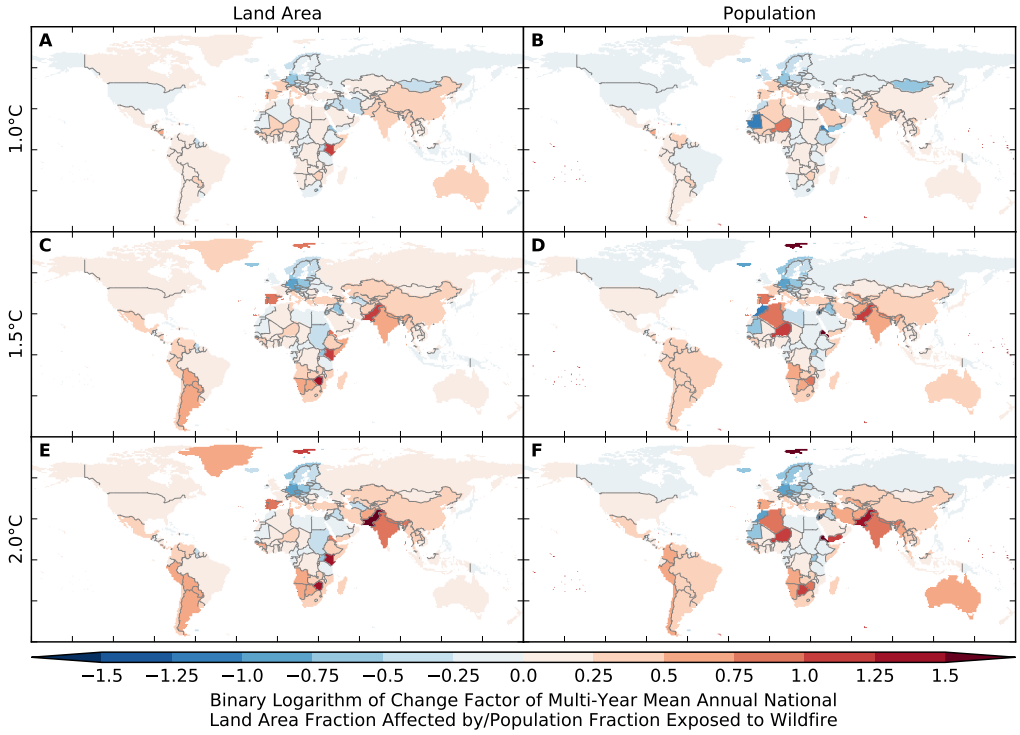

Figure S216: **Pure effect of climate change on annual national land area fraction affected by and population fraction exposed to wildfire (IPSL-CM5A-LR + LPJmL).** Analogous to Figure S202.

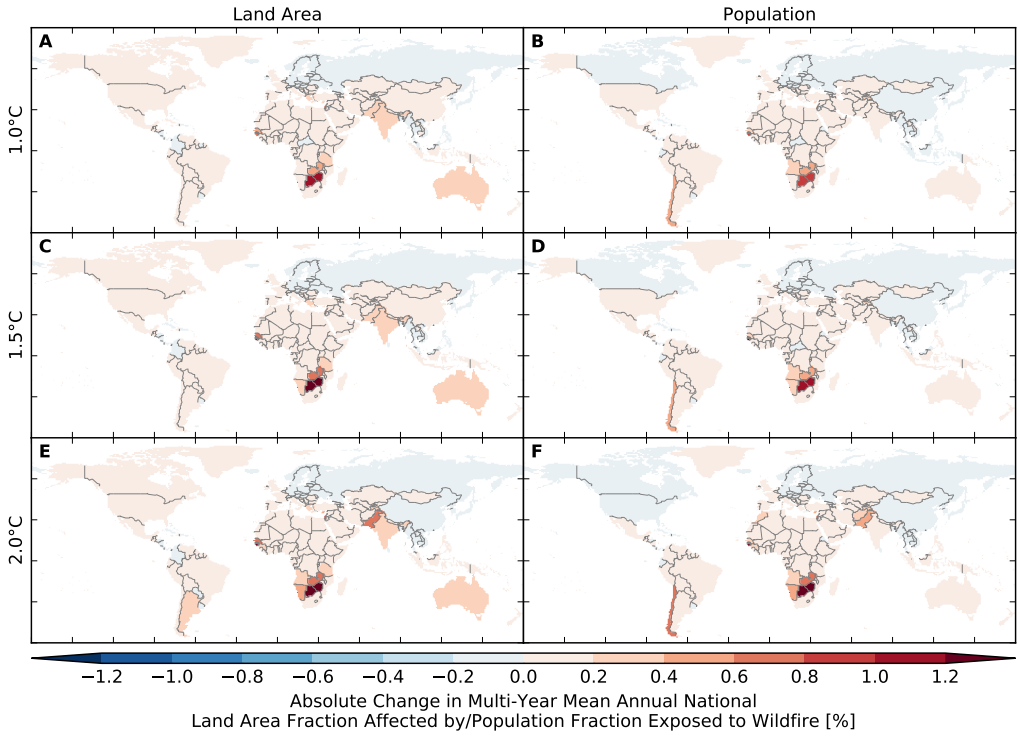

Figure S217: **Pure effect of climate change on annual national land area fraction affected by and population fraction exposed to wildfire (MIROC5 + LPJmL).** Analogous to Figure S201.

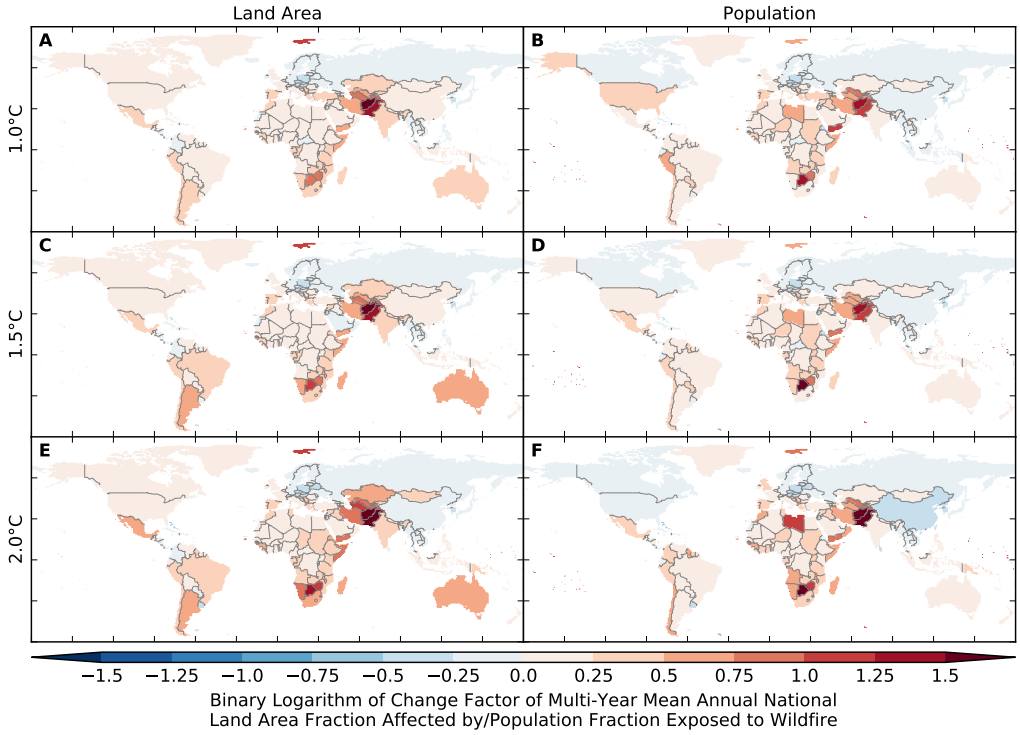

Figure S218: **Pure effect of climate change on annual national land area fraction affected by and population fraction exposed to wildfire (MIROC5 + LPJmL).** Analogous to Figure S202.

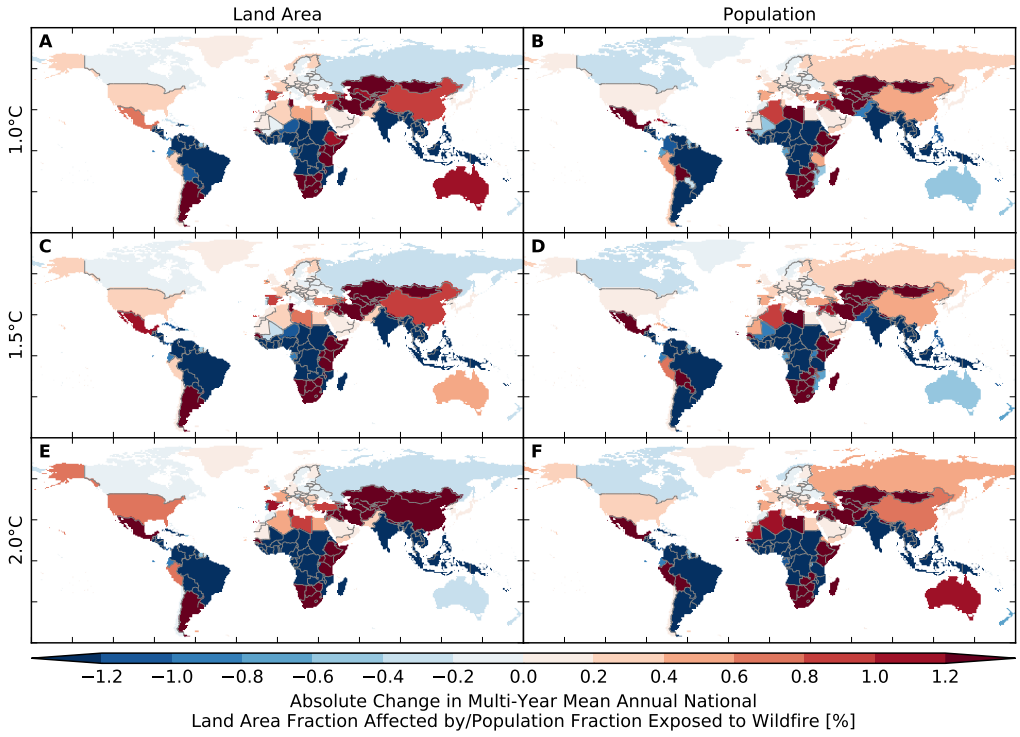

Figure S219: **Pure effect of climate change on annual national land area fraction affected by and population fraction exposed to wildfire (GFDL-ESM2M + ORCHIDEE).** Analogous to Figure S201.

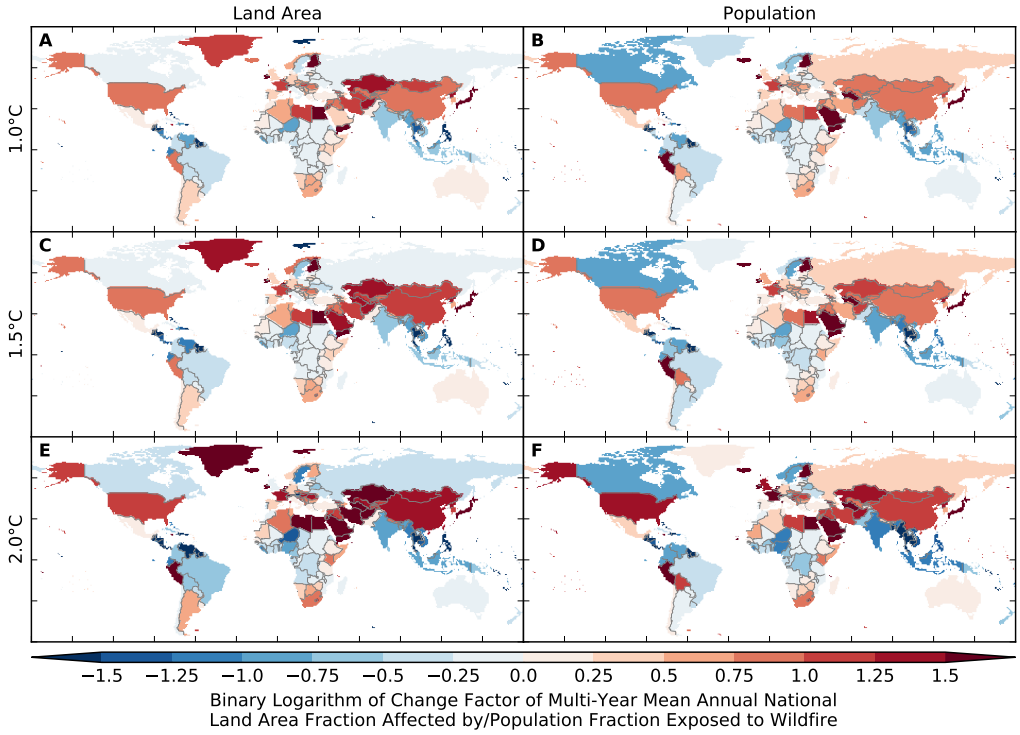

Figure S220: **Pure effect of climate change on annual national land area fraction affected by and population fraction exposed to wildfire (GFDL-ESM2M + ORCHIDEE).** Analogous to Figure S202.

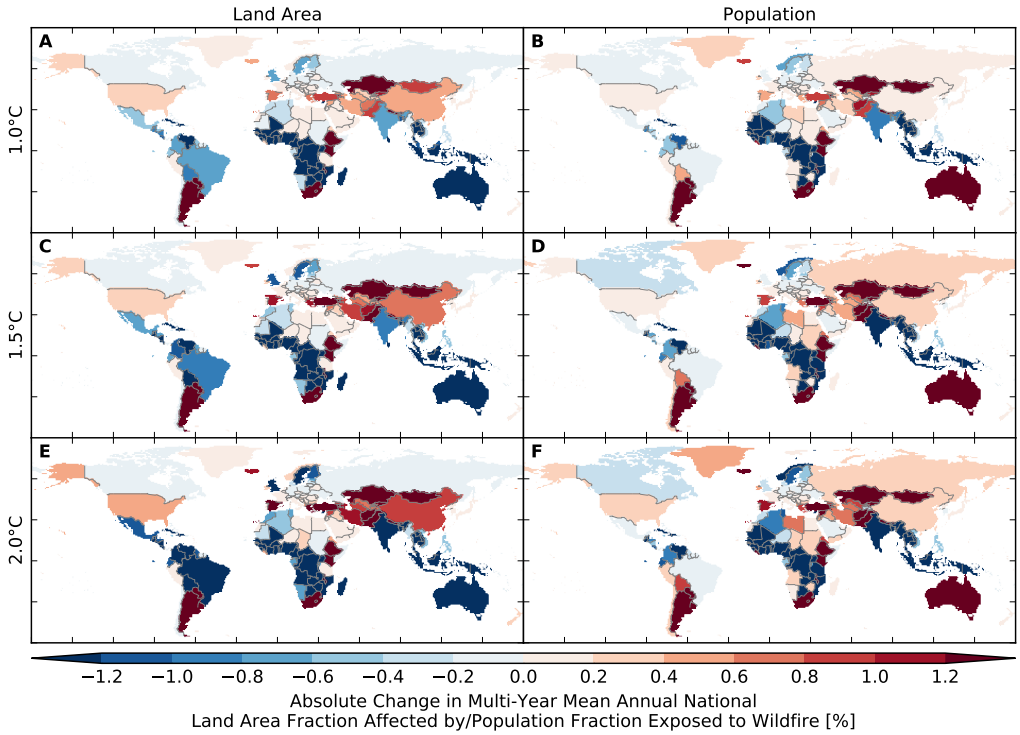

Figure S221: **Pure effect of climate change on annual national land area fraction affected by and population fraction exposed to wildfire (IPSL-CM5A-LR + ORCHIDEE).** Analogous to Figure S201.

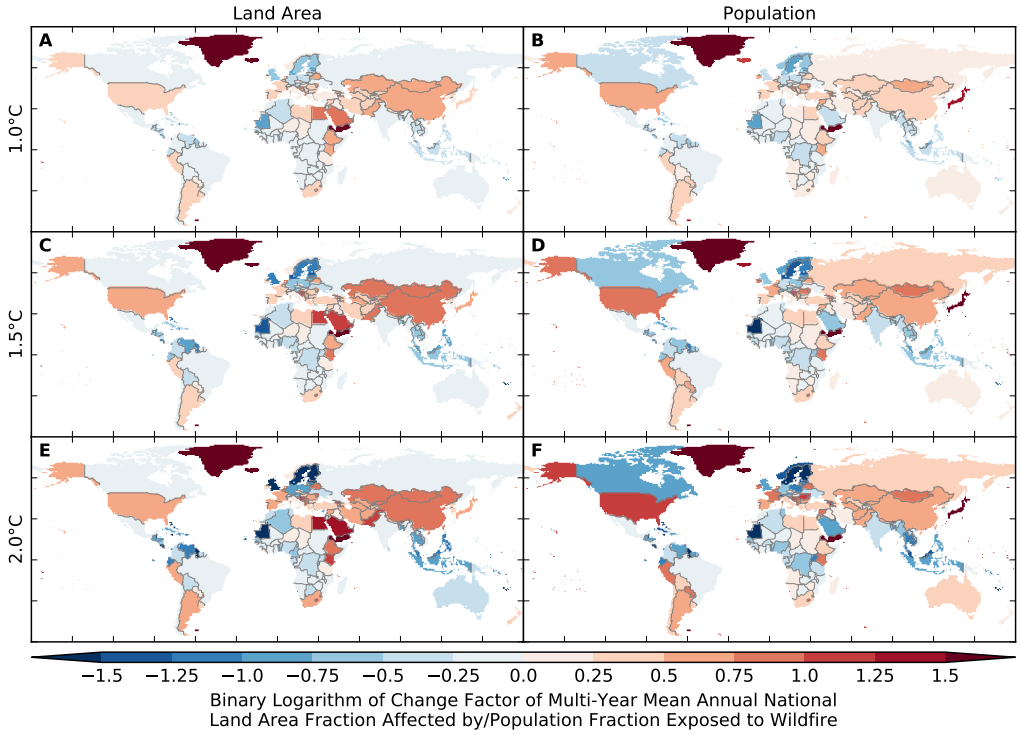

Figure S222: **Pure effect of climate change on annual national land area fraction affected by and population fraction exposed to wildfire (IPSL-CM5A-LR + ORCHIDEE).** Analogous to Figure S202.

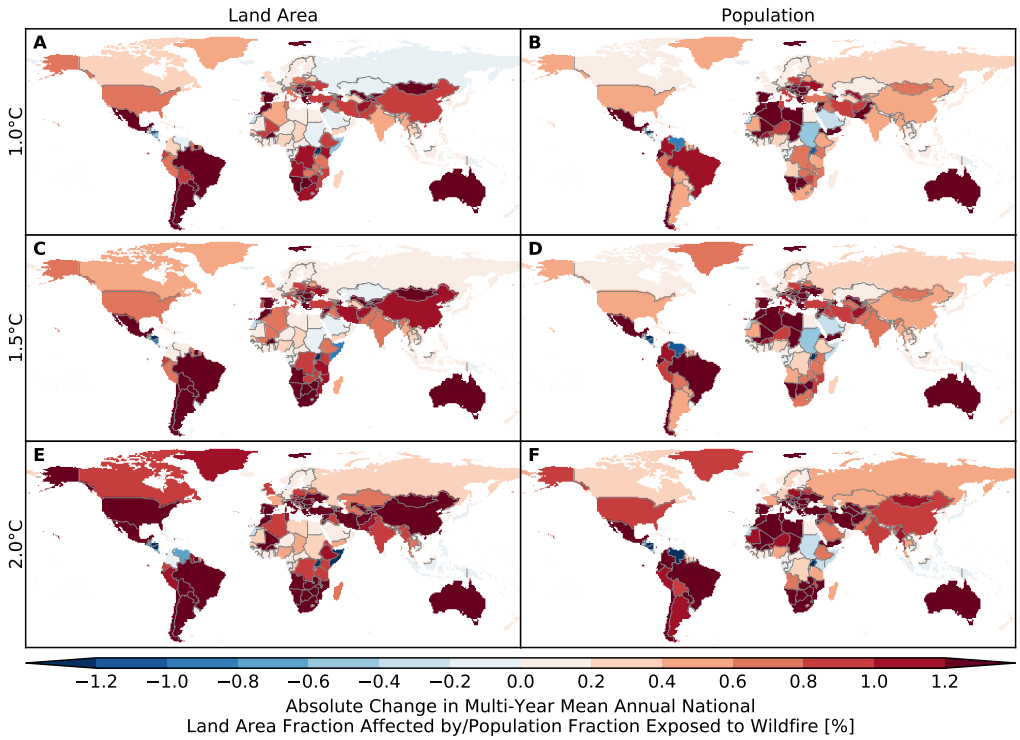

Figure S223: **Pure effect of climate change on annual national land area fraction affected by and population fraction exposed to wildfire (GFDL-ESM2M + VISIT).** Analogous to Figure S201.

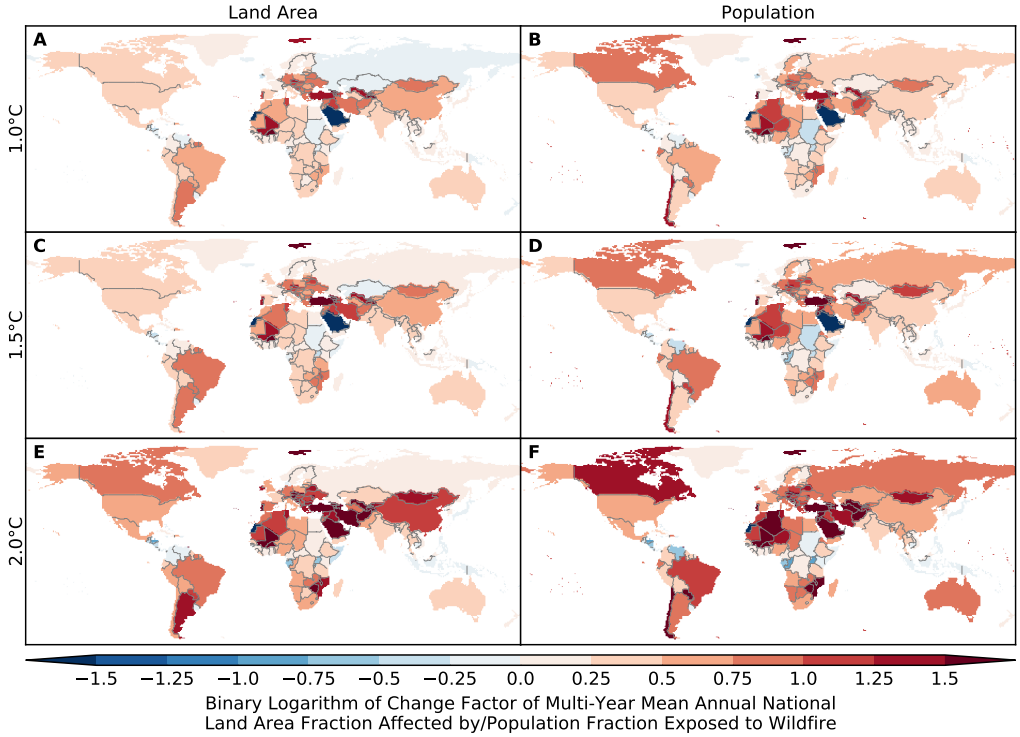

Figure S224: **Pure effect of climate change on annual national land area fraction affected by and population fraction exposed to wildfire (GFDL-ESM2M + VISIT).** Analogous to Figure S202.

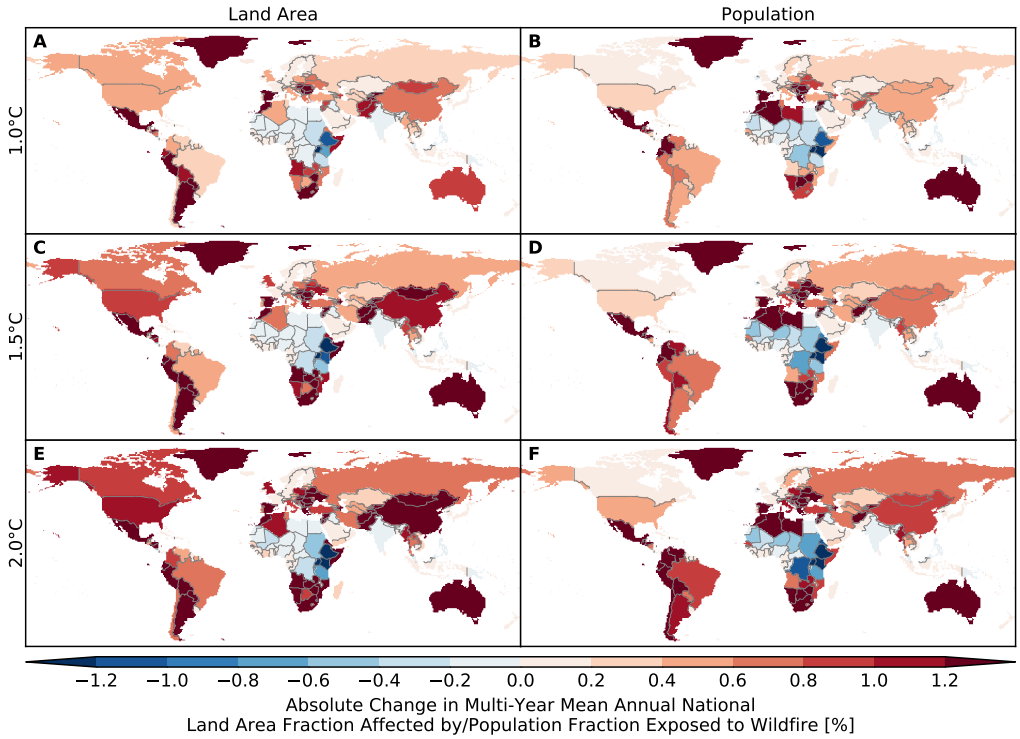

Figure S225: **Pure effect of climate change on annual national land area fraction affected by and population fraction exposed to wildfire (IPSL-CM5A-LR + VISIT).** Analogous to Figure S201.

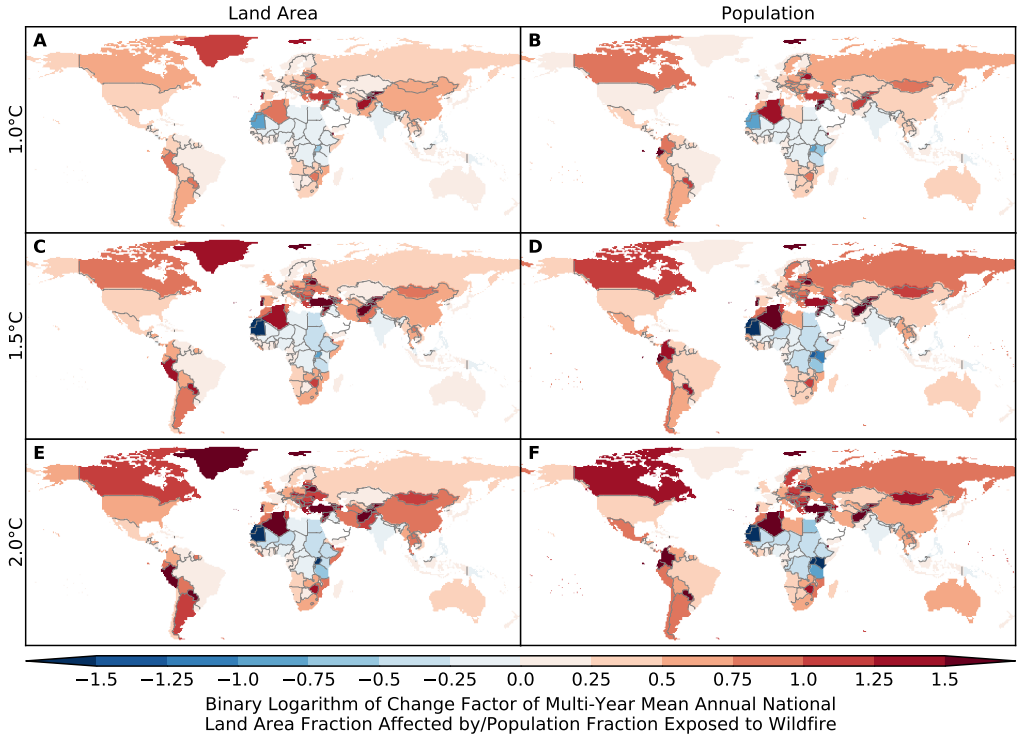

Figure S226: **Pure effect of climate change on annual national land area fraction affected by and population fraction exposed to wildfire (IPSL-CM5A-LR + VISIT).** Analogous to Figure S202.

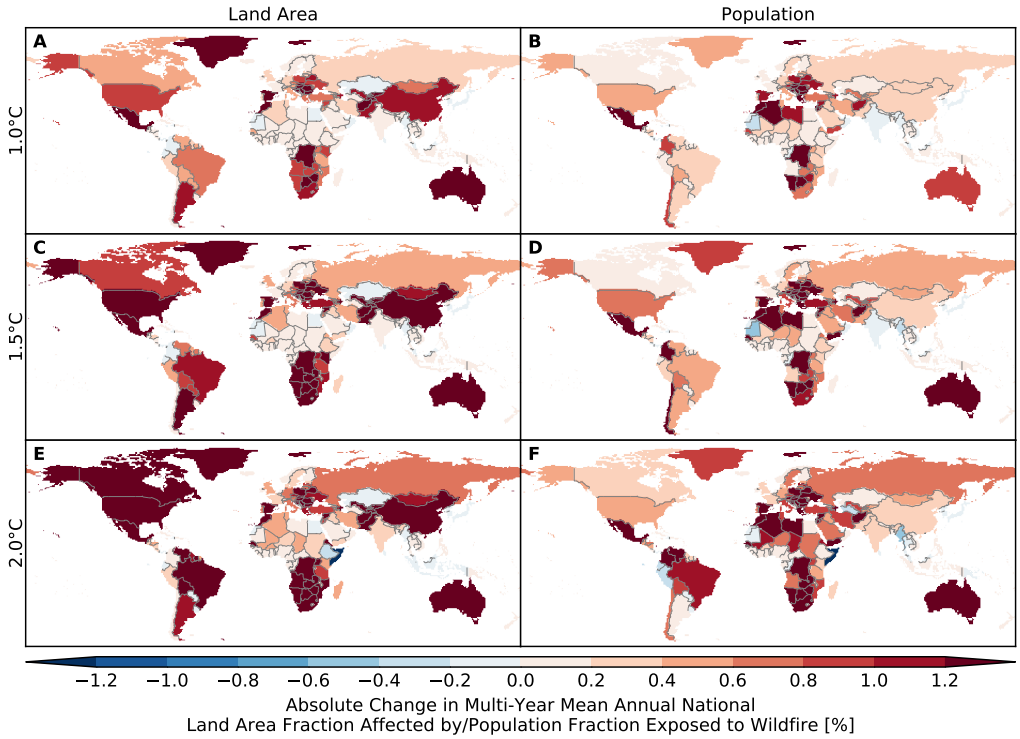

Figure S227: **Pure effect of climate change on annual national land area fraction affected by and population fraction exposed to wildfire (MIROC5 + VISIT).** Analogous to Figure S201.

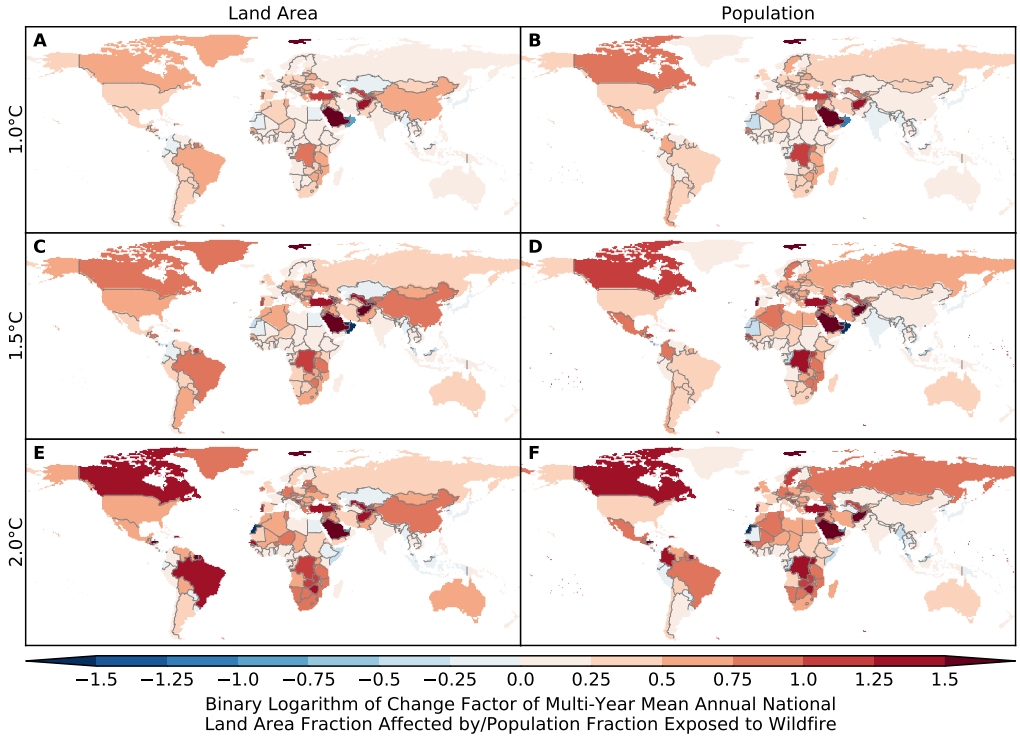

Figure S228: **Pure effect of climate change on annual national land area fraction affected by and population fraction exposed to wildfire (MIROC5 + VISIT).** Analogous to Figure S202.

9.5 Droughts

Land area affected

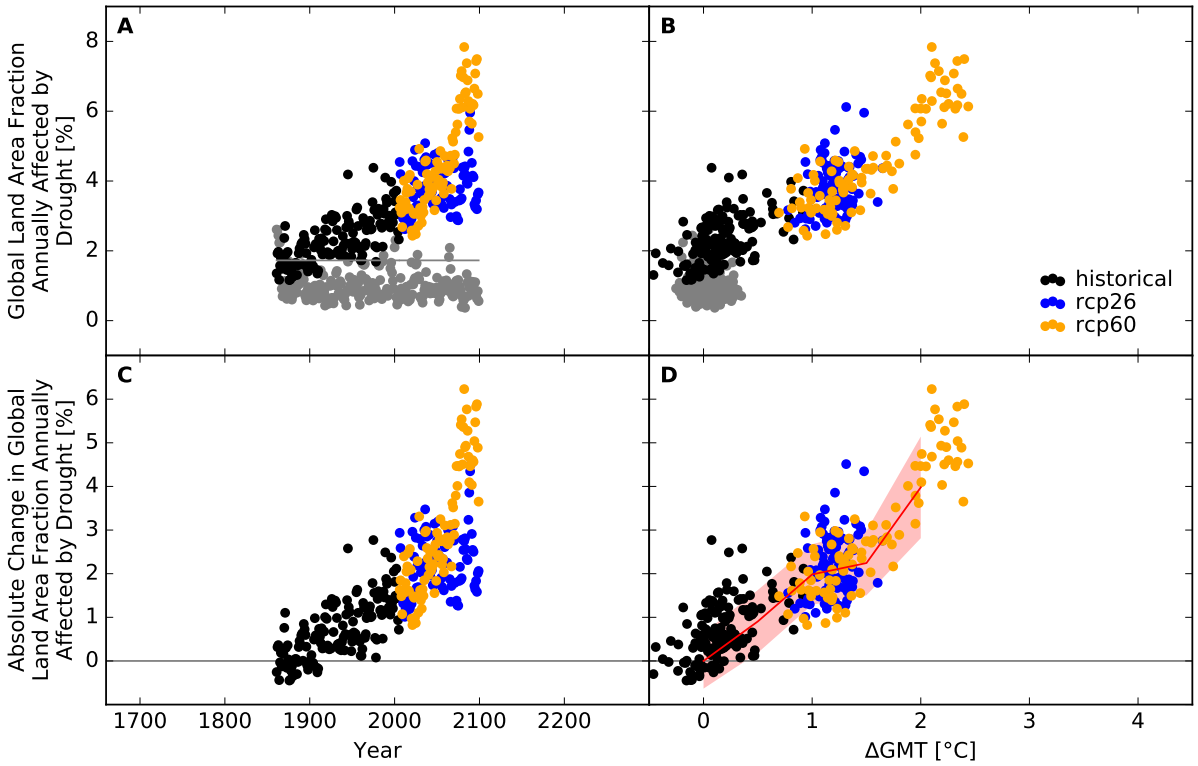

Figure S229: **Derivation of the pure effect of climate change on the global land area fraction annually affected by drought (GFDL-ESM2M + CLM45).** Panel A: Time series of annual global land area fraction affected (AFA) by drought for preindustrial climate (grey dots), historical climate (black dots), climate projections for RCP2.6 (blue dots), and RCP6.0 (orange dots). In all simulations, socioeconomic conditions are varied according to the historically observed development between 1860 and 2005, and held fixed at 1860 conditions before 1860 and at 2005 conditions after 2005. The horizontal gray lines before 1860 and after 2005 represent the multi-year mean global land area fraction annually affected by drought under preindustrial climate conditions and socioeconomic conditions of 1860 and 2005, respectively. The gray line between 1860 and 2005 is a linear interpolation of these mean values. Panel B: Data shown in Panel A plotted against the associated GCM-specific annual global mean temperature (GMT) change relative to the long-term preindustrial mean GMT. Panel C: Pure effect of climate change on AFA, calculated as the difference between the annual data shown in Panel A and the multi-year mean AFA under preindustrial climate conditions (gray line in Panel A). Panel D: Data shown in Panel C plotted against annual GMT change. The red line represents the mean values of the annual data points per 1 °C-wide GMT change bin, with bins centered at GMT change levels increasing from 0 °C to 4 °C in steps of 0.5 °C. The area shaded in red represents the mean value ±1 standard deviation ranges of the annual data points per GMT change bin.

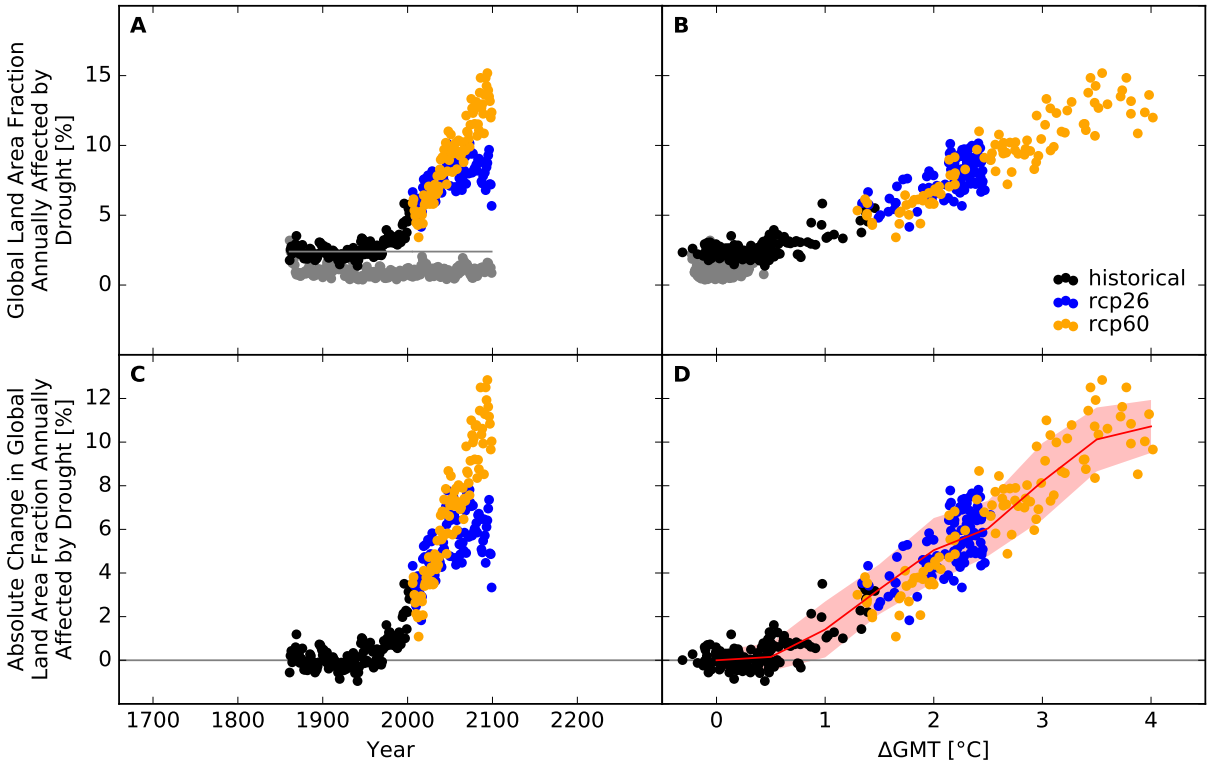

Figure S230: **Derivation of the pure effect of climate change on the global land area fraction annually affected by drought (IPSL-CM5A-LR + CLM45).** Analogous to Figure S229.

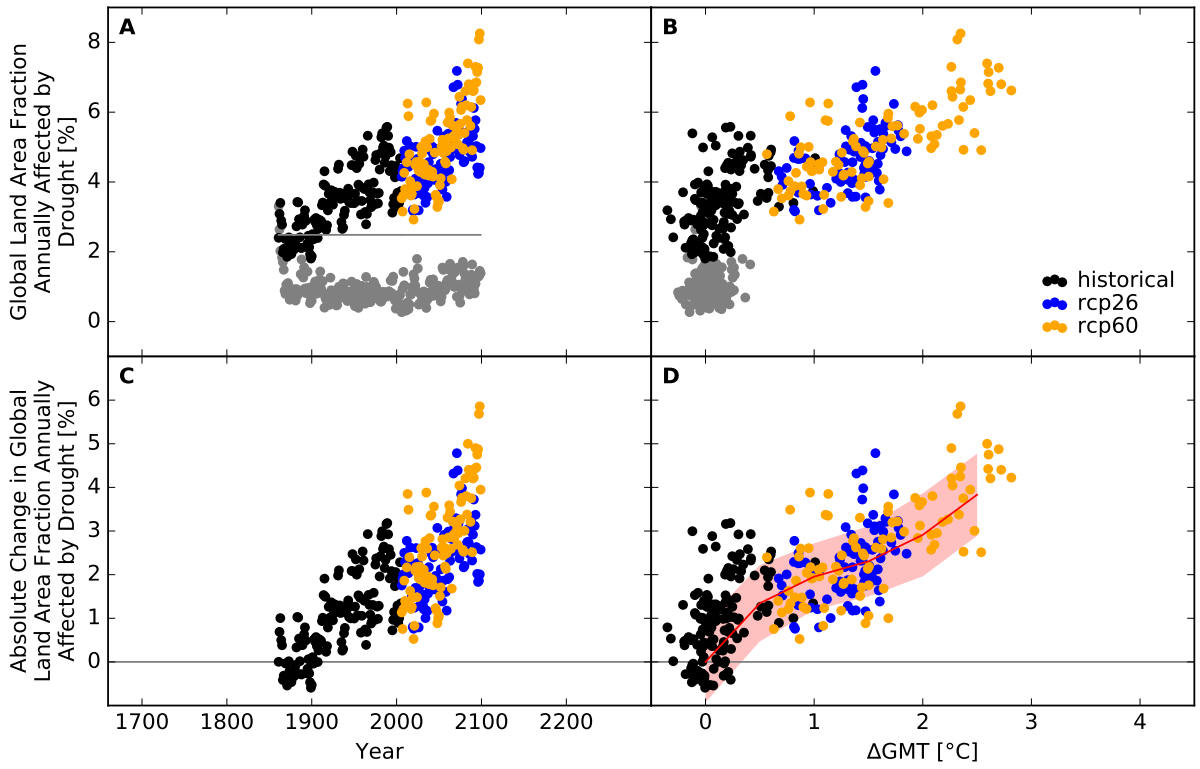

Figure S231: **Derivation of the pure effect of climate change on the global land area fraction annually affected by drought (MIROC5 + CLM45).** Analogous to Figure S229.

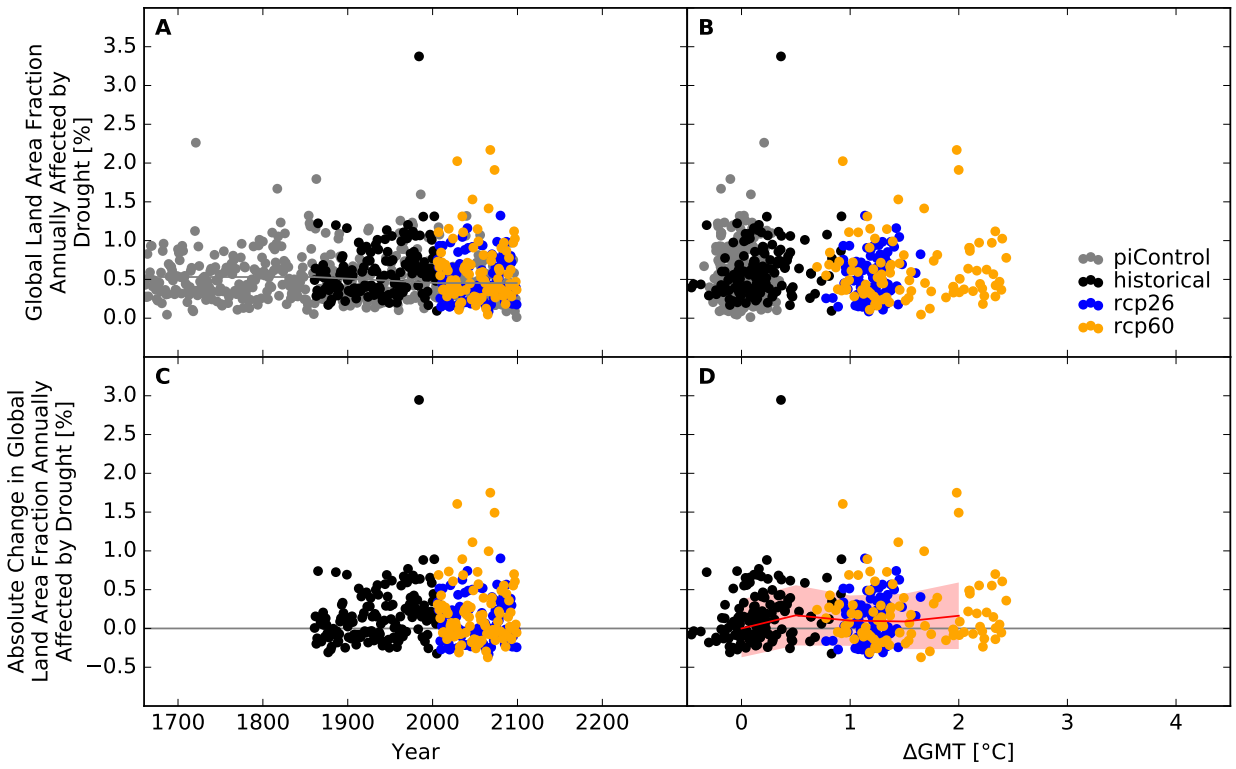

Figure S232: **Derivation of the pure effect of climate change on the global land area fraction annually affected by drought (GFDL-ESM2M + H08).** Analogous to Figure S229.

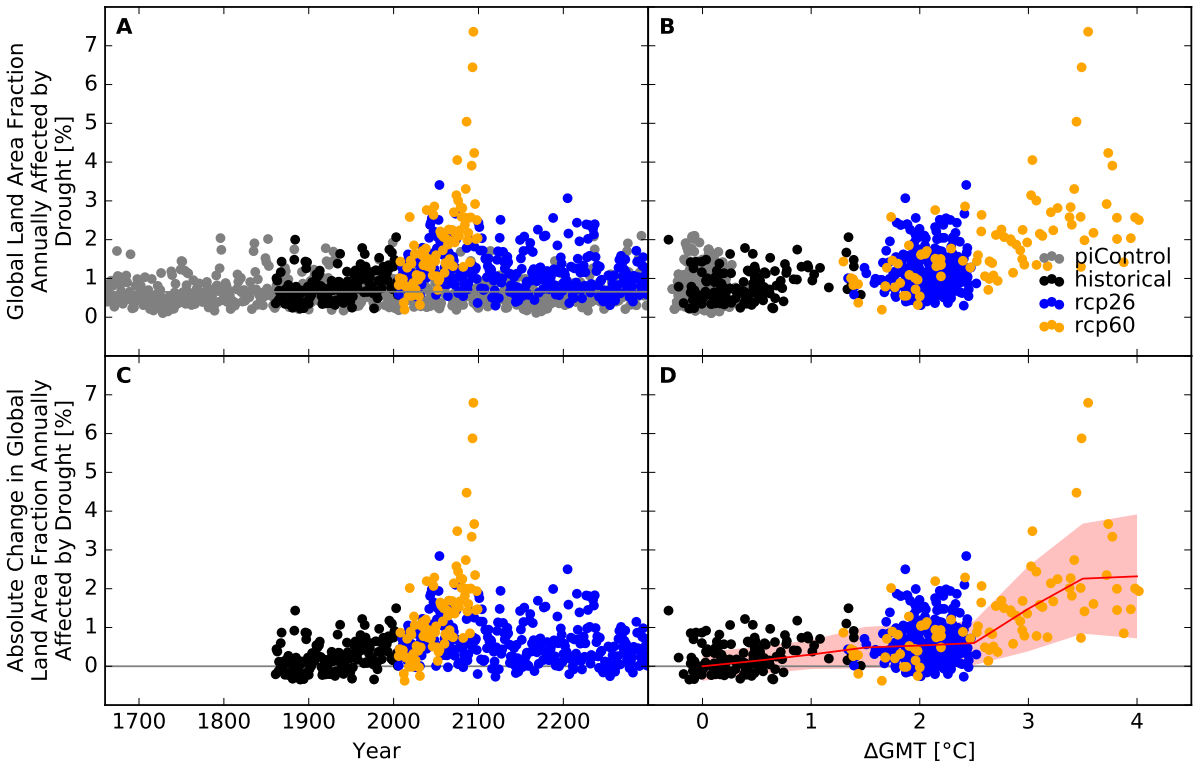

Figure S233: **Derivation of the pure effect of climate change on the global land area fraction annually affected by drought (IPSL-CM5A-LR + H08).** Analogous to Figure S229.

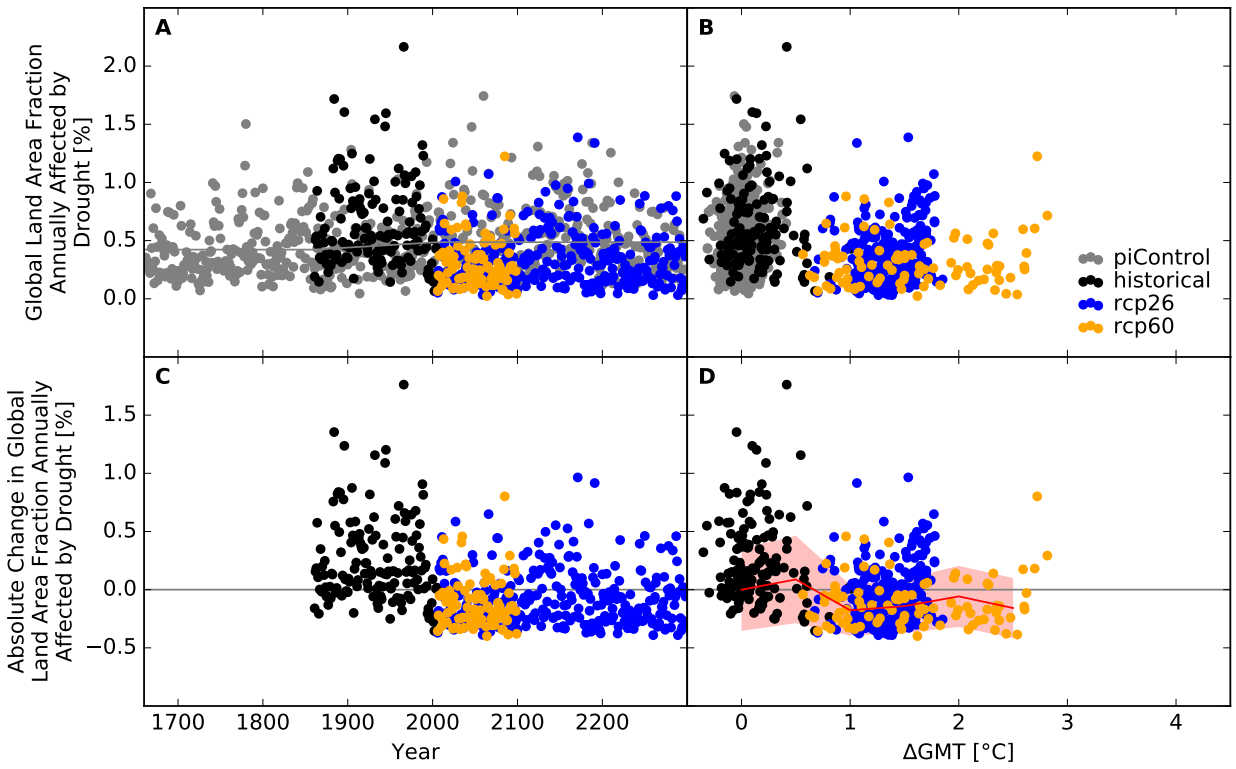

Figure S234: **Derivation of the pure effect of climate change on the global land area fraction annually affected by drought (MIROC5 + H08).** Analogous to Figure S229.

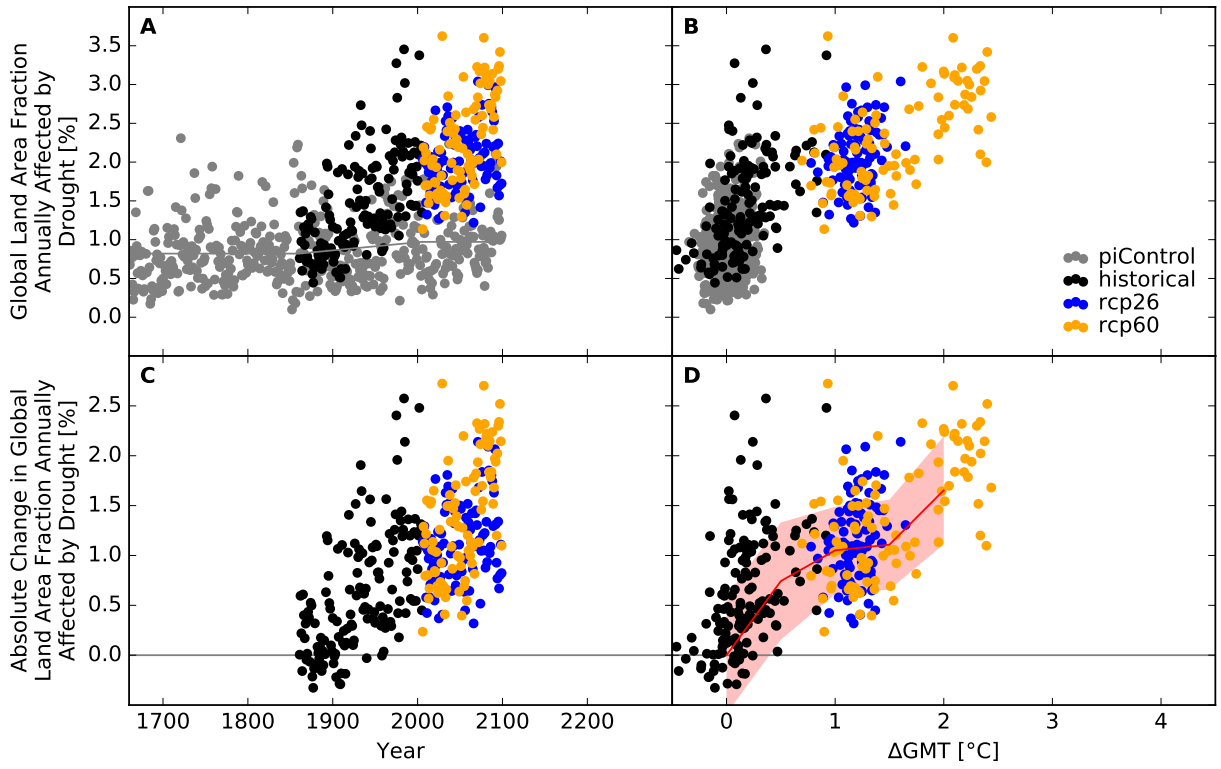

Figure S235: **Derivation of the pure effect of climate change on the global land area fraction annually affected by drought (GFDL-ESM2M + JULES-W1).** Analogous to Figure S229.

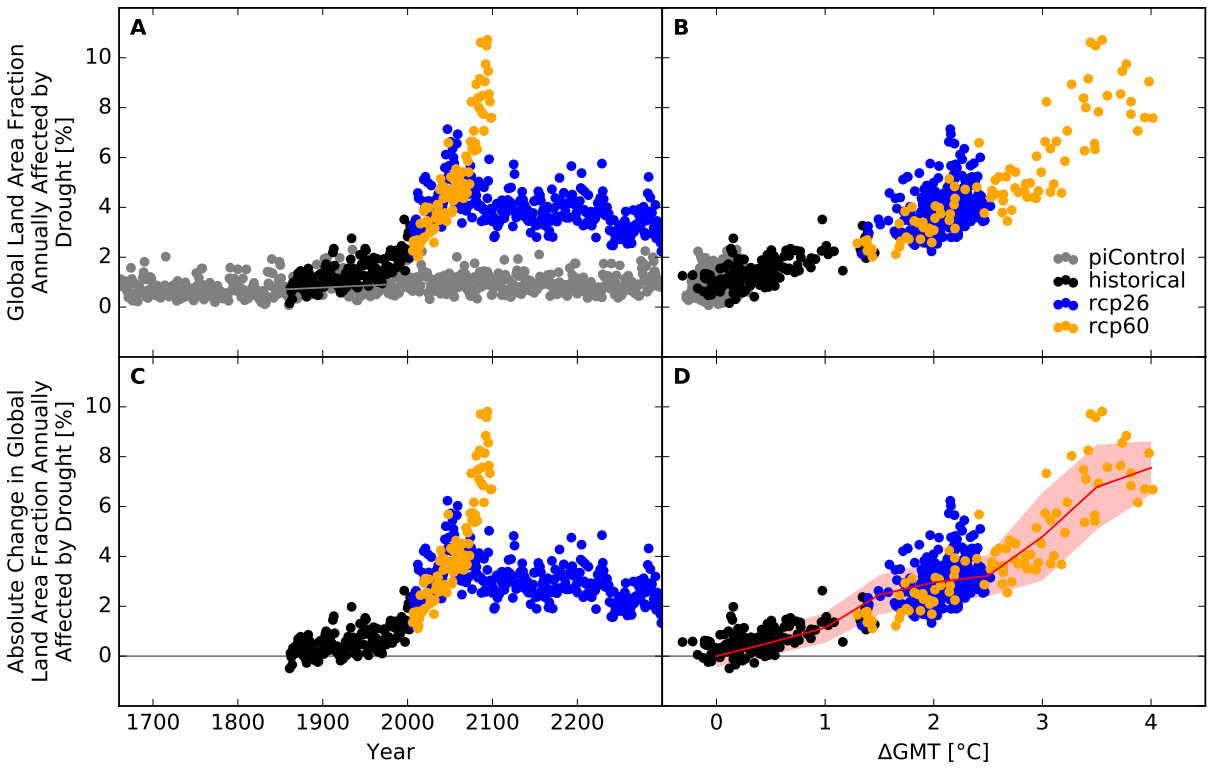

Figure S236: **Derivation of the pure effect of climate change on the global land area fraction annually affected by drought (IPSL-CM5A-LR + JULES-W1).** Analogous to Figure S229.

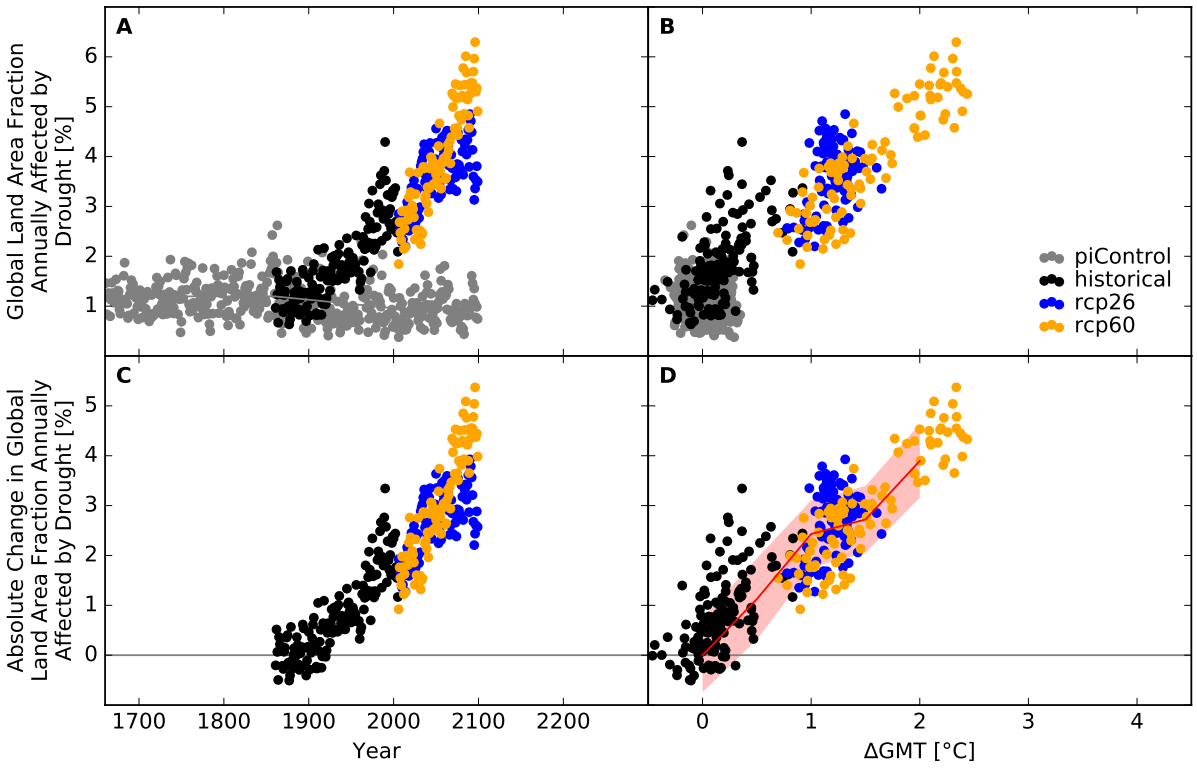

Figure S237: **Derivation of the pure effect of climate change on the global land area fraction annually affected by drought (GFDL-ESM2M + LPJmL).** Analogous to Figure S229.

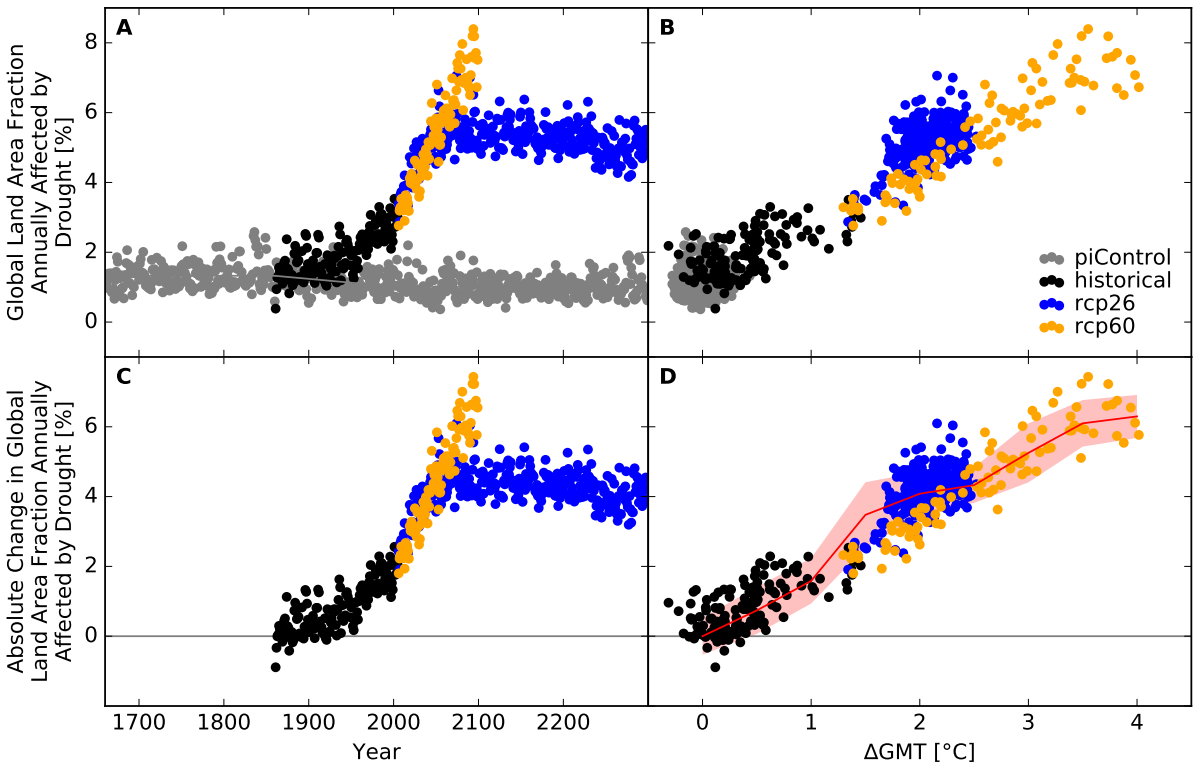

Figure S238: **Derivation of the pure effect of climate change on the global land area fraction annually affected by drought (IPSL-CM5A-LR + LPJmL).** Analogous to Figure S229.

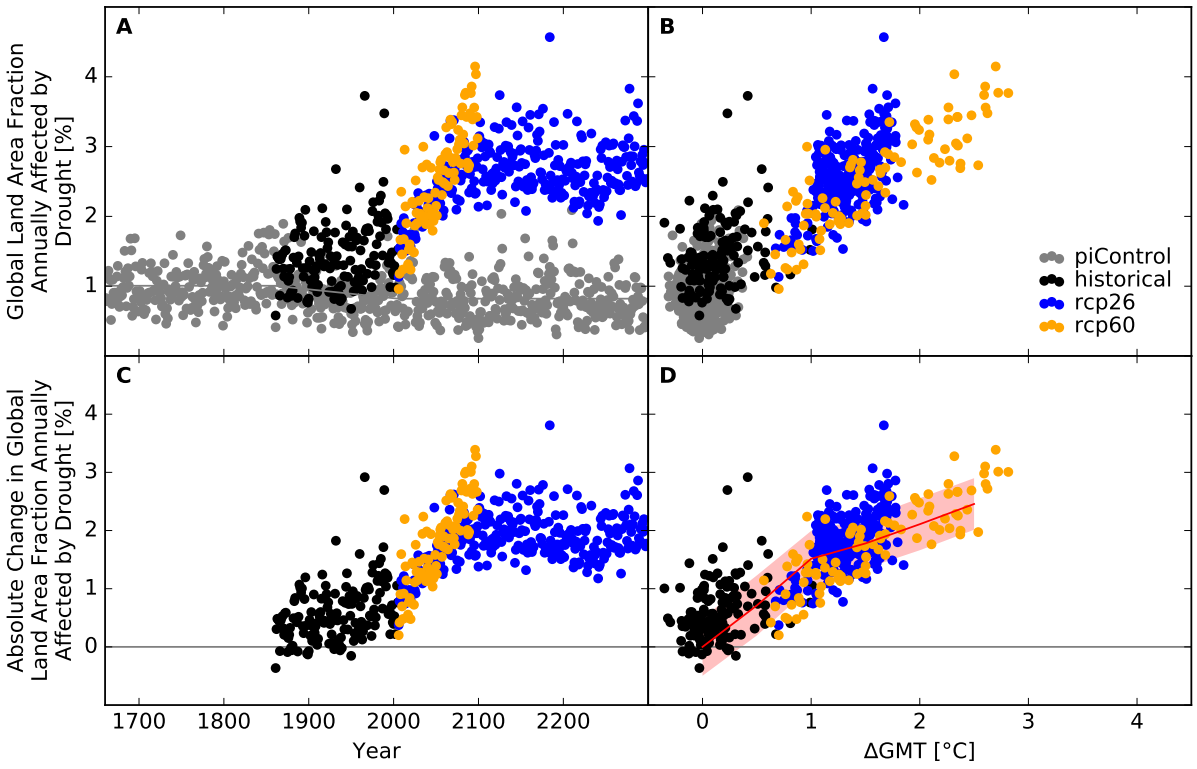

Figure S239: **Derivation of the pure effect of climate change on the global land area fraction annually affected by drought (MIROC5 + LPJmL).** Analogous to Figure S229.

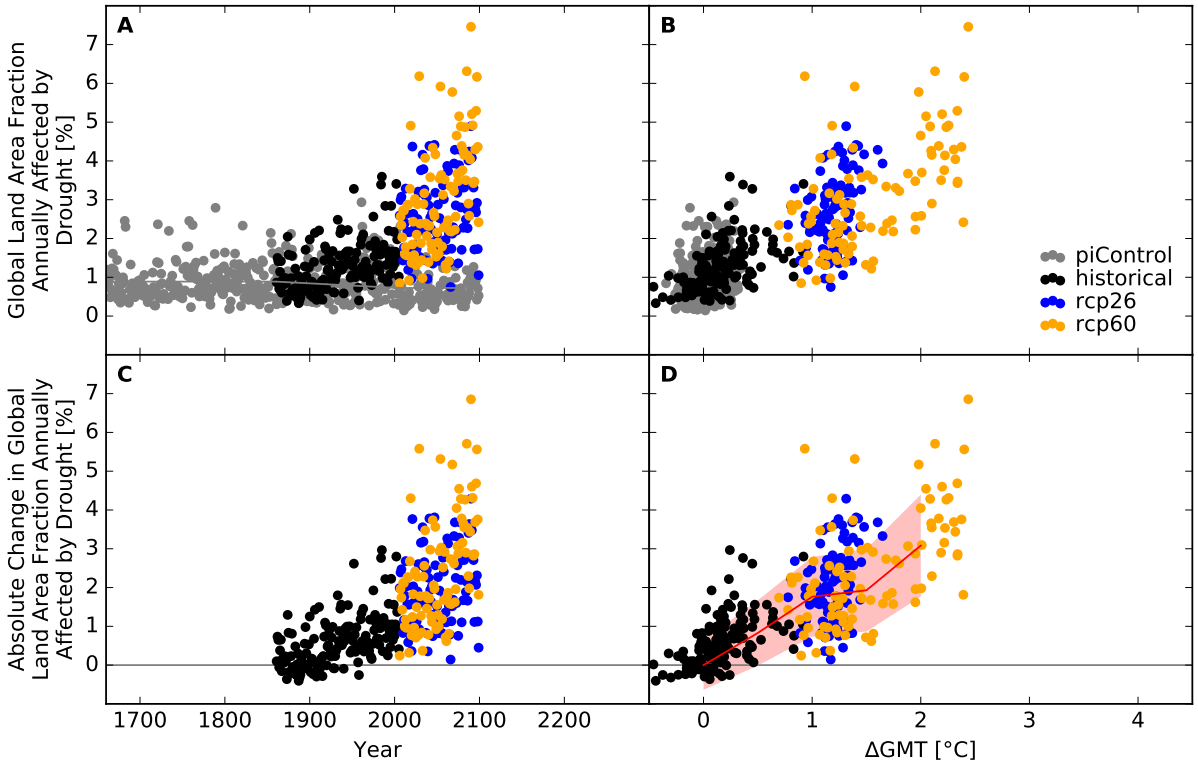

Figure S240: **Derivation of the pure effect of climate change on the global land area fraction annually affected by drought (GFDL-ESM2M + MPI-HM).** Analogous to Figure S229.

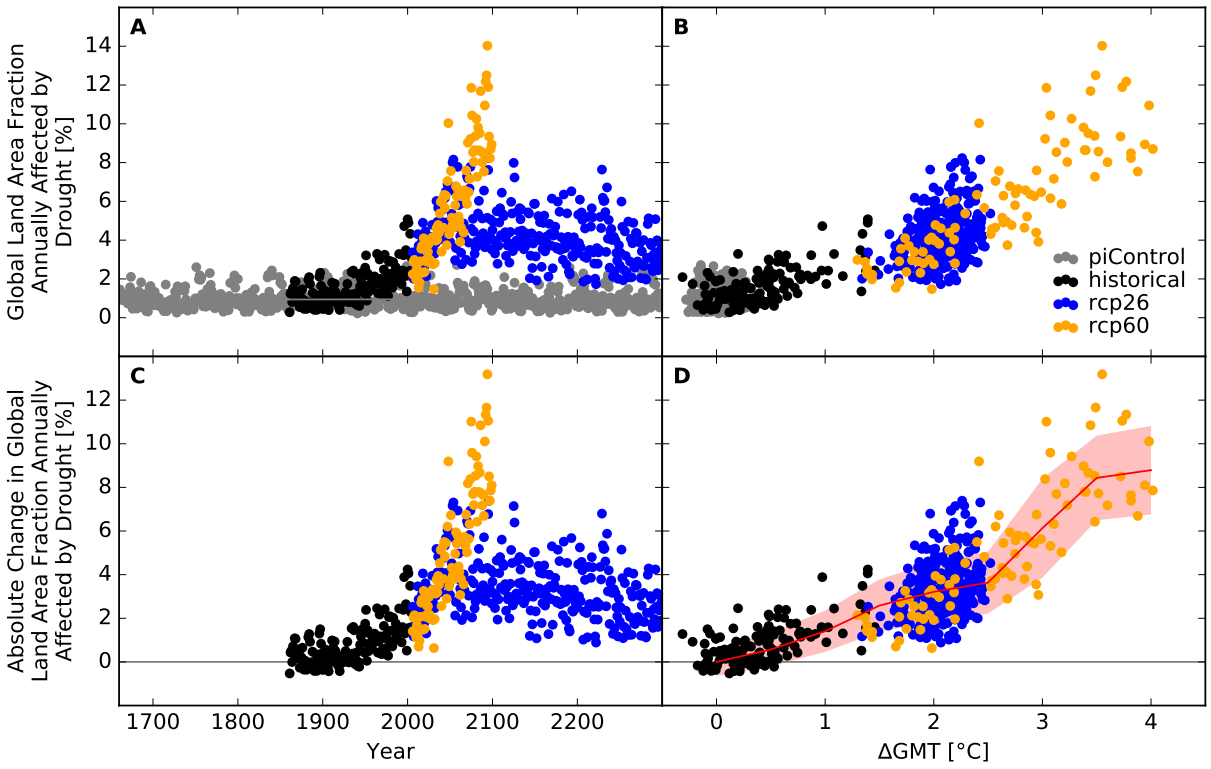

Figure S241: **Derivation of the pure effect of climate change on the global land area fraction annually affected by drought (IPSL-CM5A-LR + MPI-HM).** Analogous to Figure S229.

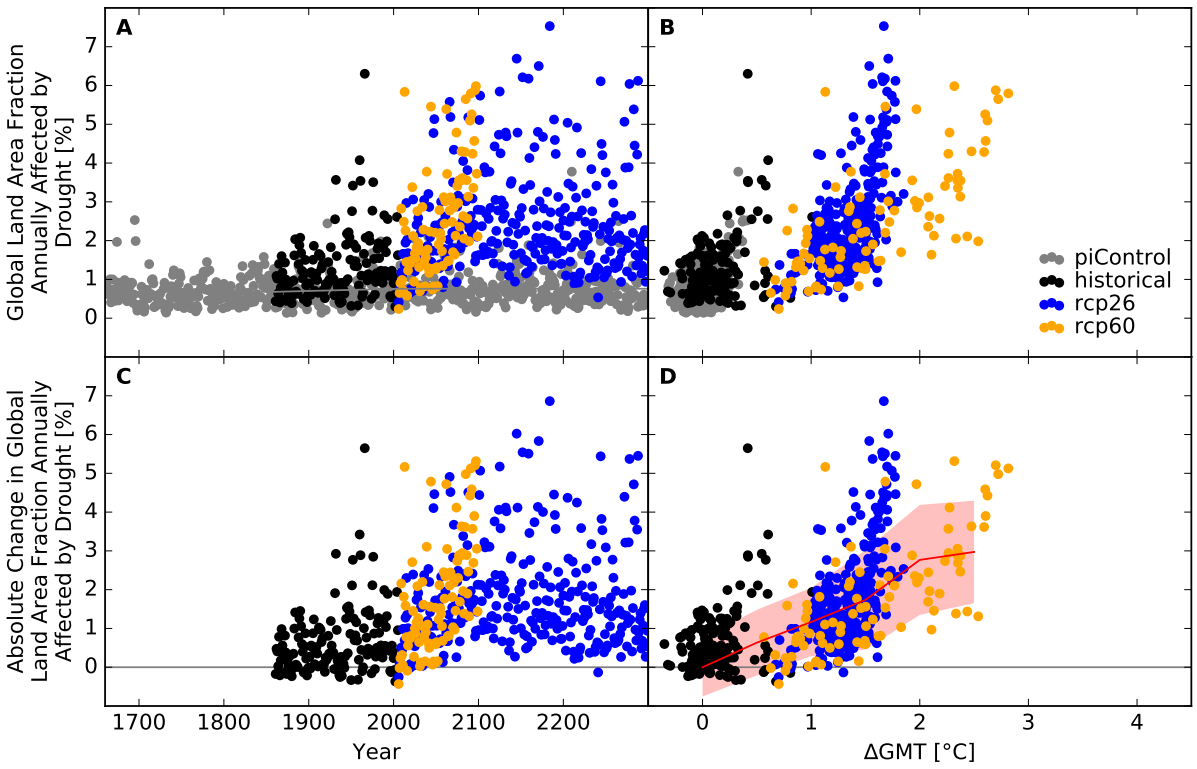

Figure S242: **Derivation of the pure effect of climate change on the global land area fraction annually affected by drought (MIROC5 + MPI-HM).** Analogous to Figure S229.

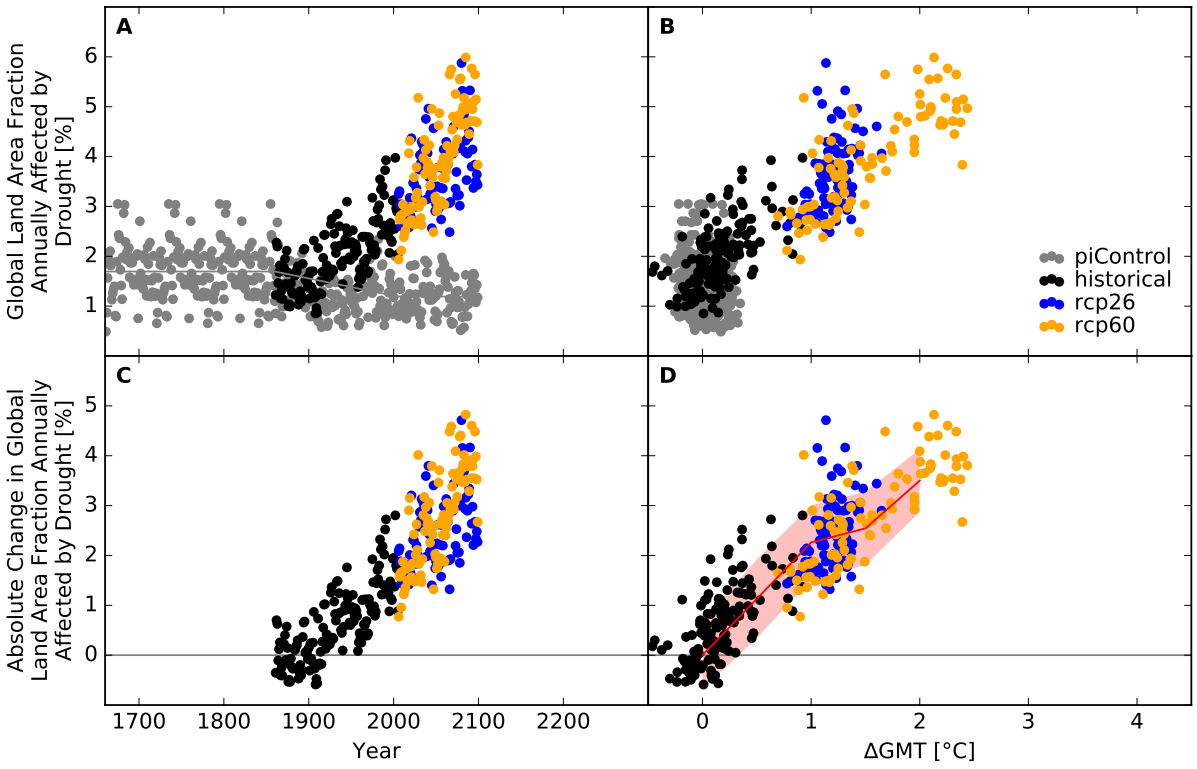

Figure S243: **Derivation of the pure effect of climate change on the global land area fraction annually affected by drought (GFDL-ESM2M + ORCHIDEE).** Analogous to Figure S229.

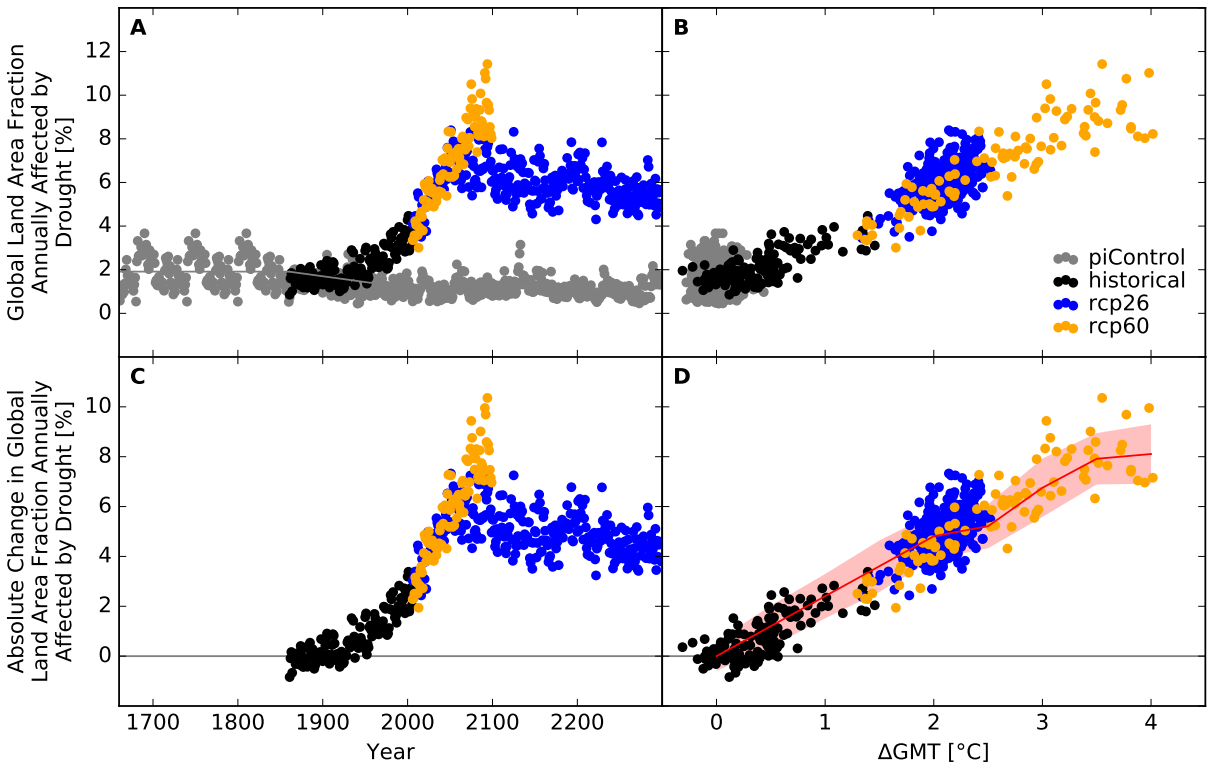

Figure S244: **Derivation of the pure effect of climate change on the global land area fraction annually affected by drought (IPSL-CM5A-LR + ORCHIDEE).** Analogous to Figure S229.

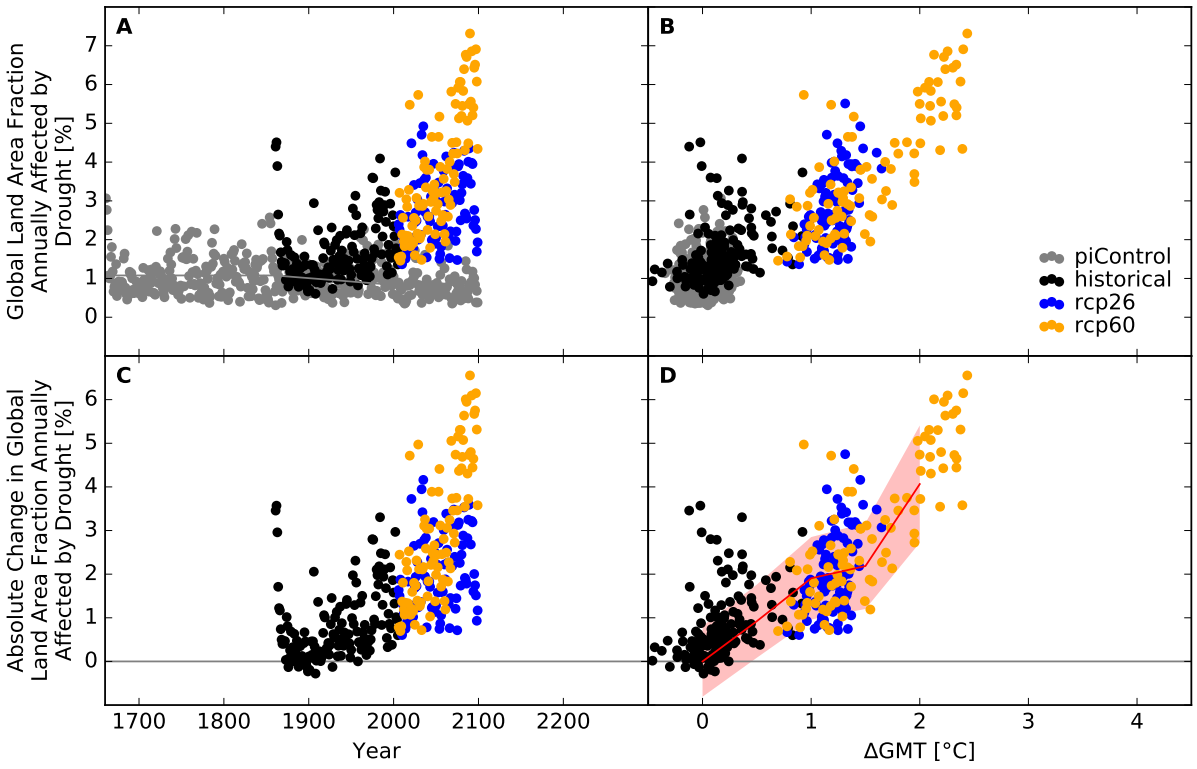

Figure S245: **Derivation of the pure effect of climate change on the global land area fraction annually affected by drought (GFDL-ESM2M + PCR-GLOBWB).** Analogous to Figure S229.

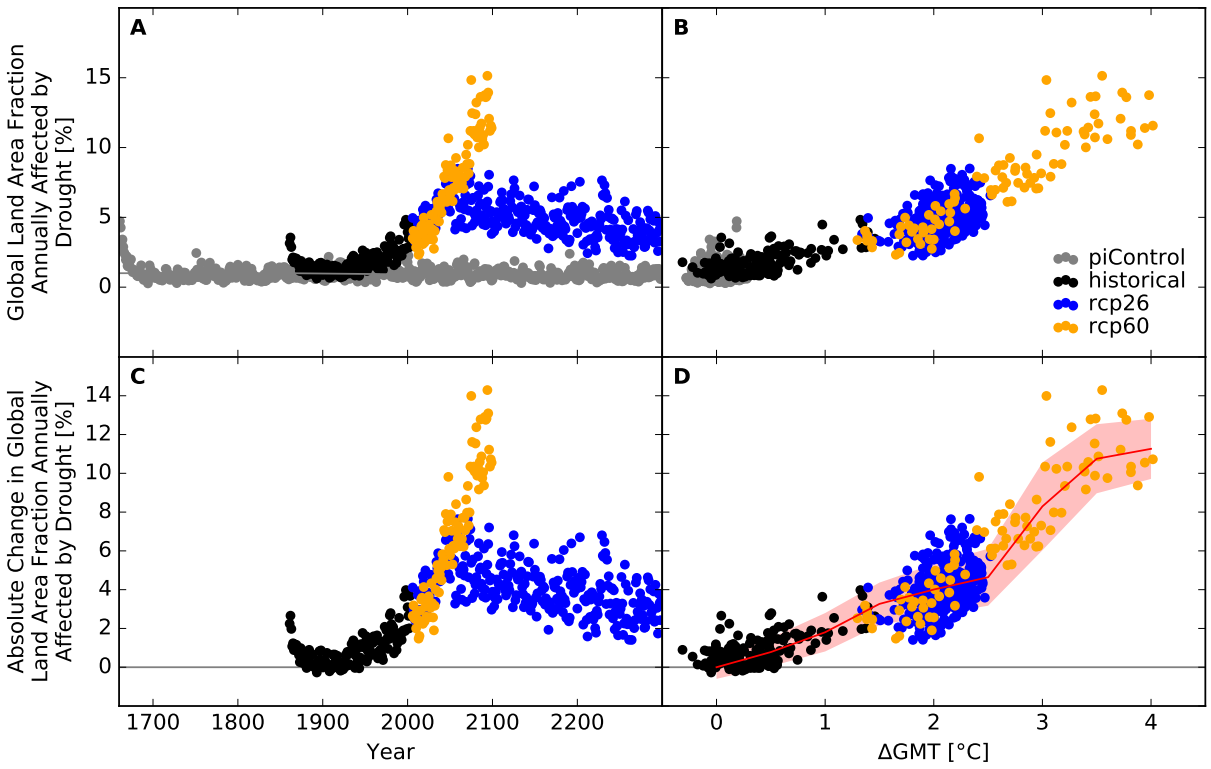

Figure S246: **Derivation of the pure effect of climate change on the global land area fraction annually affected by drought (IPSL-CM5A-LR + PCR-GLOBWB).** Analogous to Figure S229.

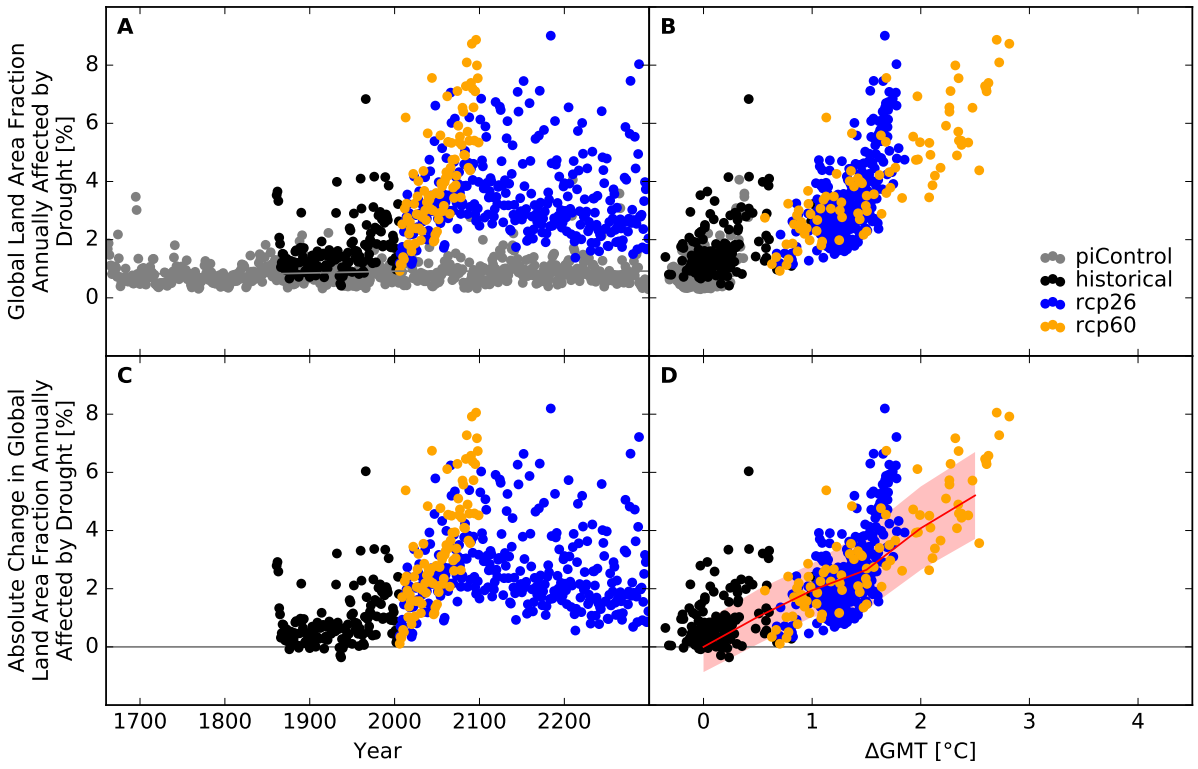

Figure S247: **Derivation of the pure effect of climate change on the global land area fraction annually affected by drought (MIROC5 + PCR-GLOBWB).** Analogous to Figure S229.

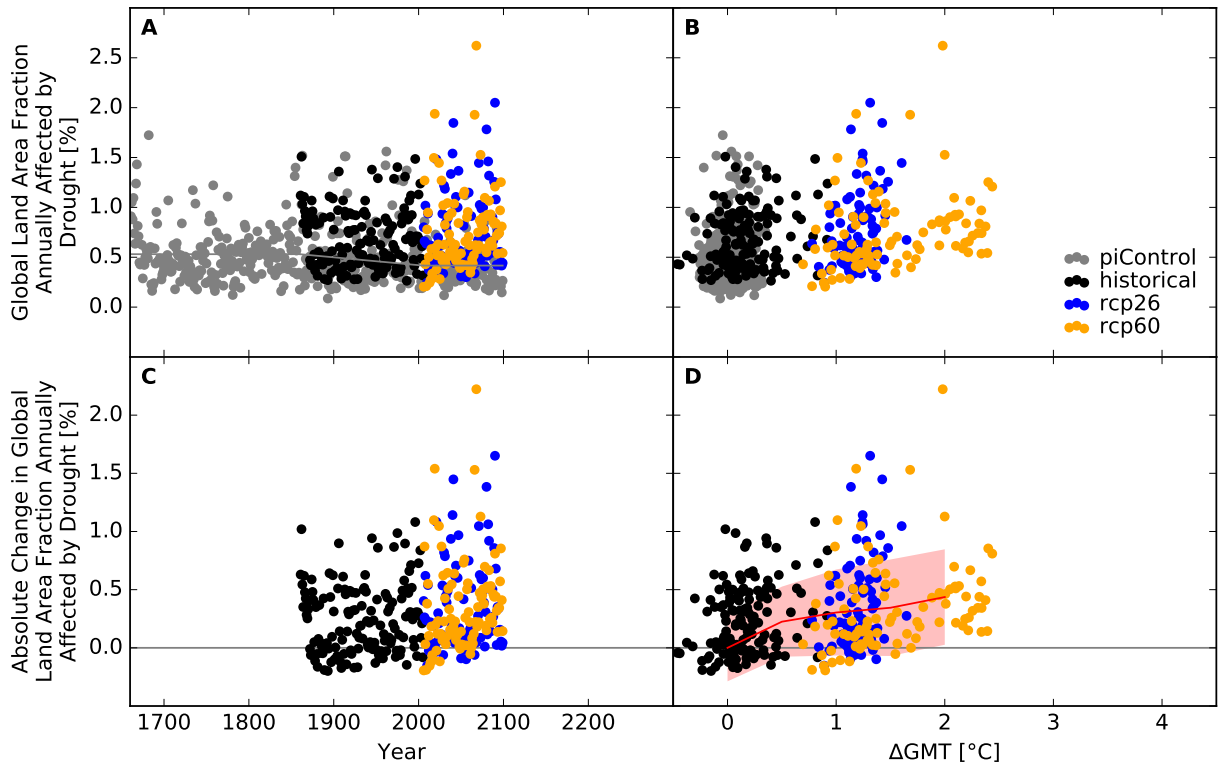

Figure S248: **Derivation of the pure effect of climate change on the global land area fraction annually affected by drought (GFDL-ESM2M + WaterGAP2).** Analogous to Figure S229.

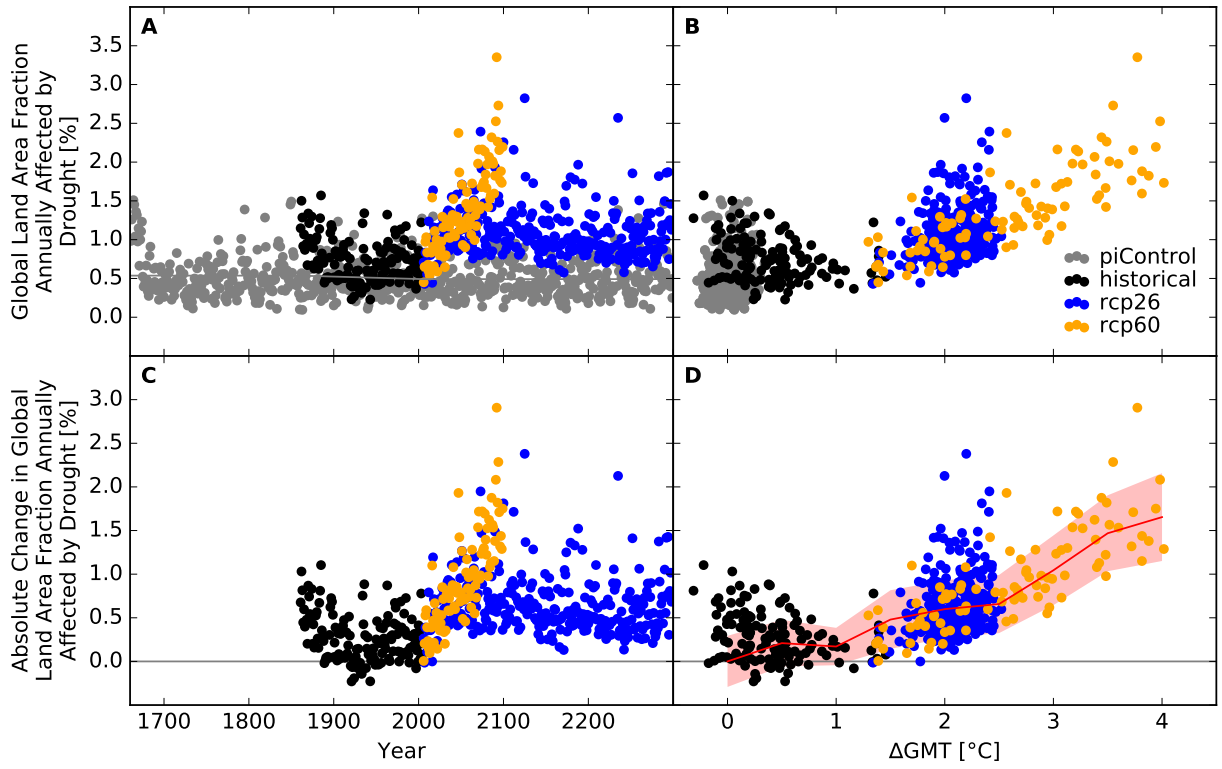

Figure S249: **Derivation of the pure effect of climate change on the global land area fraction annually affected by drought (IPSL-CM5A-LR + WaterGAP2).** Analogous to Figure S229.

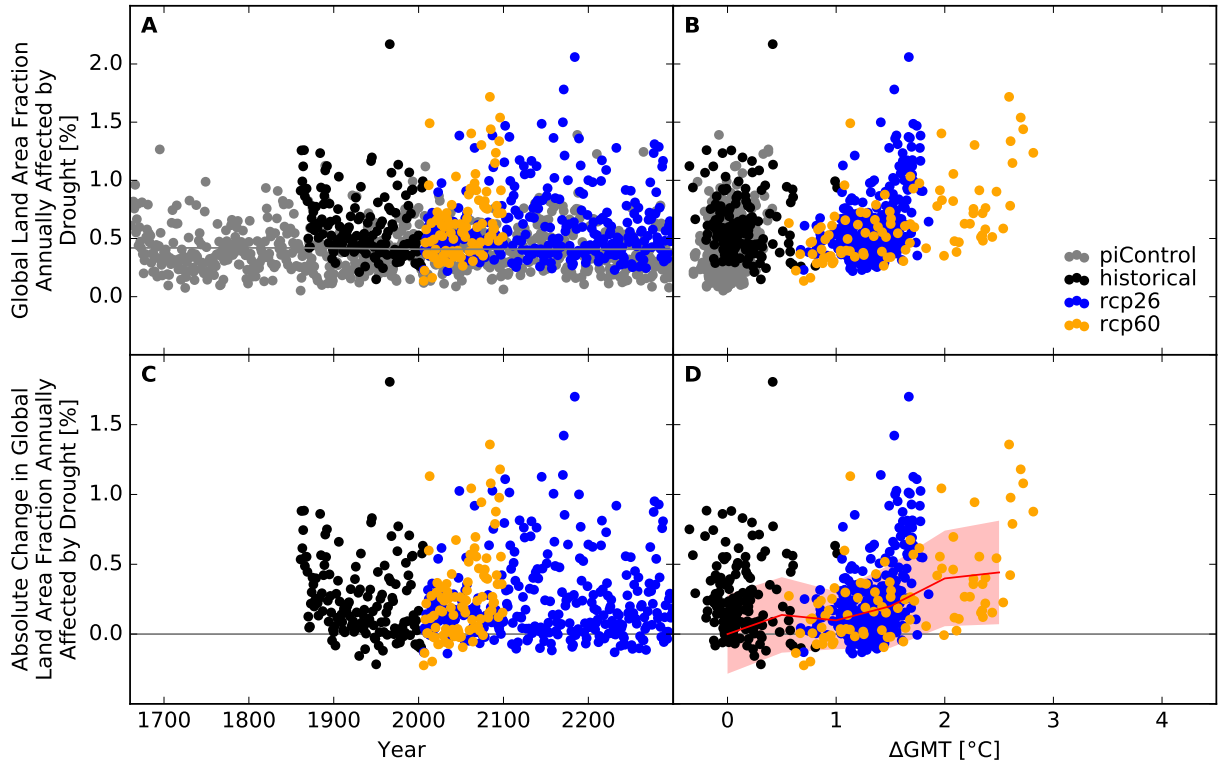

Figure S250: **Derivation of the pure effect of climate change on the global land area fraction annually affected by drought (MIROC5 + WaterGAP2).** Analogous to Figure S229.

Number of people exposed

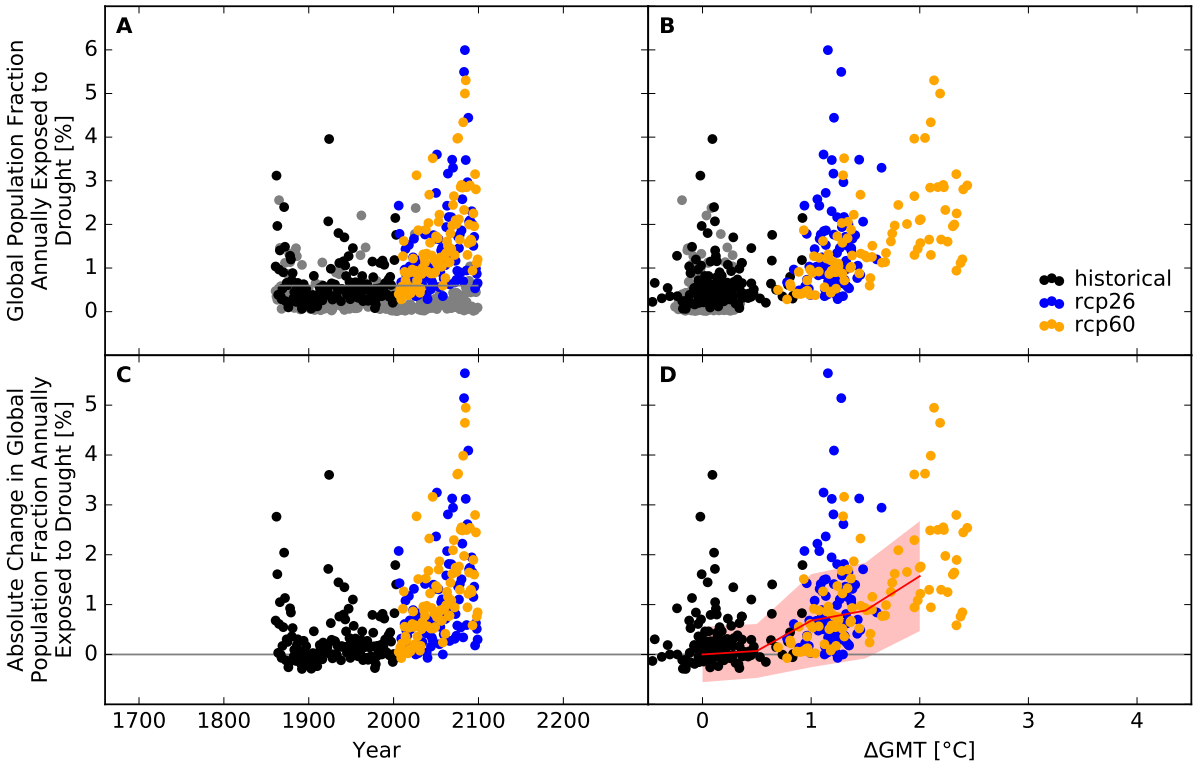

Figure S251: **Derivation of the pure effect of climate change on the global population fraction annually exposed to drought (GFDL-ESM2M + CLM45).** Panel A: Time series of annual global population fraction exposed (PFE) to drought for preindustrial climate (grey dots), historical climate (black dots), climate projections for RCP2.6 (blue dots), and RCP6.0 (orange dots). In all simulations, socioeconomic conditions are varied according to the historically observed development between 1860 and 2005, and held fixed at 1860 conditions before 1860 and at 2005 conditions after 2005. The horizontal gray lines before 1860 and after 2005 represent the multi-year mean global population fraction annually exposed to drought under preindustrial climate conditions and socioeconomic conditions of 1860 and 2005, respectively. The gray line between 1860 and 2005 is a linear interpolation of these mean values. Panel B: Data shown in Panel A plotted against the associated GCM-specific annual global mean temperature (GMT) change relative to the long-term preindustrial mean GMT. Panel C: Pure effect of climate change on PFE, calculated as the difference between the annual data shown in Panel A and the multi-year mean PFE under preindustrial climate conditions (gray line in Panel A). Panel D: Data shown in Panel C plotted against annual GMT change. The red line represents the mean values of the annual data points per 1 °C-wide GMT change bin, with bins centered at GMT change levels increasing from 0 °C to 4 °C in steps of 0.5 °C. The area shaded in red represents the mean value ±1 standard deviation ranges of the annual data points per GMT change bin.

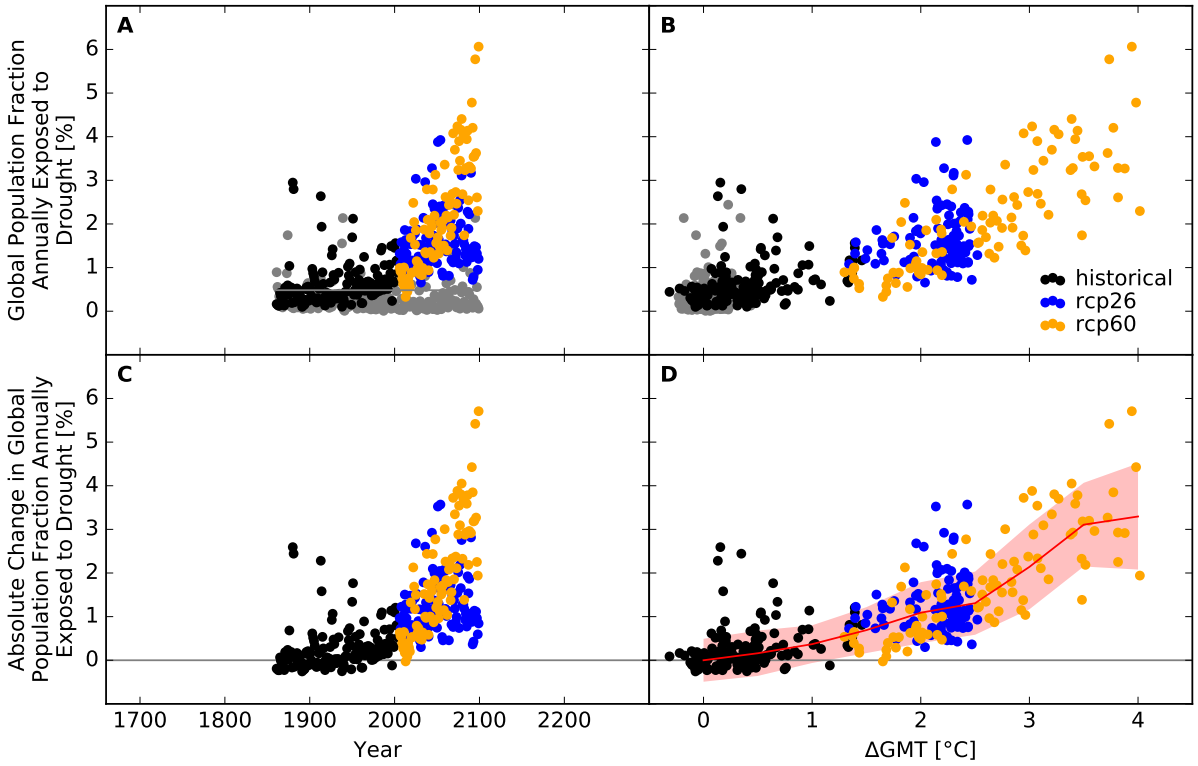

Figure S252: **Derivation of the pure effect of climate change on the global population fraction annually exposed to drought (IPSL-CM5A-LR + CLM45).** Analogous to Figure S251.

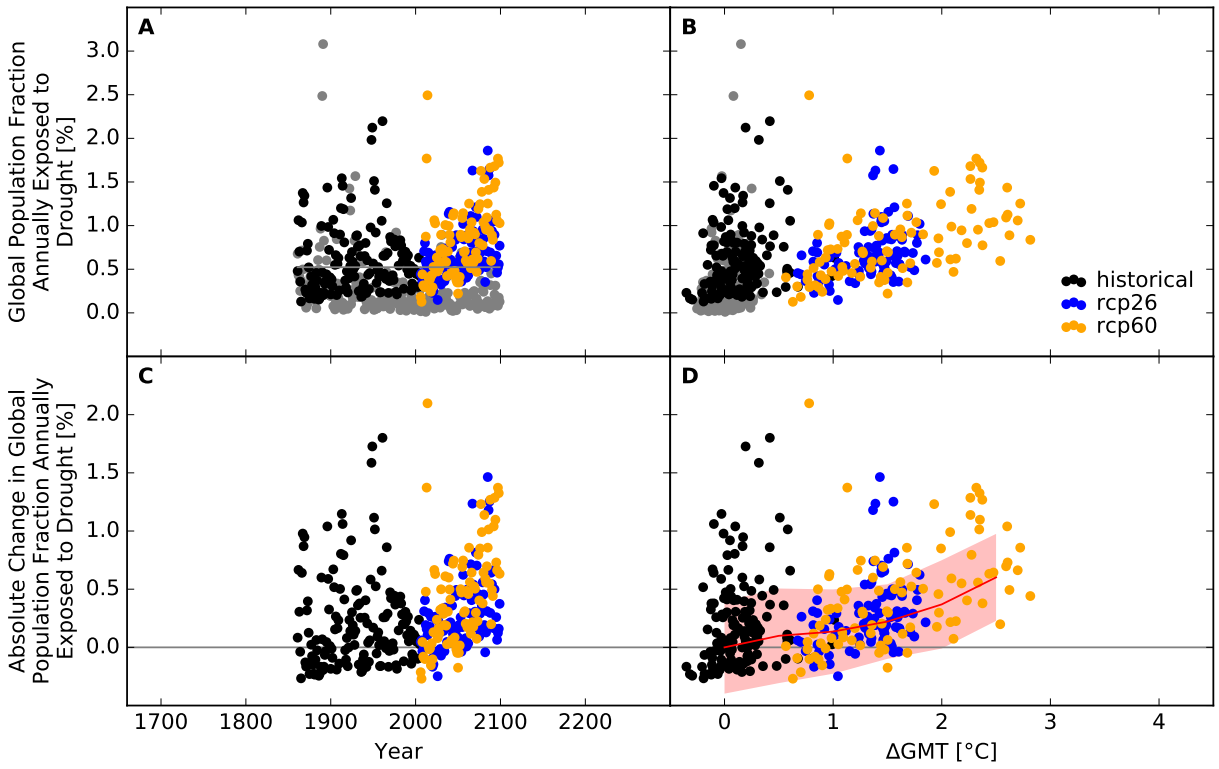

Figure S253: **Derivation of the pure effect of climate change on the global population fraction annually exposed to drought (MIROC5 + CLM45).** Analogous to Figure S251.

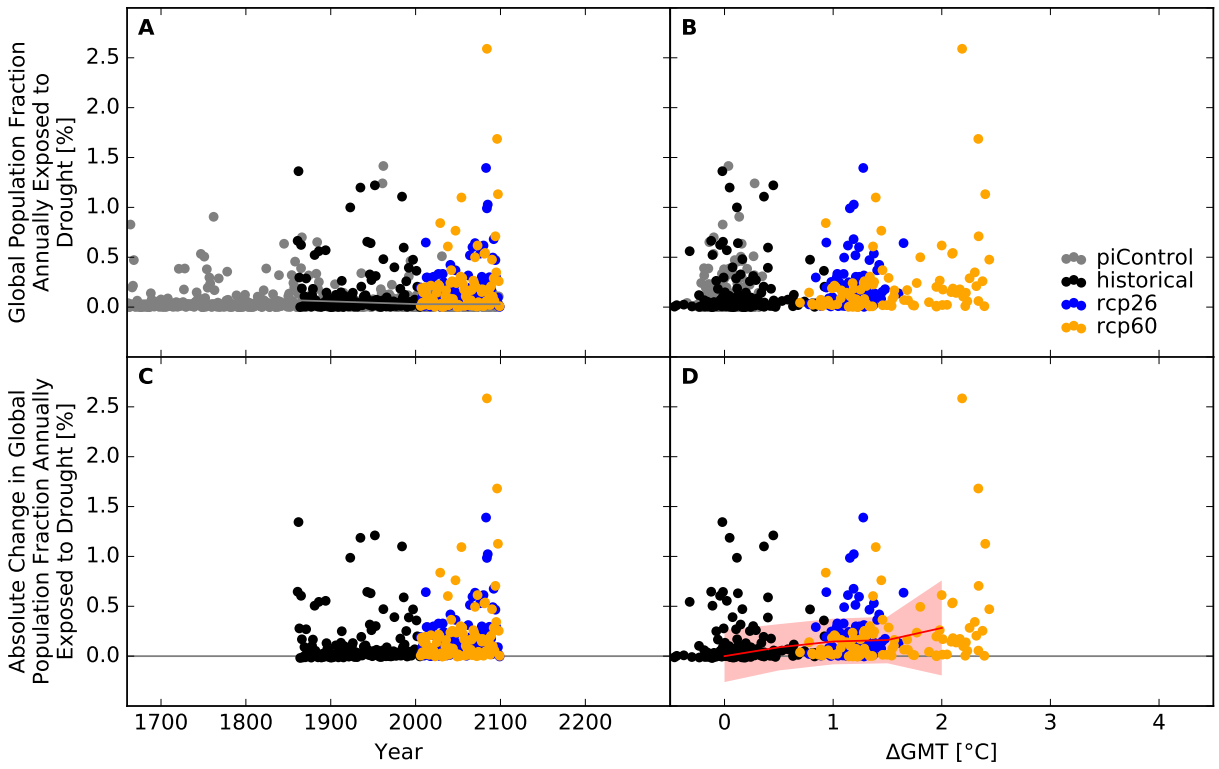

Figure S254: **Derivation of the pure effect of climate change on the global population fraction annually exposed to drought (GFDL-ESM2M + H08).** Analogous to Figure S251.

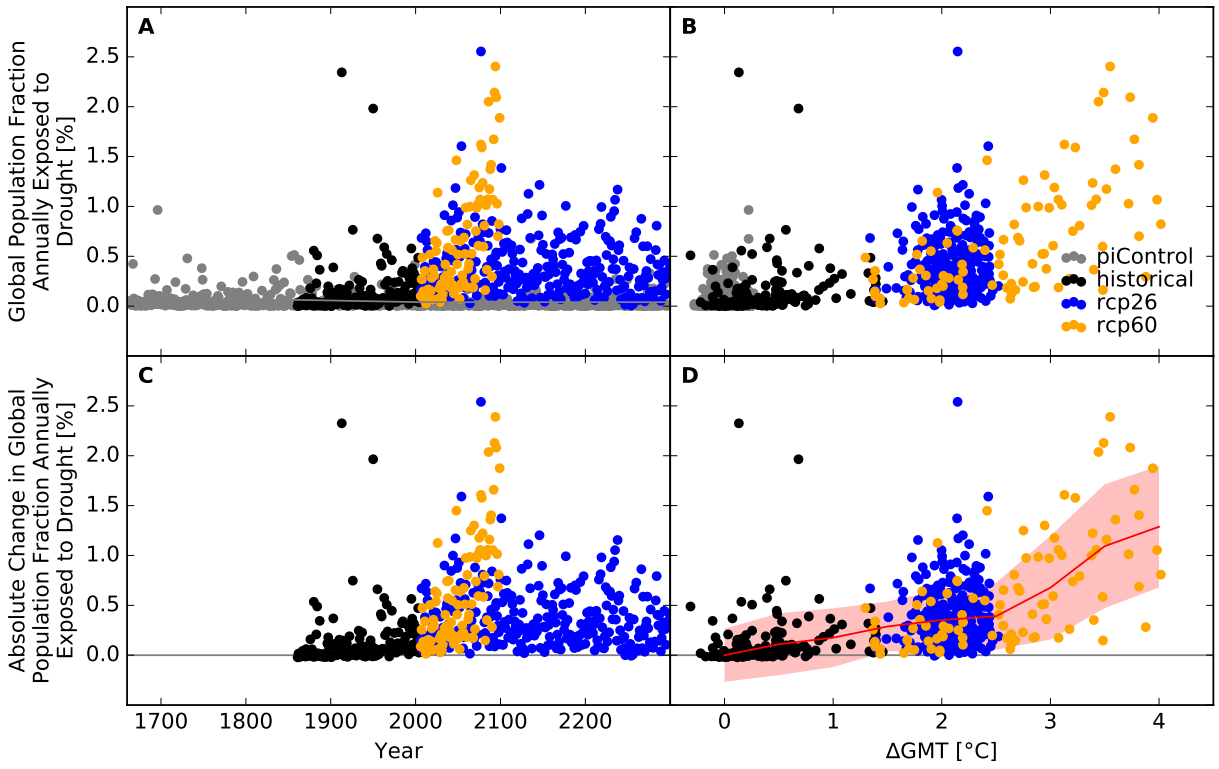

Figure S255: **Derivation of the pure effect of climate change on the global population fraction annually exposed to drought (IPSL-CM5A-LR + H08).** Analogous to Figure S251.

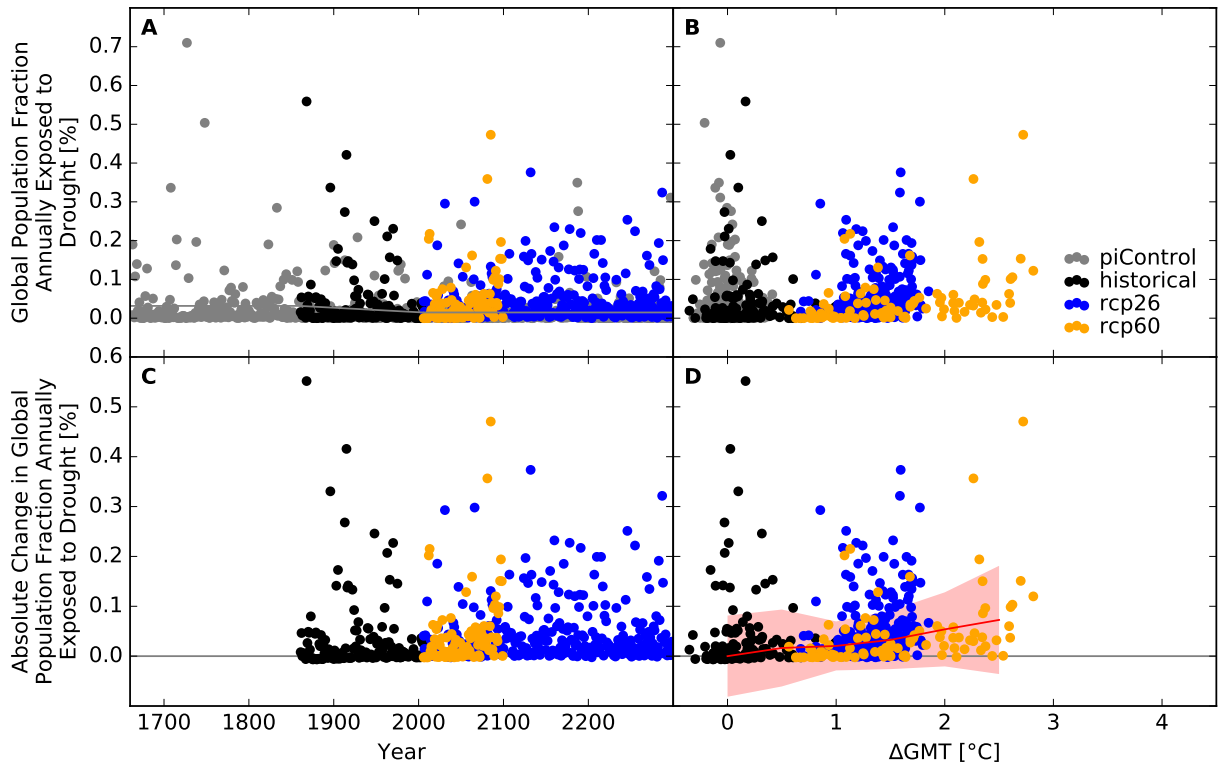

Figure S256: **Derivation of the pure effect of climate change on the global population fraction annually exposed to drought (MIROC5 + H08).** Analogous to Figure S251.

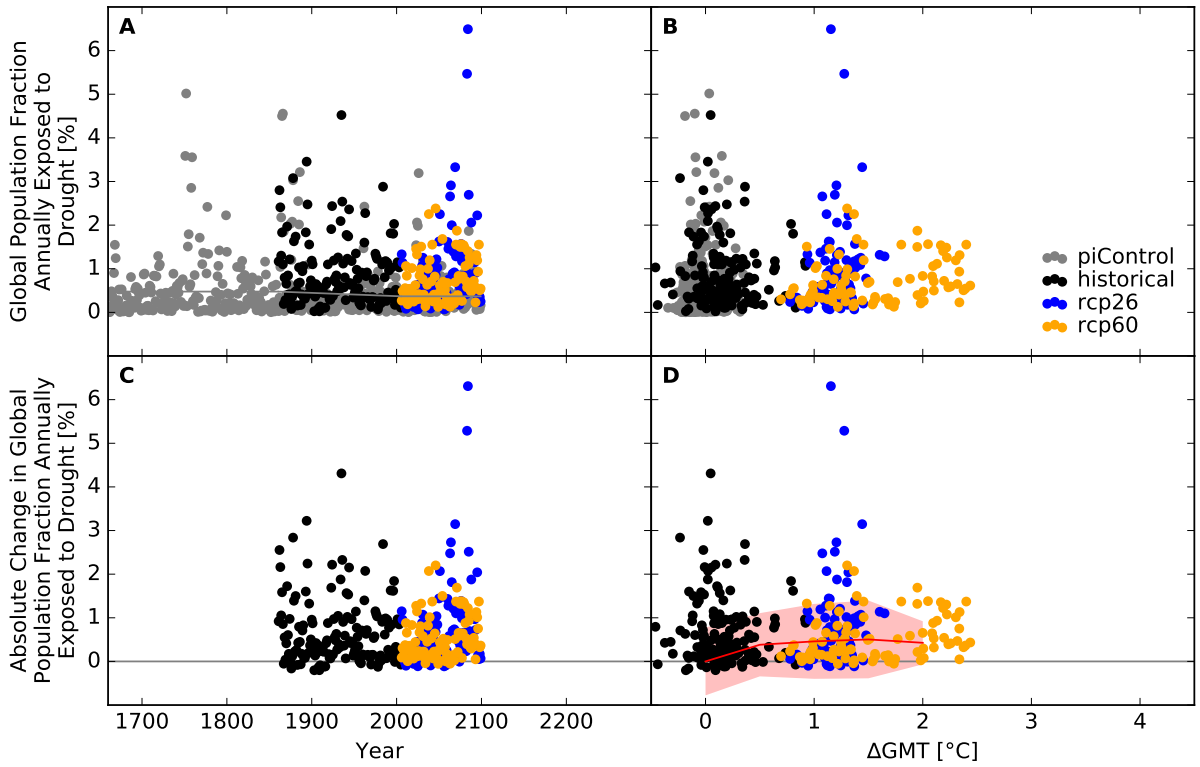

Figure S257: **Derivation of the pure effect of climate change on the global population fraction annually exposed to drought (GFDL-ESM2M + JULES-W1).** Analogous to Figure S251.

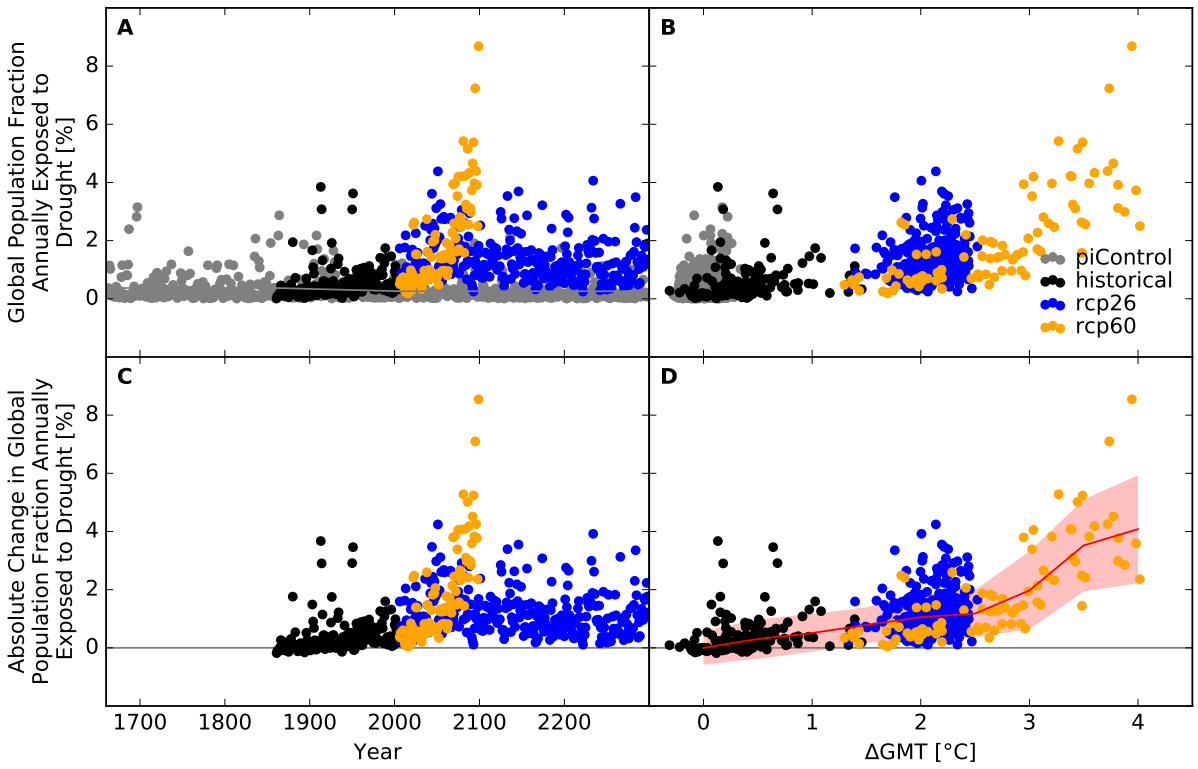

Figure S258: **Derivation of the pure effect of climate change on the global population fraction annually exposed to drought (IPSL-CM5A-LR + JULES-W1).** Analogous to Figure S251.

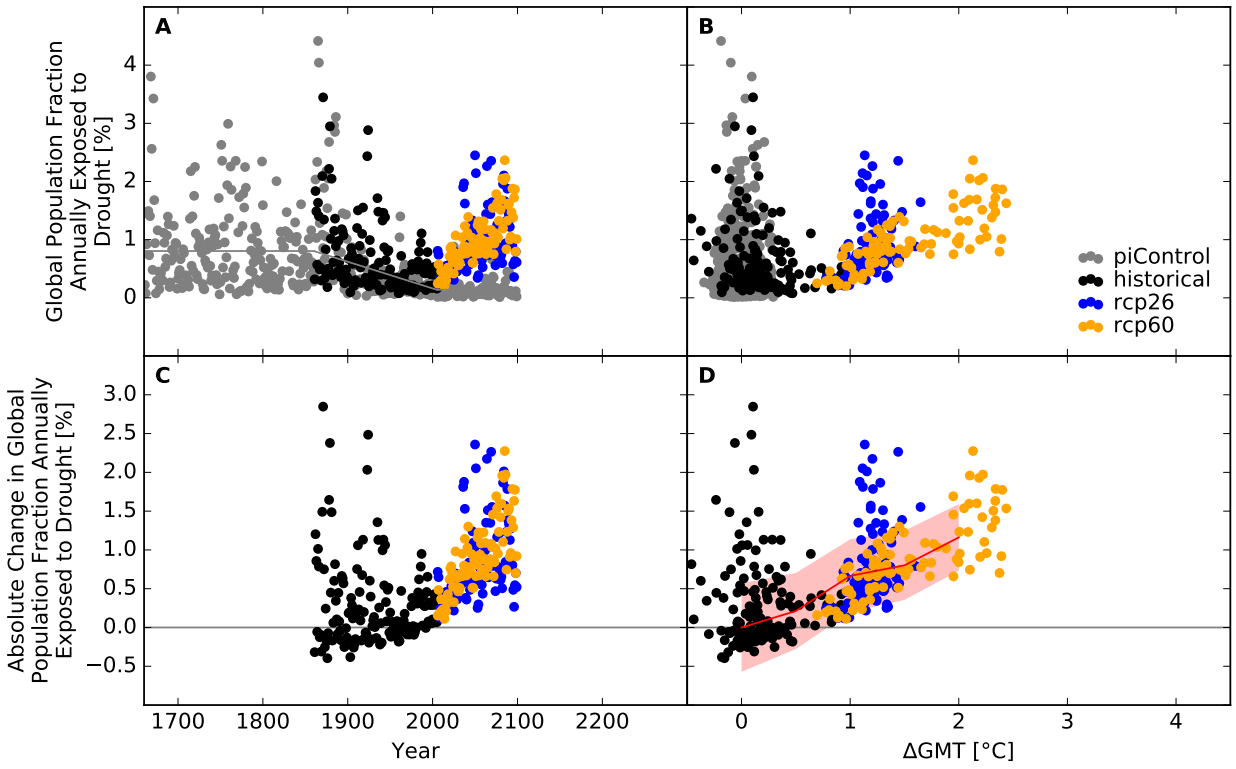

Figure S259: **Derivation of the pure effect of climate change on the global population fraction annually exposed to drought (GFDL-ESM2M + LPJmL).** Analogous to Figure S251.

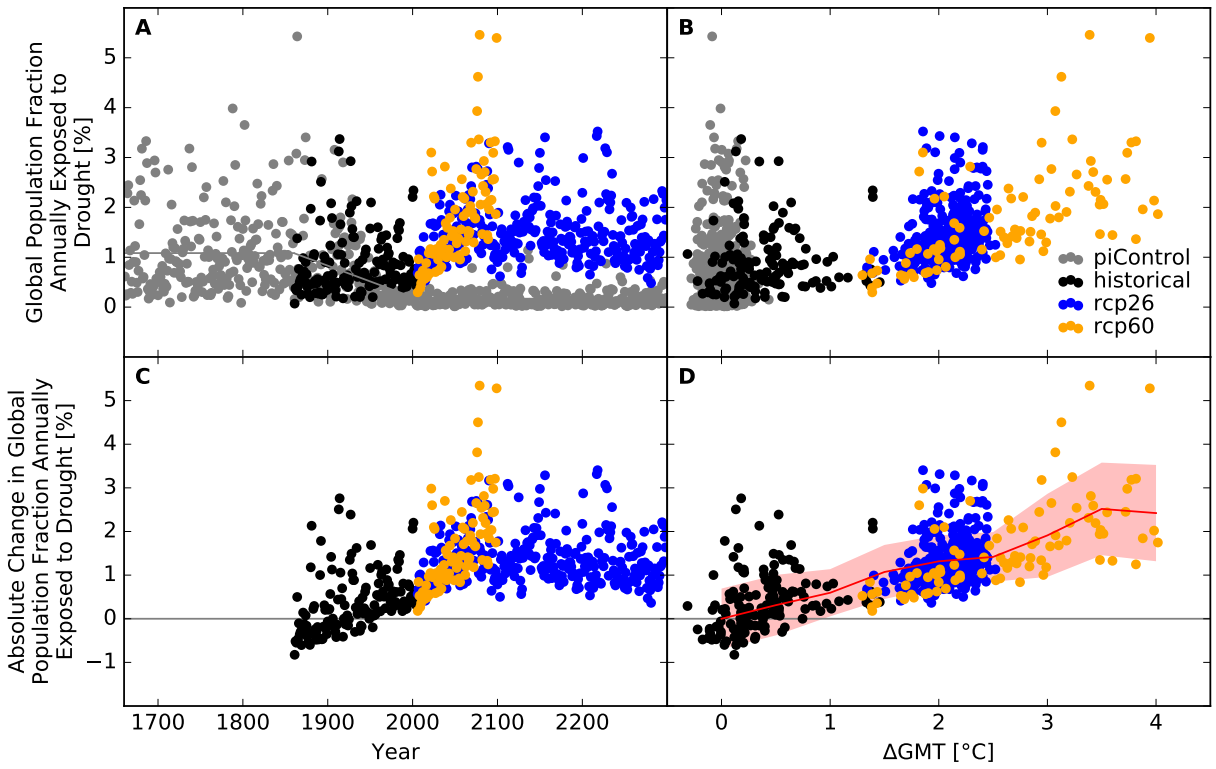

Figure S260: **Derivation of the pure effect of climate change on the global population fraction annually exposed to drought (IPSL-CM5A-LR + LPJmL).** Analogous to Figure S251.

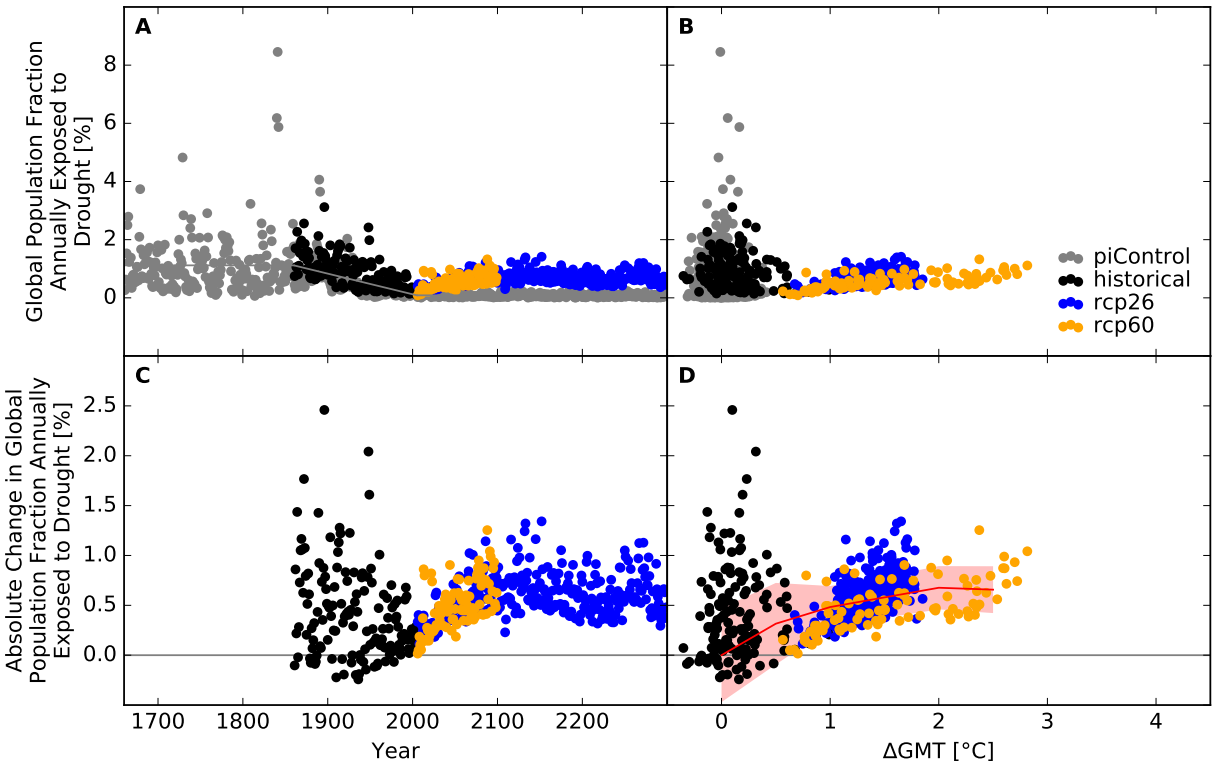

Figure S261: **Derivation of the pure effect of climate change on the global population fraction annually exposed to drought (MIROC5 + LPJmL).** Analogous to Figure S251.

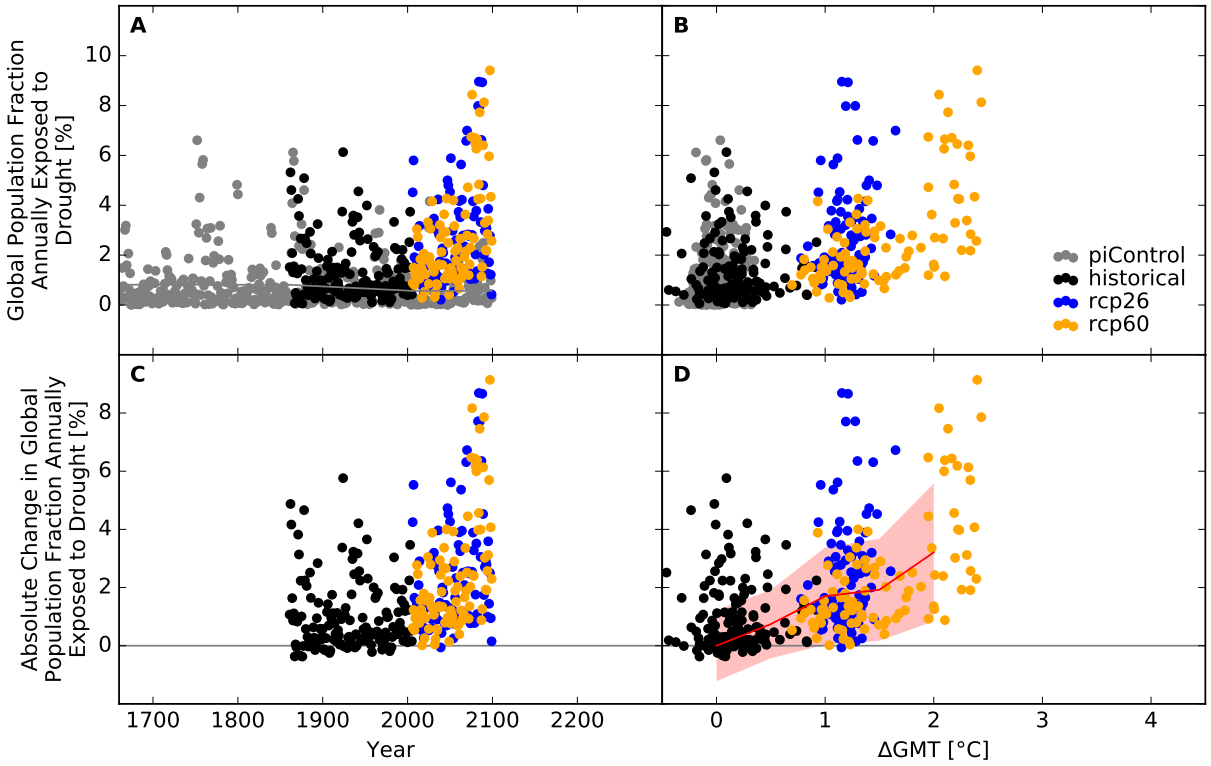

Figure S262: **Derivation of the pure effect of climate change on the global population fraction annually exposed to drought (GFDL-ESM2M + MPI-HM).** Analogous to Figure S251.

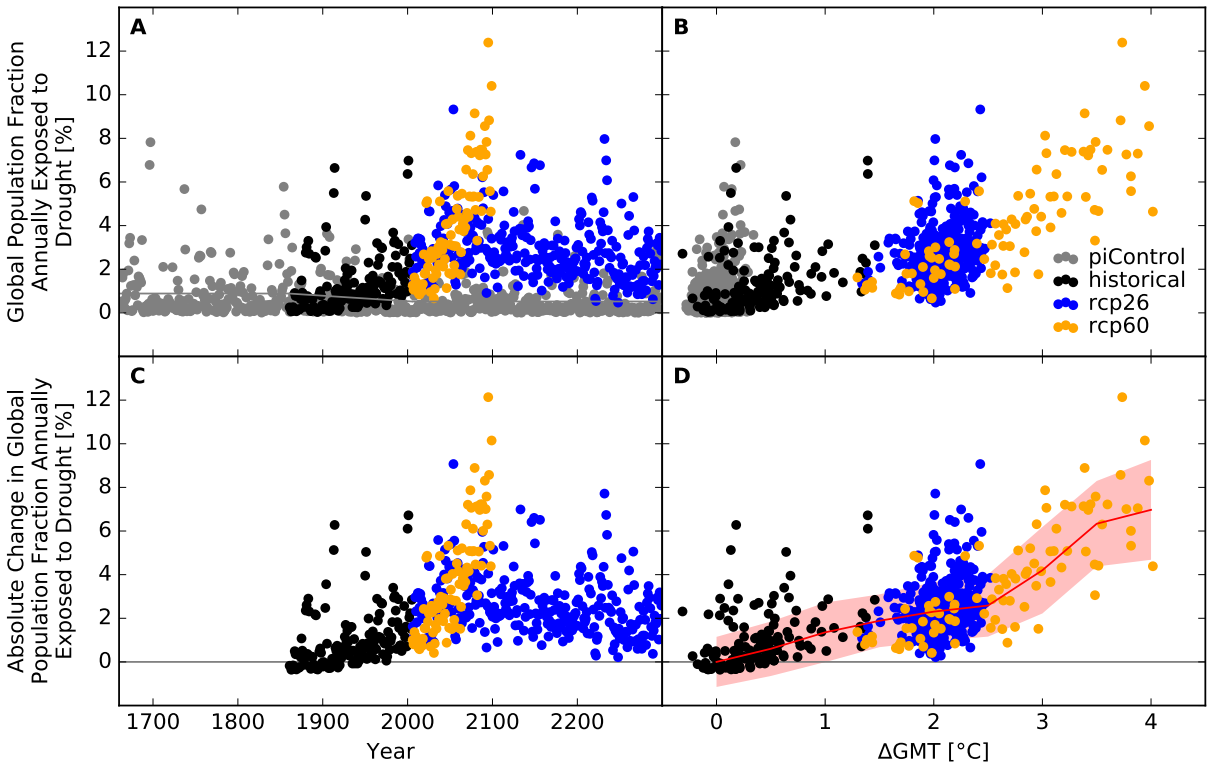

Figure S263: **Derivation of the pure effect of climate change on the global population fraction annually exposed to drought (IPSL-CM5A-LR + MPI-HM).** Analogous to Figure S251.

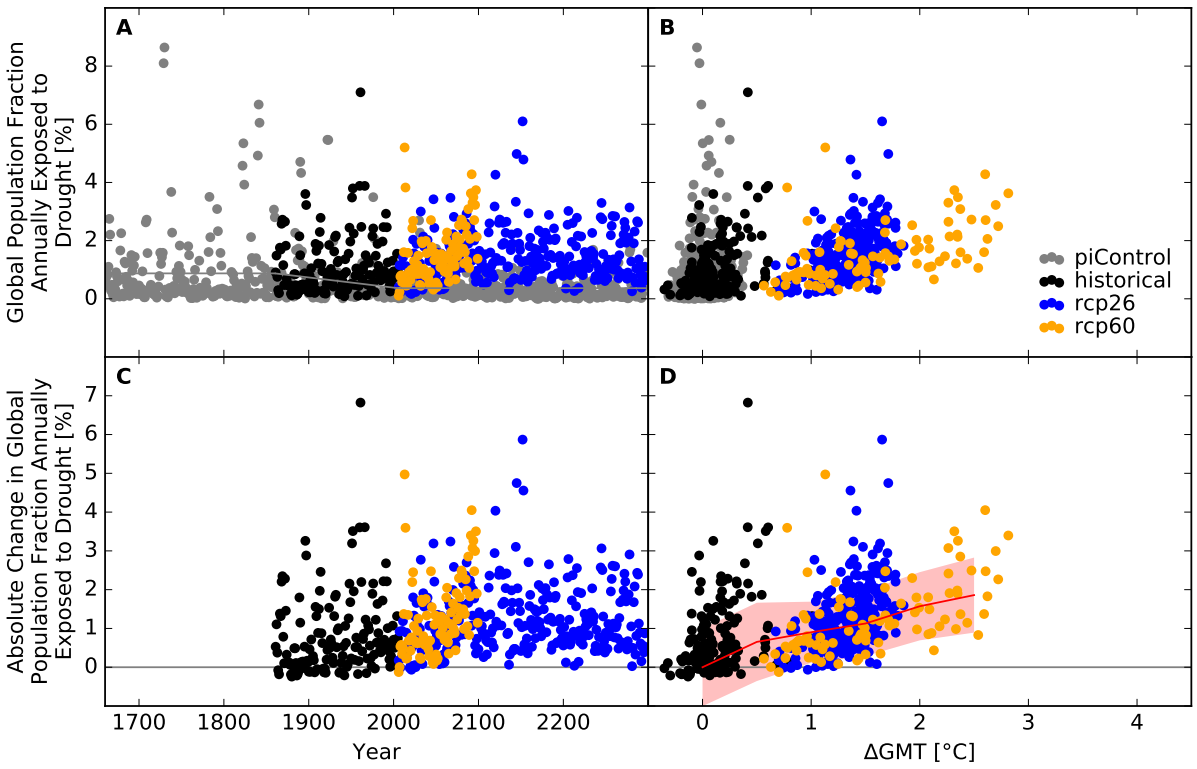

Figure S264: **Derivation of the pure effect of climate change on the global population fraction annually exposed to drought (MIROC5 + MPI-HM).** Analogous to Figure S251.

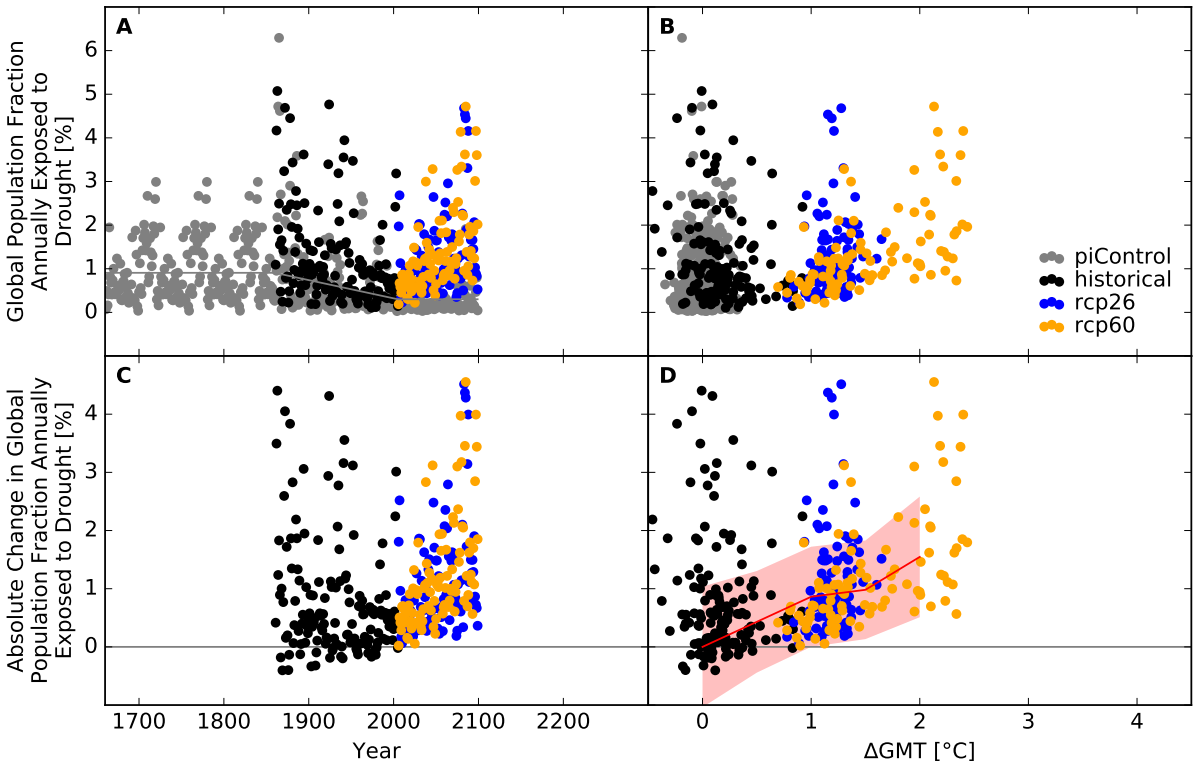

Figure S265: **Derivation of the pure effect of climate change on the global population fraction annually exposed to drought (GFDL-ESM2M + ORCHIDEE).** Analogous to Figure S251.

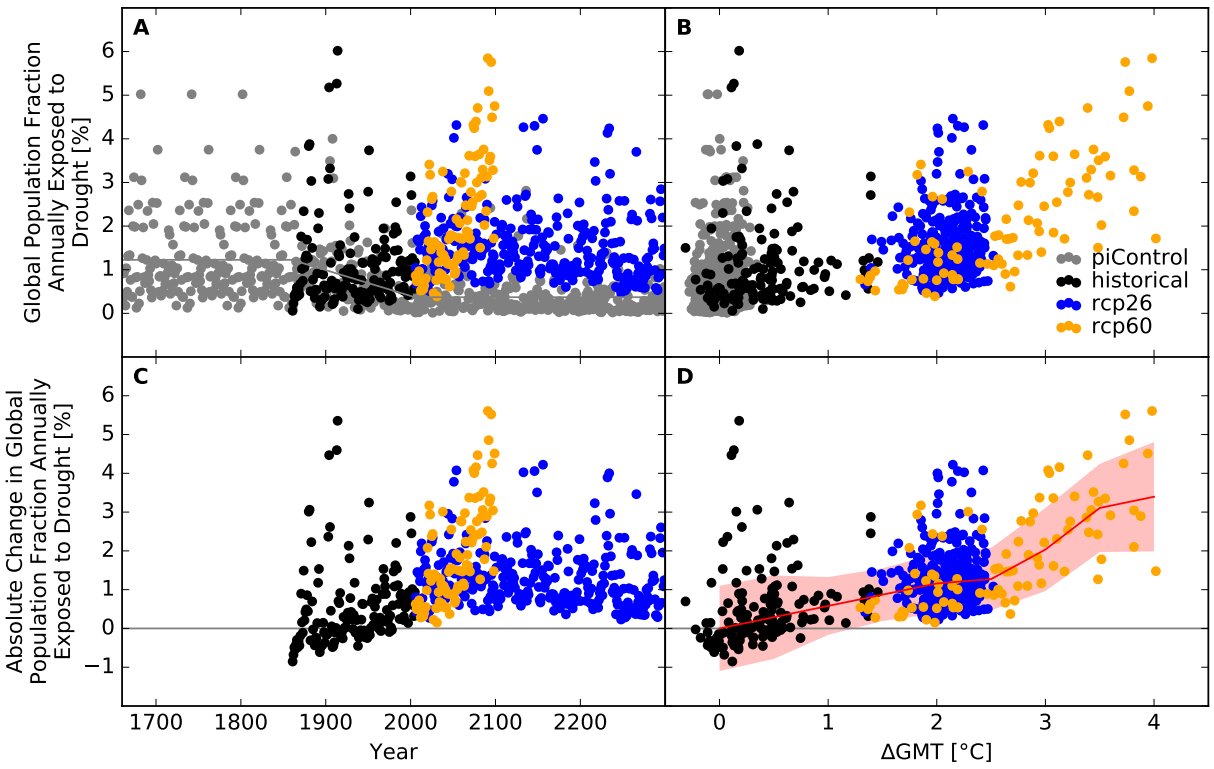

Figure S266: **Derivation of the pure effect of climate change on the global population fraction annually exposed to drought (IPSL-CM5A-LR + ORCHIDEE).** Analogous to Figure S251.

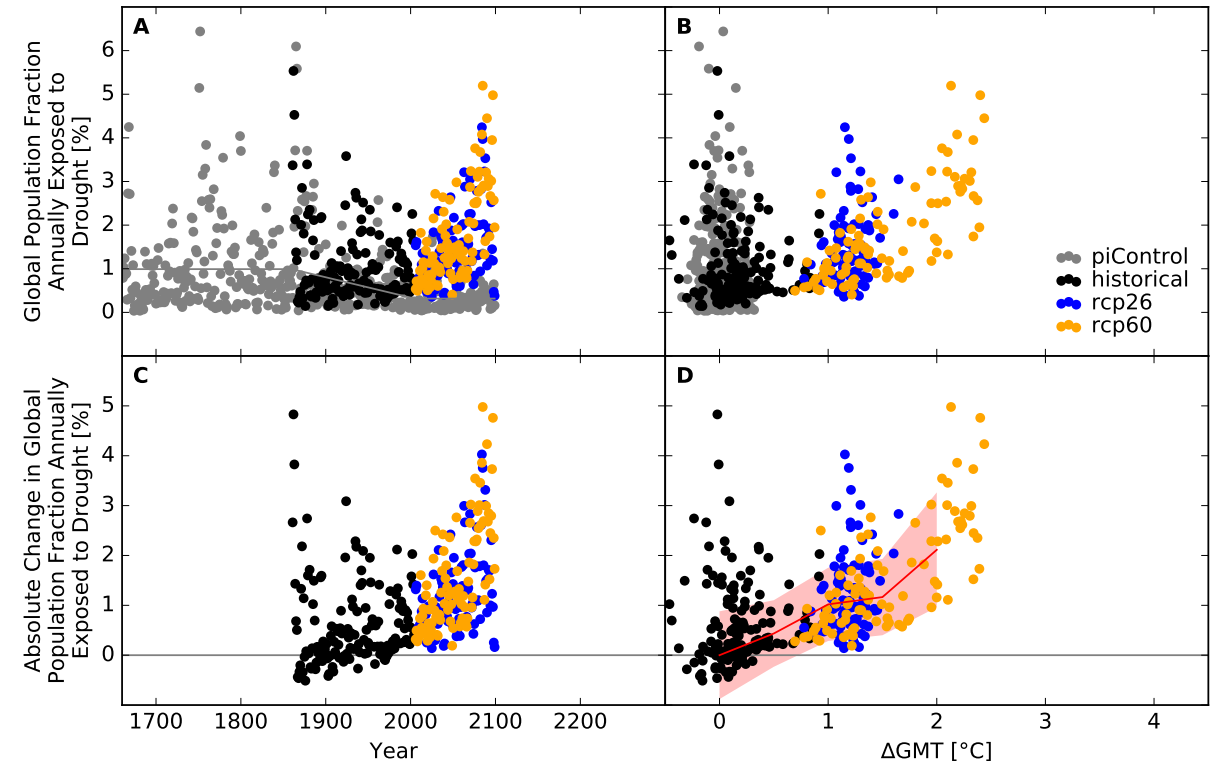

Figure S267: **Derivation of the pure effect of climate change on the global population fraction annually exposed to drought (GFDL-ESM2M + PCR-GLOBWB).** Analogous to Figure S251.

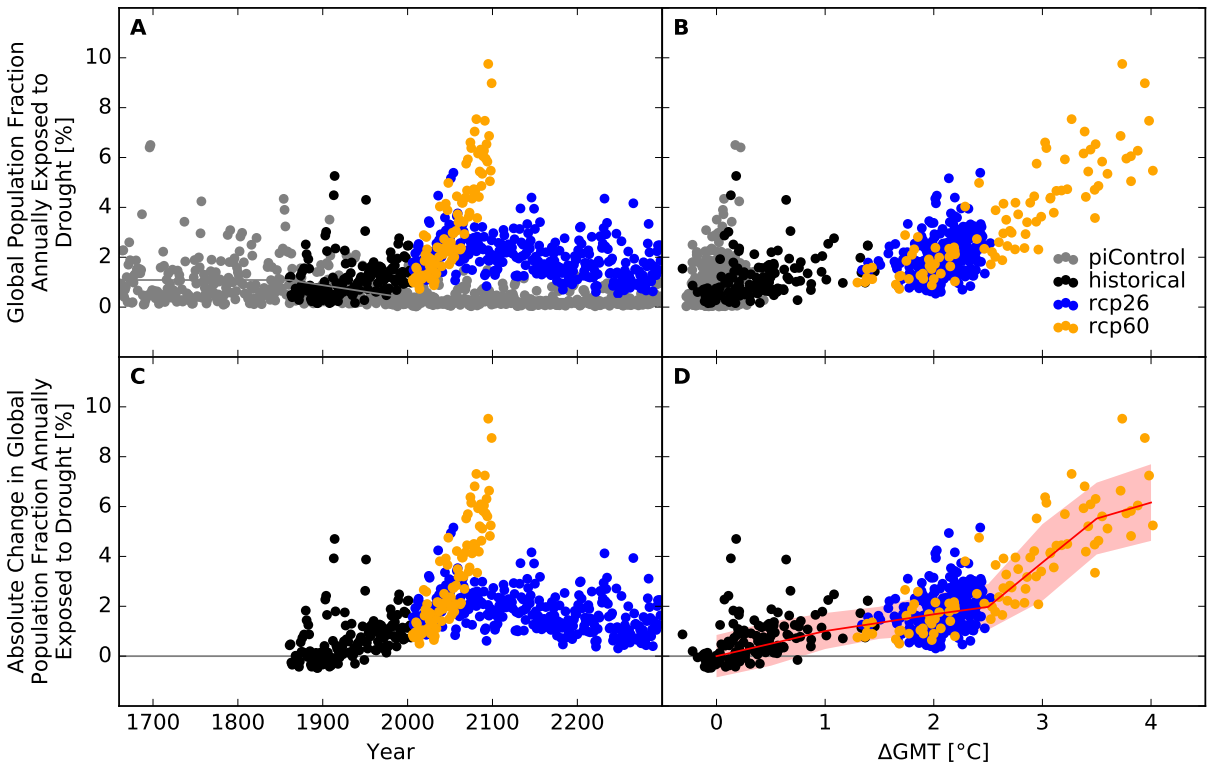

Figure S268: **Derivation of the pure effect of climate change on the global population fraction annually exposed to drought (IPSL-CM5A-LR + PCR-GLOBWB).** Analogous to Figure S251.

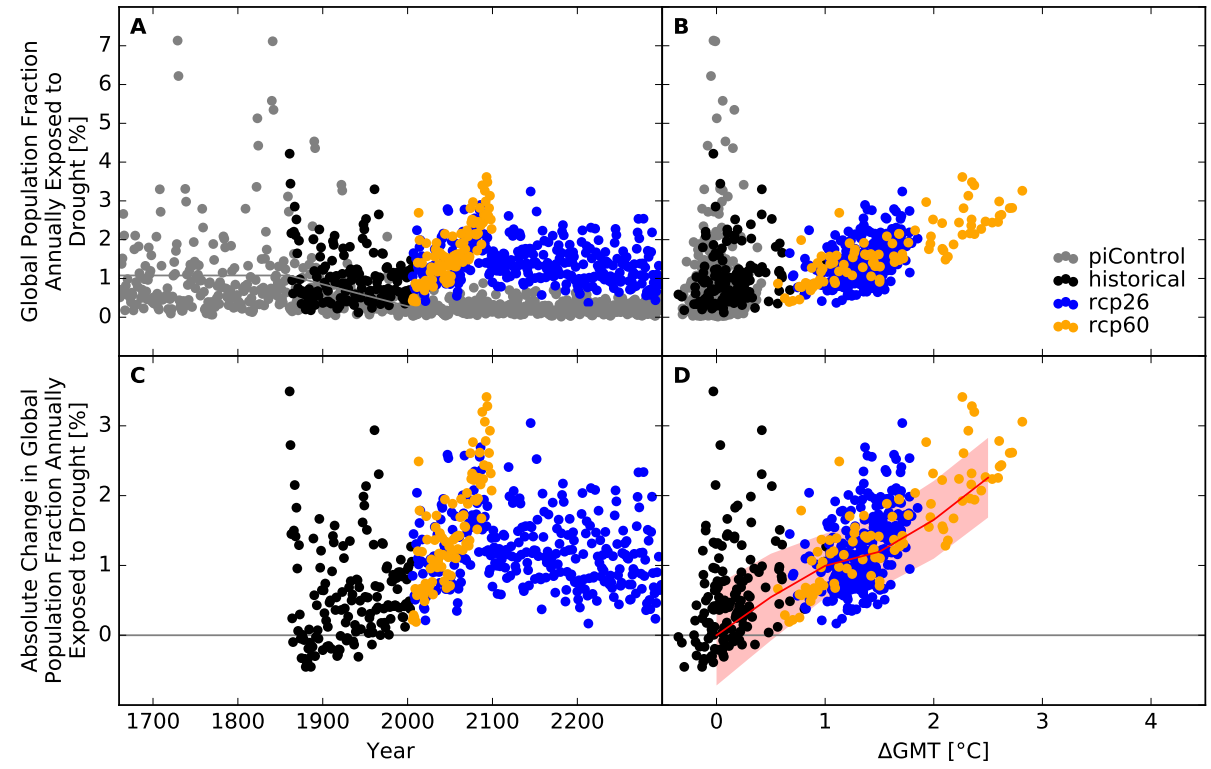

Figure S269: **Derivation of the pure effect of climate change on the global population fraction annually exposed to drought (MIROC5 + PCR-GLOBWB).** Analogous to Figure S251.

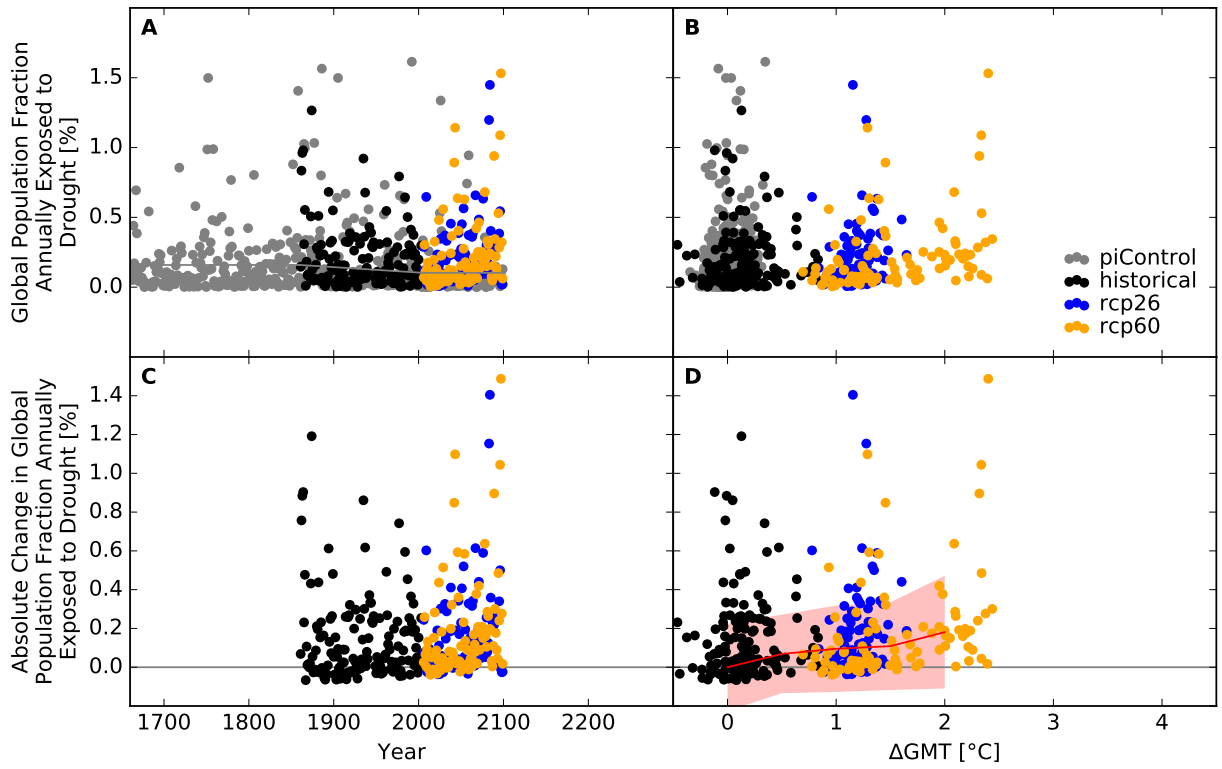

Figure S270: **Derivation of the pure effect of climate change on the global population fraction annually exposed to drought (GFDL-ESM2M + WaterGAP2).** Analogous to Figure S251.

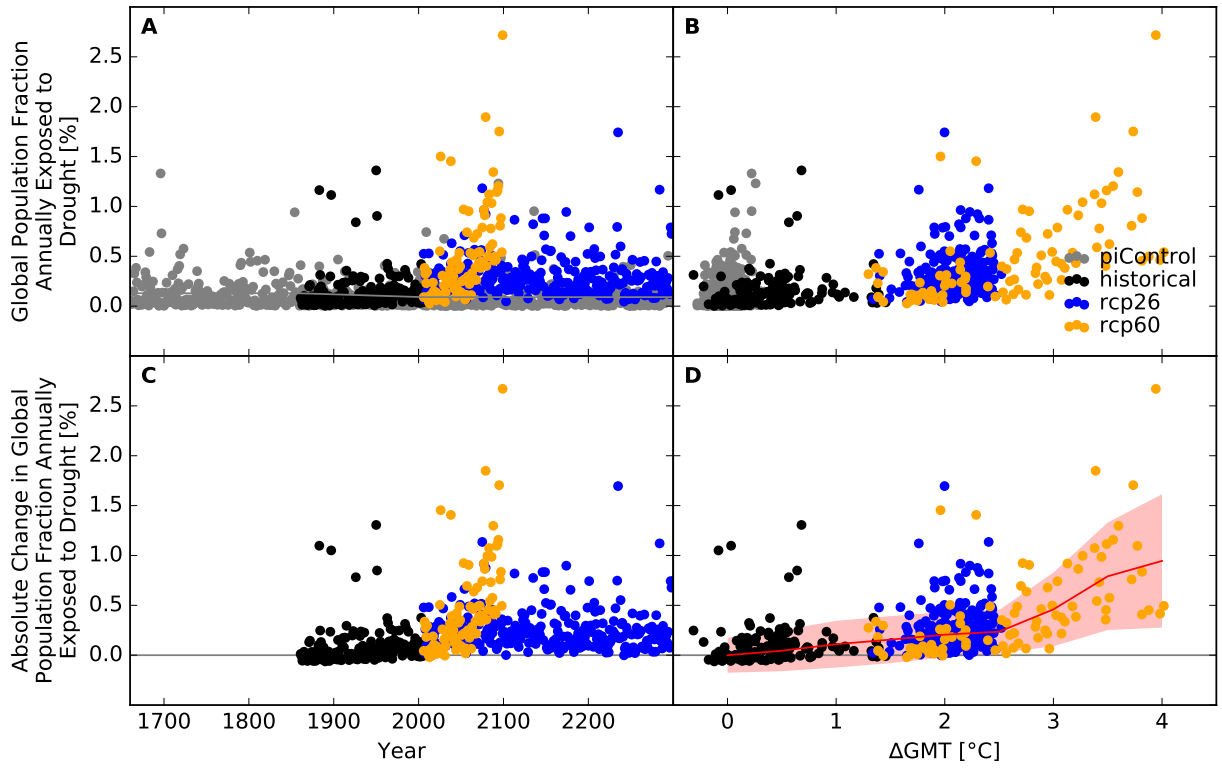

Figure S271: **Derivation of the pure effect of climate change on the global population fraction annually exposed to drought (IPSL-CM5A-LR + WaterGAP2).** Analogous to Figure S251.

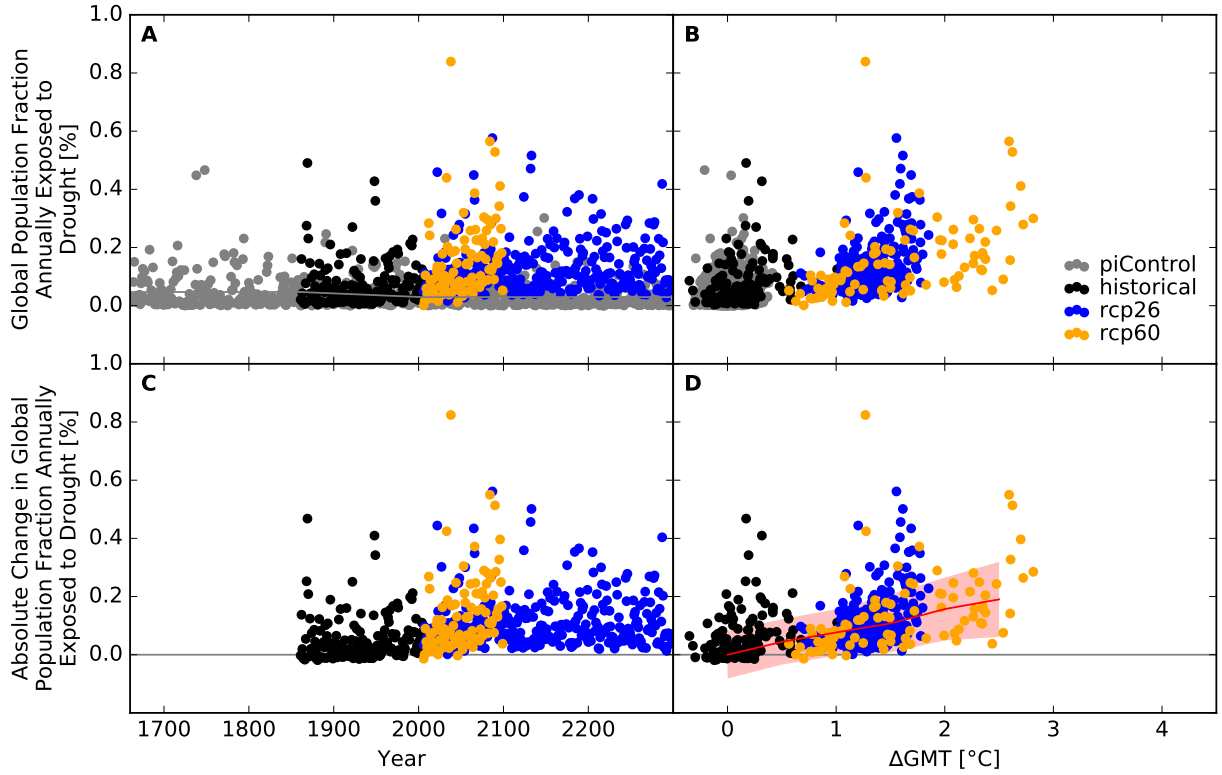

Figure S272: **Derivation of the pure effect of climate change on the global population fraction annually exposed to drought (MIROC5 + WaterGAP2).** Analogous to Figure S251.

Land area affected and number of people exposed at the national scale

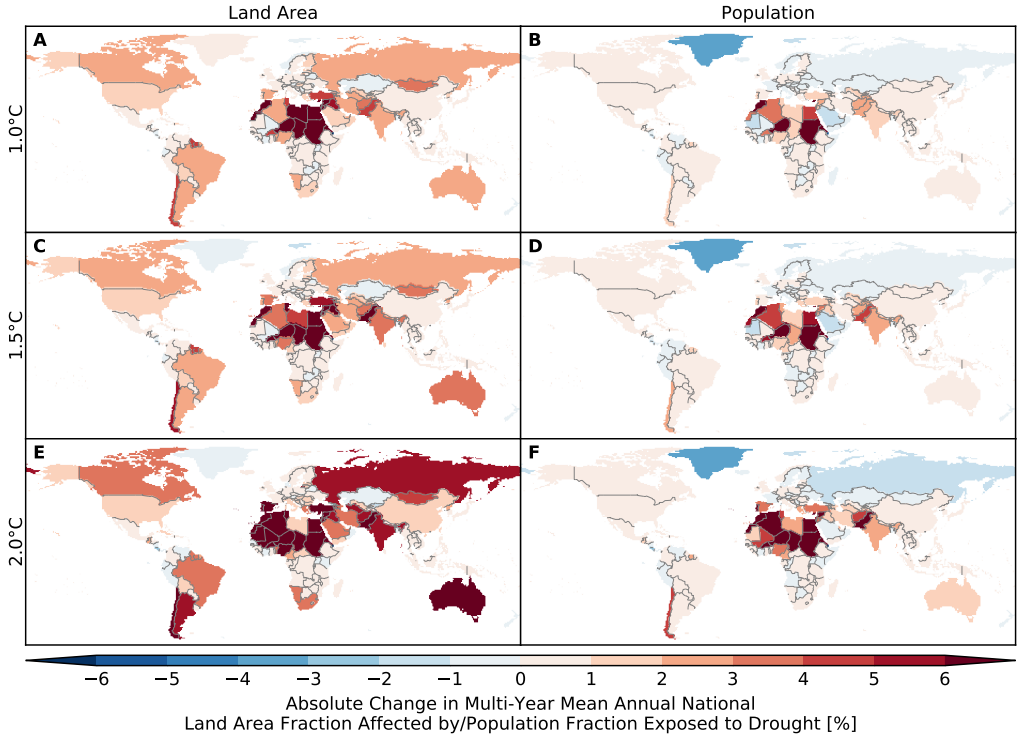

Figure S273: **Pure effect of climate change on annual national land area fraction affected by and population fraction exposed to drought (GFDL-ESM2M + CLM45).** Absolute changes in multi-year mean annual national (A, C, E) land area fraction affected by and (B, D, F) population fraction exposed to drought at (A, B) 1 °C, (C, D) 1.5 °C and (E, F) 2 °C global warming.

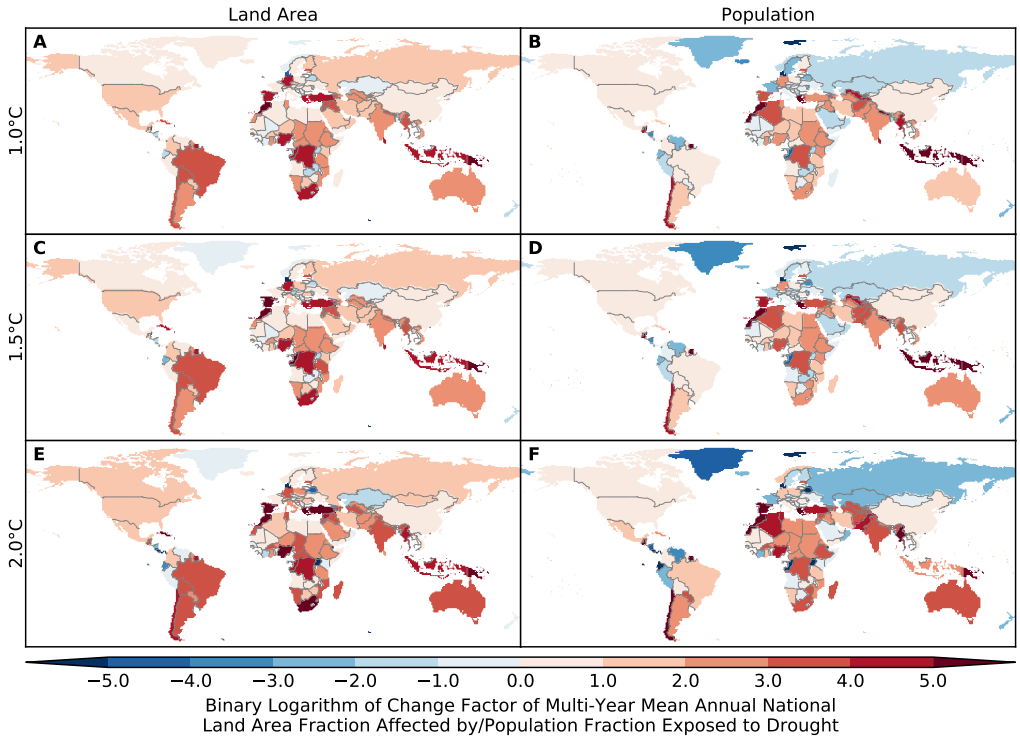

Figure S274: **Pure effect of climate change on annual national land area fraction affected by and population fraction exposed to drought (GFDL-ESM2M + CLM45).** Same as Figure S273 but for relative changes expressed in terms of binary logarithms of change factors, i.e. −1 means a change by a factor of 0.5, 0 means no change, and 1 means a change by a factor of 2. White indicates undefined relative changes due to division by zero.

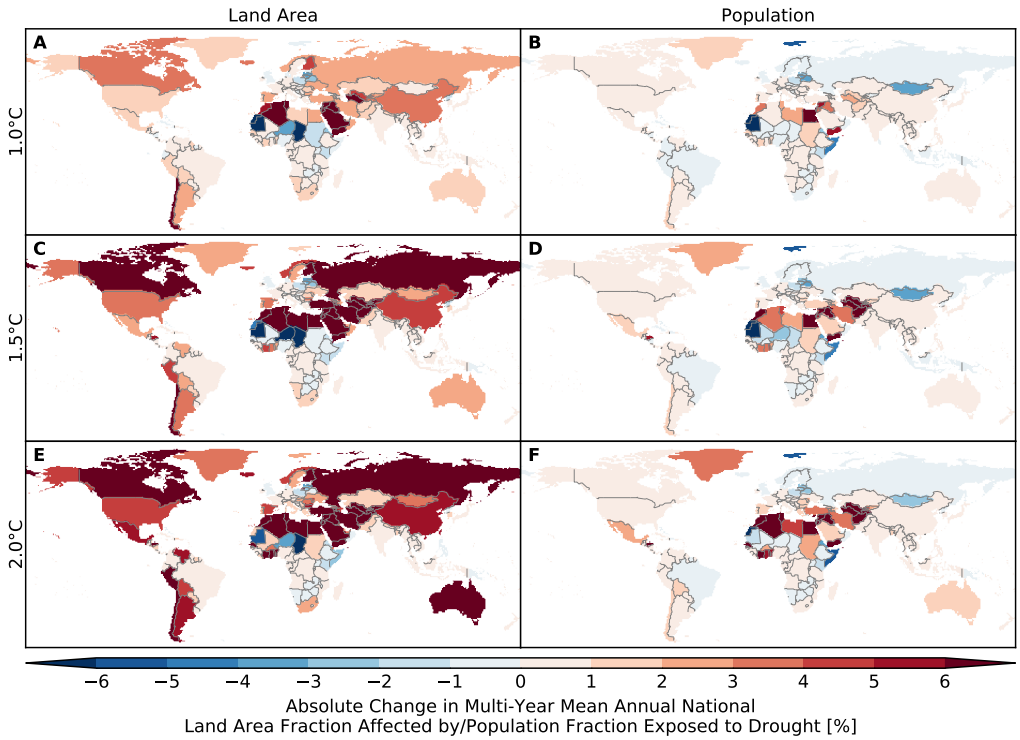

Figure S275: **Pure effect of climate change on annual national land area fraction affected by and population fraction exposed to drought (IPSL-CM5A-LR + CLM45).** Analogous to Figure S273.

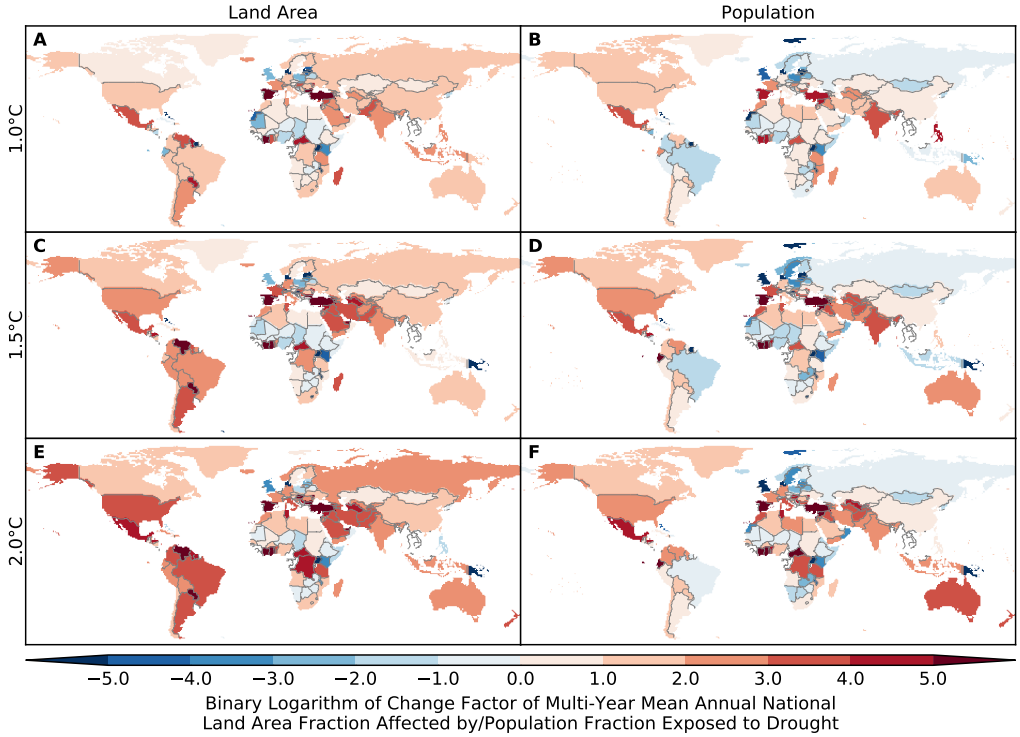

Figure S276: **Pure effect of climate change on annual national land area fraction affected by and population fraction exposed to drought (IPSL-CM5A-LR + CLM45).** Analogous to Figure S274.

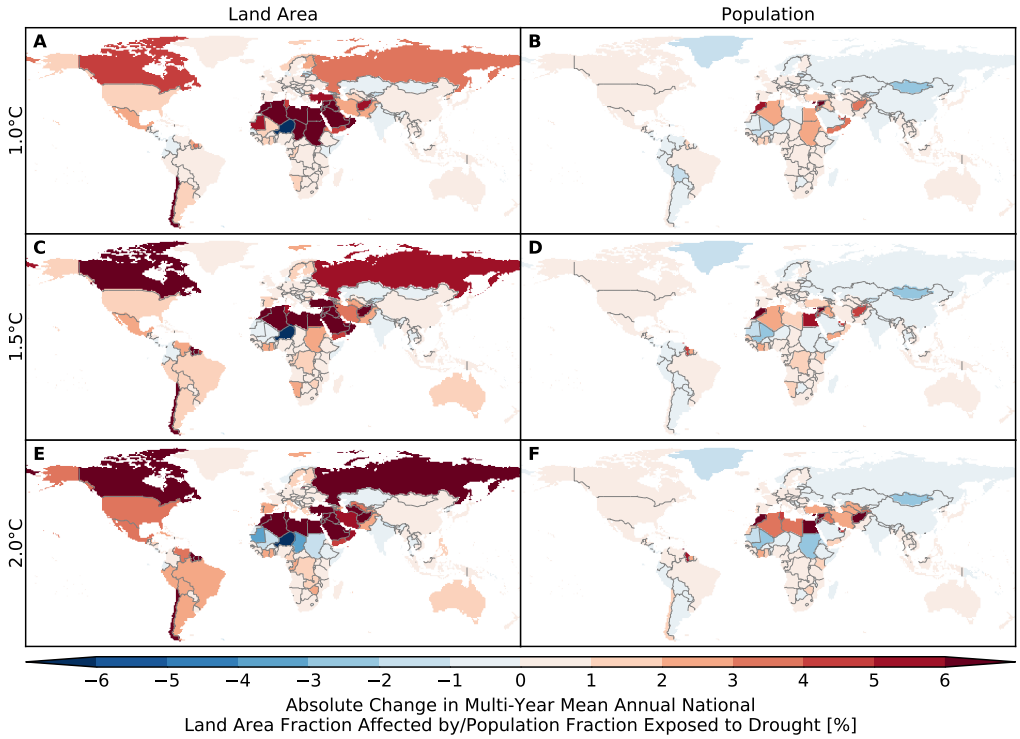

Figure S277: **Pure effect of climate change on annual national land area fraction affected by and population fraction exposed to drought (MIROC5 + CLM45).** Analogous to Figure S273.

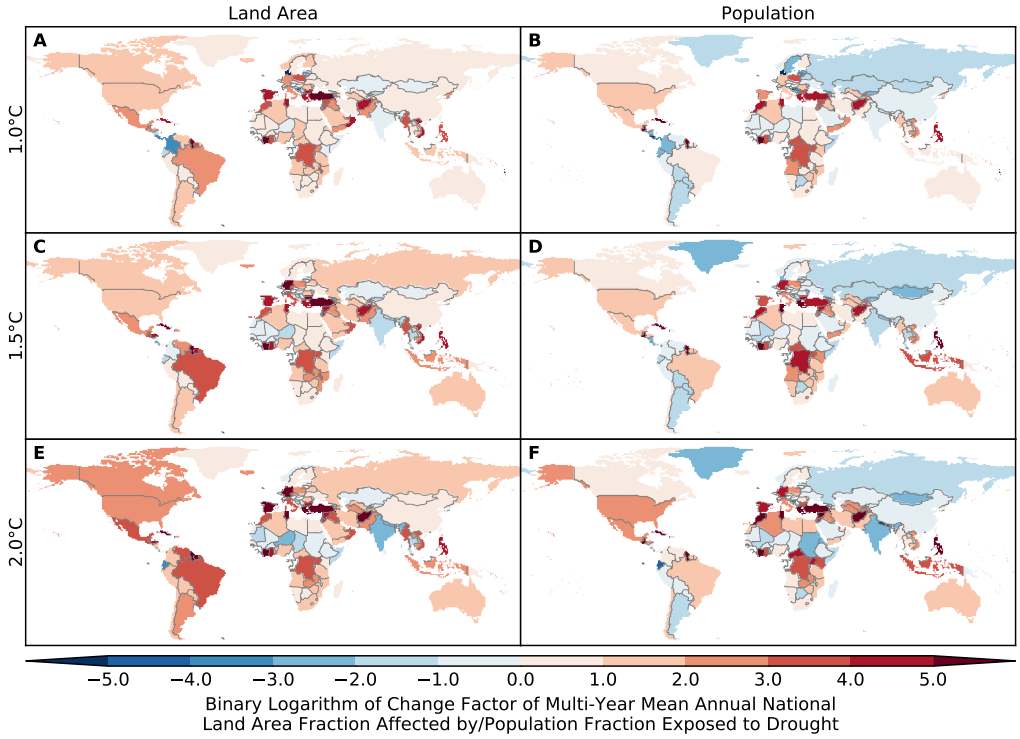

Figure S278: **Pure effect of climate change on annual national land area fraction affected by and population fraction exposed to drought (MIROC5 + CLM45).** Analogous to Figure S274.

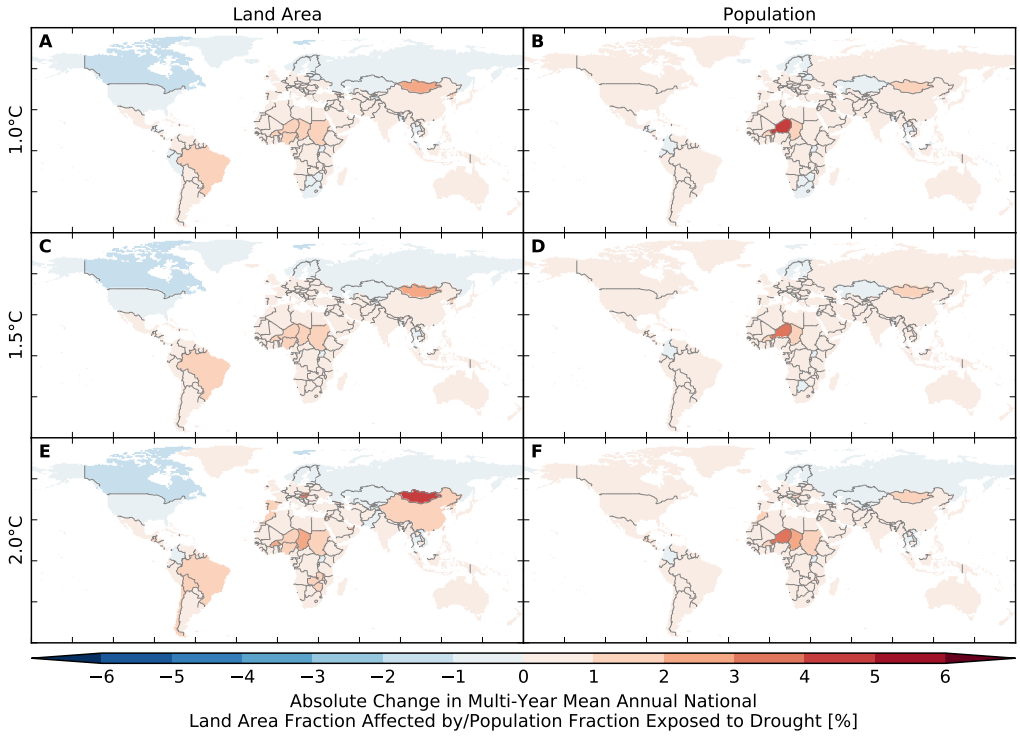

Figure S279: **Pure effect of climate change on annual national land area fraction affected by and population fraction exposed to drought (GFDL-ESM2M + H08).** Analogous to Figure S273.

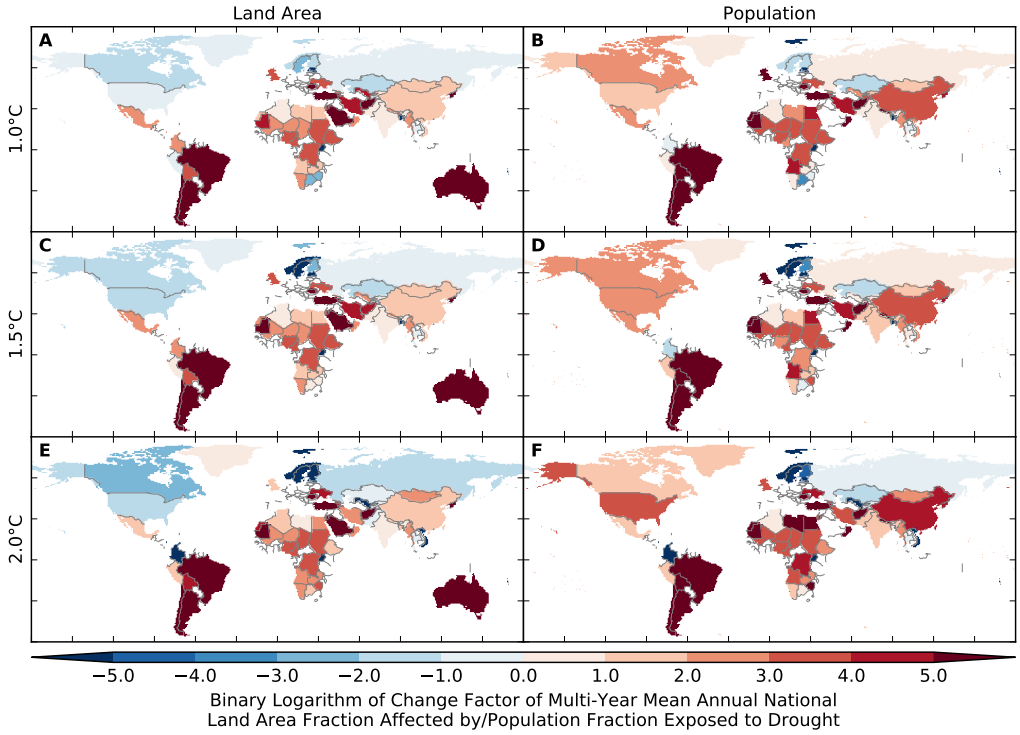

Figure S280: **Pure effect of climate change on annual national land area fraction affected by and population fraction exposed to drought (GFDL-ESM2M + H08).** Analogous to Figure S274.

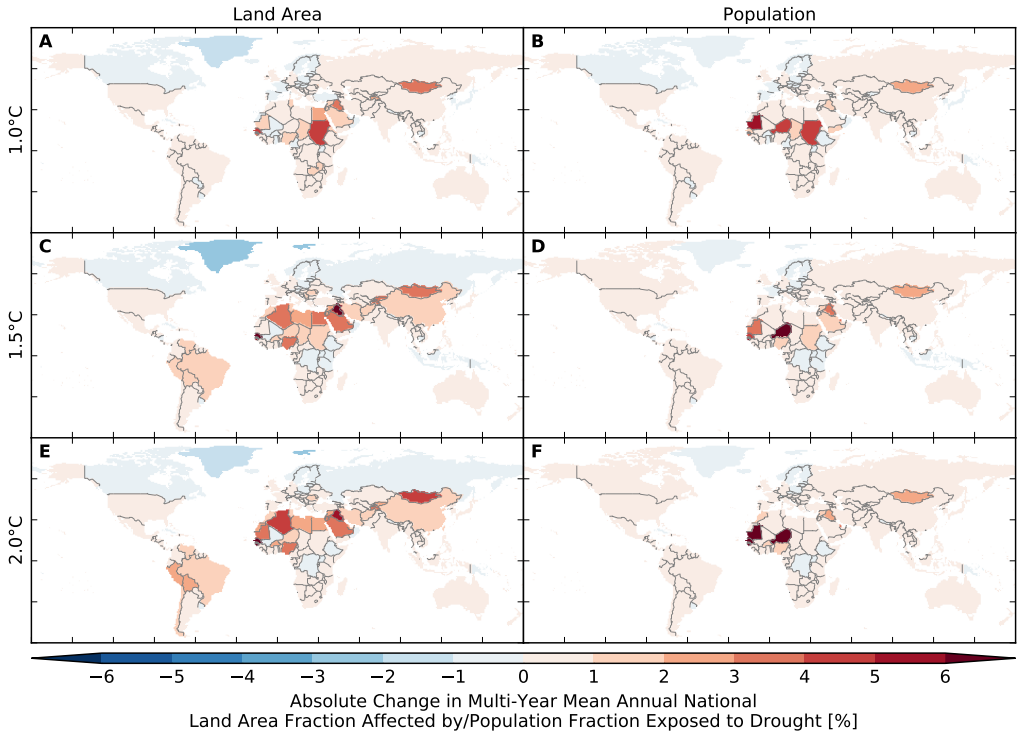

Figure S281: **Pure effect of climate change on annual national land area fraction affected by and population fraction exposed to drought (IPSL-CM5A-LR + H08).** Analogous to Figure S273.

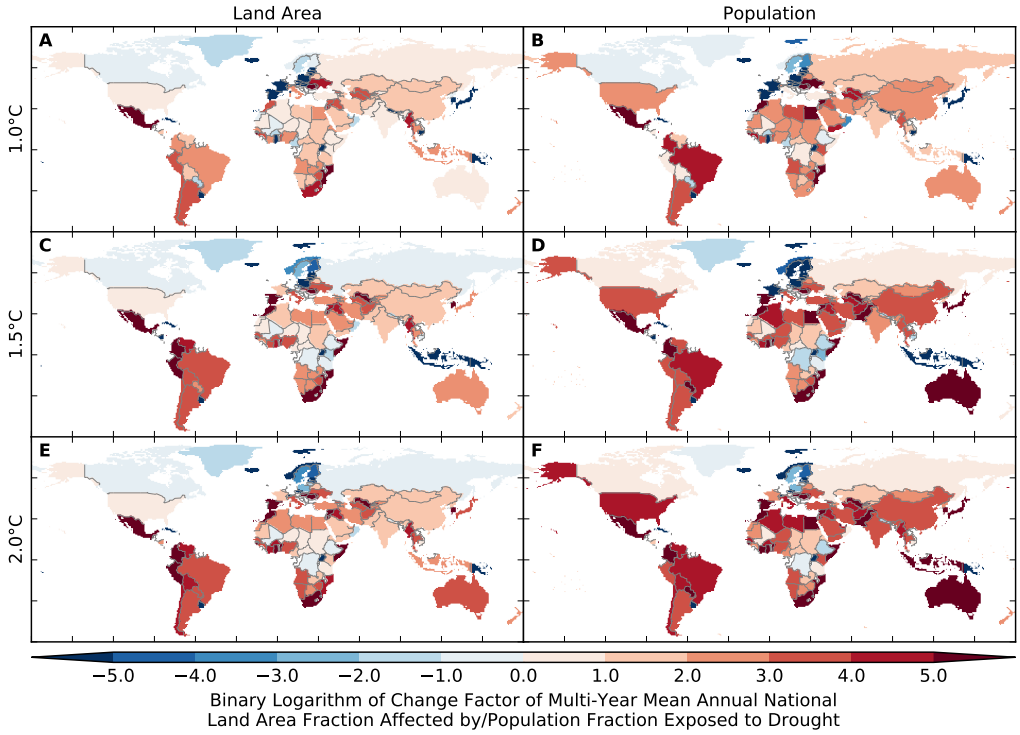

Figure S282: **Pure effect of climate change on annual national land area fraction affected by and population fraction exposed to drought (IPSL-CM5A-LR + H08).** Analogous to Figure S274.

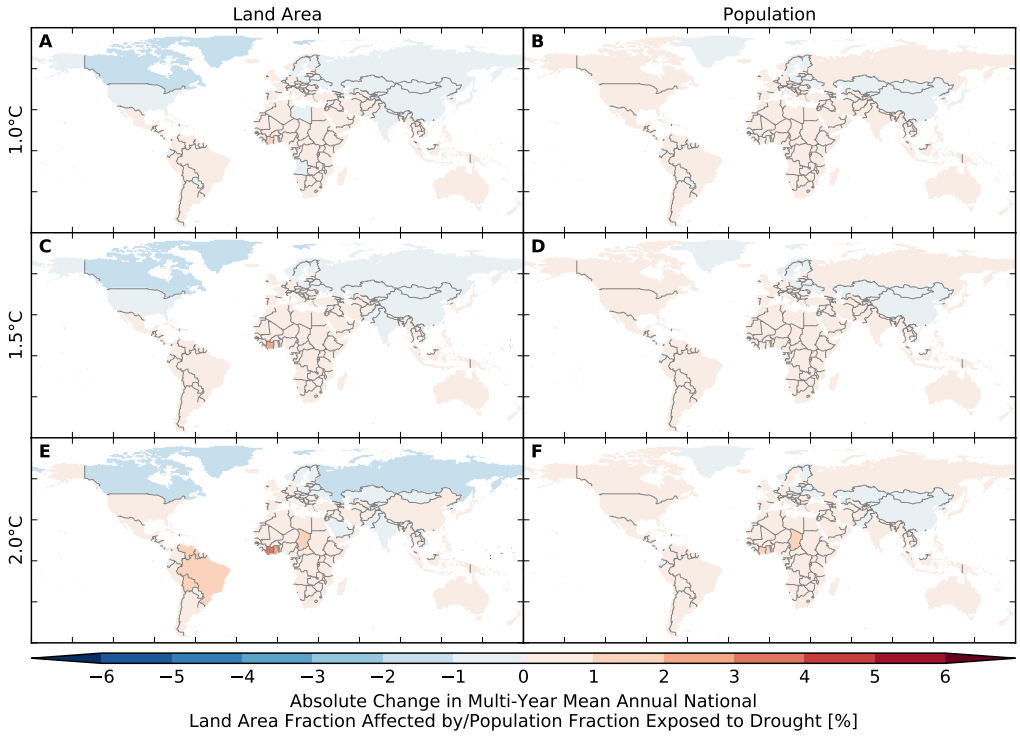

Figure S283: **Pure effect of climate change on annual national land area fraction affected by and population fraction exposed to drought (MIROC5 + H08).** Analogous to Figure S273.

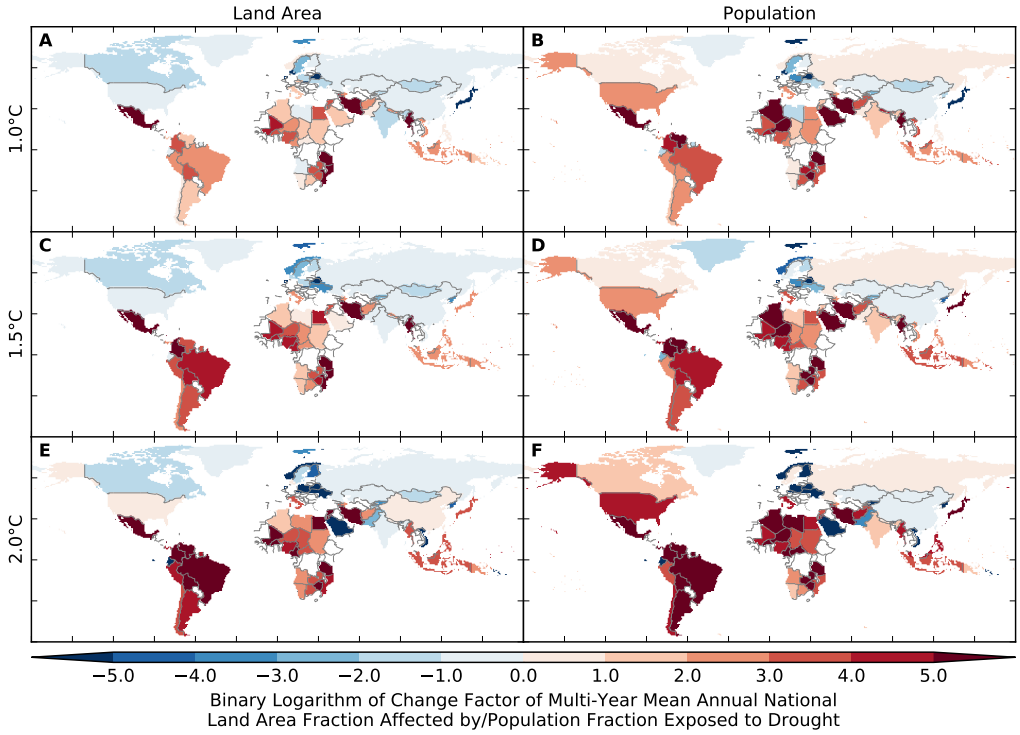

Figure S284: **Pure effect of climate change on annual national land area fraction affected by and population fraction exposed to drought (MIROC5 + H08).** Analogous to Figure S274.

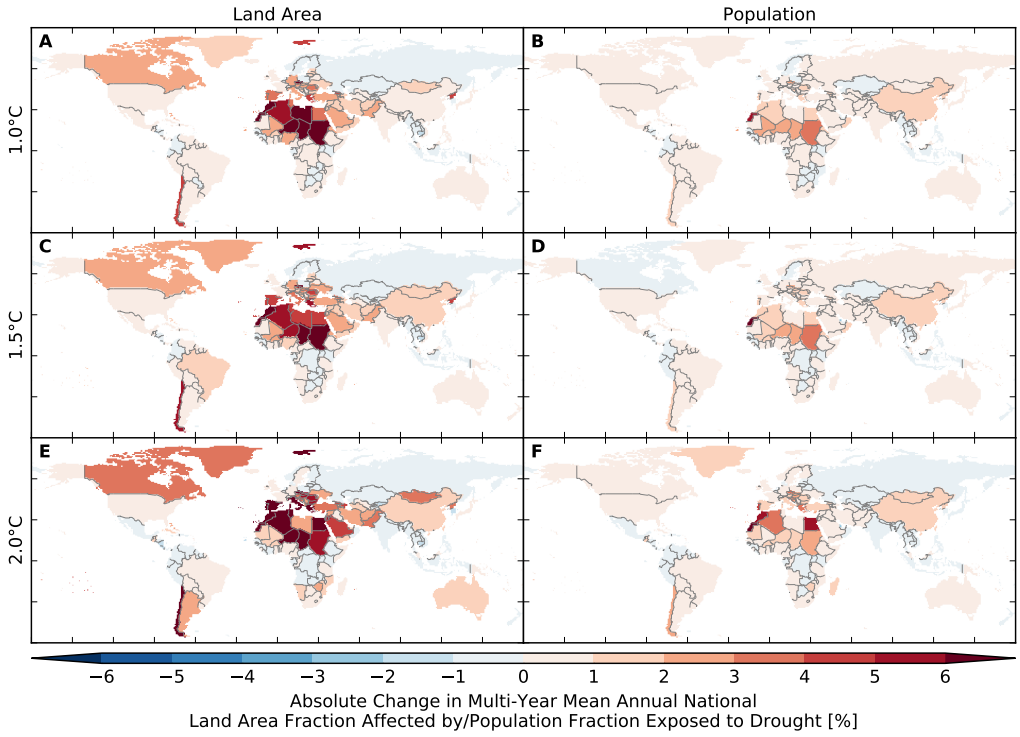

Figure S285: **Pure effect of climate change on annual national land area fraction affected by and population fraction exposed to drought (GFDL-ESM2M + JULES-W1).** Analogous to Figure S273.

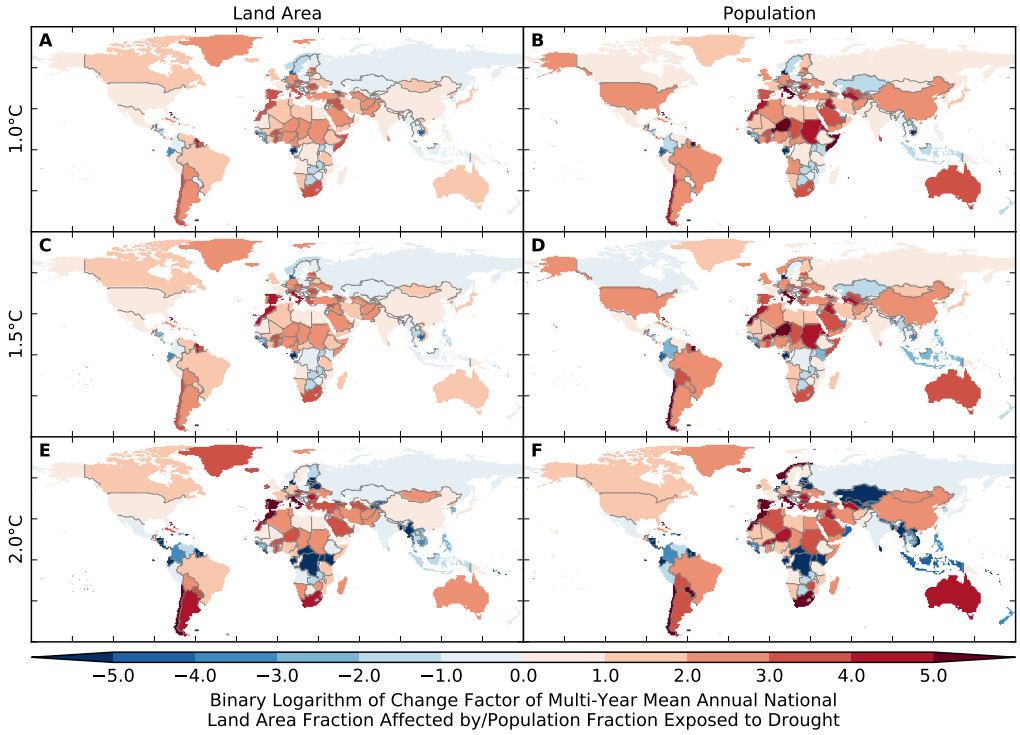

Figure S286: **Pure effect of climate change on annual national land area fraction affected by and population fraction exposed to drought (GFDL-ESM2M + JULES-W1).** Analogous to Figure S274.

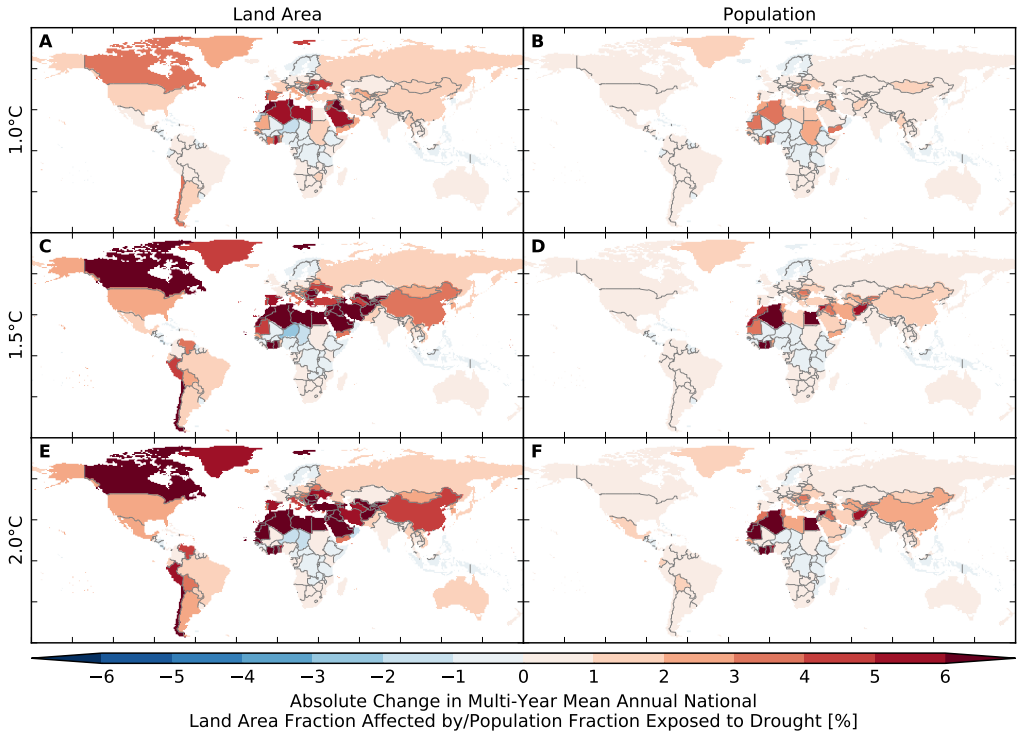

Figure S287: **Pure effect of climate change on annual national land area fraction affected by and population fraction exposed to drought (IPSL-CM5A-LR + JULES-W1).** Analogous to Figure S273.

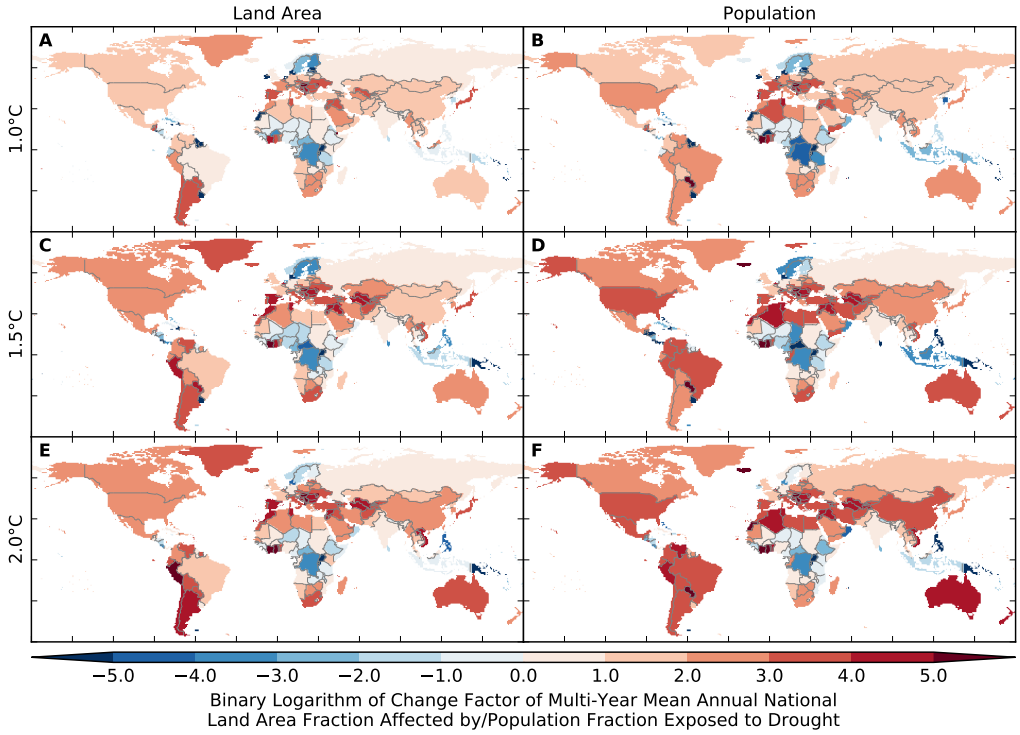

Figure S288: **Pure effect of climate change on annual national land area fraction affected by and population fraction exposed to drought (IPSL-CM5A-LR + JULES-W1).** Analogous to Figure S274.

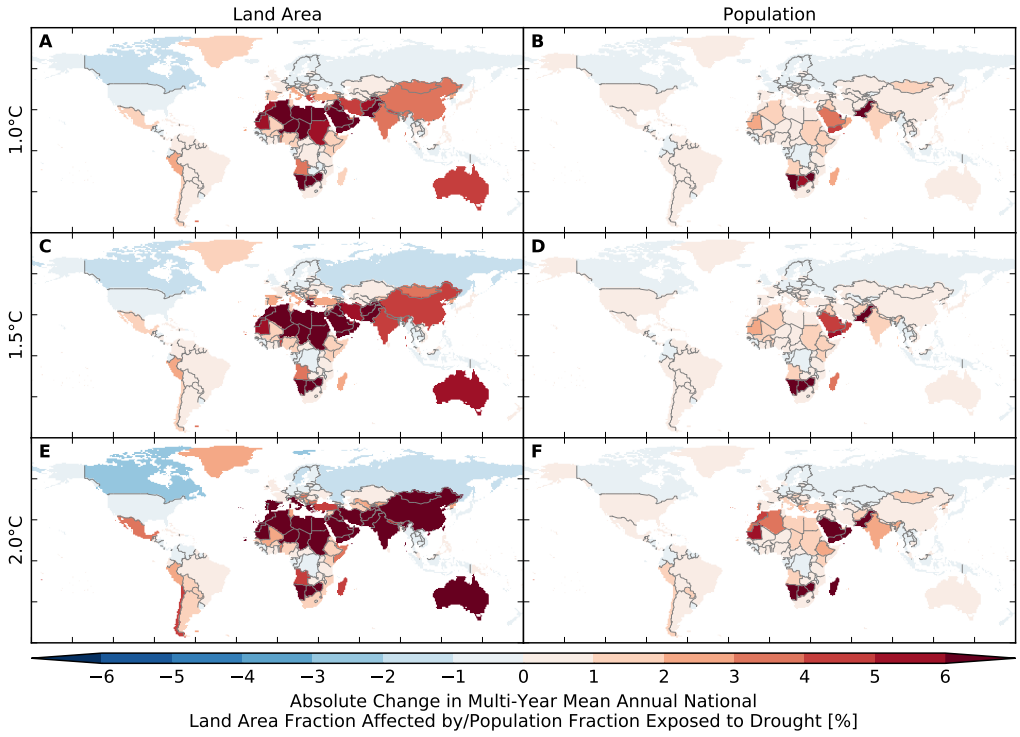

Figure S289: **Pure effect of climate change on annual national land area fraction affected by and population fraction exposed to drought (GFDL-ESM2M + LPJmL).** Analogous to Figure S273.

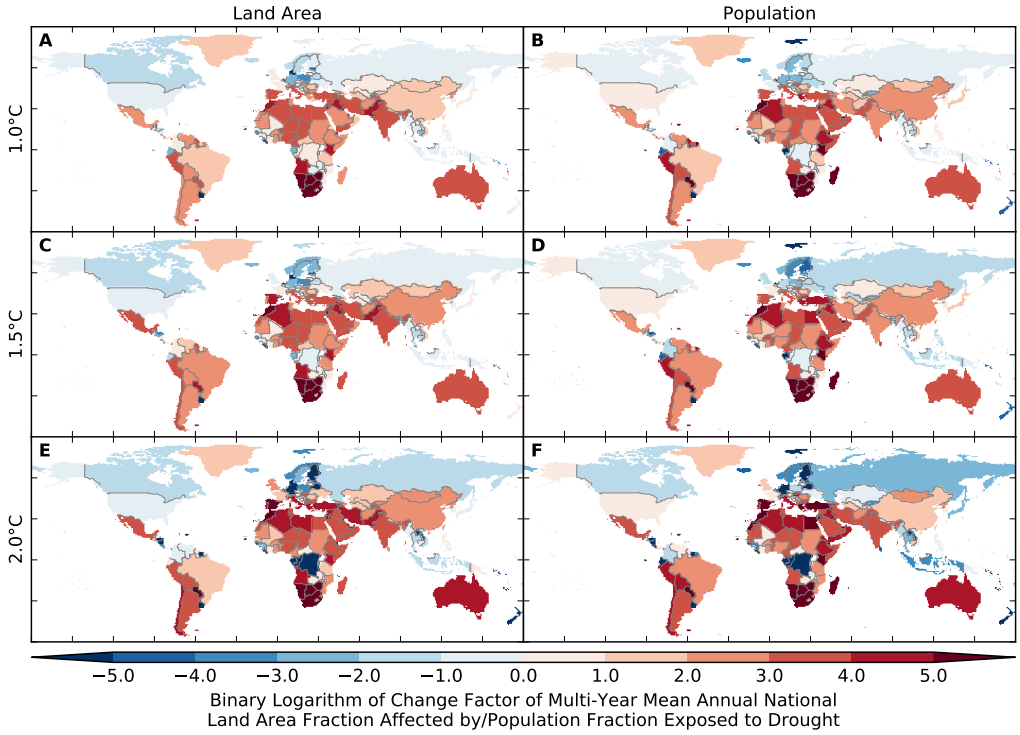

Figure S290: **Pure effect of climate change on annual national land area fraction affected by and population fraction exposed to drought (GFDL-ESM2M + LPJmL).** Analogous to Figure S274.

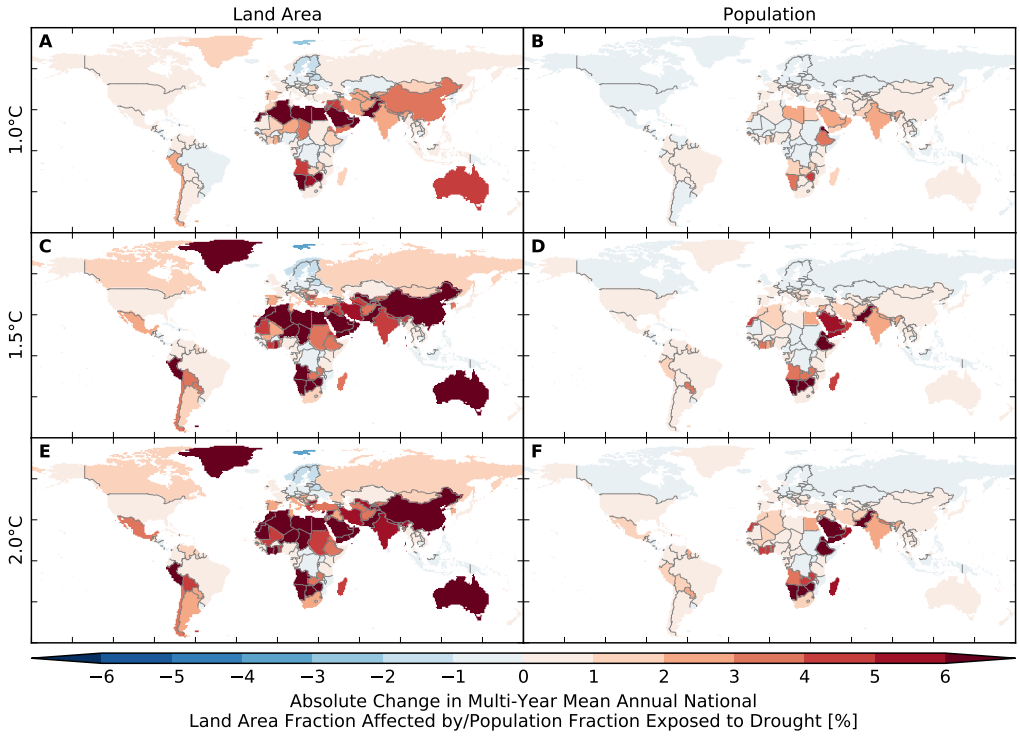

Figure S291: **Pure effect of climate change on annual national land area fraction affected by and population fraction exposed to drought (IPSL-CM5A-LR + LPJmL).** Analogous to Figure S273.

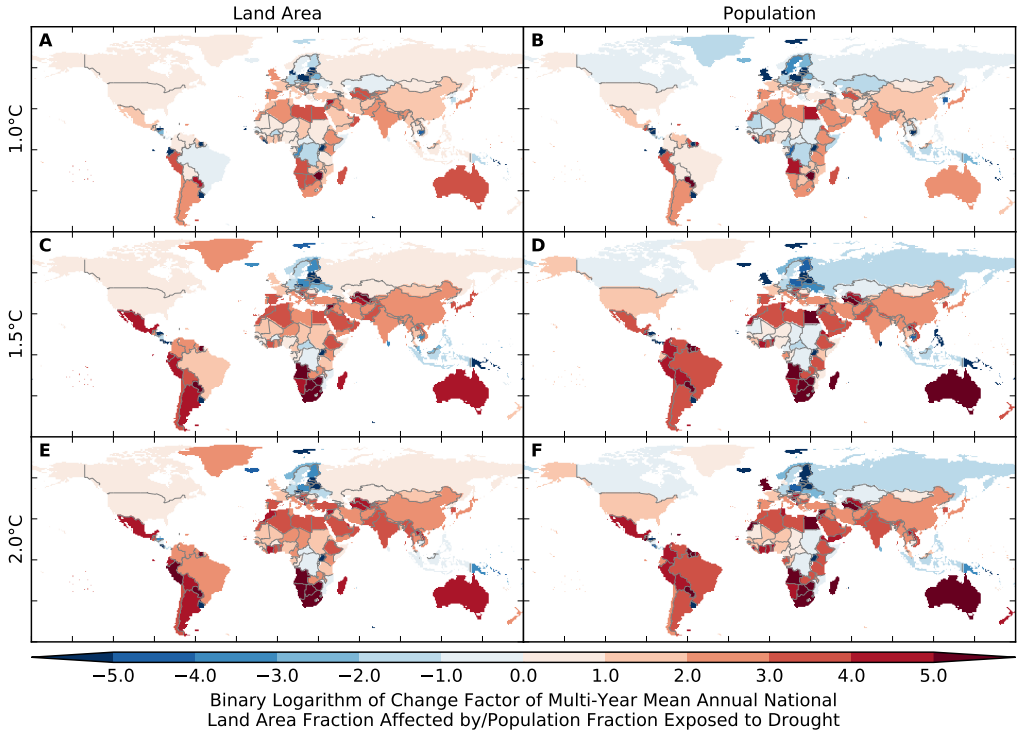

Figure S292: **Pure effect of climate change on annual national land area fraction affected by and population fraction exposed to drought (IPSL-CM5A-LR + LPJmL).** Analogous to Figure S274.

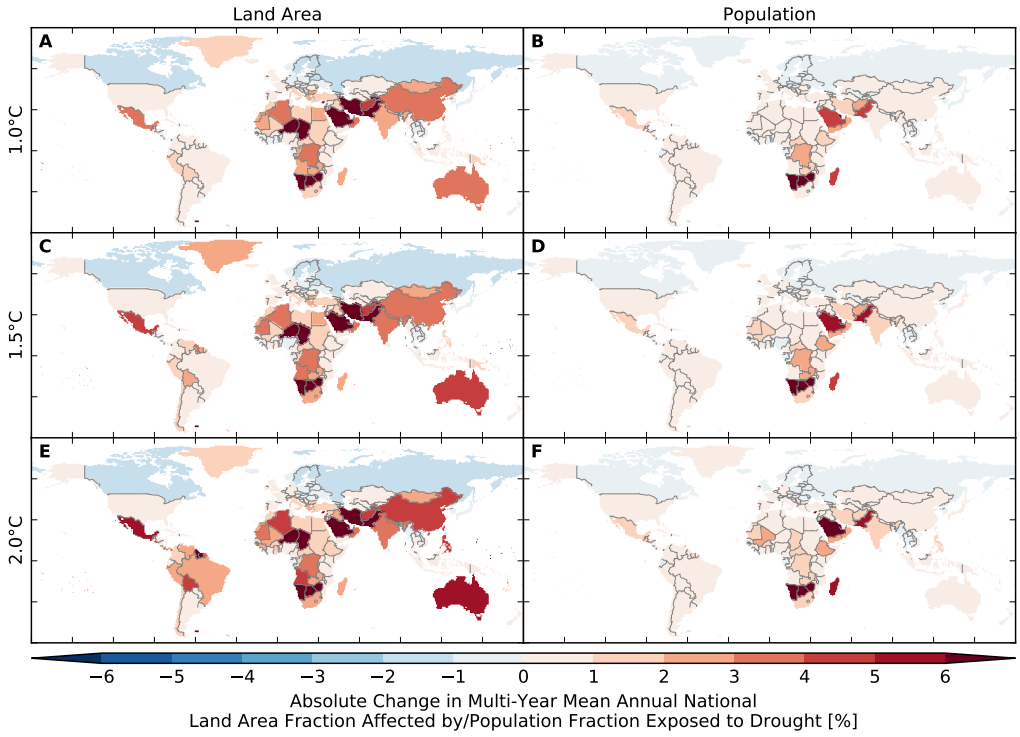

Figure S293: **Pure effect of climate change on annual national land area fraction affected by and population fraction exposed to drought (MIROC5 + LPJmL).** Analogous to Figure S273.

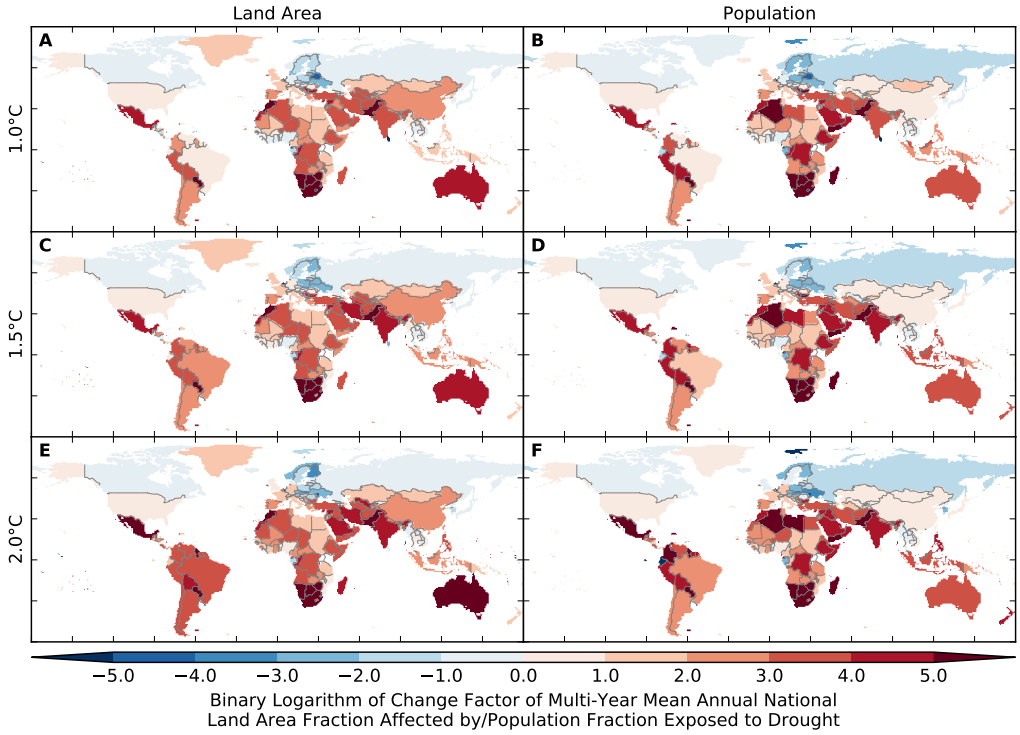

Figure S294: **Pure effect of climate change on annual national land area fraction affected by and population fraction exposed to drought (MIROC5 + LPJmL).** Analogous to Figure S274.

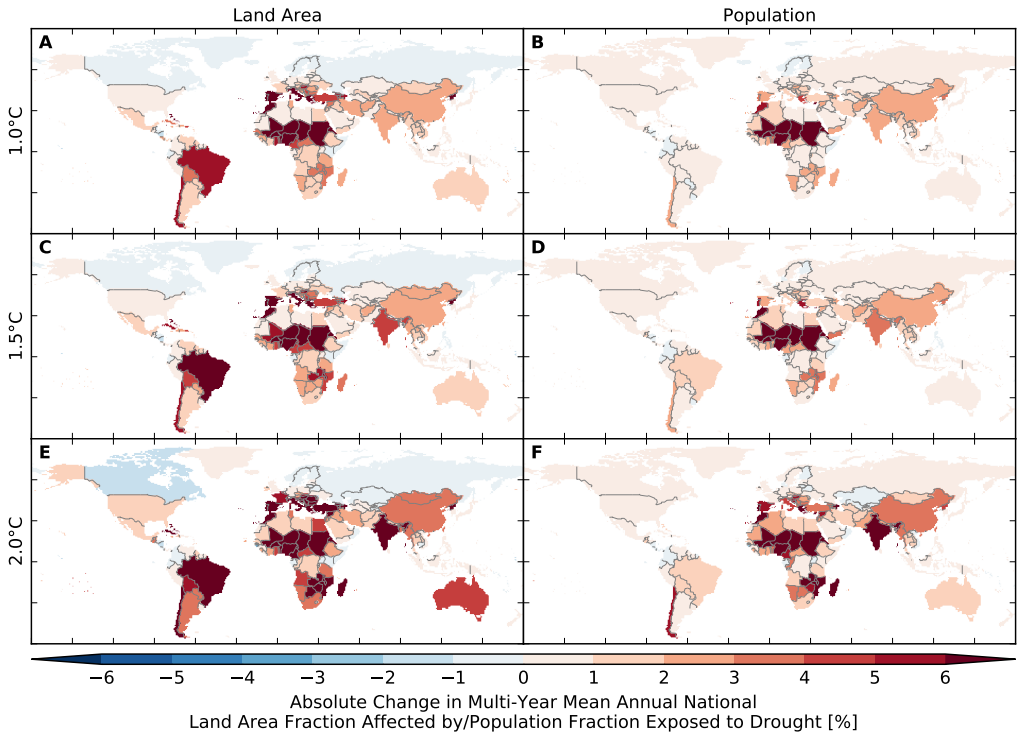

Figure S295: **Pure effect of climate change on annual national land area fraction affected by and population fraction exposed to drought (GFDL-ESM2M + MPI-HM).** Analogous to Figure S273.

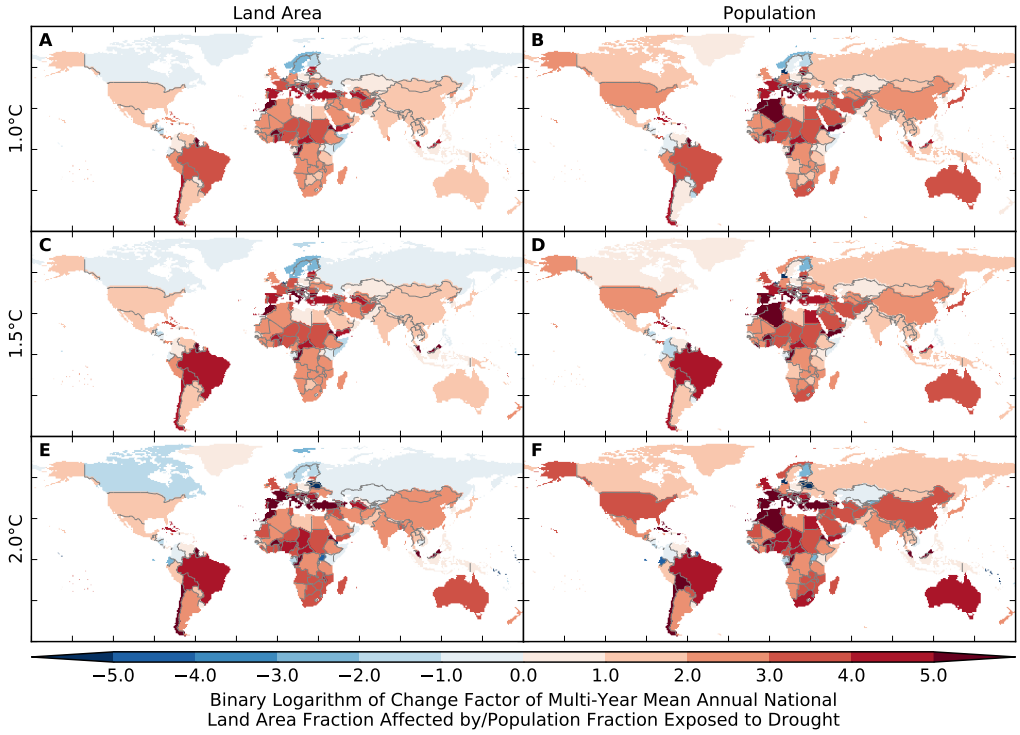

Figure S296: **Pure effect of climate change on annual national land area fraction affected by and population fraction exposed to drought (GFDL-ESM2M + MPI-HM).** Analogous to Figure S274.

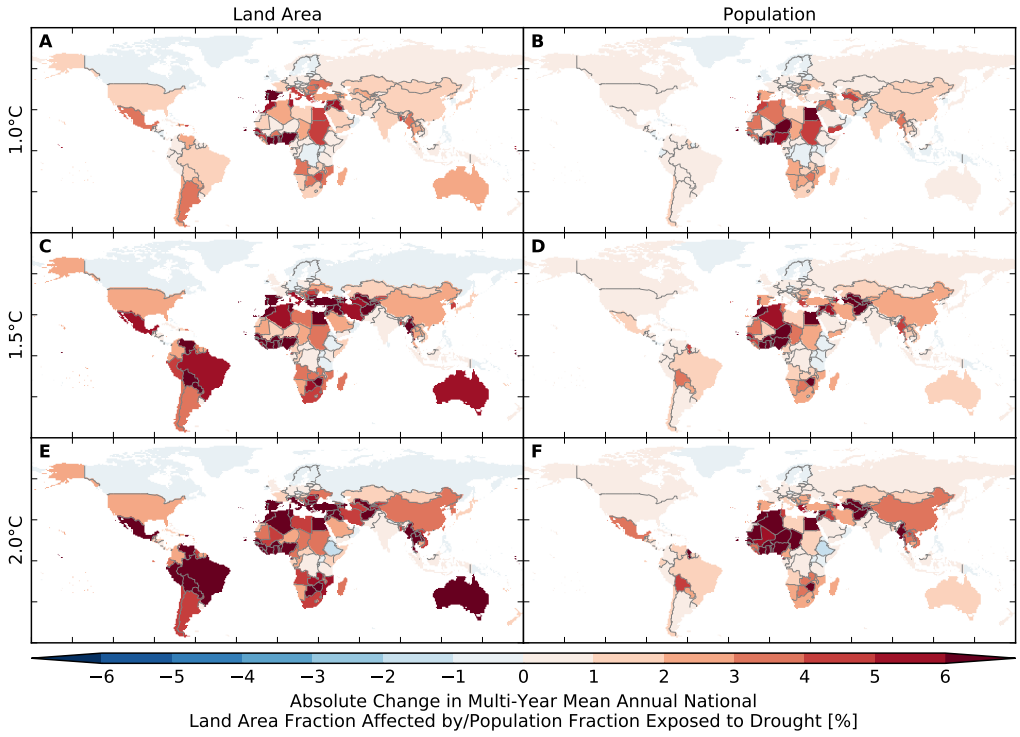

Figure S297: **Pure effect of climate change on annual national land area fraction affected by and population fraction exposed to drought (IPSL-CM5A-LR + MPI-HM).** Analogous to Figure S273.

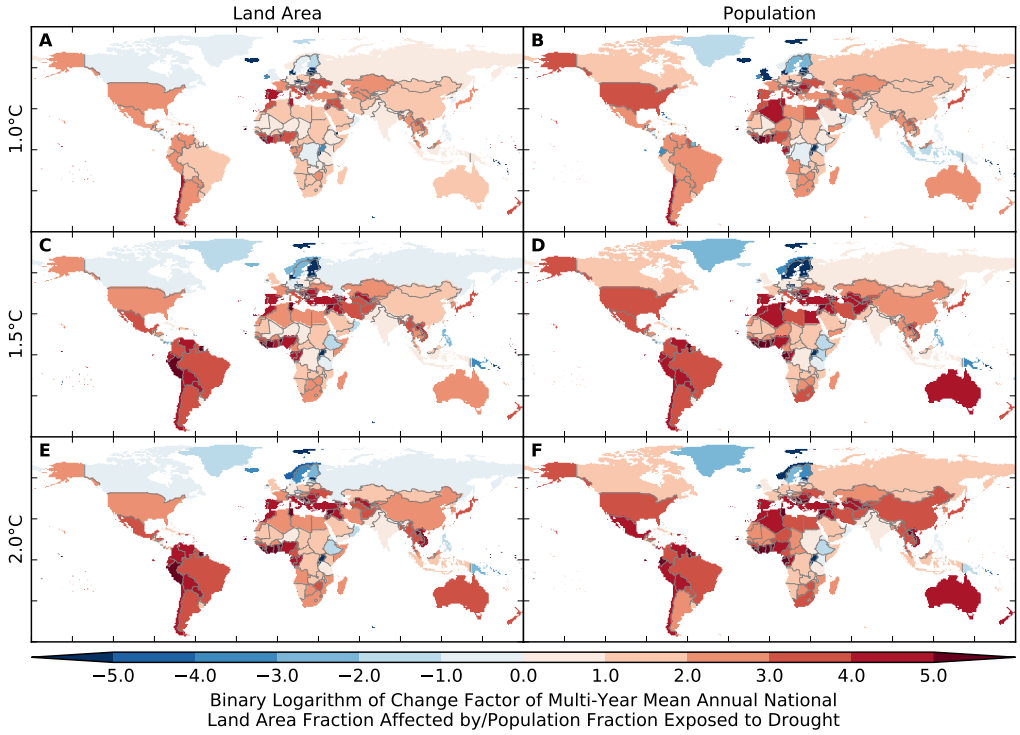

Figure S298: **Pure effect of climate change on annual national land area fraction affected by and population fraction exposed to drought (IPSL-CM5A-LR + MPI-HM).** Analogous to Figure S274.

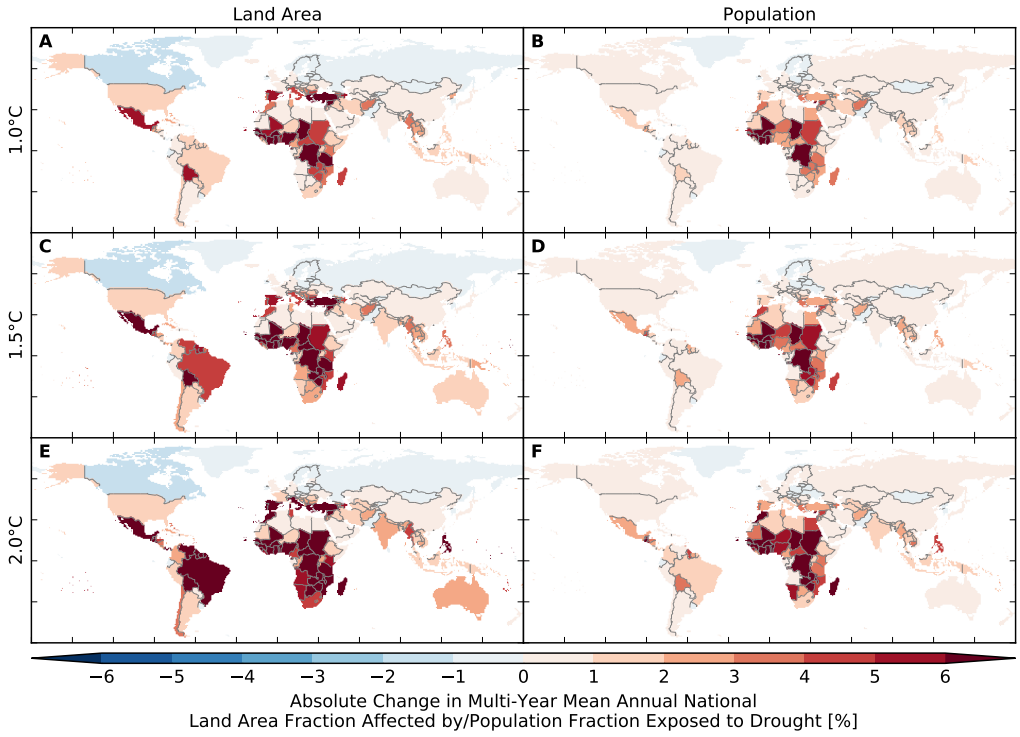

Figure S299: **Pure effect of climate change on annual national land area fraction affected by and population fraction exposed to drought (MIROC5 + MPI-HM).** Analogous to Figure S273.

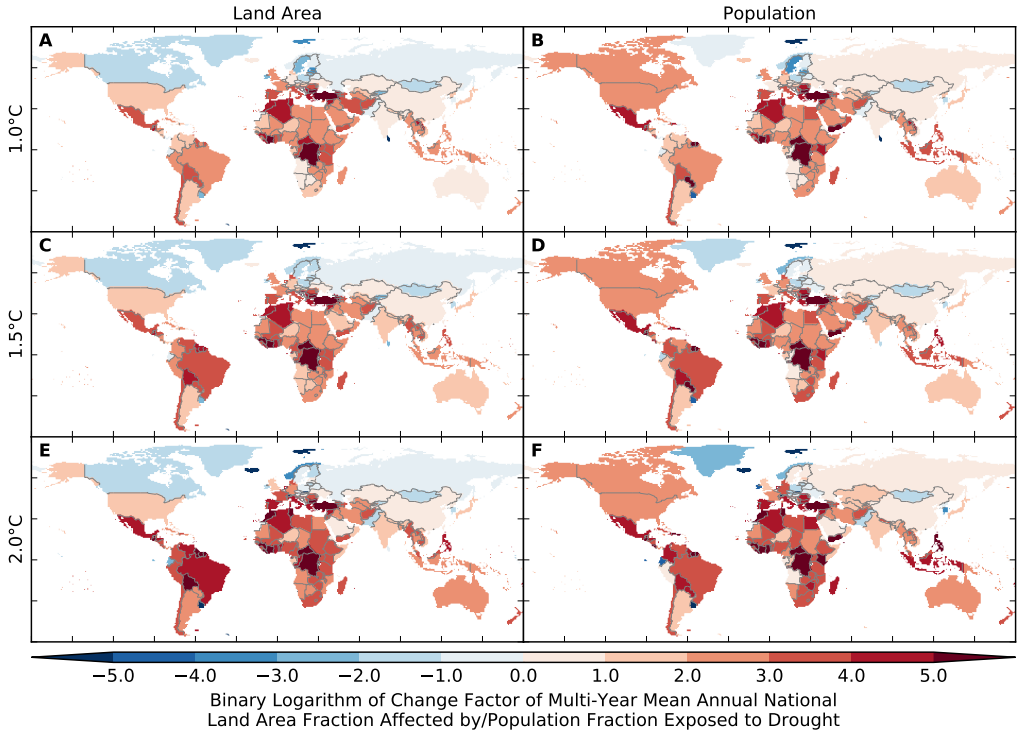

Figure S300: **Pure effect of climate change on annual national land area fraction affected by and population fraction exposed to drought (MIROC5 + MPI-HM).** Analogous to Figure S274.

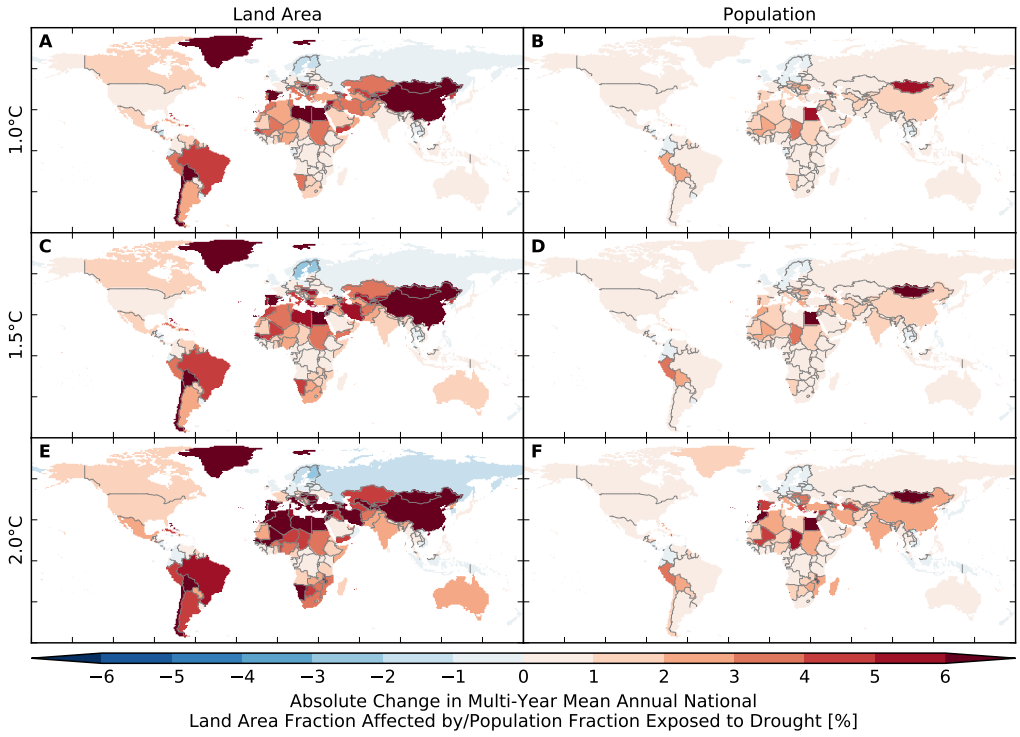

Figure S301: **Pure effect of climate change on annual national land area fraction affected by and population fraction exposed to drought (GFDL-ESM2M + ORCHIDEE).** Analogous to Figure S273.

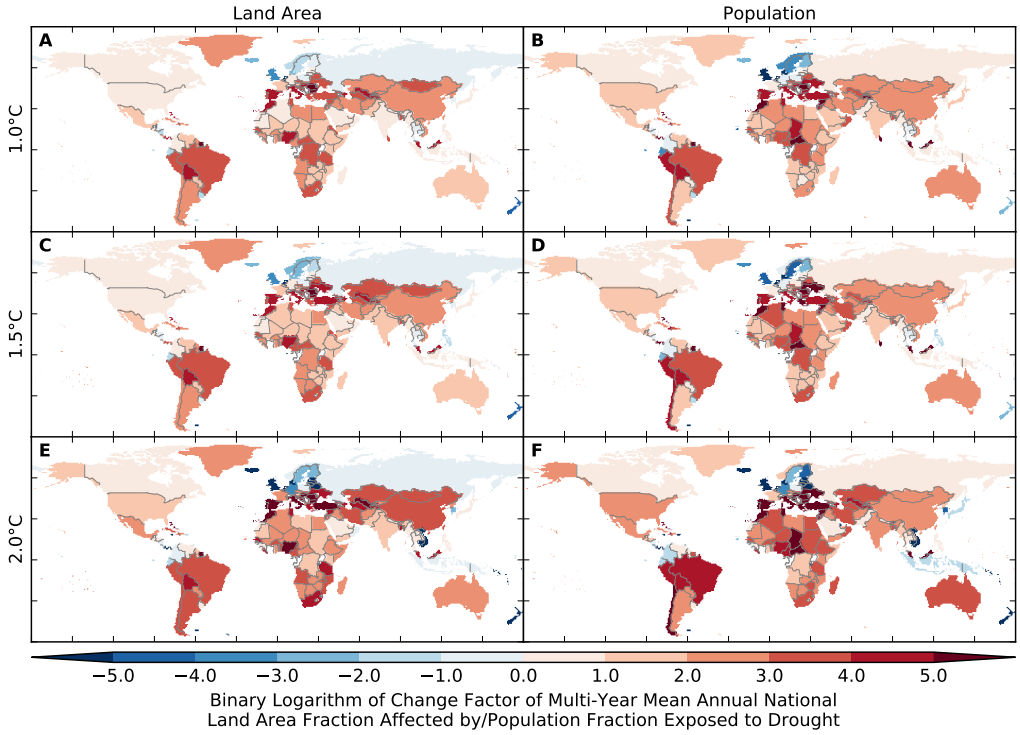

Figure S302: **Pure effect of climate change on annual national land area fraction affected by and population fraction exposed to drought (GFDL-ESM2M + ORCHIDEE).** Analogous to Figure S274.

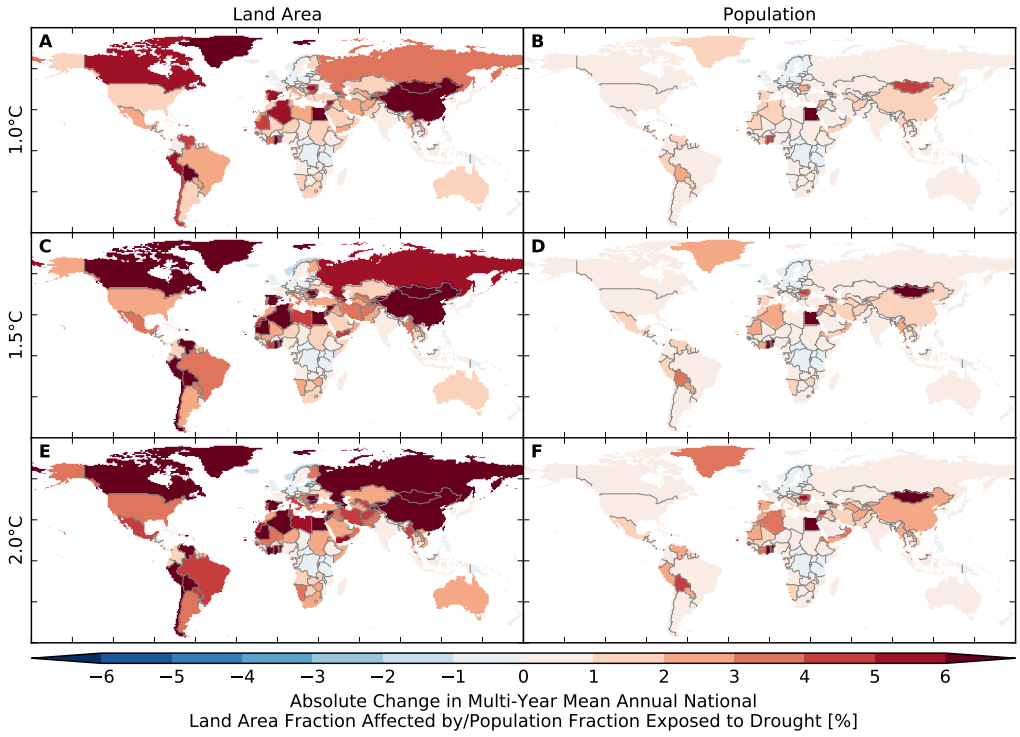

Figure S303: **Pure effect of climate change on annual national land area fraction affected by and population fraction exposed to drought (IPSL-CM5A-LR + ORCHIDEE).** Analogous to Figure S273.

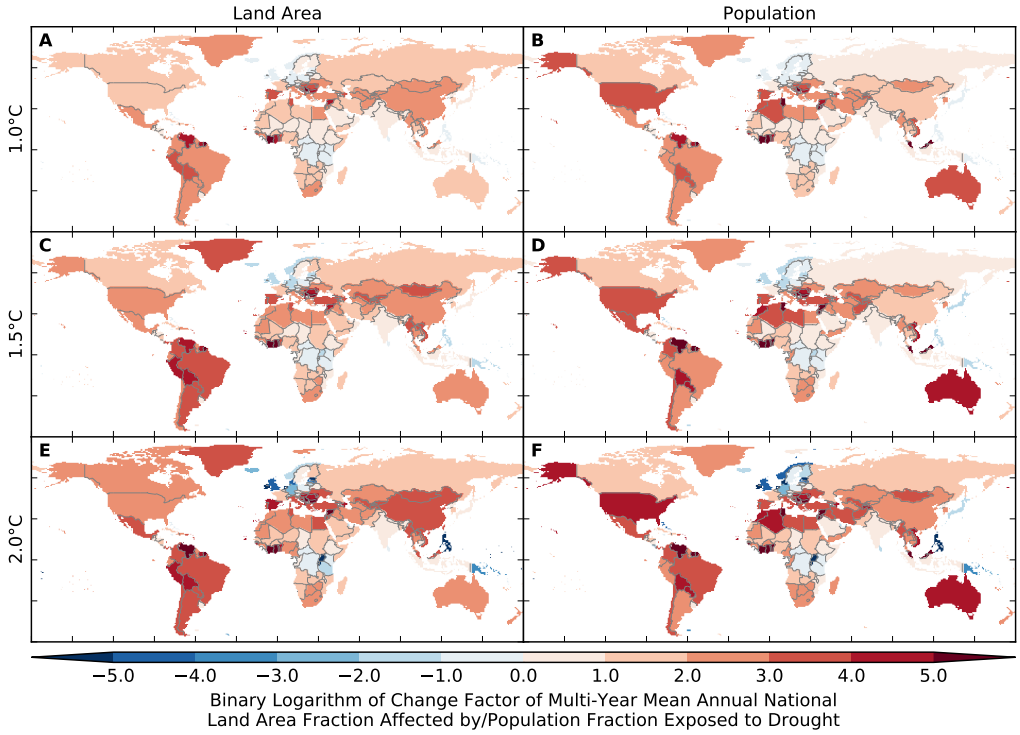

Figure S304: **Pure effect of climate change on annual national land area fraction affected by and population fraction exposed to drought (IPSL-CM5A-LR + ORCHIDEE).** Analogous to Figure S274.

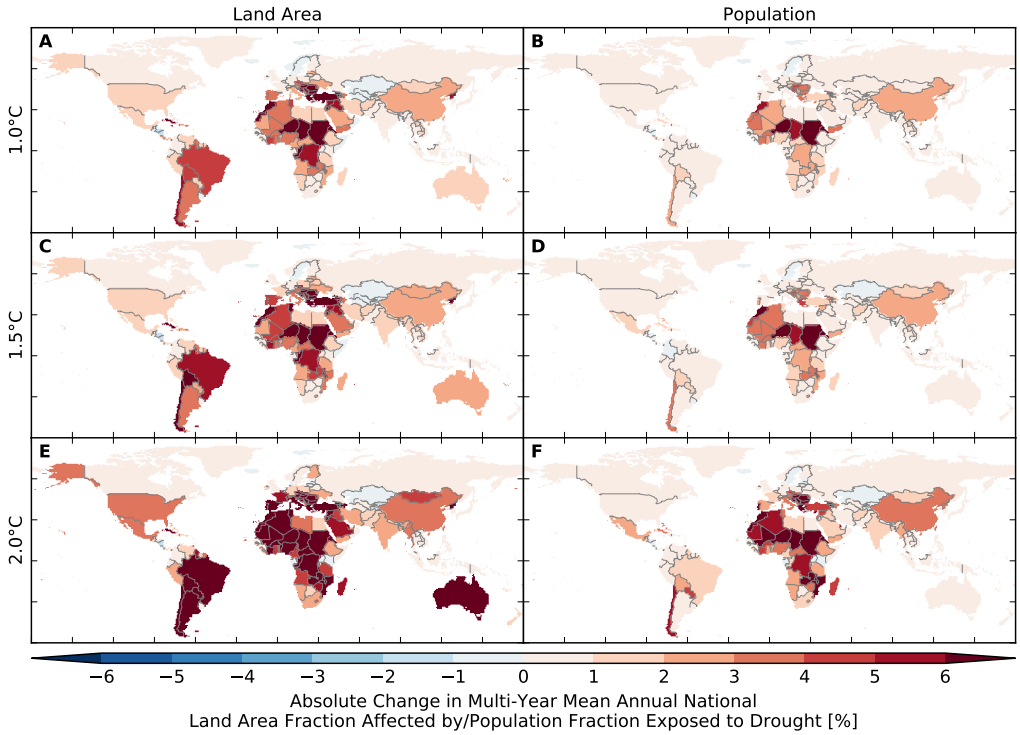

Figure S305: **Pure effect of climate change on annual national land area fraction affected by and population fraction exposed to drought (GFDL-ESM2M + PCR-GLOBWB).** Analogous to Figure S273.

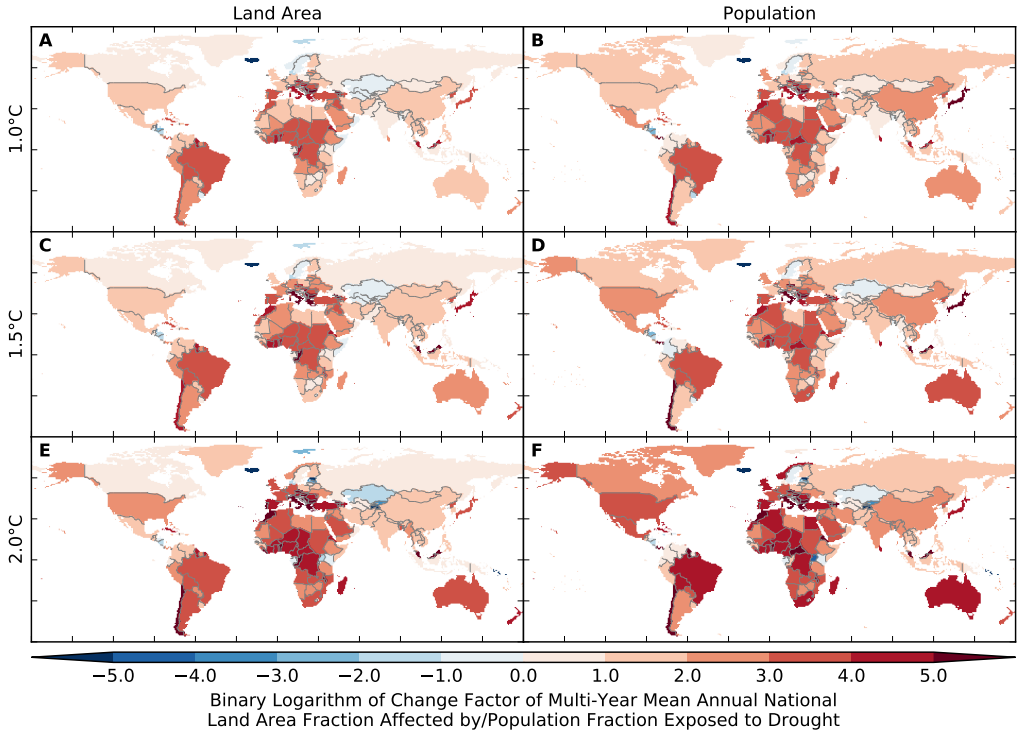

Figure S306: **Pure effect of climate change on annual national land area fraction affected by and population fraction exposed to drought (GFDL-ESM2M + PCR-GLOBWB).** Analogous to Figure S274.

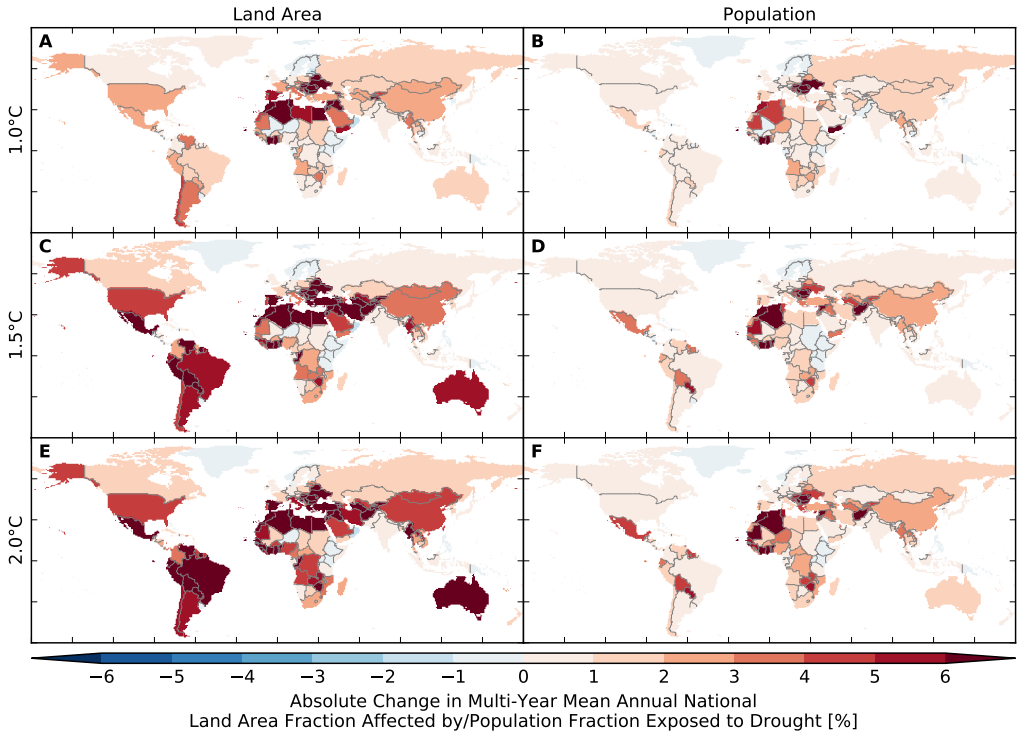

Figure S307: **Pure effect of climate change on annual national land area fraction affected by and population fraction exposed to drought (IPSL-CM5A-LR + PCR-GLOBWB).** Analogous to Figure S273.

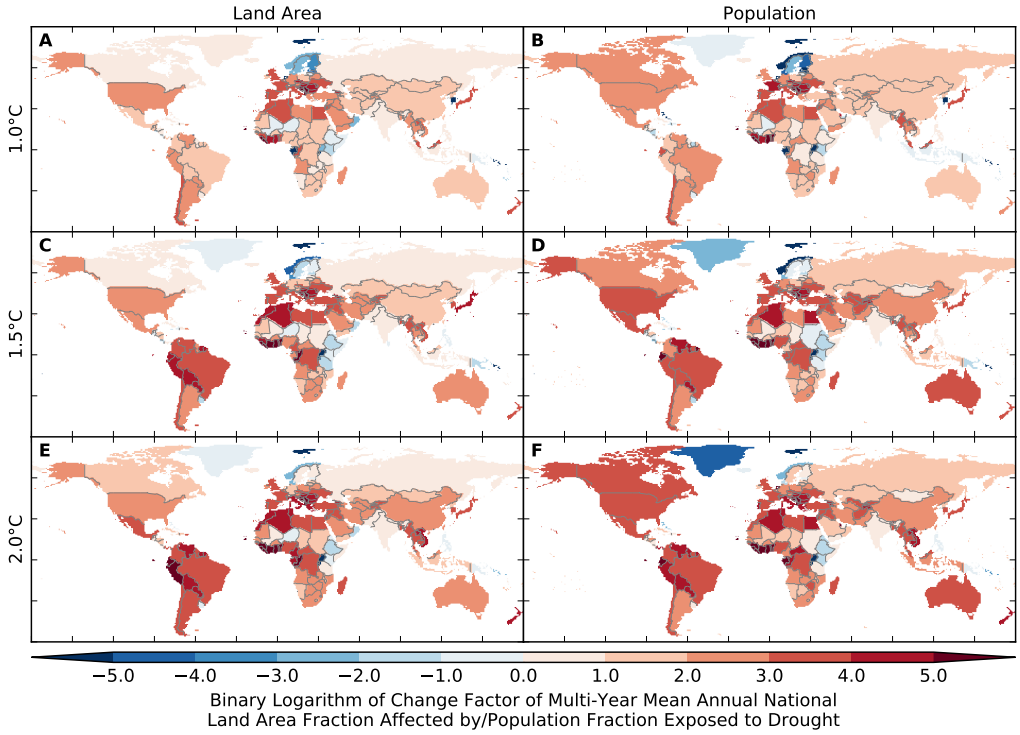

Figure S308: **Pure effect of climate change on annual national land area fraction affected by and population fraction exposed to drought (IPSL-CM5A-LR + PCR-GLOBWB).** Analogous to Figure S274.

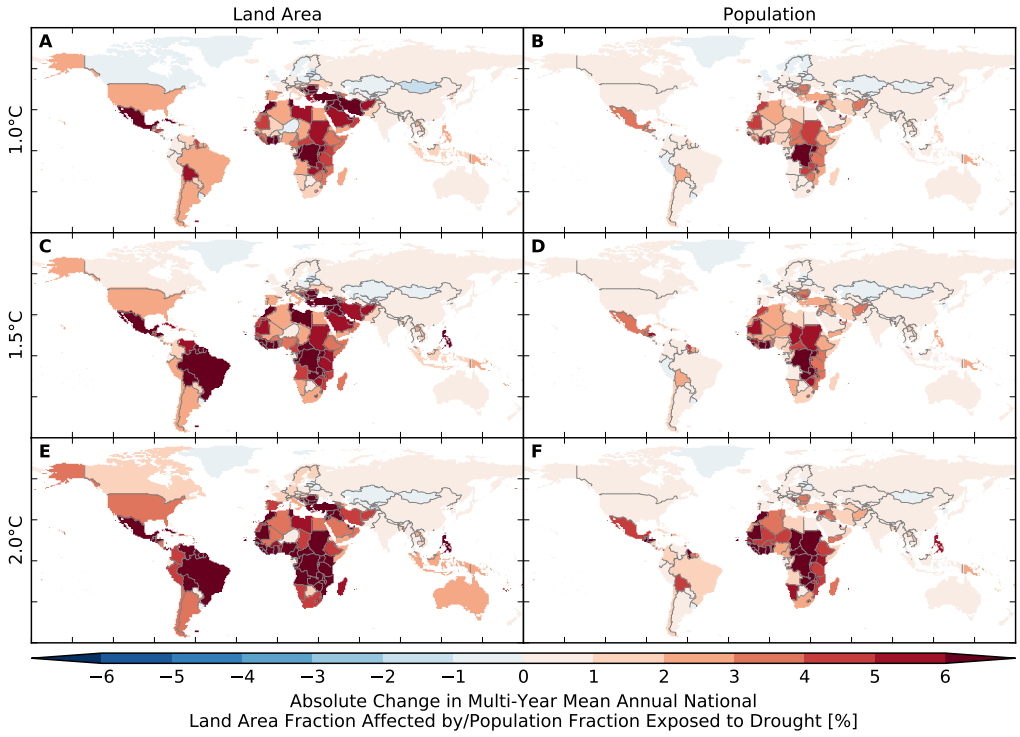

Figure S309: **Pure effect of climate change on annual national land area fraction affected by and population fraction exposed to drought (MIROC5 + PCR-GLOBWB).** Analogous to Figure S273.

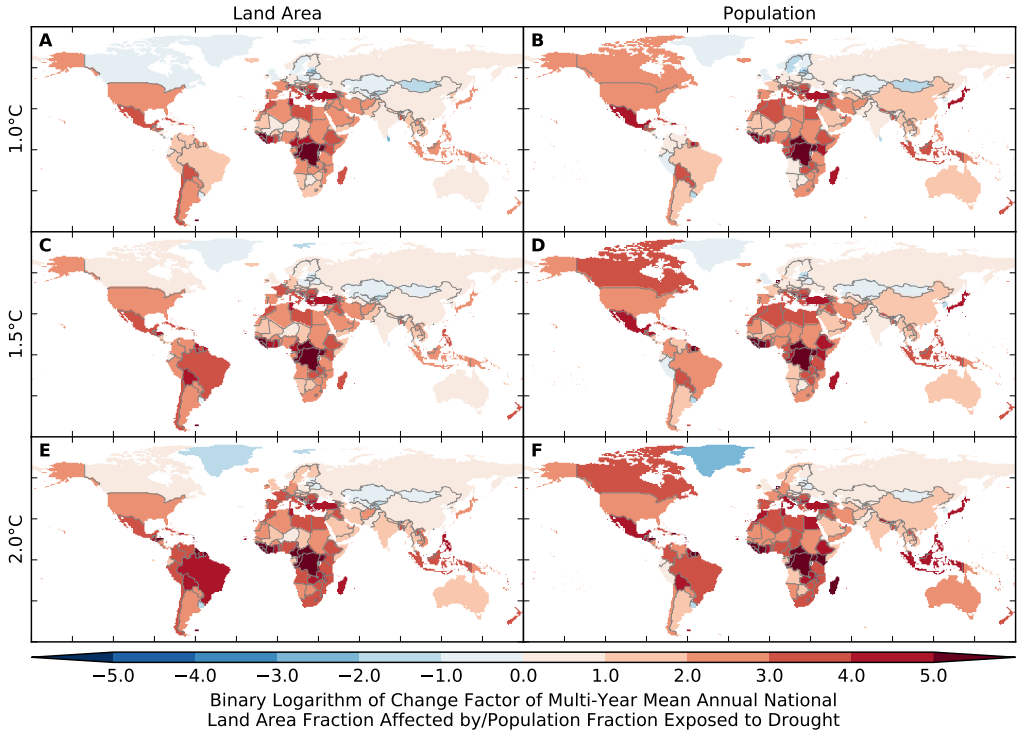

Figure S310: **Pure effect of climate change on annual national land area fraction affected by and population fraction exposed to drought (MIROC5 + PCR-GLOBWB).** Analogous to Figure S274.

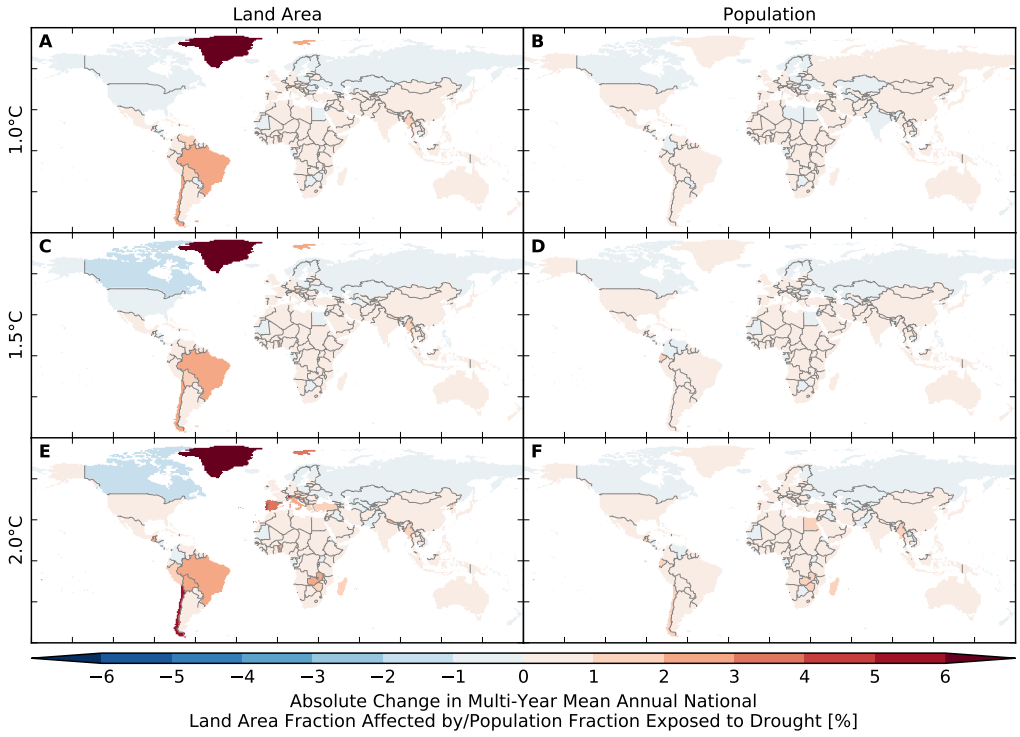

Figure S311: **Pure effect of climate change on annual national land area fraction affected by and population fraction exposed to drought (GFDL-ESM2M + WaterGAP2).** Analogous to Figure S273.

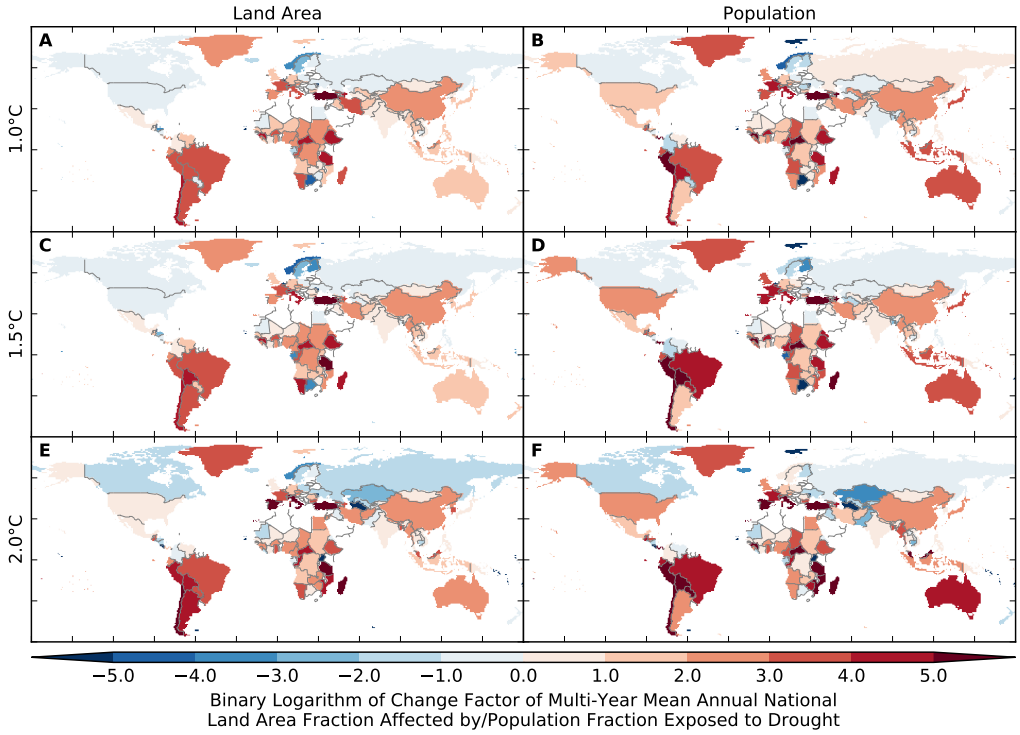

Figure S312: **Pure effect of climate change on annual national land area fraction affected by and population fraction exposed to drought (GFDL-ESM2M + WaterGAP2).** Analogous to Figure S274.

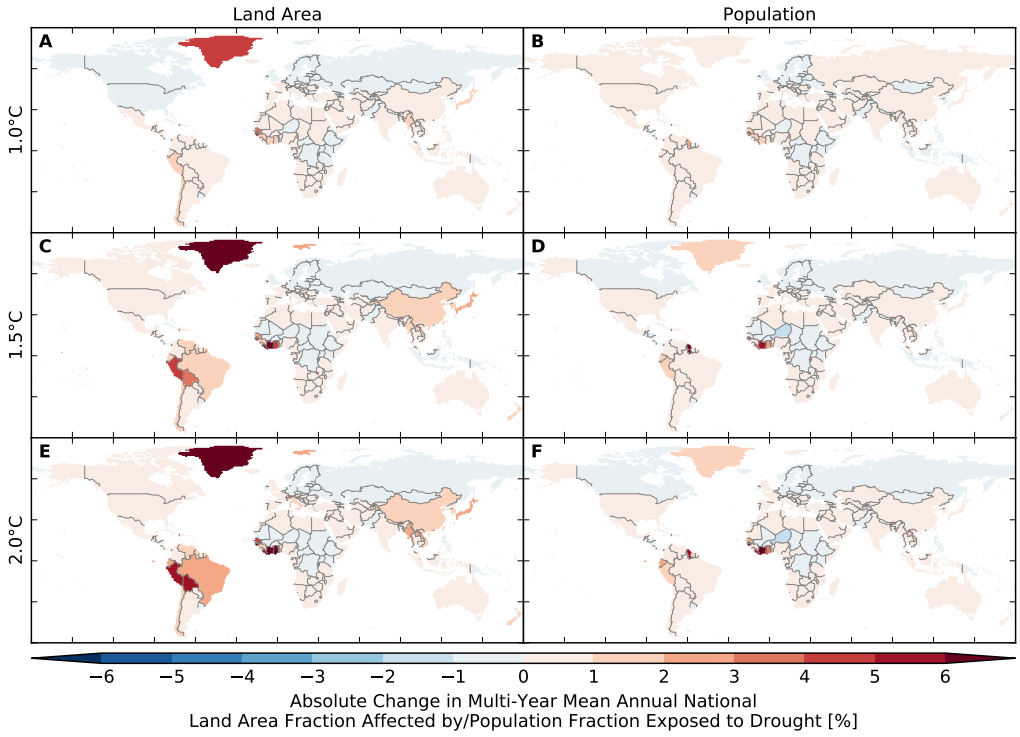

Figure S313: **Pure effect of climate change on annual national land area fraction affected by and population fraction exposed to drought (IPSL-CM5A-LR + WaterGAP2).** Analogous to Figure S273.

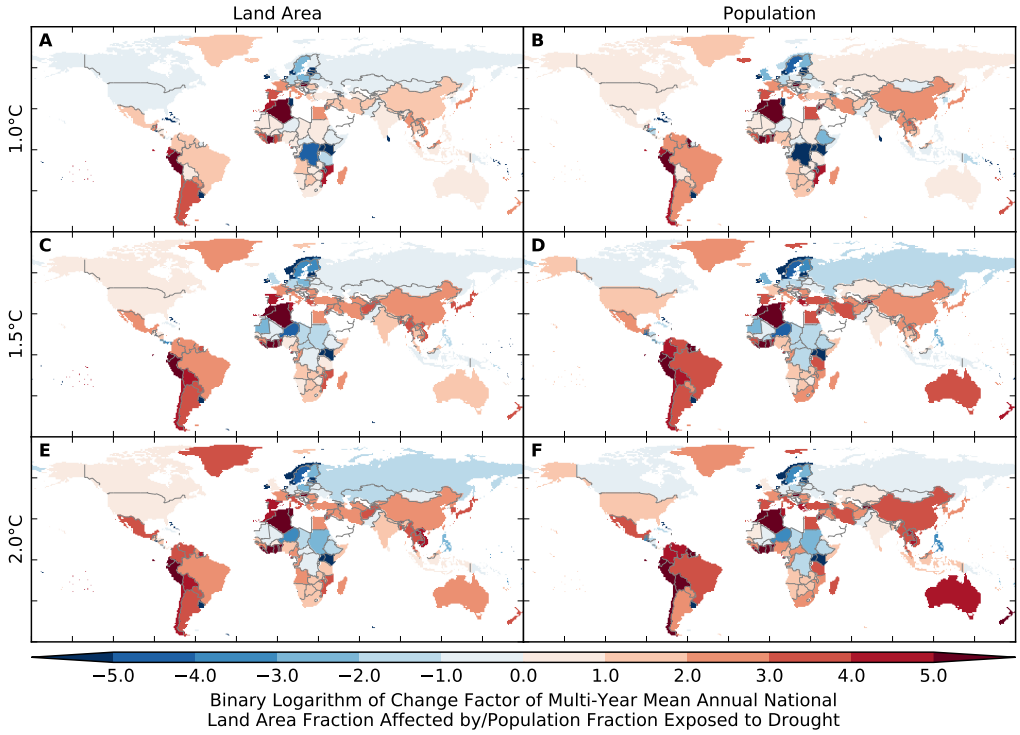

Figure S314: **Pure effect of climate change on annual national land area fraction affected by and population fraction exposed to drought (IPSL-CM5A-LR + WaterGAP2).** Analogous to Figure S274.

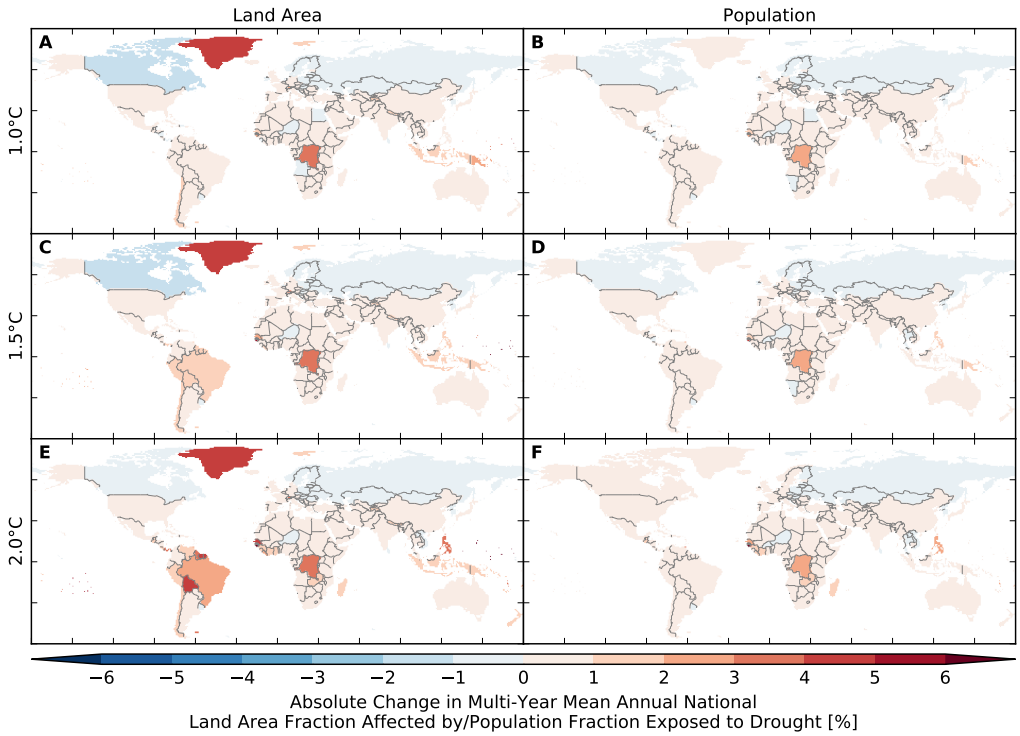

Figure S315: **Pure effect of climate change on annual national land area fraction affected by and population fraction exposed to drought (MIROC5 + WaterGAP2).** Analogous to Figure S273.

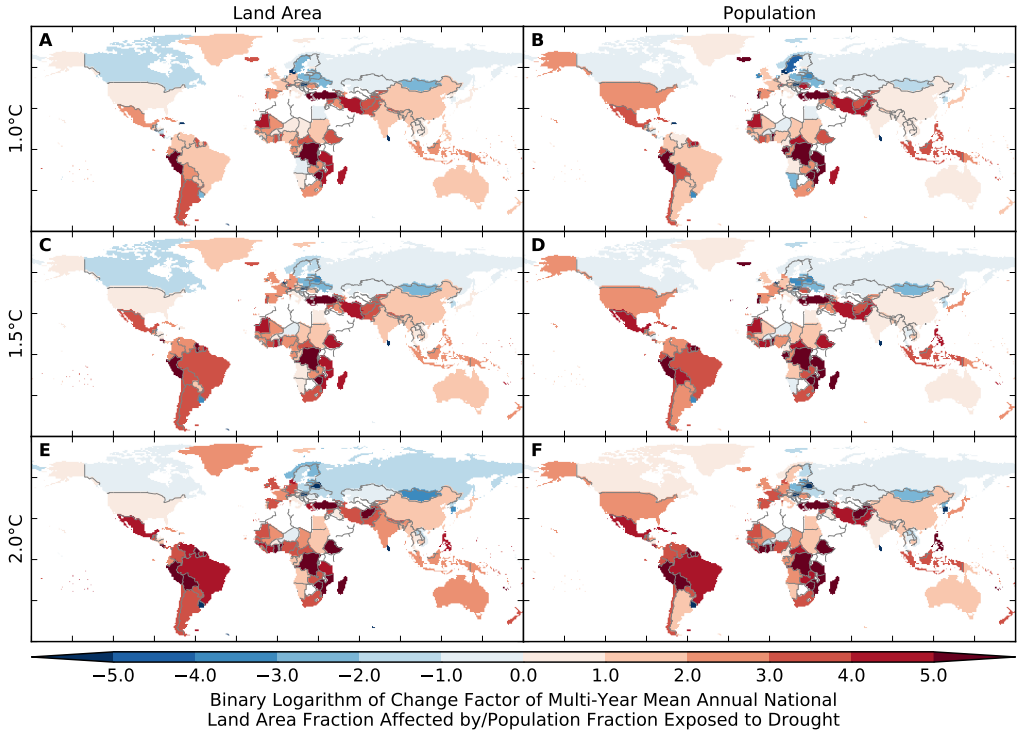

Figure S316: **Pure effect of climate change on annual national land area fraction affected by and population fraction exposed to drought (MIROC5 + WaterGAP2).** Analogous to Figure S274.

9.6 Heatwaves

Land area affected

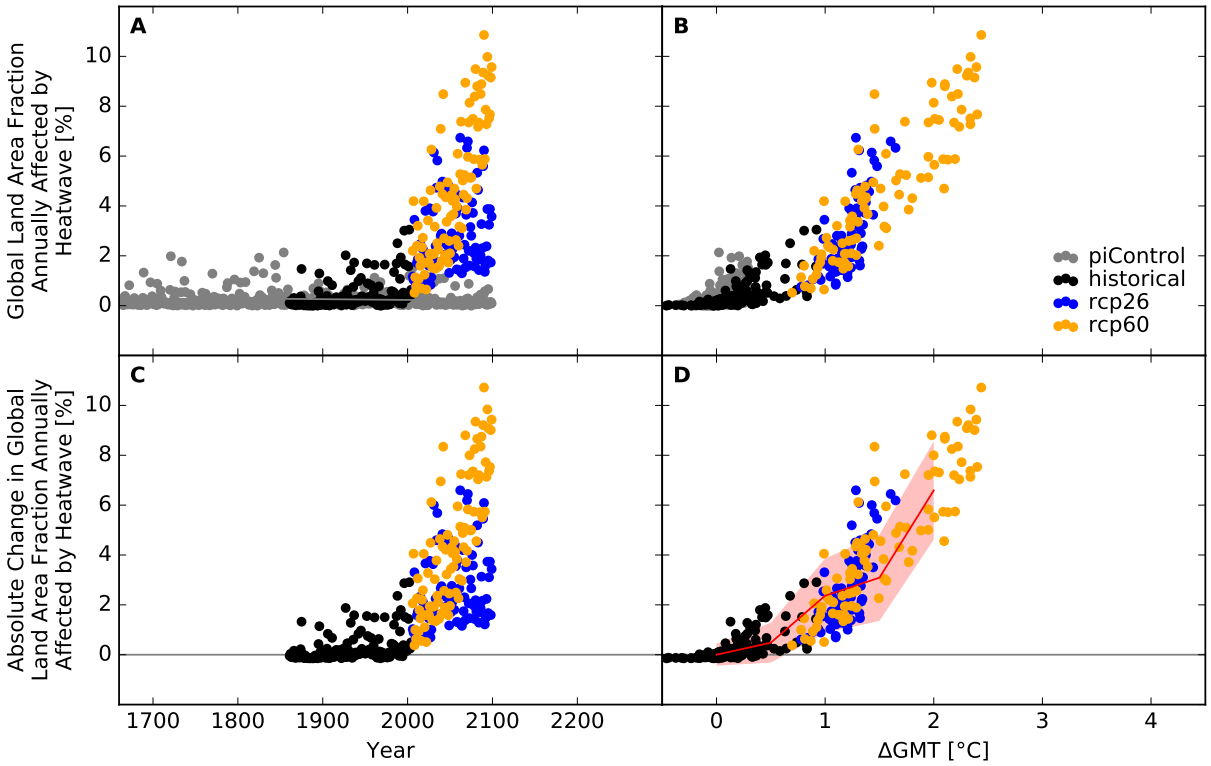

Figure S317: **Derivation of the pure effect of climate change on the global land area fraction annually affected by heatwave (GFDL-ESM2M + HWMId-humidex).** Panel A: Time series of annual global land area fraction affected (AFA) by heatwave for preindustrial climate (grey dots), historical climate (black dots), climate projections for RCP2.6 (blue dots), and RCP6.0 (orange dots). In all simulations, socioeconomic conditions are varied according to the historically observed development between 1860 and 2005, and held fixed at 1860 conditions before 1860 and at 2005 conditions after 2005. The horizontal gray lines before 1860 and after 2005 represent the multi-year mean global land area fraction annually affected by heatwave under preindustrial climate conditions and socioeconomic conditions of 1860 and 2005, respectively. The gray line between 1860 and 2005 is a linear interpolation of these mean values. Panel B: Data shown in Panel A plotted against the associated GCM-specific annual global mean temperature (GMT) change relative to the long-term preindustrial mean GMT. Panel C: Pure effect of climate change on AFA, calculated as the difference between the annual data shown in Panel A and the multi-year mean AFA under preindustrial climate conditions (gray line in Panel A). Panel D: Data shown in Panel C plotted against annual GMT change. The red line represents the mean values of the annual data points per 1 °C-wide GMT change bin, with bins centered at GMT change levels increasing from 0 °C to 4 °C in steps of 0.5 °C. The area shaded in red represents the mean value ±1 standard deviation ranges of the annual data points per GMT change bin.

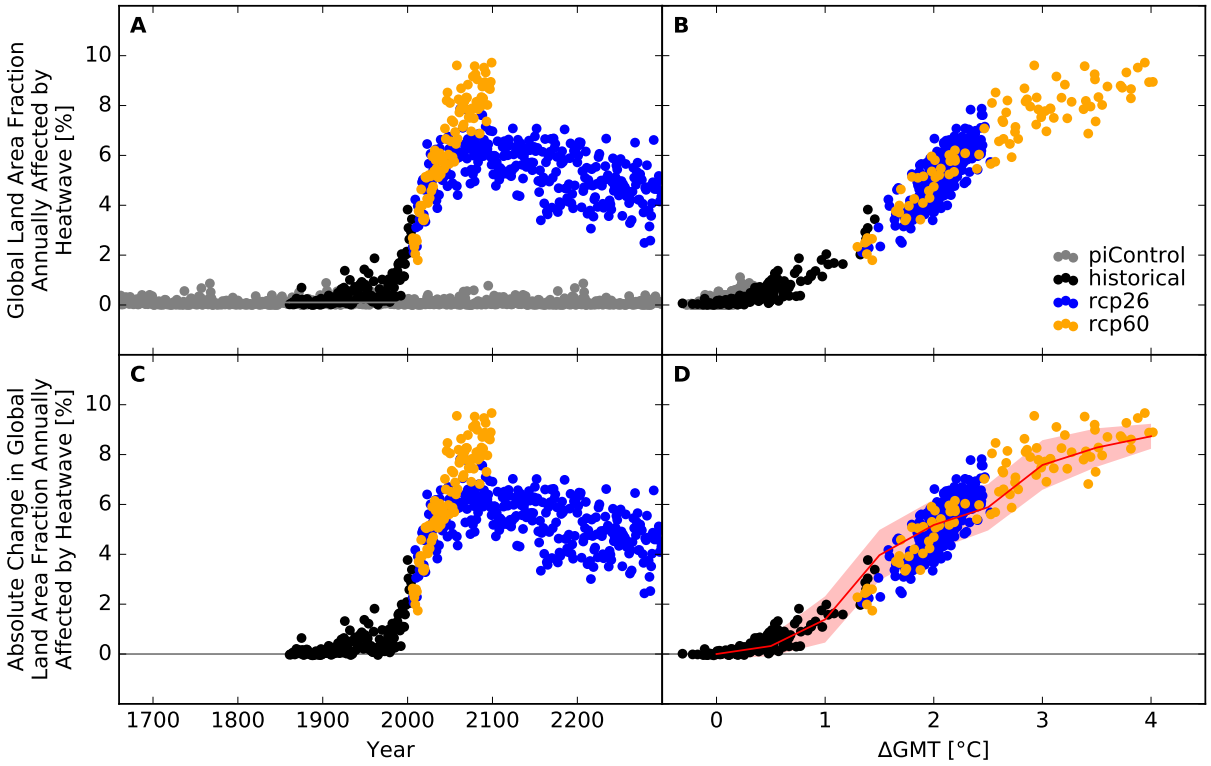

Figure S318: **Derivation of the pure effect of climate change on the global land area fraction annually affected by heatwave (IPSL-CM5A-LR + HWMId-humidex).** Analogous to Figure S317.

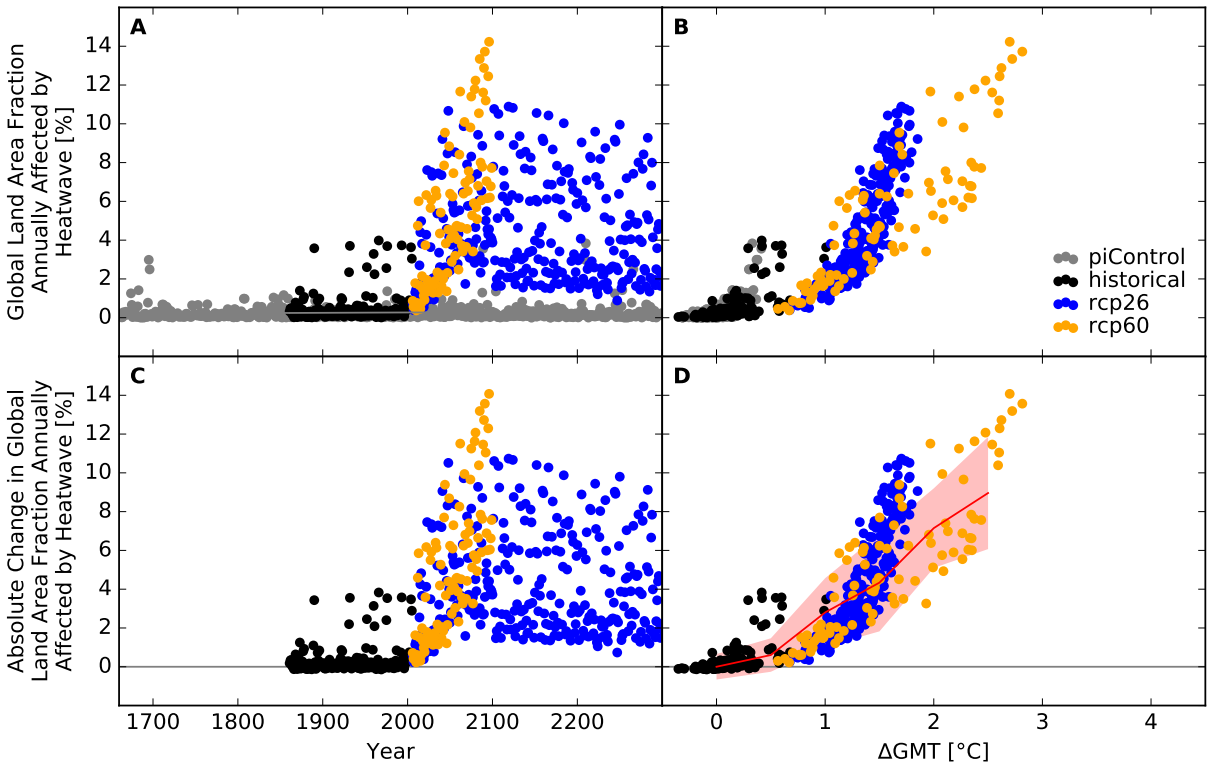

Figure S319: **Derivation of the pure effect of climate change on the global land area fraction annually affected by heatwave (MIROC5 + HWMId-humidex).** Analogous to Figure S317.

Number of people exposed

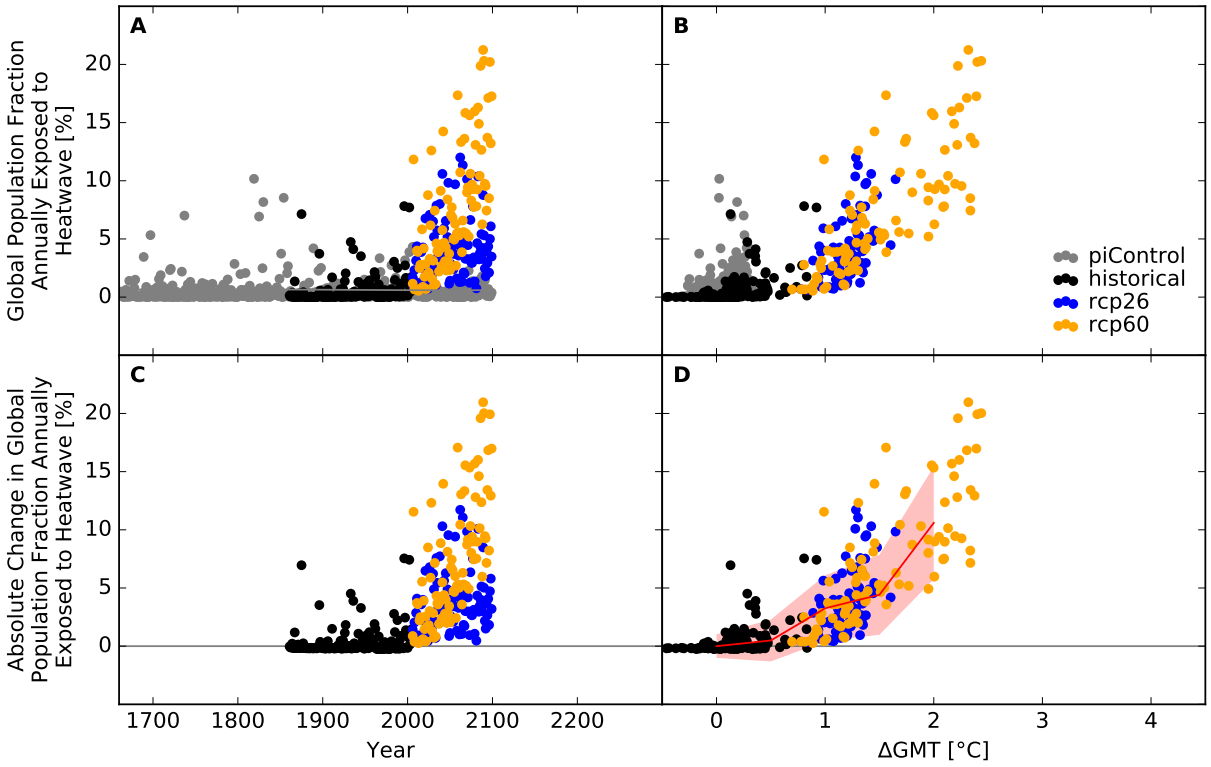

Figure S320: **Derivation of the pure effect of climate change on the global population fraction annually exposed to heatwave (GFDL-ESM2M + HWMId-humidex).** Panel A: Time series of annual global population fraction exposed (PFE) to heatwave for preindustrial climate (grey dots), historical climate (black dots), climate projections for RCP2.6 (blue dots), and RCP6.0 (orange dots). In all simulations, socioeconomic conditions are varied according to the historically observed development between 1860 and 2005, and held fixed at 1860 conditions before 1860 and at 2005 conditions after 2005. The horizontal gray lines before 1860 and after 2005 represent the multi-year mean global population fraction annually exposed to heatwave under preindustrial climate conditions and socioeconomic conditions of 1860 and 2005, respectively. The gray line between 1860 and 2005 is a linear interpolation of these mean values. Panel B: Data shown in Panel A plotted against the associated GCM-specific annual global mean temperature (GMT) change relative to the long-term preindustrial mean GMT. Panel C: Pure effect of climate change on PFE, calculated as the difference between the annual data shown in Panel A and the multi-year mean PFE under preindustrial climate conditions (gray line in Panel A). Panel D: Data shown in Panel C plotted against annual GMT change. The red line represents the mean values of the annual data points per 1 °C-wide GMT change bin, with bins centered at GMT change levels increasing from 0 °C to 4 °C in steps of 0.5 °C. The area shaded in red represents the mean value ±1 standard deviation ranges of the annual data points per GMT change bin.

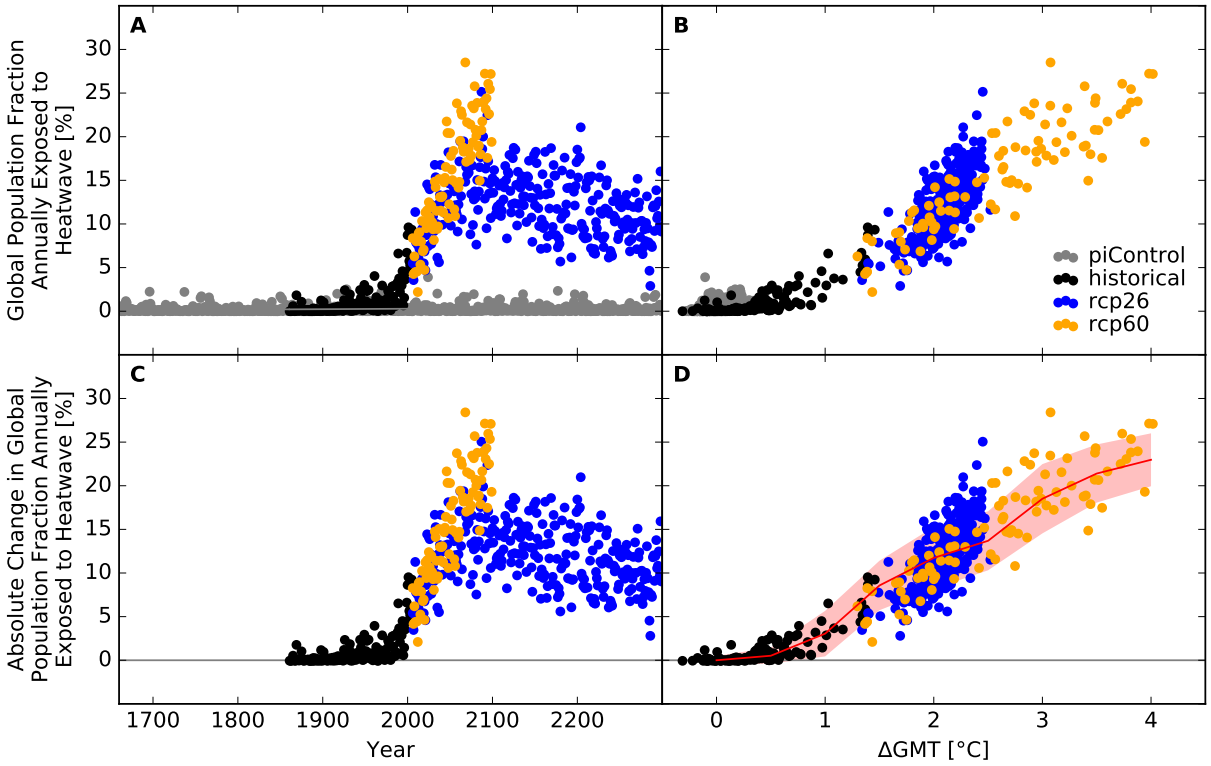

Figure S321: **Derivation of the pure effect of climate change on the global population fraction annually exposed to heatwave (IPSL-CM5A-LR + HWMId-humidex).** Analogous to Figure S320.

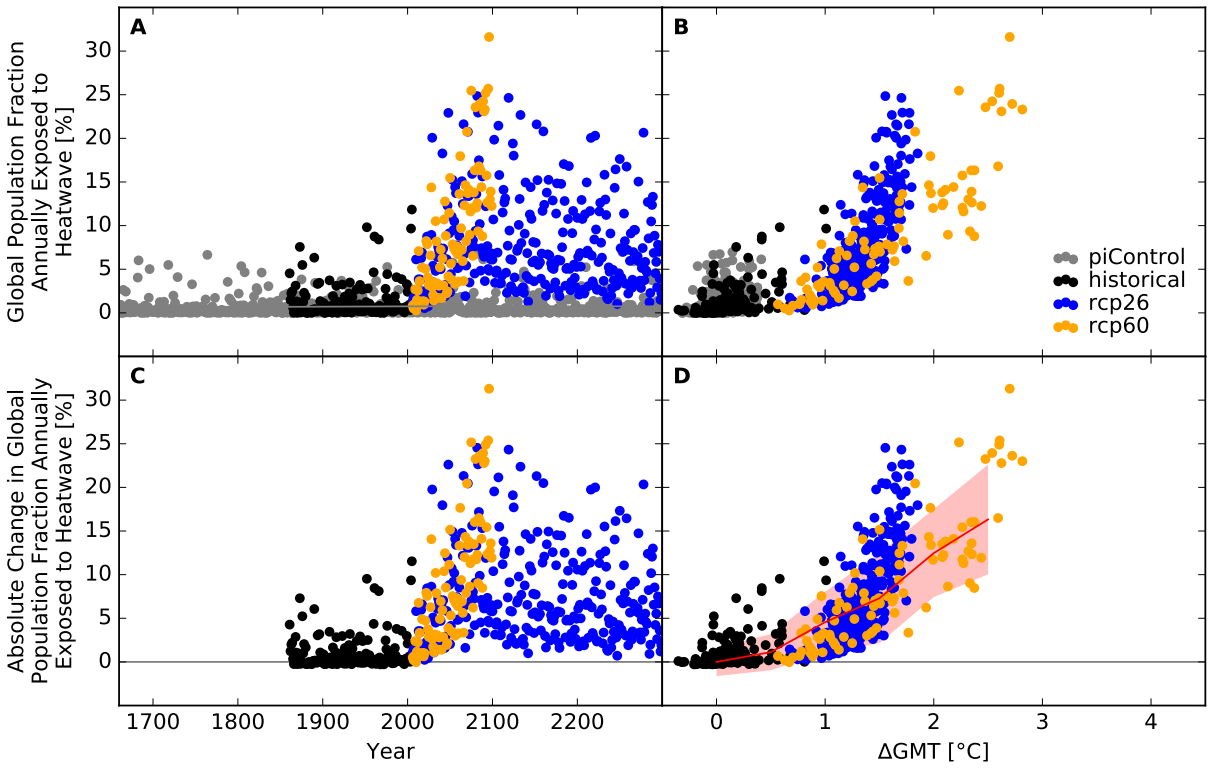

Figure S322: **Derivation of the pure effect of climate change on the global population fraction annually exposed to heatwave (MIROC5 + HWMId-humidex).** Analogous to Figure S320.

Land area affected and number of people exposed at the national scale

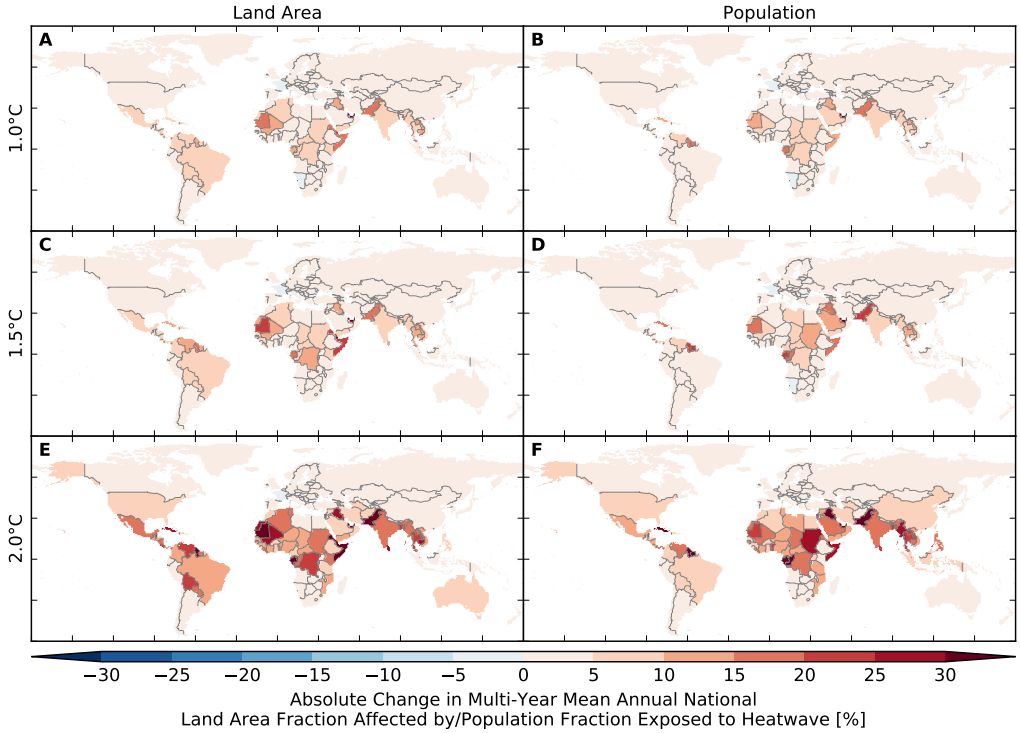

Figure S323: **Pure effect of climate change on annual national land area fraction affected by and population fraction exposed to heatwave (GFDL-ESM2M + HWMId-humidex).** Absolute changes in multi-year mean annual national (A, C, E) land area fraction affected by and (B, D, F) population fraction exposed to heatwave at (A, B) 1 °C, (C, D) 1.5 °C and (E, F) 2 °C global warming.

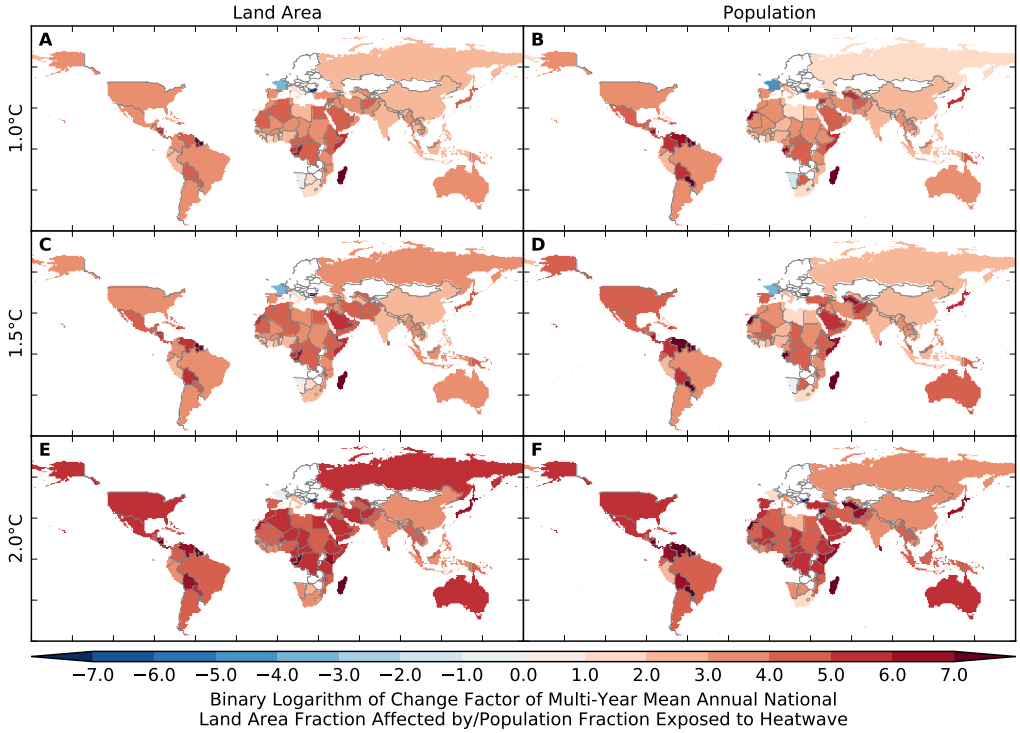

Figure S324: **Pure effect of climate change on annual national land area fraction affected by and population fraction exposed to heatwave (GFDL-ESM2M + HWMId-humidex).** Same as Figure S323 but for relative changes expressed in terms of binary logarithms of change factors, i.e. −1 means a change by a factor of 0.5, 0 means no change, and 1 means a change by a factor of 2. White indicates undefined relative changes due to division by zero.

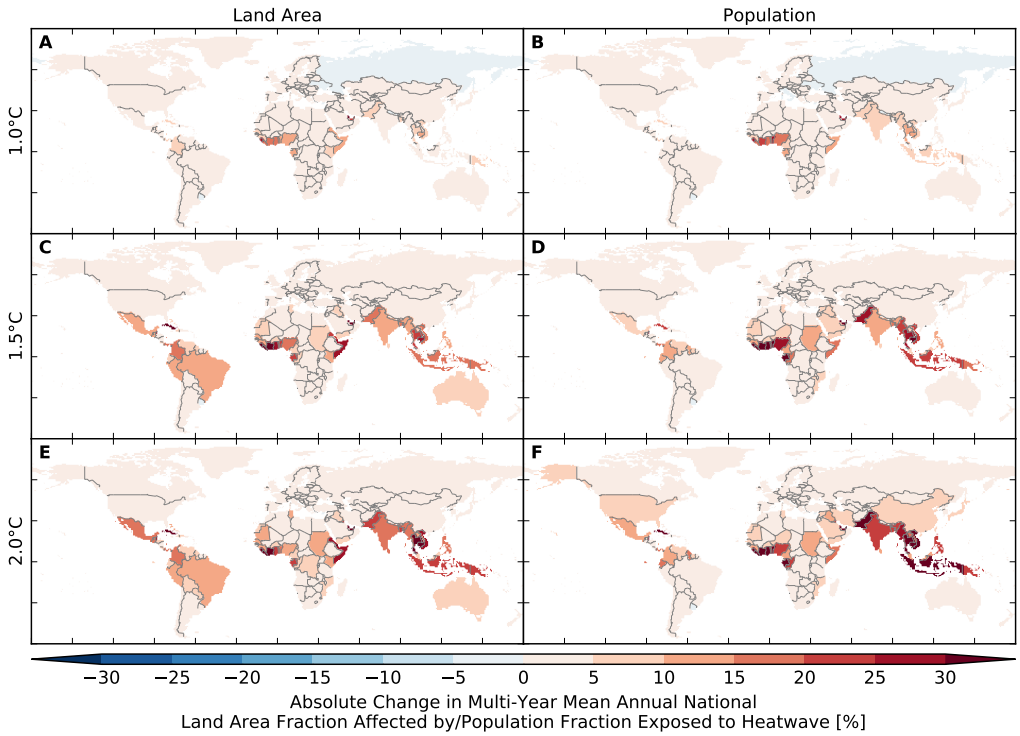

Figure S325: **Pure effect of climate change on annual national land area fraction affected by and population fraction exposed to heatwave (IPSL-CM5A-LR + HWMId-humidex).** Analogous to Figure S323.

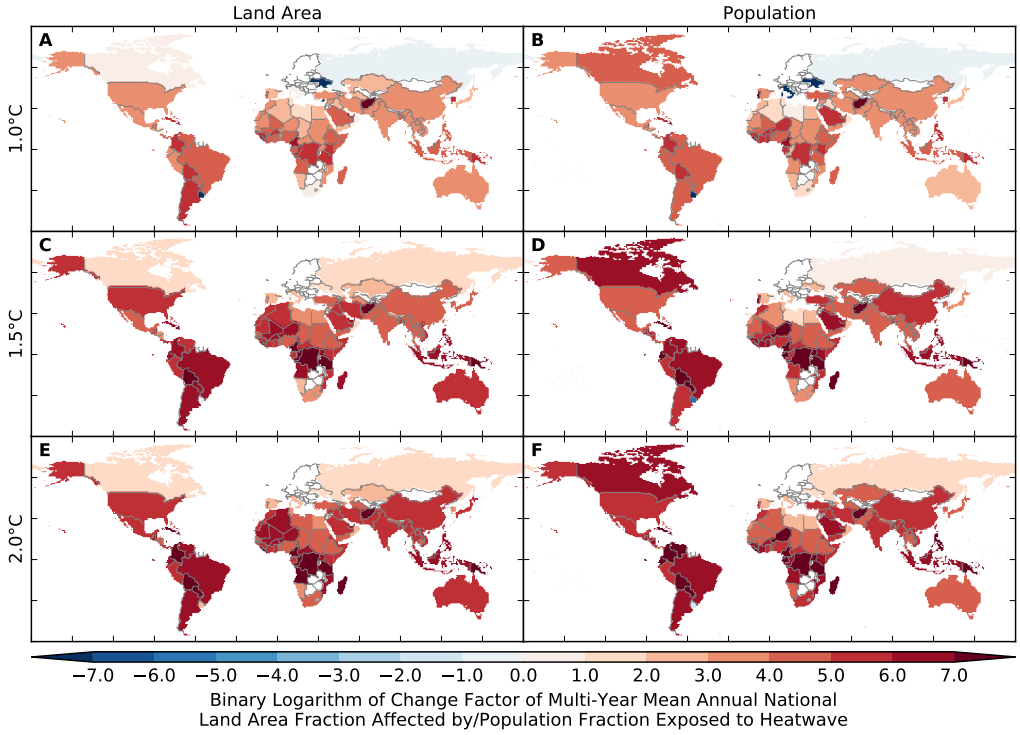

Figure S326: **Pure effect of climate change on annual national land area fraction affected by and population fraction exposed to heatwave (IPSL-CM5A-LR + HWMId-humidex).** Analogous to Figure S324.

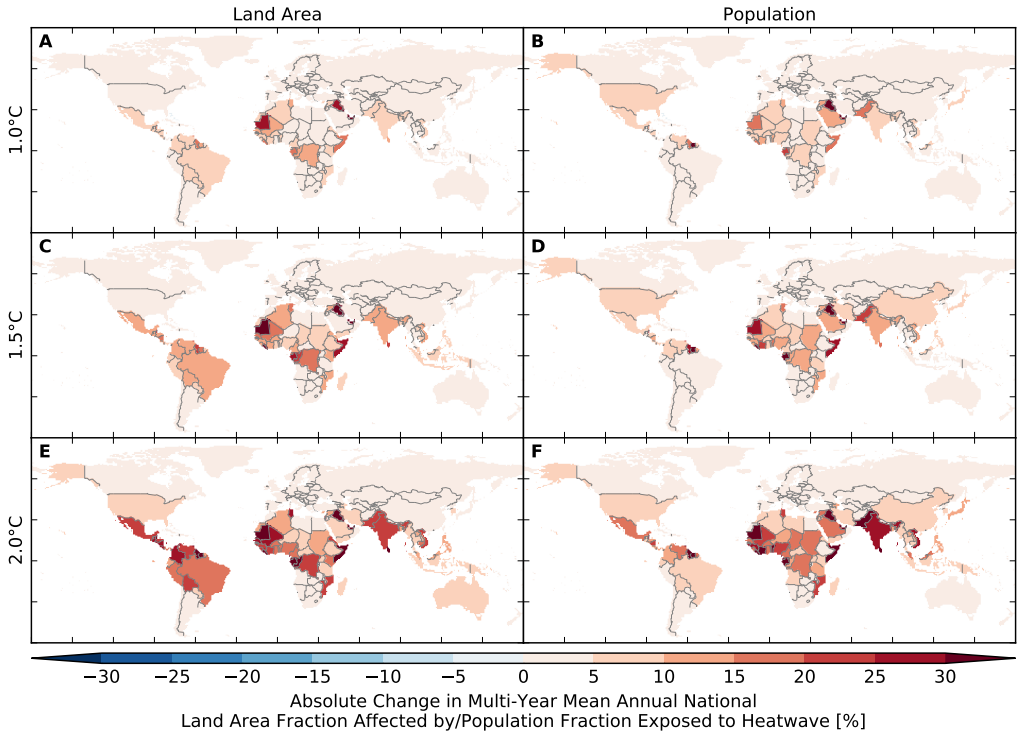

Figure S327: **Pure effect of climate change on annual national land area fraction affected by and population fraction exposed to heatwave (MIROC5 + HWMId-humidex).** Analogous to Figure S323.

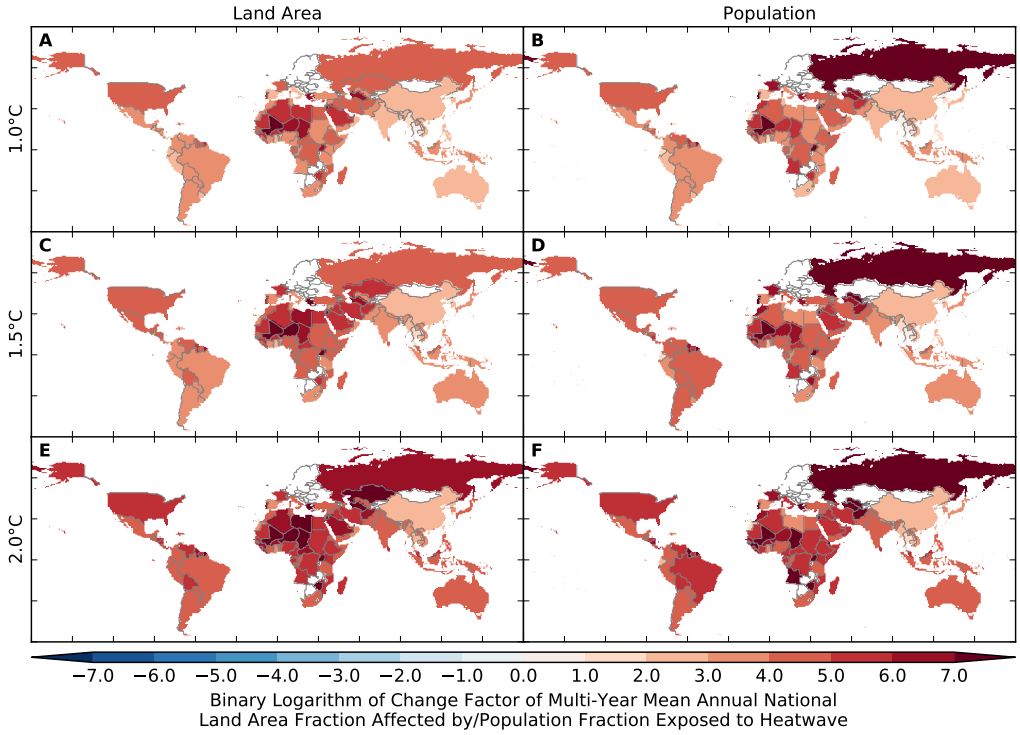

Figure S328: **Pure effect of climate change on annual national land area fraction affected by and population fraction exposed to heatwave (MIROC5 + HWMId-humidex).** Analogous to Figure S324.

References

[1] N. Andela, D. C. Morton, L. Giglio, Y. Chen, G. R. van der Werf, P. S. Kasibhatla, R. S. DeFries, G. J. Collatz, S. Hantson, S. Kloster, D. Bachelet, M. Forrest, G. Lasslop, F. Li, S. Mangeon, J. R. Melton, C. Yue, and J. T. Randerson. A human-driven decline in global burned area. *Science*, 356(6345):1356–1362, 2017. doi:10.1126/science.aal4108.

[2] S. Archibald, R.J. Scholes, D.P. Roy, G. Roberts, and L. Boschetti. Southern African fire regimes as revealed by remote sensing, 2010. doi:10.1071/WF10008.

[3] Sally Archibald, Caroline E. R. Lehmann, Jose L. Gómez-Dans, and Ross A. Bradstock. Defining pyromes and global syndromes of fire regimes. *Proceedings of the National Academy of Sciences*, 110(16):6442–6447, 2013. URL: http://www.pnas.org/content/110/16/6442.abstract, arXiv:http://www.pnas.org/content/110/16/6442.full.pdf, doi:10.1073/pnas.1211466110.

[4] M. J. Best, M. Pryor, D. B. Clark, G. G. Rooney, R .L. H. Essery, C. B. Ménard, J. M. Edwards, M. A. Hendry, A. Porson, N. Gedney, L. M. Mercado, S. Sitch, E. Blyth, O. Boucher, P. M. Cox, C. S. B. Grimmond, and R. J. Harding. The Joint UK Land Environment Simulator (JULES), model description – Part 1: Energy and water fluxes. *Geoscientific Model Development*, 4(3):677–699, sep 2011. URL: http://www.geosci-model-dev.net/4/677/2011/gmd-4-677-2011.html, doi:10.5194/gmd-4-677-2011.

[5] Alberte Bondeau, Pascalle c. Smith, Sönke Zaehle, Sibyll Schaphoff, Wolfgang Lucht, Wolfgang Cramer, Dieter Gerten, Hermann Lotze-Campen, Christoph Müller, Markus Reichstein, and Benjamin Smith. Modelling the role of agriculture for the 20th century global terrestrial carbon balance. *Global Change Biology*, 13(3):679–706, 2007. URL: http://dx.doi.org/10.1111/j.1365-2486.2006.01305.x, doi:10.1111/j.1365-2486.2006.01305.x.

[6] T. Bosshard, M. Carambia, K. Goergen, S. Kotlarski, P. Krahe, M. Zappa, and C. Schär. Quantifying uncertainty sources in an ensemble of hydrological climate-impact projections. *Water Resources Research*, 49(3):1523–1536, 2013. doi:10.1029/2011WR011533.

[7] David M. J. S. Bowman, Jennifer K. Balch, Paulo Artaxo, William J. Bond, Jean M. Carlson, Mark A. Cochrane, Carla M. D'Antonio, Ruth S. DeFries, John C. Doyle, Sandy P. Harrison, Fay H. Johnston, Jon E. Keeley, Meg A. Krawchuk, Christian A. Kull, J. Brad Marston, Max A. Moritz, I. Colin Prentice, Christopher I. Roos, Andrew C. Scott, Thomas W. Swetnam, Guido R. van der Werf, and Stephen J. Pyne. Fire in the Earth System. *Science*, 324(5926):481–484, 2009. URL: http://science.sciencemag.org/content/324/5926/481, arXiv:http://science.sciencemag.org/content/324/5926/481.full.pdf, doi:10.1126/science.1163886.

[8] David N. Bresch. Shaping Climate Resilient Development: Economics of Climate Adaptation. In *Climate Change Adaptation Strategies – An Upstream-downstream Perspective*, pages 241–254. Springer International Publishing, Cham, 2016. URL: http://link.springer.com/10.1007/978-3-319-40773-9{_}13, doi:10.1007/978-3-319-40773-9_13.

[9] A. J. Challinor, J. Watson, D. B. Lobell, S. M. Howden, D. R. Smith, and N. Chhetri. A meta-analysis of crop yield under climate change and adaptation. *Nature Clim. Change*, 4(4):287–291, 2014. URL: http://dx.doi.org/10.1038/nclimate2153, doi:10.1038/nclimate2153.

[10] Aiguo Dai. Increasing drought under global warming in observations and models. *Nature Clim. Change*, 3:52–58, 2013. doi:10.1038/nclimate1633.

[11] John P. Dunne, Ronald J. Stouffer, and Jasmin G. John. Reductions in labour capacity from heat stress under climate warming. *Nature Climate Change*, 3:563–, February 2013. doi:10.1038/nclimate1827.

[12] Warnant P Henrot A Favre E Ouberdous M Dury M, Hambuckers A and François L. Responses of European forest ecosystems to 21st century climate: assessing changes in interannual variability and fire intensity. *iForest – Biogeosciences and Forestry*, (2):82–99, 2011. URL: http://www.sisef.it/iforest/contents/?id=ifor0572-004, arXiv:http://www.sisef.it/iforest/pdf/?id=ifor0572-004, doi:10.3832/ifor0572-004.

[13] J. Elliott, C. Müller, D. Deryng, J. Chryssanthacopoulos, K. J. Boote, M. Büchner, I. Foster, M. Glotter, J. Heinke, T. Iizumi, R. C. Izaurralde, N. D. Mueller, D. K. Ray, C. Rosenzweig, A. C. Ruane, and J. Sheffield. The Global Gridded Crop Model Intercomparison: data and modeling protocols for Phase 1 (v1.0). *Geoscientific Model Development*, 8(2):261–277, 2015. URL: https://www.geosci-model-dev.net/8/261/2015/, doi:10.5194/gmd-8-261-2015.

[14] Kerry Emanuel. Downscaling CMIP5 climate models shows increased tropical cyclone activity over the 21st century. *Proceedings of the National Academy of Sciences of the United States of America*, 110(30):12219–24, jul 2013. URL: http://www.ncbi.nlm.nih.gov/pubmed/23836646, doi:10.1073/pnas.1301293110.

[15] Kerry Emanuel, Ragoth Sundararajan, and John Williams. Hurricanes and Global Warming: Results from Downscaling IPCC AR4 Simulations. *Bulletin of the American Meteorological Society*, 89(3):347–367, mar 2008. URL: http://journals.ametsoc.org/doi/abs/10.1175/BAMS-89-3-347, doi:10.1175/BAMS-89-3-347.

[16] C. Folberth, J. Elliott, C. Müller, J. Balkovic, J. Chryssanthacopoulos, R. C. Izaurralde, C. D. Jones, N. Khabarov, W. Liu, A. Reddy, E. Schmid, R. Skalský, H. Yang, A. Arneth, P. Ciais, D. Deryng, P. J. Lawrence, S. Olin, T. A. M. Pugh, A. C. Ruane, and X. Wang. Uncertainties in global crop model frameworks: effects of cultivar distribution, crop management and soil handling on crop yield estimates. *Biogeosciences Discussions*, 2016:1–30, 2016. URL: https://www.biogeosciences-discuss.net/bg-2016-527/, doi:10.5194/bg-2016-527.

[17] Christian Folberth, Thomas Gaiser, Karim C. Abbaspour, Rainer Schulin, and Hong Yang. Regionalization of a large-scale crop growth model for sub-Saharan Africa: Model setup, evaluation, and estimation of maize yields. *Agriculture, Ecosystems & Environment*, 151(Supplement C):21 – 33, 2012. URL: http://www.sciencedirect.com/science/article/pii/S0167880912000497, doi:https://doi.org/10.1016/j.agee.2012.01.026.

[18] Canadian Center for Occupational Health and Safety. Humidex Rating and Work. https://www.ccohs.ca/oshanswers/phys_agents/humidex.html, 2017. [retrieved on 10/27/2017].

[19] William M. Frank, George S. Young, William M. Frank, and George S. Young. The Interannual Variability of Tropical Cyclones. *Monthly Weather Review*, 135(10):3587–3598, oct 2007. URL: http://journals.ametsoc.org/doi/abs/10.1175/MWR3435.1, doi:10.1175/MWR3435.1.

[20] K Frieler, R Betts, E Burke, P Ciais, S Denvil, D Deryng, K Ebi, T Eddy, K Emanuel, J Elliot, E Galbraith, S Gosling, K Halladay, F Hatermann, T Hickler, J Hinkel, V Huber, C Jones, V Krysanova, S Lange, H Lotze, H Lotze-Campen, M Mengel, I Mouratiadou, H Müller Schmied, S Ostberg, F Piontek, A Popp, C Reyer, J Schewe, M Stevanovic, K Suzuki, T andThonicke, H Tian, D. T. Tittensor, R Vautard, M van Vliet, L Warszawski, and F Zhao. Assessing the impacts of 1.5°C global warming - simulation protocol of the Inter-Sectoral Model Intercomparison Project (ISIMIP2b). *Geoscientific Model Development*, (October):submitted, 2016. doi:10.5194/gmd-2016-229.

[21] R. Sahajpal S. Frolking et al. G. Hurtt, L. Chini. Harmonization of global land-use change and management for the period 850-2100. *Geoscientific Model Development*, in prep.

[22] T. Geiger, K. Frieler, and D. N. Bresch. A global historical data set of tropical cyclone exposure (TCE-DAT). *Earth System Science Data Discussions*, 2017:1–15, 2017. URL: https://www.earth-syst-sci-data-discuss.net/essd-2017-78/, doi:10.5194/essd-2017-78.

[23] Tobias Geiger, Katja Frieler, and Anders Levermann. High-income does not protect against hurricane losses. *Environmental Research Letters*, 11(8):084012, aug 2016. URL: http://stacks.iop.org/1748-9326/11/i=8/a=084012?key=crossref.055882ddb8d15bdf74e8b0433b2b8f6b, doi:10.1088/1748-9326/11/8/084012.

[24] A. Gettelman, D. N. Bresch, C. C. Chen, J. E. Truesdale, and J. T. Bacmeister. Projections of future tropical cyclone damage with a high-resolution global climate model. *Climatic Change*, pages 1–11, 2017. doi:10.1007/s10584-017-1902-7.

[25] L. Giglio, J. T. Randerson, G. R. van der Werf, P. S. Kasibhatla, G. J. Collatz, D. C. Morton, and R. S. DeFries. Assessing variability and long-term trends in burned area by merging multiple satellite fire products. *Biogeosciences*, 7(3):1171–1186, 2010. doi:10.5194/bg-7-1171-2010.

[26] Louis Giglio, James T. Randerson, and Guido R. van der Werf. Analysis of daily, monthly, and annual burned area using the fourth-generation global fire emissions database (GFED4). *Journal of Geophysical Research: Biogeosciences*, 118(1):317–328, 2013. URL: http://dx.doi.org/10.1002/jgrg.20042, doi:10.1002/jgrg.20042.

[27] Peter H. Gleick. Basic Water Requirements for Human Activities - Meeting Basic Needs. *Water International*, 21(2):83–92, 1996. doi:10.1080/02508069608686494.

[28] M Guimberteau, A Ducharne, P Ciais, J P Boisier, S Peng, M De Weirdt, H Verbeeck, and Environmental Biology. Testing conceptual and physically based soil hydrology schemes against observations for the Amazon Basin. *Geoscientific Model Development*, 7(3):1115–1136, 2014. doi:10.5194/gmd-7-1115-2014.

[29] S. Hagemann and L. Dümenil Gates. Improving a subgrid runoff parameterization scheme for climate models by the use of high resolution data derived from satellite observations. *Climate Dynamics*, 21(3-4):349–359, sep 2003. doi:10.1007/s00382-003-0349-x.

[30] N. Hanasaki, S. Yoshikawa, Y. Pokhrel, and S. Kanae. A global hydrological simulation to specify the sources of water used by humans. *Hydrology and Earth System Sciences Discussions*, 2017:1–53, 2017. URL: https://www.hydrol-earth-syst-sci-discuss.net/hess-2017-280/, doi:10.5194/hess-2017-280.

[31] Yukiko Hirabayashi, Shinjiro Kanae, Seita Emori, Taikan Oki, and Masahide Kimoto. Global projections of changing risks of floods and droughts in a changing climate. *Hydrological Sciences Journal*, 53(4):754–772, 2008. URL: http://dx.doi.org/10.1623/hysj.53.4.754, arXiv:http://dx.doi.org/10.1623/hysj.53.4.754, doi:10.1623/hysj.53.4.754.

[32] Yukiko Hirabayashi, Roobavannan Mahendran, Sujan Koirala, Lisako Konoshima, Dai Yamazaki, Satoshi Watanabe, Hyungjun Kim, and Shinjiro Kanae. Global flood risk under climate change. *Nature Climate Change*, 3(9):816–821, 2013. URL: http://dx.doi.org/10.1038/nclimate1911$\backslash$npapers3://publication/doi/10.1038/nclimate1911, doi:10.1038/nclimate1911.

[33] Greg Holland. A Revised Hurricane Pressure–Wind Model. *Monthly Weather Review*, 136(9):3432–3445, 2008. doi:10.1175/2008MWR2395.1.

[34] World Development Indicators. Employment in agriculture (percent of total employment) (modeled ILO estimate), October 2017. URL: https://data.worldbank.org/indicator/SL.AGR.EMPL.ZS.

[35] Akihiko Ito and Motoko Inatomi. Water-Use Efficiency of the Terrestrial Biosphere: A Model Analysis Focusing on Interactions between the Global Carbon and Water Cycles. *Journal of Hydrometeorology*, 13(2):681–694, 2012. URL: https://doi.org/10.1175/JHM-D-10-05034.1, arXiv:https://doi.org/10.1175/JHM-D-10-05034.1, doi:10.1175/JHM-D-10-05034.1.

[36] Akihiko Ito and Takehisa Oikawa. A simulation model of the carbon cycle in land ecosystems (Sim-CYCLE): a description based on dry-matter production theory and plot-scale validation. *Ecological Modelling*, 151(2):143 – 176, 2002. URL: http://www.sciencedirect.com/science/article/pii/S0304380001004732, doi:https://doi.org/10.1016/S0304-3800(01)00473-2.

[37] J. R. Wallis J. R. M. Hosking. *Regional Frequency Analysis*. Cambridge University Press, 1997.

[38] A F Jenkinson. The frequency distribution of the annual maximum (or minimum) values of meteorological elements. *Q. J. R. Meteorol. Soc.*, 81:158–171, 1955.

[39] Stahl K. *Hydrological drought—a study across Europe*. PhD dissertation, Albert- Ludwigs-Universität, Freiburg, Germany, 2001. URL: http://www.sciencedirect.com/science/article/pii/S1474706504001676, doi:https://doi.org/10.1016/j.pce.2004.09.018.

[40] Etsushi Kato, Tsuguki Kinoshita, Akihiko Ito, Michio Kawamiya, and Yoshiki Yamagata. Evaluation of spatially explicit emission scenario of land-use change and biomass burning using a process-based biogeochemical model. *Journal of Land Use Science*, 8(1):104–122, 2013. doi:10.1080/1747423X.2011.628705.

[41] K. Klein Goldewijk, A. Beusen, J. Doelman, and E. Stehfest. New anthropogenic land use estimates for the Holocene; HYDE 3.2. *Earth System Science Data Discussions*, 2016:1–40, 2016. URL: https://www.earth-syst-sci-data-discuss.net/essd-2016-58/, doi:10.5194/essd-2016-58.

[42] W. Knorr, A. Arneth, and L. Jiang. Demographic controls of future global fire risk. *Nature Climate Change*, 6:781–785, 2016. doi:10.1038/nclimate2999.

[43] Sujan Koirala, Pat J F Yeh, Yukiko Hirabayashi, Shinjiro Kanae, and Taikan Oki. Global-scale land surface hydrologic modeling with the representation of water table dynamics. *Journal of Geophysical Research Atmospheres*, 119(1):75–89, 2014. doi:10.1002/2013JD020398.

[44] Osamu Kunii, Shuzo Kanagawa, Iwao Yajima, Yoshiharu Hisamatsu, Sombo Yamamura, Takashi Amagai, and Ir T. Sachrul Ismail. The 1997 Haze Disaster in Indonesia: Its Air Quality and Health Effects. *Archives of Environmental Health: An International Journal*, 57(1):16–22, January 2002. doi:10.1080/00039890209602912.

[45] David M Lawrence, Keith W Oleson, Mark G Flanner, Peter E Thornton, Sean C Swenson, Peter J Lawrence, Xubin Zeng, Zong-Liang Yang, Samuel Levis, Koichi Sakaguchi, Gordon B Bonan, and Andrew G Slater. Parameterization improvements and functional and structural advances in Version 4 of the Community Land Model. *Journal of Advances in Modeling Earth Systems*, 3(1), 2011. M03001. doi:10.1029/2011MS00045.

[46] Flavio Lehner, Sloan Coats, Thomas F. Stocker, Angeline G. Pendergrass, Benjamin M. Sanderson, Christoph C. Raible, and Jason E. Smerdon. Projected drought risk in 1.5°C and 2°C warmer climates. *Geophysical Research Letters*, 44(14):7419–7428, 2017. 2017GL074117. URL: http://dx.doi.org/10.1002/2017GL074117, doi:10.1002/2017GL074117.

[47] Wenfeng Liu, Hong Yang, Christian Folberth, Xiuying Wang, Qunying Luo, and Rainer Schulin. Global investigation of impacts of PET methods on simulating crop-water relations for maize. *Agricultural and Forest Meteorology*, 221(Supplement C):164 – 175, 2016. URL: http://www.sciencedirect.com/science/article/pii/S0168192316301800, doi:https://doi.org/10.1016/j.agrformet.2016.02.017.

[48] Wenfeng Liu, Hong Yang, Junguo Liu, Ligia B. Azevedo, Xiuying Wang, Zongxue Xu, Karim C. Abbaspour, and Rainer Schulin. Global assessment of nitrogen losses and trade-offs with yields from major crop cultivations. *Science of The Total Environment*, 572(Supplement C):526 – 537, 2016. URL: http://www.sciencedirect.com/science/article/pii/S0048969716317867, doi:https://doi.org/10.1016/j.scitotenv.2016.08.093.

[49] J. M. Masterton and F. A. Richardson. *Humidex: A Method of Quantifying Human Discomfort Due to Excessive Heat and Humidity*. Environment Canada.

[50] Robert Mendelsohn, Kerry Emanuel, Shun Chonabayashi, and Laura Bakkensen. The impact of climate change on global tropical cyclone damage. *Nature Climate Change*, 2(3):205–209, jan 2012. URL: http://www.nature.com/doifinder/10.1038/nclimate1357, doi:10.1038/nclimate1357.

[51] Chad Monfreda, Navin Ramankutty, and Jonathan A. Foley. Farming the planet: 2. Geographic distribution of crop areas, yields, physiological types, and net primary production in the year 2000. *Global Biogeochemical Cycles*, 22(1):n/a–n/a, 2008. GB1022. URL: http://dx.doi.org/10.1029/2007GB002947, doi:10.1029/2007GB002947.

[52] Florent Mouillot and Christopher B. Field. Fire history and the global carbon budget: a 1°× 1° fire history reconstruction for the 20thcentury. *Global Change Biology*, 11(3):398–420, 2005. URL: http://dx.doi.org/10.1111/j.1365-2486.2005.00920.x, doi:10.1111/j.1365-2486.2005.00920.x.

[53] C. Müller, J. Elliott, J. Chryssanthacopoulos, A. Arneth, J. Balkovic, P. Ciais, D. Deryng, C. Folberth, M. Glotter, S. Hoek, T. Iizumi, R. C. Izaurralde, C. Jones, N. Khabarov, P. Lawrence, W. Liu, S. Olin, T. A. M. Pugh, D. K. Ray, A. Reddy, C. Rosenzweig, A. C. Ruane, G. Sakurai, E. Schmid, R. Skalsky, C. X. Song, X. Wang, A. de Wit, and H. Yang. Global gridded crop model evaluation: benchmarking, skills, deficiencies and implications. *Geoscientific Model Development*, 10(4):1403–1422, 2017. URL: https://www.geosci-model-dev.net/10/1403/2017/, doi:10.5194/gmd-10-1403-2017.

[54] H. Müller Schmied, L. Adam, S. Eisner, G. Fink, M. Flörke, H. Kim, T. Oki, F. T. Portmann, R. Reinecke, C. Riedel, Q. Song, J. Zhang, and P. Döll. Variations of global and continental water balance components as impacted by climate forcing uncertainty and human water use. *Hydrology and Earth System Sciences*, 20(7):2877–2898, 2016. URL: https://www.hydrol-earth-syst-sci.net/20/2877/2016/, doi:10.5194/hess-20-2877-2016.

[55] H Müller Schmied, S. Eisner, D. Franz, M. Wattenbach, F. T. Portmann, M. Flörke, and P. Döll. Sensitivity of simulated global-scale freshwater fluxes and storages to input data, hydrological model structure, human water use and calibration. *Hydrology and Earth System Sciences*, 18(9):3511–3538, 2014. doi:10.5194/hess-18-3511-2014.

[56] Washington R. Nyabeze. Estimating and interpreting hydrological drought indices using a selected catchment in Zimbabwe. *Physics and Chemistry of the Earth, Parts A/B/C*, 29(15):1173–1180, 2004. Water, Science, Technology and Policy Convergence and Action by All (A Meeting Point for Action leading to Sustainable Development). URL: http://www.sciencedirect.com/science/article/pii/S1474706504001676, doi:https://doi.org/10.1016/j.pce.2004.09.018.

[57] Keith Oleson, David M. Lawrence, Gordon B. Bonan, Beth Drewniak, Maoyi Huang, Charles D. Koven, Samuel Levis, Fang Li, William J. Riley, Zachary M. Subin, Sean Swenson, Peter E. Thornton, Anil Bozbiyik, Rosie Fisher, Colette L. Heald, Erik Kluzek, Jean-Francois Lamarque, Peter J. Lawrence, L. Ruby Leung, William Lipscomb, Stefan P. Muszala, Daniel M. Ricciuto, William J. Sacks, Ying Sun, Jinyun Tang, and Zong-Liang Yang. Technical Description of version 4.5 of the Community Land Model (CLM). Technical Report NCAR/TN-503+STR, NCAR Technical Note, July 2013. doi:10.5065/D6RR1W7M.

[58] Jerry S. Olson, Julia A. Watts, and Linda J. Allison. Carbon in live vegetation of major world ecosystems. Technical report, Oak Ridge National Laboratory, 1983.

[59] L. V. Papadimitriou, A. G. Koutroulis, M. G. Grillakis, and I. K. Tsanis. The effect of GCM biases on global runoff simulations of a land surface model. *Hydrology and Earth System Sciences*, 21(9):4379–4401, 2017. URL: https://www.hydrol-earth-syst-sci.net/21/4379/2017/, doi:10.5194/hess-21-4379-2017.

[60] F. Pappenberger, E. Dutra, F. Wetterhall, and H. L. Cloke. Deriving global flood hazard maps of fluvial floods through a physical model cascade. *Hydrology and Earth System Sciences*, 16(11):4143–4156, 2012. doi:10.5194/hess-16-4143-2012.

[61] O. Pechony and D. T. Shindell. Driving forces of global wildfires over the past millennium and the forthcoming century. *Proceedings of the National Academy of Sciences*, 107(45):19167–19170, 2010. URL: http://www.pnas.org/content/107/45/19167.abstract, arXiv:http://www.pnas.org/content/107/45/19167.full.pdf, doi:10.1073/pnas.1003669107.

[62] Leland T. Peirce. Diurnal Variation in the Dew-Point Temperature at Asheville, N. C. *Monthly Weather Review*, 62(8):289–293, 1934. doi:10.1175/1520-0493(1934)62<289:DVITDT>2.0.CO;2.

[63] Stephen Plummer, Olivier Arino, Franck Ranera, Kevin Tansey, Jing Chen, Gerard Dedieu, Hugh Eva, Isidoro Piccolini, Roland Leigh, Geert Borstlap, Bart Beusen, Freddy Fierens, Walter Heyns, Riccardo Benedetti, Roselyne Lacaze, Sebastien Garrigues, Tristan Quaife, Martin De Kauwe, Shaun Quegan, Michael Raupach, Peter Briggs, Ben Poulter, Alberte Bondeau, Peter Rayner, Martin Schultz, and Ian McCallum. An Update on the globcarbon initiative: multi-sensor estimation of global biophysical products for global terrestrial carbon studies. In *Proceedings of Envisat Symposium 2007, 23–27 April 2007, Montreux, Switzerland*. ESA Communication Production Office, ESTEC, 2007. URL: http://eprints.ucl.ac.uk/179082/.

[64] Navin Ramankutty and Jonathan A. Foley. Estimating historical changes in global land cover: Croplands from 1700 to 1992. *Global Biogeochemical Cycles*, 13(4):997–1027, 1999. doi:10.1029/1999GB900046.

[65] Cynthia Rosenzweig, Joshua Elliott, Delphine Deryng, Alex C. Ruane, Christoph Müller, Almut Arneth, Kenneth J. Boote, Christian Folberth, Michael Glotter, Nikolay Khabarov, Kathleen Neumann, Franziska Piontek, Thomas A. M. Pugh, Erwin Schmid, Elke Stehfest, Hong Yang, and James W. Jones. Assessing agricultural risks of climate change in the 21st century in a global gridded crop model intercomparison. *Proceedings of the National Academy of Sciences*, 111(9):3268–3273, 2014. URL: http://www.pnas.org/content/111/9/3268.abstract, arXiv:http://www.pnas.org/content/111/9/3268.full.pdf, doi:10.1073/pnas.1222463110.

[66] Stefanie Rost, Dieter Gerten, Alberte Bondeau, Wolfgang Lucht, Janine Rohwer, and Sibyll Schaphoff. Agricultural green and blue water consumption and its influence on the global water system. *Water Resources Research*, 44(9):1–17, sep 2008. doi:10.1029/2007WR006331.

[67] Simone Russo, Jana Sillmann, and Erich M Fischer. Top ten European heatwaves since 1950 and their occurrence in the coming decades. *Environmental Research Letters*, 10(12):124003, 2015. doi:10.1088/1748-9326/10/12/124003.

[68] Simone Russo, Jana Sillmann, and Andreas Sterl. Humid heat waves at different warming levels. *Scientific Reports*, 7(1):7477, 2017. doi:10.1038/s41598-017-07536-7.

[69] Sacks, William J. and Deryng, Delphine and Foley, Jonathan A. and Ramankutty, Navin. Crop planting dates: an analysis of global patterns. *Global Ecology and Biogeography*, 19(5):607–620, 2010. URL: http://dx.doi.org/10.1111/j.1466-8238.2010.00551.x, doi:10.1111/j.1466-8238.2010.00551.x.

[70] Sibyll Schaphoff, Ursula Heyder, Sebastian Ostberg, Dieter Gerten, Jens Heinke, and Wolfgang Lucht. Contribution of permafrost soils to the global carbon budget. *Environmental Research Letters*, 8(1):014026, 2013. URL: http://stacks.iop.org/1748-9326/8/i=1/a=014026?key=crossref.0e7839a06a4152bf5363c45a8727a5a1, doi:10.1088/1748-9326/8/1/014026.

[71] Sibyll Schaphoff, Ursula Heyder, Sebastian Ostberg, Dieter Gerten, Jens Heinke, and Wolfgang Lucht. Contribution of permafrost soils to the global carbon budget. *Environmental Research Letters*, 8(1):014026, 2013. URL: http://stacks.iop.org/1748-9326/8/i=1/a=014026.

[72] Peter D. Schwartzman, Patrick J. Michaels, and Paul C. Knappenberger. Observed changes in the diurnal dewpoint cycles across North America. *Geophysical Research Letters*, 25(13):2265–2268, 1998. doi:10.1029/98GL01843.

[73] Paolo Scussolini, Jeroen C. J. H. Aerts, Brenden Jongman, Laurens M. Bouwer, Hessel C. Winsemius, Hans de Moel, Philip J. Ward, Hans de Moel, and Philip J. Ward. FLOPROS: an evolving global database of flood protection standards. *Natural Hazards and Earth System Sciences*, 16(5):1049–1061, may 2016. doi:10.5194/nhess-16-1049-2016.

[74] Sonia I. Seneviratne, Thierry Corti, Edouard L. Davin, Martin Hirschi, Eric B. Jaeger, Irene Lehner, Boris Orlowsky, and Adriaan J. Teuling. Investigating soil moisture–climate interactions in a changing climate: A review. *Earth-Science Reviews*, 99(3):125–161, 2010. URL: http://www.sciencedirect.com/science/article/pii/S0012825210000139, doi:https://doi.org/10.1016/j.earscirev.2010.02.004.

[75] J. Sheffield and E. F. Wood. Characteristics of global and regional drought, 1950–2000: Analysis of soil moisture data from off-line simulation of the terrestrial hydrologic cycle. *J. Geophys. Res.-Atmos.*, 112:D17115, 2007. doi:10.1029/2006JD008288.

[76] Justin Sheffield and Eric F. Wood. Projected changes in drought occurrence under future global warming from multi-model, multi-scenario, IPCC AR4 simulations. *Climate Dynamics*, 31(1):79–105, 2008. doi:10.1007/s00382-007-0340-z.

[77] Steven C. Sherwood and Matthew Huber. An adaptability limit to climate change due to heat stress. *Proceedings of the National Academy of Sciences*, 107(21):9552–9555, 2010. doi:10.1073/pnas.0913352107.

[78] B. Smith, D. Wårlind, A. Arneth, T. Hickler, P. Leadley, J. Siltberg, and S. Zaehle. Implications of incorporating N cycling and N limitations on primary production in an individual-based dynamic vegetation model. *Biogeosciences*, 11(7):2027–2054, 2014. URL: https://www.biogeosciences.net/11/2027/2014/, doi:10.5194/bg-11-2027-2014.

[79] Aditya Sood and Vladimir Smakhtin. Global hydrological models: a review. *Hydrological Sciences Journal*, 60(4):549–565, 2015. URL: http://dx.doi.org/10.1080/02626667.2014.950580, arXiv:http://dx.doi.org/10.1080/02626667.2014.950580, doi:10.1080/02626667.2014.950580.

[80] T Stacke and S Hagemann. Development and validation of a global dynamical wetlands extent scheme. *Hydrology and Earth System Sciences Discussions*, 9(1):405–440, 2012. doi:10.5194/hessd-9-405-2012.

[81] Elke Stehfest, Maik Heistermann, Joerg A. Priess, Dennis S. Ojima, and Joseph Alcamo. Simulation of global crop production with the ecosystem model DayCent. *Ecological Modelling*, 209(2):203–219, 2007. doi:10.1016/j.ecolmodel.2007.06.028.

[82] Kumiko Takata, Seita Emori, and Tsutomu Watanabe. Development of the minimal advanced treatments of surface interaction and runoff. *Global and Planetary Change*, 38(1-2):209–222, jul 2003. doi:10.1016/S0921-8181(03)00030-4.

[83] Kevin Tansey, Jean-Marie Grégoire, Pierre Defourny, Roland Leigh, Jean-François Pekel, Eric van Bogaert, and Etienne Bartholomé. A new, global, multi-annual (2000–2007) burnt area product at 1 km resolution. *Geophysical Research Letters*, 35(1), 2008. L01401. doi:10.1029/2007GL031567.

[84] K. Thonicke, A. Spessa, I. C. Prentice, S. P. Harrison, L. Dong, and C. Carmona-Moreno. The influence of vegetation, fire spread and fire behaviour on biomass burning and trace gas emissions: results from a process-based model. *Biogeosciences*, 7(6):1991–2011, 2010. URL: https://www.biogeosciences.net/7/1991/2010/, doi:10.5194/bg-7-1991-2010.

[85] Kirsten Thonicke, Sergey Venevsky, Stephen Sitch, and Wolfgang Cramer. The role of fire disturbance for global vegetation dynamics: coupling fire into a Dynamic Global Vegetation Model. *Global Ecology and Biogeography*, 10(6):661–677, 2001. URL: http://dx.doi.org/10.1046/j.1466-822X.2001.00175.x, doi:10.1046/j.1466-822X.2001.00175.x.

[86] Kirsten Thonicke, Sergey Venevsky, Stephen Sitch, and Wolfgang Cramer. The role of fire disturbance for global vegetation dynamics: coupling fire into a Dynamic Global Vegetation Model. *Global Ecology and Biogeography*, 10(6):661–677, 2001. doi:10.1046/j.1466-822X.2001.00175.x.

[87] G. R. van der Werf, J. T. Randerson, L. Giglio, T. T. van Leeuwen, Y. Chen, B. M. Rogers, M. Mu, M. J. E. van Marle, D. C. Morton, G. J. Collatz, R. J. Yokelson, and P. S. Kasibhatla. Global fire emissions estimates during 1997–2016. *Earth System Science Data*, 9(2):697–720, 2017. doi:10.5194/essd-9-697-2017.

[88] Anne F. Van Loon. Hydrological drought explained. *Wiley Interdisciplinary Reviews: Water*, 2(4):359–392, 2015. URL: http://dx.doi.org/10.1002/wat2.1085, doi:10.1002/wat2.1085.

[89] J.P. Vidal, E. Martin, L. Franchistéguy, Florence Habets, Jean-Michel Soubeyroux, M. Blanchard, and M. Baillon. Multilevel and multiscale drought reanalysis over France with the Safran-Isba-Modcou hydrometeorological suite. *Hydrol. Earth Syst. Sci.*, 14(3):459–478, 2010. doi:10.5194/hess-14-459-2010.

[90] Y. Wada, D. Wisser, and M. F P Bierkens. Global modeling of withdrawal, allocation and consumptive use of surface water and groundwater resources. *Earth System Dynamics*, 5(1):15–40, 2014. doi:10.5194/esd-5-15-2014.

[91] Yoshihide Wada, Inge E. M. de Graaf, and Ludovicus P. H. van Beek. High-resolutionmodeling of human and climate impacts on global water resources. *Journal of Advances in Modeling Earth Systems*, 8:735–763, 2016. doi:10.1002/2013MS000282.Received.

[92] P.J. Ward, B. Jongman, M. Kummu, M.D. Dettinger, F.C. Sperna Weiland, and H.C. Winsemius. Strong influence of El Niño Southern Oscillation on flood risk around the world. *Proceedings of the National Academy of Science of the USA*, pages 1–6, 2014. doi:10.1073/pnas.1409822111.

[93] J.R. Williams. *The EPIC Model*, pages 909–1000. Water Resources Publications, Littleton, USA, 1995.

[94] Dai Yamazaki, Gustavo A M De Almeida, and Paul D. Bates. Improving computational efficiency in global river models by implementing the local inertial flow equation and a vector-based river network map. *Water Resources Research*, 49(11):7221–7235, 2013. doi:10.1002/wrcr.20552.

[95] Dai Yamazaki, Shinjiro Kanae, Hyungjun Kim, and Taikan Oki. A physically based description of floodplain inundation dynamics in a global river routing model. *Water Resources Research*, 47(4):1–21, 2011. doi:10.1029/2010WR009726.

[96] C. Yue, P. Ciais, P. Cadule, K. Thonicke, S. Archibald, B. Poulter, W. M. Hao, S. Hantson, F. Mouillot, P. Friedlingstein, F. Maignan, and N. Viovy. Modelling the role of fires in the terrestrial carbon balance by incorporating SPITFIRE into the global vegetation model ORCHIDEE – Part 1: simulating historical global burned area and fire regimes. *Geoscientific Model Development*, 7(6):2747–2767, 2014. URL: https://www.geosci-model-dev.net/7/2747/2014/, doi:10.5194/gmd-7-2747-2014.

[97] C. Yue, P. Ciais, P. Cadule, K. Thonicke, and T. T. van Leeuwen. Modelling the role of fires in the terrestrial carbon balance by incorporating SPITFIRE into the global vegetation model ORCHIDEE – Part 2: Carbon emissions and the role of fires in the global carbon balance. *Geoscientific Model Development*, 8(5):1321–1338, 2015. URL: https://www.geosci-model-dev.net/8/1321/2015/, doi:10.5194/gmd-8-1321-2015.

[98] Fang Zhao, Ted I E Veldkamp, Katja Frieler, Jacob Schewe, Sebastian Ostberg, Sven Willner, Bernhard Schauberger, Simon N Gosling, Hannes Müller Schmied, Felix T Portmann, Guoyong Leng, Maoyi Huang, Xingcai Liu, Qiuhong Tang, Naota Hanasaki, Hester Biemans, Dieter Gerten, Yusuke Satoh, Yadu Pokhrel, Tobias Stacke, Philippe Ciais, Jinfeng Chang, Agnes Ducharne, Matthieu Guimberteau, Yoshihide Wada, Hyungjun Kim, and Dai Yamazaki. The critical role of the routing scheme in simulating peak river discharge in global hydrological models. *Environmental Research Letters*, 12(7):075003, jul 2017. URL: http://stacks.iop.org/1748-9326/12/i=7/a=075003?key=crossref.63f02148d4abaa19c17d3bacfa731598, doi:10.1088/1748-9326/aa7250.